Mathematics of Super-Resolution Biomedical Imaging

H. Ammari and J. Garnier and H. Kang and L. H. Nguyen and

L. Seppecher

Habib Ammari, Josselin Garnier, Hyeonbae
Kang, Loc Hoang Nguyen, Laurent Seppecher

Mathematics of Super-Resolution Biomedical Imaging

Contents

Part II Single-Wave Imaging

Part III Anomaly Imaging

1

Introduction

Inverse problems in medical imaging are in their most general form ill-posed. They literally have no solution. If, however, in advance one has additional structural information or can supply missing information, then one may be able to determine specific features about what one wishes to image with a satisfactory resolution and accuracy. One such type of information can be that the imaging problem is to find unknown small anomalies with significantly different parameters from those of the surrounding medium. These anomalies may represent potential tumors at an early stage. Over the last few years, an expansion technique has been developed for the imaging of such anomalies. It has proven useful in dealing with many medical imaging problems. The method relies on linearizing the data with respect to the characteristic size of the anomalies. A remarkable feature of this method is that it allows a stable and accurate reconstruction of the location and of some geometric features of the anomalies, even with moderately noisy data [64]. This is because the method reduces the set of admissible solutions and the number of unknowns. It can be seen as a kind of regularization in comparison with (nonlinear) iterative approaches.

More recently, assuming that the material properties of the tissues have known or partially known frequency profiles or spatial regularity, signal separation techniques have been successfully used for the robust solution of biomedical imaging problems from multifrequency or multi-measurement settings [12, 13, 48].

Another promising technique for efficient imaging is to combine into one tomographic process different physical types of waves. Doing so, one alleviates deficiencies of each separate type of waves, while combining their strengths. Again, asymptotic analysis plays a key role in the design of robust and efficient imaging techniques based on this concept of multi-waves. In the last decade or so, work on multi-wave imaging in biomedical applications has come a long way [24, 322]. The motivation is to achieve high-resolution and high-contrast imaging. Multi-wave imaging modalities include photoacoustic and thermoacoustic imaging [345], magnetic resonance elastography [262],

magneto-acousto-electrical tomography [308], magnetoacoustic tomography with magnetic induction [346], and impediography [208].

Recently, driven by the search for new materials with interesting and unique optical properties, the field of nanoparticle research has grown immensely [256]. Nanoparticles have been proposed to be used as labels in molecular biology. New types of cancer diagnostic nanoparticles are constantly being developed. Plasmon resonant nanoparticles have unique capabilities of enhancing the brightness and directivity of light and confining strong electromagnetic fields. Their optical response is dominated by the appearance of plasmon resonances over a wide range of wavelengths [256]. Plasmon resonant nanoparticles are also being used in thermotherapy as nanometric heat-generators that can be activated remotely by external electromagnetic fields [90]. Second-harmonic generation contrast mechanisms have been also used in biomedical imaging. These emerging nonlinear optical contrast mechanisms reveal new information from biological specimens and tissues [326].

Properties of Biological Tissues

Dielectric Properties

Dielectric properties of a material basically reflect the electric charge movement inside the material in response to an external electric field. Dielectric response of biological materials is always frequency dependent. It results from the interaction of electromagnetic radiation with their constituents at the cellular and molecular level. Information about tissue structure and composition can be obtained by measuring the dielectric properties of the tissues [265].

Low-frequency, radio-frequency, and microwave dielectric properties of biological materials are of interest in electrical impedance tomography and microwave imaging. They are important for our understanding of the mechanism of interaction of electromagnetic fields with biological systems in these frequency ranges. The two electrical properties which define the electrical characteristics are the dielectric constant and the conductivity. These dielectric properties are frequency-dependent or dispersive. A significant change in them over a frequency range is called a dielectric dispersion. Although the dielectric properties of the tissues vary greatly from tissue to tissue, their typical behavior is characterized by three distinctly large dielectric dispersions, referred to as α-, β-, and γ-dispersions [265]. The α-dispersion usually occurs below a few kHz (low-frequencies), the β-dispersion in the frequency region from tens of kHz to tens of MHz (radio-frequencies), and the γ-dispersion in the microwave frequency region from 0.1 to 100 GHz. The mechanism of the α-dispersion is associated with polarization in the tissue. The β-dispersion is caused by the cellular structure of tissues, with poorly conducting membranes separating intracellular and extracellular domains. It arises principally

from interfacial polarization of cell membranes (Maxwell-Wagner-Fricke effect). The γ-dispersion arises mainly from polarization due to reorientation of water molecules.

Assume a time-harmonic electric field $\Re(E(x)e^{i\omega t})$ is applied to a biological material. The total induced current density $\Re(J_{\text{tot}}(x)e^{i\omega t})$ inside the material is given by

$$J_{\text{tot}} = (\sigma_0 + i\omega\varepsilon)E = (\sigma_0 + \omega\varepsilon'')E + i\omega\varepsilon'E\,,$$

where ω is the angular frequency of the applied field, σ_0 is the conductivity of the material at very low frequencies, $\varepsilon := \varepsilon' - i\varepsilon''$ is the complex permittivity of the material, ε' is the dielectric constant, and ε'' is the loss factor of the material. The (frequency-dependent) conductivity σ of the material is given by

$$\sigma(\omega) = \sigma_0 + \omega\varepsilon''(\omega)\,.$$

We call

$$\kappa(\omega) = \sigma(\omega) + i\omega\varepsilon'(\omega)$$

the electrical admittivity of the material.

The dielectric constant ε' and the loss factor ε'' are not independent of each other. For linear and causal dielectric response, the Kramers-Kronig relations give a necessary connection between them. We have

$$\varepsilon'(\omega) - \varepsilon_\infty = \frac{2}{\pi}\text{p.v.}\int_0^{+\infty} \frac{s\varepsilon''(s)}{s^2 - \omega^2}ds\,,$$

$$\varepsilon''(\omega) = -\frac{2\omega}{\pi}\text{p.v.}\int_0^{+\infty} \frac{\varepsilon'(s) - \varepsilon_\infty}{s^2 - \omega^2}ds\,,$$

where ε_∞ is the dielectric constant at very high frequencies and p.v. denotes the Cauchy principal value. A linear response means that the dielectric properties are independent of the applied field strength, which is true for biological tissue when the external electric field is not very strong. On the other hand, causality is one of the fundamental principles in physics. It states that the effect cannot precede the cause. For scattering of electromagnetic waves, it indicates that no scattered wave can exist before the incident wave has reached the scattering object, whose size is assumed to be finite.

Idealized approaches have been used to interpret experimental data for the frequency-dependence of the dielectric constant and the conductivity:

- Debye model:
$$\varepsilon(\omega) = \varepsilon_\infty + \frac{\varepsilon_0 - \varepsilon_\infty}{1 + i\omega\tau}\,;$$

- Cole-Cole model:
$$\varepsilon(\omega) = \varepsilon_\infty + \frac{\varepsilon_0 - \varepsilon_\infty}{1 + (i\omega\tau)^{1-\eta}}\,,$$

where ε_0 is the dielectric constant at very low frequencies, τ is a relaxation time, and τ and $0 < \eta < 1$ depend on the nature of the biological material.

As will shown later, membranes are responsible of the dielectric properties of tissues at low- and radio-frequencies (α- and β-dispersion ranges). Charges accumulate at membranes from extra and intracellular fluids and lead to anisotropic overall dielectric properties because of the orientation of cells. The pertinent mathematical theory for analyzing this fundamental mechanism is based on homogenization of double layers.

Dielectric properties at microwave frequencies are largely determined by the strongly dispersive behavior of water. The cell membranes impose no hindrance on the flow of electricity through the cell interior for frequencies in the γ-dispersion range. Consequently, since cell structure does not affect microwave data, dielectric properties of tissues at microwave frequencies can be considered isotropic. Moreover, they are solely determined by water and macromolecular content of tissues.

The interaction of electromagnetic radiation with (nonmagnetic) biological tissues can be modeled by using Maxwell's equations. Let Ω denote the medium. In the time-domain, these governing equations in $\Omega \times \mathbb{R}^+$ are

$$\begin{cases} \nabla \times E = -\dfrac{\partial H}{\partial t}, \quad \nabla \times H = J + \dfrac{\partial D}{\partial t}, \\ \nabla \cdot H = 0, \quad \nabla \cdot D = \rho, \end{cases} \tag{1.1}$$

where E is the electric field, H is the magnetic field, D is the electric flux density, $\partial D/\partial t$ is the displacement current, ρ and J are the electric charge and current densities, and t denotes time. The charge and current densities ρ and J are the sources of the electromagnetic fields. For wave propagation, they are localized in space. From (1.1), they satisfy in $\Omega \times \mathbb{R}^+$ the equation of conservation of charges:

$$\nabla \cdot J + \frac{\partial \rho}{\partial t} = 0. \tag{1.2}$$

On the other hand, Ohm's law is valid and is expressed as

$$J = \sigma_0 E \quad \text{in } \Omega \times \mathbb{R}_+. \tag{1.3}$$

The total current density $J_{\text{tot}} = J + \partial D/\partial t = \sigma_0 E + \partial D/\partial t$. The electric flux density D is related to the electric field E via the so-called constitutive relation, whose precise form depends on the material in which the fields exist. When a time-varying electric field is applied, the polarization response of the biological material is local but not instantaneous. Such (dispersive) response can be described by the causal constitutive relationship:

$$D(x,t) = \int_{-\infty}^{t} \varepsilon(x, t-s) E(x,s) ds, \quad (x,t) \in \Omega \times \mathbb{R}^+. \tag{1.4}$$

Through the inverse Fourier transform, general solutions of Maxwell's equation can be built as linear combinations of single-frequency (or time-harmonic) solutions. We assume that the fields are time-harmonic

$$E(x,t) = \Re(E(x,\omega)e^{i\omega t}), \quad H(x,t) = \Re(H(x,\omega)e^{i\omega t}),$$

$$D(x,t) = \Re(D(x,\omega)e^{i\omega t}), \quad \text{etc}$$

where $E(x,\omega), H(x,\omega), D(x,\omega)$, etc, are complex-valued functions. Replacing time derivatives $\partial/\partial t$ by $i\omega$, and writing here

$$\varepsilon(x,\omega) = \int_{-\infty}^{\infty} \varepsilon(x,t)e^{-i\omega t}\, dt\,,$$

the constitutive relation (1.4) becomes multiplicative in the frequency domain:

$$D(x,\omega) = \varepsilon(x,\omega)E(x,\omega)\,.$$

As said earlier, the Kramers-Kronig relations are the frequency-domain expression of causality and relate the real and imaginary parts, ε' and $-\varepsilon''$, of ε as functions of ω. The Maxwell equations (1.1) can be written in the form:

$$\nabla \times \nabla \times E - \omega^2\big(\varepsilon' + \frac{\sigma}{i\omega}\big)E = 0\,. \tag{1.5}$$

At $\omega \to 0$, $\nabla \times E = 0$, and therefore, $E = \nabla u$, where the electric potential u is solution to the conductivity equation

$$\nabla \cdot \big(\sigma + i\omega\varepsilon'\big)\nabla u = 0\,.$$

On the other hand, at microwave frequencies, the Helmholtz equation can be used to approximate (1.5). Let

$$n^2 = \big(\varepsilon' + \frac{\sigma}{i\omega}\big)\,.$$

Using the vectorial identity $\nabla \times \nabla = -\Delta + \nabla\nabla\cdot$, it follows that

$$\Delta E + \omega^2 n^2 E + 2\nabla\big(\frac{\nabla n}{n} \cdot E\big) = 0\,.$$

Assume that

$$\omega \Big|\frac{\nabla n}{n}\Big| \ll 1\,,$$

which means that ε' and ε'' vary slowly on the scale of the wavelength $2\pi/\omega$. Then, any of the components E_j of E satisfies (approximately) the Helmholtz equation:

$$\Delta E_j + \omega^2 n^2 E_j = 0\,. \tag{1.6}$$

We refer to (1.6) as the scalar approximation of Maxwell's equations.

Optical Properties

Electromagnetic fields can be transmitted through a biological medium with varying degrees of absorption, reflection, and scattering. Absorption is a function of the molecular composition of tissue and is therefore sensitive to tissue pathologies and functions, reflection occurs at tissues boundaries and scattering is caused by inhomogeneities of the order of a wavelength in tissues. At optical wavelengths, electromagnetic wave propagation is dominated by scattering because the inhomogeneities of cellular structures and particle sizes are of the order of an optical wavelength. Optical propagation in biological materials can be investigated in three scales [82]. The mathematical description of light propagation changes according to the length scale of interest [307]. Maxwell's equations in random media are valid on the microscopic scale. The mesoscale, in which the characteristic scale is set by the scattering length, can be described by the radiative transport equation. The radiative transfer equation can be derived by considering the high-frequency asymptotics of wave propagation in a random medium. The random medium is assumed to be statistically homogeneous and its dielectric properties are described by a random field and are weakly fluctuating. Finally, the macroscale can be described by the diffusion approximation to the radiative transfer approximation.

In radiative transport theory, the propagation of light through a material medium is formulated in terms of a conservation law that accounts for gains and losses of photons due to scattering and absorption. The fundamental quantity of interest is the specific intensity $I(x, \xi)$, defined as the intensity at the position x in the direction ξ. The specific intensity obeys the radiative transfer equation (RTE):

$$\frac{1}{c}\frac{\partial I}{\partial t} + \xi \cdot \nabla I + (\mu_a + \mu_s)I = \mu_s \int_S p(\xi', \xi)I(x, \xi', t)d\xi' \qquad (1.7)$$

for $(x, \xi, t) \in \Omega \times S \times \mathbb{R}^+$, where μ_a and μ_s are the absorption and scattering coefficients, c is the speed of light, and S is the unit sphere. The specific intensity I also satisfies the half-range boundary condition

$$I(x, \xi, t) = I^{\text{in}}(x, \xi, t) , \quad \xi \cdot \nu < 0 , \quad (x, t) \in \partial\Omega \times \mathbb{R}^+ , \qquad (1.8)$$

where I^{in} is the incident specific intensity at the boundary and ν is the outward normal to $\partial\Omega$. The phase function p is symmetric with respect to interchange of its arguments and obeys the normalization condition

$$\int_S p(\xi, \xi')d\xi' = 1 , \qquad (1.9)$$

for all ξ. For scattering by spherically-symmetric particles, $p(\xi, \xi')$ depends only upon the angle between ξ and ξ'. For isotropic scattering, $p = 1/(4\pi)$.

If the medium is composed of spatially uncorrelated point particles with number density ρ, then

$$\mu_a = \rho\sigma_a \ , \quad \mu_s = \rho\sigma_s \ , \quad p = \frac{d\sigma_s}{d\Theta}/\sigma_s \ , \tag{1.10}$$

where σ_a and σ_s are the absorption and scattering cross sections of the particles and $d\sigma_s/d\Theta$ is the differential scattering cross section. Here, Θ is the solid angle. Note that σ_a, σ_s and p are wavelength dependent quantities.

The diffusion approximation (DA) to the RTE is widely used in applications. It is valid in the regime where the scattering mean free path $1/\mu_s$ is small compared to the distance of propagation. The diffusion approximation is derived using asymptotic methods. The advantage of this approach is that it leads to error estimates and treats the problem of boundary conditions for the resulting diffusion equation in a natural way.

The diffusion approximation holds when the scattering coefficient is large, the absorption coefficient is small, the point of observation is far from the boundary of the medium and the time-scale is sufficiently long. Accordingly, we perform the rescaling

$$\mu_a \to \epsilon\mu_a \ , \quad \mu_s \to \frac{1}{\epsilon}\mu_s \ , \quad t \to \frac{1}{\epsilon}t \ , \tag{1.11}$$

where $\epsilon \ll 1$. Thus the RTE (1.7) becomes

$$\frac{\epsilon^2}{c}\frac{\partial I}{\partial t} + \epsilon\xi \cdot \nabla I + \epsilon^2\mu_a I + \mu_s I = \mu_s \int_S p(\xi,\xi')I(x,\xi',t)d\xi' \ . \tag{1.12}$$

We then introduce the asymptotic expansion for the specific intensity

$$I(x,\xi,t) = I_0(x,\xi,t) + \epsilon I_1(x,\xi,t) + \epsilon^2 I_2(x,\xi,t) + \cdots \tag{1.13}$$

which we substitute into (1.12). Upon collecting terms of $O(1)$, $O(\epsilon)$ and $O(\epsilon^2)$ we have

$$\int_S p(\xi,\xi')I_0(x,\xi',t)d\xi' = I_0(x,\xi,t) \ , \tag{1.14}$$

$$\xi \cdot \nabla I_0 + \mu_s I_1 = \mu_s \int_S p(\xi,\xi')I_1(x,\xi',t)d\xi' \ , \tag{1.15}$$

$$\xi \cdot \nabla I_1 + \mu_a I_0 + \mu_s I_2 = \mu_s \int_S p(\xi,\xi')I_2(x,\xi',t)d\xi' \ . \tag{1.16}$$

The normalization condition (1.9) forces I_0 to be independent of ξ. If $p(\xi,\xi')$ depends only upon the quantity $\xi \cdot \xi'$, it can be seen that

$$I_1(x,\xi,t) = -\frac{1}{1-g}\xi \cdot \nabla I_0(x,t) \ , \tag{1.17}$$

where the anisotropy g is given by

$$g = \int_S \xi \cdot \xi' p(\xi \cdot \xi')d\xi' \ , \tag{1.18}$$

with $-1 < g < 1$. Note that $g = 0$ corresponds to isotropic scattering and $g = 1$ to extreme forward scattering. If we insert the above expression for I_1 into (1.16) and integrate over ξ, we obtain the (approximate) diffusion equation for the energy density $\Phi(x,t) = \frac{1}{c} \int I(x,\xi,t)\, d\xi$:

$$\frac{\partial \Phi(x,t)}{\partial t} - \nabla \cdot [D(x)\nabla \Phi(x,t)] + c\mu_a(x)\Phi(x,t) = 0 \ . \qquad (1.19)$$

Here the diffusion coefficient is defined by

$$D = \frac{c}{3(1-g)\mu_t} \ , \qquad (1.20)$$

where $\mu_t = \mu_a + \mu_s$ is the extinction coefficient. The above derivation of the diffusion approximation holds in an infinite medium. In a bounded domain, it is necessary to account for boundary layers, since the boundary conditions for the diffusion equation and the RTE are not compatible. In addition to (1.19), the energy density must satisfy the boundary condition

$$\Phi + \ell_{\text{ext}}\nu \cdot \nabla \Phi = f \quad \text{on} \quad \partial\Omega \times \mathbb{R}^+ \ , \qquad (1.21)$$

where f is the source and the extrapolation length ℓ_{ext} can be computed from radiative transport theory. We note that $\ell_{\text{ext}} = 0$ corresponds to an absorbing boundary and $\ell_{\text{ext}} \to \infty$ to a reflecting boundary.

Assuming a time-harmonic source $f(x,t) = \Re(f(x)e^{i\omega t})$ with modulation frequency ω, the energy density is of the form $|Phi(x,t) = \Re(|Phi(x)e^{i\omega t})$ where the density $\Phi(x)$ obeys the equation

$$-\nabla \cdot [D(x)\nabla \Phi(x)] + (c\mu_a(\boldsymbol{r}) + i\omega)\Phi(x) = 0 \quad \text{in} \quad \Omega \ , \qquad (1.22)$$

with the boundary condition (1.21) on $\partial\Omega$.

Elastic Properties

Elasticity imaging for medical diagnosis aims at providing a quantitative visualization of mechanical properties of tissues. Biological tissues are linear, isotropic (visco-)elastic materials. The elastic properties of tissues carry information about their composition, micro-structure, physiology, and pathology. Changes in tissue elasticity are generally correlated with pathological phenomena such as weakening of vessel walls or cirrhosis of the liver. Many cancers appear as extremely hard nodules because of the recruitment of collagen during tumorigenesis. It is therefore very interesting and challenging for diagnostic applications to find ways for generating resolved images that depict tissue elasticity or stiffness [262].

Let (λ, μ) be the Lamé coefficients of the medium and let ρ be its density. We also introduce the bulk modulus $\beta := \lambda + 2\mu/d$. The compression modulus λ measures the resistance of the material to compression and the shear modulus μ measures the resistance to shearing.

Let F be a mechanical force. Assuming that we can use the linear isotropic elasticity model, the displacements inside the medium can be described by the initial boundary-value problem for the Lamé system of equations:

$$\begin{cases} \rho\dfrac{\partial^2 u}{\partial t^2} - \nabla\lambda\nabla\cdot u - \nabla\cdot\mu\nabla^s u = F & \text{in } \Omega\times\mathbb{R}_+\,, \\[2mm] \dfrac{\partial u}{\partial n} = 0 & \text{on } \partial\Omega\times\mathbb{R}_+\,, \\[2mm] u(x,0) = \dfrac{\partial u}{\partial t}(x,0) = 0 & \text{in } \Omega\,, \end{cases} \qquad (1.23)$$

where $\nabla^s = (\nabla + \nabla^T)/2$ with the superscript T being the transpose. Here, $\partial/\partial\nu$ denotes the co-normal derivative defined by

$$\frac{\partial u}{\partial n} = \lambda(\nabla\cdot u)\nu + 2\mu\nabla^s u\,\nu \quad \text{on } \partial\Omega\,,$$

where ν is the outward normal at $\partial\Omega$. The symmetric gradient $\nabla^s u$ is the strain tensor with entries $(\partial_i u_j + \partial_j u_i)/2$. If we define the elasticity tensor $\mathbb{C} = (C_{ijkl})_{i,j,k,l=1}^d$ for by

$$C_{ijkl} = \lambda\delta_{ij}\delta_{kl} + \mu(\delta_{ik}\delta_{jl} + \delta_{il}\delta_{jk})\,,$$

the stress tensor is given by

$$\sigma(u) = \mathbb{C}\nabla^s u\,.$$

The Neumann boundary condition, $\partial u/\partial n = 0$ on $\partial\Omega$, comes from the fact that the sample is embedded in air and can move freely at the boundary.

Under some physical assumptions, the Lamé system of equations (1.23) can be reduced to an acoustic wave equation. For doing so, we neglect the shear effects in the medium by taking $\mu = 0$. The acoustic approximation says that the dominant wave type is a compressional wave. Equation (1.23) becomes

$$\begin{cases} \rho\dfrac{\partial^2 u}{\partial t^2} - \nabla\lambda\nabla\cdot u = F & \text{in } \Omega\times\mathbb{R}_+\,, \\[2mm] \dfrac{\partial u}{\partial n} = 0 & \text{on } \partial\Omega\times\mathbb{R}_+\,, \\[2mm] u(x,0) = \dfrac{\partial u}{\partial t}(x,0) = 0 & \text{in } \Omega\,. \end{cases} \qquad (1.24)$$

Introduce the pressure

$$p = \lambda\nabla\cdot u \quad \text{in } \Omega\times\mathbb{R}_+\,.$$

Taking the divergence of (1.24) yields the acoustic wave equation

$$\begin{cases} \dfrac{1}{\lambda}\dfrac{\partial^2 p}{\partial t^2} - \nabla \cdot \dfrac{1}{\rho}\nabla p = \nabla \cdot F & \text{in } \Omega \times \mathbb{R}_+ \,, \\[2mm] \qquad\qquad\qquad p = 0 & \text{on } \partial\Omega \times \mathbb{R}_+ \,, \\[2mm] p(x,0) = \dfrac{\partial p}{\partial t}(x,0) = 0 & \text{in } \Omega \,. \end{cases} \tag{1.25}$$

Note that acoustic wave reflection in soft tissue by an interface with air can be modeled well by a homogeneous Dirichlet boundary condition.

Through the inverse Fourier transform, time-harmonic solutions to the elasticity and the acoustic wave equations respectively satisfy

$$\begin{cases} \nabla \cdot \mu \nabla^s u + \nabla \lambda \nabla \cdot u + \omega^2 \rho u = F & \text{in } \Omega \,, \\[2mm] \qquad\qquad\qquad\qquad \dfrac{\partial u}{\partial n} = 0 & \text{on } \partial\Omega \,, \end{cases}$$

and

$$\begin{cases} \nabla \cdot \dfrac{1}{\rho}\nabla p + \dfrac{\omega^2}{\lambda}p = -\nabla \cdot F & \text{in } \Omega \,, \\[2mm] \qquad\qquad\quad p = 0 & \text{on } \partial\Omega \,, \end{cases}$$

where, by abuse of notation, F denotes the inverse Fourier transform of the source term.

In elasticity imaging of biological media, the compression modulus λ is four to six orders of magnitude higher than the shear modulus μ [262]. As $\lambda \to +\infty$, the Lamé system converges to the modified Stokes system given by

$$\begin{cases} \nabla \cdot \mu \nabla^s u + \nabla p + \omega^2 \rho u = F & \text{in } \Omega \,, \\[2mm] \qquad\qquad\qquad \nabla \cdot u = 0 & \text{in } \Omega \,, \\[2mm] \qquad\quad p\nu + \mu \dfrac{\partial u}{\partial \nu} = 0 & \text{on } \partial\Omega \,. \end{cases}$$

By reducing the elasticity system to the modified Stokes system, one removes the compression modulus from consideration [47]. Viscosity tissue properties can be included by considering the shear modulus μ to depend on the frequency ω. Again, Kramers-Kronig relations give a necessary connection between the real and imaginary parts of μ as functions of ω.

Super-Resolution Biomedical Imaging

Super-resolution imaging is a collective name for a number of emerging techniques that achieve resolution below the conventional resolution limit, defined as the minimum distance that two point-source objects have to be in order to distinguish the two sources from each other. In this book we describe recent advances in scale separation techniques, spectroscopic approaches, multi-wave

imaging, and nanoparticle imaging. The objective is fivefold: (i) To provide asymptotic expansions for both internal and boundary perturbations that are due to the presence of small anomalies; (ii) To apply those asymptotic formulas for the purpose of identifying the material parameters and certain geometric features of the anomalies; (iii) To design efficient inversion algorithms in multi-wave modalities; (iv) to develop inversion techniques using multi-frequency measurements; (v) to develop a mathematical and numerical framework for nanoparticle imaging.

Applications of the anomaly detection and multi-wave approaches in medical imaging are described in some detail. In particular, the use of asymptotic analysis to improve a multitude of emerging imaging techniques is highlighted. These imaging modalities include both single-wave and multi-wave approaches. They can be divided into three groups: (i) Those using boundary or scattering measurements such as electrical impedance tomography, ultrasound, and infrared tomographies; (ii) Those using internal measurements such as magnetic resonance elastography; (iii) Those using boundary measurements obtained from internal perturbations of the medium such as photoacoustic tomography, impediography, and magnetoacoustic imaging.

Multi-wave imaging is based on thermo-elastic, acousto-electric, and Lorentz force effects.

When a tissue absorbs and is heated by laser energy, the resulting nonuniform temperature distribution causes internal forces, which lead to thermo-elastic deformation. This deformation is determined (in a solid body) by the thermo-elastic wave equation subject to the appropriate boundary and initial conditions. Thermoacoustic phenomenon consists of two processes: microwave energy absorption and acoustic wave generation. Thermal diffusion in the thermoacoustic process can be neglected because the microwave pulse width is much shorter than the thermal diffusion time in biological tissues, that is, the thermal confinement condition is satisfied. Accordingly, the acoustic wave generated by heat and thermo-elastic expansion from the absorbed microwave is governed by

$$\frac{1}{c^2}\frac{\partial^2 p}{\partial t^2} - \Delta p = \frac{\beta}{C_p}\sigma|E|^2\,\delta_{t=0}\,,$$

where $c = \sqrt{\lambda/\rho}$ is the speed of sound, C_p is the specific heat capacity, β is the thermal expansion coefficient, and $\delta_{t=0}$ is the Dirac mass at $t = 0$. The electric field E is solution to the Helmholtz equation

$$\Delta E + \omega^2(\varepsilon' + \frac{\sigma}{i\omega})E = 0\,,$$

with the permittivity ε' being known. Quantitative thermoacoustic imaging is to determine σ from measurements of $\sigma|E|^2$ in the domain Ω.

Photoacoustic imaging is a hybrid emerging modality, combining the high contrast and spectroscopic-based specificity of optical imaging with the high spatial resolution of ultrasound imaging. It consists in measuring outside the

object the acoustic signals emitted by the thermo-elastic effect by use of ultrasonic transducers. Its objective is to produce an image that represents a map of spatially variant electromagnetic absorption properties of the tissues, from knowledge of the measured acoustic signals [345].

Superresolution imaging of electrical activities and properties of biological tissues can be achieved using the acousto-electric effect [208]. The acousto-electric effect was first presented after studying the effects of ultrasonic pressure changes on conductivity on electrolytes. As an ultrasound wave distributes through an aqueous solution it produces periodic change in pressure and temperature and therefore modifies the conductivity of the solution inside the insonified volume determined by the ultrasound source. By applying electric current to the solution, the change in conductivity gives rise to a change in voltage, producing the acousto-electric interaction signal. The interaction signal is proportional to the pressure change and the amount of current lowing through the medium and has the same frequency as the acoustic pressure wave. The phenomena causing the modulation of the conductivity are periodic acoustic pressure change and change in temperature. The resulting effects are a change in molar concentration due to the bulk compressibility and thermal expansion effect, and a change in ion mobility due to the changes in solvent viscosity against pressure and temperature.

The Lorentz force is the force acting on currents in a magnetic field. It plays a key role in ultrasonically-induced Lorentz force imaging of conductivity and magnetoacoustic tomography with magnetic induction [346]. The Lorentz force per unit volume, F, arising from the current density J and the magnetic field B is given by

$$F = J \times B \,.$$

In general, magnetoacoustic effects are small, but small effects underlie many emerging biomedical imaging techniques [308].

The aim of this book is to review recent developments in the mathematical and numerical modelling of anomaly detection, spectroscopic imaging, and multi-wave biomedical imaging.

The book is divided into four parts:

- Anomaly Imaging: Scale Separation Techniques
- Multi-Wave Imaging
- Spectroscopic Imaging
- Nanoparticle Imaging

The four approaches described in this book allow one to overcome the severe ill-posedness character of imaging reconstruction in biomedical applications and to achieve superresolution imaging. Their robustness with respect to incomplete data, measurement, and medium noises is also investigated.

The bibliography provides a list of relevant references. It is by no means comprehensive. However, it should provide the reader with some useful guidance in searching for further details on the main ideas and approaches discussed in this book.

The material in this book is taught as a graduate course in applied mathematics at ETH. Tutorial notes and Matlab codes can be downloaded at `http://www.sam.math.ethz.ch/~hammari/`. We are very grateful to Giovanni Alberti and Francisco Romero for preparing them. Some of the material in this book is from our wonderful collaborations with Giovanni Alberti, Eric Bonnetier, Elie Bretin, Yves Capdeboscq, Mathias Fink, Pierre Garapon, Laure Giovangigli, Bangti Jin, Wenjia Jing, Vincent Jugnon, Eunjung Lee, Hyundae Lee, Pierre Millien, Matias Ruiz, Jin Keun Seo, Mickael Tanter, Faouzi Triki, Abdul Wahab, Han Wang, Eung Je Woo, and Hai Zhang. We feel indebted to all of them.

Part I

Mathematical and Probabilistic Tools

2

Basic Mathematical Concepts

This chapter reviews some mathematical concepts essential for understanding imaging principles. We first review commonly used special functions, function spaces, and integral transforms: the Fourier transform and the spherical mean Radon transform. We then collect basic facts about the Kramers-Kronig relations, the Moore-Penrose generalized inverse, singular value decomposition, and compact operators. The theory of regularization of ill-posed inverse problems is briefly discussed.

2.1 Special Functions

2.1.1 Bessel Functions

Bessel functions of the first kind of real order ν, denoted by $J_\nu(x)$, are useful for describing some imaging effects. One definition of $J_\nu(x)$ is given in terms of the series representation

$$J_\nu(x) = (\frac{x}{2})^\nu \sum_{l=0}^{+\infty} \frac{(-x^2/4)^l}{l!\Gamma(\nu+l+1)} \, , \qquad (2.1)$$

where the gamma function Γ is defined by

$$\Gamma(z) = \int_0^{+\infty} e^{-t} t^{z-1} \, dt \quad \text{for } \Re(z) > 0 \, .$$

Another formula, valid for $\Re\nu > -\frac{1}{2}$, is

$$J_\nu(x) = [\Gamma(\frac{1}{2})\Gamma(\nu+\frac{1}{2})]^{-1}(\frac{x}{2})^\nu \int_{-1}^1 (1-t^2)^{\nu-\frac{1}{2}} e^{ixt} \, dt \, . \qquad (2.2)$$

Some useful identities for Bessel functions are summarized below. For further details, we refer the reader to [331, pages 225-233].

We have the recurrence relation

$$(\frac{d}{dx} + \frac{\nu}{x})J_\nu(x) = J_{\nu-1}(x) \ . \tag{2.3}$$

For $n \in \mathbb{Z}$, we have the integral representation

$$J_n(x) = \frac{1}{2\pi} \int_{-\pi}^{\pi} e^{ix \sin \phi - in\phi} d\phi \ , \tag{2.4}$$

i.e., the functions $J_n(x)$ are the Fourier coefficients of $e^{ix \sin \phi}$. Therefore, the Jacobi-Anger expansion holds:

$$e^{ix \sin \phi} = \sum_{n \in \mathbb{Z}} J_n(x) e^{in\phi} \ . \tag{2.5}$$

Formula (2.5) can be used in two dimensions to expand a plane wave as a sum of cylindrical waves. We have

$$e^{i\xi \cdot x} = \sum_{n \in \mathbb{Z}} e^{in(\frac{\pi}{2} - \theta_\xi)} J_n(|\xi||x|) e^{in\theta_x} \ , \tag{2.6}$$

where $x = (|x|, \theta_x)$ and $\xi = (|\xi|, \theta_\xi)$ in the polar coordinates. The function $x \mapsto J_n(|\xi||x|) e^{in\theta_x}$ is called a cylindrical wave.
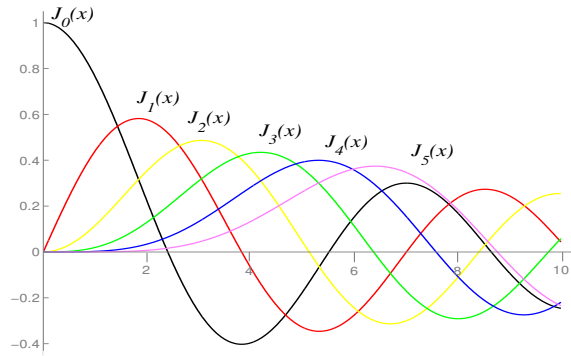
Fig. 2.1. Plots of Bessel functions $J_n(x), n = 0, \ldots, 5$.

For $n, l \in \mathbb{Z}$, we have

$$\int_0^{\pi/2} J_{2n}(2x \sin \phi) \, d\phi = \frac{\pi}{2} J_n^2(x) \ , \tag{2.7}$$

and

$$\int_0^\pi J_l(2x\cos\phi)\cos((2n-l)\phi)\,d\phi = 2\pi J_n(x)J_{l-n}(x)\ . \tag{2.8}$$

Formula (2.8) is known as Neumann's formula.

Bessel functions appear in an approximation of the Dirac function δ_0 at the origin. Let $\mathcal{F}$ be the Fourier transform defined for $f \in L^1(\mathbb{R}^d)$ by

$$\mathcal{F}[f](\xi) = (2\pi)^{-d/2}\int_{\mathbb{R}^d} e^{-ix\cdot\xi}f(x)\,dx\ . \tag{2.9}$$

An approximation $\tilde\delta_K$ to δ_0 can be defined by

$$\mathcal{F}[\tilde\delta_K](\xi) = \begin{cases} (2\pi)^{-d/2}, & |\xi| < K\ , \\ 0, & |\xi| \geq K\ , \end{cases} \tag{2.10}$$

or equivalently by

$$\tilde\delta_K(x) = (2\pi)^{-d/2}\frac{J_{d/2}(K|x|)}{(K|x|)^{d/2}}\ , \tag{2.11}$$

where $J_{d/2}$ is the Bessel function of the first kind of order $d/2$.

For arguments $x < \nu$, the Bessel functions look qualitatively like simple power law, with the asymptotic form for $0 < x \ll \nu$

$$J_\nu(x) \approx \frac{1}{\Gamma(\nu+1)}\left(\frac{x}{2}\right)^\nu \approx \frac{1}{\sqrt{2\pi\nu}}\left(\frac{ex}{2\nu}\right)^\nu\ . \tag{2.12}$$

For $x > \nu$, the Bessel functions look qualitatively like cosine waves whose amplitude decay as $x^{-1/2}$. The asymptotic form for $x \gg \nu$ is

$$J_\nu(x) \approx \sqrt{\frac{2}{\pi x}}\cos\left(x - \frac{\nu\pi}{2} - \frac{\pi}{4}\right)\ . \tag{2.13}$$

In the transition region where $x \approx \nu$, the typical amplitude of the Bessel functions is

$$J_\nu(\nu) \approx \frac{2^{1/3}}{3^{2/3}\Gamma\left(\frac{2}{3}\right)}\frac{1}{\nu^{1/3}} \approx \frac{0.4473}{\nu^{1/3}}\ ,$$

which holds asymptotically for large ν.

The Bessel function J_ν solves the ODE, known as Bessel's equation,

$$\left(\frac{d^2}{dx^2} + \frac{1}{x}\frac{d}{dx} + (1 - \frac{\nu^2}{x^2})\right)J_\nu(x) = 0\ , \tag{2.14}$$

or equivalently,

$$\left(\frac{d}{dx} - \frac{\nu-1}{x}\right)\left(\frac{d}{dx} + \frac{\nu}{x}\right)J_\nu(x) = -J_\nu(x)\ . \tag{2.15}$$

Note that adding and subtracting (2.3) and (2.15) produce the identities

$$2J'_\nu(x) = J_{\nu-1}(x) - J_{\nu+1}(x) \, ,$$

$$\frac{2\nu}{x} J_\nu(x) = J_{\nu-1}(x) + J_{\nu+1}(x) \, .$$

Equation (2.14), for each ν, has a two-dimensional solution space. Note that $J_{-\nu}$ is also a solution. From the expression (2.1) it is clear that J_ν and $J_{-\nu}$ are linearly independent provided ν is not an integer. On the other hand, comparison of power series shows

$$J_{-n}(x) = (-1)^n J_n(x), \quad n \in \mathbb{N} \, .$$

A calculation of the Wronskian shows that

$$W(J_\nu, J_{-\nu})(x) = -2\frac{\sin \pi\nu}{\pi x} \, .$$

Therefore, J_ν and $J_{-\nu}$ are linearly independent, and consequently they form a basis of solutions to (2.14), if and only if ν is not an integer. To construct a basis of solutions uniformly good for all ν, it is natural to set

$$Y_\nu(x) = \frac{J_\nu(x)\cos\pi\nu - J_{-\nu}(x)}{\sin\pi\nu} \tag{2.16}$$

when ν is not an integer, and define for integer n

$$Y_n(x) = \lim_{\nu \to n} Y_\nu(x) \, .$$

We have

$$W(J_\nu, Y_\nu)(x) = \frac{2}{\pi x} \, ,$$

for all ν.

2.1.2 Hankel Functions

Another important pair of solutions to Bessel's equation is that of Hankel functions

$$H_\nu^{(1)}(x) = J_\nu(x) + iY_\nu(x), \quad H_\nu^{(2)}(x) = J_\nu(x) - iY_\nu(x) \, . \tag{2.17}$$

The following behavior of $H_\nu^{(1)}$ for fixed ν and $x \to 0$ holds:

$$H_\nu^{(1)}(x) \approx -\frac{i2^\nu \Gamma(\nu)}{\pi} x^{-\nu} \, . \tag{2.18}$$

For n an integer, it is also known that, as $x \to 0$,

$$J_n(x) = \frac{x^n}{2^n} \left(\frac{1}{\Gamma(n+1)} - \frac{\frac{1}{4}x^2}{\Gamma(n+2)} + \frac{(\frac{1}{4}x^2)^2}{2!\Gamma(n+3)} - \frac{(\frac{1}{4}x^2)^3}{3!\Gamma(n+4)} + \cdots \right),$$

$$(2.19)$$

$$Y_n(x) = -\frac{(\frac{1}{2}x)^{-n}}{\pi} \sum_{l=0}^{n-1} \frac{(n-l-1)!}{l!} (\frac{1}{4}x^2)^l + \frac{2}{\pi} \log(\frac{1}{2}x) J_n(x)$$

$$- \frac{(\frac{1}{2}x)^n}{\pi} \sum_{l=0}^{\infty} (\psi(l+1) + \psi(n+l+1)) \frac{(-\frac{1}{4}x^2)^l}{l!(n+l)!},$$

$$(2.20)$$

where $\psi(1) = -\gamma$ and

$$\psi(n) = -\gamma + \sum_{l=1}^{n-1} \frac{1}{l} \quad \text{for } n \geq 2$$

with γ being the Euler constant. In particular, if $n = 0$, we have

$$J_0(x) = 1 - \frac{1}{4}x^2 + \frac{1}{64}x^4 + O(x^6),$$

$$Y_0(x) = \frac{2}{\pi} \log x + \frac{2}{\pi}(\gamma - \log 2) - \frac{1}{2\pi}x^2 \log x + \left(\frac{1}{2\pi} - \frac{1}{2\pi}(\gamma - \log 2) \right) x^2$$

$$+ O(x^4 \log x).$$

It is worth pointing out that the Bessel functions $J_{n+1/2}(x)$, for n an integer, are elementary functions. For $\nu = n + 1/2$, the integrand in (2.2) involves $(1 - t^2)^n$, so the integral can be evaluated explicitly. We have, in particular,

$$J_{1/2}(x) = (\frac{2}{\pi x})^{1/2} \sin x.$$

Then (2.3) gives

$$J_{-1/2}(x) = (\frac{2}{\pi x})^{1/2} \cos x,$$

which by (2.16) is equal to $-Y_{1/2}(x)$. Applying (2.15) and (2.3) repeatedly gives

$$J_{n+1/2}(x) = (-1)^n \prod_{l=1}^{n} (\frac{d}{dx} - \frac{l - \frac{1}{2}}{x}) \frac{\sin x}{\sqrt{2\pi x}}$$

and the same sort of formula for $J_{-n-1/2}(x)$, with the $(-1)^n$ removed, and $\sin x$ replaced by $\cos x$.

The functions

$$j_n(x) := \sqrt{\frac{\pi}{2}} \frac{J_{n+\frac{1}{2}}(x)}{\sqrt{x}},$$

$$(2.21)$$

and

$$y_n(x) := \sqrt{\frac{\pi}{2}} \frac{Y_{n+\frac{1}{2}}(x)}{\sqrt{x}}$$

$$(2.22)$$

are known as the spherical Bessel functions and form a basis for the solution space of the spherical Bessel equation

$$\left(\frac{d^2}{dx^2} + \frac{2}{x}\frac{d}{dx} + (1 - \frac{n(n+1)}{x^2})\right)f(x) = 0 .$$

Analogously to (2.17), we define $h_n^{(1)}$ and $h_n^{(2)}$ by

$$h_n^{(1)}(x) = j_n(x) + iy_n(x), \quad h_n^{(2)}(x) = j_n(x) - iy_n(x) . \qquad (2.23)$$

In three dimensions, there is an analogue to (2.6). The following plane wave expansion, also known as the Rayleigh equation, holds:

$$e^{i\xi \cdot x} = 4\pi \sum_{l=0}^{+\infty} \sum_{m=-l}^{l} i^l j_l(|\xi||x|)Y_{lm}(\theta_x, \phi_x)\overline{Y}_{lm}(\theta_\xi, \phi_\xi) , \qquad (2.24)$$

where Y_{lm} are the spherical harmonic functions and $\xi = (|\xi|, \theta_\xi, \phi_\xi), x = (|x|, \theta_x, \phi_x)$ in the spherical coordinates.

The closure relation,

$$\int_0^{+\infty} xJ_\nu(tx)J_\nu(sx)\, dx = \frac{1}{t}\delta_0(t - s) \qquad (2.25)$$

for $\nu > -1/2$, holds and is equivalent to

$$\int_0^{+\infty} x^2 j_\nu(tx)j_\nu(sx)\, dx = \frac{\pi}{2t^2}\delta_0(t - s) .$$

The cylindrical waves form a complete set. We have the completeness relation

$$\frac{\delta_0(r - r_0)\delta_0(\theta - \theta_0)}{r} = \sum_{m\in\mathbb{Z}} \frac{1}{2\pi} \int_0^{+\infty} tJ_m(tr)J_m(tr_0)\, dt\, e^{im(\theta-\theta_0)} , \qquad (2.26)$$

which is the analogue of the completeness relation for plane waves

$$\delta_0(x - x_0)\delta_0(y - y_0) = (\frac{1}{2\pi})^2 \int_\mathbb{R}\int_\mathbb{R} e^{i(\xi_x x + \xi_y y)}e^{-i(\xi_x x_0 + \xi_y y_0)}\, d\xi_x d\xi_y$$
$$= \frac{1}{2\pi}\mathcal{F}^{-1}(1)(x - x_0, y - y_0) .$$

The connecting link between these two relations is the plane wave expansion (2.5).

Finally, we recall that

$$\int_0^{+\infty} x^2 j_0(tx)\, dx = 2\pi^2\delta_0(t) , \qquad (2.27)$$

which can be obtained by integrating the spherical plane wave representation (2.24).

2.2 Function Spaces

The following functional spaces are needed for the study of mapping properties of layer potentials.

For ease of notation we will sometimes use ∂ and ∂^2 to denote the gradient and the Hessian, respectively.

Let $D \subset \mathbb{R}^d$ be a bounded smooth domain. We define the Banach spaces $W^{1,p}(D), 1 \leq p < +\infty$, by

$$W^{1,p}(D) = \left\{ u \in L^p(D) : \int_D |u|^p + \int_D |\nabla u|^p < +\infty \right\},$$

where ∇u is interpreted as a distribution, and $L^p(D)$ is defined in the usual way, with the norm

$$||u||_{L^p(D)} = \left(\int_D |u|^p \right)^{1/p}.$$

The space $W^{1,p}(D)$ is equipped with the norm

$$||u||_{W^{1,p}(D)} = \left(\int_D |u|^p + \int_D |\nabla u|^p \right)^{1/p}.$$

Another Banach space $W_0^{1,p}(D)$ arises by taking the closure of $\mathcal{C}_0^\infty(D)$, the set of infinitely differentiable functions with compact support in D, in $W^{1,p}(D)$. The spaces $W^{1,p}(D)$ and $W_0^{1,p}(D)$ do not coincide for bounded D. The case $p = 2$ is special, since the spaces $W^{1,2}(D)$ and $W_0^{1,2}(D)$ are Hilbert spaces under the scalar product

$$(u, v) = \int_D \overline{u}\, v + \int_D \nabla \overline{u} \cdot \nabla v,$$

where $\overline{\cdot}$ stands for complex conjugation. We will also need the space $W_{\mathrm{loc}}^{1,2}(\mathbb{R}^d \setminus \overline{D})$ of functions $u \in L_{\mathrm{loc}}^2(\mathbb{R}^d \setminus \overline{D})$, the set of locally square summable functions in $\mathbb{R}^d \setminus \overline{D}$, such that

$$hu \in W^{1,2}(\mathbb{R}^d \setminus \overline{D}), \forall\, h \in \mathcal{C}_0^\infty(\mathbb{R}^d \setminus \overline{D}).$$

We let $W^{-1,2}(D)$ to be the dual of $W_0^{1,2}(D)$. Further, we define $W^{2,2}(D)$ as the space of functions $u \in W^{1,2}(D)$ such that $\partial^2 u \in L^2(D)$ and the space $W^{s,2}(D)$ as the interpolation space $[W^{1,2}(D), W^{2,2}(D)]_s$ for $1 < s < 2$ and $[L^2(D), W^{1,2}(D)]_s$ for $0 < s < 1$; see, for example, the book by Bergh and Löfström [104].

It is known that the trace operator $u \mapsto u|_{\partial D}$ is a bounded linear surjective operator from $W^{1,2}(D)$ into $W_{1/2}^2(\partial D)$, where $f \in W_{1/2}^2(\partial D)$ if and only if $f \in L^2(\partial D)$ and

$$\int_{\partial D} \int_{\partial D} \frac{|f(x) - f(y)|^2}{|x - y|^d} \, d\sigma(x) \, d\sigma(y) < +\infty.$$

We set $W^2_{-1/2}(\partial D) = (W^2_{1/2}(\partial D))^*$ and let $(\,,\,)_{-1/2,1/2}$ denote the duality pair between these dual spaces.

We introduce a weighted norm, $\|u\|_{W^{1,2}_w(\mathbb{R}^d \setminus \overline{D})}$, in two dimensions. Let

$$\|u\|^2_{W^{1,2}_w(\mathbb{R}^2 \setminus \overline{D})} := \int_{\mathbb{R}^2 \setminus \overline{D}} \frac{|u(x)|^2}{\sqrt{1+|x|^2}} dx + \int_{\mathbb{R}^2 \setminus \overline{D}} |\nabla u(x)|^2 dx. \qquad (2.28)$$

This weighted norm is introduced because the solutions of the static elasticity equation behave like $O(|x|^{-1})$ in two dimensions as $|x| \to \infty$. For convenience, we set

$$W(\mathbb{R}^d \setminus \overline{D}) := \begin{cases} W^{1,2}_w(\mathbb{R}^2 \setminus \overline{D}) & \text{for } d = 2, \\ W^{1,2}(\mathbb{R}^3 \setminus \overline{D}) & \text{for } d = 3. \end{cases} \qquad (2.29)$$

In three dimensions, $W(\mathbb{R}^d \setminus \overline{D})$ is the usual Sobolev space.

Finally, let $\{\tau_1, \ldots, \tau_{d-1}\}$ be an orthonormal basis for the tangent plane to ∂D at x and let

$$\partial/\partial\tau = \sum_{p=1}^{d-1} (\partial/\partial\tau_p)\, \tau_p$$

denote the tangential derivative on ∂D. We say that $f \in W^2_1(\partial D)$ if $f \in L^2(\partial D)$ and $\partial f/\partial\tau \in L^2(\partial D)$.

2.3 Fourier Analysis

2.3.1 Fourier Transform

The Fourier transform plays an important role in imaging and in the analysis of waves. In both cases, the notion of frequency content of a signal is important.

For $f \in L^1(\mathbb{R}^d)$, the Fourier transform $\mathcal{F}[f]$ and the inverse Fourier transform $\mathcal{F}^{-1}[f]$ are defined by

$$\mathcal{F}[f](\xi) = (2\pi)^{-d/2} \int_{\mathbb{R}^d} e^{-ix\cdot\xi} f(x)\, dx\,, \qquad (2.30)$$

$$\mathcal{F}^{-1}[f](\xi) = (2\pi)^{-d/2} \int_{\mathbb{R}^d} e^{i\xi\cdot x} f(x)\, dx\,. \qquad (2.31)$$

We use both transforms for other classes of functions, such as for functions in $L^2(\mathbb{R}^d)$ and even for the tempered distributions $\mathcal{S}'(\mathbb{R}^d)$, the dual of the Schwartz space of rapidly decreasing functions:

$$\mathcal{S}(\mathbb{R}^d) = \left\{ u \in \mathcal{C}^\infty(\mathbb{R}^d) : x^\beta \partial^\alpha u \in L^\infty(\mathbb{R}^d) \text{ for all } \alpha, \beta \geq 0 \right\},$$

where $x^\beta = x_1^{\beta_1} \ldots x_d^{\beta_d}, \partial^\alpha = \partial_1^{\alpha_1} \ldots \partial_d^{\alpha_d}$, with $\partial_j = \partial/\partial x_j$.

We list a few properties of the Fourier transform. It is easy to verify that $\mathcal{F} : \mathcal{S}(\mathbb{R}^d) \to \mathcal{S}(\mathbb{R}^d)$ and

$$i^{|\alpha|} \xi^\alpha \partial_\xi^\beta \mathcal{F}[f](\xi) = (-i)^{|\beta|} \mathcal{F}[\partial^\alpha(x^\beta f)](\xi) .$$

If $f_r(x) = f(rx), r > 0$, we have

$$\mathcal{F}[f_r](\xi) = r^{-d} \mathcal{F}[f](r^{-1}\xi) .$$

Likewise, if $f_y(x) = f(x + y)$ for $y \in \mathbb{R}^d$, then

$$\mathcal{F}[f_y](\xi) = e^{i\xi \cdot y} \mathcal{F}[f](\xi) .$$

We have the inversion formula: $\mathcal{F}\mathcal{F}^{-1} = \mathcal{F}^{-1}\mathcal{F} = I$ on both $\mathcal{S}(\mathbb{R}^d)$ and $\mathcal{S}'(\mathbb{R}^d)$. If $f \in L^2(\mathbb{R}^d)$, then $\mathcal{F}[f] \in L^2(\mathbb{R}^d)$, too. Plancherel's theorem says that $\mathcal{F} : L^2(\mathbb{R}^d) \to L^2(\mathbb{R}^d)$ is unitary, so that $\mathcal{F}^{-1}$ is the adjoint.

In general, if $f, g \in L^2(\mathbb{R}^d)$, then we have Parseval's relation:

$$\int_{\mathbb{R}^d} \mathcal{F}[f]g \, dx = \int_{\mathbb{R}^d} f\mathcal{F}[g] \, dx . \tag{2.32}$$

Since $\mathcal{F}^{-1}[\overline{f}] = \overline{\mathcal{F}[f]}$, this relation has its counterpart for $\mathcal{F}^{-1}$. This indeed also gives

$$\int_{\mathbb{R}^d} \overline{f}g \, dx = \int_{\mathbb{R}^d} \overline{\mathcal{F}[f]}\mathcal{F}[g] \, d\xi ,$$

and hence

$$\int_{\mathbb{R}^d} |f|^2 \, dx = \int_{\mathbb{R}^d} |\mathcal{F}[f]|^2 \, d\xi .$$

We now make some comments on the relation between the Fourier transform and convolutions. For $f \in \mathcal{S}'(\mathbb{R}^d)$, $g \in \mathcal{S}(\mathbb{R}^d)$, the convolution is defined by

$$(f \star g)(x) = \int_{\mathbb{R}^d} f(x - y)g(y) \, dy ,$$

and we have

$$\mathcal{F}[f \star g] = (2\pi)^{d/2} \mathcal{F}[f]\mathcal{F}[g], \quad \mathcal{F}[fg] = (2\pi)^{-d/2} \mathcal{F}[f] \star \mathcal{F}[g] .$$

Moreover, for a real-valued function f, we have

$$\mathcal{F}[f(-x)] = \overline{\mathcal{F}[f]} , \tag{2.33}$$

and

$$\mathcal{F}\Big[\int_{\mathbb{R}^d} f(y)g(x + y) \, dy\Big] = (2\pi)^{d/2} \overline{\mathcal{F}[f]}\mathcal{F}[g] . \tag{2.34}$$

Fourier transforms of a few special functions will be needed. For h a Gaussian function,

$$h(x) := e^{-|x|^2/2}, \quad x \in \mathbb{R}^d ,$$

we have

$$\mathcal{F}[h](\xi) = e^{-|\xi|^2/2}, \quad \xi \in \mathbb{R}^d . \tag{2.35}$$

For δ_0 the Dirac function at the origin, *i.e.*, $\delta_0 \in \mathcal{S}'(\mathbb{R}^d)$ and $\delta_0(f) = f(0)$ for $f \in \mathcal{S}(\mathbb{R}^d)$, we have

$$\mathcal{F}[\delta_0] = (2\pi)^{-d/2} . \tag{2.36}$$

Another useful result is the classification of distributions supported at a single point. If $f \in \mathcal{S}'(\mathbb{R}^d)$ is supported at $\{0\}$, then there exist an integer n and real numbers a_α such that

$$f = \sum_{|\alpha| \leq n} a_\alpha \partial^\alpha \delta_0 .$$

Let $\mathbb{Z}$ denote the set of all integers. The Shah distribution

$$\mathrm{shah}_K = \sum_{l \in \mathbb{Z}^d} \delta_{Kl} ,$$

where $\delta_y(f) = f(y)$, has the Fourier transform

$$\mathcal{F}[\mathrm{shah}_{2\pi/K}] = (2\pi)^{-d/2} K^d \mathrm{shah}_K .$$

This is Poisson's formula. More generally, we have for $f \in \mathcal{S}(\mathbb{R}^d)$

$$\sum_{l \in \mathbb{Z}^d} \mathcal{F}[f](\xi - \frac{2\pi l}{K}) = (2\pi)^{-d/2} K^d \sum_{l \in \mathbb{Z}^d} f(Kl) e^{-iK\xi \cdot l} . \tag{2.37}$$

Physicists consider that a progressive plane wave is of the form $e^{i(\xi \cdot x - \omega t)}$. Accordingly the convention for the Fourier transform in time is different than in space (compare with (2.30)–(2.31)):

$$\mathcal{F}_{\mathrm{t}}[f](\omega) = \frac{1}{\sqrt{2\pi}} \int_{-\infty}^{\infty} f(t) e^{i\omega t} dt , \tag{2.38}$$

$$\mathcal{F}_{\mathrm{t}}^{-1}[f](t) = \frac{1}{\sqrt{2\pi}} \int_{-\infty}^{\infty} f(\omega) e^{-i\omega t} d\omega . \tag{2.39}$$

The properties listed above still hold true, in particular (2.33) and (2.34):

$$\mathcal{F}_{\mathrm{t}}[f(-t)](\omega) = \overline{\mathcal{F}_{\mathrm{t}}[f](\omega)} , \tag{2.40}$$

$$\mathcal{F}_{\mathrm{t}}\Big[\int f(s)g)t + s)ds\Big](\omega) = \sqrt{2\pi}\overline{\mathcal{F}_{\mathrm{t}}[f](\omega)}\mathcal{F}_{\mathrm{t}}[g](\omega) . \tag{2.41}$$

These simple formulas have important interpretations in imaging. Identity (2.40) expresses the fact that the time reversal operation in the time domain ($x \in \mathbb{R}$ variable) is equivalent to the complex conjugation in the frequency domain (ξ variable). Identity (2.41) shows that the cross correlation of two

signals involves a product of the two Fourier transforms in the frequency domain, one of the transform being complex conjugated.

Finally, we recall the Paley-Wiener theorem. Let $f \in L^2(\mathbb{R}^+), f \equiv 0$ on $\mathbb{R}^-$. Then $\mathcal{F}_{\mathrm{t}}[f]$ is holomorphic in $\mathbb{C}^+$ defined by

$$\mathbb{C}^+ = \left\{ \omega : \Im \omega > 0 \right\}, \tag{2.42}$$

and there exists $C > 0$ such that

$$\left| \mathcal{F}_{\mathrm{t}}[f](\xi + i\eta) \right| \leq \frac{C}{\sqrt{\eta}}, \quad \eta > 0.$$

Moreover, $\mathcal{F}_{\mathrm{t}}[f]$ is L^2 in any horizontal stripe in the upper half-plane. The converse also holds. If F is holomorphic in $\mathbb{C}^+$, $||F|_{\Im \omega = \eta}||_{L^2} \leq C$ for $\eta \geq 0$, then F is a holomorphic Fourier transform of a function $f \in L^2(\mathbb{R}^+)$, $F = \mathcal{F}_{\mathrm{t}}[f]$.

2.3.2 Shannon's Sampling Theorem

We call a function (or distribution) in $\mathbb{R}^d, d \geq 1$, whose Fourier transform vanishes outside $|\xi| \leq K$ band-limited with bandwidth K. Shannon's sampling theorem for $d = 1$ is the following. The reader is referred to [261, page 41] for a proof.

Theorem 2.1 (Shannon's Sampling Theorem) *Let $f \in L^2(\mathbb{R})$ be band-limited with bandwidth K, and let $0 < \Delta x \leq \pi/K$. Then f is uniquely determined by the values $f(l\Delta x), l \in \mathbb{Z}$. The smallest detail represented by such a function is then of size $2\pi/K$. We also have the explicit formula*

$$f(x) = \sum_{l \in \mathbb{Z}} f\left(\frac{l\pi}{K} \right) \frac{\sin(Kx - l\pi)}{Kx - l\pi} . \tag{2.43}$$

The sampling interval π/K is often imposed by computation or storage constraints. Moreover, if the support of $\mathcal{F}[f]$ is not included in $[-K, K]$, then the interpolation formula (2.43) does not recover f. We give a filtering procedure to reduce the resulting error, known as the aliasing artifact. To apply Shannon's sampling theorem, f is approximated by the closest function $\tilde{f}$ whose Fourier transform has a support in $[-K, K]$. Plancherel's theorem gives that

$$||f - \tilde{f}||^2 = \int_{-\infty}^{+\infty} |\mathcal{F}[f](\xi) - \mathcal{F}[\tilde{f}](\xi)|^2 \, d\xi$$

$$= \int_{|\xi| > K} |\mathcal{F}[f](\xi)|^2 \, d\xi + \int_{|\xi| < K} |\mathcal{F}[f](\xi) - \mathcal{F}[\tilde{f}](\xi)|^2 \, d\xi .$$

The distance is minimal when the second integral is zero and hence

$$\mathcal{F}[\tilde{f}](\xi) = \mathcal{F}[f](\xi)\chi([-K, K])(\xi) = \sqrt{2\pi}\mathcal{F}[\tilde{\delta}_K](\xi)\mathcal{F}[f](\xi) \ ,$$

where $\chi([-K, K])$ is the characteristic function of the interval $[-K, K]$ and

$$\tilde{\delta}_K(x) = \sin(K|x|)/(\pi K|x|) \ ;$$

see (2.10). This corresponds to $\tilde{f} = f \star \tilde{\delta}_K$. The filtering of $f(x)$ by $\tilde{\delta}_K(x)$ removes any frequency larger than K. Since $\mathcal{F}[\tilde{f}]$ has a support in $[-K, K]$, the sampling theorem proves that $\tilde{f}$ can be recovered from the samples $\tilde{f}(l\pi/K)$.

In the two-dimensional case, we use the separable extension principle. This not only simplifies the mathematics but also leads to faster numerical algorithms along the rows and columns of images. If $\mathcal{F}[f]$ has a support included in $[-K_1, K_1] \times [-K_2, K_2]$, then the following two-dimensional sampling formula holds:

$$f(x, y) = \sum_{l=(l_1,l_2)\in\mathbb{Z}^2} f\left(\frac{l_1\pi}{K_1}, \frac{l_2\pi}{K_2}\right) \frac{\sin(K_1 x - l_1\pi)}{K_1 x - l_1\pi} \frac{\sin(K_2 y - l_2\pi)}{K_2 y - l_2\pi} \ . \quad (2.44)$$

If the support of $\mathcal{F}[f]$ is not included in the low-frequency rectangle $[-K_1, K_1] \times [-K_2, K_2]$, then we have to filter f with the low-pass separable filter $\tilde{\delta}_{K_1}(x) \, \tilde{\delta}_{K_2}(y)$.

2.4 Kramers-Kronig Relations and Causality

Causal linear systems, with input $H(t)$, output $S(t)$, and transfer function $f(t)$ are characterized by the relation

$$S(t) = \int_{-\infty}^{t} f(t - s)H(s)\, ds \ .$$

If we assume that $f \in L^2(\mathbb{R}^+)$, we can investigate the Fourier transform

$$F(\omega) = \mathcal{F}_{\mathrm{t}}[f](\omega) = \frac{1}{\sqrt{2\pi}} \int_{0}^{+\infty} f(t)e^{i\omega t}\, dt \ .$$

By the Paley-Wiener theorem, $F(\omega)$ is analytic for $\omega = \xi + i\eta \in \mathbb{C}^+$ and satisfies the integrability property

$$\sup_{\eta > 0} \int_{-\infty}^{+\infty} |F(\xi + i\eta)|^2 \, d\xi = \int_{-\infty}^{+\infty} |F(\xi)|^2 \, d\xi < +\infty \ . \quad (2.45)$$

Functions analytic in the upper half plane, and satisfying (2.45) are referred to as Hardy functions ($F \in \mathcal{H}^2(\mathbb{R})$). The converse also holds: all Hardy functions may be obtained as Fourier transforms of L^2-functions supported on $\mathbb{R}^+$.

The real and imaginary parts of Hardy functions obey the Kramers-Kronig relations. The following integral identities hold by applying a limiting procedure to the Cauchy integral representation for analytic functions.

Theorem 2.2 (Kramers-Kronig relations) *Let $F(\omega) \in \mathcal{H}^2(\mathbb{R})$. Then*

$$
\begin{aligned}
\Re F(\omega) &= -\frac{1}{\pi}\text{p.v.}\int_{-\infty}^{+\infty} \frac{\Im F(\omega')}{\omega - \omega'}\, d\omega' = -\mathcal{H}[\Im F(\omega)]\,, \\
\Im F(\omega) &= \frac{1}{\pi}\text{p.v.}\int_{-\infty}^{+\infty} \frac{\Re F(\omega')}{\omega - \omega'}\, d\omega' = \mathcal{H}[\Re F(\omega)]\,,
\end{aligned}
\tag{2.46}
$$

where $\mathcal{H}$, bounded operator from $L^2(\mathbb{R}) \to L^2(\mathbb{R})$, is the Hilbert transform and is given by

$$
\mathcal{H}[G(\omega)] = \frac{1}{\pi}\text{p.v.}\int_{-\infty}^{+\infty} \frac{G(\omega')}{\omega - \omega'}\, d\omega',\quad G \in L^2(\mathbb{R})\,.
\tag{2.47}
$$

If the transfer function $f(t)$ is real-valued, then the real and imaginary parts of its Fourier transform $F(\omega) = \mathcal{F}_{\text{t}}[f](\omega)$ are respectively even and odd. Incorporating these symmetries into the Kramers-Kronig relations (2.46) gives

$$
\begin{aligned}
\Re F(\omega) &= \frac{2}{\pi}\text{p.v.}\int_{0}^{+\infty} \frac{\omega'\Im F(\omega')}{(\omega')^2 - \omega^2}\, d\omega'\,, \\
\Im F(\omega) &= -\frac{2\omega}{\pi}\text{p.v.}\int_{0}^{+\infty} \frac{\Re F(\omega')}{(\omega')^2 - \omega^2}\, d\omega'\,,
\end{aligned}
\tag{2.48}
$$

from which we can deduce that $F(-\omega) = \overline{F(\omega)}$ for $\omega \in \mathbb{R}$. Thus, the causality of a real-valued transfer function $f(t)$ implies that its Fourier transform $F(\omega)$ is analytic in $\mathbb{C}^+$ and that the real and imaginary parts of $F(\omega)$ are not independent but are connected by the non-local integral relations (2.48). We refer to (2.48) as dispersion relations. Kramers-Kronig relations express the equivalence between causality and the existence of dispersion relations, and so between the mathematical properties of the functions describing the physics in the domains of time and frequency. They give necessary connections between the real and imaginary parts of the complex permittivity and the complex shear modulus of tissues and therefore, constitute a fundamental test of self-consistency since any set of experimental (or reconstructed) data of the real and imaginary parts of the complex permittivity or the complex shear modulus must respect the Kramers-Kronig relations.

From the Kramers-Kronig relations, it is possible to deduce the value of the zero-order moment of the real part and the value of the first-order moment of the imaginary part of $F(\omega)$. This can be obtained by using the fact that if

$$
g(y) = \text{p.v.}\int_{0}^{+\infty} \frac{h(x)}{y^2 - x^2}\, dx\,,
$$

where h is continuously differentiable and $h(x) = O((x \log x)^{-1})$, then

$$
\int_{0}^{+\infty} h(x)\, dx = \lim_{y \to +\infty} y^2 g(y)\,.
$$

Therefore, from (2.48), it follows that

$$
\begin{cases}
\displaystyle\int_0^{+\infty} \omega' \Im F(\omega')\, d\omega' = -\frac{\pi}{2} \lim_{\omega \to +\infty} \omega^2 \Re F(\omega)\,, \\[2ex]
\displaystyle\int_0^{+\infty} \Re F(\omega')\, d\omega' = \frac{\pi}{2} \lim_{\omega \to +\infty} \omega \Im F(\omega)\,.
\end{cases}
\tag{2.49}
$$

Similarly, other useful identities can be obtained. Taking the limit of the first identity in (2.48) as $\omega \to 0$ yields

$$
\Re F(0) = \frac{2}{\pi} \text{p.v.} \int_0^{+\infty} \frac{\Im F(\omega')}{\omega'}\, d\omega'\,.
\tag{2.50}
$$

Since $\Re F(\omega')$ is an even function of ω', $\Re F(\omega') - \Re F(0) = O((\omega')^2)$ as $\omega' \to 0$. Using

$$
\text{p.v.} \int_0^{+\infty} \frac{1}{(\omega')^2 - \omega^2}\, d\omega' = 0\,,
$$

and taking the limit of the second identity in (2.48) as $\omega \to 0$, we obtain

$$
\lim_{\omega \to 0} \frac{1}{\omega} \Im F(\omega) = -\frac{2}{\pi} \text{p.v.} \int_0^{+\infty} \frac{(\Re F(\omega') - \Re F(0))}{(\omega')^2}\, d\omega'\,.
\tag{2.51}
$$

We refer to (2.49), (2.50), and (2.51) as sum rules.

2.5 Singular Value Decomposition

One of the most fruitful tools in the theory of linear inverse and imaging problems is the singular value decomposition of a matrix and its extension to certain classes of linear operators. It allows for both understanding the ill-posedness of inverse and imaging problems and describing the effect of the regularization methods.

Let A be a bounded linear operator from a separable Hilbert space H into a separable Hilbert space K. By the singular value decomposition (SVD) we mean a representation of A in the form

$$
Af = \sum_l \sigma_l \left(f_l, f\right) g_l\,,
$$

where $(f_l), (g_l)$ are orthonormal systems in H, K, respectively, and σ_l are nonnegative numbers, the singular values of A. The sum may be finite or infinite. The adjoint of A is given by

$$
A^* g = \sum_l \sigma_l \left(g_l, g\right) f_l\,,
$$

and the operators

$$A^*Af = \sum_l \sigma_l^2 \left(f_l, f\right) f_l \,,$$

$$AA^*g = \sum_l \sigma_l^2 \left(g_l, g\right) g_l \,,$$

are self-adjoint operators in H, K, respectively. The spectrum of A^*A, AA^* consists of the eigenvalues σ_l^2 and possibly the eigenvalue 0, whose multiplicity may be infinite.

The Moore-Penrose generalized inverse is given by

$$A^+g = \sum_l \sigma_l^{-1} \left(g_l, g\right) f_l \,,$$

where the sum is over the indices l such that $\sigma_l > 0$. Indeed this is the least-squares solution to $Af = g$ of minimum norm.

Let us now review the basic concepts of singular value decomposition of a matrix. Let $M_{m,n}(\mathbb{C})$ denote the set of all m-by-n matrices over $\mathbb{C}$. The set $M_{n,n}(\mathbb{C})$ is abbreviated to $M_n(\mathbb{C})$. The spectral theorem applied to the positive semi-definite matrices AA^* and A^*A gives the following singular value decomposition of a matrix $A \in M_{m,n}(\mathbb{C})$. Here $A^* := \overline{A}^T$, where T denotes the transpose.

Theorem 2.3 (Spectral Theorem) *Let $A \in M_{m,n}(\mathbb{C})$ be given, and let $q = \min\{m, n\}$. There is a matrix $\Sigma = (\Sigma_{ij}) \in M_{m,n}(\mathbb{R})$ with $\Sigma_{ij} = 0$ for all $i \neq j$ and $\Sigma_{11} \geq \Sigma_{22} \geq \ldots \geq \Sigma_{qq} \geq 0$, and there are two unitary matrices $V \in M_m(\mathbb{C})$ and $W \in M_n(\mathbb{C})$ such that $A = V\Sigma W^*$. The numbers $\{\Sigma_{ii}\}$ are the nonnegative square roots of the eigenvalues of AA^*, and hence are uniquely determined. The columns of V are eigenvectors of AA^* and the columns of W are eigenvectors of A^*A (arranged in the same order as the corresponding eigenvalues Σ_{ii}^2).*

The diagonal entries Σ_{ii}, $i = 1, \ldots, q = \min\{m, n\}$ of Σ are called the singular values of A, and the columns of V and the columns of W are the (respectively, left and right) singular vectors of A.

The SVD has the following desirable computational properties:

(i) The rank of A can be easily determined from its SVD. Specifically, $\mathrm{rank}(A)$ equals to the number of nonzero singular values of A.

(ii) The Frobenius norm of A, $||A||_F := \sqrt{\mathrm{Tr}(A\overline{A}^T)}$ with Tr being the trace, is given by $||A||_F = \sqrt{\sum_{m=1}^q \Sigma_{mm}^2}$.

(iii) SVD is an effective computational tool for finding lower-rank approximations to a given matrix. Specifically, let $p < \mathrm{rank}(A)$. Then the rank p matrix A_p minimizing $||A - A_p||_F$ is given by $A_p = V\Sigma_p W^*$, where the matrix Σ_p is obtained from Σ after the singular values $\Sigma_{nn}, p+1 \leq n \leq q$, are set to zero.

2.6 Compact Operators

Let H be a Banach space. A bounded linear operator A on H is compact if whenever $\{x_j\}$ is a bounded sequence in H, the sequence $\{Ax_j\}$ has a convergent subsequence. The operator A is said to be of finite rank if $\mathrm{Range}(A)$ is finite-dimensional. Clearly every operator of finite rank is compact.

We recall some basic results on compact operators.

(i) The set of compact operators on H is a closed two-sided ideal in the algebra of bounded operators on H with the norm topology.

(ii) If A is a linear bounded operator on the Banach space H and there is a sequence $\{A_N\}_{N\in\mathbb{N}}$ of linear operators of finite rank such that $\|A_N - A\| \to 0$, then A is compact.

(iii) The operator A is compact on the Banach space H if and only if the dual operator A^* is compact on the dual space H^*.

We also recall the main structure theorem for compact operators. Let A be a compact operator on the Hilbert space H (which we identify with its dual). For each $\lambda \in \mathbb{C}$, let $V_\lambda = \{x \in H : Ax = \lambda x\}$ and $V_{\bar\lambda} = \{x \in H : A^*x = \bar\lambda x\}$. Then

(i) The set of $\lambda \in \mathbb{C}$ for which $V_\lambda \neq \{0\}$ is finite or countable, and in the latter case its only accumulation point is zero. Moreover, $\dim(V_\lambda) < +\infty$ for all $\lambda \neq 0$.

(ii) If $\lambda \neq 0$, $\dim(V_\lambda) = \dim(V_{\bar\lambda})$.

(iii) If $\lambda \neq 0$, the range of $\lambda I - A$ is closed.

Suppose $\lambda \neq 0$. Then

(i) The equation $(\lambda I - A)x = y$ has a solution if and only if $y \perp V_{\bar\lambda}$.

(ii) $(\lambda I - A)$ is surjective if and only if it is injective.

We recall the concept of a Fredholm operator acting between Banach spaces H and K. We say that a bounded linear operator $A : H \to K$ is Fredholm if the subspace $\mathrm{Range}(A)$ is closed in K and the subspace $\mathrm{Ker}(A)$ and the quotient space $K/\mathrm{Range}(A)$ are finite-dimensional. In this case, the index of A is the integer defined by

$$\mathrm{index}\ (A) = \dim \mathrm{Ker}(A) - \dim(K/\mathrm{Range}(A))\ .$$

In the sequel, we encapsulate the main conclusion of Fredholm's original theory. If $A = I + B$, where $B : H \to H$ is compact, then $A : H \to H$ is Fredholm with index zero. If $A : H \to K$ is Fredholm and $B : H \to K$ is compact, then their sum $A + B : H \to K$ is Fredholm, and index $(A+B) =$ index (A). This shows that the index is stable under compact perturbations.

Finally, we recall that a compact operator A on a separable Hilbert space H is a Hilbert-Schmidt operator if the sequence of its singular values is square summable. An equivalent characterization is $\sum_n \|A\varphi_n\|^2 < \infty$ or $\sum_{m,n} |(\varphi_m, A\varphi_n)|^2 < \infty$ for any orthonormal basis (φ_n) of H.

2.7 Spherical Mean Radon Transform

The spherical mean Radon transform, which integrates a function over all spheres centered at points of a given set, is useful in multi-wave tomographies. For instance, in photoacoustic imaging, under some simplifications, the spherical mean data of an unknown function (the absorbed optical energy density) is measured by acoustic transducers, and the imaging problem is to invert that transform. For the spherical mean transform, uniqueness and stability reconstruction, explicit inversion formulas, incomplete data problems are challenging issues. Most of the known inversion formulas pertain to the spherical acquisition geometry, *i.e.*, to the situation when centers of integration spheres (the detector positions) lie on a sphere surrounding the support of the function to be imaged.

Let Ω be a bounded open set of $\mathbb{R}^d$. The spherical mean Radon transform $\mathcal{R} : \mathcal{C}^0(\mathbb{R}^d) \to \mathcal{C}^0(\partial\Omega \times \mathbb{R}^+)$ with centers on $\partial\Omega$ is given for $f \in \mathcal{C}^0(\mathbb{R}^d)$ by

$$\mathcal{R}[f](x,s) = \frac{1}{\omega_d} \int_S f(x + s\xi)\, d\sigma(\xi), \quad (x,s) \in \partial\Omega \times \mathbb{R}^+, \tag{2.52}$$

where S denotes the unit sphere in $\mathbb{R}^d$ and ω_d its area.

Let B be the unit ball of center 0 and radius 1 ($\partial B = S$). If we look at $\mathcal{R}$ as the map from $\mathcal{C}_0^\infty(B) \to \mathcal{C}^\infty(S \times \mathbb{R}^+)$, then we have the following inversion formula for $d = 3$ [166]:

$$f(x) = \frac{1}{2\pi} \nabla \cdot \int_S y \frac{\frac{\partial}{\partial s}(s\mathcal{R}[f])(y, |x - y|)}{|x - y|}\, d\sigma(y), \tag{2.53}$$

while for $d = 2$ [165],

$$f(x) = \frac{1}{2\pi} \int_S \int_0^2 \left[\frac{d}{ds} s \frac{d}{ds} \mathcal{R}[f] \right](y,s) \log |s^2 - |y - x|^2|\, ds\, d\sigma(y), \tag{2.54}$$

or equivalently,

$$f(x) = \frac{1}{2\pi} \text{p.v.} \int_S \int_{-2}^2 \frac{(t \frac{\partial}{\partial t}(\mathcal{R}[f]))(y,t)}{|x - y| - t}\, dt\, d\sigma(y)$$

with $\mathcal{R}[f]$ being extended on negative time as an odd function.

We now connect the spherical mean Radon transform to the wave equation. Let $y \in \mathbb{R}^3$ and let

$$U_y(x,t) := \frac{\delta_0(t - |x - y|)}{4\pi|x - y|} \quad \text{for } x \neq y. \tag{2.55}$$

The function U_y is the outgoing fundamental solution (also called retarded fundamental solution) to the wave equation in three dimensions:

$$(\partial_t^2 - \Delta)U_y(x,t) = \delta_y(x)\delta_0(t) \quad \text{in } \mathbb{R}^3 \times \mathbb{R}. \tag{2.56}$$

Moreover, U_y satisfies the conditions: $U_y(x,t) = \partial_t U_y(x,t) = 0$ for $x \neq y$ and $t < 0$. The function U_y corresponds to a spherical wave generated at the source point y and propagating at speed 1.

In the two-dimensional case, the fundamental solution is given by

$$U_y(x,t) := \frac{H(t - |x - y|)}{2\pi\sqrt{t^2 - |x - y|^2}} \quad \text{for } |x - y| \neq t \,, \tag{2.57}$$

where H is the Heaviside step function.

Consider the wave equation in $\mathbb{R}^d$, $d = 2, 3$,

$$\frac{\partial^2 p}{\partial t^2}(x,t) - \Delta p(x,t) = 0 \quad \text{in } \mathbb{R}^d \times \mathbb{R}^+ \,,$$

with the initial conditions

$$p(x,0) = p_0(x) \quad \text{and} \quad \frac{\partial p}{\partial t}(x,0) = 0 \,.$$

Assume that the support of $p_0 \in C^0(\mathbb{R}^d)$ is contained in a bounded set Ω of $\mathbb{R}^d$. With the outgoing fundamental solution U_y, p can be written as

$$p(x,t) = \int_\Omega \partial_t U_y(x,t) p_0(y) \, dy, \quad (x,t) \in \mathbb{R}^d \times \mathbb{R}^+ \,. \tag{2.58}$$

Therefore, the following Kirchhoff formulas follow from (2.58):

$$p(x,t) = \begin{cases} \partial_t \int_0^t \dfrac{s\mathcal{R}[p_0](x,s)}{\sqrt{t^2 - s^2}} \, ds, & d = 2 \,, \\ \partial_t (t\mathcal{R}[p_0])(x,t), & d = 3 \,. \end{cases} \tag{2.59}$$

When Ω is the unit disk ($\partial\Omega = S$), from (2.54) it follows that

$$p_0(x) = \mathcal{R}^* \mathcal{B} \mathcal{R}[p_0](x) \,, \tag{2.60}$$

where $\mathcal{R}^*$ is the adjoint of $\mathcal{R}$,

$$\mathcal{R}^*[g](x) = \frac{1}{2\pi} \int_S \frac{g(y, |x - y|)}{|x - y|} \, d\sigma(y) \,, \tag{2.61}$$

and $\mathcal{B}$ is defined by

$$\mathcal{B}[g](x,t) = \int_0^2 \frac{\partial^2 g}{\partial s^2}(x,s) \log(|s^2 - t^2|) \, ds \tag{2.62}$$

for $g : S \times \mathbb{R}^+ \to \mathbb{R}$.

In order to extend the definition (2.52) of the spherical mean Radon transform to distributions, we introduce the dual operator $\mathcal{R}^* : \mathcal{S}(\partial\Omega \times \mathbb{R}^+) \to \mathcal{S}(\mathbb{R}^d)$ defined for $g \in \mathcal{S}(\partial\Omega \times \mathbb{R}^+)$ by

$$\mathcal{R}^*[g](x) = \frac{1}{\omega_d} \int_{\partial\Omega} \frac{g(y, |x-y|)}{|x-y|^{d-1}} \, d\sigma(y)$$

with $\mathcal{S}$ being the Schwartz space. Then, for any tempered distribution $f \in \mathcal{S}'(\mathbb{R}^d)$ (the dual of $\mathcal{S}(\mathbb{R}^d)$), we define its spherical mean Radon transform $\mathcal{R}[f] \in \mathcal{S}'(\partial\Omega \times \mathbb{R}^+)$ as follows:

$$(\mathcal{R}[f], g)_{\mathcal{S}'(\partial\Omega \times \mathbb{R}^+), \mathcal{S}(\partial\Omega \times \mathbb{R}^+)} = (f, \mathcal{R}^*[g])_{\mathcal{S}'(\mathbb{R}^d), \mathcal{S}(\mathbb{R}^d)}, \qquad \forall g \in \mathcal{S}(\partial\Omega \times \mathbb{R}^+).$$

The following stability result holds [293].

Lemma 2.4 *Let $0 < \eta < 1$. Suppose that for any $f \in W^{\eta,2}(\mathbb{R}^d)$ with compact support, $\mathcal{R}[f] = 0$ implies that $f = 0$. Then there exists a positive constant C such that*

$$\frac{1}{C} ||f||_{W^{\eta,2}(\mathbb{R}^d)} \le ||\mathcal{R}[f]||_{W^{\eta+(d-1)/2,2}(\partial\Omega \times \mathbb{R}^+)} \le C ||f||_{W^{\eta,2}(\mathbb{R}^d)}.$$

2.8 Regularization of Ill-Posed Problems

In this section we review some of the most commonly used methods for solving ill-posed inverse problems. These methods are called regularization methods. Although the emphasis in this book is not on classical regularization techniques, it is quite important to understand the philosophy behind them and how they work in practice.

2.8.1 Stability

Problems in image reconstruction are usually not well-posed in the sense of Hadamard. This means that they suffer from one of the following deficiencies:

(i) They may not be solvable (in the strict sense) at all.
(ii) The solution, if exists, may not be unique.
(iii) The solution may not depend continuously on the data.

A classical ill-posed inverse problem is the deconvolution problem. Define the compact operator $A : L^2(\mathbb{R}) \to L^2(\mathbb{R})$ by

$$(Af)(x) := \int_{-\infty}^{+\infty} h(x-y) f(y) \, dy \,,$$

where h is a Gaussian convolution kernel,

$$h(x) := \frac{1}{\sqrt{2\pi}} e^{-x^2/2} \,.$$

The operator A is injective, which can be seen by applying the Fourier transform on Af, yielding

$$\mathcal{F}[Af] = \mathcal{F}[h \star f] = \mathcal{F}[h]\mathcal{F}[f] \ ,$$

with $\mathcal{F}[h]$ given by (2.35). Therefore, if $Af = 0$, we have $\mathcal{F}[f] = 0$, hence $f = 0$. Formally, the solution to the equation $Af = g$ is

$$f(x) = \mathcal{F}^{-1}\left[\frac{\mathcal{F}(g)}{\mathcal{F}(h)}\right](x), \quad x \in \mathbb{R} \ . \tag{2.63}$$

However, the above formula is not well defined for general $g \in L^2(\mathbb{R})$ (or even in $\mathcal{S}'(\mathbb{R})$) since $1/\mathcal{F}[h]$ grows as $e^{\xi^2/2}$.

To explain the basic ideas of regularization, let A be a bounded linear operator from a Hilbert space H into a Hilbert space K. Consider the problem of solving

$$Af = g \tag{2.64}$$

for f. Item (i) means that g may not be in the range of A, (ii) means that A may not be injective, and (iii) means that A^{-1} may not be continuous.

One could do away with (i) and (ii) by using the generalized inverse A^+. But A^+ does not have to be continuous. Thus, small error in g may cause errors of arbitrary size in f. To restore continuity, we introduce the notion of a regularization of A^+. This is a family $(T_\gamma)_{\gamma>0}$ of linear continuous operators $T_\gamma : K \to H$, which are defined on all of K and for which

$$\lim_{\gamma \to 0} T_\gamma g = A^+ g$$

on the domain of A^+. Obviously, $||T_\gamma|| \to +\infty$ as $\gamma \to 0$ if A^+ is unbounded. With the help of regularization, we can solve (2.64) in the following way. Let $g^\epsilon \in K$ be an approximation to g such that $||g - g^\epsilon|| \le \epsilon$. Let $\gamma(\epsilon)$ be such that, as $\epsilon \to 0$,

$$\gamma(\epsilon) \to 0, \quad ||T_{\gamma(\epsilon)}|| \epsilon \to 0 \ .$$

Then, as $\epsilon \to 0$,

$$\begin{aligned}
||T_{\gamma(\epsilon)}g^\epsilon - A^+ g|| &\le ||T_{\gamma(\epsilon)}(g^\epsilon - g)|| + ||T_{\gamma(\epsilon)}g - A^+ g|| \\
&\le ||T_{\gamma(\epsilon)}|| \epsilon + ||T_{\gamma(\epsilon)}g - A^+ g|| \\
&\to 0 \ .
\end{aligned}$$

Hence $T_{\gamma(\epsilon)}g^\epsilon$ is close to $A^+ g$ if g^ϵ is close to g.

The number γ is called a regularization parameter. Determining a good regularization parameter is a major issue in the theory of ill-posed problems.

Measurement errors of arbitrarily small L^2-norm in g may cause g to be not in Range(A) and the inversion formula (2.63) practically useless. Therefore, instead of trying to solve (2.64) exactly, one seeks to find a nearby problem that is uniquely solvable and that is robust in the sense that small errors in the data do not corrupt excessively this approximate solution.

We briefly discuss three families of classical regularization methods: (i) regularization by singular value truncation, (ii) the Tikhonov-Phillips regularization and (iii) regularization by truncated iterative methods.

2.8.2 The Truncated SVD

Let

$$Af = \sum_l \sigma_l \,(f_l, f)\, g_l$$

be the SVD of A. Then

$$T_\gamma g = \sum_{\sigma_l \geq \gamma} \sigma_l^{-1} \,(g_l, g)\, f_l \tag{2.65}$$

is a regularization with $||T_\gamma|| \leq 1/\gamma$.

A good measure for the degree of ill-posedness of (2.64) is the rate of decay of the singular values σ_l. It is clear from (2.65) that the ill-posedness is more pronounced as the rate of decay increases. A polynomial decay is usually considered manageable, while an exponential decay indicates that only very poor approximations to f in (2.64) can be computed. The SVD gives us all the information we need about an ill-posed problem.

There is a rule for choosing the truncation level, that is often referred to as the discrepancy principle. This principle states that we cannot expect the approximate solution f_γ to yield a smaller residual error, $Af_\gamma - g$, than the noise level ϵ, since otherwise we would be fitting the solution to the noise. This leads to the following selection criterion for γ: choose the largest γ that satisfies $||g - \sum_{\sigma_l \geq \gamma}(g_l, g)g_l|| \leq \epsilon$.

2.8.3 Tikhonov-Phillips Regularization

Linear Problems

The discussion in the previous subsection demonstrates that when solving the equation (2.64) for a compact operator A, serious problems occur when the singular values of A tend to zero rapidly, causing the norm of the approximate solution to go to infinity as the regularization parameter γ goes to zero. The idea in the basic Tikhonov-Phillips regularization scheme is to control simultaneously the norm of the residual, $Af_\gamma - g$, and the norm of the approximate solution f_γ.

To do so, we set

$$T_\gamma = (A^*A + \gamma I)^{-1} A^* \ .$$

Equivalently, $f_\gamma = T_\gamma g$ can be defined by minimizing $||Af - g||^2 + \gamma ||f||^2$. Here the regularization parameter γ plays essentially the role of a Lagrange multiplier. In terms of the SVD of A presented in Section 2.5, we have

$$T_\gamma g = \sum_l F_\gamma(\sigma_l)\sigma_l^{-1} \,(g_l, g)\, f_l \ , \tag{2.66}$$

where $F_\gamma(\sigma) = \sigma^2/(\sigma^2 + \gamma)$.

The choice of the value of the regularization parameter γ based on the noise level of the measurement g is a central issue in the literature discussing Tikhonov-Phillips regularization. Several methods for choosing γ have been proposed. The most common one is known as the Morozov discrepancy principle. This principle is essentially the same as the discrepancy principle discussed in connection with the singular value truncation principle. It is rather straightforward to implement the principle numerically.

Let ϵ be the measurement error. Let

$$\varphi : \mathbb{R}^+ \to \mathbb{R}^+, \quad \varphi(\gamma) = ||Af_\gamma - g||$$

be the discrepancy related to the regularization parameter γ. The Morozov discrepancy principle says that γ should be chosen from the condition

$$\varphi(\gamma) = \epsilon \, , \tag{2.67}$$

if possible, *i.e.*, the regularized solution should not try to satisfy the data more accurately than up to the noise level ϵ. Equation (2.67) has a unique solution $\gamma = \gamma(\epsilon)$ if and only if (i) any component in the data g that is orthogonal to Range(A) must be due to noise and (ii) the error level ϵ should not exceed the signal level $||g||$.

Nonlinear Problems

Tikhonov-Phillips regularization method is sometimes applicable also when non-linear problems are considered. Let H and K be Hilbert spaces. Let $A : H \to K$ be a nonlinear mapping. We want to find $f \in H$ satisfying

$$A(f) = g + \epsilon \, , \tag{2.68}$$

where ϵ is observation noise. If A is such that large changes in f may produce small changes in $A(f)$, the problem of finding f a solution to (2.68) is ill-posed and numerical methods, typically, iterative ones, may fail to find a satisfactory estimate of f.

The nonlinear Tikhonov-Phillips regularization scheme amounts to searching for f that minimizes the functional

$$||A(f) - g||^2 + \gamma G(f) \, , \tag{2.69}$$

where $G : H \to \mathbb{R}$ is a nonnegative functional. The most common penalty term is $G(f) = ||f||^2$ although a lot of work has been recently devoted to the analysis of nonquadratic-type penalization methods; see, for instance, [315]. We first restrict ourselves to this choice and suppose that A is Fréchet differentiable. In this case, the most common method to search for a minimizer of (2.69) is to use an iterative scheme based on successive linearizations of A. The linearization of A around a given point f_0 leads that the minimizer of (2.69) (around f_0) is

$$f = (R_{f_0}^* R_{f_0} + \gamma I)^{-1} R_{f_0}^* \left(g - A(f_0) + R_{f_0} f_0 \right) ,$$

where R_{f_0} is the Fréchet derivative of A at f_0. We recall that A is Fréchet differentiable at f_0 if it allows an expansion of the form

$$A(f_0 + h) = A(f_0) + R_{f_0} h + o(||h||) ,$$

where R_{f_0} is a continuous linear operator.

2.8.4 Regularization by Truncated Iterative Methods

The most common iterative methods to solve (2.64) are Landweber iteration, Kaczmarz iteration, and Krylov subspace methods. The best known of the Krylov iterative methods when the matrix A is symmetric and positive definite is the conjugate gradient method. In this section, we only discuss regularizing properties of Landweber and Kaczmarz iterations. We refer to [209] and the references therein concerning the Krylov subspace methods.

Linear Landweber Iteration

The drawback of the Thikhonov-Phillips regularization is that it requires to invert the regularized normal operator $A^*A + \gamma I$. This inversion may be costly in practice. The linear Landweber iteration method is an iterative technique in which no inversion is necessary. It is defined to solve the linear equation $Af = g$ as follows:

$$f^0 = 0, \quad f^{k+1} = f^k + \eta A^* \left(g - A f^k \right), \quad k \geq 0 ,$$

for some $\eta > 0$. By induction, since

$$f^{k+1} = (I - \eta A^* A) f^k + \eta A^* g, \quad k \geq 0 ,$$

we verify that $f^k = T_\gamma g$, with $\gamma = 1/k, k \geq 1$, and

$$T_\gamma g = \eta \sum_{l=0}^{1/\gamma - 1} (I - \eta A^* A)^l A^* g .$$

Let $q \leq +\infty$ be the number of singular values of A. Let σ_l be the singular values arranged in a decreasing sequence and g_l and f_l be respectively the associated left and right singular vectors. Since

$$\eta \sum_{l=0}^{1/\gamma - 1} (I - \eta A^* A)^l A^* g = \sum_{l=1}^{q} \frac{1}{\sigma_l} (1 - (1 - \eta \sigma_l^2)^{1/\gamma})(g_l, g) f_l ,$$

where $f_l = (f, g_l)$, a good choice of η is thus $\eta \approx \sigma_1^{-2}$.

Kaczmarz Iteration

Kaczmarz's method (also known as the algebraic reconstruction technique) is an iterative method for solving linear systems of equations. Let $H, H_j, j = 1, \ldots, p$, be Hilbert spaces, and let

$$A_j : H \to H_j, \quad j = 1, \ldots, p \,,$$

be bounded linear maps from H onto H_j with $\mathrm{Range}(A_j) = H_j$. Let $g_j \in H_j$ be given. We want to compute $f \in H$ such that

$$A_j f = g_j, \quad j = 1, \ldots, p \,. \tag{2.70}$$

Kaczmarz's method for the solution of (2.70) reads:

Algorithm 2.1 Kaczmarz's method

---
1. $f_0 = f^k$,
2. $f_j = f_{j-1} + \gamma A_j^* (A_j A_j^*)^{-1} (g_j - A_j f_{j-1}), \quad j = 1, \ldots, p$,
3. $f^{k+1} = f_p$, with $f^0 \in H$ arbitrary.

Here γ is a regularization parameter. Under certain assumptions, f^k converges to a solution of (2.70) if (2.70) has a solution and to a generalized solution if not.

2.8.5 Regularizations by Nonquadratic Constraints

L^1-Regularization

Regularization methods rely on a regularization term that is adapted to the a prior knowledge on the solution to be recovered. In some biomedical imaging applications, the a prior knowledge is that the solution has a sparse expansion with respect to some given basis. Sparsity means that only a few coefficients of the solution are nonzero.

In order to promote sparsity, an L^1 penalization can be added, $G(f) = ||f||_{L^1} := \sum_j |(\varphi_j, f)|$, where (φ_j) is an orthonormal basis of H. When compared to the classical (L_2-) Tikhonov-Phillips regularization, the L^1-regularization puts a lesser penalty on functions f with large but few components with respect to the basis (φ_j), and a higher penalty on sums of many small components. The L^1-minimization procedure promotes then sparsity of the expansion of f with respect to the basis (φ_j).

Total Variation Regularization

When the solution of the imaging problem is piecewise constant, total variation regularization can be used.

Let Ω be a bounded smooth domain. The total variation of a real-valued function f on Ω is defined by

$$\left|f\right|_{\mathrm{TV}(\Omega)} := \sup\left\{ \int_\Omega f(x)\Phi(x)\,dx, \Phi \in \mathcal{C}_0^1(\Omega), \sup|\Phi| \le 1 \right\}.$$

A function f in Ω is of bounded variation on Ω if $\left|f\right|_{\mathrm{TV}(\Omega)} < +\infty$. If $f \in \mathcal{C}^1(\overline{\Omega})$, then $\left|f\right|_{\mathrm{TV}(\Omega)} = \|\nabla f\|_{L^1(\Omega)}$. The total variation of the characteristic function $\chi(\Omega)$ is the length of $\partial\Omega$.

Consider the minimization problem (2.69). The total variation regularization is nonquadratic and given by $G(f) = \int_\Omega |\nabla f|$. If A is Fréchet differentiable, then the gradient of the discrepancy function at f_0 is given by

$$\gamma\nabla \cdot \frac{\nabla f_0}{|\nabla f_0|} + 2R_{f_0}^*\left(g - A(f_0)\right),$$

where R_{f_0} is the Fréchet derivative of A at f_0.

Direct computation of a solution to the minimization problem (2.69) can be complicated as the gradient is not continuous. Nevertheless, an approximate solution can be obtained via an iterative shrinkage-thresholding algorithm [97].

Algorithm 2.2 Iterative shrinkage-thresholding algorithm

---

1. Data g; initial set: $f^{(0)} = x^{(0)} = 0$, $t_0 = 1$;
2. $x^{(k)} = T_\gamma\left(f^{(k)} - \eta R_{f^{(k)}}^*\left(g - A(f^{(k)})\right)\right)$ with $\eta > 0$ being the step size and

$$T_\gamma[y] = \arg\min_x \left\{ \frac{1}{2}\|y - x\|_{L^2}^2 + \gamma\|\nabla x\|_{L^1} \right\}. \tag{2.71}$$

3. $f^{(k+1)} = x^{(k)} + \frac{t_k - 1}{t_{k+1}}\left(x^{(k)} - x^{(k-1)}\right)$ with $t_{k+1} = \frac{1+\sqrt{1+4t_k^2}}{2}$.

2.9 Optimal Control

Let H be a Banach space. In biomedical imaging, H stands either for a set of admissible properties of a biological material or for a set of geometric shapes. Consider a discrepancy functional $J(u(h))$ depending on $h \in H$ via the solution $u(h)$ to a system where h acts as a parameter, say: $A(h)u(h) = g$. Here,

g represents the data. In order to minimize J we need to compute its Fréchet derivative

$$\frac{\partial J}{\partial u}(u(h))\frac{\partial u}{\partial h}\,,$$

which is not explicit in h. The introduction of the adjoint system

$$A(h)^*p(h) = \frac{\partial J}{\partial u}(u(h))\,, \tag{2.72}$$

where $A(h)^*$ denotes the adjoint of $A(h)$ makes this explicit. Multiplying (2.72) by $\frac{\partial u}{\partial h}\delta h$ we obtain

$$\frac{\partial J}{\partial u}(u(h))\frac{\partial u}{\partial h}\delta h = -p(h)\frac{\partial A}{\partial h}\delta h u(h)\,,$$

and therefore, the Fréchet derivative of J is given by

$$-p(h)\frac{\partial A^*}{\partial h}u(h)\,.$$

Algorithm 2.3 Optimal control algorithm

---
1. Data g; initial set: $h^{(0)}$;
2. Compute $p(h^{(k)})$ solution to (2.72);
3. $h^{(k+1)} = h^{(k)} + \eta p(h^{(k)})\frac{\partial A^*}{\partial h}u(h^{(k)})$ with $\eta > 0$ being the step size.

2.10 Convergence of Nonlinear Landweber Iterations

We state a convergence result concerning nonlinear Landweber iterations. This result will be useful in studying optimal control approaches for hybrid tomographies.

Let H be a Hilbert space and $F : K \to H$ be a differentiable map where K is an closed and convex subset of H. Given $y_* \in H$, assume that we want to solve the equation

$$F(x_*) = y_*, \quad x_* \in K\,. \tag{2.73}$$

It is natuaral to minimize

$$J(x) = \frac{1}{2}\|F(x) - y_*\|^2 \tag{2.74}$$

with $x \in K$. Assume that F is Fréchet differentiable. So is J. The derivative of J is given by

$$dJ(x)h = \big(dF(x)h, F(x) - y_*\big) = \big(h, dF(x)^*(F(x) - y_*)\big)\,, \tag{2.75}$$

where the superscript * indicates the dual map. The iteration sequence due to the descent gradient method is given by the so-called (nonlinear) Landweber iterations:

$$x^{(n+1)} = Tx^{(n)} - \eta dF(Tx^{(n)})^*(F(Tx^{(n)}) - y_*) . \qquad (2.76)$$

Here, T is the Hilbert projection of H onto K

$$T : H \ni x \mapsto \operatorname{argmin}\{\|x - a\} : a \in K\} \qquad (2.77)$$

and η is a small positive number. The presence of T in (2.76) is necessary because $x^{(n)}$ might not be in K and $F(x^{(n)})$ might not be well-defined. The map T above also increases the rate of convergence of $(x^{(n)})$ to x_* due to

$$\|Tx^{(n)} - x_*\| \le \|x^{(n)} - x_*\| \quad n \ge 1 . \qquad (2.78)$$

We have the proposition.

Proposition 2.5 *Assume that the Fréchet derivative dF is Lipschitz continuous and that for all $x \in K$,*

$$\|dF(x)\|_{H^*} \ge c , \qquad (2.79)$$

for some positive constant c. Then the sequence defined in (2.76) converges to x_* provided that $x^{(0)}$ is a "good" initial guess for x_* and η is sufficiently small.

Proof. Since dF is Lipschitz continuous, we have for all x such that $\|x - x_*\|$ is small

$$\begin{aligned}
\|F(x) - F(x_*) - dF(x)(x - x_*)\| &\le C\|x - x_*\|^2 \\
&\le C\|x - x_*\|\|F(x) - F(x_*)\| \\
&\le \mu\|F(x) - F(x_*)\| \qquad (2.80)
\end{aligned}$$

for small constant μ. For all $n \ge 1$, let F_n denote the nth error quantity $F(Tx^{(n)}) - y_*$. We have

$$\begin{aligned}
\|x^{(n+1)} - x_*\|^2 - \|x^{(n)} - x_*\|^2 &\le \|x^{(n+1)} - x_*\|^2 - \|Tx^{(n)} - x_*\|^2 \\
&= 2\langle x^{(n+1)} - Tx^{(n)}, Tx^{(n)} - x_*\rangle + \|x^{(n+1)} - Tx^{(n)}\|^2 \\
&= 2\eta\langle -dF(Tx^{(n)})^*F_n, Tx^{(n)} - x_*\rangle \\
&\qquad + \langle \eta F_n, \mu dF(Tx^{(n)})dF(Tx^{(n)})^*\rangle \\
&= \langle F_n, 2\eta F_n - 2\eta dF(Tx^{(n)})(Tx^{(n)} - x_*)\rangle - \eta\|F_n\|^2 \\
&\qquad + \langle \sqrt{\eta}F_n, (-I + \eta dF(Tx^{(n)})dF(\sqrt{\mu}Tx^{(n)})^*))F_n\rangle \\
&\le \eta(2\mu - 1)\|F_n\|^2 .
\end{aligned}$$

It then follows that

$$\|x^{(n+1)} - x_*\|^2 + \eta(1 - 2\mu)\|F_n\|^2 \le \|x^{(n)} - x_*\|^2 , \qquad (2.81)$$

and therefore,

$$\sum_{n=1}^{\infty} \|FT(x^{(n)}) - y_*\|^2 \leq \frac{\|x^{(0)} - x_*\|^2}{\eta(1 - 2\mu)} . \tag{2.82}$$

We now obtain the convergence of $(x^{(n)})$ to x_* using the mean value theorem and condition (2.79)

$$c\|Tx^{(n)} - x_*\| \leq \|dF(\tilde{x}^{(n)})(Tx^{(n)} - x_*)\| = \|F(Tx^{(n)}) - F(x_*)\| \to 0 \tag{2.83}$$

for some $\tilde{x}^{(n)} = tTx^{(n)} + (1 - t)x_*$, $t \in (0, 1)$. $\square$

2.11 Level Set Method

Let H be a set of geometric shapes and consider the minimization over H of a discrepancy functional J. The main idea of the level set approach is to represent the boundary of the domain D as the zero level set of a continuous function ϕ, *i.e.*,

$$D = \left\{ x : \phi(x) < 0 \right\},$$

to work with function ϕ instead of D, and to derive an evolution equation for ϕ to solve the minimization problem. In fact, by allowing additional time-dependence of ϕ, we can compute the geometric motion of D in time by evolving the level set function ϕ. A geometric motion with normal velocity $V = V(x, t)$ can be realized by solving the Hamilton-Jacobi equation

$$\frac{\partial \phi}{\partial t} + V|\nabla \phi| = 0. \tag{2.84}$$

Minimization within the level set framework consists of choosing a velocity V driving the evolution towards a minimum (or at least increasing the discrepancy functional we want to minimize).

Consider the geometry of the zero level set

$$\partial D = \left\{ x : \phi(x) = 0 \right\},$$

under a variation of ϕ. Suppose that $\phi(x)$ is perturbed by a small variation $\delta\phi(x)$. Let δx be the resulting variation of the point x. By taking the variation of the equation $\phi(x) = 0$, we find

$$\delta\phi = -\nabla\phi \cdot \delta x . \tag{2.85}$$

Observe that the unit outward normal at x is given by

$$\nu(x) = \frac{\nabla\phi(x)}{|\nabla\phi(x)|} .$$

Now, if t represents time, then the function ϕ depends on both x and t. We use the notation

$$\partial D(t) = \left\{ x : \phi(x,t) = 0 \right\}.$$

Assume that each point $x \in \partial D(t)$ moves perpendicular to the curve. That is, the variation δx satisfies

$$\delta x = V(x,t) \frac{\nabla \phi(x,t)}{|\nabla \phi(x,t)|}.$$

Suppose that J is given by (2.69) (with $\gamma = 0$) and the minimization is performed over piecewise functions $f = f_+ \chi(\mathbb{R}^d \setminus \overline{D}) + f_- \chi(D)$ with $f_\pm$ being given constants. The minimal requirement for the variations of $\phi(x,t)$ is that J be a decreasing function of t. The directional derivative of the function J in the direction δf is given by

$$\delta J(f) = J'(f)\delta f = 2R_f^* \Big(g - A(f) \Big)\delta f \,,$$

where J' is the Fréchet derivative of J and R_f^* is the Fréchet derivative of $A(f)$. Since δf is a measure on ∂D given by

$$\delta f = (f_+ - f_-)\delta x \cdot \nu(x)\,,$$

we have

$$\delta f = (f_+ - f_-)\frac{\nabla \phi(x)}{|\nabla \phi(x)|} \cdot \delta x \bigg|_{x \in \partial D}. \tag{2.86}$$

Hence,

$$\delta J(f) = (f_+ - f_-)J'(f)V\,,$$

and therefore, in order to make $\delta J(f)$ negative, we can choose

$$V(x,t) = (f_+ - f_-)R_f^* \Big(g - A(f) \Big)\,. \tag{2.87}$$

As (2.87) is only valid for $x \in \partial D$, a velocity extension to the entire domain should be performed. This leads to the Hamilton-Jacobi equation (2.84) for $\phi(x,t)$ with the initial condition $\phi(x,0) = \phi_0(x)$, and thus the problem of maximizing $J(f)$ is converted into a level set form.

3

Layer Potential Techniques

The anomaly imaging algorithms described in this book rely on asymptotic expansions of the fields when the medium contains particles of small volume. Such asymptotics will be investigated in the cases of the conductivity equation, which models the quasi-static limit for electromagnetic waves, the Helmholtz equations, which are used for the scalar theory of electromagnetic waves and for the propagation of acoustic waves, and the elasticity equations. The use of Helmholtz equations in electromagnetic theory can be justified when there is no depolarization as the electromagnetic wave propagates through the medium. The depolarization effects can be ignored only if the wavelength is much smaller than the typical size of the inhomogeneities in the medium.

We prepare the way in this chapter by reviewing a number of basic facts on the layer potentials for these equations which are very useful for robust imaging of small anomalies. The most important results in this chapter are on integral representations for solutions to transmission scattering problems and, on the other hand, the Helmholtz-Kirchhoff identities. The results on the transmission scattering problems will be used to provide asymptotic expansions of the solution perturbations due to presence of small particles. As will be shown later, the Helmholtz-Kirchhoff identities play a key role in the analysis of resolution in wave imaging.

We begin with the conductivity equation and study the Neumann-Poincaré operator. We then discuss the transmission scattering problem for the Helmholtz equation. Compared to the conductivity equation, the only new difficulty in establishing integral representation formulas for the Helmholtz equation is that the equations inside and outside the particle are not the same. We should then consider two unknowns and solve a system of equations on the boundary of the particle instead of just one equation. We also note that when dealing with the Helmholtz equation, one should introduce a radiation condition, known as the Sommerfeld radiation condition, to select the physical solution to the problem. Then we derive the Helmholtz-Kirchhoff identity, which plays

a key role in the resolution analysis. Finally, we recall useful results on layer potential techniques for the elasticity equations.

3.1 The Laplace Equation

This section deals with the Laplace operator (or Laplacian) in $\mathbb{R}^d$, denoted by Δ. The Laplacian models the quasi-static approximation for electromagnetic wave propagation. After deriving the fundamental solution for the Laplacian, we shall introduce the single- and double-layer potentials as well as the Neumann-Poincaré operator. We then provide the jump relations and mapping properties of these surface potentials. We review the spectral properties of the Neumann-Poincaré operator. We recall a Calderón identity (also known as Plemelj's symmetrization principle) and apply the symmetrization principle to the Neumann-Poincaré operator. Finally, we investigate the transmission problem.

3.1.1 Fundamental Solution

To give a fundamental solution to the Laplacian in the general case of the dimension d, we denote by ω_d the area of the unit sphere S in $\mathbb{R}^d$.

Lemma 3.1 *A fundamental solution to the Laplacian is given by*

$$\Gamma(x) = \begin{cases} \dfrac{1}{2\pi}\log|x| \, , & d = 2 \, , \\[2ex] \dfrac{1}{(2-d)\omega_d}|x|^{2-d} \, , & d \geq 3 \, . \end{cases} \tag{3.1}$$

It satisfies in the sense of distributions $\Delta\Gamma = \delta_0$.

Let $a \in \mathbb{R}^d$ and $q \in \mathbb{R}$. Let $\Gamma(x,z) := \Gamma(x-z)$ for $x \neq z$ be the fundamental solution for a source point at z. The function $q\Gamma(x,z)$ is called the potential due to charges q at the source point z. The function $a \cdot \nabla_z \Gamma(x,z)$ is called the dipole of moment $|a|$ and direction $a/|a|$ at the source point z. It is known that using point charges one can obtain a dipole only approximately (two large charges a small distance apart). See [295].

We next state Green's identity.

Lemma 3.2 *Assume that D is a bounded $\mathcal{C}^2$-domain in $\mathbb{R}^d, d \geq 2$, and let $u \in W^{1,2}(D)$ be a harmonic function. Then for any $x \in D$,*

$$u(x) = \int_{\partial D} \left(u(y)\frac{\partial\Gamma}{\partial\nu_y}(x,y) - \frac{\partial u}{\partial\nu_y}(y)\Gamma(x,y) \right) d\sigma(y) \, . \tag{3.2}$$

Particularly useful solutions to the Laplace equation in $\mathbb{R}^2$ are homogeneous harmonic polynomials $r^n e^{\pm in\theta}$ with (r,θ) being the polar coordinates.

3.1.2 Layer Potentials

In this subsection we show how important the fundamental solution is to potential theory. It gives rise to integral operators that invert the Laplacian. We need these integral operators (also called layer potentials) in solving the transmission problem.

Given a bounded $\mathcal{C}^2$-domain D in $\mathbb{R}^d, d \geq 2$, we denote respectively the single- and double-layer potentials of a function $\phi \in L^2(\partial D)$ as $\mathcal{S}_D[\phi]$ and $\mathcal{D}_D[\phi]$, where

$$\mathcal{S}_D[\phi](x) := \int_{\partial D} \Gamma(x,y)\phi(y)\,d\sigma(y)\,, \quad x \in \mathbb{R}^d\,, \tag{3.3}$$

$$\mathcal{D}_D[\phi](x) := \int_{\partial D} \frac{\partial}{\partial \nu_y}\Gamma(x,y)\phi(y)\,d\sigma(y)\,, \quad x \in \mathbb{R}^d \setminus \partial D\,. \tag{3.4}$$

We begin with recalling their basic properties. We note that for $x \in \mathbb{R}^d \setminus \partial D$ and $y \in \partial D$, $\partial \Gamma/\partial \nu_y(x,y)$ is an L^∞-function in y and harmonic in x, and it is $O(|x|^{1-d})$ as $|x| \to +\infty$. Therefore we readily see that $\mathcal{D}_D[\phi]$ and $\mathcal{S}_D[\phi]$ are well-defined and harmonic in $\mathbb{R}^d \setminus \partial D$. Let us list their behavior at $+\infty$.

Lemma 3.3 *The following holds:*

(i) $\mathcal{D}_D[\phi](x) = O(|x|^{1-d})$ *as* $|x| \to +\infty$.
(ii) $\mathcal{S}_D[\phi](x) = O(|x|^{2-d})$ *as* $|x| \to +\infty$ *when* $d \geq 3$.
(iii) *If* $d = 2$, *we have*

$$\mathcal{S}_D[\phi](x) = \frac{1}{2\pi}\int_{\partial D}\phi(y)\,d\sigma(y)\,\log|x| + O(|x|^{-1}) \quad as\ |x| \to +\infty\,.$$

(iv) *If* $\int_{\partial D}\phi(y)\,d\sigma = 0$, *then* $\mathcal{S}_D[\phi](x) = O(|x|^{1-d})$ *as* $|x| \to +\infty$ *for* $d \geq 2$.

Lemma 3.2 shows that if $u \in W^{1,2}(D)$ is harmonic, then for any $x \in D$,

$$u(x) = \mathcal{D}_D[u|_{\partial D}](x) - \mathcal{S}_D\left[\frac{\partial u}{\partial \nu}\bigg|_{\partial D}\right](x)\,. \tag{3.5}$$

To solve the Dirichlet and Neumann problems, where either u or $\partial u/\partial \nu$ on ∂D is prescribed, we need to understand well the subtle behaviors of the functions $\mathcal{D}_D[\phi](x \pm t\nu_x)$ and $\nabla \mathcal{S}_D[\phi](x \pm t\nu_x)$ for $x \in \partial D$ as $t \to 0^+$. A detailed discussion of the behavior near the boundary ∂D of $\mathcal{D}_D[\phi]$ and $\nabla \mathcal{S}_D[\phi]$ for a $\mathcal{C}^2$-domain D and a density $\phi \in L^2(\partial D)$ is given below. We shall follow [168].

Throughout this book, we use the dot for the scalar product in $\mathbb{R}^d$. Assume that D is a bounded $\mathcal{C}^2$-domain. Then we have the bound

$$\left|\frac{(x-y)\cdot\nu_x}{|x-y|^d}\right| \leq C\frac{1}{|x-y|^{d-2}} \quad \text{for } x,y \in \partial D, x \neq y\,, \tag{3.6}$$

which shows that there exists a positive constant C depending only on D such that

$$\int_{\partial D} \left(\frac{|(x-y) \cdot \nu_x|}{|x-y|^d} + \frac{|(x-y) \cdot \nu_y|}{|x-y|^d} \right) d\sigma(y) \le C , \tag{3.7}$$

and

$$\int_{|y-x|<\epsilon} \left(\frac{|(x-y) \cdot \nu_x|}{|x-y|^d} + \frac{|(x-y) \cdot \nu_y|}{|x-y|^d} \right) d\sigma(y) \le C \int_0^\epsilon \frac{1}{r^{d-2}} r^{d-2} \, dr$$
$$\le C\epsilon , \tag{3.8}$$

for any $x \in \partial D$, by integration in polar coordinates.

Introduce the operator $\mathcal{K}_D : L^2(\partial D) \to L^2(\partial D)$ given by

$$\mathcal{K}_D[\phi](x) = \frac{1}{\omega_d} \int_{\partial D} \frac{(y-x) \cdot \nu_y}{|x-y|^d} \phi(y) \, d\sigma(y) . \tag{3.9}$$

We refer to $\mathcal{K}_D$ as the Neumann-Poincaré operator.

The estimate (3.7) proves that this operator is bounded. In fact, for $\phi, \psi \in L^2(\partial D)$, we estimate

$$\left| \int_{\partial D} \int_{\partial D} \frac{(y-x) \cdot \nu_y}{|x-y|^d} \phi(y) \, \psi(x) \, d\sigma(y) \, d\sigma(x) \right| \tag{3.10}$$

via the inequality $2ab \le a^2 + b^2$. Then, by (3.7), (3.10) is dominated by

$$C \left(||\phi||^2_{L^2(\partial D)} + ||\psi||^2_{L^2(\partial D)} \right) .$$

Replacing ϕ, ψ, by $t\phi, (1/t)\psi$, we see that (3.10) is bounded by

$$C \left(t^2 ||\phi||^2_{L^2(\partial D)} + \frac{1}{t^2} ||\psi||^2_{L^2(\partial D)} \right) ;$$

minimizing over $t \in (0, +\infty)$, via elementary calculus, we see that (3.10) is dominated by $C||\phi||_{L^2(\partial D)}||\psi||_{L^2(\partial D)}$, proving that $\mathcal{K}_D$ is a bounded operator on $L^2(\partial D)$.

On the other hand, it is easily checked that the operator defined by

$$\mathcal{K}_D^*[\phi](x) = \frac{1}{\omega_d} \int_{\partial D} \frac{(x-y) \cdot \nu_x}{|x-y|^d} \phi(y) \, d\sigma(y) , \tag{3.11}$$

is the L^2-adjoint of $\mathcal{K}_D$. Furthermore, the operator $\mathcal{K}_D^*$ is scale invariant:

$$\mathcal{K}_{sD}^*[\widetilde{\phi}](\widetilde{x}) = \mathcal{K}_D^*[\phi](x), \quad x \in \partial D ,$$

where sD denotes the dilation of D by $s > 0$, $\widetilde{x} = sx, \widetilde{\phi}(\widetilde{y}) = \phi(sy), y \in \partial D$.

It is now important to ask about the compactness of these operators. Indeed, to apply the Fredholm theory for solving the Dirichlet and Neumann problems for the Laplace equation, we will need the following lemma.

Lemma 3.4 *If D is a bounded C^2-domain, then the operators $\mathcal{K}_D$ and $\mathcal{K}_D^*$ are compact operators in $L^2(\partial D)$.*

The Neumann-Poincaré operator $\mathcal{K}_D^*$ is not self-adjoint on $L^2(\partial D)$ unless D is a disk or a ball. In these cases, we may simplify the expressions defining the operators $\mathcal{K}_D$ and $\mathcal{K}_D^*$. The following results hold.

Lemma 3.5 (i) *Suppose that D is a two dimensional disk with radius r_0. Then,*

$$\frac{(x-y)\cdot\nu_x}{|x-y|^2} = \frac{1}{2r_0} \quad \forall\, x, y \in \partial D, x \neq y ,$$

and therefore, for any $\phi \in L^2(\partial D)$,

$$\mathcal{K}_D^*[\phi](x) = \mathcal{K}_D[\phi](x) = \frac{1}{4\pi r_0}\int_{\partial D} \phi(y)\, d\sigma(y) , \qquad (3.12)$$

for all $x \in \partial D$.

(ii) *For $d \geq 3$, if D is a ball with radius r_0, then, we have*

$$\frac{(x-y)\cdot\nu_x}{|x-y|^d} = \frac{1}{2r_0}\frac{1}{|x-y|^{d-2}} \quad \forall\, x, y \in \partial D, x \neq y ,$$

and for any $\phi \in L^2(\partial D)$ and $x \in \partial D$,

$$\mathcal{K}_D^*[\phi](x) = \mathcal{K}_D[\phi](x) = \frac{(2-d)}{2r_0}\mathcal{S}_D[\phi](x) . \qquad (3.13)$$

In two dimensions, we also remark that if the disk D of radius r_0 is centered at the origin, then one can easily see that for each integer n

$$\mathcal{S}_D[e^{in\theta}](x) = \begin{cases} -\dfrac{r_0}{2|n|}\left(\dfrac{r}{r_0}\right)^{|n|} e^{in\theta} & \text{if } |x| = r < r_0 , \\[3mm] -\dfrac{r_0}{2|n|}\left(\dfrac{r_0}{r}\right)^{|n|} e^{in\theta} & \text{if } |x| = r > r_0 , \end{cases} \qquad (3.14)$$

and hence

$$\frac{\partial}{\partial r}\mathcal{S}_D[e^{in\theta}](x) = \begin{cases} -\dfrac{1}{2}\left(\dfrac{r}{r_0}\right)^{|n|-1} e^{in\theta} & \text{if } |x| = r < r_0 , \\[3mm] \dfrac{1}{2}\left(\dfrac{r_0}{r}\right)^{|n|+1} e^{in\theta} & \text{if } |x| = r > r_0 . \end{cases} \qquad (3.15)$$

It follows from (3.12) that

$$\mathcal{K}_D^*[e^{in\theta}] = 0 \quad \forall n \neq 0 . \qquad (3.16)$$

We also get

$$\mathcal{D}_D[e^{in\theta}](x) = \begin{cases} \dfrac{1}{2}\left(\dfrac{r}{r_0}\right)^{|n|} e^{in\theta} & \text{if } |x| = r < r_0 \text{ ,} \\[3mm] -\dfrac{1}{2}\left(\dfrac{r_0}{r}\right)^{|n|} e^{in\theta} & \text{if } |x| = r > r_0 \text{ .} \end{cases}$$

Another useful formula in two dimensions is the expression of $\mathcal{K}_D[\phi](x)$, where D is an ellipse whose semi-axes are on the x_1- and x_2-axes and of length a and b, respectively. Using the parametric representation $X(t) = (a\cos t, b\sin t), 0 \le t \le 2\pi$, for the boundary ∂D, we find that

$$\mathcal{K}_D[\phi](x) = \frac{ab}{2\pi(a^2 + b^2)} \int_0^{2\pi} \frac{\phi(X(t))}{1 - Q\cos(t+\theta)}\, dt \text{ ,} \tag{3.17}$$

where $x = X(\theta)$ and $Q = (a^2 - b^2)/(a^2 + b^2)$.

Turning now to the behavior of the double layer potential at the boundary, we first recall that the double layer potential with constant density has a jump.

Lemma 3.6 *If D is a bounded $\mathcal{C}^2$-domain, then $\mathcal{D}_D[1](x) = 0$ for $x \in \mathbb{R}^d \setminus \overline{D}$, $\mathcal{D}_D[1](x) = 1$ for $x \in D$, and $\mathcal{K}_D[1](x) = 1/2$ for $x \in \partial D$.*

Lemma 3.6 can be extended to general densities $\phi \in L^2(\partial D)$. For convenience we introduce the following notation. For a function u defined on $\mathbb{R}^d \setminus \partial D$, we denote

$$u|_\pm(x) := \lim_{t \to 0^+} u(x \pm t\nu_x), \quad x \in \partial D \text{ ,}$$

and

$$\left.\frac{\partial u}{\partial \nu_x}\right|_\pm(x) := \lim_{t \to 0^+} \nabla u(x \pm t\nu_x) \cdot \nu_x \text{ ,} \quad x \in \partial D \text{ ,}$$

if the limits exist. Here ν_x is the outward unit normal to ∂D at x.

We relate in the next lemma the traces $\mathcal{D}_D|_\pm$ of the double-layer potential to the operator $\mathcal{K}_D$ defined by (3.9).

Lemma 3.7 *If D is a bounded $\mathcal{C}^2$-domain, then for $\phi \in L^2(\partial D)$*

$$(\mathcal{D}_D[\phi])\big|_\pm(x) = \left(\mp\frac{1}{2}I + \mathcal{K}_D\right)[\phi](x) \quad a.e. \ x \in \partial D \text{ .} \tag{3.18}$$

In a similar way, we can describe the behavior of the gradient of the single layer potential at the boundary. The following lemma reveals the connection between the traces $\partial \mathcal{S}_D/\partial \nu|_\pm$ and the operator $\mathcal{K}_D^*$ defined by (3.11).

Lemma 3.8 *If D is a bounded $\mathcal{C}^2$-domain, then for $\phi \in L^2(\partial D)$*

$$\left.\frac{\partial}{\partial T}\mathcal{S}_D[\phi]\right|_+(x) = \left.\frac{\partial}{\partial T}\mathcal{S}_D[\phi]\right|_-(x) \quad a.e. \ x \in \partial D \text{ ,} \tag{3.19}$$

where $\partial/\partial T$ is the tangential derivative and

$$\left.\frac{\partial}{\partial \nu}\mathcal{S}_D[\phi]\right|_\pm(x) = \left(\pm\frac{1}{2}I + \mathcal{K}_D^*\right)[\phi](x) \quad a.e. \ x \in \partial D \text{ .} \tag{3.20}$$

It is worth emphasizing that the signs in (3.18) and (3.20) are opposite.

We now consider the integral equations

$$\left(\frac{1}{2}I + \mathcal{K}_D\right)[\phi] = f \quad \text{and} \quad \left(\frac{1}{2}I - \mathcal{K}_D^*\right)[\psi] = g \tag{3.21}$$

for $f, g \in L^2(\partial D)$.

By the trace formulas (3.20) and (3.18) for the single- and double-layer potentials, it is easily seen that if ϕ and ψ are solutions to these equations then $\mathcal{D}_D[\phi]$ solves the Dirichlet problem with Dirichlet data f:

$$\begin{cases} \Delta U = 0 & \text{in } D\,, \\ U = f & \text{on } \partial D\,, \end{cases}$$

and $-\mathcal{S}_D[\psi]$ solves the Neumann problem with Neumann data g:

$$\begin{cases} \Delta V = 0 & \text{in } D\,, \\ \dfrac{\partial V}{\partial \nu} = g & \text{on } \partial D\,, \end{cases}$$

if g and ψ satisfy $\int_{\partial D} g\,d\sigma = \int_{\partial D} \psi\,d\sigma = 0$.

In view of Lemma 3.4, we can apply the Fredholm theory to study the solvability of the two integral equations in (3.21).

We conclude this section by investigating the invertibility of the single layer potential. We shall see that complications arise when $d = 2$.

Lemma 3.9 *Let D be a bounded smooth domain in $\mathbb{R}^d$. Let $\phi \in L^2(\partial D)$ satisfy $\mathcal{S}_D[\phi] = 0$ on ∂D.*

(i) *If $d \geq 3$, then $\phi = 0$.*
(ii) *If $d = 2$ and $\int_{\partial D} \phi = 0$, then $\phi = 0$.*

Lemma 3.10 *Let D be a bounded $\mathcal{C}^2$-domain in $\mathbb{R}^d$.*

(i) *If $d \geq 3$, then $\mathcal{S}_D : L^2(\partial D) \to W_1^2(\partial D)$ has a bounded inverse.*
(ii) *If $d = 2$, then the operator $A : L^2(\partial D) \times \mathbb{R} \to W_1^2(\partial D) \times \mathbb{R}$ defined by*

$$A(\phi, a) = \left(\mathcal{S}_D[\phi] + a, \int_{\partial D} \phi\right)$$

has a bounded inverse.
(iii) *Suppose $d = 2$ and let $(\phi_e, a) \in L^2(\partial D) \times \mathbb{R}$ denote the solution of the system*

$$\begin{cases} \mathcal{S}_D[\phi_e] + a = 0\,, \\ \int_{\partial D} \phi_e = 1\,, \end{cases} \tag{3.22}$$

then $\mathcal{S}_D : L^2(\partial D) \to W_1^2(\partial D)$ has a bounded inverse if and only if $a \neq 0$.

3.1.3 Invertibility of $\lambda I - \mathcal{K}_D^*$

Let D be a bounded domain, and let

$$L_0^2(\partial D) := \left\{ \phi \in L^2(\partial D) : \int_{\partial D} \phi \, d\sigma = 0 \right\} .$$

Let $\lambda \neq 0$ be a real number. Of particular interest for solving the transmission problem for the Laplacian would be the invertibility of the operator $\lambda I - \mathcal{K}_D^*$ on $L^2(\partial D)$ or $L_0^2(\partial D)$ for $|\lambda| \geq 1/2$. The case $|\lambda| = 1/2$ corresponds to the integral equations in (3.21).

It was proved by Kellogg in [219] that the eigenvalues of $\mathcal{K}_D^*$ on $L^2(\partial D)$ lie in $(-1/2, 1/2]$. The following injectivity result holds.

Lemma 3.11 *Let λ be a real number and let D be a bounded $\mathcal{C}^2$-domain. The operator $\lambda I - \mathcal{K}_D^*$ is one to one on $L_0^2(\partial D)$ if $|\lambda| \geq 1/2$, and for $\lambda \in (-\infty, -1/2] \cup (1/2, +\infty)$, $\lambda I - \mathcal{K}_D^*$ is one to one on $L^2(\partial D)$.*

We now turn to the surjectivity of the operator $\lambda I - \mathcal{K}_D^*$ on $L^2(\partial D)$ or $L_0^2(\partial D)$. Since D is a bounded $\mathcal{C}^2$-domain, as shown in Lemma 3.4, the operators $\mathcal{K}_D$ and $\mathcal{K}_D^*$ are compact operators in $L^2(\partial D)$. Therefore, the surjectivity of $\lambda I - \mathcal{K}_D^*$ holds, by applying the Fredholm alternative.

3.1.4 Symmetrization of $\mathcal{K}_D^*$

Lemma 3.11 shows that the spectrum of $\mathcal{K}_D^*$ lies in the interval $(-1/2, 1/2]$. In this subsection we symmetrize the non-self-adjoint operator $\mathcal{K}_D^*$ and prove that it can be realized as a self-adjoint operator on $W_{-1/2}^2(\partial D)$ by introducing a new inner product.

We first state the following result.

Lemma 3.12 *Let $d \geq 2$. The operator $\mathcal{S}_D$ in $W_{-1/2}^2(\partial D)$ is self-adjoint and $-\mathcal{S}_D \geq 0$ on $L^2(\partial D)$.*

By Lemma 3.12, there exists a unique square root of $-\mathcal{S}_D$ which we denote by $\sqrt{-\mathcal{S}_D}$; furthermore, $\sqrt{-\mathcal{S}_D}$ is self-adjoint and $\sqrt{-\mathcal{S}_D} \geq 0$.

Next we look into the kernel of $\mathcal{S}_D$. If $d \geq 3$, then it is known that $\mathcal{S}_D : W_{-1/2}^2(\partial D) \rightarrow W_{1/2}^2(\partial D)$ has a bounded inverse. Suppose now that $d = 2$. If $\phi_0 \in \text{Ker}(\mathcal{S}_D)$, then the function u defined by

$$u(x) := \mathcal{S}_D[\phi_0](x), \quad x \in \mathbb{R}^2$$

satisfies $u = 0$ on ∂D. Therefore, $u(x) = 0$ for all $x \in D$. It then follows from (3.20) that

$$\mathcal{K}_D^*[\phi_0] = \frac{1}{2}\phi_0 \quad \text{on } \partial D . \tag{3.23}$$

Let $(\cdot, \cdot)_{-\frac{1}{2}, \frac{1}{2}}$ denote the duality pairing between $W_{-1/2}^2(\partial D)$ and $W_{1/2}^2(\partial D)$. If $(\phi_0, 1)_{-1/2, 1/2} = 0$, then $u(x) \rightarrow 0$ as $|x| \rightarrow \infty$, and hence $u(x) = 0$ for

$x \in \mathbb{R}^2 \setminus D$ as well. Thus $\phi_0 = 0$. The eigenfunctions of (3.23) make a one dimensional subspace of $W^2_{-1/2}(\partial D)$, which means that $\text{Ker}(\mathcal{S}_D)$ is of at most one dimension.

Let $(\phi_e, a) \in W^2_{-1/2}(\partial D) \times \mathbb{R}$ denote the solution of the system (3.22), then it can be shown that $\mathcal{S}_D : W^2_{-1/2}(\partial D) \to W^2_{1/2}(\partial D)$ has a bounded inverse if and only if $a \neq 0$.

The following result is well-known. It shows that $\mathcal{K}_D \mathcal{S}_D$ is self-adjoint on $W^2_{-1/2}(\partial D)$.

Lemma 3.13 *The following Calderón identity (also known as Plemelj's symmetrization principle) holds:*

$$\mathcal{S}_D \mathcal{K}_D^* = \mathcal{K}_D \mathcal{S}_D \quad on \ W^2_{-1/2}(\partial D) . \tag{3.24}$$

Consider the three-dimensional case. Since the single layer potential becomes a unitary operator from $W^2_{-1/2}(\partial D)$ onto $W^2_{1/2}(\partial D)$, the operator $\mathcal{K}_D^*$ can be symmetrized using Calderón identity (3.24) and hence becomes self-adjoint. It is then possible to write its spectral decomposition. Let $\mathcal{H}^*(\partial D)$ be the space $W^2_{-1/2}(\partial D)$ with the inner product

$$(u, v)_{\mathcal{H}^*} = -(u, \mathcal{S}_D[v])_{-\frac{1}{2}, \frac{1}{2}} , \tag{3.25}$$

which is equivalent to the original one (on $W^2_{-1/2}(\partial D)$).

Theorem 3.14 *For $d = 3$, the following results hold:*

(i) The operator $\mathcal{K}_D^*$ is self-adjoint in the Hilbert space $\mathcal{H}^*(\partial D)$;
(ii) Let (λ_j, φ_j), $j = 0, 1, 2, \ldots$ be the eigenvalue and normalized eigenfunction pair of $\mathcal{K}_D^*$ in $\mathcal{H}^*(\partial D)$, then $\lambda_0 = 1/2$, $\lambda_j \in (-\frac{1}{2}, \frac{1}{2})$ for $j \geq 1$, and $\lambda_j \to 0$ as $j \to \infty$;
(iii) The following spectral representation formula holds: for any $\psi \in W^2_{-1/2}(\partial D)$,

$$\mathcal{K}_D^*[\psi] = \sum_{j=0}^{\infty} \lambda_j (\varphi_j, \psi)_{\mathcal{H}^*} \varphi_j .$$

Moreover, it is clear that the following result holds.

Lemma 3.15 *Let $d = 3$. Let $\mathcal{H}(\partial D)$ be the space $W^2_{1/2}(\partial D)$ equipped with the following equivalent inner product*

$$(u, v)_{\mathcal{H}} = ((-\mathcal{S}_D)^{-1}[u], v)_{-\frac{1}{2}, \frac{1}{2}}. \tag{3.26}$$

Then, $\mathcal{S}_D$ is an isometry between $\mathcal{H}^*(\partial D)$ and $\mathcal{H}(\partial D)$.

Furthermore, we list other useful observations and basic results in three dimensions.

Lemma 3.16 *Let $d = 3$. The following results hold:*

(i) We have $(-\frac{1}{2}I + \mathcal{K}_D^*)\mathcal{S}_D^{-1}[\chi(\partial D)] = 0$ with $\chi(\partial D)$ being the characteristic function of ∂D.

(ii) The corresponding eigenspace to $\lambda_0 = \frac{1}{2}$ has dimension one and is spanned by the function $\varphi_0 = c\mathcal{S}_D^{-1}[\chi(\partial D)]$ for some constant c such that $||\varphi_0||_{\mathcal{H}^*} = 1$.

(iii) Moreover, $\mathcal{H}^*(\partial D) = \mathcal{H}_0^*(\partial D) \oplus \{\mu\varphi_0, \ \mu \in \mathbb{C}\}$, where $\mathcal{H}_0^*(\partial D)$ is the zero mean subspace of $\mathcal{H}^*(\partial D)$ and $\varphi_j \in \mathcal{H}_0^*(\partial D)$ for $j \geq 1$, i.e., $(\varphi_j, \chi(\partial D))_{-\frac{1}{2},\frac{1}{2}} = 0$ for $j \geq 1$. Here, $\{\varphi_j\}_j$ is the set of normalized eigenfunctions of $\mathcal{K}_D^*$.

In two dimensions, again based on (3.24), we show that $\mathcal{K}_D^*$ can be realized as a self-adjoint operator by introducing a new inner product, slightly different from the one introduced in the three-dimensional case.

Recall that the single-layer potential $\mathcal{S}_D : W_{-1/2}^2(\partial D) \to W_{1/2}^2(\partial D)$ is not, in general, invertible nor injective. Hence, $-(u, \mathcal{S}_D[v])_{-\frac{1}{2},\frac{1}{2}}$ does not define an inner product and the symmetrization technique described in Theorem 3.14 is no longer valid. To overcome this difficulty, a substitute of $\mathcal{S}_D$ can be introduced as in [80] by

$$\widetilde{\mathcal{S}}_D[\psi] = \begin{cases} \mathcal{S}_D[\psi] & \text{if } (\psi, \chi(\partial D))_{-\frac{1}{2},\frac{1}{2}} = 0, \\ \chi(\partial D) & \text{if } \psi = \varphi_0, \end{cases} \tag{3.27}$$

where φ_0 is the unique eigenfunction of $\mathcal{K}_D^*$ associated with eigenvalue $1/2$ such that $(\varphi_0, \chi(\partial D))_{-\frac{1}{2},\frac{1}{2}} = 1$. Note that, from the jump relations of the layer potentials, $\mathcal{S}_D[\varphi_0]$ is constant.

The operator $\widetilde{\mathcal{S}}_D : W_{-1/2}^2(\partial D) \to W_{1/2}^2(\partial D)$ is invertible. Moreover, the following Calderón identity holds $\mathcal{K}_D\widetilde{\mathcal{S}}_D = \widetilde{\mathcal{S}}_D\mathcal{K}_D^*$. With this, define

$$(u,v)_{\mathcal{H}^*} = -(u, \widetilde{\mathcal{S}}_D[v])_{-\frac{1}{2},\frac{1}{2}}.$$

Thanks to the invertibility and positivity of $-\widetilde{\mathcal{S}}_D$, this defines an inner product for which $\mathcal{K}_D^*$ is self-adjoint and $\mathcal{H}^*$ is equivalent to $W_{-1/2}^2(\partial D)$. Then, if D is $\mathcal{C}^2$, we have the following results.

Theorem 3.17 *Let $d = 2$. Let D be a $\mathcal{C}^2$ bounded simply connected domain of $\mathbb{R}^2$ and let $\widetilde{\mathcal{S}}_D$ be the operator defined in (3.27). Then,*

(i) *The operator $\mathcal{K}_D^*$ is compact self-adjoint in the Hilbert space $\mathcal{H}^*(\partial D)$ equipped with the inner product defined by*

$$(u,v)_{\mathcal{H}^*} = -(u, \widetilde{\mathcal{S}}_D[v])_{-\frac{1}{2},\frac{1}{2}}; \tag{3.28}$$

(ii) *Let (λ_j, φ_j), $j = 0, 1, 2, \ldots$, be the eigenvalue and normalized eigenfunction pair of $\mathcal{K}_D^*$ with $\lambda_0 = \frac{1}{2}$. Then, $\lambda_j \in (-\frac{1}{2}, \frac{1}{2}]$ and $\lambda_j \to 0$ as $j \to \infty$;*

(iii) *$\mathcal{H}^*(\partial D) = \mathcal{H}_0^*(\partial D) \oplus \{\mu\varphi_0, \ \mu \in \mathbb{C}\}$, where $\mathcal{H}_0^*(\partial D)$ is the zero mean subspace of $\mathcal{H}^*(\partial D)$;*

(iv) The following representation formula holds: for any $\psi \in W^2_{-1/2}(\partial D)$,

$$\mathcal{K}^*_D[\psi] = \sum_{j=0}^{\infty} \lambda_j (\varphi_j, \psi)_{\mathcal{H}^*} \, \varphi_j.$$

Lemma 3.18 *Let $\mathcal{H}(\partial D)$ be the space $W^2_{1/2}(\partial D)$ equipped with the following equivalent inner product*

$$(u, v)_{\mathcal{H}} = (-\widetilde{\mathcal{S}}^{-1}_D[u], v)_{-\frac{1}{2}, \frac{1}{2}}. \tag{3.29}$$

Then, $\widetilde{\mathcal{S}}_D$ is an isometry between $\mathcal{H}^*(\partial D)$ and $\mathcal{H}(\partial D)$.

Note that $\widetilde{\mathcal{S}}^{-1}_D[\chi(\partial D)] = \varphi_0$ and $(-\frac{1}{2}I + \mathcal{K}^*_D) = (-\frac{1}{2}I + \mathcal{K}^*_D)\mathcal{P}_{\mathcal{H}^*_0}$, where $\mathcal{P}_{\mathcal{H}^*_0}$ is the orthogonal projection onto $\mathcal{H}^*_0(\partial D)$. In particular, we have $(-\frac{1}{2}I + \mathcal{K}^*_D)\widetilde{\mathcal{S}}^{-1}_D[\chi(\partial D)] = 0$.

Note also that using (3.12), it follows that if D is a disk, then the spectrum of $\mathcal{K}^*_D$ is $\{0, 1/2\}$. Furthermore, by using (3.13) it can be shown that the spectrum of $\mathcal{K}^*_D$ in the case where D is a ball is $1/(2(2j + 1)), j = 0, 1, \ldots$. If D is an ellipse of semi-axes a and b, then $1/2$ and $\pm(1/2)((a-b)/(a+b))^j, j = 1, 2, \ldots$ are the eigenvalues of $\mathcal{K}^*_D$, which can be expressed by (3.17). The eigenvalues of $\mathcal{K}^*_D$ for D being an ellipsoid can be expressed explicitly in terms of Lamé functions.

3.1.5 Neumann Function

Let Ω be a smooth bounded domain in $\mathbb{R}^d, d \geq 2$. Let $N(x, z)$ be the Neumann function for $-\Delta$ in Ω corresponding to a Dirac mass at z. That is, N is the solution to

$$\begin{cases} -\Delta_x N(x, z) = \delta_z & \text{in } \Omega, \\ \left.\dfrac{\partial N}{\partial \nu_x}\right|_{\partial\Omega} = -\dfrac{1}{|\partial\Omega|}, \displaystyle\int_{\partial\Omega} N(x, z)\, d\sigma(x) = 0 & \text{for } z \in \Omega. \end{cases} \tag{3.30}$$

Note that the Neumann function $N(x, z)$ is defined as a function of $x \in \overline{\Omega}$ for each fixed $z \in \Omega$.

The operator defined by $N(x, z)$ is the solution operator for the Neumann problem

$$\begin{cases} \Delta U = 0 & \text{in } \Omega, \\ \left.\dfrac{\partial U}{\partial \nu}\right|_{\partial\Omega} = g. \end{cases} \tag{3.31}$$

Namely, the function U defined by

$$U(x) := \int_{\partial\Omega} N(x, z)g(z)\, d\sigma(z) \tag{3.32}$$

is the solution to (3.31) satisfying $\int_{\partial\Omega} U \, d\sigma = 0$.

Now we discuss some properties of N as a function of x and z.

Lemma 3.19 (Neumann Function) *The Neumann function N is symmetric in its arguments, that is, $N(x, z) = N(z, x)$ for $x \neq z \in \Omega$. Furthermore, it has the form*

$$
N(x, z) = \begin{cases} -\dfrac{1}{2\pi} \log |x - z| + R_2(x, z) & \text{if } d = 2 , \\ \dfrac{1}{(d-2)\omega_d} \dfrac{1}{|x - z|^{d-2}} + R_d(x, z) & \text{if } d \geq 3 , \end{cases} \tag{3.33}
$$

where $R_d(\cdot, z)$ belongs to $W^{\frac{3}{2}, 2}(\Omega)$ for any $z \in \Omega, d \geq 2$ and solves

$$
\begin{cases} \Delta_x R_d(x, z) = 0 & \text{in } \Omega , \\ \dfrac{\partial R_d}{\partial \nu_x}\big|_{\partial\Omega} = -\dfrac{1}{|\partial\Omega|} + \dfrac{1}{\omega_d} \dfrac{(x-z) \cdot \nu_x}{|x-z|^d} & \text{for } x \in \partial\Omega . \end{cases}
$$

Note that, because of (3.33), the formula

$$
U(x) \approx -\mathcal{S}_\Omega[g](x) \quad \text{in } \Omega
$$

is obtained as a first approximation of the solution to the Neumann problem (3.31).

For D, a subset of Ω, let

$$
N_D[f](x) := \int_{\partial D} N(x, y) f(y) \, d\sigma(y), \quad x \in \Omega .
$$

The following lemma relates the fundamental solution Γ to the Neumann function N.

Lemma 3.20 *For $z \in \Omega$ and $x \in \partial\Omega$, let $\Gamma_z(x) := \Gamma(x, z)$ and $N_z(x) := N(x, z)$. Then*

$$
\left(-\frac{1}{2}I + \mathcal{K}_\Omega\right)[N_z](x) = \Gamma_z(x) \quad \text{modulo constants}, \quad x \in \partial\Omega , \tag{3.34}
$$

or, to be more precise, for any simply connected smooth domain D compactly contained in Ω and for any $g \in L_0^2(\partial D)$, we have for any $x \in \partial\Omega$

$$
\int_{\partial D} \left(-\frac{1}{2}I + \mathcal{K}_\Omega\right)[N_z](x) g(z) \, d\sigma(z) = \int_{\partial D} \Gamma_z(x) g(z) \, d\sigma(z) , \tag{3.35}
$$

or equivalently,

$$
\left(-\frac{1}{2}I + \mathcal{K}_\Omega\right)\left[(N_D[g])\big|_{\partial\Omega}\right](x) = \mathcal{S}_D[g]\big|_{\partial\Omega}(x) . \tag{3.36}
$$

The following simple observation is useful.

Lemma 3.21 *Let $f \in L^2(\partial\Omega)$ satisfy $\left(\frac{1}{2}I - \mathcal{K}_\Omega\right)[f] = 0$. Then f is constant.*

We mention that the Neumann function for the ball $B_R(0)$ is given, for any $x, z \in B_R(0)$, by

$$
\begin{aligned}
N(x,z) = {} & \frac{1}{4\pi|x-z|} + \frac{1}{4\pi|\frac{R}{|x|}x - \frac{|x|}{R}z|} \\
& + \frac{1}{4\pi R}\log\frac{2}{1 - \frac{x\cdot z}{R^2} + \frac{1}{R}|\frac{|x|}{R}z - \frac{R}{|x|}x|} - \frac{1}{2\pi R} \quad \text{for } d=3,
\end{aligned}
\tag{3.37}
$$

and by

$$
N(x,z) = -\frac{1}{2\pi}\left(\log|x-z| + \log\left|\frac{R}{|x|}x - \frac{|x|}{R}z\right|\right) + \frac{\log R}{\pi} \quad \text{for } d=2. \tag{3.38}
$$

3.1.6 Transmission Problems

Consider a bounded domain $D \Subset \mathbb{R}^d$ with a connected smooth boundary and conductivity $0 < k \neq 1 < +\infty$.

Let H be a harmonic function in $\mathbb{R}^d$, and let u be the solution of the transmission problem

$$
\begin{cases}
\nabla \cdot \left(1 + (k-1)\chi(D)\right)\nabla u = 0 & \text{in } \mathbb{R}^d, \\
(u - H)(x) = O(|x|^{1-d}) & \text{as } |x| \to +\infty.
\end{cases}
\tag{3.39}
$$

We have the following result.

Theorem 3.22 *Suppose that D is a domain compactly contained in $\mathbb{R}^d$ with a connected smooth boundary and conductivity $0 < k \neq 1 < +\infty$. Then the solution u of the transmission problem (3.42) is given by*

$$
u(x) = H(x) + \mathcal{S}_D[\phi](x), \quad x \in \mathbb{R}^d, \tag{3.40}
$$

where $\phi \in L_0^2(\partial D)$ is the unique solution to the integral equation

$$
\left(\lambda I - \mathcal{K}_D^*\right)[\phi] = \frac{\partial H}{\partial \nu}\bigg|_{\partial D} \quad \text{on } \partial D, \tag{3.41}
$$

where $\lambda = (k+1)/(2(k-1))$.

Let Ω be a bounded domain in $\mathbb{R}^d$ with a connected smooth boundary and conductivity equal to 1. Consider a bounded domain $D \Subset \Omega$ with a connected smooth boundary and conductivity $0 < k \neq 1 < +\infty$. Let $g \in L_0^2(\partial\Omega)$, and let u be the solution of the Neumann problem

$$
\begin{cases}
\nabla \cdot \left(1 + (k-1)\chi(D)\right)\nabla u = 0 & \text{in } \Omega, \\
\dfrac{\partial u}{\partial \nu}\bigg|_{\partial\Omega} = g, \\
\displaystyle\int_{\partial\Omega} u(x)\, d\sigma(x) = 0.
\end{cases}
\tag{3.42}
$$

We state a decomposition formula of the steady-state voltage potential u into a harmonic part and a refraction part. This decomposition formula is unique and inherits geometric properties of the inclusion D. We refer to [64, 214] for its proof.

Theorem 3.23 (Decomposition Formula) *Suppose that D is a domain compactly contained in Ω with a connected smooth boundary and conductivity $0 < k \neq 1 < +\infty$. Then the solution u of the Neumann problem (3.42) has the representation*

$$u(x) = H(x) + \mathcal{S}_D[\phi](x), \quad x \in \Omega , \tag{3.43}$$

where the harmonic function H is given by

$$H(x) = -\mathcal{S}_\Omega[g](x) + \mathcal{D}_\Omega[f](x), \quad x \in \Omega , \quad f := u|_{\partial\Omega} \in W^2_{1/2}(\partial\Omega) , \tag{3.44}$$

and $\phi \in L^2_0(\partial D)$ satisfies the integral equation

$$\left(\frac{k+1}{2(k-1)} I - \mathcal{K}_D^* \right)[\phi] = \left. \frac{\partial H}{\partial \nu} \right|_{\partial D} \quad on \ \partial D . \tag{3.45}$$

The decomposition (3.43) into a harmonic part and a refraction part is unique. Moreover, $\forall \, n \in \mathbb{N}$, there exists a constant $C_n = C(n, \Omega, dist(D, \partial\Omega))$ independent of D and the conductivity k such that

$$\|H\|_{\mathcal{C}^n(\overline{D})} \leq C_n \|g\|_{L^2(\partial\Omega)} . \tag{3.46}$$

Furthermore, the following holds

$$H(x) + \mathcal{S}_D[\phi](x) = 0, \quad \forall \, x \in \mathbb{R}^d \setminus \overline{\Omega} . \tag{3.47}$$

Another useful expression of the harmonic part H of u is given in the following lemma.

Lemma 3.24 *We have*

$$H(x) = \begin{cases} u(x) - (k-1) \displaystyle\int_D \nabla_y \Gamma(x,y) \cdot \nabla u(y) \, dy, & x \in \Omega , \\[4mm] -(k-1) \displaystyle\int_D \nabla_y \Gamma(x,y) \cdot \nabla u(y) \, dy, & x \in \mathbb{R}^d \setminus \overline{\Omega} . \end{cases} \tag{3.48}$$

Let $g \in L^2_0(\partial\Omega)$ and

$$U(y) := \int_{\partial\Omega} N(x,y)g(x) \, d\sigma(x) .$$

Then U is the solution to the Neumann problem (3.31) and the following representation holds.

Theorem 3.25 *The solution u of (3.42) can be represented as*

$$u(x) = U(x) - N_D[\phi](x), \quad x \in \partial\Omega , \tag{3.49}$$

where ϕ is defined in (3.45).

3.2 Helmholtz Equation

Consider the scalar wave equation $\partial_t^2 U - \Delta U = 0$. We obtain a time-harmonic solution $U(x,t) = \Re(e^{-ikt}u(x))$ if the space-dependent part u satisfies the Helmholtz equation, $\Delta u + k^2 u = 0$.

Mathematical models for acoustical and microwave soundings of biological media involve the Helmholtz equation.

This section begins by discussing the well-known Sommerfeld radiation condition, and by deriving a fundamental solution. We then introduce the single- and double-layer potentials, and state Rellich's lemma. Then, we establish an integral representation for the solution to the transmission scattering problem. We also discuss the reciprocity property and derive the Helmholtz-Kirchhoff identity for fundamental solutions of the Helmholtz equations.

3.2.1 Fundamental Solution

A fundamental solution $\Gamma_k(x)$ to the Helmholtz operator $\Delta + k^2$ in $\mathbb{R}^d$ is a solution (in the sense of distributions) of

$$(\Delta + k^2)\Gamma_k = \delta_0 \ , \tag{3.50}$$

where δ_0 is the Dirac mass at 0. Solutions are not unique, since we can add to a solution any plane wave (of the form $e^{ik\theta \cdot x}, \theta \in \mathbb{R}^d : |\theta| = 1$) or any combination of such plane waves. So, we need to specify the behavior of the solutions at infinity. It is natural to look for radial solutions of the form $\Gamma_k(x) = w_k(r)$ that is subject to the extra Sommerfeld radiation condition or outgoing wave condition

$$\left| \frac{dw_k}{dr} - ikw_k \right| \leq Cr^{-(d+1)/2} \quad \text{at infinity.} \tag{3.51}$$

If $d = 3$, equation (3.50) becomes

$$\frac{1}{r^2}\frac{d}{dr}r^2\frac{dw_k}{dr} + k^2 w_k = 0, \quad r > 0 \ ,$$

whose solution is

$$w_k(r) = c_1 \frac{e^{ikr}}{r} + c_2 \frac{e^{-ikr}}{r} \ .$$

It is easy to check that the Sommerfeld radiation condition (3.51) leads to $c_2 = 0$ and then (3.50) leads to $c_1 = -1/(4\pi)$.

If $d = 2$, equation (3.50) becomes

$$\frac{1}{r}\frac{d}{dr}r\frac{dw_k}{dr} + k^2 w_k = 0, \quad r > 0 \ .$$

This is a Bessel equation whose solutions are not elementary functions. From Section 2.1, we know that the Hankel functions of the first and second kinds of

order 0, $H_0^{(1)}(kr)$ and $H_0^{(2)}(kr)$, form a basis for the solution space. At infinity $(r \to +\infty)$, only $H_0^{(1)}(kr)$ satisfies the outgoing radiation condition (3.51). At the origin $(r \to 0)$, $H_0^{(1)}(kr)$ behaves like $(2i/\pi)\log(r)$. The following lemma holds.

Lemma 3.26 (Fundamental Solution) *The outgoing fundamental solution $\Gamma_k(x)$ to the operator $\Delta + k^2$ is given by*

$$\Gamma_k(x) = \begin{cases} -\dfrac{i}{4}H_0^{(1)}(k|x|) \,, & d = 2 \,, \\[2mm] -\dfrac{e^{ik|x|}}{4\pi|x|} \,, & d = 3 \,, \end{cases} \qquad (3.52)$$

for $x \neq 0$, where $H_0^{(1)}$ is the Hankel function of the first kind of order 0.

Note that the time-harmonic fundamental solution Γ_k satisfies the identity

$$\Gamma_k(x - y) = -\sqrt{2\pi}\mathcal{F}_t(U_y(x,t))(x,k) \,,$$

where $\mathcal{F}_t$ is defined by (2.38) and U_y is respectively defined by (2.55) and (2.57) for $d = 3$ and $d = 2$.

The following Graf's addition formula for $d = 2$ will be useful [337].

Lemma 3.27 *For $|x| > |y|$, we have*

$$H_0^{(1)}(k|x-y|) = \sum_{n \in \mathbb{Z}} H_n^{(1)}(k|x|)e^{in\theta_x}J_n(k|y|)e^{-in\theta_y} \,, \qquad (3.53)$$

where $x = (|x|, \theta_x)$ and $y = (|y|, \theta_y)$ in polar coordinates. Here $H_n^{(1)}$ is the Hankel function of the first kind of order n and J_n is the Bessel function of order n; see (2.2) and (2.17).

In three dimensions, the following addition formula holds for $|x| > |y|$:

$$\frac{e^{ik|x-y|}}{4\pi|x-y|} = ik\sum_{l=0}^{+\infty}\sum_{m=-l}^{l} h_l^{(1)}(k|x|)j_l(k|y|)Y_{lm}(\theta_x, \phi_x)Y_{lm}(\theta_y, \phi_y) \,, \qquad (3.54)$$

where $x = (|x|, \theta_x, \phi_x)$, $y = (|y|, \theta_y, \phi_y)$ in the spherical coordinates and Y_{lm} is the spherical harmonic function. Here, j_l and $h_l^{(1)}$ are defined by (2.21) and (2.23). Formulas (3.53) and (3.54) are particularly useful since they will allow us to introduce the notion of scattering coefficients for the solutions to the Helmholtz equation.

Another useful decomposition of Γ_k is into plane waves. The following decomposition, known as the Weyl representation of cylindrical and spherical waves holds:

$$\Gamma_k(x) = -ic_d \int_{\mathbb{R}^{d-1}} \frac{1}{\beta(\alpha)}e^{i(\beta(\alpha)|x_d|+\alpha\cdot\tilde{x})} \, d\alpha \,, \qquad (3.55)$$

where $x = (\tilde{x}, x_d)$, $\tilde{x} = (x_1, \ldots, x_{d-1})$,

$$\beta(\alpha) = \begin{cases} \sqrt{k^2 - |\alpha|^2}, & |\alpha| < k \ , \\ i\sqrt{|\alpha|^2 - k^2}, & |\alpha| \geq k \ , \end{cases}$$

and

$$c_2 = \frac{1}{4\pi}, \quad c_3 = \frac{1}{8\pi^2} \ .$$

As will be shown later, (3.55) plays a key role in diffraction tomography. From now on, we denote by $\Gamma_k(x, y) := \Gamma_k(x - y)$ for $x \neq y$.

Particular solutions to the Helmholtz equation in $\mathbb{R}^d, d = 2, 3$, are plane waves given by $e^{ik\theta \cdot x}$ where θ is a unit real vector, and cylindrical and spherical waves defined by $\Gamma_k(x, y)$ with y being the source point for respectively $d = 2$ and 3. These particular solutions will be very useful in the subsequent chapters.

3.2.2 Layer Potentials

For a bounded smooth domain D in $\mathbb{R}^d$ and $k > 0$ let $\mathcal{S}_D^k$ and $\mathcal{D}_D^k$ be the single- and double-layer potentials defined by Γ_k, that is,

$$\mathcal{S}_D^k[\phi](x) = \int_{\partial D} \Gamma_k(x, y)\phi(y)\, d\sigma(y) \ , \quad x \in \mathbb{R}^d \ ,$$

$$\mathcal{D}_D^k[\phi](x) = \int_{\partial D} \frac{\partial \Gamma_k(x, y)}{\partial \nu_y}\phi(y)\, d\sigma(y) \ , \quad x \in \mathbb{R}^d \setminus \partial D \ ,$$

for $\phi \in L^2(\partial D)$. Because $\Gamma_k - \Gamma$, where Γ is defined by (3.1), is a smooth function, we can easily prove from (3.20) and (3.18) that

$$\left.\frac{\partial(\mathcal{S}_D^k[\phi])}{\partial \nu}\right|_{\pm}(x) = \left(\pm \frac{1}{2}I + (\mathcal{K}_D^k)^* \right)[\phi](x) \quad \text{a.e. } x \in \partial D \ , \tag{3.56}$$

$$\left.(\mathcal{D}_D^k[\phi])\right|_{\pm}(x) = \left(\mp \frac{1}{2}I + \mathcal{K}_D^k \right)[\phi](x) \quad \text{a.e. } x \in \partial D \ , \tag{3.57}$$

for $\phi \in L^2(\partial D)$, where $\mathcal{K}_D^k$ is the operator defined by

$$\mathcal{K}_D^k[\phi](x) = \int_{\partial D} \frac{\partial \Gamma_k(x, y)}{\partial \nu_y}\phi(y)d\sigma(y) \ , \tag{3.58}$$

and $(\mathcal{K}_D^k)^*$ is given by

$$(\mathcal{K}_D^k)^*[\phi](x) = \int_{\partial D} \frac{\partial \Gamma_k(x, y)}{\partial \nu_x}\phi(y)d\sigma(y) \ . \tag{3.59}$$

Moreover, the integral operators $\mathcal{K}_D^k$ and $(\mathcal{K}_D^k)^*$ are compact on $L^2(\partial D)$. Note that $(\mathcal{K}_D^k)^*$ is the L^2-adjoint of $\mathcal{K}_D^{-k}$.

We will need the following important result from the theory of the Helmholtz equation. It will help us to prove uniqueness of the solution to exterior Helmholtz problems. For its proof we refer to [140, Lemma 2.11] or [270, Lemma 9.8].

Lemma 3.28 (Rellich's Lemma) *Let* $R_0 > 0$ *and* $B_R(0) = \{|x| < R\}$. *Let* u *satisfy the Helmholtz equation* $\Delta u + k^2 u = 0$ *for* $|x| > R_0$. *Assume, furthermore, that*

$$\lim_{R \to +\infty} \int_{\partial B_R(0)} |u(x)|^2 \, d\sigma(x) = 0 \,.$$

Then, $u \equiv 0$ *for* $|x| > R_0$.

Note that the assertion of this lemma does not hold if k is imaginary or $k = 0$.

Now we can state the following uniqueness result for the Helmholtz equation.

Lemma 3.29 *Suppose* $d = 2$ *or* 3. *Let* D *be a bounded* $\mathcal{C}^2$-*domain in* $\mathbb{R}^d$. *Let* $u \in W^{1,2}_{\mathrm{loc}}(\mathbb{R}^d \setminus \overline{D})$ *satisfy*

$$\begin{cases} \Delta u + k^2 u = 0 \quad in \ \mathbb{R}^d \setminus \overline{D} \,, \\[2mm] \left| \dfrac{\partial u}{\partial r} - iku \right| = O\left(r^{-(d+1)/2} \right) \quad as \ r = |x| \to +\infty \quad uniformly \ in \ \dfrac{x}{|x|} \,, \\[2mm] \Im \displaystyle\int_{\partial D} \overline{u} \dfrac{\partial u}{\partial \nu} \, d\sigma = 0 \,. \end{cases}$$

Then, $u \equiv 0$ *in* $\mathbb{R}^d \setminus \overline{D}$.

3.2.3 Transmission Problem

Introduce the piecewise constant functions

$$\mu(x) = \begin{cases} \mu_0 \,, & x \in \Omega \setminus \overline{D} \,, \\ \mu_\star \,, & x \in D \,, \end{cases} \tag{3.60}$$

and

$$\varepsilon(x) = \begin{cases} \varepsilon_0 \,, & x \in \Omega \setminus \overline{D} \,, \\ \varepsilon_\star \,, & x \in D \,, \end{cases} \tag{3.61}$$

where $\mu_0, \mu_\star, \varepsilon_0$, and $\varepsilon_\star$ are positive constants.

Let $f \in W^2_{1/2}(\partial\Omega)$, and let u and U denote the solutions to the Helmholtz equations

$$\begin{cases} \nabla \cdot (\dfrac{1}{\mu} \nabla u) + \omega^2 \varepsilon u = 0 \ \ in \ \Omega \,, \\[2mm] u = f \ \ on \ \partial\Omega \,, \end{cases} \tag{3.62}$$

and

$$\begin{cases} \Delta U + \omega^2 \varepsilon_0 \mu_0 U = 0 & \text{in } \Omega \,, \\ U = f & \text{on } \partial\Omega \,. \end{cases} \tag{3.63}$$

In electromagnetics, ε_0 and $\varepsilon_\star$ are electrical permittivities, μ_0 and $\mu_\star$ are magnetic permeabilities, and u and U are electric potentials. In acoustics, one replaces permittivity and permeability by compressibility and volume density of mass, and the scalar electric potential by the scalar acoustic pressure.

We now present two decompositions of the solution of (3.62) similar to the representation formula (3.43) for the transmission problem for the harmonic equation. To do so, we first state the following theorem which is of importance to us for establishing our decomposition formulas. We refer the reader to [64] for its proof.

Theorem 3.30 *Let $k_\star^2 := \omega^2 \mu_\star \varepsilon_\star$. Suppose that $k_0^2 := \omega^2 \mu_0 \varepsilon_0$ is not a Dirichlet eigenvalue for $-\Delta$ on D. For each $(F, G) \in W_1^2(\partial D) \times L^2(\partial D)$, there exists a unique solution $(f, g) \in L^2(\partial D) \times L^2(\partial D)$ to the system of integral equations*

$$\begin{cases} \mathcal{S}_D^{k_\star}[f] - \mathcal{S}_D^{k_0}[g] = F \\ \dfrac{1}{\mu_\star} \dfrac{\partial(\mathcal{S}_D^{k_\star}[f])}{\partial\nu}\bigg|_- - \dfrac{1}{\mu_0} \dfrac{\partial(\mathcal{S}_D^{k_0}[g])}{\partial\nu}\bigg|_+ = G \end{cases} \quad on \; \partial D \,. \tag{3.64}$$

Furthermore, there exists a constant C independent of F and G such that

$$\|f\|_{L^2(\partial D)} + \|g\|_{L^2(\partial D)} \le C\left(\|F\|_{W_1^2(\partial D)} + \|G\|_{L^2(\partial D)} \right) . \tag{3.65}$$

The following decomposition formula holds.

Theorem 3.31 (Decomposition Formula) *Suppose that k_0^2 is not a Dirichlet eigenvalue for $-\Delta$ on D. Let u be the solution of (3.62) and $g := \frac{\partial u}{\partial\nu}|_{\partial\Omega}$. Define*

$$H(x) := -\mathcal{S}_\Omega^{k_0}[g](x) + \mathcal{D}_\Omega^{k_0}[f](x) \,, \quad x \in \mathbb{R}^d \setminus \partial\Omega \,, \tag{3.66}$$

and let $(\phi, \psi) \in L^2(\partial D) \times L^2(\partial D)$ be the unique solution of

$$\begin{cases} \mathcal{S}_D^{k_\star}[\phi] - \mathcal{S}_D^{k_0}[\psi] = H \\ \dfrac{1}{\mu_\star} \dfrac{\partial(\mathcal{S}_D^{k_\star}[\phi])}{\partial\nu}\bigg|_- - \dfrac{1}{\mu_0} \dfrac{\partial(\mathcal{S}_D^{k_0}[\psi])}{\partial\nu}\bigg|_+ = \dfrac{1}{\mu_0} \dfrac{\partial H}{\partial\nu} \end{cases} \quad on \; \partial D \,. \tag{3.67}$$

Then u can be represented as

$$u(x) = \begin{cases} H(x) + \mathcal{S}_D^{k_0}[\psi](x) \,, & x \in \Omega \setminus \overline{D} \,, \\ \mathcal{S}_D^{k_\star}[\phi](x) \,, & x \in D \,. \end{cases} \tag{3.68}$$

Moreover, there exists $C > 0$ independent of H such that

$$\|\phi\|_{L^2(\partial D)} + \|\psi\|_{L^2(\partial D)} \le C\left(\|H\|_{L^2(\partial D)} + \|\nabla H\|_{L^2(\partial D)} \right) . \tag{3.69}$$

The following proposition is also of importance to us. We refer again to [64] for a proof.

Proposition 3.32 *For each $n \in \mathbb{N}$ there exists C_n independent of D (but depending on $\mathrm{dist}(D, \partial\Omega)$) such that*

$$\|H\|_{\mathcal{C}^n(\overline{D})} \leq C_n \|f\|_{W^2_{1/2}(\partial\Omega)} .$$

We now transform the decomposition formula (3.68) into the one using Green's function and the background solution U, that is, the solution of (3.63).

Suppose that k_0^2 is not a Dirichlet eigenvalue for $-\Delta$ on D. Let $G_{k_0}(x,y)$ be the Dirichlet Green function for $\Delta + k_0^2$ in Ω, *i.e.*, for each $y \in \Omega$, G_{k_0} is the solution of

$$\begin{cases} (\Delta + k_0^2) G_{k_0}(x,y) = \delta_y(x) , & x \in \Omega , \\ G_{k_0}(x,y) = 0 , & x \in \partial\Omega . \end{cases} \tag{3.70}$$

Then,

$$U(x) = \int_{\partial\Omega} \frac{\partial G_{k_0}(x,y)}{\partial\nu_y} f(y) d\sigma(y) , \quad x \in \Omega .$$

We need to introduce some more notation. For a $\mathcal{C}^2$-domain $D \Subset \Omega$ and $\phi \in L^2(\partial D)$, let

$$G_D^{k_0}[\phi](x) := \int_{\partial D} G_{k_0}(x,y)\phi(y)\, d\sigma(y) , \quad x \in \overline{\Omega} .$$

Our second decomposition formula is the following.

Theorem 3.33 *Let ψ be the function defined in (3.67). Then*

$$\frac{\partial u}{\partial\nu}(x) = \frac{\partial U}{\partial\nu}(x) + \frac{\partial(G_D^{k_0}[\psi])}{\partial\nu}(x) , \quad x \in \partial\Omega . \tag{3.71}$$

Note that if $x \in \mathbb{R}^d \setminus \Omega$ and $z \in \Omega$, then

$$\int_{\partial\Omega} \Gamma_{k_0}(x,y) \frac{\partial G_{k_0}(z,y)}{\partial\nu_y}\bigg|_{\partial\Omega} d\sigma(y) = \Gamma_{k_0}(x,z) . \tag{3.72}$$

As a consequence of (3.72), we have

$$\left(\frac{1}{2} I + (\mathcal{K}_\Omega^{k_0})^* \right) \left[\frac{\partial G_{k_0}(z,\cdot)}{\partial\nu_y}\bigg|_{\partial\Omega} \right](x) = \frac{\partial \Gamma_{k_0}(x,z)}{\partial\nu_x} , \tag{3.73}$$

for all $x \in \partial\Omega$ and $z \in \Omega$.

Finally, we will need the Neumann function N_{k_0}, which is defined by

$$\begin{cases} \Delta_x N_{k_0}(x,z) + {k_0}^2 N_{k_0}(x,z) = \delta_z & \text{in } \Omega , \\ \dfrac{\partial N_{k_0}}{\partial\nu_x}\bigg|_{\partial\Omega} = 0 & \text{for } z \in \Omega . \end{cases} \tag{3.74}$$

Here, we assume that k_0^2 is not a Neumann eigenvalue of $-\Delta$ in Ω. Recall that the following useful relation between the Neumann function and the fundamental solution Γ_{k_0} holds:

$$(\frac{1}{2}I - \mathcal{K}_\Omega^{k_0})[N_{k_0}(\cdot, z)](x) = \Gamma_{k_0}(x, z), \quad x \in \partial\Omega, \ z \in \Omega . \tag{3.75}$$

3.2.4 Reciprocity

Let μ and ε be two piecewise smooth functions such that $\mu(x) = \mu_0$ and $\varepsilon(x) = \varepsilon_0$ for $|x| \geq R_0$ for some positive R_0. For $y \in \mathbb{R}^d$, introduce the fundamental solution $\Phi_{k_0}(x, y)$ to be the solution to

$$(\nabla_x \cdot \frac{1}{\mu}\nabla_x + \omega^2\varepsilon)\Phi_{k_0} = \frac{1}{\mu_0}\delta_y , \tag{3.76}$$

subject to the Sommerfeld radiation condition.

An important property satisfied by the fundamental solution Φ_{k_0} is the reciprocity property. The following holds.

Lemma 3.34 *We have, for $x \neq y$,*

$$\Phi_{k_0}(x, y) = \Phi_{k_0}(y, x) . \tag{3.77}$$

Identity (3.77) means that the wave recorded at x when there is a time-harmonic source at y is equal to the wave recorded at y when there is a time-harmonic source at x.

Proof. We consider the equations satisfied by the fundamental solution with the source at y_2 and with the source at y_1 (with $y_1 \neq y_2$):

$$(\nabla_x \cdot \frac{1}{\mu}\nabla_x + \omega^2\varepsilon)\Phi_{k_0}(x, y_2) = \frac{1}{\mu_0}\delta_{y_2} ,$$

$$(\nabla_x \cdot \frac{1}{\mu}\nabla_x + \omega^2\varepsilon)\Phi_{k_0}(x, y_1) = \frac{1}{\mu_0}\delta_{y_1} .$$

We multiply the first equation by $\Phi_{k_0}(x, y_1)$ and subtract the second equation multiplied by $\Phi_{k_0}(x, y_2)$:

$$\nabla_x \cdot \frac{\mu_0}{\mu}\Big[\Phi_{k_0}(x, y_1)\nabla_x\Phi_{k_0}(x, y_2) - \Phi_{k_0}(x, y_2)\nabla_x\Phi_{k_0}(x, y_1)\Big]$$
$$= -\Phi_{k_0}(x, y_2)\delta_{y_1} + \Phi_{k_0}(x, y_1)\delta_{y_2}$$
$$= -\Phi_{k_0}(y_1, y_2)\delta_{y_1} + \Phi_{k_0}(y_2, y_1)\delta_{y_2} .$$

We next integrate over the ball B_R of center 0 and radius R which contains both y_1 and y_2 and use the divergence theorem:

$$\int_{\partial B_R} \nu \cdot \Big[\Phi_{k_0}(x, y_1)\nabla_x\Phi_{k_0}(x, y_2) - \Phi_{k_0}(x, y_2)\nabla_x\Phi_{k_0}(x, y_1)\Big]d\sigma(x)$$
$$= -\Phi_{k_0}(y_1, y_2) + \Phi_{k_0}(y_2, y_1) ,$$

where ν is the unit outward normal to the ball B_R, which is $\nu = x/|x|$.

If $x \in \partial B_R$ and $R \to \infty$, then we have by the Sommerfeld radiation condition:

$$\nu \cdot \nabla_x \Phi_{k_0}(x, y) = ik_0 \Phi_{k_0}(x, y) + O\Big(\frac{1}{R^{(d+1)/2}}\Big) \, .$$

Therefore, as $R \to \infty$,

$$-\Phi_{k_0}(y_1, y_2) + \Phi_{k_0}(y_2, y_1)$$
$$= ik_0 \int_{\partial B_R} \Big[\Phi_{k_0}(x, y_1)\Phi_{k_0}(x, y_2) - \Phi_{k_0}(x, y_2)\Phi_{k_0}(x, y_1) \Big] d\sigma(x)$$
$$= 0 \, ,$$

which is the desired result.   □

3.2.5 Lippmann-Schwinger Representation Formula

The following Lippmann-Schwinger representation formula for Φ_{k_0} holds.

Lemma 3.35 *For any $x \neq y$, we have*

$$\Phi_{k_0}(x, y) = \Gamma_{k_0}(x, y) + \int (\frac{\mu_0}{\mu(z)} - 1)\nabla \Phi_{k_0}(z, x) \cdot \nabla \Gamma_{k_0}(z, y) \, dz$$
$$+ k_0^2 \int (1 - \frac{\varepsilon(z)}{\varepsilon_0})\Phi_{k_0}(z, x)\Gamma_{k_0}(z, y) \, dz \, . \tag{3.78}$$

Proof. We multiply (3.76) by Γ_{k_0} and subtract the equation satisfied by Γ_{k_0} multiplied by $\frac{1}{\mu_0}\Phi_{k_0}$:

$$\nabla_z \cdot \Big[\frac{1}{\mu(z)}\Gamma_{k_0}(z, y)\nabla_z\Phi_{k_0}(z, x) - \frac{1}{\mu_0}\Phi_{k_0}(z, x)\nabla_z\Gamma_{k_0}(z, y) \Big]$$
$$= (\frac{1}{\mu(z)} - \frac{1}{\mu_0})\nabla_z\Phi_{k_0}(z, x) \cdot \nabla_z\Gamma_{k_0}(z, y)$$
$$+ \omega^2\varepsilon_0\big(1 - \frac{\varepsilon(z)}{\varepsilon_0}\big)\Phi_{k_0}(z, x)\Gamma_{k_0}(z, y)$$
$$+ \frac{1}{\mu_0}(\Gamma_{k_0}(x, y)\delta_x(z) - \Phi_{k_0}(x, y)\delta_y(z)) \, .$$

We integrate over B_R (with R large enough so that it encloses the support of $\mu - \mu_0$ and $\varepsilon - \varepsilon_0$) and send R to infinity to obtain thanks to the Sommerfeld radiation condition the desired result.   □

Lippmann-Schwinger representation formula (3.78) is used as a basis for expanding the fundamental solution Φ_{k_0} when $\mu \approx \mu_0$ and $\varepsilon \approx \varepsilon_0$. If Φ_{k_0} in the right-hand side is replaced by Γ_{k_0}, then we obtain:

$$\Phi_{k_0}(x, y) \approx \Gamma_{k_0}(x, y) + \int (\frac{\mu_0}{\mu(z)} - 1)\nabla \Gamma_{k_0}(z, y) \cdot \nabla \Gamma_{k_0}(z, y) \, dz$$
$$+ k_0^2 \int (1 - \frac{\varepsilon(z)}{\varepsilon_0})\Gamma_{k_0}(z, y)\Gamma_{k_0}(z, y) \, dz \, , \tag{3.79}$$

which is the (first-order) Born approximation for Φ_{k_0}.

3.2.6 The Helmholtz-Kirchhoff Theorem

The Helmholtz-Kirchhoff theorem plays a key role in understanding the resolution limit in imaging with waves. The following holds.

Lemma 3.36 *Let ∂B_R be the sphere of radius R and center 0. We have*

$$\int_{\partial B_R} \left(\frac{\partial \overline{\Gamma_{k_0}}}{\partial \nu}(x,y)\Gamma_{k_0}(z,y) - \overline{\Gamma_{k_0}}(x,y)\frac{\partial \Gamma_{k_0}}{\partial \nu}(z,y) \right) d\sigma(y) = 2i\Im m \Gamma_{k_0}(x,z) \ ,$$

(3.80)

which yields

$$\lim_{R \to +\infty} \int_{\partial B_R} \overline{\Gamma_{k_0}}(x,y)\Gamma_{k_0}(z,y)\,d\sigma(y) = -\frac{1}{k_0}\Im \Gamma_{k_0}(x,z) \ ,$$

(3.81)

by using the radiation outgoing condition.

Identity (3.81) is valid even in inhomogeneous media. The following identity holds, which as we will see shows that the sharper the behavior of the imaginary part of the fundamental solution Φ_{k_0} around the source is, the higher is the resolution.

Theorem 3.37 *Let Φ_{k_0} be the fundamental solution defined in (3.76). We have*

$$\lim_{R \to +\infty} \int_{|y|=R} \overline{\Phi_{k_0}}(x,y)\Phi_{k_0}(z,y)\,d\sigma(y) = -\frac{1}{k_0}\Im \Phi_{k_0}(x,z) \ .$$

(3.82)

Proof. The proof is based essentially on the second Green's identity and the Sommerfeld radiation condition. Let us consider

$$(\nabla_y \cdot \tfrac{1}{\mu}\nabla_y + \omega^2 \varepsilon)\Phi_{k_0}(y,x_2) = \frac{1}{\mu_0}\delta_{x_2} \ ,$$

$$(\nabla_y \cdot \tfrac{1}{\mu}\nabla_y + \omega^2 \varepsilon)\Phi_{k_0}(y,x_1) = \frac{1}{\mu_0}\delta_{x_1} \ .$$

We multiply the first equation by $\overline{\Phi_{k_0}}(y,x_1)$ and we subtract the second equation multiplied by $\Phi_{k_0}(y,x_2)$:

$$\nabla_y \frac{\mu_0}{\mu} \cdot \left[\overline{\Phi_{k_0}}(y,x_1)\nabla_y \Phi_{k_0}(y,x_2) - \Phi_{k_0}(y,x_2)\nabla_y\overline{\Phi_{k_0}}(y,x_1) \right]$$

$$= -\Phi_{k_0}(y,x_2)\delta_{x_1} + \overline{\Phi_{k_0}}(y,x_1)\delta_{x_2}$$

$$= -\Phi_{k_0}(x_1,x_2)\delta_{x_1} + \overline{\Phi_{k_0}}(x_1,x_2)\delta_{x_2} \ ,$$

using the reciprocity property $\Phi_{k_0}(x_1,x_2) = \Phi_{k_0}(x_2,x_1)$.

We integrate over the ball B_R and we use the divergence theorem:

$$\int_{\partial B_R} \nu \cdot \left[\overline{\Phi_{k_0}}(y,x_1)\nabla_y \Phi_{k_0}(y,x_2) - \Phi_{k_0}(y,x_2)\nabla_y\overline{\Phi_{k_0}}(y,x_1) \right] d\sigma(y)$$

$$= -\Phi_{k_0}(x_1,x_2) + \overline{\Phi_{k_0}}(x_1,x_2) \ .$$

This equality can be viewed as an application of the second Green's identity. The Green's function also satisfies the Sommerfeld radiation condition

$$\lim_{|y|\to\infty} |y|\Big(\frac{y}{|y|} \cdot \nabla_y - ik_0\Big)\Phi_{k_0}(y, x_1) = 0 \ ,$$

uniformly in all directions $y/|y|$. Using this property, we substitute $ik_0\Phi_{k_0}(y, x_2)$ for $\nu \cdot \nabla_y \Phi_{k_0}(y, x_2)$ in the surface integral over ∂B_R, and $-ik_0\overline{\Phi_{k_0}}(y, x_1)$ for $\nu \cdot \nabla_y \overline{\Phi_{k_0}}(y, x_1)$, and we obtain the desired result. □

3.2.7 Scattering Amplitude and the Optical Theorem

Scattering Coefficients

We first define the scattering coefficients of a particle. Assume that k_0^2 is not a Dirichlet eigenvalue for $-\Delta$ on D. Then, from Theorem 3.30 we know that the solution to

$$\begin{cases} \nabla \cdot \frac{1}{\mu}\nabla u + \omega^2 \varepsilon u = 0 \quad \text{in } \mathbb{R}^2 \ , \\ (u - U) \text{ satisfies the outgoing radiation condition,} \end{cases} \tag{3.83}$$

can be represented using the single layer potentials $\mathcal{S}_D^{k_0}$ and $\mathcal{S}_D^{k_\star}$ as follows:

$$u(x) = \begin{cases} U(x) + \mathcal{S}_D^{k_0}[\psi](x), & x \in \mathbb{R}^2 \setminus \overline{D} \ , \\ \mathcal{S}_D^{k_\star}[\varphi](x), & x \in D \ , \end{cases} \tag{3.84}$$

where the pair $(\varphi, \psi) \in L^2(\partial D) \times L^2(\partial D)$ is the unique solution to

$$\begin{cases} \mathcal{S}_D^{k_\star}[\varphi] - \mathcal{S}_D^{k_0}[\psi] = U \\ \dfrac{1}{\mu_\star}\dfrac{\partial(\mathcal{S}_D^{k_\star}[\varphi])}{\partial\nu}\bigg|_{-} - \dfrac{1}{\mu_0}\dfrac{\partial(\mathcal{S}_D^{k_0}[\psi])}{\partial\nu}\bigg|_{+} = \dfrac{1}{\mu_0}\dfrac{\partial U}{\partial\nu} \quad \text{on } \partial D \ . \end{cases} \tag{3.85}$$

Moreover, there exists a constant $C = C(k_\star, k_0, D)$ such that

$$\|\varphi\|_{L^2(\partial D)} + \|\psi\|_{L^2(\partial D)} \le C(\|U\|_{L^2(\partial D)} + \|\nabla U\|_{L^2(\partial D)}) \ . \tag{3.86}$$

Furthermore, the constant C can be chosen to be scale independent. There exists δ_0 such that if one denotes by $(\varphi_\delta, \psi_\delta)$ the solution of (3.85) with $k_\star$ and k_0 respectively replaced by $\delta k_\star$ and δk_0, then

$$\|\varphi_\delta\|_{L^2(\partial D)} + \|\psi_\delta\|_{L^2(\partial D)} \le C(\|U\|_{L^2(\partial D)} + \|\nabla U\|_{L^2(\partial D)}) \ . \tag{3.87}$$

Note that the following asymptotic formula holds as $|x| \to \infty$, which can be seen from (3.84) and Graf's formula (3.53):

$$u(x) - U(x) = -\frac{i}{4} \sum_{n\in\mathbb{Z}} H_n^{(1)}(k_0|x|)e^{in\theta_x} \int_{\partial D} J_n(k_0|y|)e^{-in\theta_y}\psi(y)d\sigma(y) \ . \tag{3.88}$$

Let (φ_m, ψ_m) be the solution to (3.85) with $J_m(k_0|x|)e^{im\theta_x}$ in the place of $U(x)$. We define the *scattering coefficient* as follows.

Definition 3.38 *The scattering coefficients W_{nm}, $m, n \in \mathbb{Z}$, associated with the permittivity and permeability distributions ε, μ and the frequency ω (or $k_\star, k_0, D$) are defined by*

$$W_{nm} = W_{nm}[\varepsilon, \mu, \omega] := \int_{\partial D} J_n(k_0|y|)e^{-in\theta_y}\psi_m(y)d\sigma(y) . \qquad (3.89)$$

We derive the exponential decay of the scattering coefficients. We have the following lemma for the size of $|W_{nm}|$.

Lemma 3.39 *There is a constant C depending on $(\varepsilon, \mu, \omega)$ such that*

$$|W_{nm}[\varepsilon, \mu, \omega]| \leq \frac{C^{|n|+|m|}}{|n|^{|n|}|m|^{|m|}} \quad \text{for all } n, m \in \mathbb{Z} . \qquad (3.90)$$

Moreover, there exists δ_0 such that, for all $\delta \leq \delta_0$,

$$|W_{nm}[\varepsilon, \mu, \delta\omega]| \leq \frac{C^{|n|+|m|}}{|n|^{|n|}|m|^{|m|}}\delta^{|n|+|m|} \quad \text{for all } n, m \in \mathbb{Z} , \qquad (3.91)$$

where the constant C depends on $(\varepsilon, \mu, \omega)$ but is independent of δ.

Proof. Let $U(x) = J_m(k_0|x|)e^{im\theta_x}$ and (φ_m, ψ_m) be the solution to (3.85). Since

$$J_m(t) \sim \frac{(-1)^m}{\sqrt{2\pi|m|}}\left(\frac{et}{2|m|}\right)^{|m|} \qquad (3.92)$$

as $m \to \infty$ (see (2.12)), we have

$$\|U\|_{L^2(\partial D)} + \|\nabla U\|_{L^2(\partial D)} \leq \frac{C^{|m|}}{|m|^{|m|}}$$

for some constant C. Thus it follows from (3.86) that

$$\|\psi_m\|_{L^2(\partial D)} \leq \frac{C^{|m|}}{|m|^{|m|}} \qquad (3.93)$$

for another constant C. So we get (3.90) from (3.89).

On the other hand, one can see from (3.87) that (3.93) still holds for some C independent of δ as long as $\delta \leq \delta_0$ for some δ_0. Note that

$$W_{nm}[\varepsilon, \mu, \delta\omega] = \int_{\partial D} J_n(\delta k_0|y|)e^{-in\theta_y}\psi_{m,\delta}(y)d\sigma(y) , \qquad (3.94)$$

where $(\varphi_{m,\delta}, \psi_{m,\delta})$ is the solution to (3.85) with $k_\star$ and k_0 respectively replaced by $\delta k_\star$ and δk_0 and $J_m(\delta k_0|x|)e^{im\theta_x}$ in the place of $U(x)$. So one can use (3.92) to obtain (3.91). This completes the proof. $\square$

Recall from (2.26) that the family of cylindrical waves $\{J_n(k_0|y|)e^{-in\theta_y}\}_n$ is complete. If U is given as

$$U(x) = \sum_{m \in \mathbb{Z}} a_m(U) J_m(k_0|x|) e^{im\theta_x} \ , \tag{3.95}$$

where $a_m(U)$ are constants, it follows from the principle of superposition that the solution (φ, ψ) to (3.85) is given by

$$\psi = \sum_{m \in \mathbb{Z}} a_m(U) \psi_m \ .$$

Then one can see from (3.88) that the solution u to (3.83) can be represented as

$$u(x) - U(x) = -\frac{i}{4} \sum_{n \in \mathbb{Z}} H_n^{(1)}(k_0|x|) e^{in\theta_x} \sum_{m \in \mathbb{Z}} W_{nm} a_m(U) \quad \text{as } |x| \to \infty \ . \tag{3.96}$$

In particular, if U is given by a plane wave $e^{ik_0\xi \cdot x}$ with ξ being on the unit circle, then

$$u(x) - e^{ik_0\xi \cdot x} = -\frac{i}{4} \sum_{n \in \mathbb{Z}} H_n^{(1)}(k_0|x|) e^{in\theta_x} \sum_{m \in \mathbb{Z}} W_{nm} e^{im(\frac{\pi}{2} - \theta_\xi)} \quad \text{as } |x| \to \infty \ , \tag{3.97}$$

where $\xi = (\cos\theta_\xi, \sin\theta_\xi)$ and $x = (|x|, \theta_x)$. In fact, from the Jacobi-Anger expansion of plane waves (2.6) it follows that

$$e^{ik_0\xi \cdot x} = \sum_{m \in \mathbb{Z}} e^{im(\frac{\pi}{2} - \theta_\xi)} J_m(k_0|x|) e^{im\theta_x} \ , \tag{3.98}$$

and

$$\psi = \sum_{m \in \mathbb{Z}} e^{im(\frac{\pi}{2} - \theta_\xi)} \psi_m \ . \tag{3.99}$$

Thus (3.97) holds. It is worth emphasizing that the expansion formula (3.96) or (3.97) determines uniquely the scattering coefficients W_{nm}, for $n, m \in \mathbb{Z}$.

Scattering Amplitude

Let D be a bounded domain in $\mathbb{R}^2$ with smooth boundary ∂D, and let (ε_0, μ_0) be the pair of electromagnetic parameters (permittivity and permeability) of $\mathbb{R}^2 \setminus \overline{D}$ and $(\varepsilon_\star, \mu_\star)$ be that of D. Then the permittivity and permeability distributions are given by

$$\varepsilon = \varepsilon_0 \chi(\mathbb{R}^2 \setminus \overline{D}) + \varepsilon_\star \chi(D) \quad \text{and} \quad \mu = \mu_0 \chi(\mathbb{R}^2 \setminus \overline{D}) + \mu_\star \chi(D) \ . \tag{3.100}$$

Given a frequency ω, set $k_\star = \omega\sqrt{\varepsilon_\star \mu_\star}$ and $k_0 = \omega\sqrt{\varepsilon_0 \mu_0}$. For a function U satisfying $(\Delta + k_0^2)U = 0$ in $\mathbb{R}^2$, we consider the scattered wave u, *i.e.*, the solution to (3.83).

Suppose that U is given by a plane wave $e^{ik_0\xi \cdot x}$ with ξ being on the unit circle, then (3.97) yields

$$u(x) - e^{ik_0 \xi \cdot x} = -\frac{i}{4} \sum_{n \in \mathbb{Z}} H_n^{(1)}(k_0|x|) e^{in\theta_x} \sum_{m \in \mathbb{Z}} W_{nm} e^{im(\frac{\pi}{2} - \theta_\xi)} \quad \text{as } |x| \to \infty ,$$

$$(3.101)$$

where W_{nm}, given by (3.89), are the scattering coefficients, $\xi = (\cos\theta_\xi, \sin\theta_\xi)$, and $x = (|x|, \theta_x)$.

The far-field pattern $A_\infty[\varepsilon, \mu, \omega]$, when the incident field is given by $e^{ik_0 \xi \cdot x}$, is defined to be

$$u(x) - e^{ik_0 \xi \cdot x} = -ie^{-\frac{\pi i}{4}} \frac{e^{ik_0|x|}}{\sqrt{8\pi k_0|x|}} A_\infty[\varepsilon, \mu, \omega](\theta_\xi, \theta_x) + o(|x|^{-\frac{1}{2}}) \quad \text{as } |x| \to \infty .$$

$$(3.102)$$

Recall that

$$H_0^{(1)}(t) \sim \sqrt{\frac{2}{\pi t}} e^{i(t - \frac{\pi}{4})} \quad \text{as } t \to \infty , \qquad (3.103)$$

where $\sim$ indicates that the difference between the right-hand and left-hand side is $O(t^{-1})$. If $|x|$ is large while $|y|$ is bounded, then we have

$$|x - y| = |x| - |y| \cos(\theta_x - \theta_y) + O(\frac{1}{|x|}),$$

and hence

$$H_0^{(1)}(k_0|x - y|) \sim e^{-\frac{\pi i}{4}} \sqrt{\frac{2}{\pi k_0|x|}} e^{ik_0(|x| - |y|\cos(\theta_x - \theta_y))} \quad \text{as } |x| \to \infty .$$

Thus, from (3.84), we get

$$u(x) - e^{ik_0 \xi \cdot x} \sim -ie^{-\frac{\pi i}{4}} \frac{e^{ik_0|x|}}{\sqrt{8\pi k_0|x|}} \int_{\partial D} e^{-ik_0|y|\cos(\theta_x - \theta_y)} \psi(y) \, d\sigma(y) \quad (3.104)$$

as $|x| \to \infty$ and infer that the far-field pattern is given by

$$A_\infty[\varepsilon, \mu, \omega](\theta_\xi, \theta_x) = \int_{\partial D} e^{-ik_0|y|\cos(\theta_x - \theta_y)} \psi(y) \, d\sigma(y) , \qquad (3.105)$$

where ψ is given by (3.99).

We now show that the scattering coefficients are basically the Fourier coefficients of the far-field pattern (the scattering amplitude) which is 2π-periodic function in two dimensions.

Let

$$A_\infty[\varepsilon, \mu, \omega](\theta_\xi, \theta_x) = \sum_{n \in \mathbb{Z}} b_n(\theta_\xi) e^{in\theta_x}$$

be the Fourier series of $A_\infty[\varepsilon, \mu, \omega](\theta_\xi, \cdot)$. From (3.105) it follows that

$$b_n(\theta_\xi) = \frac{1}{2\pi} \int_0^{2\pi} \int_{\partial D} e^{-ik_0|y|\cos(\theta_x - \theta_y)} \psi(y) \, d\sigma(y) \, e^{-in\theta_x} \, d\theta_x$$

$$= \frac{1}{2\pi} \int_{\partial D} \int_0^{2\pi} e^{-ik_0|y|\cos(\theta_x - \theta_y)} e^{-in\theta_x} \, d\theta_x \, \psi(y) \, d\sigma(\theta_y) .$$

Since

$$\frac{1}{2\pi} \int_0^{2\pi} e^{-ik_0|y|\cos(\theta_x - \theta_y)} e^{-in\theta_x} \, d\theta_x = J_n(k_0|y|) e^{-in(\theta_y + \frac{\pi}{2})} \; ,$$

we deduce that

$$b_n(\theta_\xi) = \int_{\partial D} J_n(k_0|y|) e^{-in(\theta_y + \frac{\pi}{2})} \psi(y) \, d\sigma(\theta_y) \; .$$

Using (3.99) we now arrive at the following theorem.

Theorem 3.40 *Let θ and θ' be respectively the incident and scattered direction. Then we have*

$$A_\infty[\varepsilon, \mu, \omega](\theta, \theta') = \sum_{n,m \in \mathbb{Z}} i^{(m-n)} e^{in\theta'} W_{nm}[\varepsilon, \mu, \omega] e^{-im\theta} \; , \qquad (3.106)$$

where the scattering coefficients W_{nm} are defined by (3.89).

We emphasize that the series in (3.106) is well-defined provided that k_0^2 is not a Dirichlet eigenvalue for $-\Delta$ on D. Moreover, it converges uniformly in θ and θ' thanks to (3.90). Furthermore, there exists $\delta_0 > 0$ such that for any $\delta \le \delta_0$ the series expansion of $A_\infty[\varepsilon, \mu, \delta\omega](\theta, \theta')$ is well-defined and its convergence is uniform in δ. This is the key point of our construction of near-cloaking structures. We also note that if U is given by (3.95) then the scattering amplitude, which we denote by $A_\infty[\varepsilon, \mu, \omega](U, \theta')$, is given by

$$A_\infty[\varepsilon, \mu, \omega](U, \theta') = \sum_{n \in \mathbb{Z}} i^{-n} e^{in\theta'} \sum_{m \in \mathbb{Z}} W_{nm} a_m(U) \; . \qquad (3.107)$$

The conversion of the far-field to the near field is achieved via formula (3.101).

Optical Theorem

Let $d = 3$. The analogous quantity of the Poynting vector in scalar wave theory is the energy flux vector [112]. For $\Re\left[u(x) e^{-ik_0 t}\right]$, the averaged value of the energy flux vector, taken over an interval which is long compared to the period of the oscillations, is given by

$$F(x) = -ik_0 \left[\overline{u}(x) \nabla u(x) - u(x) \nabla \overline{u}(x) \right] \; .$$

Consider the outward flow of energy through the sphere ∂B_R of radius R and center the origin:

$$\mathcal{W} = \int_{\partial B_R} F(x) \cdot \nu(x) d\sigma(x) \; ,$$

where $\nu(x)$ is the outward normal at $x \in \partial B_R$.

As the total field can be written as $u = U + u^s$, the flow can be decomposed into three parts:

$$\mathcal{W} = \mathcal{W}^i + \mathcal{W}^s + \mathcal{W}' ,$$

where

$$\mathcal{W}^i = -i\beta \int_{\partial B_R} \left[\overline{U}(x)\nabla U(x) - U(x)\nabla \overline{U}(x) \right] \cdot \nu(x)\, d\sigma(x) ,$$

$$\mathcal{W}^s = -i\beta \int_{\partial B_R} \left[\overline{u^s}(x)\nabla u^s(x) - u^s(x)\nabla \overline{u^s}(x) \right] \cdot \nu(x)\, d\sigma(x) ,$$

$$\mathcal{W}' = -i\beta \int_{\partial B_R} \left[\overline{U}(x)\nabla u^s(x) - u^s(x)\nabla \overline{U}(x) - U(x)\nabla \overline{u^s}(x) + \overline{u^s}(x)\nabla U(x) \right] \cdot \nu(x)\, d\sigma(x) ,$$

where β is a positive constant.

In the case where $U(x) = e^{ik_0\xi \cdot x}$ is a plane wave, we can see that $\mathcal{W}^i = 0$:

$$\mathcal{W}^i = -i\beta \int_{\partial B_R} \left[\overline{U}(x)\nabla U(x) - U(x)\nabla \overline{U}(x) \right]\, d\sigma(x) ,$$

$$= -i\beta \int_{\partial B_R} \left[e^{-ik_0\xi \cdot x} ik_0\xi e^{ik_0\xi \cdot x} + e^{ik_0\xi \cdot x} k_0 d e^{-ik_0\xi \cdot x} \right] \cdot \nu(x)\, d\sigma(x) ,$$

$$= 2\beta k_0\xi \cdot \int_{\partial B_R} \nu(x)\, d\sigma(x) ,$$

$$= 0 .$$

In a non absorbing medium with non absorbing scatterers, $\mathcal{W}$ is equal to zero because the electromagnetic energy would be conserved by the scattering process. However, if there is an absorbing scatterer inside the medium, the conservation of energy gives the rate of absorption as

$$\mathcal{W}^a = -\mathcal{W} .$$

Therefore, we have

$$\mathcal{W}^a + \mathcal{W}^s = -\mathcal{W}' .$$

Here, $\mathcal{W}'$ is called the extinction rate. It is the rate at which the energy is removed by the scatterer from the illuminating plane wave, and it is the sum of the rate of absorption and the rate at which energy is scattered.

Denote by V the quantity $V(x) = \beta \left| \overline{U}(x)\nabla U(x) - U(x)\nabla \overline{U}(x) \right|$. In the case of a plane wave illumination, $V(x)$ is independent of x and is given by $V = 2\beta k_0$.

Definition 3.41 *The scattering cross-section Q^s, the absorption cross-section Q^a and the extinction cross-section are defined by*

$$Q^s = \frac{\mathcal{W}^s}{V}, \quad Q^a = \frac{\mathcal{W}^a}{V}, \quad Q^{ext} = \frac{-\mathcal{W}'}{V} .$$

Note that these quantities are independent of x in the case of a plane wave illumination.

Theorem 3.42 (Optical theorem) *Let $d = 3$. If $U(x) = e^{ik_0\xi \cdot x}$, where ξ is a unit direction of incidence, then*

$$Q^{ext}[\varepsilon, \mu, \omega](\xi) = Q^s[\varepsilon, \mu, \omega](\xi) + Q^a[\varepsilon, \mu, \omega](\xi) = \frac{4\pi}{k_0}\Im\left[A_\infty[\varepsilon, \mu, \omega](\xi, \xi)\right] ,$$

(3.108)

$$Q^s[\varepsilon, \mu, \omega](\xi) = \int_{|\hat{x}|=1} |A_\infty[\varepsilon, \mu, \omega](\xi, \hat{x})|^2 d\sigma(\hat{x})$$

(3.109)

with A_∞ being the scattering amplitude defined by

$$(u - U)(x) = \frac{e^{ik_0|x|}}{|x|}A_\infty[\varepsilon, \mu, \omega]\left(\xi, \frac{x}{|x|}\right) + O\left(\frac{1}{|x|^2}\right) .$$

(3.110)

Proof. The Sommerfeld radiation condition gives, for any $x \in \partial B_R$,

$$\nabla u^s(x) \cdot \nu(x) \sim ik_0 u^s(x) .$$

(3.111)

Hence, from (3.110) we get

$$u^s(x)\nabla\overline{u^s}(x) \cdot \nu(x) - \overline{u^s}(x)\nabla u^s(x) \cdot \nu(x) \sim \frac{-2ik_0}{|x|^2}\left|A_\infty[\varepsilon, \mu, \omega]\left(\xi, \frac{x}{|x|}\right)\right|^2 ,$$

which yields (3.109). We now compute the extinction rate. We have

$$\nabla U(x) \cdot \nu(x) = ik_0\xi \cdot \nu(x)e^{ik_0\xi \cdot x} .$$

(3.112)

Therefore, using (3.111) and (3.112), it follows that

$$\overline{U}(x)\nabla u^s(x) \cdot \nu(x) - u^s(x)\nabla\overline{U}(x) \cdot \nu(x) \sim \left[ik_0\frac{e^{ik_0(|x|-\xi\cdot x)}}{|x|}\xi \cdot \nu + ik_0\frac{e^{ik_0(|x|-\xi\cdot x)}}{|x|}\right]A_\infty[\varepsilon, \mu, \omega]\left(\xi, \frac{x}{|x|}\right)$$
$$\sim \frac{ik_0 e^{ik_0|x|-\xi\cdot\nu(x)}}{|x|}\left(\xi \cdot \nu(x) + 1\right)A_\infty[\varepsilon, \mu, \omega]\left(\xi, \frac{x}{|x|}\right) .$$

For $x \in \partial B_R$, we can write

$$\overline{U}(x)\nabla u^s(x) \cdot \nu(x) - u^s(x)\nabla\overline{U}(x) \cdot \nu(x) \sim \frac{ik_0 e^{-ik_0 R\nu(x)\cdot(\xi-\nu(x))}}{R}\left(\xi \cdot \nu(x) + 1\right)A_\infty[\varepsilon, \mu, \omega]\left(\xi, \frac{x}{|x|}\right) .$$

We now use Jones' lemma (see, for instance, [112, Appendix XII])

$$\frac{1}{R}\int_{\partial B_R} \mathcal{G}(\nu(x))e^{-ik_0\xi\cdot\nu(x)}d\sigma(x) \sim \frac{2\pi i}{k_0}\left(\mathcal{G}(\xi)e^{-ik_0 R} - \mathcal{G}(-\xi)e^{ik_0 R}\right)$$

as $R \to \infty$, to obtain

$$\int_{\partial B_R} \left[\overline{U}(x)\nabla u^s(x) - u^s(x)\nabla\overline{U}(x)\right] \cdot \nu(x) \sim -4\pi A_\infty[\varepsilon, \mu, \omega](\xi, \xi) \quad \text{as } R \to \infty .$$

Therefore,

$$\mathcal{W}' = i4\pi\beta\left[A_\infty[\varepsilon,\mu,\omega](\xi,\xi) - \overline{A_\infty}[\varepsilon,\mu,\omega](\xi,\xi)\right] = -8\pi\beta\Im\left[A_\infty[\varepsilon,\mu,\omega](\xi,\xi)\right] .$$

Since

$$\beta\left|\overline{U}(x)\nabla U(x) - U(x)\nabla\overline{U}(x)\right| = 2\beta k_0 ,$$

we get the result. $\square$

In two dimensions, the scattering cross-section $Q^s[\varepsilon,\mu,\omega]$ is defined by

$$Q^s[\varepsilon,\mu,\omega](\theta') := \int_0^{2\pi}\left|A_\infty[\varepsilon,\mu,\omega](\theta,\theta')\right|^2 d\theta . \qquad (3.113)$$

As an immediate consequence of Theorem 3.40 we obtain

$$Q^s[\varepsilon,\mu,\omega](\theta') = 2\pi\sum_{m\in\mathbb{Z}}\left|\sum_{n\in\mathbb{Z}}i^{-n}W_{nm}[\varepsilon,\mu,\omega]e^{in\theta'}\right|^2 . \qquad (3.114)$$

Analogously to Theorem 3.42, we can prove that

$$\Im A_\infty[\varepsilon,\mu,\omega](\theta',\theta') = -\sqrt{\frac{k_0}{8\pi}}Q^{\text{ext}}[\varepsilon,\mu,\omega](\theta'), \quad \forall\,\theta'\in[0,2\pi] . \qquad (3.115)$$

Therefore, for non absorbing scatterers, *i.e.*, $Q^a = 0$, the above optical theorem leads to a natural constraint on W_{nm}. From (3.114) and (3.115), we obtain

$$\Im\sum_{n,m\in\mathbb{Z}}i^{m-n}e^{i(n-m)\theta'}W_{nm}[\varepsilon,\mu,\omega] = -\sqrt{\frac{\pi k_0}{2}}\sum_{m\in\mathbb{Z}}\left|\sum_{n\in\mathbb{Z}}i^{-n}W_{nm}[\varepsilon,\mu,\omega]e^{in\theta'}\right|^2 ,$$
$$(3.116)$$

$\forall\,\theta'\in[0,2\pi]$.

Since $\omega\mapsto A_\infty[\varepsilon,\mu,\omega]$ is analytic in $\mathbb{C}^+$, A_∞ vanishes efficiently rapidly as $\omega\to+\infty$, and $A_\infty[\varepsilon,\mu,-\omega] = \overline{A_\infty[\varepsilon,\mu,\omega]}$ for real values of ω, the real and imaginary parts of the scattering amplitude are connected by the Kramers-Kronig relations (2.48) and we have for $\xi\in\mathbb{R}^d, |\xi| = 1, d = 2, 3$,

$$\Re A_\infty[\varepsilon,\mu,\omega](\xi,\xi) = c_d\,\text{p.v.}\int_0^{+\infty}\frac{(\omega')^{(d+1)/2}Q^{\text{ext}}[\varepsilon,\mu,\omega'](\xi)}{(\omega')^2 - \omega^2}\,d\omega' , \quad (3.117)$$

and

$$Q^{\text{ext}}[\varepsilon,\mu,\omega](\xi) = -\frac{2}{\pi\sqrt{\varepsilon_0\mu_0}}\,\text{p.v.}\int_0^{+\infty}\frac{\Re A_\infty[\varepsilon,\mu,\omega'](\xi,\xi)}{(\omega')^2 - \omega^2}\,d\omega' , \qquad (3.118)$$

where $c_3 = \sqrt{\varepsilon_0\mu_0}/(2\pi^2)$ and $c_2 = -\sqrt{\sqrt{\varepsilon_0\mu_0}/(2\pi^3)}$. Moreover, from (2.50) and (2.51), we obtain by respectively taking the limits of (3.117) and (3.118) as $\omega\to 0$ the following sum rules:

$$\Re A_\infty[\varepsilon,\mu,0](\xi,\xi) = c_d \,\text{p.v.} \int_0^{+\infty} (\omega')^{(d-3)/2} Q^{\text{ext}}[\varepsilon,\mu,\omega'](\xi)\,d\omega' , \quad (3.119)$$

and

$$Q^{\text{ext}}[\varepsilon,\mu,0](\xi) = -\frac{2}{\pi\sqrt{\varepsilon_0\mu_0}} \,\text{p.v.} \int_0^{+\infty} \frac{\Re A_\infty[\varepsilon,\mu,\omega'](\xi,\xi) - \Re A_\infty[\varepsilon,\mu,0](\xi,\xi)}{(\omega')^2}\,d\omega' .$$
$$(3.120)$$

3.3 Elasticity Equations

Let Ω be a domain in $\mathbb{R}^d$, $d = 2,3$. Let λ and μ be the Lamé constants for Ω satisfying the strong convexity condition

$$\mu > 0 \quad \text{and} \quad d\lambda + 2\mu > 0. \quad (3.121)$$

The constants λ and μ are respectively referred to as the compression modulus and the shear modulus. We also introduce the bulk modulus $\beta := \lambda + 2\mu/d$. We refer the reader to [243, p.11] for an explanation of the physical significance of (3.121).

In a homogeneous isotropic elastic medium, the elastostatic operator corresponding to the Lamé constants λ, μ is given by

$$\mathcal{L}^{\lambda,\mu} u := \mu\Delta u + (\lambda + \mu)\nabla\nabla \cdot u, \quad u : \Omega \to \mathbb{R}^d . \quad (3.122)$$

If Ω is bounded with a connected smooth boundary, then we define the conormal derivative $\partial u/\partial n$ by

$$\frac{\partial u}{\partial n} = \lambda(\nabla \cdot u)\nu + \mu(\nabla u + \nabla u^T)\nu , \quad (3.123)$$

where ∇u is the matrix $(\partial_j u_i)_{i,j=1}^d$ with u_i being the i-th component of u, and ν is the outward unit normal to the boundary $\partial\Omega$.

Note that the conormal derivative has a direct physical meaning:

$$\frac{\partial u}{\partial n} = \text{traction on } \partial\Omega.$$

The vector u is the displacement field of the elastic medium having the Lamé coefficients λ and μ, and the symmetric gradient

$$\nabla^s u := (\nabla u + \nabla u^T)/2 \quad (3.124)$$

is the strain tensor.

In $\mathbb{R}^d$, $d = 2,3$, let

$$I := \delta_{jl} e_j \otimes e_l,$$
$$\mathbb{I} := \frac{1}{2}(\delta_{jl}\delta_{km} + \delta_{jm}\delta_{kl}) e_j \otimes e_k \otimes e_l \otimes e_m,$$

with $(e_1, \ldots, e_d)$ being the canonical basis of $\mathbb{R}^d$ and $\otimes$ denoting the tensor product between vectors in $\mathbb{R}^d$. Here, I is the $d \times d$ identity matrix or 2-tensor while $\mathbb{I}$ is the identity 4-tensor.

Define the elasticity tensor $\mathbb{C} = (C_{jklm})_{i,j,k,l=1}^d$ for $\mathbb{R}^d$ by

$$C_{jklm} = \lambda \delta_{jk} \delta_{lm} + \mu(\delta_{jl} \delta_{km} + \delta_{jm} \delta_{kl}), \qquad (3.125)$$

which can be written as

$$\mathbb{C} := \lambda I \otimes I + 2\mu \mathbb{I}.$$

With this notation, we have

$$\mathcal{L}^{\lambda,\mu} u = \nabla \cdot \mathbb{C} \nabla^s u,$$

and

$$\frac{\partial u}{\partial n} = (\mathbb{C} \nabla^s u)\nu = \sigma(u)\nu,$$

where $\sigma(u)$ is the stress tensor given by

$$\sigma(u) = \mathbb{C} \nabla^s u.$$

Now, we consider the elastic wave equation

$$\rho \partial_t^2 U - \mathcal{L}^{\lambda,\mu} U = 0,$$

where the positive constant ρ is the density of the medium. Then, we obtain a time-harmonic solution $U(x,t) = \Re e[e^{-i\omega t} u(x)]$ if the space-dependent part u satisfies the time-harmonic elasticity equation for the displacement field,

$$(\mathcal{L}^{\lambda,\mu} + \omega^2 \rho)u = 0, \qquad (3.126)$$

with ω being the angular frequency.

The time-harmonic elasticity equation (3.126) has a special family of solutions called p- and s-plane waves:

$$U^p(x) = e^{i\omega \sqrt{\rho/(\lambda+2\mu)} x \cdot \theta} \theta \quad \text{and} \quad U^s(x) = e^{i\omega \sqrt{\rho/\mu} x \cdot \theta} \theta^{\perp} \qquad (3.127)$$

for $\theta \in \mathbb{S}^{d-1} := \{\theta \in \mathbb{R}^d : |\theta| = 1\}$ the direction of the wavevector and $\theta^{\perp}$ is such that $|\theta^{\perp}| = 1$ and $\theta^{\perp} \cdot \theta = 0$. Note that U^p is irrotational while U^s is solenoidal.

Taking the limit $\omega \to 0$ in (3.126) yields the static elasticity equation

$$\mathcal{L}^{\lambda,\mu} u = 0. \qquad (3.128)$$

In a bounded domain Ω, the equations (3.126) and (3.128) need to be supplemented with boundary conditions at $\partial\Omega$. If $\partial\Omega$ is a stress-free surface, the traction acting on $\partial\Omega$ vanishes:

$$\frac{\partial u}{\partial n} = 0.$$

This boundary condition is appropriate when the surface $\partial\Omega$ forms the outer boundary on the elastic body that is surrounded by empty space.

In a homogeneous, isotropic medium, using the Helmholtz decomposition theorem, the displacement field can be decomposed into the sum of an irrotational and a solenoidal field. Assume that Ω is simply connected and its boundary $\partial\Omega$ is connected. The Helmholtz decomposition states that for $w \in L^2(\Omega)^d$ there exist $\phi_w \in W^{1,2}(\Omega)$ and $\psi_w \in H_{\mathrm{curl}}(\Omega) \cap H_{\mathrm{div}}(\Omega)$ such that

$$w = \nabla\phi_w + \nabla \times \psi_w. \tag{3.129}$$

The Helmholtz decomposition (3.129) can be found by solving the following weak Neumann problem in Ω [79, 148]:

$$\int_\Omega \overline{\nabla\phi_w} \cdot \nabla q \, dx = \int_\Omega \overline{w} \cdot \nabla q \, dx \quad \forall\, q \in W^{1,2}(\Omega). \tag{3.130}$$

The function $\phi_w \in W^{1,2}(\Omega)$ is uniquely defined up to an additive constant. In order to uniquely define the function ψ_w, we impose that it satisfies the following properties [111]:

$$\begin{cases} \nabla \cdot \psi_w = 0 & \text{in } \Omega, \\ \psi_w \cdot \nu = (\nabla \times \psi_w) \cdot \nu = 0 & \text{on } \partial\Omega. \end{cases} \tag{3.131}$$

The boundary condition $(\nabla \times \psi_w) \cdot \nu = 0$ on $\partial\Omega$ shows that the gradient and curl parts in (3.129) are orthogonal.

We define, respectively, the Helmholtz decomposition operators $\mathcal{H}^p$ and $\mathcal{H}^s$ for $w \in L^2(\Omega)^d$ by

$$\mathcal{H}^p[w] := \nabla\phi_w \quad \text{and} \quad \mathcal{H}^s[w] := \nabla \times \psi_w, \tag{3.132}$$

where ϕ_w is a solution to (3.130) and ψ_w satisfy $\nabla \times \psi_w = w - \nabla\phi_w$ together with (3.131).

The following lemma holds.

Lemma 3.43 (Properties of the Helmholtz decomposition operators)
Let the Lamé parameters (λ, μ) be constants satisfying (3.121). We have the orthogonality relations

$$\mathcal{H}^s\mathcal{H}^p = \mathcal{H}^p\mathcal{H}^s = 0. \tag{3.133}$$

Moreover, $\mathcal{H}^s$ and $\mathcal{H}^p$ commute with $\mathcal{L}^{\lambda,\mu}$: For any smooth vector field w in Ω,

$$\mathcal{H}^\alpha[\mathcal{L}^{\lambda,\mu}w] = \mathcal{L}^{\lambda,\mu}\mathcal{H}^\alpha[w], \quad \alpha = p, s. \tag{3.134}$$

Proof. We only prove (3.134). The orthogonality relations (3.133) are easy to see. Let $\mathcal{H}^s[w] = \nabla\phi_w$ and let $\mathcal{H}^p[w] = \nabla \times \psi_w$. Then we have

$$\mathcal{L}^{\lambda,\mu}w = (\lambda + 2\mu)\nabla\Delta\phi_w + \mu\nabla \times \Delta\psi_w,$$

and therefore,

$$\mathcal{H}^s[\mathcal{L}^{\lambda,\mu}w] = (\lambda + 2\mu)\nabla\Delta\phi_w = \mathcal{L}^{\lambda,\mu}\mathcal{H}^s[w],$$

and

$$\mathcal{H}^p[\mathcal{L}^{\lambda,\mu}w] = \mu\nabla \times \Delta\psi_w = \mathcal{L}^{\lambda,\mu}\mathcal{H}^p[w]$$

as desired.   □

It is worth emphasizing that in the exterior (unbounded) domain $\mathbb{R}^d \setminus \overline{\Omega}$ or in the free space $\mathbb{R}^d$, the Helmholtz decomposition (3.129) stays valid with $W^{1,2}(\Omega)$ replaced by $\{v \in L^2_{\mathrm{loc}} : \nabla v \in L^2\}$; see, for instance, [177, 163].

In the time-harmonic regime, if the medium is infinite, then the irrotational and solenoidal fields solve two separate Helmholtz equations with different wavenumbers. As will be shown in the next section, radiation conditions should be imposed in order to select the physical solutions. The irrotational field is called compressional wave (p-wave) and the solenoidal field is called shear wave (s-wave). The displacement field associated with the p-wave is in the same direction as the wave propagates while the displacement field associated with the s-wave propagates orthogonally to the direction of propagation of the wave. Note that, in three dimensions, the s-wave has two directions of oscillations. Note also that if the medium is bounded, then the p- and s-waves are coupled by the boundary conditions at the boundary of the medium.

Let the wave numbers κ_s and κ_p be given by

$$\kappa_s = \frac{\omega}{c_s} \quad \text{and} \quad \kappa_p = \frac{\omega}{c_p}, \tag{3.135}$$

where c_s is the wave velocity for shear waves and c_p is the wave velocity for compressive waves:

$$c_s = \sqrt{\frac{\mu}{\rho}} \quad \text{and} \quad c_p = \sqrt{\frac{\lambda + 2\mu}{\rho}}. \tag{3.136}$$

The α-wave, $\alpha = p, s$, propagates with a wave number κ_α, through space and the corresponding wave velocity is given by c_α. Note that if $\lambda > 0$, then c_p is larger than c_s provided that (3.121) holds. This means that the p-wave arrives faster than the s-wave in the time domain.

Finally, it is worth mentioning that by antiplane elasticity equation we mean the conductivity equation $\nabla \cdot \mu\nabla u_3 = 0$, where u_3 is the x_3-component of the displacement field u in three dimensions. When the elastic material is invariant under the transformation $x_3 \to -x_3$, the equations of linearized elasticity can be reduced to the antiplane elasticity equation.

3.3.1 Radiation Condition

Let us formulate the *radiation condition* for the time-harmonic elastic waves when Im $\omega \geq 0$ and $\omega \neq 0$.

Since $\mathcal{H}^s$ and $\mathcal{H}^p$ commute with $\mathcal{L}^{\lambda,\mu}$, as shown in Lemma 3.43, it follows from the Helmholtz decomposition (3.129) that any smooth solution u to the constant-coefficient equation $(\mathcal{L}^{\lambda,\mu}+\omega^2\rho)u = 0$ can be decomposed as follows:

$$u = u_p + u_s, \tag{3.137}$$

where u_p and u_s satisfy the equations

$$\begin{cases} (\triangle + \kappa_p^2)u_p = 0, & \nabla \times u_p = 0, \\ (\triangle + \kappa_s^2)u_s = 0, & \nabla \cdot u_s = 0. \end{cases} \tag{3.138}$$

In fact, u_p and u_s are given by $u_p = \mathcal{H}^p[u]$ and $u_s = \mathcal{H}^s[u]$.

In order to select the physical solutions, we impose on u_p and u_s the radiation condition for solutions of the Helmholtz equation by requiring, as $r = |x| \to +\infty$, that

$$\begin{cases} \partial_r u_p(x) - i\kappa_p u_p(x) = O(r^{-(d+1)/2}), \\ \partial_r u_s(x) - i\kappa_s u_s(x) = O(r^{-(d+1)/2}). \end{cases} \tag{3.139}$$

We say that u satisfies the Sommerfeld-Kupradze radiation condition if it can be decomposed in the form (3.137) with u_p and u_s satisfying (3.138) and (3.139).

We recall the following uniqueness results for the exterior problem [235].

Lemma 3.44 (Uniqueness result) *Let u be a solution to $(\mathcal{L}^{\lambda,\mu}+\omega^2\rho)u = 0$ in $\mathbb{R}^d \setminus \overline{\Omega}$ satisfying the Sommerfeld-Kupradze radiation condition (3.139). If either $u = 0$ or $\partial u/\partial n = 0$ on $\partial\Omega$, then u is identically zero in $\mathbb{R}^d \setminus \overline{\Omega}$.*

3.3.2 Integral Representation of Solutions to the Lamé System

Fundamental Solutions

In dimension d, the Kupradze matrix $\Gamma^\omega = (\Gamma_{jl}^\omega)_{j,l=1}^d$ of the fundamental solution to the operator $\mathcal{L}^{\lambda,\mu} + \omega^2\rho$ satisfies

$$(\mathcal{L}^{\lambda,\mu} + \omega^2\rho)\Gamma^\omega(x - y) = \delta_y(x)I, \qquad x \in \mathbb{R}^d, x \neq y, \tag{3.140}$$

where δ_y is the Dirac mass at y and I is the $d \times d$ identity matrix. The function Γ^ω can be decomposed into shear and pressure components:

$$\Gamma^\omega(x) = \Gamma_s^\omega(x) + \Gamma_p^\omega(x), \quad x \in \mathbb{R}^d, \quad x \neq 0, \tag{3.141}$$

where

$$\Gamma_p^\omega(x) = -\frac{1}{\mu\kappa_s^2}D\Gamma_p^\omega(x) \quad \text{and} \quad \Gamma_s^\omega(x) = \frac{1}{\mu\kappa_s^2}(\kappa_s^2 I + D)\Gamma_s^\omega(x). \tag{3.142}$$

Here, the tensor D is defined by

$$D = \nabla \otimes \nabla = (\partial_{jl}^2)_{j,l=1}^d, \tag{3.143}$$

where the function Γ_α^ω is the fundamental solution to the Helmholtz operator, i.e.,

$$(\Delta + \kappa_\alpha^2)\Gamma_\alpha^\omega(x) = \delta_0(x), \quad x \in \mathbb{R}^d, x \neq 0,$$

subject to the Sommerfeld radiation condition:

$$\partial_r \Gamma_\alpha^\omega(x) - i\kappa_\alpha \Gamma_\alpha^\omega(x) = O(r^{-(d+1)/2}) \quad \text{as } r = |x| \to +\infty.$$

Note that $\nabla \cdot \Gamma_s^\omega = 0$ and $\nabla \times \Gamma_p^\omega = 0$. Moreover, Γ^ω satisfies the Sommerfeld-Kupradze radiation condition (3.139). Here, the vector field $\nabla \cdot \Gamma_s^\omega$ and the matrix field $\nabla \times \Gamma_p^\omega$ are defined by

$$\begin{cases} (\nabla \cdot \Gamma_s^\omega)q = \nabla \cdot (\Gamma_s^\omega q), \\ (\nabla \times \Gamma_p^\omega)q = \nabla \times (\Gamma_p^\omega q) \end{cases}$$

for all $q \in \mathbb{R}^d$.

The function Γ_α^ω, for $\alpha = p, s$, is given by

$$\Gamma_\alpha^\omega(x) = \begin{cases} -\dfrac{i}{4}H_0^{(1)}(\kappa_\alpha|x|), & d = 2, \\ -\dfrac{e^{i\kappa_\alpha|x|}}{4\pi|x|}, & d = 3, \end{cases} \tag{3.144}$$

where $H_0^{(1)}$ is the Hankel function of the first kind of order 0. We recall the following behavior of the Hankel function near 0:

$$-\frac{i}{4}H_0^{(1)}(\kappa_\alpha|x|) = \frac{1}{2\pi}\log(\kappa_\alpha|x|) + \tau + \sum_{n=1}^{+\infty}(b_n \log(\kappa_\alpha|x|) + c_n)(\kappa_\alpha|x|)^{2n} \tag{3.145}$$

for $\alpha = p, s$, where

$$b_n = \frac{(-1)^n}{2\pi}\frac{1}{2^{2n}(n!)^2}, \quad c_n = -b_n\left(\gamma - \log 2 - \frac{\pi i}{2} - \sum_{j=1}^n \frac{1}{j}\right),$$

and the constant $\tau = (1/2\pi)(\gamma - \log 2) - i/4$, γ being the Euler constant. Moreover, as $t \to +\infty$, we have

$$\begin{aligned}
H_0^{(1)}(t) &= \sqrt{\frac{2}{\pi t}}e^{i(t-\frac{\pi}{4})}\left[1 + O\left(\frac{1}{t}\right)\right], \\
\frac{d}{dt}H_0^{(1)}(t) &= \sqrt{\frac{2}{\pi t}}e^{i(t+\frac{\pi}{4})}\left[1 + O\left(\frac{1}{t}\right)\right].
\end{aligned} \tag{3.146}$$

Using (3.146), one can see that in the two-dimensional case

$$\hat{x} \cdot \nabla H_0^{(1)}(\kappa_\alpha |x|) - i\kappa_\alpha H_0^{(1)}(\kappa_\alpha |x|) = O(|x|^{-3/2}), \qquad (3.147)$$

where $\hat{x} := x/|x|$. This is exactly the two-dimensional Sommerfeld radiation condition one should impose in order to select the physical solution of the Helmholtz equation.

In the three-dimensional case, the Kupradze matrix $\Gamma^\omega = (\Gamma_{jl}^\omega)_{j,l=1}^3$ is given by

$$\Gamma_{jl}^\omega(x) = -\frac{\delta_{jl}}{4\pi\mu|x|} e^{i\kappa_s|x|} + \frac{1}{4\pi\omega^2\rho} \partial_j\partial_l \frac{e^{i\kappa_p|x|} - e^{i\kappa_s|x|}}{|x|}, \qquad (3.148)$$

where κ_α, $\alpha = p, s$, is given by (3.135). One can easily show that Γ_{jl}^ω has the series representation:

$$\Gamma_{jl}^\omega(x) = -\frac{1}{4\pi} \sum_{n=0}^{+\infty} \frac{i^n}{(n+2)n!} \left(\frac{n+1}{c_s^{n+2}} + \frac{1}{c_p^{n+2}} \right) \omega^n \delta_{jl} |x|^{n-1} \qquad (3.149)$$

$$+ \frac{1}{4\pi\rho} \sum_{n=0}^{+\infty} \frac{i^n(n-1)}{(n+2)n!} \left(\frac{1}{c_s^{n+2}} - \frac{1}{c_p^{n+2}} \right) \omega^n |x|^{n-3} x_j x_l .$$

If $\omega = 0$, then $\Gamma := \Gamma^0$ is the Kelvin matrix of the fundamental solution to the Lamé system; *i.e.*,

$$\Gamma_{jl}(x) = -\frac{\gamma_1}{4\pi} \frac{\delta_{jl}}{|x|} - \frac{\gamma_2}{4\pi} \frac{x_j x_l}{|x|^3}, \qquad (3.150)$$

where

$$\gamma_1 = \frac{1}{2}\left(\frac{1}{\mu} + \frac{1}{2\mu+\lambda} \right) \quad \text{and} \quad \gamma_2 = \frac{1}{2}\left(\frac{1}{\mu} - \frac{1}{2\mu+\lambda} \right). \qquad (3.151)$$

In the two-dimensional case, the Kupradze matrix $\Gamma^\omega = (\Gamma_{jl}^\omega)_{j,l=1}^2$ of the fundamental solution to the operator $\mathcal{L}^{\lambda,\mu} + \omega^2\rho$, $\omega \neq 0$, is given by

$$\Gamma_{ij}^\omega(x) = -\frac{i}{4\mu}\delta_{jl} H_0^{(1)}(\kappa_s|x|) + \frac{i}{4\omega^2\rho} \partial_j\partial_l \left(H_0^{(1)}(\kappa_p|x|) - H_0^{(1)}(\kappa_s|x|) \right).$$
$$(3.152)$$

For $\omega = 0$, we set Γ to be the Kelvin matrix of fundamental solutions to the Lamé system; *i.e.*,

$$\Gamma_{jl}(x) = \frac{\gamma_1}{2\pi}\delta_{jl} \log|x| - \frac{\gamma_2}{2\pi} \frac{x_j x_l}{|x|^2}. \qquad (3.153)$$

Single- and Double-Layer Potentials

Let Ω be a bounded domain in $\mathbb{R}^d$, $d = 2, 3$, with a connected smooth boundary. The single- and double-layer potentials for the operator $\mathcal{L}^{\lambda,\mu} + \omega^2 \rho$ are given by

$$\mathcal{S}_\Omega^\omega[\varphi](x) = \int_{\partial\Omega} \Gamma^\omega(x - y)\varphi(y)\, d\sigma(y), \quad x \in \mathbb{R}^d, \tag{3.154}$$

$$\mathcal{D}_\Omega^\omega[\varphi](x) = \int_{\partial\Omega} \frac{\partial\Gamma^\omega}{\partial n(y)}(x - y)\varphi(y)\, d\sigma(y), \quad x \in \mathbb{R}^d \setminus \partial\Omega, \tag{3.155}$$

for $\varphi \in L^2(\partial\Omega)^d$, where $\partial/\partial n$ denotes the conormal derivative defined in (3.123). Thus, for $j = 1, \ldots, d$,

$$(\mathcal{D}_\Omega^\omega[\varphi](x))_j = \int_{\partial\Omega} \lambda \frac{\partial\Gamma_{jl}^\omega}{\partial y_l}(x - y)\varphi(y) \cdot \nu(y)$$
$$+ \mu\Big(\frac{\partial\Gamma_{jl}^\omega}{\partial y_k} + \frac{\partial\Gamma_{jk}^\omega}{\partial y_l}\Big)(x - y)\nu_l(y)\varphi_k(y)\, d\sigma(y).$$

The following formulas give the jump relations satisfied by the conormal derivative of the single-layer potential and by the double-layer potential:

$$\frac{\partial(\mathcal{S}_\Omega^\omega[\varphi])}{\partial n}\Big|_\pm(x) = \Big(\pm \frac{1}{2}I + (\mathcal{K}_\Omega^\omega)^* \Big)[\varphi](x) \quad \text{a.e. } x \in \partial\Omega, \tag{3.156}$$

$$(\mathcal{D}_\Omega^\omega[\varphi])\Big|_\pm(x) = \Big(\mp \frac{1}{2}I + \mathcal{K}_\Omega^\omega \Big)[\varphi](x) \quad \text{a.e. } x \in \partial\Omega, \tag{3.157}$$

where $\mathcal{K}_\Omega^\omega$ is the operator defined by

$$\mathcal{K}_\Omega^\omega[\varphi](x) = \text{p.v.} \int_{\partial\Omega} \frac{\partial\Gamma^\omega}{\partial n(y)}(x - y)\varphi(y)\, d\sigma(y) \tag{3.158}$$

and $(\mathcal{K}_\Omega^\omega)^*$ is the L^2-adjoint of $\mathcal{K}_\Omega^{-\omega}$; that is,

$$(\mathcal{K}_\Omega^\omega)^*[\varphi](x) = \text{p.v.} \int_{\partial\Omega} \frac{\partial\Gamma^\omega}{\partial n(x)}(x - y)\varphi(y)\, d\sigma(y).$$

The operators $(\mathcal{K}_\Omega^\omega)^*$ and $\mathcal{K}_\Omega^\omega$ are called the Neumann-Poincaré operators.

By a straightforward calculation, one can see that the single- and double-layer potentials, $\mathcal{S}_\Omega^\omega[\varphi]$ and $\mathcal{D}_\Omega^\omega[\varphi]$ for $\varphi \in L^2(\partial\Omega)^d$, satisfy the time-harmonic elasticity equation in Ω and $\mathbb{R}^d \setminus \overline{\Omega}$ together with the Sommerfeld-Kupradze radiation condition (3.139).

Let $\mathcal{S}_\Omega$, $\mathcal{D}_\Omega$, $(\mathcal{K}_\Omega)^*$, and $\mathcal{K}_\Omega$ be the layer potentials for the operator $\mathcal{L}^{\lambda,\mu}$. Analogously to (3.156) and (3.157), the following formulas give the jump relations obeyed by $\mathcal{D}_\Omega[\varphi]$ and by $\partial(\mathcal{S}_\Omega[\varphi])/\partial n$ on $\partial\Omega$ for $\varphi \in L^2(\partial\Omega)^d$:

$$\frac{\partial(\mathcal{S}_\Omega[\varphi])}{\partial n}\Big|_\pm(x) = \Big(\pm \frac{1}{2}I + (\mathcal{K}_\Omega)^* \Big)[\varphi](x) \quad \text{a.e. } x \in \partial\Omega, \tag{3.159}$$

$$(\mathcal{D}_\Omega[\varphi])\Big|_\pm(x) = \Big(\mp \frac{1}{2}I + \mathcal{K}_\Omega \Big)[\varphi](x) \quad \text{a.e. } x \in \partial\Omega. \tag{3.160}$$

Again, the layer potentials $\mathcal{S}_\Omega[\varphi]$, $\mathcal{D}_\Omega[\varphi]$ for $\varphi \in L^2(\partial\Omega)^d$ satisfy

$$\mathcal{L}^{\lambda,\mu}\mathcal{S}_\Omega[\varphi] = \mathcal{L}^{\lambda,\mu}\mathcal{D}_\Omega[\varphi] = 0 \quad \text{in } \Omega \cup (\mathbb{R}^d \setminus \overline{\Omega}).$$

We emphasize that the singular integral operators $\mathcal{K}_\Omega$ and $\mathcal{K}_\Omega^\omega$ are not compact, even on smooth domains. This causes some difficulties in solving the elasticity system using layer potential techniques.

Let Ψ be the vector space of all linear solutions to the equation $\mathcal{L}^{\lambda,\mu}u = 0$ satisfying $\partial u/\partial n = 0$ on $\partial\Omega$, or, equivalently,

$$\begin{aligned}
\Psi &= \left\{ \psi \in W^{1,2}(\Omega)^d : \partial_j\psi_l + \partial_l\psi_j = 0,\ 1 \le j,l \le d \right\}, \\
&= \left\{ \psi(x) = a + Bx, a \in \mathbb{C}^d, B \in M_d^A \right\},
\end{aligned} \tag{3.161}$$

where M_d^A is the space of antisymmetric matrices. One has

$$\dim \Psi = d(d+1)/2.$$

Define a subspace of $L^2(\partial\Omega)^d$ by

$$L_\Psi^2(\partial\Omega) = \left\{ f \in L^2(\partial\Omega)^d : \int_{\partial\Omega} \overline{f} \cdot \psi \, d\sigma = 0 \ \forall \ \psi \in \Psi \right\}. \tag{3.162}$$

In particular, since Ψ contains constant functions, we get

$$\int_{\partial\Omega} f \, d\sigma = 0$$

for any $f \in L_\Psi^2(\partial\Omega)$.

Define

$$W_\Psi^{-1/2}(\partial\Omega) := \left\{ \varphi \in W_{-1/2}^2(\partial\Omega)^d : (\varphi, \psi)_{-1/2,1/2} = 0 \ \forall \ \psi \in \Psi \right\}. \tag{3.163}$$

Then the following result holds.

Lemma 3.45 (Mapping properties of $\mathcal{K}_\Omega^*$) *The operator $\pm\frac{1}{2}I + \mathcal{K}_\Omega^*$ is invertible on $W_\Psi^{-1/2}(\partial\Omega)$. Moreover, there exists a positive constant C such that*

$$\|\mathcal{S}_\Omega[\varphi]\|_{W(\mathbb{R}^d)} \le C\|\varphi\|_{W_{-1/2}^2(\partial\Omega)} \tag{3.164}$$

for all $\varphi \in W_{-1/2}^2(\partial\Omega)^d$. Furthermore, the null space of $-\frac{1}{2}I + \mathcal{K}_\Omega$ on $W_{-1/2}^2(\partial\Omega)$ is Ψ.

The following invertibility results will be also needed.

Lemma 3.46 (Mapping properties of $(\mathcal{K}_\Omega^\omega)^*$) *The operator $\frac{1}{2}I + (\mathcal{K}_\Omega^\omega)^*$ is invertible on $W_{-1/2}^2(\partial\Omega)^d$. If $\omega^2\rho$ is not a Dirichlet eigenvalue for $-\mathcal{L}^{\lambda,\mu}$ on Ω, then $-\frac{1}{2}I + (\mathcal{K}_\Omega^\omega)^*$ is invertible on $W_{-1/2}^2(\partial\Omega)^d$ as well.*

Next, we recall Green's formulas for the Lamé system, which can be obtained by integration by parts. The first formula is

$$\int_{\partial\Omega} \overline{u} \cdot \frac{\partial v}{\partial n}\, d\sigma = \int_{\Omega} \overline{u} \cdot \mathcal{L}^{\lambda,\mu} v\, dx + Q(u,v), \qquad (3.165)$$

where $u \in W^{1,2}(\Omega)^d$, $v \in W^{3/2,2}(\Omega)^d$, and

$$Q(u,v) = \int_{\Omega} \left(\lambda(\overline{\nabla \cdot u})(\nabla \cdot v) + 2\mu \overline{\nabla^s u} : \nabla^s v \right) dx. \qquad (3.166)$$

Here and throughout this book $A : B = \sum_{j,l=1}^{d} a_{jl} b_{jl}$ for matrices $A = (a_{jl})$ and $B = (b_{jl})$.

The strong convexity condition (3.121) shows that the quadratic form

$$u \mapsto Q(u,u)$$

is positive definite. Note that $W^{1,2}(\Omega)^d$ is the closure of this quadratic form since $u \mapsto \nabla^s u$ is elliptic of order 1.

Formula (3.165) yields Green's second formula

$$\int_{\partial\Omega} \left(\overline{u} \cdot \frac{\partial v}{\partial n} - v \cdot \overline{\frac{\partial u}{\partial n}} \right) d\sigma(x) = \int_{\Omega} \left(\overline{u} \cdot \mathcal{L}^{\lambda,\mu} v - v \cdot \overline{\mathcal{L}^{\lambda,\mu} u} \right) dx \qquad (3.167)$$

for $u, v \in W^{3/2,2}(\Omega)^d$.

Formula (3.167) shows that if $u \in W^{3/2,2}(\Omega)^d$ satisfies $\mathcal{L}^{\lambda,\mu} u = 0$ in Ω, then $\partial u/\partial n|_{\partial\Omega} \in L^2_\Psi(\partial\Omega)$.

The following formulation of Korn's inequality will be of interest to us.

Lemma 3.47 (Korn's inequality) *Let Ω be a bounded smooth domain in $\mathbb{R}^d$. Let $u \in W^{1,2}(\Omega)^d$ satisfy*

$$\int_{\Omega} \left(\overline{u} \cdot \psi + \overline{\nabla u} : \nabla \psi \right) dx = 0 \quad \text{for all } \psi \in \Psi. \qquad (3.168)$$

Then there is a constant C depending only on the Lipschitz character of Ω such that

$$\int_{\Omega} \left(|u|^2 + |\nabla u|^2 \right) dx \le C \int_{D} |\nabla^s u|^2\, dx. \qquad (3.169)$$

Here, $|\nabla u|^2 = \overline{\nabla u} : \nabla u$ and $|\nabla^s u|^2 = \overline{\nabla^s u} : \nabla^s u$.

Finally, using Green's formulas one can prove that $-\mathcal{S}_\Omega$ is positive.

Lemma 3.48 *The operator $-\mathcal{S}_\Omega : L^2(\partial\Omega)^d \to L^2(\partial\Omega)^d$ is positive and self-adjoint.*

Transmission Problem

In this subsection we consider a smooth bounded inclusion D with Lamé parameters $\widetilde{\lambda}, \widetilde{\mu}$ different from those λ and μ of the background medium. We assume that the pair of Lamé parameters $\widetilde{\lambda}, \widetilde{\mu}$ satisfy the strong convexity condition (3.121) and is such that

$$(\lambda - \widetilde{\lambda})(\mu - \widetilde{\mu}) \geq 0, \quad (\lambda - \widetilde{\lambda})^2 + (\mu - \widetilde{\mu})^2 \neq 0. \qquad (3.170)$$

Let $\widetilde{\mathcal{S}}_D^\omega$ denote the single-layer potential defined by (3.154) with λ, μ replaced by $\widetilde{\lambda}, \widetilde{\mu}$. We also denote by $\partial u/\partial\widetilde{n}$ the conormal derivative associated with $\widetilde{\lambda}, \widetilde{\mu}$. We now have the following solvability result which can be viewed as a compact perturbation result of the case $\omega = 0$.

Theorem 3.49 *Let D be a smooth bounded domain in $\mathbb{R}^d$. Suppose that $(\lambda - \widetilde{\lambda})(\mu - \widetilde{\mu}) \geq 0$ and $0 < \widetilde{\lambda}, \widetilde{\mu} < +\infty$. Suppose that $\Im\omega \geq 0$ and $\omega^2\rho$ is not a Dirichlet eigenvalue for $-\mathcal{L}^{\lambda,\mu}$ on D. For any given $(F, G) \in W^{1,2}(\partial D)^d \times L^2(\partial D)^d$, there exists a unique pair $(f, g) \in L^2(\partial D)^d \times L^2(\partial D)^d$ such that*

$$\begin{cases} \widetilde{\mathcal{S}}_D^\omega[f]|_- - \mathcal{S}_D^\omega[g]|_+ = F, \\ \dfrac{\partial}{\partial\widetilde{n}}\widetilde{\mathcal{S}}_D^\omega[f]\Big|_- - \dfrac{\partial}{\partial n}\mathcal{S}_D^\omega[g]\Big|_+ = G. \end{cases}$$

A positive constant C exists such that

$$||f||_{L^2(\partial D)^d} + ||g||_{L^2(\partial D)^d} \leq C\bigg(||F||_{W^{1,2}(\partial D)^d} + ||G||_{L^2(\partial D)^d} \bigg). \qquad (3.171)$$

Moreover, if $\omega = 0$ and $G \in L_\Psi^2(\partial D)$, then $g \in L_\Psi^2(\partial D)$.

Consider the following transmission problem:

$$\begin{cases} \mathcal{L}^{\lambda,\mu}u + \omega^2\rho u = 0 & \text{in } \Omega \setminus \overline{D}, \\ \mathcal{L}^{\widetilde{\lambda},\widetilde{\mu}}u + \omega^2\rho u = 0 & \text{in } D, \\ \dfrac{\partial u}{\partial n} = g & \text{on } \partial\Omega, \\ u\big|_+ - u\big|_- = 0 & \text{on } \partial D, \\ \dfrac{\partial u}{\partial n}\big|_+ - \dfrac{\partial u}{\partial\widetilde{n}}\big|_- = 0 & \text{on } \partial D, \end{cases} \qquad (3.172)$$

where D and Ω are smooth bounded domains in $\mathbb{R}^d$ with $\overline{D} \subset \Omega$. Note that the p- and s-waves cannot be decoupled because of the boundary and transmission conditions.

For problem (3.172) the following representation formula holds.

Theorem 3.50 (Representation formula) *Let $\Im\omega \geq 0$. Suppose that $\omega^2\rho$ is not a Dirichlet eigenvalue for $-\mathcal{L}^{\lambda,\mu}$ on D. Let u be a solution of (3.172) and $f := u|_{\partial\Omega}$. Define*

$$H(x) := \mathcal{D}_\Omega^\omega[f](x) - \mathcal{S}_\Omega^\omega[g](x), \quad x \in \mathbb{R}^d \setminus \partial\Omega. \qquad (3.173)$$

Then u can be represented as

$$u(x) = \begin{cases} H(x) + \mathcal{S}_D^\omega[\psi](x), & x \in \Omega \setminus \overline{D}, \\ \widetilde{\mathcal{S}}_D^\omega[\varphi](x), & x \in D, \end{cases} \qquad (3.174)$$

where the pair $(\varphi, \psi) \in L^2(\partial D)^d \times L^2(\partial D)^d$ is the unique solution of

$$\begin{cases} \widetilde{\mathcal{S}}_D^\omega[\varphi] - \mathcal{S}_D^\omega[\psi] = H|_{\partial D}, \\ \dfrac{\partial}{\partial\widetilde{n}}\widetilde{\mathcal{S}}_D^\omega[\varphi] - \dfrac{\partial}{\partial n}\mathcal{S}_D^\omega[\psi] = \dfrac{\partial H}{\partial n}\Big|_{\partial D}. \end{cases} \qquad (3.175)$$

Moreover, we have

$$H(x) + \mathcal{S}_D^\omega[\psi](x) = 0, \quad x \in \mathbb{R}^d \setminus \overline{\Omega}. \qquad (3.176)$$

3.3.3 Reciprocity Property and Helmholtz-Kirchhoff Identities

We now discuss the reciprocity property and derive the Helmholtz-Kirchhoff identities for elastic media.

Note first that the conormal derivative tensor $\partial\Gamma^\omega/\partial n$ means that for all constant vectors q,

$$\left[\frac{\partial\Gamma^\omega}{\partial n}\right] q := \frac{\partial\left[\Gamma^\omega q\right]}{\partial n}.$$

From now on, we set $\Gamma^\omega(x, y) := \Gamma^\omega(x - y)$ for $x \neq y$.

An important property satisfied by the fundamental solution Γ^ω is the reciprocity property. If the medium is not homogeneous, then the following holds:

$$\Gamma^\omega(y, x) = \left[\Gamma^\omega(x, y)\right]^T, \quad x \neq y. \qquad (3.177)$$

If the medium is homogeneous, then one can see from (3.148) and (3.152) that $\Gamma^\omega(x, y)$ is symmetric and

$$\Gamma^\omega(y, x) = \Gamma^\omega(x, y), \quad x \neq y. \qquad (3.178)$$

Identity (3.177) states that the nth component of the displacement at x due to a point source excitation at y in the mth direction is identical to the mth component of the displacement at y due to a point source excitation at x in the nth direction.

The following results are the building block of the resolution analysis in elasticity imaging.

Proposition 3.51 *Let Ω be a bounded smooth domain.*

(i) For all $x, z \in \Omega$, we have

$$\int_{\partial\Omega} \left[\frac{\partial \Gamma^\omega(x, y)}{\partial n(y)} \overline{\Gamma}_\omega(y, z) - \Gamma^\omega(x, y) \frac{\partial \overline{\Gamma}^\omega(y, z)}{\partial n(y)} \right] d\sigma(y) = -2i\Im m \left\{ \Gamma^\omega(x, z) \right\}.$$
(3.179)

(ii) For all $x, z \in \Omega$, we have

$$\int_{\partial\Omega} \left[\frac{\partial \Gamma_s^\omega(x, y)}{\partial n(y)} \overline{\Gamma_p^\omega}(y, z) - \Gamma_s^\omega(x, y) \frac{\partial \overline{\Gamma_p^\omega}(y, z)}{\partial n(y)} \right] d\sigma(y) = 0. \qquad (3.180)$$

(iii) For all $x, z \in \Omega$ and $\alpha = p, s$,

$$\int_{\partial\Omega} \left[\frac{\partial \Gamma_\alpha^\omega(x, y)}{\partial n(y)} \overline{\Gamma_\alpha^\omega}(y, z) - \Gamma_\alpha^\omega(x, y) \frac{\partial \overline{\Gamma_\alpha^\omega}(y, z)}{\partial n(y)} \right] d\sigma(y) = -2i\Im m \left\{ \Gamma_\alpha^\omega(x, z) \right\}.$$
(3.181)

In order to simplify Helmholtz-Kirchhoff identities , we derive an approximation of the conormal derivative

$$\partial \Gamma^\omega(x, y) / \partial n(y), \quad y \in \partial\Omega, x \in \Omega,$$

when Ω is a ball with very large radius

If $\nu(y) = \widehat{y - x}$ ($:= (y - x)/|x - y|$) and $|x - y| \gg 1$, then, for $\alpha = p, s$, we have

$$\frac{\partial \Gamma_\alpha^\omega(x, y)}{\partial n} = i\omega c_\alpha \Gamma_\alpha^\omega(x, y) + o\left(\frac{1}{|x - y|^{(d-1)/2}} \right), \qquad (3.182)$$

and the following result holds.

Proposition 3.52 (Helmholtz-Kirchhoff Identities) *Let $\Omega \subset \mathbb{R}^d$ be a ball with radius R. Then, for all $x, z \in \Omega$, we have*

$$\lim_{R \to +\infty} \int_{\partial\Omega} \Gamma_\alpha^\omega(x, y) \overline{\Gamma_\alpha^\omega}(y, z) d\sigma(y) = -\frac{1}{\omega c_\alpha} \Im m \left\{ \Gamma_\alpha^\omega(x, z) \right\}, \; \alpha = p, s, \quad (3.183)$$

and

$$\lim_{R \to +\infty} \int_{\partial\Omega} \Gamma_s^\omega(x, y) \overline{\Gamma_p^\omega}(y, z) d\sigma(y) = 0. \qquad (3.184)$$

3.3.4 Incompressible Limit

Let D be an elastic inclusion which is a bounded domain in $\mathbb{R}^d$ ($d = 2, 3$) with smooth boundary. Let $(\widetilde{\lambda}, \widetilde{\mu})$ be the pair of Lamé parameters of D while (λ, μ) is that of the background $\mathbb{R}^d \setminus D$. Then the elasticity tensors for the inclusion and the background can be written respectively as $\widetilde{\mathbb{C}} = (\widetilde{C}_{jklm})$ and

$\mathbb{C} = (C_{jklm})$ where $\widetilde{C}_{jklm}$ and C_{jklm} are defined according to (3.125) and the elasticity tensor for $\mathbb{R}^d$ in the presence of the inclusion D is given by

$$\chi(D)\widetilde{\mathbb{C}} + \chi(\mathbb{R}^d \setminus \overline{D})\mathbb{C}. \tag{3.185}$$

We assume that the strong convexity conditions (3.121) and (3.170) hold for the pairs (λ, μ) and $(\widetilde{\lambda}, \widetilde{\mu})$ respectively, that are in turn required to have the representation of the displacement vectors in terms of the single layer potential in what follows. We also denote by $\widetilde{\beta}$ the bulk modulus given by $\widetilde{\beta} = \widetilde{\lambda} + 2\widetilde{\mu}/d$.

We consider the problem of the Lamé system of the linear elasticity: For a given function h satisfying $\nabla \cdot \mathbb{C}\nabla^s h = 0$ in $\mathbb{R}^d$,

$$\begin{cases} \nabla \cdot (\chi(D)\widetilde{\mathbb{C}} + \chi(\mathbb{R}^d \setminus \overline{D})\mathbb{C})\nabla^s u = 0 & \text{in } \mathbb{R}^d, \\ u(x) - h(x) = O(|x|^{1-d}) & \text{as } |x| \to \infty, \end{cases} \tag{3.186}$$

where $\nabla^s u$ is the symmetric gradient (or the strain tensor). Equation (3.186) is equivalent to the following problem:

$$\begin{cases} \mathcal{L}^{\lambda,\mu} u = 0 & \text{in } \mathbb{R}^d \setminus \overline{D}, \\ \mathcal{L}^{\widetilde{\lambda},\widetilde{\mu}} u = 0 & \text{in } D, \\ u|_- = u|_+ & \text{on } \partial D, \\ \left.\dfrac{\partial u}{\partial \widetilde{\nu}}\right|_- = \left.\dfrac{\partial u}{\partial \nu}\right|_+ & \text{on } \partial D, \\ u(x) - h(x) = O(|x|^{1-d}) & \text{as } |x| \to \infty. \end{cases} \tag{3.187}$$

We show that if $\widetilde{\lambda} \to \infty$ and $\widetilde{\mu}$ is fixed, then (3.187) approaches to the Stokes system. Roughly speaking, if $\widetilde{\lambda} \to \infty$, then $\nabla \cdot u$ is approaching to 0 while $\widetilde{\lambda}\nabla \cdot u$ stays bounded. So (3.187) approaches to the Stokes problem.

The following result from [47] holds.

Theorem 3.53 *Suppose that λ and $\widetilde{\lambda}$ go to $+\infty$ with $\widetilde{\lambda}/\lambda = O(1)$. Suppose that $\nabla \cdot h = 0$ in $\mathbb{R}^d$. Let (u_∞, p) be the solution to*

$$\begin{cases} \mu\Delta u_\infty + \nabla p = 0 & \text{in } \mathbb{R}^d \setminus \overline{D}, \\ \widetilde{\mu}\Delta u_\infty + \nabla p = 0 & \text{in } D, \\ u_\infty\big|_- = u_\infty\big|_+ & \text{on } \partial D, \\ \left(p\nu + \widetilde{\mu}\dfrac{\partial u_\infty}{\partial \nu}\right)\Big|_- = \left(p\nu + \mu\dfrac{\partial u_\infty}{\partial \nu}\right)\Big|_+ & \text{on } \partial D, \\ \nabla \cdot u_\infty = 0 & \text{in } \mathbb{R}^d, \\ u_\infty(x) - h(x) = O(|x|^{1-d}) & \text{as } |x| \to +\infty, \\ p(x) = O(|x|^{-d}) & \text{as } |x| \to +\infty, \end{cases} \tag{3.188}$$

where $\partial u_\infty / \partial \nu|_\pm = \nabla^s u_\infty|_\pm \nu$. There exists a positive constant C independent of λ and $\widetilde\lambda$ such that the following error estimate holds for λ and $\widetilde\lambda$ large enough:

$$\left\| u - u_\infty \right\|_{W(\mathbb{R}^d)} \le \frac{C}{\sqrt\lambda} \left\| \frac{\partial h}{\partial \nu} \right\|_{W^2_{-1/2}(\partial D)}, \tag{3.189}$$

where $W(\mathbb{R}^d)$ is defined by (2.29).

Equations (3.188) are the linearized equations of incompressible fluids or the Stokes system. Existence and uniqueness of a solution to (3.188) can be proved using layer potential techniques; see [47]. We refer the reader to [161, 162] for a unique continuation and regularity results for (3.188).

A complete asymptotic expansion can be constructed. For doing so, let u_j for $j \ge 1$ be defined by

$$\begin{cases} \mu \Delta u_j + \nabla p_j + \mu \nabla p_{j-1} = 0 & \text{in } \mathbb{R}^d \setminus \overline{D}, \\ \widetilde\mu \Delta u_j + \nabla p_j + \widetilde\mu \nabla p_{j-1} = 0 & \text{in } D, \\ u_j\big|_- = \left(\dfrac{\widetilde\lambda}{\lambda}\right)^j u_j\big|_+ & \text{on } \partial D, \\ \left(\dfrac{\widetilde\lambda}{\lambda}\right)^j \left(p_j\big|_+ \nu + \mu \dfrac{\partial u_j}{\partial \nu}\Big|_+ \right) - \left(p_j\big|_- \nu + \widetilde\mu \dfrac{\partial u_j}{\partial \nu}\Big|_- \right) = 0 & \text{on } \partial D, \\ \nabla \cdot u_j = p_{j-1} & \text{in } \mathbb{R}^d, \\ u_j(x) = O(|x|^{1-d}) & \text{as } |x| \to +\infty, \\ p_j(x) = O(|x|^{-d}) & \text{as } |x| \to +\infty. \end{cases} \tag{3.190}$$

Here, $p_0 = p$ given by (3.188). Equations (3.190) are nonhomogeneous. In [47], the following theorem is proved.

Theorem 3.54 *There exists a positive constant C independent of λ and $\widetilde\lambda$ such that the following error estimate holds for λ and $\widetilde\lambda$ large enough and for all integers J:*

$$\left\| u - u_\infty - \sum_{j=1}^J \left(\frac{1}{\lambda^j} \chi(\mathbb{R}^d \setminus D) + \frac{1}{\widetilde\lambda^j} \chi(D) \right) u_j \right\|_{W(\mathbb{R}^d)} \le C \left(\frac{1}{\lambda^{J+\frac12}} + \frac{1}{\widetilde\lambda^{J+\frac12}} \right) \left\| \frac{\partial h}{\partial \nu} \right\|_{W^2_{-1/2}(\partial D)}. \tag{3.191}$$

4

Probabilistic Tools

In this chapter we introduce useful probabilistic tools for imaging in the presence of noise. In particular, we examine image characteristics with respect to various data acquisition and processing schemes. We focus specifically on issues related to image resolution, signal-to-noise ratio, and image artifacts.

The noise models discussed in this book are measurement and medium (or cluttered) noises. They affect the stability and resolution of the imaging functionals in very different ways.

Imaging involves measurement and processing of activated signals emanating from an object. Any practical measurement always contains an undesirable component that is uncorrelated with (*i.e.*, independent of) the desired signal. This component is referred to as measurement noise. On the other hand, medium noise models the uncertainty in the physical parameters of the background medium. In many practical situations, the physical parameters of the background medium fluctuate spatially around a known background. Of great concern in imaging is the question of how measurement and medium noises are modeled and how the imaging process handles them-that is, whether they are suppressed or amplified. We give in this section an introduction to probability theory that provides the basic tools for modeling imaging schemes with waves in the presence of noise.

4.1 Random Variables

A characteristic of measurement noise is that it does not have fixed values in repeated measurements. Such a quantity is described by a random variable. The statistical distribution of a continuous random variable can be characterized by its probability density function (PDF). The PDF of a (real-valued) random variable ξ is often denoted by $p_\xi(x)$, which represents the probability density of obtaining a specific value x for ξ in a particular measurement:

$$\mathbb{P}(\xi \in [a, b]) = \int_a^b p_\xi(x)dx \ .$$

Note that p_ξ is a nonnegative function whose total integral is equal to one. Given the PDF it is possible to compute the expectation of a nice function (bounded or positive) of the random variable $\phi(\xi)$, which is the weighted average of ϕ with respect to the PDF p_ξ:

$$\mathbb{E}[\phi(\xi)] = \int_\mathbb{R} \phi(x) p_\xi(x) dx \ .$$

The most important expectations are the first- and second-order moments. The mean of the random variable ξ is defined as

$$\mathbb{E}[\xi] = \int x p_\xi(x) \, dx \ .$$

It is the first-order statistical moment. The variance is defined as

$$\mathrm{Var}[\xi] = \mathbb{E}[|\xi - \mathbb{E}[\xi]|^2] = \mathbb{E}[\xi^2] - \mathbb{E}[\xi]^2 \ ,$$

which is a second-order statistical moment. The variable $\sigma_\xi := \sqrt{\mathrm{Var}[\xi]}$ is called the standard deviation, which is a measure of the average deviation from the mean.

The PDF of measurement noise is not always known in practical situations. We often use parameters such as mean and variance to describe it. It is then usual to assume that the noise has Gaussian PDF. This can be justified by the maximum of entropy principle, which assumes that the PDF maximizes the entropy $-\int p_\xi(x) \log p_\xi(x) \, dx$ with the constraints $\int p_\xi(x) dx = 1$, $\int x p_\xi(x) \, dx = x_0$, and $\int (x - x_0)^2 p_\xi(x) dx = \sigma^2$. This PDF is nothing else than the Gaussian PDF

$$p_\xi(x) = \frac{1}{\sqrt{2\pi}\sigma} \exp\left(-\frac{(x - x_0)^2}{2\sigma^2}\right) \ , \tag{4.1}$$

with mean x_0 and variance σ^2. Moreover, the measurement error often results from the cumulative effect of many uncorrelated sources of uncertainty. As a consequence, based on the central limit theorem, most measurement noise can be treated as Gaussian noise. Recall here the central limit theorem: When a random variable ξ is the sum of n independent and identically distributed random variables (with finite variance), then the distribution of ξ is a Gaussian distribution with the appropriate mean and variance in the limit $n \to +\infty$. In terms of PDFs, this means that, if a function $h(x)$ is convolved with itself n times, in the limit $n \to +\infty$, the convolution product is a Gaussian function with a variance that is n times the variance of $h(x)$, provided the area, mean, and variance of $h(x)$ are finite.

The following theorem, which is a consequence of Slutsky's theorem, will be useful.

Theorem 4.1 *Let (ξ_n) and (ζ_n) be sequences of random variables. If ξ_n converges in distribution to a random variable ξ and ζ_n converges in probability to a non zero constant c, then $\zeta_n^{-1}\xi_n$ converges in distribution to $c^{-1}\xi$.*

Throughout this book, if ξ has the PDF (4.1), then we write $\xi \sim \mathcal{N}(x_0, \sigma^2)$ with $\mathcal{N}(x_0, \sigma^2)$ being the normal distribution of mean x_0 and variance σ^2.

4.2 Random Vectors

A d-dimensional random vector ξ is collection of d (real-valued) random variables $(\xi_1, \ldots, \xi_d)^T$. The distribution of a continuous random vector is characterized by the PDF p_ξ:

$$\mathbb{P}(\xi \in [a_1, b_1] \times \cdots \times [a_d, b_d]) = \int_{[a_1, b_1] \times \cdots \times [a_d, b_d]} p_\xi(x) dx, \qquad \forall a_j \le b_j .$$

The vector $\xi = (\xi_1, \ldots, \xi_d)^T$ is independent if its PDF can be written as a product of the one-dimensional PDFs of the components of the vector:

$$p_\xi(x) = \prod_{j=1}^{d} p_{\xi_j}(x_j) \text{ for all } x = (x_1, \ldots, x_d) \in \mathbb{R}^d ,$$

or equivalently,

$$\mathbb{E}\big[\phi_1(\xi_1) \cdots \phi_d(\xi_d)\big] = \mathbb{E}\big[\phi_1(\xi_1)\big] \cdots \mathbb{E}\big[\phi_d(\xi_d)\big], \qquad \forall \phi_1, \ldots, \phi_d \in \mathcal{C}_b(\mathbb{R}, \mathbb{R}) .$$

Here, $\mathcal{C}_b(\mathbb{R}, \mathbb{R})$ denotes the space of all bounded continuous real-valued functions.

Example: a d-dimensional normalized Gaussian random vector ξ has the Gaussian PDF

$$p_\xi(x) = \frac{1}{\sqrt{(2\pi)^d}} \exp(-\frac{|x|^2}{2}) .$$

This PDF can be factorized into the product of one-dimensional Gaussian PDFs, which shows that ξ is a vector of independent random normalized Gaussian variables $(\xi_1, \ldots, \xi_d)^T$.

In the general case, two formulas are of interest. The marginal formula gives the PDF of a subvector extracted from a random vector: If $\begin{pmatrix} \xi_1 \\ \xi_2 \end{pmatrix}$ is a random vector with PDF $p_{\xi_1, \xi_2}(x_1, x_2)$, then ξ_2 is a random vector with PDF

$$p_{\xi_2}(x_2) = \int p_{\xi_1, \xi_2}(x_1, x_2) dx_1 ,$$

since for any test function ϕ we have

$$\mathbb{E}[\phi(\xi_2)] = \iint \phi(x_2) p_{\xi_1, \xi_2}(x_1, x_2) dx_1 dx_2 = \int \phi(x_2) p_{\xi_2}(x_2) dx_2 .$$

The conditioning formula gives the PDF of a subvector extracted from a random vector given the observation of the complementary subvector: If

$\begin{pmatrix} \xi_1 \\ \xi_2 \end{pmatrix}$ is a random vector with PDF $p_{\xi_1, \xi_2}(x_1, x_2)$, then, given $\xi_2 = x_2$, ξ_1 is a random vector with PDF

$$p_{\xi_1}(x_1 | \xi_2 = x_2) = \frac{p_{\xi_1, \xi_2}(x_1, x_2)}{p_{\xi_2}(x_2)} \ . \tag{4.2}$$

Indeed, this can be seen by taking the limit $\delta x_1 \to 0$ and $\delta x_2 \to 0$ in

$$\mathbb{P}(\xi_1 \in [x_1, x_1 + \delta x_1] | \xi_2 \in [x_2, x_2 + \delta x_2])$$
$$= \frac{\mathbb{P}(\xi_1 \in [x_1, x_1 + \delta x_1], \xi_2 \in [x_2, x_2 + \delta x_2])}{\mathbb{P}(\xi_2 \in [x_2, x_2 + \delta x_2])} \approx \frac{p_{\xi_1, \xi_2}(x_1, x_2) \delta x_1 \delta x_2}{p_{\xi_2}(x_2) \delta x_2} \ .$$

It is worth emphasizing that formula (4.2) holds if $p_{\xi_2}(x_2) > 0$, otherwise one defines $p_{\xi_1}(x_1 | \xi_2 = x_2) = p_0(x_1)$, where p_0 is an arbitrary PDF which plays no role.

Of course, if the vectors ξ_1 and ξ_2 are independent, then $p_{\xi_1}(x_1 | \xi_2 = x_2) = p_{\xi_1}(x_1)$ since the knowledge of ξ_2 does not bring any information about ξ_1.

As in the case of random variables, we may not always require or may not be able to give a complete statistical description of a random vector. In such cases, we work only with the first and second statistical moments. Let $\xi = (\xi_i)_{i=1,\dots,d}$ be a random vector. The mean of ξ is the vector $\mu = (\mu_j)_{j=1,\dots,d}$:

$$\mu_j = \mathbb{E}[\xi_j] \ .$$

The covariance matrix of ξ is the matrix $C = (C_{jl})_{j,l=1,\dots,d}$:

$$C_{jl} = \mathbb{E}\big[(\xi_j - \mathbb{E}[\xi_j])(\xi_l - \mathbb{E}[\xi_l])\big] \ .$$

These statistical moments are enough to characterize the first two moments of any linear combination of the components of ξ. Indeed, if $\beta = (\beta_j)_{j=1,\dots,d} \in \mathbb{R}^d$, then the random variable $Z = \beta \cdot \xi = \sum_{j=1}^{d} \beta_j \xi_j$ has mean:

$$\mathbb{E}[Z] = \beta \cdot \mu = \sum_{j=1}^{d} \beta_j \mathbb{E}[\xi_j] \ ,$$

and variance:

$$\mathrm{Var}(Z) = \beta \cdot C\beta = \sum_{j,l=1}^{d} C_{jl} \beta_j \beta_l \ .$$

As a byproduct of this result, we can see that the matrix C is positive semi-definite.

If the variables are independent, then the covariance matrix is diagonal. In particular:

$$\mathrm{Var}\Big(\sum_{j=1}^{d} \xi_j \Big) = \sum_{j=1}^{d} \mathrm{Var}(\xi_j) \ .$$

The reciprocal is false in general (*i.e.*, the fact that the covariance matrix is diagonal does not ensure that the vector is independent).

4.3 Gaussian Random Vectors

A Gaussian random vector $\xi = (\xi_1, \ldots, \xi_d)^T$ with mean μ and covariance matrix R (we write $\xi \sim \mathcal{N}(\mu, R)$ with $\mathcal{N}(\mu, R)$ being the normal distribution of mean μ and covariance matrix R) has the PDF

$$p(x) = \frac{1}{(2\pi)^{d/2}\sqrt{\det R}} \exp\left(-\frac{(x-\mu)\cdot R^{-1}(x-\mu)}{2}\right),$$

provided R is symmetric and positive definite. As mentioned in the case of random variables, the Gaussian statistics is the one that is obtained from the maximum entropy principle (given that the first- and second-order moments of the random vector are specified) and also from the central limit theorem. This distribution is characterized by

$$\mathbb{E}[e^{i\lambda\cdot\xi}] = \int_{\mathbb{R}^d} e^{i\lambda\cdot x} p(x)dx = \exp\left(i\lambda\cdot\mu - \frac{\lambda\cdot R\lambda}{2}\right), \qquad \lambda \in \mathbb{R}^d, \qquad (4.3)$$

which also shows that, if $\lambda \in \mathbb{R}^d$, then the linear combination $\lambda\cdot\xi$ is a Gaussian random variable $\mathcal{N}(\lambda\cdot\mu, \lambda\cdot R\lambda)$.

The Gaussian property is robust: it is stable with respect to any linear transform, and it is also stable with respect to conditioning. Indeed, if $\mathcal{L}$ denotes the distribution and $\binom{\xi_1}{\xi_2}$ is a Gaussian random vector (with ξ_1 a $\mathbb{R}^{d_1}$-valued random vector and ξ_2 a $\mathbb{R}^{d_2}$-valued random vector):

$$\mathcal{L}\left(\binom{\xi_1}{\xi_2}\right) = \mathcal{N}\left(\binom{\mu_1}{\mu_2}, \begin{pmatrix} R_{11} & R_{12} \\ R_{21} & R_{22} \end{pmatrix}\right),$$

with the means $\mu_1 \in \mathbb{R}^{d_1}$ and $\mu_2 \in \mathbb{R}^{d_2}$, the covariance matrices R_{11} of size $d_1 \times d_1$, R_{12} of size $d_1 \times d_2$, $R_{21} = R_{12}^T$ of size $d_2 \times d_1$, and R_{22} of size $d_2 \times d_2$, then the distribution of ξ_1 conditionally on $\xi_2 = x_2$ is Gaussian:

$$\mathcal{L}(\xi_1|\xi_2 = x_2) = \mathcal{N}(\mu_1 + R_{12}R_{22}^{-1}(x_2 - \mu_2), R_{11} - R_{12}R_{22}^{-1}R_{21}). \qquad (4.4)$$

This result is obtained from the application of the general conditioning formula (4.2) and from the use of the block inversion formula

$$\begin{pmatrix} R_{11} & R_{12} \\ R_{21} & R_{22} \end{pmatrix}^{-1} = \begin{pmatrix} Q^{-1} & -Q^{-1}R_{12}R_{22}^{-1} \\ -R_{22}^{-1}R_{21}Q^{-1} & R_{22}^{-1} + R_{22}^{-1}R_{21}Q^{-1}R_{12}R_{22}^{-1} \end{pmatrix},$$

where $Q = R_{11} - R_{12}R_{22}^{-1}R_{21}$ is the Schur complement.

The extension to complex-valued random vectors is straightforward: a complex-valued random vector $\xi = (\xi_1, \ldots, \xi_d)^T$ has Gaussian statistics if $(\Re\xi_1, \ldots, \Re\xi_d, \Im\xi_1, \ldots, \Im\xi_d)^T$ is a real-valued Gaussian random vector.

Let $\xi = (\xi_1, \ldots, \xi_d)^T$ be a complex Gaussian random vector. We say that ξ is circularly symmetric if its mean is zero and if its relation matrix

$(\mathbb{E}[\xi_j\xi_l])_{j,l=1}^d$ is zero. Its distribution is characterized by its covariance matrix $(\mathbb{E}[\overline{\xi_j}\xi_l])_{j,l=1}^d$. For $d = 1$, *i.e.*, for the case where ξ is a complex Gaussian random variable, circular symmetry holds if and only if $\Re\xi$ and $\Im\xi$ are statistically independent and identically distributed Gaussian statistics with mean zero and equal variance.

4.4 Random Processes

Random signals measured in an imaging experiment are conveniently modeled as random functions of time, which are known as random (or stochastic) processes.

Remember that a random variable is a random number, in the sense that a realization of the random variable is a real number and that the statistical distribution of the random variable is characterized by its PDF. In the same way, a random process $(\xi(t))_{t\in\mathbb{R}^d}$ is a random function, in the sense that a realization of the random process is a function from $\mathbb{R}^d$ to $\mathbb{R}$, and that the distribution of $(\xi(t))_{t\in\mathbb{R}^d}$ is characterized by the finite-dimensional distributions $(\xi(t_1), \ldots, \xi(t_n))$, for any n, $t_1, \ldots, t_n \in \mathbb{R}^d$.

As in the case of real random variables, we may not always require a complete statistical description of a random process, or we may not be able to obtain it even if desired. In such cases, we work with the first and second statistical moments. The most important ones are

(i)   Mean: $m(t) = \mathbb{E}[\xi(t)]$;
(ii) Variance: $\mathrm{Var}[\xi(t)] = \mathbb{E}[(\xi(t) - \mathbb{E}[\xi(t)])^2]$;
(iii) Covariance function: $R(t, t') = \mathbb{E}[(\xi(t) - \mathbb{E}[\xi(t)])(\xi(t') - \mathbb{E}[\xi(t')])]$.

4.4.1 Gaussian Random Processes

We say that a random process $(\xi(t))_{t\in\mathbb{R}^d}$ is a real-valued Gaussian if any linear combination $\xi_\lambda = \displaystyle\sum_{i=1}^n \lambda_i \xi(t_i)$ has Gaussian distribution. In this case ξ_λ has Gaussian distribution with PDF

$$p_{\xi_\lambda}(x) = \frac{1}{\sqrt{2\pi}\sigma_\lambda} \exp\left(-\frac{(x - m_\lambda)^2}{2\sigma_\lambda^2}\right), \qquad x \in \mathbb{R},$$

where the mean and variance are given by

$$m_\lambda = \sum_{i=1}^n \lambda_i \mathbb{E}[\xi(t_i)] = \sum_{i=1}^n \lambda_i m(t_i),$$

$$\sigma_\lambda^2 = \sum_{i,j=1}^n \lambda_i \lambda_j \mathbb{E}[\xi(t_i)\xi(t_j)] - m_\lambda^2 = \sum_{i,j=1}^n \lambda_i \lambda_j R(t_i, t_j).$$

The first two moments $(m(t))_{t \in \mathbb{R}^d}$ and $(R(t, t'))_{t,t' \in \mathbb{R}^d}$ characterize the finite-dimensional distribution of the process $(\xi(t))_{t \in \mathbb{R}^d}$. Indeed, the finite-dimensional distribution of $(\xi(t_1), \ldots, \xi(t_n))$ has PDF $p(x_1, \ldots, x_n)$ that can be obtained by applying an inverse Fourier transform to

$$\int e^{i \sum_{j=1}^n \lambda_j x_j} p(x_1, \ldots, x_n) dx_1 \cdots dx_n$$

$$= \mathbb{E}[e^{i \sum_{j=1}^n \lambda_j \xi(t_j)}] = \mathbb{E}[e^{i\xi_\lambda}] = \int e^{ix} p_{\xi_\lambda}(x) dx = \exp\left(im_\lambda - \frac{\sigma_\lambda^2}{2}\right)$$

$$= \exp\left(i \sum_{j=1}^n \lambda_j m(t_j) - \frac{1}{2} \sum_{j,l=1}^n \lambda_j \lambda_l R(t_j, t_l)\right),$$

which shows with (4.3) that $(\xi(t_1), \ldots, \xi(t_n))$ has a Gaussian PDF with mean $(m(t_j))_{j=1,\ldots,n}$ and covariance matrix $(R(t_j, t_l))_{j,l=1,\ldots,n}$. As a consequence the distribution of a Gaussian process is characterized by the mean function $(m(t))_{t \in \mathbb{R}^d}$ and the covariance function $(R(t, t))_{t,t' \in \mathbb{R}^d}$.

It is rather easy to simulate a realization of a Gaussian process $(\xi(t))_{t \in \mathbb{R}^d}$ whose mean $m(t)$ and covariance function $R(t, t')$ are given. If $(t_1, \ldots, t_n)$ is a grid of points, then the following algorithm (Cholesky's method) is a random generator of $(\xi(t_1), \ldots, \xi(t_n))$:

Algorithm 4.1 Random generator

1. Compute the mean vector $M_i = \mathbb{E}[\xi(t_i)]$ and the covariance matrix $C_{ij} = \mathbb{E}[\xi(t_i)\xi(t_j)] - \mathbb{E}[\xi(t_i)]\mathbb{E}[\xi(t_j)]$.
2. Generate a random vector $Z = (Z_1, \ldots, Z_n)$ of n independent Gaussian random variables with mean 0 and variance 1 (use `randn` in MATLAB, or use the Box-Müller algorithm).
3. Compute $Y = M + C^{1/2} Z$.
Output: The vector Y has the distribution of $(\xi(t_1), \ldots, \xi(t_n))$ because it has Gaussian distribution and it has the correct mean and covariance.

Note that the computation of the square root of the matrix C is expensive from the computational point of view, and one usually chooses the Cholesky method to compute it.

4.4.2 Stationary Gaussian Random Processes

We say that $(\xi(t))_{t \in \mathbb{R}^d}$ is a stationary stochastic process if the statistics of the process is invariant to a shift in the origin: for any $t_0 \in \mathbb{R}^d$,

$$(\xi(t_0 + t))_{t \in \mathbb{R}^d} \stackrel{\text{distribution}}{=} (\xi(t))_{t \in \mathbb{R}^d} .$$

Let us consider a stationary Gaussian process $(\xi(t))_{t \in \mathbb{R}^d}$ with mean zero and autocovariance function $C(\tau) = \mathbb{E}[\xi(t)\xi(t + \tau)]$. The spectral representation of the real-valued stationary Gaussian process $(\xi(t))_{t \in \mathbb{R}^d}$ is

$$\xi(t) = \frac{1}{(2\pi)^{d/4}} \int_{\mathbb{R}^d} e^{ik\cdot t} \sqrt{\mathcal{F}[C](k)}\,\hat{n}_k dk \;,$$

with $\hat{n}_k$ is a complex white noise, *i.e.*, $\hat{n}_k$ is complex-valued, Gaussian, $\hat{n}_{-k} = \overline{\hat{n}_k}$, $\mathbb{E}\left[\hat{n}_k\right] = 0$, $\mathbb{E}\left[\hat{n}_k \hat{n}_{k'}\right] = 0$, and $\mathbb{E}\left[\hat{n}_k \overline{\hat{n}_{k'}}\right] = \delta(k - k')$ (the representation is formal, one should in fact use stochastic integrals $d\hat{W}_k = \hat{n}_k dk$). A complex white noise is actually the Fourier transform of a real white noise: we have $\hat{n}_k = (2\pi)^{-d/2} \int e^{-ik\cdot t} n(t) dt$ where $n(t)$ is a real white noise, *i.e.*, $n(t)$ real-valued, Gaussian, $\mathbb{E}\left[n(t)\right] = 0$, and $\mathbb{E}\left[n(t)n(t')\right] = \delta(t - t')$.

It is straightforward to simulate a realization of a stationary Gaussian process (with mean zero and autocovariance c) using its spectral representation and Fast Fourier Transforms. In dimension $d = 1$, if we fix a grid of points $t_i = (i-1)\Delta t$, $i = 1, \ldots, n$, then one can simulate the vector $(\xi(t_1), \ldots, \xi(t_n))$ by the following algorithm:

Algorithm 4.2 Realization of a stationary Gaussian process

---

1. Evaluate the covariance vector $c = (C(t_1), \ldots, C(t_n))$.
2. Generate a random vector $Z = (Z_1, \ldots, Z_n)$ of n independent Gaussian random variables with mean 0 and variance 1.
3. Filter with the element-wise square root of the (discrete) Fourier transform of c:
$$Y = \text{IFT}\left(\sqrt{\text{DFT}(c)} \times \text{DFT}(Z)\right) .$$

Output: The vector Y is a realization of $(\xi(t_1), \ldots, \xi(t_n))$.

In practice one uses FFT and IFFT instead of DFT and IFT, and one obtains a periodized version of the random vector $(\xi(t_1), \ldots, \xi(t_n))$, due to the FFT. This algorithm is much more efficient than the Cholesky's method.

In imaging problems, a commonly used covariance function is of the form $C(\tau) = \exp(-|\tau|^2/l^2)$. Here l is said to be the correlation length of the random process. In this book, to model clutter (or medium noise), we use such a choice for the covariance function.

4.4.3 Local Maxima of a Gaussian Random Field

Let $\Omega \Subset \mathbb{R}^3$ be a bounded domain and let $(\xi(x))_{x\in\Omega}$ be a stationary Gaussian random field with mean zero. The statistical distribution of the random field is characterized by the covariance function:

$$C(x) = \mathbb{E}\left[\xi(x')\xi(x' + x)\right].$$

From now on we assume that C is smooth, so that the realizations of the random field are smooth [5, Theorem 1.4.2]. As we will see below, the relevant statistical information about local and global maxima of the field is in the variance

$$u_0^2 = C(0) = \mathbb{E}[\xi(x)^2]$$

and in the Hessian matrix of the correlation function

$$\Lambda = \left(\frac{\mathbb{E}\big[\partial_{x_j}\xi(x)\partial_{x_l}\xi(x)\big]}{\mathbb{E}\big[\xi(x)^2\big]} \right)_{j,l=1,\dots,3} = \left(-\frac{\partial^2_{x_j x_l} C(0)}{C(0)} \right)_{j,l=1,\dots,3}.$$

Let us denote by M_u^Ω the number of local maxima of $\xi(x)$ in Ω with values larger than u:

$$M_u^\Omega = \mathrm{Card}\big\{ \text{ local maxima of } (\xi(x))_{x\in\Omega} \text{ with values larger than } u \big\}.$$

We have [4, Theorem 6.3.1]

$$\mathbb{E}[M_u^\Omega] = \frac{|\Omega|}{V_c}\frac{u^2}{u_0^2} \exp\big(-\frac{u^2}{2u_0^2}\big)\Big(1 + O\Big(\frac{u_0}{u}\Big)\Big), \text{ for } u \gg u_0,$$

where V_c is the hotspot volume defined in terms of the determinant of the Hessian of the correlation function as:

$$V_c = \frac{4\pi^2}{(\det \Lambda)^{1/2}}.$$

4.4.4 Global Maximum of a Gaussian Random Field

Let us denote by $\xi_{\max}^\Omega$ the global maximum of the field over the domain Ω:

$$\xi_{\max}^\Omega = \max_{x\in\Omega} \xi(x).$$

Using [4, Theorem 6.9.4] when $|\Omega| \gg V_c$, the statistical distribution of $\xi_{\max}^\Omega$ is of the form

$$\xi_{\max}^\Omega = u_0\Big[A\Big(\frac{|\Omega|}{V_c}\Big) + B\Big(\frac{|\Omega|}{V_c}\Big)Z_0\Big],$$

where Z_0 follows a Gumbel distribution with cumulative distribution function $\mathbb{P}(Z_0 \leq x) = \exp(-e^{-x})$,

$$A(V) = \sqrt{2\log(V)} + \frac{\log\big[2\log(V)\big]}{\sqrt{2\log(V)}},$$

$$B(V) = \frac{1}{\sqrt{2\log(V)}}.$$

To leading order, the value of the global maximum is deterministic and given by

$$\xi_{\max}^\Omega \simeq u_0\sqrt{2\log\Big(\frac{|\Omega|}{V_c}\Big)}.$$

4.4.5 The local Shape of a Local Maximum

Using Eq. (4.4) one can show that, given that the random field $\xi(x)$ has a local extremum at x_0 with peak amplitude u (with $u \gg u_0$), then we have locally around x_0:

$$\xi(x) \simeq u\Big[\frac{C(x - x_0)}{u_0^2} + o(1)\Big], \qquad [u \gg u_0].$$

To prove this, let us fix $x_0 \in \mathbb{R}^3$. The random vector

$$\begin{pmatrix} \xi(x) \\ \xi(x_0) \\ \nabla\xi(x_0) \end{pmatrix}$$

has Gaussian distribution:

$$\mathcal{N}\left(\begin{pmatrix} 0 \\ 0 \\ 0 \end{pmatrix}, \begin{pmatrix} C(0) & C(x - x_0) & -\nabla C(x - x_0)^T \\ C(x - x_0) & C(0) & 0 \\ -\nabla C(x - x_0) & 0 & C(0)\Lambda \end{pmatrix}\right).$$

Applying Eq. (4.4), the distribution of $\xi(x)$ given $\xi(x_0) = u$ and $\nabla\xi(x_0) = 0$ is

$$\mathcal{N}\Big(\frac{C(x - x_0)}{C(0)}u, C(0) - \frac{\nabla C(x - x_0)^T \Lambda^{-1} \nabla C(x - x_0)}{C(0)}\Big).$$

This gives the desired result when $u \gg u_0 = C(0)^{1/2}$.

4.4.6 Realization of a Cluttered Medium

Let Ω be a bounded smooth domain. Let $y \in \mathbb{R}^d \setminus \overline{\Omega}$. We consider the Helmholtz equation:

$$\Big(\Delta_x + k_0^2(1 + \nu_{\text{noise}}(x))\Big)\Phi_{k_0}(x, y) = \delta_y \quad \text{in } \mathbb{R}^d,$$

subject to the Sommerfeld radiation condition. Here, $\nu_{\text{noise}}(x)$ is a random process with mean zero. For instance, it may be a smooth, odd, and bounded function of a stationary Gaussian process with mean zero and given covariance function, multiplied by a characteristic function of a compact domain within Ω. The composition by the smooth and bounded function ensures that the process $1 + \nu_{\text{noise}}(x)$ remains bounded and bounded away from zero almost surely. The multiplication by the characteristic function ensures that the fluctuations of the medium are compactly supported.

The random process $\nu_{\text{noise}}(x)$ describes the random fluctuations of the index of refraction in the medium. Since the coefficient of the equation is random, the fundamental solution $\Phi_{k_0}(x, y)$ is itself random. The relation between the statistics of the fluctuations of the index of refraction and the

statistics of $\Phi_{k_0}(x, y)$ is highly nontrivial and nonlinear. In particular cluttered noise, that is the difference between the random fundamental solution and the background homogeneous fundamental solution, is not an additive white noise.

In order to simulate ν_{noise} (and Φ_{k_0}), we first generate on a grid of points that covers the support of the characteristic function a realization of a stationary Gaussian random process using the method described in Section 4.4. Then we apply the smooth and bounded function and we multiply by the characteristic function.

Figure 4.1 shows a typical realization of a medium noise and its projection on the finite-element mesh.
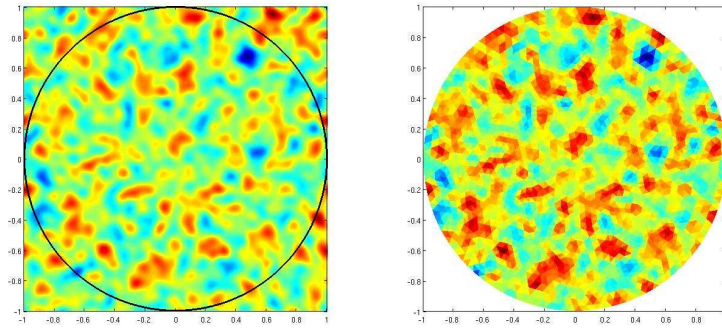
Fig. 4.1. Realization of a medium noise.

5

General Image Characteristics

Irrespectively of the methods used to acquire images, there are a number of criteria by which the image characteristics can be evaluated and compared. The most important of these criteria are spatial resolution and the signal-to-noise ratio. This section covers a number of general concepts applicable to multistatic imaging.

5.1 Spatial Resolution

There are a number of measures used to describe the spatial resolution of an imaging modality. We focus on describing a point spread function (PSF) concept and show how to use it to analyze resolution limitation in several practical imaging schemes.

5.1.1 Point Spread Function

Consider an idealized object consisting of a single point. It is likely that the image we obtain from it is a blurred point. Nevertheless, we are still able to identify it as a point. Now, we add another point to the object. If the two points are farther apart, we will see two blurred points. However, as the two points are moving closer to each other, the image looks less like two points. In fact, the two points will merge together to become a single blob when their separation is below a certain threshold. We call this threshold value the resolution limit of the imaging system. Formally stated, the spatial resolution of an imaging system is the smallest separation of two point sources necessary for them to remain resolvable in the resultant image.

In order to arrive at a more quantitative definition of the resolution, we next introduce the point spread function concept. The relationship between an arbitrary object function $I(x)$ and its image $\hat{I}$ can typically be described by $\hat{I}(x) = (I \star h)(x)$, where the convolution kernel function $h(x)$ is known as the point spread function since $\hat{I}(x) = h(x)$ for $I(x) = \delta_0(x)$. In a perfect

imaging system, the PSF $h(x)$ would be a delta function, and in this case the image would be a perfect representation of the object. If $h(x)$ deviates from a $\delta-$function, $\hat{I}(x)$ will be a blurred version of $I(x)$. The amount of blurring introduced in $\hat{I}(x)$ by an imperfect $h(x)$ can be quantified by the width of $h(x)$. The spatial resolution, W_h, is clearly related to the PSF. It is defined as the full width of $h(x)$ at its half maximum; alternatively the half width of $h(x)$ at its first zero.

If the PSF is a Gaussian function,

$$h(x) = e^{-\frac{x^2}{2\sigma^2}} \, ,$$

where σ is the standard deviation of the distribution, then the resolution, defined as the full width at the half maximum, is given by $2\sqrt{2\log 2}\sigma \approx 2.35\,\sigma$.

Consider now the problem of reconstructing a one-dimensional image from its truncated Fourier series. The image reconstructed based on the truncated Fourier series is given by

$$\hat{I}(x) = \frac{1}{\sqrt{2\pi}}\Delta k \sum_{n=-N/2}^{N/2-1} S(n\Delta k)e^{in\Delta k\,x} \, ,$$

where $S(n\Delta k) = \frac{1}{\sqrt{2\pi}}\int_{\mathbb{R}} I(x)e^{-in\Delta k\,x}\,dx$. The underlying PSF is given by

$$h(x) = \Delta k\,\frac{\sin(\pi N\Delta k\,x)}{\sin(\pi\Delta k\,x)} \, ,$$

with Δk being the fundamental frequency and N the number of Fourier samples. Then the resolution (defined as the half width of h at its first zero) is $W_h = 1/(N\Delta k)$. Therefore, we cannot improve image resolution and reduce the number of measured data points at the same time. This assertion is often referred to as the uncertainty relation of Fourier imaging, and in practice, one chooses N as large as signal-to-noise ratio as long as imaging time permits.

5.1.2 Rayleigh Resolution Limit

In imaging with waves, the Rayleigh resolution limit is defined as the minimum distance that two point-source objects have to be in order to distinguish the two sources from each other.

Using the Helmholtz-Kirchhoff identity (3.80), it can be seen that in three dimensions the PSF is a sinc function,

$$h(x) = \text{sinc}(k_0 x) = \frac{\sin k_0 x}{k_0 x}(= j_0(k_0 x)) \, .$$

Therefore, the two point sources can be resolved if the peak intensity of the sinc PSF from one source coincides with the first zero-crossing point of the

PSF of the other, *i.e.*, if the two source points are separated by (at least) one-half the wavelength $\lambda := 2\pi/k_0$. If the PSF is given by

$$h(x) = \frac{J_1(k_0 x)}{k_0 x} \; ,$$

J_1 being the Bessel function of the first-order, then the resolution is given by $W_h \approx 0.61\lambda$ since the first positive zero of J_1 is approximately 3.83.

5.2 Signal-To-Noise Ratio

In imaging it is useful to measure the relative strength of a signal or information versus noise level. For doing so, we define the concept of signal-to-noise ratio.

Let $\hat{I} = I + \xi$ be a measured quantity containing the true signal I and the noise component ξ with zero mean and standard deviation σ_ξ. The signal-to-noise ratio (SNR) for $\hat{I}$ from a single measurement is defined by

$$(\text{SNR})_{\hat{I}} = \frac{|I|}{\sigma_\xi} \; .$$

We remark that the signal-to-noise ratio is sometimes defined by $(|I|/\sigma_\xi)^2$ and that the signal-to-noise ratio in logarithmic decibel scale (dB) is $20\log(|I|/\sigma_\xi)$.

If N measurements are taken such that $\hat{I}_n = I + \xi_n$ are obtained to produce

$$\frac{1}{N} \sum_{n=1}^{N} \hat{I}_n = I + \frac{1}{N} \sum_{n=1}^{N} \xi_n \; ,$$

then the signal-to-noise ratio for $(1/N) \sum_{n=1}^{N} \hat{I}_n$ is

$$\frac{|I|}{\sqrt{\text{Var}[\frac{1}{N} \sum_{n=1}^{N} \xi_n]}} = \sqrt{N} \frac{|I|}{\sigma_\xi} = \sqrt{N}(\text{SNR})_{\hat{I}} \; ,$$

assuming that the noise for different measurements is uncorrelated. Thus N signal averaging yields an improvement by a factor of $\sqrt{N}$ in the signal-to-noise ratio. Recall that two signals, ξ_1 and ξ_2, are said to be uncorrelated if

$$\mathbb{E}\big[(\xi_1 - \mathbb{E}[\xi_1])(\xi_2 - \mathbb{E}[\xi_2])\big] = 0 \; .$$

Part II

Single-Wave Imaging

6

Electrical Impedance Tomography

There are a variety of medical problems for which it would be useful to know the distribution of the electrical properties inside the body. By electrical properties we mean specifically the electric conductivity and permittivity. The electric conductivity is a measure of the ease with which a material conducts electricity; the electric permittivity is a measure of how readily the charges within a material separate under an imposed electric field. Both of these properties are of interest in medical applications, because different tissues have different conductivities and permittivities.

One important medical problem for which knowledge of internal electrical properties would be useful is the detection of breast cancer. Experimental results show that the conductivity of the cancerous tissue is 5 to 8 times larger than the one of normal tissue [176, 207]. In this chapter we describe general algorithms used in electrical impedance tomography (EIT).

6.1 Mathematical Model

In this section we present the mathematical model for EIT. We use this model to describe some reconstruction algorithms.

The electric potential or voltage u in the body Ω is governed by

$$\nabla \cdot \kappa(x, \omega) \nabla u = 0, \quad x \in \Omega . \tag{6.1}$$

Here the (frequency dependent) admittivity κ is given by $\kappa(x, \omega) = \sigma(x, \omega) + i\omega\varepsilon(x, \omega)$, where σ is the electric conductivity, ε is the electric permittivity, and ω is the angular frequency of the applied current.

In practice, we apply currents to electrodes on the surface $\partial\Omega$ of the body. These currents produce a current density on the surface whose inward pointing normal component is denoted by g. Thus,

$$\kappa \frac{\partial u}{\partial \nu} = g \quad \text{on } \partial\Omega . \tag{6.2}$$

The mathematical model of EIT is (6.1) and (6.2), together with the conservation of charge condition $\int_{\partial\Omega} g = 0$ and the condition $\int_{\partial\Omega} u = 0$, which amounts to choosing a reference voltage. The injected currents can be approximated by linear combinations of dipoles. A dipole at a point $z \in \partial\Omega$ is given by $-|\partial\Omega|\, \partial\delta_z/\partial T$, $\partial/\partial T$ being the tangential derivative at $\partial\Omega$. The operator

$$\Lambda_\kappa : \widetilde{W}^2_{-1/2}(\partial\Omega) \to \widetilde{W}^2_{1/2}(\partial\Omega)$$
$$g \qquad \mapsto \quad u|_{\partial\Omega}$$

is called the Neumann-to-Dirichlet boundary map. Here, $\widetilde{W}^2_{-1/2}(\partial\Omega)$ is the set of functions g in $W^2_{-1/2}(\partial\Omega)$ satisfying $(g,1)_{-1/2,1/2} = 0$ and $\widetilde{W}^2_{1/2}(\partial\Omega)$ is the set of functions in $W^2_{1/2}(\partial\Omega)$ with mean-value zero.

Green's formula yields the reciprocity property of the Neumann-to-Dirichlet data:

$$(\overline{f}, \Lambda_\kappa[g])_{-1/2,1/2} = (\overline{g}, \Lambda_\kappa[f])_{-1/2,1/2}, \qquad (6.3)$$

for $f,g \in \widetilde{W}^2_{-1/2}(\partial\Omega)$.

The reconstruction problem in EIT is to obtain an approximation of κ in Ω from the boundary measurements of u on $\partial\Omega$. This problem is challenging because it is not only nonlinear, but also severely ill-posed, which means that large changes in the interior can correspond to very small changes in the measured data.

From a theoretical point of view, all possible boundary measurements uniquely determine κ in Ω. However, in practice we are limited to a finite number of current-to-voltage patterns.

Before describing classical reconstruction algorithms in EIT, we explain the fundamental shortcomings of EIT in detail by use of its discretized version.

6.2 Ill-Conditioning

For simplicity, we suppose that Ω is a square region in $\mathbb{R}^2$. We divide Ω uniformly into $N \times N$ sub-squares Ω_{ij} with the center point (x_i, y_j), where $i,j = 0, \ldots, N-1$. The goal of EIT is to determine $N \times N$ admittivity values under the assumption that the admittivity κ is constant on each subsquare Ω_{ij}, say κ_{ij}. Let

$$\Sigma = \left\{ \kappa : \kappa|_{\Omega_{ij}} = \text{constant for } i,j = 0, \ldots, N-1 \right\}.$$

For a given $\kappa \in \Sigma$, the solution u of the direct problem (6.1) and (6.2) can be approximated by a vector $U = (u_0, u_1, \ldots, u_{N^2-1})$ such that each interior voltage $u_k, k = i + jN$ is determined by the weighted average (depending on κ) of the four neighboring potentials. More precisely, a discretized form of (6.1) is given by

$$u_k = \frac{1}{a_{kk}}\left[a_{kk_N}u_{k_N} + a_{kk_S}u_{k_S} + a_{kk_E}u_{k_E} + a_{kk_W}u_{k_W}\right],$$

with

$$a_{kk} = -\sum_l a_{kk_l} \quad \text{and } a_{kk_l} = \frac{\kappa_k \kappa_{k_l}}{\kappa_k + \kappa_{k_l}} \quad \text{for } l = N, S, E, W .$$

Here k_N, k_S, k_E, k_W denote north, south, east, and west neighboring of $k-$th point. The discretized equation (6.1) with the Neumann boundary condition (6.2) can be written as a linear system $A_\kappa U = G$, where G is the injection current vector associated with g. Let F denote the small-size sub-vector of U restricted to $\partial\Omega$, which corresponds to the boundary voltage potential on $\partial\Omega$. Then the inverse problem is to determine κ, or equivalently A_κ, from one or several measurements of current-to-voltage pairs $(G^m, F^m), m = 1, \ldots, M$.

The fundamental shortcoming of EIT for providing high resolution images is due to the fact that reconstructing A_κ from $(G^m, F^m), m = 1, \ldots, M$, is exponentially difficult as the matrix size A_κ increases. More precisely, the value of the potential at each Ω_{ij} inside Ω can be expressed as the weighted average of its neighboring potentials where weights are determined by the admittivity distribution. Therefore, the measured data F is entangled in the global structure of the admittivity distribution in a highly nonlinear way and any internal admittivity value κ_{ij} has a little influence on boundary measurements if Ω_{ij} is away from the boundary. This phenomenon causes the ill-posedness nature of EIT. Nevertheless, as it will be shown later, a multifrequency approach can be successfully employed to recover stably admittivity distributions and to eliminate modeling errors.

6.2.1 Static Imaging

Static image reconstruction problem is based on iterative methods. An image reconstruction algorithm iteratively updates the admittivity distribution until it minimizes in the least-squares sense the difference between measured data and computed boundary voltages. As part of each iteration in the minimization, a forward solver is used to determine the boundary voltages that would be produced given the applied currents. This technique was first introduced in EIT in the 80's following a number of variations and improvements. These include utilization of a priori information, various forms of regularization (Tikhonov, l^1, or total variation regularizations) and adaptive mesh refinement. Even though this approach is widely adopted for static imaging by many researchers, it requires a large amount of computation time for producing static images even with low spatial resolution and poor accuracy.

Because of the fundamental limitations of EIT, it seems from a practical point of view reasonable to restrict ourselves to find the deviation of the admittivity from an assumedly known admittivity.

6.2.2 Dynamic Imaging

The algorithms described here are based on approximations to the linearized
EIT problem.

Barber-Brown Backprojection Algorithm

The Barber-Brown Backprojection algorithm is the first fast and useful al-
gorithm in EIT although it provides images with very low resolution. It is
based on the assumption that the admittivity does not differ very much from
a constant.

For simplicity, suppose that Ω is the unit disk in $\mathbb{R}^2$ and κ is a small
perturbation of a constant $\kappa = \kappa_0 + \delta\kappa$ in Ω. In the simplest case we assume
$\kappa_0 = 1$, so that

$$\kappa(x) = 1 + \delta\kappa(x), \quad |\delta\kappa(x)| \ll 1, \, x \in \Omega \, , \tag{6.4}$$

and we further assume that $\delta\kappa = 0$ on $\partial\Omega$. Let u_0 and u denote the po-
tentials corresponding to κ_0 and κ with the same Neumann boundary data
$g = -2\pi\partial\delta_z/\partial\theta$ at a point $z \in \partial\Omega$. Writing $u = u_0 + \delta u$, δu satisfies approxi-
mately the equation

$$-\Delta\delta u \approx \nabla\delta\kappa \cdot \nabla u_0 \quad \text{in } \Omega \, , \tag{6.5}$$

with the homogeneous boundary condition. Here, the term $\nabla\delta\kappa \cdot \nabla\delta u$ is ne-
glected.

Observe that

$$u_0(x) = \frac{x \cdot z^\perp}{|x - z|^2} \, ,$$

where $z^\perp$ is the rotate of z by $\pi/2$. Next, we introduce a holomorphic function
in Ω whose real part is $-u_0$:

$$\Psi_z(x) := s + it := -\frac{x \cdot z^\perp}{|x - z|^2} + i\frac{1 - z \cdot x}{|x - z|^2} \, .$$

Then we can view Ψ_z as a transform which maps the unit disk Ω onto the upper
half plane $\widetilde{\Omega} := \{s + it : t > 1/2\}$. Hence, we can view x as a function with
respect to $\Psi_z = s + it$ defined in $\widetilde{\Omega}$. Let $\widetilde{\delta u}_z(\Psi_z(x)) = \delta u(x)$ and $\widetilde{\delta\kappa}_z(\Psi_z(x)) = \delta\kappa(x)$. Using the fact that $\nabla s \cdot \nabla t = 0$ and $|\nabla s| = |\nabla t|$, it follows from (6.5)
that

$$\begin{cases} \Delta\widetilde{\delta u}_z = -\dfrac{\partial\widetilde{\delta\kappa}_z}{\partial s} \quad \text{in } \widetilde{\Omega} \, , \\[2mm] \dfrac{\partial\widetilde{\delta u}_z}{\partial t}\bigg|_{t=1/2} = 0 \, . \end{cases}$$

Hence, if $\widetilde{\delta\kappa}_z$ is independent of the $t-$variable, $\widetilde{\delta u}_z$ depends only on s and
$\widetilde{\delta\kappa}_z$. With the notation $z = (\cos\theta, \sin\theta)$, Barber and Brown derived from this
idea the following reconstruction formula:

$$\delta\kappa(x) = \widetilde{\delta\kappa}_z(\Psi_z(x)) = \frac{1}{2\pi}\int_0^{2\pi}\frac{\partial}{\partial s}\widetilde{\delta u}_z(s + \frac{i}{2})\,d\theta\ .$$

Dynamic Imaging

Suppose that currents $g^n, n = 1, \ldots, N$, are applied on $\partial\Omega$. Application of g^n gives rise to the potential u^n inside Ω. In dynamic imaging, we measure the boundary voltage potential $f^n = u^n|_\Omega$ to reconstruct the change of the admittivity $\delta\kappa$ from the relation between g^n and f^n. Let u_0^n denote the background potential, that is, the solution to

$$\begin{cases} \Delta u_0^n = 0 \quad \text{in } \Omega\ , \\ \dfrac{\partial u_0^n}{\partial\nu} = g^n \quad \text{on } \partial\Omega\ , \\ \int_{\partial\Omega} u_0^n = 0\ . \end{cases}$$

Set $\delta u^n = u^n - u_0^n$. The reconstruction algorithm is based on the following identity

$$\int_\Omega \delta\kappa\nabla u_0^n\cdot\nabla u_0^m = \int_{\partial\Omega}(g^n f_0^m - f^n g^m) - \int_\Omega \delta\kappa\nabla\delta u^n\cdot\nabla u_0^m\ .$$

Since the last term in the above identity can be regarded as negligibly small, the perturbation $\delta\kappa$ can be computed from

$$\int_\Omega \delta\kappa\nabla u_0^n\cdot\nabla u_0^m = b[n,m]\ , \tag{6.6}$$

where $b[n,m] = \int_{\partial\Omega}(g^n f_0^m - f^n g^m)$.

In order to construct $\delta\kappa$, we divide the domain Ω into L small subregions as $\Omega = \cup_{l=1}^L \Omega_l$ and assume that $\delta\kappa$ is constant $(= \delta\kappa_l)$ in each subregion Ω_l. With this kind of discretization, we can transform (6.6) into matrix form. To do this, we use a single index $j = 1,\ldots,J$ with $J = N^2$ for the index pair (m,n) with $j = N(m-1) + n$, and introduce the sensitivity matrix $M = [M_{jl}] \in \mathbb{R}^{J\times L}$ with its entries M_{jl} given by

$$M_{jl} = \int_{\Omega_l}\nabla u_0^n\cdot\nabla u_0^m\,dx \quad (j\leftrightarrow(m,n))\ ,$$

and a data vector $X \in \mathbb{R}^J$ with its jth entry X_j given by

$$X_j = b[n,m] \quad (j\leftrightarrow(m,n)).$$

Upon writing the vector $A = (\delta\kappa_l)_l \in \mathbb{C}^L$, we obtain the following linear system

$$MA = X\ . \tag{6.7}$$

The matrix M is called the sensitivity matrix. It depends on the data collection. The distribution of its singular values determines the spatial image resolution.

6.2.3 Electrode Model

The continuum model (6.1) and (6.2) is a poor model for real experiments, because we do not know the current density g. In practice, we know only the currents that are sent down wires attached to discrete electrodes, which in turn are attached to the body. One might approximate the unknown current density as a constant over each electrode, but this model also turns out to be inadequate. We need to account for two main effects: the discreteness of the electrodes, and the extra conductive material (the electrodes themselves) we have added. We should account for the electrochemical effect that takes place at the contact between the electrode and the body. This effect is the formation of a thin, highly resistive layer between the electrode and the body. The impedance of this layer is characterized by a number z_n, called the effective contact impedance.

Let E_n denote the part of $\partial\Omega$ that corresponds to the nth electrode and let I_n be the current sent to the electrode E_n. The electrode model consists of (6.1),

$$\int_{E_n} \kappa \frac{\partial u}{\partial \nu} = I_n, \quad n = 1, \ldots, N ,$$

$$\kappa \frac{\partial u}{\partial \nu} = 0 \quad \text{in the gap between the electrodes,}$$

the constraint

$$u + z_n \kappa \frac{\partial u}{\partial \nu} = V_n \quad \text{on } E_n, \quad n = 1, \ldots, N ,$$

where V_n, for $n = 1, \ldots, N$, is the measured potential on the electrode E_n and z_n is the contact impedance assumed to be known, together with the conditions

$$\sum_{n=1}^{N} I_n = 0 \quad \text{(conservation of charge)}$$

and

$$\sum_{n=1}^{N} V_n = 0 \quad \text{(choice of a ground).}$$

This model has been shown to have a unique solution and able to predict the experimental measurements.

Ultrasound and Microwave Tomographies

Propagation of acoustical and electromagnetic waves in biological tissue is described by linear wave equations. Although the physical interpretation varies, these equations largely coincide. Ultrasound and microwave tomographies can be done in the time domain and the frequency domain. A standard inversion technique in ultrasound and microwave imaging in the frequency domain is the diffraction tomography.

7.1 Born Approximation

In ultrasound and microwave imaging, the object to be imaged is irradiated by a plane wave $U(x) = e^{i\omega x \cdot \theta}$, with the wavelength $\lambda := 2\pi/\omega$, travelling in the direction of the unit vector θ. The relevant equation is the Helmholtz equation

$$\Delta u + \omega^2 (1 + V) u = 0 \quad \text{in } \mathbb{R}^d \ ,$$

subject to the Sommerfeld radiation condition on the scattered field

$$u^s := u - U$$

at infinity, where the object is given by the function V, which vanishes outside the object. The total field u is measured outside the object for many directions θ. From all these measurements, the function V has to be determined.

The scattered field $u^{(s)}$ satisfies the Sommerfeld radiation condition and the Helmholtz equation

$$\Delta u^{(s)}(x) + \omega^2 u^{(s)}(x) = -\omega^2 (e^{i\omega x \cdot \theta} + u^{(s)}(x)) V(x), \quad x \in \mathbb{R}^d \ . \qquad (7.1)$$

Now we consider the Born approximation for weakly scattering target. We assume that the function V is supported in $|x| < \rho$ and $|V| \ll 1$. Then we can neglect $u^{(s)}$ on the right-hand side of (7.1), obtaining

$$\Delta u^{(s)}(x) + \omega^2 u^{(s)}(x) \approx -\omega^2 e^{i\omega x \cdot \theta} V(x), \quad x \in \mathbb{R}^d \ .$$

This equation can be solved for $u^{(s)}$ with the help of the outgoing fundamental solution Γ_ω for the Helmholtz operator $\Delta + \omega^2$. We have

$$u^{(s)}(x) \approx -\omega^2 \int_{|y|<\rho} \Gamma_\omega(x,y) e^{i\omega\theta \cdot y} V(y)\, dy, \quad x \in \mathbb{R}^d \,. \qquad (7.2)$$

Γ_ω is the outgoing fundamental solution to the Helmholtz equation in $\mathbb{R}^d$:

$$(\Delta + \omega^2)\Gamma_\omega(x,y) = \delta_x(y) \quad \text{in } \mathbb{R}^d \,, \qquad (7.3)$$

subject to the outgoing radiation condition. Here δ_x is the Dirac mass at x. We have $\Gamma_\omega(x,y) = \Gamma_\omega(x-y,0)$ and, in dimension $d = 2$ or 3, $\Gamma_\omega(x,0)$ is given by (3.52) and it has the plane wave decomposition (3.55).

7.2 Diffraction Tomography Algorithm

In the frequency domain, from measurements at a single frequency or bandlimited measurements, diffraction tomography can be used to reconstruct within the Born approximation a low-pass version of the electromagnetic target. The principal of diffraction tomography computes the Fourier transform of the reflectivity function of the weakly scattering target from the Fourier transform of the measured scattered data. The computation is based on the Weyl representation (3.55) of cylindrical and spherical waves.

To present the basics of diffraction tomography, we first recall that the fundamental solution Γ_ω has the plane wave decomposition (3.55). Substituting (3.55) into the Born approximation (7.2) for the scattered field $u^{(s)}$ yields

$$u^{(s)}(x) \approx i\omega^2 c_d \int_{\mathbb{R}^{d-1}} \int_{|y|<\rho} \frac{V(y)}{\beta(\alpha)} e^{i(\beta(\alpha)|x_d - y_d| + \alpha \cdot (\tilde{x} - \tilde{y}))} e^{i\omega\theta \cdot y}\, dy\, d\alpha \,, \quad (7.4)$$

where $y = (\tilde{y}, y_d)$.

Suppose for simplicity that $d = 2$, $\theta = (0,1)$ and $u^{(s)}$ is measured on the line $x_2 = l$, where l is greater than any y_2-coordinate within the object. Then (7.4) may be rewritten as

$$u^{(s)}(x_1, l) \approx \frac{i\omega^2}{4\pi} \int_{-\infty}^{+\infty} d\alpha \int_{|y|<\rho} \frac{V(y)}{\beta(\alpha)} e^{i(\beta(\alpha)(l-y_2) + \alpha(x_1 - y_1))} e^{i\omega y_2}\, dy \,.$$

Recognizing part of the inner integral as the two-dimensional Fourier transform of the reflectivity function V evaluated at $(\alpha, \beta(\alpha) - \omega)$ we find

$$u^{(s)}(x_1, l) \approx \frac{i\omega^2}{2} \int_{-\infty}^{+\infty} \frac{1}{\beta(\alpha)} e^{i(\beta(\alpha)l + \alpha x_1)} \mathcal{F}V(\alpha, \beta(\alpha) - \omega)\, d\alpha \,,$$

where

$$\mathcal{F}(V)(\alpha, \beta) = \frac{1}{2\pi} \int V(y) e^{-i\alpha y_1 - i\beta y_2} dy \; .$$

Taking the one-dimensional Fourier transform $\mathcal{F}_1$ of $u^{(s)}(x_1, l)$,

$$\mathcal{F}_1(u^{(s)})(\alpha, l) = \frac{1}{\sqrt{2\pi}} \int u^{(s)}(y_1, l) e^{-i\alpha y_1} dy_1 \; ,$$

we obtain

$$\mathcal{F}_1(u^{(s)})(\alpha, l) \approx i\omega^2 \sqrt{\frac{\pi}{2}} \frac{1}{\sqrt{\omega^2 - \alpha^2}} e^{i\sqrt{\omega^2 - \alpha^2} l} \mathcal{F}(V)(\alpha, \sqrt{\omega^2 - \alpha^2} - \omega) \; ,$$

for $|\alpha| < \omega$.

This expression relates the two-dimensional Fourier transform of V to the one-dimensional Fourier transform of the scattered field at the receiver line $x_2 = l$.

The factor

$$i\omega^2 \sqrt{\frac{\pi}{2}} \frac{1}{\sqrt{\omega^2 - \alpha^2}} e^{i\sqrt{\omega^2 - \alpha^2} l}$$

is a simple function of α for a fixed receiver line and operating frequency ω. As α varies from $-\omega$ to ω, the coordinates $(\alpha, \sqrt{\omega^2 - \alpha^2} - \omega)$ in the Fourier transform of V trace out a semicircular arc. The endpoints of this semicircular arc are at the distance $\sqrt{2}\,\omega$ from the origin in the Fourier domain. Therefore, if the object is illuminated from many different θ-directions, we can fill up a disk of diameter $\sqrt{2}\,\omega$ in the Fourier domain and then approximately reconstruct $V(x)$ by direct Fourier inversion. The reconstructed object is a low-pass filtered version of the original one.

7.3 Time-Reversal Techniques

From time-domain or broadband measurements, time-reversal techniques yield direct reconstruction of V within the Born approximation. The main idea of time-reversal is to take advantage of the reversibility of the wave equation in order to back-propagate signals to the support of V that reflected them. In the context of inverse source problems, one measures the scattered wave on a closed surface surrounding the support of V, and retransmits it through the background medium in a time-reversed chronology. Then the perturbation will travel back to the support of V.

Consider the wave equation in the free space $\mathbb{R}^d$, $d = 2$ or 3,

$$\begin{cases} \dfrac{\partial^2 u}{\partial t^2}(x, t) - \Delta u(x, t) = \dfrac{d\delta_0}{dt}(t) f(x), & (x, t) \in \mathbb{R}^d \times \mathbb{R} \; , \\[2ex] u(x, t) = 0 \quad \text{and} \quad \dfrac{\partial u(x, t)}{\partial t} = 0, & t < 0 \; , \end{cases} \tag{7.5}$$

where δ_0 is the Dirac mass at 0 and the source f is real-valued, smooth and has a smooth compact support.

Let Ω be a smooth bounded domain in $\mathbb{R}^d$ containing the support of f. Let $g(y, t)$ be defined as $g(y, t) := u(y, t)$ for all $y \in \partial\Omega$ and $t \in [0, T]$, where, in three dimensions, T is supposed to be sufficiently large such that

$$u(x, t) = \frac{\partial u(x, t)}{\partial t} = 0$$

for $t \geq T$ and $x \in \Omega$. It is easy to see that g is smooth.

Our aim in this section is to reconstruct an approximation of the source f from g on $\partial\Omega \times [0, T]$.

We introduce the time-dependent Green function

$$\Gamma(x, y, s, t) = \frac{1}{2\pi} \int_{\mathbb{R}} \Gamma_\omega(x, y) \exp(-i\omega(t - s)) d\omega \ , \qquad (7.6)$$

where Γ_ω is the outgoing fundamental solution (7.3) to the Helmholtz equation $(\Delta + \omega^2)$ in $\mathbb{R}^d$ subject to the outgoing radiation condition. The time-dependent Green function is the solution of the free space wave equation

$$\begin{cases} \dfrac{\partial^2 \Gamma}{\partial t^2}(x, y, s, t) - \Delta_y \Gamma(x, y, s, t) = -\delta_x(y)\delta_s(t), & (y, t) \in \mathbb{R}^d \times \mathbb{R} \ , \\ \Gamma(x, y, s, t) = \dfrac{\partial \Gamma}{\partial t}(x, y, s, t) = 0, & y \in \mathbb{R}^d, \quad t < s \ , \end{cases}$$

where δ_x and δ_s are the Dirac masses at x and at s. Note that $U_y(x, t)$ introduced in (2.56) is nothing else than $\Gamma(x, y, 0, t)$. Moreover,

$$g(y, t) = -\int_\Omega \frac{\partial \Gamma}{\partial t}(z, y, 0, t) f(z) \, dz, \quad y \in \partial\Omega, \quad t \in [0, T] \ . \qquad (7.7)$$

7.3.1 Ideal Time-Reversal Imaging Technique

We introduce the solution v of the following wave problem

$$\begin{cases} \dfrac{\partial^2 v}{\partial t^2}(x, t) - \Delta_x v(x, t) = 0, & (x, t) \in \Omega \times [0, T] \ , \\ v(x, 0) = \dfrac{\partial v}{\partial t}(x, 0) = 0, & x \in \Omega \ , \\ v(x, t) = \dfrac{1}{2} g(x, T - t), & (x, t) \in \partial\Omega \times [0, T] \ . \end{cases} \qquad (7.8)$$

The time-reversal imaging functional $\mathcal{I}_{\mathrm{TR}}^{(1)}(x)$ is defined by

$$\mathcal{I}_{\mathrm{TR}}^{(1)}(x) = v(x, T), \quad x \in \Omega \ . \qquad (7.9)$$

In order to make $\mathcal{I}_{\mathrm{TR}}^{(1)}(x)$ explicit, we introduce the causal Dirichlet Green function (also called retarded Dirichlet Green function) $G^{\mathrm{c}}(x, y, s, t)$ defined as the solution of the following wave equation

$$\begin{cases} \dfrac{\partial^2 G^c}{\partial t^2}(x,y,s,t) - \Delta_y G^c(x,y,s,t) = -\delta_x(y)\delta_s(t), & (y,t) \in \Omega \times \mathbb{R}\,, \\ G^c(x,y,s,t) = 0, \quad \dfrac{\partial G^c}{\partial t}(x,y,s,t) = 0, & y \in \Omega, \quad t < s\,, \\ G^c(x,y,s,t) = 0, & (y,t) \in \partial\Omega \times \mathbb{R}\,. \end{cases}$$

We also introduce the anticausal Dirichlet Green function (also called advanced Dirichlet Green function) $G^a(x,y,s,t)$ defined as the solution of the following wave equation

$$\begin{cases} \dfrac{\partial^2 G^a}{\partial t^2}(x,y,s,t) - \Delta_y G^a(x,y,s,t) = -\delta_x(y)\delta_s(t), & (y,t) \in \Omega \times \mathbb{R}\,, \\ G^a(x,y,s,t) = 0, \quad \dfrac{\partial G^a}{\partial t}(x,y,s,t) = 0, & y \in \Omega, \quad t > s\,, \\ G^a(x,y,s,t) = 0, & (y,t) \in \partial\Omega \times \mathbb{R}\,. \end{cases}$$

Using the time-reversibility of the wave equation, the anticausal Green function is given in terms of the causal Green function by

$$G^a(x,y,s,t) = G^c(x,y,s,2s-t) = G^c(x,y,t,s)\,. \tag{7.10}$$

Finally we introduce the symmetric Dirichlet Green function:

$$G(x,y,s,t) = \frac{1}{2}\Big(G^a(x,y,s,t)\chi((-\infty,s))(t) + G^c(x,y,s,t)\chi((s,\infty))(t)\Big)\,,$$

where $\chi((-\infty,s))$ and $\chi((s,\infty))$ are the characteristic functions of the intervals $(-\infty,s)$ and (s,∞), respectively. The function G contains both the causal and anticausal Green functions and it is a solution of

$$\begin{cases} \dfrac{\partial^2 G}{\partial t^2}(x,y,s,t) - \Delta_y G(x,y,s,t) = -\delta_x(y)\delta_s(t), & (y,t) \in \Omega \times \mathbb{R}, \\ G(x,y,s,t) = 0, & (y,t) \in \partial\Omega \times \mathbb{R}\,. \end{cases}$$

We can then express the time-reversal imaging functional $\mathcal{I}_{\mathrm{TR}}^{(1)}$ as

$$\mathcal{I}_{\mathrm{TR}}^{(1)}(x) = v(x,T) = \frac{1}{2}\int_0^T \int_{\partial\Omega} \frac{\partial G^c(x,y,s,T)}{\partial \nu_y} g(y,T-s)d\sigma(y)ds\,,$$

where $\partial/\partial\nu_y$ denotes the outward normal derivative at $y \in \partial\Omega$. The relation (7.10) yields

$$\begin{aligned} \mathcal{I}_{\mathrm{TR}}^{(1)}(x) &= \frac{1}{2}\int_0^T \int_{\partial\Omega} \frac{\partial G^a(x,y,T,s)}{\partial \nu_y} g(y,T-s)d\sigma(y)ds \\ &= \int_0^T \int_{\partial\Omega} \frac{\partial G(x,y,T,s)}{\partial \nu_y} g(y,T-s)d\sigma(y)ds \\ &= \int_0^T \int_{\partial\Omega} \frac{\partial G(x,y,0,t)}{\partial \nu_y} g(y,t)d\sigma(y)dt\,, \end{aligned}$$

because G is even. Since $g(x,t) = 0$ for $t \geq T$ and for $t \leq 0$,

$$\mathcal{I}_{\mathrm{TR}}^{(1)}(x) = \int_{\mathbb{R}} \int_{\partial\Omega} \frac{\partial G(x,y,0,t)}{\partial\nu_y} g(y,t) d\sigma(y) dt . \tag{7.11}$$

In identity (7.11), the dependence of the time-reversal functional $\mathcal{I}_{\mathrm{TR}}^{(1)}$ on the boundary data g is explicitly shown. Moreover, it follows from (7.7) that

$$\mathcal{I}_{\mathrm{TR}}^{(1)}(x) = -\int_\Omega f(z) \int_{\mathbb{R}} \int_{\partial\Omega} \frac{\partial G(x,y,0,t)}{\partial\nu_y} \frac{\partial\Gamma}{\partial t}(z,y,0,t) d\sigma(y) dt \, dz . \tag{7.12}$$

The reason why we have chosen to express the functional $\mathcal{I}_{\mathrm{TR}}^{(1)}$ in terms of the symmetric Green function G rather than in terms of the causal Green function G^c will be clear later.

Now we prove that $\mathcal{I}_{\mathrm{TR}}^{(1)}(x)$ gives a perfect image of $f(x)$. For doing so, we denote

$$G_\omega(x,y) = \int_{\mathbb{R}} G(x,y,0,t)e^{i\omega t} dt .$$

Then from (7.6), (7.12), and Parseval's relation (2.32), we have

$$\mathcal{I}_{\mathrm{TR}}^{(1)}(x) = -\frac{i}{2\pi} \int_\Omega f(z) \int_{\mathbb{R}} \omega \int_{\partial\Omega} \frac{\partial G_\omega}{\partial\nu_y}(x,y)\overline{\Gamma_\omega}(z,y) d\sigma(y) \, d\omega \, dz .$$

Moreover, by integrating by parts over Ω we get

$$\int_{\partial\Omega} \frac{\partial G_\omega}{\partial\nu_y}(x,y)\overline{\Gamma_\omega}(z,y) d\sigma(y) = \overline{\Gamma_\omega}(z,x) - G_\omega(x,z) = \overline{\Gamma_\omega}(x,z) - G_\omega(x,z) ,$$

and recalling that G_ω is real-valued because $t \to G(x,y,0,t)$ is real and even, we have

$$\Im \int_{\partial\Omega} \frac{\partial G_\omega}{\partial\nu_y}(x,y)\overline{\Gamma_\omega}(z,y) d\sigma(y) = \Im\left\{\overline{\Gamma_\omega}(x,z)\right\} = -\Im\left\{\Gamma_\omega(x,z)\right\} .$$

Therefore,

$$\mathcal{I}_{\mathrm{TR}}^{(1)}(x) = -\frac{1}{2\pi} \int_\Omega f(z) \int_{\mathbb{R}} \omega\Im\left\{\Gamma_\omega(x,z)\right\} d\omega \, dz . \tag{7.13}$$

Recall that

$$\frac{1}{\pi} \int_{\mathbb{R}} \omega\Im\left\{\Gamma_\omega(x,z)\right\} d\omega = -\delta_z(x) , \tag{7.14}$$

which follows from (2.27) or equivalently, from using

$$\lim_{t\to 0^+} \frac{\partial\Gamma}{\partial t}(x,z,0,0) = -\delta_z(x)$$

and (7.6).

Finally, from (7.13) it follows that

$$2\mathcal{I}_{\text{TR}}^{(1)}(x) = f(x) \ .$$

Note that the choice of the symmetric Dirichlet Green function is justified by the fact that its Fourier transform is real-valued. The ideal time-reversal imaging functional $\mathcal{I}_{\text{TR}}^{(1)}$ yields a perfect image of f. However, we need to compute the symmetric Dirichlet Green function G associated with the domain Ω. In the general case, it may be difficult to find an explicit expression for G. In the next section we introduce a modified time-reversal imaging functional where G is replaced with the free space fundamental solution Γ and show that the modified functional yields a good approximation of the source term f.

7.3.2 A Modified Time-Reversal Imaging Technique

In this section, we present a modified approach to the time-reversal concept using "free boundary conditions". For $s \in [0, T]$ we introduce the function v_s defined as the solution to the wave problem

$$\begin{cases} \dfrac{\partial^2 v_s}{\partial t^2}(x, t) - \Delta_x v_s(x, t) = \dfrac{d\delta_s}{dt}(t)g(x, T - s)\delta_{\partial\Omega}(x), & (x, t) \in \mathbb{R}^d \times \mathbb{R} \ , \\[2ex] v_s(x, t) = 0, \quad \dfrac{\partial v_s}{\partial t}(x, t) = 0, & x \in \mathbb{R}^d, \quad t < s \ . \end{cases}$$

Here, $\delta_{\partial\Omega}$ is the surface Dirac measure on $\partial\Omega$ and g is the measured data.

We define a modified time-reversal imaging functional by

$$\mathcal{I}_{\text{TR}}^{(2)}(x) = \int_0^T v_s(x, T)ds, \quad x \in \Omega \ . \tag{7.15}$$

Note that

$$v_s(x, t) = -\int_{\partial\Omega} \frac{\partial\Gamma}{\partial t}(x, y, s, t)g(y, T - s) \, d\sigma(y) \ .$$

Consequently, the functional $\mathcal{I}_{\text{TR}}^{(2)}$ can be expressed in terms of the free-space fundamental solution Γ as follows:

$$\mathcal{I}_{\text{TR}}^{(2)}(x) = -\int_0^T \int_{\partial\Omega} \frac{\partial\Gamma}{\partial t}(x, y, s, T)g(y, T - s)d\sigma(y)ds,$$

$$= -\int_{\mathbb{R}} \int_{\partial\Omega} \frac{\partial\Gamma}{\partial t}(x, y, 0, t)g(y, t)d\sigma(y)dt \quad x \in \Omega \ . \tag{7.16}$$

Note that $\mathcal{I}_{\text{TR}}^{(2)}$ is not exactly equivalent to $\mathcal{I}_{\text{TR}}^{(1)}$ but is an approximation. Indeed, denoting by

$$g_\omega(y) = \int g(y, s)e^{i\omega s}ds$$

the Fourier transform of $g(s, y)$, we have from (7.6) and (7.7)

$$g_\omega(y) = i\omega \int_\Omega \Gamma_\omega(z, y) f(z) \, dz \ .$$

Parseval's relation and (7.6) give

$$
\begin{aligned}
\mathcal{I}_{\text{TR}}^{(2)}(x) &= -\int_0^T \int_{\partial\Omega} \frac{\partial \Gamma}{\partial t}(x, y, 0, t) g(y, t) d\sigma(y) dt \\
&= \frac{1}{2\pi} \int_{\mathbb{R}} \int_{\partial\Omega} i\omega \Gamma_\omega(x, y) \overline{g}_\omega(y) d\sigma(y) d\omega \ , \\
&= \frac{1}{2\pi} \int_{\mathbb{R}^d} f(z) \int_{\mathbb{R}} \int_{\partial\Omega} \omega^2 \Gamma_\omega(x, y) \overline{\Gamma}_\omega(z, y) d\sigma(y) d\omega dz \ .
\end{aligned}
$$

Using the Helmholtz-Kirchhoff identity (3.82)

$$\int_{\partial\Omega} \Gamma_\omega(x, y) \overline{\Gamma}_\omega(z, y) d\sigma(y) \approx -\frac{1}{\omega} \Im\left\{\Gamma_\omega(x, z)\right\} \ ,$$

which is valid when Ω is a sphere with a large radius in $\mathbb{R}^d$, we find

$$2\mathcal{I}_{\text{TR}}^{(2)}(x) \approx -\frac{1}{\pi} \int_{\mathbb{R}^d} f(z) \int_{\mathbb{R}} \omega \Im\left\{\Gamma_\omega(x, z)\right\} d\omega dz \ .$$

Using (7.14), we finally obtain that

$$2\mathcal{I}_{\text{TR}}^{(2)}(x) \approx f(x) \ ,$$

which yields

$$\mathcal{I}_{\text{TR}}^{(2)}(x) \approx \mathcal{I}_{\text{TR}}^{(1)}(x) \ .$$

Note that, from (7.7), the operator $\mathcal{T} : f \to g$ can be expressed in the form

$$\mathcal{T}(f)(y, t) = g(y, t) = -\int_{\mathbb{R}^d} \frac{\partial \Gamma}{\partial t}(x, y, 0, t) f(x) dx, \quad (y, t) \in \partial\Omega \times [0, T] \ .$$

Then its adjoint $\mathcal{T}^*$ satisfies

$$\mathcal{T}^*(g)(x) = -\int_{\mathbb{R}} \int_{\partial\Omega} \frac{\partial \Gamma}{\partial t}(x, y, 0, t) g(y, t) d\sigma(y) dt \ ,$$

which can be seen from (7.16) to be the time-reversal functional $\mathcal{I}_{\text{TR}}^{(2)}$.

8

Time-Harmonic Reverse-Time Imaging With Additive Noise

In this chapter we consider acoustic and microwave imaging in the presence of measurement noise. Within the Born approximation, we analyze the stability and the resolution properties of reverse-time imaging.

8.1 The Data Set

Let us consider the propagation of scalar waves in a three-dimensional medium. In the presence of a localized reflector, the speed of propagation can be modeled by

$$\frac{1}{c^2(x)} = \frac{1}{c_0^2}\left(1 + V_{\text{ref}}(x)\right). \tag{8.1}$$

Here
- the constant c_0 is the known background speed. For simplicity, we assume that $c_0 = 1$;
- the local variation $V_{\text{ref}}(x)$ of the speed of propagation induced by the reflector at z_{ref} is of the form

$$V_{\text{ref}}(x) = \sigma_{\text{ref}}\chi(\Omega_{\text{ref}})(x - z_{\text{ref}}), \tag{8.2}$$

where σ_{ref} is the reflectivity of the reflector, z_{ref} is its center, and Ω_{ref} is a compactly supported domain with volume l_{ref}^3 that models its spatial support.

Suppose that we have co-localized time-harmonic transmitter and receiver arrays $\{x_1, \ldots, x_n\}$ of n elements, used to detect the reflector. In the presence of a reflector, the field received by the jth receiving element x_j when the transmitter at x_l emits a unitary time-harmonic wave is $u(\omega, x_j, x_l)$, where $u(\omega, x, y)$ the solution to the Helmholtz equation

$$\Delta_x u + \frac{\omega^2}{c^2(x)}u = \delta(x - y), \tag{8.3}$$

with the Sommerfeld radiation condition imposed on u.

The data set collected by the array describes the transmit-receive process performed at this array. If we remove the incident field then it can be defined as

$$\{v(\omega, x_j, x_l),\ j, l = 1, \ldots, n\}, \tag{8.4}$$

with

$$v(\omega, x_j, x_l) = u(\omega, x_j, x_l) - \Gamma_\omega(x_j, x_l) + W_{j,l}. \tag{8.5}$$

Here $W_{j,l}$ represents the additive measurement noise. The incident field is given in terms of the homogeneous Green's function $\Gamma_\omega(x, y)$ defined by (7.3).

8.2 The Forward Problem

A reflector is embedded at z_{ref} and is modeled by the local variation $V_{\mathrm{ref}}(x)$ of the propagation speed as in (8.1). The full Green function Φ_ω, that is to say, the Green function of the medium in the presence of the reflector at z_{ref}, is solution of

$$\Delta_x \Phi_\omega(x, y) + \frac{\omega^2}{c^2(x)} \Phi_\omega(x, y) = \delta(x - y). \tag{8.6}$$

From Lemma 3.35, it follows that the Lippmann-Schwinger integral equation for the full Green function Φ_ω is

$$\Phi_\omega(x, y) = \Gamma_\omega(x, y) - \omega^2 \int \Phi_\omega(x, z) V_{\mathrm{ref}}(z) \Gamma_\omega(z, y) dz. \tag{8.7}$$

Using the Born approximation, we get

$$\Phi_\omega(x, y) = \Gamma_\omega(x, y) - \omega^2 \int \Gamma_\omega(x, z) V_{\mathrm{ref}}(z) \Gamma_\omega(z, y) dz. \tag{8.8}$$

Therefore the full Green's function can be written as the sum

$$\Phi_\omega(x, y) = \Gamma_\omega(x, y) + G_{\mathrm{ref}}(\omega, x, y). \tag{8.9}$$

The term G_{ref} is the term in the data set that corresponds to the reflector:

$$G_{\mathrm{ref}}(\omega, x, y) = -\omega^2 \int \Gamma_\omega(x, z) V_{\mathrm{ref}}(z) \Gamma_\omega(z, y) dz.$$

The approximation (8.9) is formally valid if the correction G_{ref} is small compared to Γ_ω, i.e., in the regime in which $\sigma_{\mathrm{ref}} \ll 1$, with an error that is formally of order $O(\sigma_{\mathrm{ref}}^2)$. We also assume that the diameter l_{ref} of the scattering region Ω_{ref} is small compared to the typical wavelength. We can then model the reflector by a point reflector (the point interaction approximation)

$$V_{\mathrm{ref}}(x) \approx \sigma_{\mathrm{ref}} l_{\mathrm{ref}}^3 \delta(x - z_{\mathrm{ref}}), \tag{8.10}$$

and we can write the correction in the form

$$G_{\mathrm{ref}}(\omega, x, y) = -\omega^2 \sigma_{\mathrm{ref}} l_{\mathrm{ref}}^3 \Gamma_\omega(x, z_{\mathrm{ref}}) \Gamma_\omega(z_{\mathrm{ref}}, y). \tag{8.11}$$

The data set is therefore of the form

$$v(\omega, x_j, x_l) = v_{\mathrm{ref}}(\omega, x_j, x_l) + W_{jl}, \tag{8.12}$$

with v_{ref} the ideal data set in the absence of measurement noise

$$\begin{aligned} v_{\mathrm{ref}}(\omega, x_j, x_l) &= G_{\mathrm{ref}}(\omega, x_j, x_l) \\ &= -\omega^2 \sigma_{\mathrm{ref}} l_{\mathrm{ref}}^3 \Gamma_\omega(x_j, z_{\mathrm{ref}}) \Gamma_\omega(z_{\mathrm{ref}}, x_l), \end{aligned} \tag{8.13}$$

and W_{jl} is the measurement noise. We assume that the random variables W_{jl} are independent and identically distributed, with a circular complex Gaussian distribution with variance σ_{mes}^2, that is to say, $\Re(W_{jl})$ and $\Im(W_{jl})$ are independent and identically distributed real-valued Gaussian random variables with mean zero and variance $\sigma_{\mathrm{mes}}^2/2$.

8.3 Imaging Functionals

Define, for a smooth compactly supported V,

$$[\mathcal{A}(\omega)V]_{jl} = -\int_{\mathbb{R}^3} \Gamma_\omega(x_j, z) V(z) \Gamma_\omega(z, x_l) dz . \tag{8.14}$$

$\mathcal{A}(\omega)$ is the frequency-dependent, linear operator that maps the function V to the array data (up to the factor ω^2).

In order to image the support of V, a least-squares method can be used. The least-squares inverse problem under the Born approximation consists in minimizing over the functions V the misfit functional $J_{\mathrm{LS}}[V]$:

$$J_{\mathrm{LS}}[V] := \sum_{j,l=1}^{n} \left| A_{jl}^{\mathrm{meas}}(\omega) - [\mathcal{A}(\omega)V]_{jl} \right|^2 ,$$

where $A^{\mathrm{meas}}(\omega)$ is the measured data matrix (8.12). The solution of the least-squares linearized inverse problem is

$$V_{\mathrm{LS}} = \left(\mathcal{A}^*(\omega)\mathcal{A}(\omega) \right)^{-1} \left(\mathcal{A}^*(\omega) A^{\mathrm{meas}}(\omega) \right) .$$

Here the adjoint operator $\mathcal{A}^*(\omega)$ is defined for $n \times n$ matrices $A = (A_{jl})$ by

$$\left[\mathcal{A}^*(\omega)A \right](x) = -\sum_{j,l=1}^{n} \overline{\Gamma_\omega(x, x_j) \Gamma_\omega(x_l, x)} A_{jl} .$$

Remember that the complex conjugation in the frequency domain corresponds to the time-reversal operation in the time domain. This shows that the adjoint

operator corresponds to the backpropagation of the array data both from the receiver point x_j and from the source point x_l to the test point x.

The least-squares imaging functional is

$$\mathcal{I}_{\mathrm{LS}}(x) = \left[\left(\mathcal{A}^*(\omega)\mathcal{A}(\omega)\right)^{-1}\left(\mathcal{A}^*(\omega)A^{\mathrm{meas}}(\omega)\right)\right](x) . \tag{8.15}$$

Motivated by the fact that we often have $\mathcal{A}^*(\omega)\mathcal{A}(\omega) \approx I$, where I is the identity operator (in particular, this is a consequence of the Helmholtz-Kirchhoff identity when the array completely surrounds the region of interest), we can drop this term to get a simplified imaging functional. The Reverse-Time migration imaging functional for the search point x is defined by

$$\mathcal{I}_{\mathrm{RT}}(x) := \left[\mathcal{A}^*(\omega)A^{\mathrm{meas}}(\omega)\right](x)$$
$$= -\sum_{j,l=1}^{n} \overline{\Gamma_\omega(x,x_j)\Gamma_\omega(x_l,x)}A_{jl}^{\mathrm{meas}}(\omega) . \tag{8.16}$$

The Kirchhoff migration (or travel time migration) is obtained as a simplification of the Reverse-Time migration imaging functional in which we replace $\Gamma_\omega(x,y)$ with $e^{i\omega\mathcal{T}(x,y)}$, where $\mathcal{T}(x,y) = |x - y|$ is the travel time from x to y (since $c_0 = 1$). Therefore the Kirchhoff migration imaging functional has the form:

$$\mathcal{I}_{\mathrm{KM}}(x) := -\sum_{j,l=1}^{n} e^{-i\omega(\mathcal{T}(x_j,x)+\mathcal{T}(x_l,x))}A_{jl}^{\mathrm{meas}}(\omega) .$$

8.4 The RT-Imaging Function

In the presence of a point reflector at z_{ref} and in the presence of additive noise the data set is of the form (8.12). We study the effect of the measurement noise on the time-harmonic reverse-time imaging function defined by

$$\mathcal{I}_{\mathrm{RT}}(x) = -\sum_{j,l=1}^{n} \overline{\Gamma_\omega(x,x_j)\Gamma_\omega(x,x_l)}v(\omega,x_j,x_l). \tag{8.17}$$

8.4.1 The Imaging Function Without Measurement Noise

In the absence of noise $\sigma_{\mathrm{mes}} = 0$ the imaging function is given by

$$\mathcal{I}_{\mathrm{RT}}(x) = \mathcal{I}_0(x), \qquad \mathcal{I}_0(x) = \sigma_{\mathrm{ref}}l_{\mathrm{ref}}^3 n^2\omega^2\mathcal{H}(x, z_{\mathrm{ref}}), \tag{8.18}$$

where

$$\mathcal{H}(x,y) = \left(\frac{1}{n}\sum_{j=1}^{n}\Gamma_\omega(x,x_j)\overline{\Gamma_\omega(y,x_j)}\right)^2 . \tag{8.19}$$

The function $x \to \mathcal{H}(x, z_{\text{ref}})$ is the point spread function that describes the spatial profile of the peak obtained at the reflector location z_{ref} in the imaging function when the reflector is point-like.

Full-Aperture Array

If the sensor array is dense (i.e. the inter-sensor distance is smaller than half a wavelength) and completely surrounds the region of interest (for instance, it covers the surface of the ball with center at 0 and radius L) then Helmholtz-Kirchhoff theorem states that $\mathcal{H}(x, y)$ is proportional to the square of the imaginary part of the Green's function $\Gamma_\omega(x, y)$. We find

$$\mathcal{H}(x, y) = C_L \widetilde{\mathcal{H}}(x - y), \text{ where } \widetilde{\mathcal{H}}(x) = \text{sinc}^2(\omega|x|), \tag{8.20}$$

and $C_L = 1/(4\pi L)^4$. Therefore we have

$$\mathcal{I}_0(x) = \sigma_0 \widetilde{\mathcal{H}}(x - z_{\text{ref}}), \tag{8.21}$$

where

$$\sigma_0 = \frac{\sigma_{\text{ref}} l_{\text{ref}}^3 n^2 \omega^2}{(4\pi L)^4}, \qquad \widetilde{\mathcal{H}}(x) = \text{sinc}^2\left(\frac{2\pi|x|}{\lambda}\right), \tag{8.22}$$

and $\lambda = 2\pi/\omega$ is the wavelength. This shows that the width of the point spread function $\widetilde{\mathcal{H}}(x)$ is of the order of $\lambda/2$, which is the Abbe diffraction limit [112].

8.4.2 The Imaging Function With Measurement Noise

In the presence of measurement noise the imaging function is a complex Gaussian random field. Its mean is the unperturbed imaging function $\mathcal{I}_0$ defined by (8.18), its relation function is zero:

$$\mathbb{E}\left[\left(\mathcal{I}_{\text{RT}}(x) - \mathcal{I}_0(x)\right)\left(\mathcal{I}_{\text{RT}}(x') - \mathcal{I}_0(x')\right)\right] = 0,$$

and its covariance functions is:

$$\text{Cov}\left(\mathcal{I}_{\text{RT}}(x), \mathcal{I}_{\text{RT}}(x')\right) = \mathbb{E}\left[\left(\mathcal{I}_{\text{RT}}(x) - \mathcal{I}_0(x)\right)\left(\overline{\mathcal{I}_{\text{RT}}(x') - \mathcal{I}_0(x')}\right)\right],$$

$$= \sigma_{\text{mes}}^2 n^2 \left(\frac{1}{n} \sum_{j=1}^{n} \Gamma_\omega(x, x_j) \overline{\Gamma_\omega(x', x_j)}\right)^2$$

$$= \sigma_{\text{mes}}^2 n^2 \mathcal{H}(x, x'). \tag{8.23}$$

If we assume that $\mathcal{H}(x, y) = C_L \widetilde{\mathcal{H}}(x - y)$, with $\widetilde{\mathcal{H}}(x)$ a smooth peaked function centered at 0, as in the case of a full-aperture array discussed above, then we can see that the messurement noise creates a speckle noise $\mathcal{I}_{\text{RT}} - \mathcal{I}_0$

in the image, which is a stationary Gaussian random field with mean zero, variance

$$\sigma^2_{\text{noise}} = \sigma^2_{\text{mes}} n^2 C_L \widetilde{\mathcal{H}}(0), \tag{8.24}$$

and covariance function:

$$\text{Cov}\big(\mathcal{I}_{\text{RT}}(x), \mathcal{I}_{\text{RT}}(x')\big) = \sigma^2_{\text{noise}} \mathcal{H}_{\text{noise}}(x - x'), \tag{8.25}$$

with

$$\mathcal{H}_{\text{noise}}(x) = \frac{\widetilde{\mathcal{H}}(x)}{\widetilde{\mathcal{H}}(0)}. \tag{8.26}$$

This random field is a speckle pattern whose hotspot profiles are close to the function $\mathcal{H}_{\text{noise}}(x)$, which is (proportional to) the point spread function of the imaging function. Here the hotspot profile refers to the local shape of the speckle field around a local maximum (see Section 4.4).

The hotspot volume is defined as

$$V_c = \frac{4\pi^2}{(\det \Lambda)^{1/2}}, \qquad \Lambda = \Big(- \partial^2_{x_j x_l} \mathcal{H}_{\text{noise}}(x) \,|_{x=0} \Big)_{j,l=1,\dots,3}. \tag{8.27}$$

The maximum of the random field $\mathcal{I}_{\text{RT}}(x) - \mathcal{I}_0(x)$ over a domain Ω whose volume is much larger than the hotspot volume is a random quantity described in Section 4.4, which is equal to a deterministic value to leading order in $|\Omega|/V_c$:

$$\max_{x \in \Omega} \big\{\mathcal{I}_{\text{RT}}(x) - \mathcal{I}_0(x)\big\} = \sigma_{\text{noise}} \sqrt{2 \log \Big(\frac{|\Omega|}{V_c}\Big)}. \tag{8.28}$$

Full-Aperture Array

In the case in which the array completely surrounds the region of interest, $\mathcal{I}_{\text{RT}}(x)$ is a Gaussian random field with mean $\mathcal{I}_0(x)$ given by (9.23), variance

$$\sigma^2_{\text{noise}} = \sigma^2_{\text{mes}} n^2 \frac{1}{(4\pi L)^4}, \tag{8.29}$$

and covariance function:

$$\text{Cov}\big(\mathcal{I}_{\text{RT}}(x), \mathcal{I}_{\text{RT}}(x')\big) = \sigma^2_{\text{noise}} \mathcal{H}_{\text{noise}}(x - x'), \qquad \mathcal{H}_{\text{noise}}(x) = \text{sinc}^2\Big(\frac{2\pi|x|}{\lambda}\Big). \tag{8.30}$$

The speckle pattern is made of hotspots with typical radius λ and typical amplitude σ_{noise}. The typical shape of the hotspot is given by the function $\mathcal{H}_{\text{noise}}(x)$, that has a slow power law decay as $1/|x|^2$. The signal to noise ratio in the image is

$$\mathrm{SNR} = \frac{\mathcal{I}_0(z_{\mathrm{ref}})}{\sigma_{\mathrm{noise}}} = \frac{\sigma_0}{\sigma_{\mathrm{noise}}} = \frac{n\sigma_{\mathrm{ref}}l_{\mathrm{ref}}^3\omega^2}{\sigma_{\mathrm{mes}}(4\pi L)^2} = \frac{n\sigma_{\mathrm{ref}}l_{\mathrm{ref}}^3}{4\sigma_{\mathrm{mes}}\lambda^2 L^2}. \tag{8.31}$$

Note that:
- The SNR increases with the number n of sensors, and this is because the additive noise is independent from one sensor to the other one.
- The SNR decays with the square of the wavelength, because the scattering efficiency (and therefore the reflected signal amplitude) at small wavelengths is inversely proportional to the square of the wavelength.
- The SNR decays with the square of the distance from the array to the reflector, because the reflected signal amplitude is inversely proportional to the distance from the array to the reflector (in a three-dimensional homogeneous medium).

In the case of the full-aperture array, the matrix Λ is proportional to the identity and the hotspot volume is

$$\Lambda = \frac{8\pi^2}{3\lambda^2}I, \qquad V_c = \frac{3^{3/2}}{2^{5/2}\pi}\lambda^3. \tag{8.32}$$

This result shows that the SNR (8.31) should be considered with cautious. If σ_{noise} is of the same order as σ_0, then the speckle pattern may have a local maximum whose peak amplitude is much larger than σ_{noise} and that could be misinterpreted as a reflector.

When the SNR is large, the imaging function has the form of a peak centered at the reflector location z_{ref} that emerges from the speckle pattern. When the SNR is small, the peak centered at z_{ref} is buried into the speckle pattern.

8.4.3 Localization Error

The localization of the reflector consists in looking after the maximum of the imaging functional (the statistical approach proposed in [58] shows that the location of the maximum of the Reverse-Time imaging function is the Maximum Likelihood Estimator of the location of the reflector). In the presence of a reflector at z_{ref} the imaging functional has the form

$$\mathcal{I}_{\mathrm{RT}}(x) = \mathcal{I}_0(x) + \mathcal{I}_1(x),$$

where $\mathcal{I}_0$ is the unperturbed imaging function given by (8.18) and $\mathcal{I}_1$ is a complex Gaussian random field with mean zero, variance $\sigma_{\mathrm{noise}}^2$, and covariance function $\sigma_{\mathrm{noise}}^2 \mathcal{H}_{\mathrm{noise}}(x - x')$.

We consider the case in which $\mathcal{H}_{\mathrm{noise}}$ is real-valued, which is the case for a full-aperture array, and we denote by ℓ the width of the point spread function, which is of the order of λ for a full-aperture array. We assume $\sigma_{\mathrm{noise}} \ll \sigma_0$, so that a Taylor series expansion around z_{ref}, for $|x - z_{\mathrm{ref}}| \lesssim \ell/\mathrm{SNR} = \ell\sigma_{\mathrm{noise}}/\sigma_0$, gives:

$$\mathcal{I}_{\mathrm{RT}}(x) = \sigma_0 \Big(1 - \frac{1}{2}(x - z_{\mathrm{ref}})^T \Lambda (x - z_{\mathrm{ref}}) + \frac{1}{\sigma_0}\mathcal{I}_1(z_{\mathrm{ref}})$$

$$+ \frac{1}{\sigma_0}\nabla \mathcal{I}_1(z_{\mathrm{ref}})^T (x - z_{\mathrm{ref}}) + O\big(\frac{\sigma_{\mathrm{noise}}^3}{\sigma_0^3}\big)\Big). \qquad (8.33)$$

The estimator of the location of the maximum has the form:

$$\hat{z} = \underset{x}{\mathrm{argmax}}\left|\mathcal{I}_{\mathrm{RT}}(x)\right|^2 = z_{\mathrm{ref}} + \frac{1}{\sigma_0}\Re\big(\Lambda^{-1}\nabla \mathcal{I}_1(z_{\mathrm{ref}})\big) + O\big(\ell \frac{\sigma_{\mathrm{noise}}^2}{\sigma_0^2}\big).$$

To leading order (in $\sigma_{\mathrm{noise}}/\sigma_0$) the estimator $\hat{z}$ is unbiased, i.e. its mean is the true location z_{ref}. Moreover, using the fact that $\mathbb{E}\big[\Re\nabla\mathcal{I}_1(z_{\mathrm{ref}})\Re\nabla\mathcal{I}_1(z_{\mathrm{ref}})^T\big] = \sigma_{\mathrm{noise}}^2\Lambda/2$, the covariance matrix of the estimator $\hat{z}$ is

$$\mathbb{E}\big[(\hat{z} - z_{\mathrm{ref}})(\hat{z} - z_{\mathrm{ref}})^T\big] = \frac{\sigma_{\mathrm{noise}}^2}{2\sigma_0^2}\Lambda^{-1} = \frac{1}{2\,\mathrm{SNR}^2}\Lambda^{-1}, \qquad (8.34)$$

which is order ℓ^2/SNR^2. This means that the relative error (relative to the radius ℓ of the point spread function) in the localization of the reflector is of the order of $1/\mathrm{SNR} = \sigma_{\mathrm{noise}}/\sigma_0$. Note also that, as a byproduct of this analysis, we find that the perturbed value of the maximum of the peak is of the form

$$\left|\mathcal{I}_{\mathrm{RT}}(\hat{z})\right|^2 \simeq \sigma_0^2\Big(1 + \frac{2}{\sigma_0}\Re\big(\mathcal{I}_1(z_{\mathrm{ref}})\big) + O\big(\frac{\sigma_{\mathrm{noise}}^2}{\sigma_0^2}\big)\Big), \qquad (8.35)$$

where $\Re\big(\mathcal{I}_1(z_{\mathrm{ref}})\big)$ follows a Gaussian distribution with mean 0 and variance $\sigma_{\mathrm{noise}}^2/2$.

Full-Aperture Array

If the sensor array is dense and surrounds the region of interest, then the localization errors are independent along the three directions and their variances are

$$\mathbb{E}\big[(\hat{z}_j - z_{\mathrm{ref},j})^2\big] = \frac{\sigma_{\mathrm{noise}}^2}{\sigma_0^2}\frac{3\lambda^2}{16\pi^2} = \frac{1}{\mathrm{SNR}^2}\frac{3\lambda^2}{16\pi^2}, \quad j = 1, \ldots, 3.$$

This shows that the resolution is proportional to the wavelength and inversely proportional to the signal-to-noise ratio in the image (8.31).

Reverse-Time Imaging With Clutter Noise

9.1 The Data Set

Let us consider the propagation of scalar waves in a three-dimensional medium. In the presence of a localized reflector and small random fluctuations of the medium, the speed of propagation can be modeled by

$$\frac{1}{c^2(x)} = \frac{1}{c_0^2}\big(1 + V_{\mathrm{clu}}(x) + V_{\mathrm{ref}}(x)\big). \tag{9.1}$$

Here
- the constant c_0 is the known background speed. For simplicity, we assume that $c_0 = 1$;
- the random process $V_{\mathrm{clu}}(x)$ represents the cluttered medium;
- the local variation $V_{\mathrm{ref}}(x)$ of the speed of propagation induced by the reflector at z_{ref} is of the form

$$V_{\mathrm{ref}}(x) = \sigma_{\mathrm{ref}}\chi(\Omega_{\mathrm{ref}})(x - z_{\mathrm{ref}}), \tag{9.2}$$

where σ_{ref} is the reflectivity of the reflector, z_{ref} is its center, and Ω_{ref} is a compactly supported domain with volume l_{ref}^3 that models its spatial support.

Suppose that we have co-localized transmitter and receiver arrays $\{x_1, \ldots, x_n\}$ of n elements, used to detect the reflector. In the presence of a reflector and small random fluctuations of the medium, the field received by the jth receiving element x_j when the pulse $F(t)$ is emitted from x_l is $U(t, x_j, x_l)$, where $(t, x) \to U(t, x, y)$ is the solution to the scalar wave equation

$$\frac{1}{c^2(x)}\frac{\partial^2 U}{\partial t^2} - \Delta_x U = F(t)\delta(x - y), \tag{9.3}$$

or, in the Fourier domain, $(\omega, x) \to u(\omega, x, y)$ defined by

$$u(\omega, x, y) = \mathcal{F}_{\mathrm{t}}[u(\cdot, x, y)](\omega) = \frac{1}{\sqrt{2\pi}}\int_{-\infty}^{\infty} U(t, x, y)e^{i\omega t}dt$$

is the solution to the Helmholtz equation

$$\Delta_x u + \frac{\omega^2}{c^2(x)} u = -f(\omega)\delta(x - y), \tag{9.4}$$

with the Sommerfeld radiation condition imposed on u. Here, f is the Fourier transform of F

$$f(\omega) = \mathcal{F}_t[F](\omega) = \frac{1}{\sqrt{2\pi}} \int_{-\infty}^{\infty} F(t)e^{i\omega t}dt\,.$$

The data set collected by the array describes the transmit-receive process performed at this array. If we remove the incident field, which is here $-\Gamma_\omega(x, x_l)f(\omega)$ when the source is at x_l and emits $F(t)$, then it can be defined as

$$\{v(\omega, x_j, x_l),\ \omega \in \mathbb{R},\ j, l = 1, \ldots, n\}, \tag{9.5}$$

with

$$v(\omega, x_j, x_l) = u(\omega, x_j, x_l) + \Gamma_\omega(x_j, x_l)f(\omega). \tag{9.6}$$

The incident field is given in terms of the homogeneous Green's function $\Gamma_\omega(x, y)$ defined by (7.3).

9.2 A Model for the Scattering Medium

In this section we introduce a model for the inhomogeneous medium. We assume that the propagation speed of the medium has a homogeneous background speed value 1 and small fluctuations responsible for scattering:

$$\frac{1}{c_{\mathrm{clu}}^2(x)} = 1 + V_{\mathrm{clu}}(x)\,, \tag{9.7}$$

where $V_{\mathrm{clu}}(x)$ is a random process with mean zero and covariance function of the form

$$\mathbb{E}\big[V_{\mathrm{clu}}(x)V_{\mathrm{clu}}(x')\big] = \sigma_{\mathrm{clu}}^2 \sqrt{K_{\mathrm{clu}}(x)K_{\mathrm{clu}}(x')} H_{\mathrm{clu}}\Big(\frac{x - x'}{l_{\mathrm{clu}}}\Big). \tag{9.8}$$

Here $\mathbb{E}$ stands for the expectation with respect to the distribution of the randomly scattering medium. σ_{clu} is the standard deviation of the fluctuations. The function $x \rightarrow K_{\mathrm{clu}}(x)$ is nonnegative valued, smooth, and compactly supported, it characterizes the spatial support of the scatterers (and the typical amplitude of $K_{\mathrm{clu}}(x)$ is of order one). The function $x \rightarrow H_{\mathrm{clu}}(x/l_{\mathrm{clu}})$ is the local correlation function. It is normalized so that $H_{\mathrm{clu}}(0) = 1$ and $\int H_{\mathrm{clu}}(x)dx = 1$. Therefore l_{clu} can be considered as the correlation length of the random medium. We assume that the standard deviation σ_{clu} is small (smaller than one) and that the correlation length l_{clu} is small (smaller than the wavelength).

For simulation purposes, the random medium fluctuations can be seen as $V_{\mathrm{clu}}(x) = \sigma_{\mathrm{clu}}\sqrt{K_{\mathrm{clu}}(x)}Z_{\mathrm{clu}}(x/l_{\mathrm{clu}})$ where $Z_{\mathrm{clu}}(x)$ is a stationary random process with mean zero, variance one, and correlation length equal to one. Realizations of a stationary random process can be generated by spectral methods easily.

The clutter Green's function G_{clu}, that is to say, the Green's function of the medium with clutter noise, is the fundamental solution of

$$\Delta_x G_{\mathrm{clu}}(\omega, x, y) + \frac{\omega^2}{c_{\mathrm{clu}}^2(x)} G_{\mathrm{clu}}(\omega, x, y) = \delta(x - y), \qquad (9.9)$$

with the Sommerfeld radiation condition, where $c_{\mathrm{clu}}(x)$ is given by (9.7). The Lippmann-Schwinger integral equation for the clutter Green's function G_{clu} defined by (9.9) is

$$G_{\mathrm{clu}}(\omega, x, y) = \Gamma_\omega(x, y) - \omega^2 \int G_{\mathrm{clu}}(\omega, x, z) V_{\mathrm{clu}}(z) \Gamma_\omega(z, y) \, dz, \qquad (9.10)$$

where $V_{\mathrm{clu}}(x)$ is the random process modeling the background fluctuations as described by (9.7). We will use the Born or single-scattering approximation for the clutter Green's function solution of (9.10) by replacing G_{clu} by Γ_ω on the right-hand side. This approximation takes into account single-scattering events for the interaction of the waves with the cluttered medium:

$$G_{\mathrm{clu}}(\omega, x, y) = \Gamma_\omega(x, y) + G_1(\omega, x, y), \qquad (9.11)$$

where G_1 is given by

$$G_1(\omega, x, y) = -\omega^2 \int \Gamma_\omega(x, z) V_{\mathrm{clu}}(z) \Gamma_\omega(z, y) \, dz, \qquad (9.12)$$

and the error is formally of order $O(\sigma_{\mathrm{clu}}^2)$ where σ_{clu} is the standard deviation of $V_{\mathrm{clu}}(x)$.

9.3 The Forward Problem

We now assume that a reflector is embedded at z_{ref} in the cluttered medium. We model the reflector by a local variation $V_{\mathrm{ref}}(x)$ of the propagation speed as in (9.1). The full Green's function Φ_ω, that is to say, the Green's function of the medium with clutter in the presence of the reflector at z_{ref}, is solution of

$$\Delta_x \Phi_\omega(x, y) + \frac{\omega^2}{c^2(x)} \Phi_\omega(x, y) = \delta(x - y). \qquad (9.13)$$

The Lippmann-Schwinger integral equation for the full Green's function Φ_ω is

$$\Phi_\omega(x,y) = \Gamma_\omega(x,y) - \omega^2 \int \Phi_\omega(x,z)\big(V_{\mathrm{clu}}(z) + V_{\mathrm{ref}}(z)\big)\Gamma_\omega(z,y)dz. \quad (9.14)$$

Using again the Born approximation, we get

$$\Phi_\omega(x,y) = \Gamma_\omega(x,y) - \omega^2 \int \Gamma_\omega(x,z)\big(V_{\mathrm{clu}}(z) + V_{\mathrm{ref}}(z)\big)\Gamma_\omega(z,y)dz. \quad (9.15)$$

Therefore the full Green's function can be written as the sum

$$\Phi_\omega(x,y) = \Gamma_\omega(x,y) + G_1(\omega,x,y) + G_{\mathrm{ref}}(\omega,x,y). \quad (9.16)$$

The term G_1 is the term in the data set that will be responsible to speckle noise in the image and it is of the form (9.12). The term G_{ref} is the term in the data set that corresponds to the reflector:

$$G_{\mathrm{ref}}(\omega,x,y) = -\omega^2 \int \Gamma_\omega(x,z)V_{\mathrm{ref}}(z)\Gamma_\omega(z,y)dz.$$

The approximation (9.16) is formally valid if the correction G_{ref} is small compared to Γ_ω, i.e., in the regime in which $\sigma_{\mathrm{ref}} \ll 1$, with an error that is formally of order $O(\sigma_{\mathrm{ref}}^2)$. We also assume that the diameter l_{ref} of the scattering region Ω_{ref} is small compared to the typical wavelength. We can then model the reflector by a point reflector (the point interaction approximation)

$$V_{\mathrm{ref}}(x) \approx \sigma_{\mathrm{ref}}l_{\mathrm{ref}}^3\delta(x - z_{\mathrm{ref}}), \quad (9.17)$$

and we can write the correction in the form

$$G_{\mathrm{ref}}(\omega,x,y) = -\omega^2\sigma_{\mathrm{ref}}l_{\mathrm{ref}}^3\Gamma_\omega(x,z_{\mathrm{ref}})\Gamma_\omega(z_{\mathrm{ref}},y). \quad (9.18)$$

The data set (9.5) is therefore of the form

$$v(\omega,x_j,x_l) = v_{\mathrm{ref}}(\omega,x_j,x_l) + w(\omega,x_j,x_l), \quad (9.19)$$

with v_{ref} the ideal data set in the absence of random fluctuations of the medium

$$\begin{aligned}
v_{\mathrm{ref}}(\omega,x_j,x_l) &= -G_{\mathrm{ref}}\big(\omega,x_j,x_l\big)f(\omega) \\
&= \omega^2 f(\omega)\sigma_{\mathrm{ref}}l_{\mathrm{ref}}^3\Gamma_\omega\big(x_j,z_{\mathrm{ref}}\big)\Gamma_\omega\big(z_{\mathrm{ref}},x_l\big), \quad (9.20)
\end{aligned}$$

and w the noise due to the interaction of the wave with the random fluctuations of the medium

$$\begin{aligned}
w(\omega,x_j,x_l) &= -G_1\big(\omega,x_j,x_l\big)f(\omega) \\
&= \omega^2 f(\omega) \int \Gamma_\omega\big(x_j,z\big)V_{\mathrm{clu}}(z)\Gamma_\omega\big(z,x_l\big)dz. \quad (9.21)
\end{aligned}$$

Since l_{clu} is small, the field w is Gaussian distributed by the Central Limit Theorem.

9.4 The Imaging Function

In the presence of a point reflector at z_{ref} and in the presence of clutter noise the data set is of the form (9.19). We study the effect of the clutter noise on the reverse-time imaging function defined by

$$\mathcal{I}_{\mathrm{RT}}(x) = \frac{1}{\sqrt{2\pi}} \sum_{j,l=1}^{n} \int d\omega \, \overline{\Gamma_\omega(x,x_j)\Gamma_\omega(x,x_l)} v(\omega, x_j, x_l). \qquad (9.22)$$

9.4.1 The Imaging Function Without Clutter Noise

In the absence of noise $\sigma_{\mathrm{clu}} = 0$ the imaging function is given by

$$\mathcal{I}_{\mathrm{RT}}(x) = \mathcal{I}_0(x), \qquad \mathcal{I}_0(x) = \sigma_{\mathrm{ref}} l_{\mathrm{ref}}^3 n^2 \mathcal{H}(x, z_{\mathrm{ref}}), \qquad (9.23)$$

where

$$\mathcal{H}(x, y) = \frac{1}{\sqrt{2\pi}} \int d\omega \omega^2 f(\omega) h(\omega, x, y), \qquad (9.24)$$

$$h(\omega, x, y) = \left(\frac{1}{n} \sum_{j=1}^{n} \overline{\Gamma_\omega(x, x_j)} \Gamma_\omega(y, x_j) \right)^2. \qquad (9.25)$$

The function $x \to \mathcal{H}(x, z_{\mathrm{ref}})$ is the point spread function that describes the spatial profile of the peak obtained at the reflector location z_{ref} in the imaging function when the reflector is point-like.

Full-Aperture Array

If the sensor array is dense (i.e. the inter-sensor distance is smaller than half a wavelength) and completely surrounds the region of interest (for instance, it covers the surface of the ball with center at 0 and radius L) then Helmholtz-Kirchhoff theorem states that $h(\omega, x, y)$ is proportional to the square of the imaginary part of the Green's function $\Gamma_\omega(x, y)$. We find

$$h(\omega, x, y) = C_L \widetilde{h}(\omega, x - y), \text{ where } \widetilde{h}(\omega, x) = \operatorname{sinc}^2(\omega|x|), \qquad (9.26)$$

and $C_L = 1/(4\pi L)^4$. Therefore, when the bandwidth B of F is smaller than its central frequency ω_0, for instance, when the source is a modulated Gaussian with central frequency ω_0 and bandwidth $B \ll \omega_0$:

$$F(t) = \cos(\omega_0 t) \exp\left(-\frac{B^2 t^2}{2} \right), \qquad (9.27)$$

and

$$f(\omega) = \frac{1}{2B} e^{-\frac{(\omega - \omega)^2}{2B^2}} + \frac{1}{2B} e^{-\frac{(\omega + \omega)^2}{2B^2}}, \qquad (9.28)$$

we have

$$\mathcal{H}(x, z_{\mathrm{ref}}) = C_L \omega_0^2 \widetilde{\mathcal{H}}(x - z_{\mathrm{ref}}), \tag{9.29}$$

where

$$\widetilde{\mathcal{H}}(x) = \mathrm{sinc}^2\Big(\frac{2\pi|x|}{\lambda_0}\Big), \tag{9.30}$$

and $\lambda_0 = 2\pi/\omega_0$ is the central wavelength. This shows that the width of the point spread function $\widetilde{\mathcal{H}}(x)$ is of the order of $\lambda_0/2$, which is the Abbe diffraction limit [112]. Note also that the function $\widetilde{\mathcal{H}}(x)$ decays slowly, as $1/|x|^2$, which will turn out to be problematic when addressing scattering media.

Finite-Aperture Array

If the sensor array is dense and occupies the domain $D_a \times \{0\}$, with $D_a \subset \mathbb{R}^2$ with diameter a, and the search region is a domain Ω around $(0, 0, L)$, then in the Fresnel diffraction regime $\lambda_0 \ll a \ll L$ with $\lambda_0^{1/2} L^{3/2} \gg a^2 \gg \lambda_0 L$ we have

$$h(\omega, x, y) = C_L \widetilde{h}(\omega, x - y), \tag{9.31}$$

where, for $x = (x_\perp, x_3)$,

$$\widetilde{h}(\omega, x) = e^{-2i\omega x_3} \Big(\frac{1}{|D_a|} \int_{D_a} \exp\Big(- i\frac{\omega y_\perp}{L} \cdot x_\perp - i\frac{\omega|y_\perp|^2}{2L^2} x_3 \Big) dy_\perp \Big)^2. \tag{9.32}$$

This shows that the width of the function $\widetilde{h}(\omega, x)$ is of the order of $\lambda L/a$ in the transverse directions $(x_\perp)$ and $\lambda L^2/a^2$ in the longitudinal direction (x_3), where $\lambda = 2\pi/\omega$ is the wavelength associated to the frequency ω. These are the classical Rayleigh resolution formulas for time-harmonic waves [112, Sections 8.5 and 8.8].

   If the bandwidth B of the pulse is smaller than the central frequency ω_0 and such that $B \ll \omega_0 a^2/L^2$, for instance, when the source is a modulated Gaussian (9.27) with central frequency ω_0 and bandwidth B, then the range resolution is the same one as in the time-harmonic regime and we have

$$\mathcal{H}(x, z_{\mathrm{ref}}) = C_L \omega_0^2 \widetilde{\mathcal{H}}(x - z_{\mathrm{ref}}), \tag{9.33}$$

where

$$\widetilde{\mathcal{H}}(x) = \frac{1}{2} \exp\left(-i2\omega_0 x_3 \right) \Big(\frac{1}{|D_a|} \int_{D_a} \exp\Big(-i\frac{2\pi y_\perp}{\lambda_0 L} \cdot x_\perp - i\frac{\pi|y_\perp|^2}{\lambda_0 L^2} x_3 \Big) dy_\perp \Big)^2 + cc. \tag{9.34}$$

This shows that the width of the point spread function $\widetilde{\mathcal{H}}(x)$ is of the order of $\lambda_0 L/a$ in the transverse directions $(x_\perp)$ and $\lambda_0 L^2/a^2$ in the longitudinal direction (x_3). Note the loss of resolution compared to the full-aperture case, by a factor L/a in the transverse directions and $(L/a)^2$ in the longitudinal

direction. Note also that the function $\widetilde{\mathcal{H}}(x)$ decays slowly, as $1/|x_\perp|^2$ in the transverse direction and as $1/|x_3|$ in the longitudinal direction.

If the bandwidth B of the pulse is smaller than the central frequency ω_0 but such that $B \gg \omega_0 a^2/L^2$, for instance, when the source is a modulated Gaussian (9.27) with central frequency ω_0 and bandwidth B, then the range resolution is bandwidth-limited and we have

$$\mathcal{H}(x, z_{\mathrm{ref}}) = C_L \omega_0^2 \widetilde{\mathcal{H}}(x - z_{\mathrm{ref}}), \tag{9.35}$$

where

$$\widetilde{\mathcal{H}}(x) = \frac{1}{2} \exp\left(-i2\omega_0 x_3\right) \exp\left(-2B^2 x_3^2\right) \left(\frac{1}{|D_a|} \int_{D_a} \exp\left(-i\frac{2\pi y_\perp}{\lambda_0 L}\cdot x_\perp\right) dy_\perp\right)^2 + cc. \tag{9.36}$$

If the array is square with sidelength a, i.e.

$$D_a = [-a/2, a/2]^2, \tag{9.37}$$

then

$$\widetilde{\mathcal{H}}(x) = \cos\left(2\omega_0 x_3\right) \exp\left(-2B^2 x_3^2\right) \mathrm{sinc}^2\left(\frac{\pi a}{\lambda_0 L} x_1\right) \mathrm{sinc}^2\left(\frac{\pi a}{\lambda_0 L} x_2\right). \tag{9.38}$$

This shows that the width of the point spread function $\widetilde{\mathcal{H}}(x)$ is of the order of $\lambda_0 L/a$ in the transverse directions $(x_\perp)$ and $1/(2B)$ in the longitudinal direction (x_3). Note the loss of resolution compared to the full-aperture case, by a factor L/a in the transverse directions and ω_0/B in the longitudinal direction. Note also that the function $\widetilde{\mathcal{H}}(x)$ decays slowly, as $1/|x_\perp|^2$ in the transverse direction, but may decay fast in the longitudinal direction depending on the source.

9.4.2 The Imaging Function With Clutter Noise

In the presence of clutter noise the imaging function is a real Gaussian random field. Its mean is the unperturbed imaging function $\mathcal{I}_0$ defined by (9.23) and the covariance function of the imaging function is:

$$\mathrm{Cov}\left(\mathcal{I}_{\mathrm{RT}}(x), \mathcal{I}_{\mathrm{RT}}(x')\right) = n^4 \sigma_{\mathrm{clu}}^2 \iint dy dy' \mathcal{H}(x, y) \mathcal{H}(y', x')$$
$$\times \sqrt{K_{\mathrm{clu}}(y) K_{\mathrm{clu}}(y')} H_{\mathrm{clu}}\left(\frac{y - y'}{l_{\mathrm{clu}}}\right). \tag{9.39}$$

Using the fact that the correlation length of the medium is small, this can be simplified as

$$\mathrm{Cov}\left(\mathcal{I}_{\mathrm{RT}}(x), \mathcal{I}_{\mathrm{RT}}(x')\right) = n^4 \sigma_{\mathrm{clu}}^2 l_{\mathrm{clu}}^3 \int dy \mathcal{H}(x, y) K_{\mathrm{clu}}(y) \mathcal{H}(y, x'). \tag{9.40}$$

If we assume that the random scatterers are uniformly distributed in the search region, i.e. $K_{\mathrm{clu}} \equiv 1$, and that $\mathcal{H}(x, y) = C_L \omega_0^2 \widetilde{\mathcal{H}}(x - y)$ as in the case of a full-aperture array or finite-aperture array discussed above, then we have

$$\mathrm{Cov}\big(\mathcal{I}_{\mathrm{RT}}(x), \mathcal{I}_{\mathrm{RT}}(x')\big) = n^4 \sigma_{\mathrm{clu}}^2 l_{\mathrm{clu}}^3 C_L^2 \omega_0^4 \widetilde{\mathcal{H}} \star \widetilde{\mathcal{H}}(x - x'), \qquad (9.41)$$

where the star stands for the convolution in $\mathbb{R}^3$. This shows that the speckle noise $\mathcal{I}_{\mathrm{RT}} - \mathcal{I}_0$ in the image is a stationary Gaussian random field with mean zero, variance

$$\sigma_{\mathrm{noise}}^2 = n^4 \sigma_{\mathrm{clu}}^2 l_{\mathrm{clu}}^3 C_L^2 \omega_0^4 \widetilde{\mathcal{H}} \star \widetilde{\mathcal{H}}(0), \qquad (9.42)$$

and covariance function:

$$\mathrm{Cov}\big(\mathcal{I}_{\mathrm{RT}}(x), \mathcal{I}_{\mathrm{RT}}(x')\big) = \sigma_{\mathrm{noise}}^2 \mathcal{H}_{\mathrm{noise}}(x - x'), \qquad (9.43)$$

with

$$\mathcal{H}_{\mathrm{noise}}(x) = \frac{\widetilde{\mathcal{H}} \star \widetilde{\mathcal{H}}(x)}{\widetilde{\mathcal{H}} \star \widetilde{\mathcal{H}}(0)}. \qquad (9.44)$$

This random field is a speckle pattern whose hotspot profiles are close to the function $\mathcal{H}_{\mathrm{noise}}(x)$, which is (proportional to) the autoconvolution of the point spread function of the imaging function. Here the hotspot profile refers to the local shape of the field around a local maximum (see Section 4.4).

Note also that, when the random scatterers are not uniformly distributed in the search region, i.e. K_{clu} is not constant, then the slow decay (as a power law) of the function $\widetilde{\mathcal{H}}$ implies that the random scatterers in a far region can generate speckle noise everywhere in the image as shown by (9.40). As a consequence it is very difficult to image through a scattering layer. This is a serious drawback for reverse-time imaging.

Full-Aperture Array

In the case in which the array completely surrounds the region of interest, $\mathcal{I}_{\mathrm{RT}}(x)$ is a Gaussian random field with mean $\mathcal{I}_0(x)$ given by (9.23), variance

$$\sigma_{\mathrm{noise}}^2 = n^4 \sigma_{\mathrm{clu}}^2 l_{\mathrm{clu}}^3 C_L^2 \omega_0^4 \frac{\lambda_0^3}{8\pi}, \qquad (9.45)$$

and covariance function:

$$\mathrm{Cov}\big(\mathcal{I}_{\mathrm{RT}}(x), \mathcal{I}_{\mathrm{RT}}(x')\big) = \sigma_{\mathrm{noise}}^2 h_{\mathrm{noise}}\left(\frac{4\pi |x - x'|}{\lambda_0}\right), \qquad (9.46)$$

with the normalized function $(h_{\mathrm{noise}}(0) = 1)$

$$h_{\mathrm{noise}}(x) = \frac{\mathrm{Si}(x)}{x}, \qquad \mathrm{Si}(x) = \int_0^x \mathrm{sinc}(y)dy. \qquad (9.47)$$

The speckle pattern is made of hotspots with typical radius λ_0 and typical amplitude σ_{noise}. The typical shape of the hotspot is given by the function h_{noise}, that has a slow power law decay as $1/x$. The signal to noise ratio in the image is

$$\text{SNR} = \frac{\mathcal{I}_0(z_{\text{ref}})}{\sigma_{\text{noise}}} = \frac{2\sqrt{2\pi}\sigma_{\text{ref}}l_{\text{ref}}^3}{\sigma_{\text{clu}}l_{\text{clu}}^{3/2}\lambda_0^{3/2}}. \tag{9.48}$$

Note that it is independent of the number of sensors, because the clutter noise recorded by different receivers is correlated.

The hotspot volume is defined as

$$V_c = \frac{4\pi^2}{(\det \Lambda)^{1/2}}, \qquad \Lambda = \left(-\partial^2_{x_j x_l} h_{\text{noise}}\left(\frac{4\pi|x|}{\lambda_0}\right) |_{x=0} \right)_{j,l=1,\ldots,3}. \tag{9.49}$$

Here the matrix Λ is proportional to the identity and we have

$$\Lambda = \frac{16\pi^2}{9\lambda_0^2}I, \qquad V_c = \frac{27}{16\pi}\lambda_0^3. \tag{9.50}$$

The maximum of the function $\mathcal{I}_{\text{RT}}-\mathcal{I}_0$ over a domain Ω whose volume is much larger than the hotspot volume is a random quantity described in Section 4.4, which is equal to the deterministic value (8.28) to leading order in $|\Omega|/V_c$, with the values of σ_{noise} and V_c as given by (9.45) and (9.50). This result shows that the SNR (9.48) should be considered with cautious. The speckle pattern may have a local maximum whose peak amplitude is much larger than σ_{noise} and that can be misinterpreted as a reflector.

Finite-Aperture Array

In the case in which the sensor array is dense and occupies the square domain $D_a \times \{0\}$, with $D_a = [-a/2, a/2]^2 \subset \mathbb{R}^2$, the bandwidth B of the pulse is smaller than the central frequency ω_0 but such that $B \gg \omega_0 a^2/L^2$, and the search region is a domain Ω around $(0, 0, L)$, then the field $\mathcal{I}_{\text{RT}}(x)$ is a Gaussian random field with mean $\mathcal{I}_0(x)$ given by (9.23), variance

$$\sigma_{\text{noise}}^2 = n^4 \sigma_{\text{clu}}^2 l_{\text{clu}}^3 C_L^2 \omega_0^4 \frac{\sqrt{\pi}}{B} \frac{\lambda_0^2 L^2}{9a^2}, \tag{9.51}$$

and covariance function:

$$\text{Cov}\big(\mathcal{I}_{\text{RT}}(x), \mathcal{I}_{\text{RT}}(x')\big) = \sigma_{\text{noise}}^2 \cos\big(2\omega_0(x_3 - x_3')\big)$$
$$\times h_{\text{noise}}\Big(\frac{2\pi a(x_1 - x_1')}{\lambda_0 L}, \frac{2\pi a(x_2 - x_2')}{\lambda_0 L}, 2B(x_3 - x_3')\Big), \tag{9.52}$$

with the normalized function $(h_{\text{noise}}(0) = 1)$

$$h_{\text{noise}}(x_1, x_2, x_3) = 36\frac{1 - \text{sinc}(x_1)}{x_1^2}\frac{1 - \text{sinc}(x_2)}{x_2^2}\exp\Big(-\frac{x_3^2}{4}\Big). \tag{9.53}$$

The speckle pattern is made of hotspots with typical radius $\lambda_0 L/a$ in the transverse direction, typical radius $1/(2B)$ in the longitudinal direction, and typical amplitude σ_{noise}. The signal to noise ratio in the image is

$$\text{SNR} = \frac{\mathcal{I}_0(z_{\text{ref}})}{\sigma_{\text{noise}}} = \frac{3\sqrt{2}\sqrt[4]{\pi}\sigma_{\text{ref}}l_{\text{ref}}^3}{\sigma_{\text{clu}}l_{\text{clu}}^{3/2}\lambda_0^{3/2}}\frac{B^{1/2}a}{\omega_0^{1/2}L}. \tag{9.54}$$

Note the SNR reduction compared to the full-aperture case, by a factor of the order of $(B/\omega_0)^{1/2}(a/L)$.

The hotspot volume is defined as before as $V_c = 4\pi^2(\det \Lambda)^{-1/2}$ with

$$\Lambda = \left(-\partial^2_{x_j x_l} h_{\text{noise}}\left(\frac{2\pi a x_1}{\lambda_0 L}, \frac{2\pi a x_2}{\lambda_0 L}, 2Bx_3\right)|_{x=0}\right)_{j,l=1,\ldots,3}. \tag{9.55}$$

Here Λ is diagonal and we have

$$\Lambda_{jj} = \frac{2\pi^2 a^2}{5\lambda_0^2 L^2}, \quad j = 1,2, \qquad \Lambda_{33} = 2B^2, \qquad V_c = \frac{5\lambda_0^3}{\sqrt{2\pi}}\frac{L^2\omega_0}{a^2 B}. \tag{9.56}$$

The maximum of the function over a domain Ω whose volume is much larger than the hotspot volume is given by (8.28) as before with the values of σ_{noise} and V_c as given by (9.51) and (9.56).

10

Optical Coherence Tomography With Clutter Noise

10.1 The Principle of Optical Coherence Tomography

In Optical Coherence Tomography (OCT) a time-incoherent light beam is used in a Michelson interferometer [197]. This means that a single incident beam of incoherent light is divided by a beam splitter into two identical beams. The first beam (the reference beam 1) propagates through a homogeneous medium and it is reflected by a mirror whose longitudinal position can be adjusted (reference mirror in Figure 10.1). The second beam (the sample beam 2) is focused and backscattered by the sample to be imaged. The central position of the reference mirror corresponds (in terms of propagation distances) to the same plane as the focusing plane of the sample beam. The superposition of the reference and sample beams is then measured by a photodetector which is sensitive to the intensity.
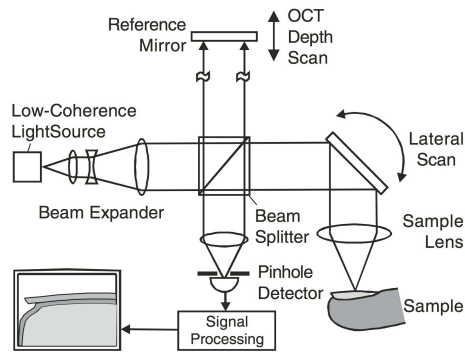

Fig. 10.1. Optical Coherence Tomography set-up. From [164].

We address the standard OCT technique, in which two scans are performed, the depth scan and the lateral scan:
- the lateral scan addresses laterally adjacent focused beams, which can be achieved by moving the sample or by using a rotating mirror which laterally shifts the probing beam (lateral scan in Figure 10.1).
- the depth scan is achieved by shifting (longitudinally) the reference mirror (depth scan in Figure 10.1).

Note that other OCT versions allow to acquire the image without scans, in particular, Fourier-domain OCT allows to get the depth-scan information by an inverse Fourier transform of the spectrum of the backscattered light by using a light source with tunable frequency.

In this section, we denote the three-dimensional spatial coordinate $x = (x_\perp, z)$ where $x_\perp \in \mathbb{R}^2$ stands for the lateral coordinates and z for the longitudinal coordinate.

In the plane of the photodetector $z = L_{\mathrm{det}}$, the reference field is

$$u(\omega, x_\perp, L_{\mathrm{det}}; \Delta x_\perp, \Delta z) = u_1(\omega, x_\perp, L_{\mathrm{det}}; \Delta z) + u_2(\omega, x_\perp, L_{\mathrm{det}}; \Delta x_\perp), \quad (10.1)$$

where $u_1(\omega, x_\perp, L_{\mathrm{det}}; \Delta z)$ is the field reflected by the mirror when the position of the mirror is shifted by Δz compared to the central position and $u_2(\omega, x_\perp, L_{\mathrm{det}}; \Delta x_\perp)$ is the field backscattered by the sample when the focused beam is laterally shifted by $\Delta x_\perp$.

The initial beam is a plane wave

$$u_{\mathrm{i}}(\omega, x_\perp, z) = f(\omega) \exp\big(i \omega z\big), \quad (10.2)$$

that is time incoherent, in the sense that $f(\omega)$ is the Fourier transform of a stationary real-valued random process with mean zero and covariance function $F(t)$, or equivalently

$$\mathbb{E}\big[f(\omega)\big] = 0, \qquad \mathbb{E}\big[f(\omega)\overline{f(\omega')}\big] = \sqrt{2\pi} P(\omega) \delta(\omega - \omega'). \quad (10.3)$$

Here $P(\omega)$ is the Fourier transform of F

$$P(\omega) = \mathcal{F}_{\mathrm{t}}[F](\omega) = \frac{1}{\sqrt{2\pi}} \int_{-\infty}^{\infty} F(t) e^{i\omega t} dt$$

it is the power spectral density of the source by Bochner's theorem, it is a nonnegative real-valued even function. It is concentrated around the central frequency ω_0 and has a bandwidth denoted by B (see (10.30) for an example).

We consider an inhomogeneous sample, with the speed of propagation:

$$\frac{1}{c^2(x)} = 1 + V_{\mathrm{sam}}(x). \quad (10.4)$$

The goal is to image the function $V_{\mathrm{sam}}(x)$.

We first describe the reference and sample beams in Section 10.2. We define the OCT imaging function in Section 10.3 and analyze its point spread function in Section 10.4. Finally in Section 10.5 we study the clutter noise in the OCT image produced by scattering.

10.2 The Reference and Sample Beams

Considering the reference beam, the propagation distance up to the photodetector is L_{det} when the mirror is at its central position, or $L_{\text{det}} + 2\Delta z$ when the mirror is shifted by Δz. Therefore the field $u_1(\omega, x_\perp, L_{\text{det}}; \Delta z)$ in the plane of the photodetector is the initial field delayed by $L_{\text{det}} + 2\Delta z$:

$$u_1(\omega, x_\perp, L_{\text{det}}; \Delta z) = f(\omega)g_1(\omega, x_\perp, L_{\text{det}}; \Delta z), \tag{10.5}$$

$$g_1(\omega, x_\perp, L_{\text{det}}; \Delta z) = \exp\big(i\omega(L_{\text{det}} + 2\Delta z)\big). \tag{10.6}$$

Considering the sample beam, it is focused by a lens in the plane $z = L_{\text{sam}}$ in the sample and it is backscattered by the sample inhomogeneities that we want to image. The propagation distance from the initial plane to the plane of the lens is L_{lens}. The propagation distance from the plane of the lens to the focusing plane is $L_{\text{foc}} = L_{\text{sam}} - L_{\text{lens}}$ (i.e. L_{foc} is the focal length of the lens). The propagation distance from the focusing plane to the photodetector is $L_{\text{det}} - L_{\text{sam}}$. So the overall propagation distance from the initial plane to the photodetector, when backscattering happens in the plane $z = L_{\text{sam}}$, is equal to L_{det}. Let us derive the expression of the sample field in the photodetector plane.

Before the lens, the field goes through a lateral scan device (a rotating mirror) that imposes a linear delay across the beam, which has the form of a linear phase shift in the Fourier domain. The lens imposes a quadratic delay across the beam, which has the form of a quadratic phase modulation, and an amplitude cut-off. As a result of these two operations, the field just after the lens reads:

$$u_{2\text{i}}(\omega, x_\perp, L_{\text{lens}}; \Delta x_\perp) = f(\omega)g_{2\text{i}}(\omega, x_\perp, L_{\text{lens}}; \Delta x_\perp), \tag{10.7}$$

$$g_{2\text{i}}(\omega, x_\perp, L_{\text{lens}}; \Delta x_\perp) = \exp\left(i\omega L_{\text{lens}} - \frac{|x_\perp|^2}{r_0^2 + r_1^2} - i\omega\frac{|x_\perp|^2 r_1}{\omega_0(r_0^2 + r_1^2)r_0}\right)$$

$$\times \exp\left(2i\omega x_\perp \cdot \frac{\Delta x_\perp}{\omega_0 r_0 r_1}\right). \tag{10.8}$$

Here:
- We have chosen a Gaussian amplitude cut-off function with radius $\sqrt{r_0^2 + r_1^2}$ because it allows for an explicit calculation below. The radius r_1 will be taken large (i.e. larger than r_0) below.
- The quadratic phase modulation is r_1/r_0 larger than the amplitude cut-off.
- The linear phase modulation is parameterized by $\Delta x_\perp$. As we will see below, $\Delta x_\perp$ turns out to be the center of the focused incident beam in the focal plane, the radius r_0 is the width of the focused incident beam in the focal plane, and the radii r_0 and r_1 determine the focal length L_{foc}:

$$L_{\text{foc}} = \frac{\omega_0 r_0 r_1}{2}. \tag{10.9}$$

We consider the Fresnel approximation for the propagation from the lens to the focal plane (which holds when the radius of the beam is larger than the

wavelength but smaller than the propagation distance, i.e. the focal length), so that the field is given by the Fresnel diffraction integral (this is also known as the paraxial approximation):

$$u_{2\mathrm{i}}(\omega, x_\perp, L_{\mathrm{lens}} + z; \Delta x_\perp) = f(\omega) g_{2\mathrm{i}}(\omega, x_\perp, L_{\mathrm{lens}} + z; \Delta x_\perp), \qquad (10.10)$$

$$g_{2\mathrm{i}}(\omega, x_\perp, L_{\mathrm{lens}} + z; \Delta x_\perp) = \frac{\omega}{2\pi i z} \exp\left(i\omega z\right)$$

$$\times \int g_{2\mathrm{i}}(\omega, y_\perp, L_{\mathrm{lens}}; \Delta x_\perp) \exp\left(i\frac{\omega}{2z}|x_\perp - y_\perp|^2\right) dy_\perp, \ (10.11)$$

that is to say,

$$g_{2\mathrm{i}}(\omega, x_\perp, L_{\mathrm{lens}} + z; \Delta x_\perp) = \frac{\omega}{2\pi i z} \exp\left(i\omega(L_{\mathrm{lens}} + z)\right)$$

$$\times \int \exp\left(-\frac{|y_\perp|^2}{r_0^2 + r_1^2}\left(1 + \frac{i\omega r_1}{\omega_0 r_0}\right) + 2i\omega y_\perp \cdot \frac{\Delta x_\perp}{\omega_0 r_0 r_1} + i\frac{\omega}{2z}|x_\perp - y_\perp|^2\right) dy_\perp. (10.12)$$

The explicit expression of the field $g_{2\mathrm{i}}(\omega, x_\perp, L_{\mathrm{lens}} + z; \Delta x_\perp)$ can be obtained by a direct calculation (involving only Gaussian integral evaluations):

$$g_{2\mathrm{i}}(\omega, x_\perp, L_{\mathrm{lens}} + z; \Delta x_\perp) = \frac{1}{1 + \frac{2iz}{\omega(r_0^2 + r_1^2)}\left(1 + \frac{i\omega r_1}{\omega_0 r_0}\right)} \exp\left(i\omega(L_{\mathrm{lens}} + z)\right)$$

$$\times \exp\left(-\frac{|x_\perp|^2}{r_0^2 + r_1^2} \frac{1 + \frac{i\omega r_1}{\omega_0 r_0}}{1 + \frac{2iz}{\omega(r_0^2 + r_1^2)}\left(1 + \frac{i\omega r_1}{\omega_0 r_0}\right)}\right)$$

$$\times \exp\left(2i\frac{\omega x_\perp \cdot \Delta x_\perp}{\omega_0 r_1 r_0} \frac{1}{1 + \frac{2iz}{\omega(r_0^2 + r_1^2)}\left(1 + \frac{i\omega r_1}{\omega_0 r_0}\right)}\right)$$

$$\times \exp\left(-\frac{2i\omega|\Delta x_\perp|^2 z}{\omega_0^2 r_1^2 r_0^2} \frac{1}{1 + \frac{2iz}{\omega(r_0^2 + r_1^2)}\left(1 + \frac{i\omega r_1}{\omega_0 r_0}\right)}\right). \qquad (10.13)$$

In the plane $L_{\mathrm{lens}} + L_{\mathrm{loc}}$ (which is equal to L_{sam}), this reads

$$g_{2\mathrm{i}}(\omega, x_\perp, L_{\mathrm{sam}}; \Delta x_\perp) = -i\frac{\omega}{\omega_0} \frac{\frac{r_1}{r_0} + \frac{r_0}{r_1}}{1 - i\frac{\omega}{\omega_0}\frac{r_0}{r_1}} \exp\left(i\omega L_{\mathrm{sam}}\right)$$

$$\times \exp\left(-\frac{|x_\perp|^2}{r_0^2}\frac{1 - i\frac{\omega_0}{\omega}\frac{r_0}{r_1}}{1 - i\frac{\omega}{\omega_0}\frac{r_0}{r_1}} + 2\frac{x_\perp \cdot \Delta x_\perp}{r_0^2}\frac{\frac{\omega^2}{\omega_0^2}\left(1 + \frac{r_0^2}{r_1^2}\right)}{1 - i\frac{\omega}{\omega_0}\frac{r_0}{r_1}}\right)$$

$$\times \exp\left(-\frac{|\Delta x_\perp|^2}{r_0^2}\frac{\frac{\omega^2}{\omega_0^2}\left(1 + \frac{r_0^2}{r_1^2}\right)}{1 - i\frac{\omega}{\omega_0}\frac{r_0}{r_1}}\right), \qquad (10.14)$$

by (10.9). For $|\omega - \omega_0| \ll \omega_0$, this can be reduced to

$$g_{2\mathrm{i}}(\omega, x_\perp, L_{\mathrm{sam}}; \Delta x_\perp) = -i\frac{r_1}{r_0}\left(1 + i\frac{r_0}{r_1}\right)\exp\left(i\omega L_{\mathrm{sam}}\right)$$

$$\times \exp\left(-\frac{|x_\perp|^2}{r_0^2} + 2\frac{x_\perp \cdot \Delta x_\perp}{r_0^2}\left(1 + i\frac{r_0}{r_1}\right) - \frac{|\Delta x_\perp|^2}{r_0^2}\left(1 + i\frac{r_0}{r_1}\right)\right) (10.15)$$

With $r_1 \gg r_0$, this simply reads

$$g_{2\mathrm{i}}(\omega, x_\perp, L_{\mathrm{sam}}; \Delta x_\perp) = \frac{r_1}{ir_0} \exp\left(i\omega L_{\mathrm{sam}}\right) \exp\left(-\frac{|x_\perp - \Delta x_\perp|^2}{r_0^2}\right), \quad (10.16)$$

which shows that the focused incident beam in the focusing plane $z = L_{\mathrm{sam}}$ has a transverse Gaussian profile with width r_0 and with center $\Delta x_\perp$, as announced above. Moreover, using again the Fresnel diffraction integral (10.13), the focused incident beam has the following form in the vicinity of the focusing plane:

$$g_{2\mathrm{i}}(\omega, x_\perp, L_{\mathrm{sam}} + z; \Delta x_\perp) = \frac{r_1}{ir_0\left(1 + \frac{2i}{\omega r_0^2}z\right)} \exp\left(i\omega(L_{\mathrm{sam}} + z)\right)$$

$$\times \exp\left(-\frac{|x_\perp - \Delta x_\perp|^2}{r_0^2(1 + \frac{2iz}{\omega r_0^2})}\right). \quad (10.17)$$

We consider a weakly inhomogeneous sample, with the speed of propagation (10.4), so that the Born approximation is valid for the backscattered sample field. The backscattered sample field in the plane $z = L_{\mathrm{sam}}$ is therefore

$$u_2(\omega, x_\perp, L_{\mathrm{sam}}; \Delta x_\perp) = f(\omega)g_2(\omega, x_\perp, L_{\mathrm{sam}}; \Delta x_\perp), \quad (10.18)$$

$$g_2(\omega, x_\perp, L_{\mathrm{sam}}; \Delta x_\perp) = -\omega^2 \iint \Gamma_\omega\left((x_\perp, L_{\mathrm{sam}}), (y_\perp, L_{\mathrm{sam}} + z)\right)$$

$$\times V_{\mathrm{sam}}(y_\perp, L_{\mathrm{sam}} + z)g_{2\mathrm{i}}\left(\omega, y_\perp, L_{\mathrm{sam}} + z; \Delta x_\perp\right)dy_\perp\, dz, \quad (10.19)$$

where $\Gamma_\omega(x, y)$ is the homogeneous Green's function and $g_{2\mathrm{i}}(\omega, y; \Delta x_\perp)$ is the focused incident beam, given by (10.17). Using again the Fresnel approximation, we have

$$\Gamma_\omega\left((x_\perp, L_{\mathrm{sam}}), (y_\perp, L_{\mathrm{sam}} + z)\right) = -\frac{1}{4\pi z} \exp\left(i\omega z + i\omega\frac{|x_\perp - y_\perp|^2}{2z}\right). \quad (10.20)$$

Finally, the backscattered sample field in the plane $z = L_{\mathrm{sam}}$ is sent to the photodetector plane $z = L_{\mathrm{det}}$ by the OCT system. Therefore the backscattered sample field $u_2(\omega, x_\perp, L_{\mathrm{det}}; \Delta x_\perp)$ in the photodetector plane is given by

$$u_2(\omega, x_\perp, L_{\mathrm{det}}; \Delta x_\perp) = f(\omega)g_2(\omega, x_\perp, L_{\mathrm{det}}; \Delta x_\perp), \quad (10.21)$$

$$g_2(\omega, x_\perp, L_{\mathrm{det}}; \Delta x_\perp) = \exp\left(i\omega(L_{\mathrm{det}} - L_{\mathrm{sam}})\right)g_2(\omega, x_\perp, L_{\mathrm{sam}}; \Delta x_\perp). \quad (10.22)$$

10.3 The Imaging Function

The imaging function is the intensity collected at the photodetector:

$$\mathcal{I}(\Delta x_\perp, \Delta z) = \frac{1}{T}\int_0^T \int_{\mathbb{R}^2} |u(t, x_\perp, L_{\mathrm{det}}; \Delta x_\perp, \Delta z)|^2 dx_\perp\, dt. \quad (10.23)$$

As $T \to \infty$, using the stationarity of the source field, the time average converges to the statistical average and we have

$$\mathcal{I}(\Delta x_\perp, \Delta z) = \int \mathbb{E}\big[|u(0, x_\perp, L_{\text{det}}; \Delta x_\perp, \Delta z)|^2\big] dx_\perp, \qquad (10.24)$$

which gives

$$\mathcal{I}(\Delta x_\perp, \Delta z) = \frac{1}{\sqrt{2\pi}} \iint P(\omega)|g_1(\omega, x_\perp, L_{\text{det}}; \Delta z) + g_2(\omega, x_\perp, L_{\text{det}}; \Delta x_\perp)|^2 dx_\perp \, d\omega. \qquad (10.25)$$

It can be decomposed into the sum of three terms:

$$\mathcal{I}(\Delta x_\perp, \Delta z) = \frac{1}{\sqrt{2\pi}} \iint P(\omega)|g_1(\omega, x_\perp, L_{\text{det}}; \Delta z)|^2 dx_\perp \, d\omega$$

$$+ \frac{\sqrt{2}}{\sqrt{\pi}} \Re \iint P(\omega)\overline{g_1(\omega, x_\perp, L_{\text{det}}; \Delta z)} g_2(\omega, x_\perp, L_{\text{det}}; \Delta x_\perp) dx_\perp \, d\omega$$

$$+ \frac{1}{\sqrt{2\pi}} \iint P(\omega)|g_2(\omega, x_\perp, L_{\text{det}}; \Delta x_\perp)|^2 dx_\perp \, d\omega. \qquad (10.26)$$

The first term is a constant background independent of Δz and $\Delta x_\perp$. The third term is negligible in the Born approximation. Therefore the image $\mathcal{I}(\Delta x_\perp, \Delta z)$ is determined by the second interference term that we study in the next section.

10.4 The Point Spread Function

Using the expressions (10.6) and (10.22) of the reference and sample fields, the imaging function (10.26) is, up to the first constant background term,

$$\mathcal{I}(\Delta x_\perp, \Delta z) = \frac{\sqrt{2}}{\sqrt{\pi}} \Re \iiint \omega^2 P(\omega) \frac{1}{4\pi z} \exp\left(i\omega \frac{|x_\perp - y_\perp|^2}{2z}\right) V_{\text{sam}}(y_\perp, L_{\text{sam}} + z)$$

$$\times e^{-2i\omega(\Delta z - z)} \frac{r_1}{ir_0\left(1 + \frac{2i}{\omega r_0^2}z\right)} \exp\left(-\frac{|y_\perp - \Delta x_\perp|^2}{r_0^2(1 + \frac{2iz}{\omega r_0^2})}\right) dy_\perp \, dz dx_\perp \, d\omega. \qquad (10.27)$$

By integrating in $x_\perp$:

$$\mathcal{I}(\Delta x_\perp, \Delta z) = \frac{1}{\sqrt{2\pi}} \Re \iiint (i\omega) P(\omega) e^{-2i\omega(\Delta z - z)} V_{\text{sam}}(y_\perp, L_{\text{sam}} + z)$$

$$\times \frac{r_1}{ir_0\left(1 + \frac{2i}{\omega r_0^2}z\right)} \exp\left(-\frac{|y_\perp - \Delta x_\perp|^2}{r_0^2(1 + \frac{2iz}{\omega r_0^2})}\right) dy_\perp \, dz d\omega. \qquad (10.28)$$

If P has central frequency ω_0 and bandwidth B with $B \ll \omega_0$, for instance,

$$F(t) = \cos(\omega_0 t)\exp\Big(-\frac{B^2 t^2}{2}\Big), \tag{10.29}$$

$$P(\omega) = \frac{1}{2B}\exp\Big(-\frac{(\omega-\omega_0)^2}{2B^2}\Big) + \frac{1}{2B}\exp\Big(-\frac{(\omega+\omega_0)^2}{2B^2}\Big), \tag{10.30}$$

and if $1/B \ll r_0^2/\lambda_0$, with $\lambda_0 = 2\pi\omega_0$, which means that the Rayleigh length r_0^2/λ_0 of the Gaussian profile is larger than the width $1/B$ of the coherent window, then

$$\mathcal{I}(\Delta x_\perp, \Delta z) = \iint \mathcal{H}(\Delta x_\perp - x_\perp, \Delta z - z; \Delta z)V_{\mathrm{sam}}(x_\perp, L_{\mathrm{sam}} + z)dx_\perp dz \tag{10.31}$$

where the point spread function is

$$\mathcal{H}(x_\perp, z; \Delta z) = \frac{\omega_0 r_1}{r_0}\frac{1}{\sqrt{1 + \frac{4\Delta z^2}{\omega_0^2 r_0^4}}}\exp\big(-2B^2 z^2\big)\exp\Big(-\frac{|x_\perp|^2}{r_0^2(1 + \frac{4\Delta z^2}{\omega_0^2 r_0^4})}\Big)$$

$$\times \cos\Big[2\omega_0 z + \arctan\big(\frac{2\Delta z}{\omega_0 r_0^2}\big) - \frac{2\Delta z}{\omega_0 r_0^2}\frac{|x_\perp|^2}{r_0^2(1 + \frac{4\Delta z^2}{\omega_0^2 r_0^4})}\Big]. \tag{10.32}$$

This shows that:

- the point spread function has longitudinal fringes (at the second harmonic $2\omega_0$) that are characteristic of OCT techniques and are sometimes called fringe bursts. In fact, these fringes can be used to extract the interference term from the background term in the imaging function, so that only the fringe envelopes are retained.
- the envelope of the point spread function decays fast in the transverse and in the longitudinal directions (here, the decay is Gaussian).
- the longitudinal resolution is $1/(2B)$, that is proportional to the width of the coherent window,
- the cross-range resolution is r_0 when the mirror position is $\Delta z = 0$, which corresponds to the scanned depth $z = L_{\mathrm{sam}}$ in the sample, and deteriorates as $r_0^2(1 + \frac{4\Delta z^2}{\omega_0^2 r_0^4})$ when the mirror position is Δz, which corresponds to the scanned depth $z = L_{\mathrm{sam}} + \Delta z$ in the sample.

Consequently:

- Longitudinal resolution depends only on the width of the coherent window, that is, the bandwidth of source.
- Lateral resolution is essentially determined by the waist of the focused beam, it is all the higher as the beam is more focused, but then the sample depths that can be scanned are reduced: if one considers that a deterioration of 50% of the lateral resolution around the depth $z = L_{\mathrm{sam}}$ is acceptable, then this means that the scanned depths should be within the interval $[L_{\mathrm{sam}} - \pi r_0^2/\lambda_0, L_{\mathrm{sam}} + \pi r_0^2/\lambda_0]$, which means around the depth $z = L_{\mathrm{sam}}$ with a thickness of the order of the Rayleigh length of the focused beam. This indicates that OCT can only scan a quite small range of depths. If one improves by a factor two the transverse resolution, then the thickness of the sample that can be scanned is reduced by a factor four.

10.5 The Clutter Noise in Optical Coherence Tomography

When there is clutter noise, that is to say, small heterogeneties in the sample, the speed of propagation can be described as

$$\frac{1}{c^2(x)} = \big[1 + V_{\text{sam}}(x) + V_{\text{clu}}(x)\big], \tag{10.33}$$

where $V_{\text{clu}}(x)$ is a random process with mean zero and covariance function (9.8). The imaging function is then of the form

$$\mathcal{I}(x) = \mathcal{I}_0(x) + \mathcal{I}_1(x), \tag{10.34}$$

$$\mathcal{I}_0(x) = \int \mathcal{H}(x_\perp - x'_\perp, z - z'; z) V_{\text{sam}}(x'_\perp, L_{\text{sam}} + z') dx'_\perp \, dz', \tag{10.35}$$

$$\mathcal{I}_1(x) = \int \mathcal{H}(x_\perp - x'_\perp, z - z'; z) V_{\text{clu}}(x'_\perp, L_{\text{sam}} + z') dx'_\perp \, dz', \tag{10.36}$$

where $\mathcal{I}_0$ is the unperturbed image described in the previous section and $\mathcal{I}_1$ is the speckle noise in the image. The speckle noise is a Gaussian random field with mean zero and with covariance

$$\text{Cov}\big(\mathcal{I}(x), \mathcal{I}(x')\big) = \sigma_{\text{clu}}^2 l_{\text{clu}}^3 \int dx'' \mathcal{H}\big(x_\perp - x''_\perp, z - z''; z\big) K_{\text{clu}}(x''_\perp, L_{\text{sam}} + z'')$$
$$\times \mathcal{H}\big(x'_\perp - x''_\perp, z' - z''; z'\big) \tag{10.37}$$

where we have used the fact that the correlation length of the random fluctuations of the sample is small.

If, additionally, the random heterogeneities are uniformly distributed, so that $K_{\text{clu}}(y) \equiv 1$, then

$$\text{Cov}\big(\mathcal{I}(x), \mathcal{I}(x')\big) = \sigma_{\text{clu}}^2 l_{\text{clu}}^3 \int dx'' \mathcal{H}\big(x_\perp - x''_\perp, z - z''; z\big)$$
$$\times \mathcal{H}\big(x'_\perp - x''_\perp, z' - z''; z'\big), \tag{10.38}$$

or equivalently (denoting the mid-point by $X = (X_\perp, Z)$ and the offset by $x = (x_\perp, z)$)

$$\text{Cov}\Big(\mathcal{I}(X + \frac{x}{2}), \mathcal{I}(X - \frac{x}{2})\Big) = \sigma_{\text{clu}}^2 l_{\text{clu}}^3 \int dx'' \mathcal{H}\Big(x''_\perp + \frac{x_\perp}{2}, z'' + \frac{z}{2}; Z + \frac{z}{2}\Big)$$
$$\times \mathcal{H}\Big(x''_\perp - \frac{x_\perp}{2}, z'' - \frac{z}{2}; Z - \frac{z}{2}\Big) \tag{10.39}$$

By computing the covariance function, we find that the random field $\mathcal{I}_1 = \mathcal{I} - \mathcal{I}_0$ is stationary (the covariance function does not depend on the mid-point X):

$$\mathrm{Cov}\Big(\mathcal{I}(X+\frac{x}{2}),\mathcal{I}(X-\frac{x}{2})\Big) = \sigma_{\mathrm{clu}}^2 l_{\mathrm{clu}}^3 \omega_0^2 r_1^2 \frac{\pi^{3/2}}{8B} \cos\big(2\omega_0 z\big)$$

$$\times \exp\big(-B^2 z^2\big)\exp\Big(-\frac{|x_\perp|^2}{2r_0^2}\Big). \quad (10.40)$$

This covariance function describes the local profile of the hotspots of the speckle pattern generated by clutter noise. The speckle hotspots, up to the high-frequency fringes, have longitudinal radius $1/B$ and transverse radius r_0 throughout the search region. Note that the covariance function, and therefore the local profile of the hotspots, is stationary throughout the scanned sample, contrarily to the point spread function that laterally spreads out away from the focal plane (see (10.32)).

If the random heterogeneities are not uniformly distributed, i.e. when K_{clu} is not constant, then the image will be speckled only in the scattering region because of the fast decay of the function $\mathcal{H}$, as shown by (10.37). This is an important difference compared to reverse-time imaging for instance. In particular the fast decay in the depth z shows that OCT is capable to image through a scattering layer, as the image beyond the scattering layer is hardly affected. If $K_{\mathrm{clu}}(x_\perp, z) = \exp(-(z - L_{\mathrm{sam}} + L_{\mathrm{clu}})^2/\Delta L_{\mathrm{clu}}^2)$, which models a scattering layer located around the depth $z = L_{\mathrm{sam}} - L_{\mathrm{clu}}$ with the width ΔL_{clu}, then the variance of the speckle pattern generated by the scattering layer is

$$\mathrm{Var}\big(\mathcal{I}(X)\big) = \sigma_{\mathrm{clu}}^2 l_{\mathrm{clu}}^3 \omega_0^2 r_1^2 \frac{\pi^{3/2}}{8B\big(1+\frac{1}{4B^2\Delta L_{\mathrm{clu}}^2}\big)^{1/2}} \exp\Big(-\frac{(L_{\mathrm{clu}}+Z)^2}{\Delta L_{\mathrm{clu}}^2 + \frac{1}{4B^2}}\Big),$$

which clearly illustrates the decay of the speckle noise in the image away from the region of the scattering layer.

Part III

Anomaly Imaging

11

Small Volume Expansions

In their most general forms imaging problems are severely ill-posed and non-linear. These are the main obstacles to find non-iterative reconstruction algorithms. If, however, in advance we have additional structural information about the profile of the material property, then we may be able to determine specific features about the conductivity distribution with a satisfactory resolution. One such type of knowledge in the conductivity case could be that the conducting body consists of a smooth background containing a number of unknown small anomalies with a significantly different conductivity.

Over the last 10 years or so, a considerable amount of interesting work has been dedicated to the imaging of such low volume fraction particles. The method of asymptotic expansions provides a useful framework to accurately and efficiently reconstruct the location and geometric features of the particles in a stable way, even for moderately noisy data.

Using the method of matched asymptotic expansions we formally derive the first-order perturbations due to the presence of the particles in the conductivity case. These perturbations are of dipole-type. A rigorous proof of these expansions is based on layer potential techniques. The concept of polarization tensor is the basic building block for the asymptotic expansion of the boundary perturbations. It is then important from an imaging point of view to precisely characterize the PT and derive some of its properties, such as symmetry, positivity, and optimal bounds on its elements, for developing efficient algorithms to reconstruct conductivity particles of small volume.

We then provide the leading-order term in this asymptotic formula of the solution to the Helmholtz equation in the presence of small electromagnetic particles. The leading-order term is the sum of a (polarized) magnetic dipole and an electric point source.

It is worth emphasizing that all the problems considered in this chapter are singularly perturbed problems. As it will be shown later, derivatives of the solution to the perturbed problem are not, inside the particle, close to those of the background solution. Consequently, the far-field expansions are not uniform in the whole background domain. Nevertheless, inner expansions

of the solution inside the particle are provided. An example of a regularly perturbed problem is the Born approximation. See (7.1).

The asymptotic expansions are first provided for bounded domains. We consider a small particle inside a bounded domain. A boundary condition (Neumann or Dirichlet) is applied and the perturbations of the (Dirichlet or Neumann) boundary data are derived. Then the asymptotic expansions are extended to monopole sources in the free space. The perturbations of the field at a receiver placed away from the particle are derived. Finally, an extension of the asymptotic approach to time-domain measurements is described. It will be shown that after truncating the high-frequency component of the measured wave, the perturbation due to the particle is a wavefront emitted by a dipolar source at the location of the particle. Such a formula will be useful for designing time-reversal techniques for particle localization.

11.1 Conductivity Problem

In this section we derive an asymptotic expansion of the voltage potentials in the presence of a diametrically small particle with conductivity different from the background conductivity.

Let $g \in L_0^2(\partial\Omega)$. Consider the solution u of

$$\begin{cases} \nabla \cdot \big(1 + (k-1)\chi(D)\big)\nabla u = 0 & \text{in } \Omega, \\ \dfrac{\partial u}{\partial \nu}\Big|_{\partial\Omega} = g, \quad \displaystyle\int_{\partial\Omega} u\, d\sigma = 0. \end{cases} \tag{11.1}$$

Let U be the background solution, that is, the solution to

$$\begin{cases} \Delta U = 0 & \text{in } \Omega, \\ \dfrac{\partial U}{\partial \nu}\Big|_{\partial\Omega} = g, \quad \displaystyle\int_{\partial\Omega} U\, d\sigma = 0. \end{cases} \tag{11.2}$$

The following asymptotic expansion expresses the fact that the conductive particle can be modeled by a dipole.

Theorem 11.1 (Voltage Boundary Perturbations) *Suppose that $D = \delta B + z$, and let u be the solution of (11.1), where $0 < k \neq 1 < +\infty$. Denote*

$$\lambda := (k+1)/(2(k-1)). \tag{11.3}$$

The following pointwise asymptotic expansion on $\partial\Omega$ holds for $d = 2, 3$:

$$u(x) = U(x) - \delta^d \nabla U(z) \cdot M(\lambda, B)\nabla_z N(x, z) + O(\delta^{d+1}), \tag{11.4}$$

where the remainder $O(\delta^{d+1})$ is dominated by $C\delta^{d+1}\|g\|_{L^2(\partial\Omega)}$ for some C independent of $x \in \partial\Omega$. Here U is the background solution, $N(x, z)$ is the

Neumann function, that is, the solution to (3.30), $M(\lambda, B) = (m_{pq})_{p,q=1}^{d}$ is the polarization tensor given by

$$m_{pq} = \int_{\partial B} (\lambda I - \mathcal{K}_B^*)^{-1}[\nu_p](\xi)\, \xi_q\, d\sigma(\xi) , \qquad (11.5)$$

where $\nu = (\nu_1, \ldots, \nu_d)$ is the outward unit normal to ∂B and $\xi = (\xi_1, \ldots, \xi_d)$.

Since $\nabla_z N(x, z) = -\nabla_x N(x, z)$, from (3.32) and (11.4), it follows that

$$\int_{\partial \Omega} (u(x) - U(x)) f(x)\, d\sigma(x) = \delta^d \nabla U(z) \cdot M(\lambda, B) \nabla V(z) + O(\delta^{d+1}) , \quad (11.6)$$

where $f \in L_0^2(\partial\Omega)$ and V is the solution to

$$\begin{cases} \Delta V = 0 & \text{in } \Omega , \\ \left.\dfrac{\partial V}{\partial \nu}\right|_{\partial\Omega} = f, & \displaystyle\int_{\partial\Omega} V\, d\sigma = 0 . \end{cases}$$

For B a smooth bounded domain in $\mathbb{R}^d$ and $0 < k \neq 1 < +\infty$ a conductivity parameter, let $v(B, k)$ be the solution to

$$\begin{cases} \Delta v = 0 & \text{in } \mathbb{R}^d \setminus \overline{B} , \\ \Delta v = 0 & \text{in } B , \\ v|_- - v|_+ = 0 & \text{on } \partial B , \\ k\left.\dfrac{\partial v}{\partial \nu}\right|_- - \left.\dfrac{\partial v}{\partial \nu}\right|_+ = 0 & \text{on } \partial B , \\ v(\xi) - \xi \to 0 & \text{as } |\xi| \to +\infty . \end{cases} \qquad (11.7)$$

The asymptotic expansion (11.4) does not hold uniformly in Ω. For internal perturbations of the voltage potential that are due to the presence of the conductivity anomaly D, the following inner asymptotic expansion holds.

Theorem 11.2 *We have*

$$u(x) \approx U(z) + \delta v\left(\frac{x - z}{\delta}, k\right) \cdot \nabla U(z) \quad \text{for } x \text{ near } z . \qquad (11.8)$$

The following result connects the polarization tensor M to the corrector v.

Lemma 11.3 *Let $M(\lambda, B) = (m_{pq})_{p,q=1}^{d}$ be defined by (11.5). Then we have*

$$M(\lambda, B) = (k - 1) \int_B \nabla v(\xi, k)\, d\xi \qquad (11.9)$$

with v being the solution to (11.7) and λ given by (11.3).

The asymptotic expansion (11.4) shows that, from an imaging point of view, the location z and the polarization tensor M of the anomaly are the only quantities that can be determined from boundary measurements of the voltage potential, assuming that the noise level is of order δ^{d+1}. It is then important to precisely characterize the polarization tensor and derive some of its properties, such as symmetry, positivity, and isoperimetric inequalities satisfied by its elements, in order to develop efficient algorithms for reconstructing conductivity anomalies of small volume.

Some important properties of the polarization tensor are listed in the next theorem.

Theorem 11.4 (Properties of the polarization tensor) *For $0 < k \neq 1 < +\infty$, let $M = M(\lambda, B) = (m_{pq})_{p,q=1}^{d}$ be the polarization tensor associated with the bounded domain B in $\mathbb{R}^d$ and the conductivity k, where λ is defined by (11.3). Then*

(i) *M is symmetric.*

(ii) *If $k > 1$, then M is positive definite, and it is negative definite if $0 < k < 1$.*

(iii) *The following isoperimetric inequalities for the polarization tensor*

$$
\begin{cases}
\dfrac{1}{k-1}\operatorname{trace}(M) \leq (d - 1 + \dfrac{1}{k})|B| \,, \\[2mm]
(k-1)\operatorname{trace}(M^{-1}) \leq \dfrac{d-1+k}{|B|} \,,
\end{cases}
\tag{11.10}
$$

hold, where trace *denotes the trace of a matrix and $|B|$ is the volume of B.*

The polarization tensor M can be explicitly computed for disks and ellipses in the plane and balls and ellipsoids in three-dimensional space. See [66, pp. 81–89]. The formula of the polarization tensor for ellipses will be useful here. Let B be an ellipse whose semi-axes are on the x_1- and x_2-axes and of length a and b, respectively. Then, $M(\lambda, B)$ takes the form

$$
M(\lambda, B) = (k-1)|B|
\begin{pmatrix}
\dfrac{a+b}{a+kb} & 0 \\[2mm]
0 & \dfrac{a+b}{b+ka}
\end{pmatrix} .
\tag{11.11}
$$

Formula (11.4) shows that from boundary measurements one can always represent and visualize an arbitrary shaped anomaly by means of an equivalent ellipse of center z with the same polarization tensor. Further, it is impossible to extract the conductivity from the polarization tensor. The information contained in the polarization tensor is a mixture of the conductivity and the volume. A small anomaly with high conductivity and a larger anomaly with lower conductivity can have the same polarization tensor.

11.2 Helmholtz Equation

Suppose that an electromagnetic medium occupies a bounded domain Ω in $\mathbb{R}^d$, with a connected $\mathcal{C}^2$-boundary $\partial\Omega$. Suppose that Ω contains a small particle of the form $D = \delta B + z$, where $z \in \Omega$ and B is a $\mathcal{C}^2$-bounded domain in $\mathbb{R}^d$ containing the origin.

Let μ_0 and ε_0 denote the permeability and the permittivity of the background medium Ω, and assume that μ_0 and ε_0 are positive constants. Let $\mu_\star$ and $\varepsilon_\star$ denote the permeability and the permittivity of D, which are also assumed to be positive constants. Introduce the piecewise constant magnetic permeability

$$\mu_\delta(x) = \begin{cases} \mu_0 , & x \in \Omega \setminus \overline{D} , \\ \mu_\star , & x \in D . \end{cases}$$

The piecewise constant electric permittivity, $\varepsilon_\delta(x)$, is defined analogously.

Let the electric field u denote the solution to the Helmholtz equation

$$\nabla \cdot (\frac{1}{\mu_\delta}\nabla u) + \omega^2 \varepsilon_\delta u = 0 \ \text{ in } \Omega , \tag{11.12}$$

with the boundary condition $u = f$ on $\partial\Omega$ with $f \in W_{\frac{1}{2}}^2(\partial\Omega)$, where $\omega > 0$ is a given frequency.

Problem (11.12) can be written as

$$\begin{cases} (\Delta + \omega^2 \varepsilon_0 \mu_0)u = 0 & \text{in } \Omega \setminus \overline{D} , \\ (\Delta + \omega^2 \varepsilon_\star \mu_\star)u = 0 & \text{in } D , \\ \dfrac{1}{\mu_\star}\dfrac{\partial u}{\partial \nu}\Big|_- - \dfrac{1}{\mu_0}\dfrac{\partial u}{\partial \nu}\Big|_+ = 0 & \text{on } \partial D , \\ u|_- - u|_+ = 0 & \text{on } \partial D , \\ u = f & \text{on } \partial\Omega . \end{cases}$$

Assuming that

$$\omega^2 \varepsilon_0 \mu_0 \text{ is not an eigenvalue for the operator } -\Delta \text{ in } L^2(\Omega)$$
$$\text{with homogeneous Dirichlet boundary conditions,} \tag{11.13}$$

we can prove existence and uniqueness of a solution to (11.12) at least for δ small enough.

With the notation of Section 3.2, the following asymptotic formula holds.

Theorem 11.5 (Boundary Perturbations) *Let $k_0 = \omega\sqrt{\varepsilon_0\mu_0}$. Suppose that (11.13) holds. Let u be the solution of (11.12) and let the function U be the background solution as before:*

$$\begin{cases} \Delta U + k_0^2 U = 0 & \text{in } \Omega , \\ U = f & \text{on } \partial\Omega . \end{cases}$$

For any $x \in \partial\Omega$,

$$\frac{\partial u}{\partial \nu}(x) = \frac{\partial U}{\partial \nu}(x) + \delta^d \left(\nabla U(z) \cdot M(\lambda, B) \frac{\partial \nabla_z G_{k_0}(x,z)}{\partial \nu_x} \right.$$
$$\left. + k_0^2 (\frac{\varepsilon_\star}{\varepsilon_0} - 1)|B|U(z)\frac{\partial G_{k_0}(x,z)}{\partial \nu_x} \right) + O(\delta^{d+1}) , \qquad (11.14)$$

where $M(\lambda, B)$ is the polarization tensor defined in (11.5) with λ given by

$$\lambda := \frac{(\mu_0/\mu_\star) + 1}{2((\mu_0/\mu_\star) - 1)} . \qquad (11.15)$$

Here G_{k_0} is the Dirichlet Green function defined by (3.70).

For internal perturbations of u that are due to the presence of the electromagnetic anomaly D, the following inner asymptotic expansion holds.

Theorem 11.6 *We have*

$$u(x) \approx U(z) + \delta v(\frac{x-z}{\delta}, \frac{\mu_0}{\mu_\star}) \cdot \nabla U(z) \quad \text{for } x \text{ near } z , \qquad (11.16)$$

where v is defined by (11.7) with $k = \mu_0/\mu_\star$.

Before concluding this section, we make a remark. Consider the Helmholtz equation with the Neumann data g in the presence of the inclusion D:

$$\begin{cases} \nabla \cdot \frac{1}{\mu_\delta} \nabla u + \omega^2 \varepsilon_\delta u = 0 \;\; \text{in } \Omega , \\ \frac{\partial u}{\partial \nu} = g \;\; \text{on } \partial\Omega . \end{cases} \qquad (11.17)$$

Let the background solution U satisfy

$$\begin{cases} \Delta U + k_0^2 U = 0 \;\; \text{in } \Omega , \\ \frac{\partial U}{\partial \nu} = g \;\; \text{on } \partial\Omega . \end{cases} \qquad (11.18)$$

The following asymptotic expansion of the solution of the Neumann problem holds. For any $x \in \partial\Omega$, we have

$$u(x) = U(x) + \delta^d \left(\nabla U(z) M(\lambda, B) \nabla_z N_{k_0}(x,z) \right.$$
$$\left. + k_0^2 (\frac{\varepsilon_\star}{\varepsilon_0} - 1)|B|U(z)N_{k_0}(x,z) \right) + O(\delta^{d+1}) , \qquad (11.19)$$

where N_{k_0} is the Neumann function defined by

$$\begin{cases} \Delta_x N_{k_0}(x,z) + k_0{}^2 N_{k_0}(x,z) = -\delta_z \;\; \text{in } \Omega , \\ \frac{\partial N_{k_0}}{\partial \nu_x}\Big|_{\partial\Omega} = 0 \;\; \text{for } z \in \Omega . \end{cases} \qquad (11.20)$$

Moreover, the inner expansion (11.16) holds true with U being defined by (11.18).

The following useful relation between the Neumann function and the fundamental solution Γ_{k_0} holds:

$$(-\frac{1}{2}I + \mathcal{K}_\Omega^{k_0})[N_{k_0}(\cdot, z)](x) = \Gamma_{k_0}(x, z), \quad x \in \partial\Omega, \; z \in \Omega . \qquad (11.21)$$

11.3 Asymptotic Formulas for Monopole Sources in Free Space

11.3.1 Conductivity Problem

Let $y \in \mathbb{R}^d \setminus \overline{D}$ and let $u_y(x)$ be the solution to the transmission problem

$$\begin{cases} \nabla \cdot (1 + (k-1)\chi(D))\nabla u_y(x) = \delta_y(x), & x \in \mathbb{R}^d , \\ u_y(x) - \Gamma(x, y) = O(|x|^{1-d}), & |x - y| \to \infty . \end{cases} \qquad (11.22)$$

Let $U_y(x) = \Gamma(x, y)$ denote the background solution. We still assume that D is of the form $D = \delta B + z$. For $y \in \partial D$ and x away from z, we can prove similarly to (11.4) that the following expansion of $u_y - U_y$ for x away from z holds:

$$(u_y - U_y)(x) = -\delta^d \nabla_z \Gamma(x, z) \cdot M(\lambda, B)\nabla_z \Gamma(y, z) + O(\delta^{d+1}) .$$

Note that, because of the symmetry of the PT, the leading-order term in the above expansion satisfies the reciprocity property, *i.e.*, $\nabla_z \Gamma(x, z) \cdot M(\lambda, B)\nabla_z \Gamma(y, z) = \nabla_y \Gamma(y, z) \cdot M(\lambda, B)\nabla_z \Gamma(x, z)$.

11.3.2 Helmholtz Equation

Suppose that D is illuminated by a time-harmonic wave generated at the point source y with the operating frequency ω. In this case, the incident field is given by

$$U_y(x) = \Gamma_{k_0}(x, y) ,$$

and the field perturbed in the presence of the particle is the solution to the following transmission problem:

$$\nabla \cdot \left(\frac{1}{\mu_0}\chi(\mathbb{R}^d \setminus \overline{D}) + \frac{1}{\mu_\star}\chi(D)\right)\nabla u_y + \omega^2 \left(\varepsilon_0 \chi(\mathbb{R}^d \setminus \overline{D}) + \varepsilon_\star \chi(D)\right) u_y = \frac{1}{\mu_0}\delta_y ,$$
$$(11.23)$$

and is subject to the outgoing radiation condition, or equivalently

$$\begin{cases} \Delta u_y + k_0^2 u_y = \delta_y & \text{in } \mathbb{R}^d \setminus \overline{D}, \\ \Delta u_y + k_\star^2 u_y = 0 & \text{in } D, \\ u_y\big|_+ - u_y\big|_- = 0 & \text{on } \partial D, \\ \dfrac{1}{\mu_0}\dfrac{\partial u_y}{\partial \nu}\bigg|_+ - \dfrac{1}{\mu_\star}\dfrac{\partial u_y}{\partial \nu}\bigg|_- = 0 & \text{on } \partial D, \\ u_y \text{ satisfies the outgoing radiation condition.} \end{cases} \tag{11.24}$$

Here, $k_\star^2 = \omega^2 \varepsilon_\star \mu_\star$.

Let u_y be the solution to (11.24) and let U_y be the solution in the absence of the target, *i.e.*, $U_y(x) = \Gamma_{k_0}(x - y)$.

As $\delta \to 0$, the following asymptotic expansion of the perturbation of the perturbation $u_y - U_y$ due to the presence of $D = \delta B + z$ can be proved analogously to (11.14):

$$\begin{aligned} u_y(x) - U_y(x) = -\delta^d \bigg[& k_0^2 (\frac{\varepsilon_\star}{\varepsilon_0} - 1)|B| \Gamma_{k_0}(x, z) \Gamma_{k_0}(y, z) \\ & + \nabla_z \Gamma_{k_0}(x, z) \cdot M(\lambda, B) \nabla_z \Gamma_{k_0}(y, z) \bigg] + O(\delta^{d+1}), \end{aligned} \tag{11.25}$$

where λ is given in this case by (11.15). Note that (11.25) is a dipolar approximation. Formula (11.25) shows that, at the leading-order in terms of the characteristic size, the effect of a small electromagnetic particle on measurements is the sum of a polarized magnetic dipole and an electric point source. Moreover, the leading-order term satisfies the reciprocity property.

11.4 Elasticity Equations

Consider an elastic medium occupying a bounded domain Ω in $\mathbb{R}^d$, with a connected smooth boundary $\partial\Omega$. Let the constants (λ, μ) denote the background Lamé coefficients, that are the elastic parameters in the absence of any inclusion. Suppose that the elastic inclusion D in Ω is given by

$$D = \delta B + z,$$

where B is a bounded smooth domain in $\mathbb{R}^d$. We assume that there exists $c_0 > 0$ such that $\inf_{x \in D} \text{dist}(x, \partial\Omega) > c_0$.

Suppose that D has the pair of Lamé constants $(\widetilde{\lambda}, \widetilde{\mu})$ satisfying (3.121) and (3.170). An asymptotic expansion for the displacement field in terms of the reference Lamé constants, the location, and the shape of the inclusion D can be derived. This expansion describes the perturbation of the solution caused by the presence of D. It is expressed in terms of the elastic moment tensor which is a geometric quantity associated with the inclusion. Based on this asymptotic expansion, we will derive the algorithms to obtain accurate

and stable reconstructions of the location and the order of magnitude of the elastic inclusion.

The elastic moment tensor (EMT) associated with the domain B and the Lamé parameters $(\lambda, \mu; \widetilde{\lambda}, \widetilde{\mu})$ is defined as follows: For $p, q = 1, \ldots, d$, let f_{pq} and g_{pq} solve

$$\begin{cases} \widetilde{\mathcal{S}}_B[f_{pq}]|_- - \mathcal{S}_B[g_{pq}]|_+ = x_p e_q|_{\partial B}, \\ \dfrac{\partial}{\partial \widetilde{n}} \widetilde{\mathcal{S}}_B[f_{pq}]\Big|_- - \dfrac{\partial}{\partial n} \mathcal{S}_B[g_{pq}]\Big|_+ = \dfrac{\partial(x_p e_q)}{\partial n}\Big|_{\partial B}, \end{cases} \tag{11.26}$$

where $(e_1, \ldots, e_d)$ is the canonical basis of $\mathbb{R}^d$. Then the EMT $\mathbb{M} := (m_{jlpq})_{j,l,p,q=1}^d$ is defined by

$$m_{jlpq} := \int_{\partial B} x_p e_q \cdot g_{jl} \, d\sigma. \tag{11.27}$$

The following lemma holds [66].

Lemma 11.7 *Suppose that* $0 < \widetilde{\lambda}, \widetilde{\mu} < +\infty$. *For* $j, l, p, q = 1, \ldots, d$,

$$m_{jlpq} = \int_{\partial B} \left[-\frac{\partial(x_p e_q)}{\partial n} + \frac{\partial(x_p e_q)}{\partial \widetilde{n}} \right] \cdot v_{jl} \, d\sigma, \tag{11.28}$$

where v_{jl} *is the unique solution of the transmission problem*

$$\begin{cases} \mathcal{L}^{\lambda,\mu} v_{jl} = 0 & \text{in } \mathbb{R}^d \setminus \overline{B}, \\ \mathcal{L}^{\widetilde{\lambda},\widetilde{\mu}} v_{jl} = 0 & \text{in } B, \\ v_{jl}|_+ - v_{jl}|_- = 0 & \text{on } \partial B, \\ \dfrac{\partial v_{jl}}{\partial n}\Big|_+ - \dfrac{\partial v_{jl}}{\partial \widetilde{n}}\Big|_- = 0 & \text{on } \partial B, \\ v_{jl}(x) - x_j e_l = O(|x|^{1-d}) & \text{as } |x| \to +\infty. \end{cases} \tag{11.29}$$

11.4.1 Static Regime

In this subsection we consider the effect of a small elastic inclusion on the boundary measurements in the static regime. For a given $g \in L^2_{\Psi}(\partial D)$ (see (3.162)), let u_δ be the solution of

$$\begin{cases} \mathcal{L}^{\lambda,\mu} u_\delta = 0 & \text{in } \Omega \setminus \overline{D}, \\ \mathcal{L}^{\widetilde{\lambda},\widetilde{\mu}} u_\delta = 0 & \text{in } D, \\ u_\delta\big|_- = u_\delta\big|_+ & \text{on } \partial D, \\ \dfrac{\partial u_\delta}{\partial \widetilde{n}}\Big|_- = \dfrac{\partial u_\delta}{\partial n}\Big|_+ & \text{on } \partial D, \\ \dfrac{\partial u_\delta}{\partial n}\Big|_{\partial \Omega} = g, \\ u_\delta\big|_{\partial \Omega} \in L^2_{\Psi}(\partial \Omega). \end{cases} \tag{11.30}$$

Let $N_\Omega(x, z)$ be the Neumann function for the Lamé system on Ω, namely, for $z \in \Omega$, $N(x, z)$ is the solution to

$$\begin{cases} \mathcal{L}^{\lambda,\mu} N_\Omega(x, z) = -\delta_z(x) I, & x \in \Omega, \\ \dfrac{\partial N_\Omega}{\partial n}(x, z) = -\dfrac{1}{|\partial\Omega|} I, & x \in \partial\Omega, \end{cases} \tag{11.31}$$

subject to the orthogonality condition:

$$\int_{\partial\Omega} N_\Omega(x, z)\psi(x) \, d\sigma(x) = 0 \quad \forall \, \psi \in \Psi. \tag{11.32}$$

We have

$$\left(-\frac{1}{2}I + \mathcal{K}_\Omega\right)^{-1} [\Gamma(\cdot - z)] (x) = N_\Omega(x, z), \quad x \in \partial\Omega, \ z \in \Omega, \tag{11.33}$$

modulo a function in Ψ.

The following outer expansion for the displacement field holds.

Theorem 11.8 *Let u_δ be the solution of (11.30) and u_0 the background solution. The following pointwise asymptotic expansion on $\partial\Omega$ holds:*

$$u_\delta(x) = u_0(x) - \delta^d \nabla u_0(z) : \mathbb{M}\nabla_z N_\Omega(x, z) + O(\delta^{d+1}), \quad x \in \partial\Omega. \tag{11.34}$$

Note that in (11.34) we have used the convention

$$\left(\nabla u_0(z) : \mathbb{M}\nabla_z N_\Omega(x, z)\right)_k = \sum_{j,l=1}^{d} \left(\partial_j(u_0)_l(z) \sum_{p,q=1}^{d} m_{jlpq}\partial_p(N_\Omega)_{kq}(x, z)\right), \tag{11.35}$$

for $k = 1, \ldots, d$.

When there are multiple well-separated inclusions

$$D_l = \delta B_l + z_l, \quad l = 1, \ldots, m,$$

where $|z_l - z_{l'}| > 2c_0$ for some $c_0 > 0$, $l \neq l'$, then by iterating formula (11.34), we obtain the following theorem.

Theorem 11.9 *The following asymptotic expansion holds uniformly for $x \in \partial\Omega$:*

$$u_\delta(x) = u_0(x) - \delta^d \sum_{l=1}^{m} \nabla u_0(z_l) : \mathbb{M}^l \nabla_z N_\Omega(x, z_l) + O(\delta^{d+1}),$$

where $\mathbb{M}^l$ is the EMT corresponding to the inclusion B_l, $l = 1, \ldots, m$.

Finally, the following inner asymptotic formula holds.

Theorem 11.10 *We have*

$$u_\delta(x) \simeq u_0(z) + \delta \sum_{j,l} v_{jl}\left(\frac{x - z}{\delta}\right)(\partial_j(u_0)_l)(z) \quad \text{for } x \text{ near } z. \tag{11.36}$$

11.4.2 Time-Harmonic Regime

Let $0 = \kappa_1 \leq \kappa_2 \leq \ldots$ be the eigenvalues of $-\mathcal{L}^{\lambda,\mu}$ in Ω with the Neumann condition on $\partial\Omega$. Note that $\kappa_1 = 0$ is of multiplicity $d(d+1)/2$, the eigenspace being Ψ. For $\omega\sqrt{\rho} \notin \{\sqrt{\kappa_j}\}_{j\geq 1}$, let u_0 be the background solution associated with (λ, μ, ρ) in Ω, $i.e.$,

$$
\begin{cases}
(\mathcal{L}^{\lambda,\mu} + \omega^2\rho)u_0 = 0 & \text{in } \Omega, \\
\dfrac{\partial u_0}{\partial n} = g & \text{on } \partial\Omega,
\end{cases}
\tag{11.37}
$$

with $g \in L^2(\partial\Omega)^d$.

Suppose that the elastic inclusion D in Ω is given by $D = \delta B + z$, where B is a bounded smooth domain in $\mathbb{R}^d$. We assume that there exists $c_0 > 0$ such that $\inf_{x \in D} \text{dist}(x, \partial\Omega) > c_0$. Suppose that D has the pair of Lamé constants $(\widetilde{\lambda}, \widetilde{\mu})$ satisfying (3.121) and (3.170) and denote by $\tilde\rho$ its density.

Let u_δ be the solution to

$$
\begin{cases}
(\mathcal{L}^{\lambda,\mu} + \omega^2\rho)u_\delta = 0 & \text{in } \Omega \setminus \overline{D}, \\
(\mathcal{L}^{\widetilde{\lambda},\widetilde{\mu}} + \omega^2\tilde\rho)u_\delta = 0 & \text{in } D, \\
u_\delta\big|_- = u_\delta\big|_+ & \text{on } \partial D, \\
\dfrac{\partial u_\delta}{\partial \tilde n}\bigg|_- = \dfrac{\partial u_\delta}{\partial n}\bigg|_+ & \text{on } \partial D, \\
\dfrac{\partial u_\delta}{\partial n} = g & \text{on } \partial\Omega.
\end{cases}
\tag{11.38}
$$

For $\omega\sqrt{\rho} \notin \{\sqrt{\kappa_j}\}_{j\geq 1}$, let $N_\Omega^\omega(x, z)$ be the Neumann function for $\mathcal{L}^{\lambda,\mu} + \omega^2\rho$ in Ω corresponding to a Dirac mass at z. That is, for $z \in \Omega$, $N_\Omega^\omega(\cdot, z)$ is the matrix-valued solution to

$$
\begin{cases}
(\mathcal{L}^{\lambda,\mu} + \omega^2\rho)N_\Omega^\omega(x, z) = -\delta_z(x)I, & x \in \Omega, \\
\dfrac{\partial N_\Omega^\omega}{\partial n}(x, z) = 0, & x \in \partial\Omega.
\end{cases}
\tag{11.39}
$$

Analogously to (11.31), the following relation holds:

$$
\left(-\frac{1}{2}I + \mathcal{K}_\Omega^\omega \right)[N_\Omega^\omega(\cdot, z)](x) = \Gamma^\omega(x, z), \quad x \in \partial\Omega, \ \ z \in \Omega.
\tag{11.40}
$$

Then, the following result can be obtained using arguments analogous to those in Theorem 11.8.

Theorem 11.11 *Let u_δ be the solution to (11.38), u_0 be the background so-lution defined by (11.37) and $\omega^2\rho$ be different from the Neumann eigenvalues of the operator $-\mathcal{L}^{\lambda,\mu}$ on Ω. Then, for $\omega\delta \ll 1$, the following asymptotic expansion holds uniformly for all $x \in \partial\Omega$:*

$$u_\delta(x) - u_0(x) = -\delta^d \Big(\nabla u_0(z) : \mathbb{M} \nabla_z N_\Omega^\omega(x, z)$$

$$+ \omega^2(\rho - \tilde{\rho})|B| N_\Omega^\omega(x, z) u_0(z) \Big) + O(\delta^{d+1}). \tag{11.41}$$

Moreover, we have

$$\left(\frac{1}{2}I - \mathcal{K}_\Omega^\omega \right) [u_\delta - u_0](x) = \delta^d \Big(\nabla u_0(z) : \mathbb{M} \nabla_z \Gamma^\omega(x - z) \tag{11.42}$$

$$+ \omega^2(\rho - \tilde{\rho})|B| \Gamma^\omega(x - z) u_0(z) \Big) + O(\delta^{d+1})$$

uniformly with respect to $x \in \partial\Omega$.

We also have an asymptotic expansion of the solutions of the Dirichlet problem.

Let $0 \leq \tau_1 \leq \tau_2 \leq \ldots$ be the eigenvalues of $-\mathcal{L}^{\lambda,\mu}$ in Ω with the Dirichlet condition on $\partial\Omega$. For $\omega\sqrt{\rho} \notin \{\sqrt{\tau_j}\}_{j \geq 1}$, let $G_\Omega^\omega(x, z)$ be the Dirichlet function for $\mathcal{L}^{\lambda,\mu} + \omega^2\rho$ in Ω corresponding to a Dirac mass at z. That is, for $z \in \Omega$, $G_\Omega^\omega(\cdot, z)$ is the matrix-valued solution to

$$\begin{cases} (\mathcal{L}^{\lambda,\mu} + \omega^2\rho)G_\Omega^\omega(x, z) = -\delta_z(x)I, & x \in \Omega, \\ G_\Omega^\omega(x, z) = 0, & x \in \partial\Omega. \end{cases} \tag{11.43}$$

Then for any $x \in \partial\Omega$, and $z \in \Omega$ we can prove in the same way as (11.40) that

$$\left(\frac{1}{2}I + (\mathcal{K}_\Omega^\omega)^* \right) [\frac{\partial G_\Omega^\omega}{\partial n}(\cdot, z)](x) = -\frac{\partial \Gamma^\omega}{\partial n}(x, z). \tag{11.44}$$

Theorem 11.12 *Let $\omega^2\rho$ be different from the Dirichlet eigenvalues of the operator $-\mathcal{L}^{\lambda,\mu}$ on Ω. Let v_δ be the solution to*

$$\begin{cases} (\mathcal{L}^{\lambda,\mu} + \omega^2\rho)v_\delta = 0 & in\ \Omega \setminus \overline{D}, \\ (\mathcal{L}^{\tilde{\lambda},\tilde{\mu}} + \omega^2\tilde{\rho})v_\delta = 0 & in\ D, \\ v_\delta|_- = v_\delta|_+ & on\ \partial D, \\ \dfrac{\partial v_\delta}{\partial \tilde{n}}\Big|_- = \dfrac{\partial v_\delta}{\partial n}\Big|_+ & on\ \partial D, \\ v_\delta = f & on\ \partial\Omega, \end{cases} \tag{11.45}$$

and let v_0 be the background solution defined by

$$\begin{cases} (\mathcal{L}^{\lambda,\mu} + \omega^2\rho)v_0 = 0 & in\ \Omega, \\ v_0 = f & on\ \partial\Omega, \end{cases} \tag{11.46}$$

with $f \in W_{1/2}^2(\partial\Omega)^d$. Then, for $\omega\delta \ll 1$, the following asymptotic expansion holds uniformly for all $x \in \partial\Omega$:

$$\frac{\partial v_\delta}{\partial \nu}(x) - \frac{\partial v_0}{\partial \nu}(x) = -\delta^d \Big(\nabla v_0(z) : \mathbb{M}\nabla_z \frac{\partial G_\Omega^\omega}{\partial \nu}(x,z) \tag{11.47}$$

$$+ \omega^2(\rho - \tilde{\rho})|B|\frac{\partial G_\Omega^\omega}{\partial \nu}(x,z)u_0(z)\Big) + O(\delta^{d+1}).$$

Moreover,

$$\Big(\frac{1}{2}I + (\mathcal{K}_\Omega^\omega)^*\Big)[\frac{\partial(v_\delta - v_0)}{\partial \nu}](x) = -\delta^d \Big(\nabla v_0(z) : \mathbb{M}\nabla_z \frac{\partial \Gamma^\omega}{\partial \nu}(x - z) \tag{11.48}$$

$$+ \omega^2(\rho - \tilde{\rho})|B|\frac{\partial \Gamma^\omega}{\partial \nu}(x - z)v_0(z)\Big) + O(\delta^{d+1})$$

uniformly with respect to $x \in \partial\Omega$.

11.4.3 Properties of the EMT

We now provide some important properties of the EMT such as symmetry, positive-definiteness, and bounds.

The following theorem holds [66, 68].

Theorem 11.13 (Symmetry) *Let $\mathbb{M}$ be the EMT associated with the domain B, and $(\widetilde{\lambda}, \widetilde{\mu})$ and (λ, μ) be the Lamé parameters of B and the background, respectively. Then, for $p, q, j, l = 1, \ldots, d$,*

$$m_{jlpq} = m_{jlqp}, \quad m_{jlpq} = m_{ljpq}, \quad and \quad m_{jlpq} = m_{pqjl}. \tag{11.49}$$

The symmetry property (11.49) implies that $\mathbb{M}$ is a symmetric linear transformation on the space M_d^S of $d \times d$ symmetric matrices.

We now recall the positive-definiteness property of the EMT. The following holds [66, 68].

Theorem 11.14 (Positivity) *Suppose that (3.170) holds. If $\widetilde{\mu} > \mu$ ($\widetilde{\mu} < \mu$, resp.), then $\mathbb{M}$ is positive (negative, resp.) definite on the space M_d^S of $d \times d$ symmetric matrices.*

Set

$$\mathbb{P}_1 := \frac{1}{d}I \otimes I, \quad \mathbb{P}_2 := \mathbb{I} - \mathbb{P}_1. \tag{11.50}$$

Since for any $d \times d$ symmetric matrix A

$$I \otimes I(A) = (A : I)\, I = \mathrm{trace}(A)\, I \quad \text{and} \quad \mathbb{I}(A) = A,$$

one can immediately see that

$$\mathbb{P}_1\mathbb{P}_1 = \mathbb{P}_1, \quad \mathbb{P}_2\mathbb{P}_2 = \mathbb{P}_2, \quad \mathbb{P}_1\mathbb{P}_2 = 0,$$

and $\mathbb{P}_2$ is then the orthonormal projection from the space of $d \times d$ symmetric matrices onto the space of symmetric matrices of trace zero.

With notation (11.50), we express the trace bounds satisfied by the EMT in the following theorem.

Theorem 11.15 (Bounds) *Set $\beta = \lambda + 2\mu/d, \widetilde{\beta} = \widetilde{\lambda} + 2\widetilde{\mu}/d$. Suppose for simplicity that $\widetilde{\mu} > \mu$. We have*

$$\frac{1}{|B|}\,\mathrm{trace}(\mathbb{P}_1\mathbb{M}\mathbb{P}_1) \leq d(\widetilde{\beta}-\beta)\frac{d\beta+2(d-1)\widetilde{\mu}}{d\widetilde{\beta}+2(d-1)\widetilde{\mu}} \tag{11.51}$$

$$\frac{1}{|B|}\,\mathrm{trace}\,(\mathbb{P}_2\mathbb{M}\mathbb{P}_2) \leq 2\,(\widetilde{\mu}-\mu)\left[\frac{d^2+d-2}{2}\right.$$
$$\left.-\,2\,(\widetilde{\mu}-\mu)\left(\frac{d-1}{2\widetilde{\mu}}+\frac{d-1}{d\widetilde{\beta}+2(d-1)\widetilde{\mu}}\right)\right], \tag{11.52}$$

$$|B|\,\mathrm{trace}\,\left(\mathbb{P}_1\mathbb{M}^{-1}\mathbb{P}_1\right) \leq \frac{1}{d(\widetilde{\beta}-\beta)}\frac{d\widetilde{\beta}+2(d-1)\mu}{d\beta+2(d-1)\mu}, \tag{11.53}$$

$$|B|\,\mathrm{trace}\,\left(\mathbb{P}_2\mathbb{M}^{-1}\mathbb{P}_2\right) \leq \frac{1}{2(\widetilde{\mu}-\mu)}\left[\frac{d^2+d-2}{2}\right.$$
$$\left.+\,2\left(\widetilde{\mu}-\mu\right)\left(\frac{d-1}{2\mu}+\frac{d-1}{d\beta+2(d-1)\mu}\right)\right], \tag{11.54}$$

where for $\mathbb{C} = (C_{pqjl})$, $\mathrm{trace}(\mathbb{C}) := \sum\limits_{j,l=1}^{d} C_{jljl}$.

Note that $\mathbb{P}_1\mathbb{M}\mathbb{P}_1$ and $\mathbb{P}_2\mathbb{M}\mathbb{P}_2$ are the bulk and shear parts of $\mathbb{M}$. We also note that

$$\mathrm{trace}(\mathbb{P}_1) = 1 \quad \text{and} \quad \mathrm{trace}(\mathbb{P}_2) = (d(d+1)-2)/2.$$

The bounds (11.51)–(11.54) are called Hashin-Shtrikman bounds for the EMT and are obtained in [124, 259].

It is worth mentioning that the dimension of the space of symmetric 4-tensors in the three dimensional space is 21, and hence the equalities (11.53) and (11.54) are satisfied on a 19 $(21-2)$ dimensional surface in tensor space. However ellipsoid geometries (with unit volume) only cover a 5 dimensional manifold within that 19 dimensional space.

EMT's under linear transformations

We recall formulas for EMT's under linear transformations. These formulas were first proved in [66].

Theorem 11.16 *Let B be a bounded domain in $\mathbb{R}^d$ and let $(m_{jlpq}(B))$ denote the EMT associated with B. Then the following holds:*

translation formula Let $z \in \mathbb{R}^d$. Then,

$$m_{jlpq}(B+z) = m_{jlpq}(B), \quad j,l,p,q = 1,\dots,d; \tag{11.55}$$

scaling formula Let $\delta > 0$. Then,

$$m_{jlpq}(\delta B) = \delta^d m_{jlpq}(B), \quad j, l, p, q = 1, \ldots, d; \tag{11.56}$$

rotation formula Let $R = (R_{jl})$ be a unitary transformation in $\mathbb{R}^d$. Then,

$$m_{jlpq}(R(B)) = \sum_{u,v=1}^{d} \sum_{k,r=1}^{d} R_{pu} R_{qv} R_{jk} R_{lr} m_{kruv}(B), \quad j, l, p, q = 1, \ldots, d. \tag{11.57}$$

EMTs for Ellipses and Balls

In dimension two, let $\mathbb{M} = (m_{jlpq})$ be the EMT for the ellipse B whose semi-axes are on the x_1- and x_2-axes and of length a and b, respectively, and let $(\widetilde{\lambda}, \widetilde{\mu})$ and (λ, μ) be the Lamé parameters of B and the background, respectively.

Then we have

$$m_{1111} = |B|(\lambda + 2\mu)\frac{(\widetilde{\mu} - \mu)(\widetilde{\lambda} - \lambda + \widetilde{\mu} - \mu)[m^2 - 2(\tau - 1)m] + c}{(\widetilde{\mu} - \mu)[3\mu + (1 - \tau)(\widetilde{\lambda} + \widetilde{\mu})]m^2 + (\mu + \widetilde{\lambda} + \widetilde{\mu})(\mu + \tau\widetilde{\mu})},$$

$$m_{2222} = |B|(\lambda + 2\mu)\frac{(\widetilde{\mu} - \mu)(\widetilde{\lambda} - \lambda + \widetilde{\mu} - \mu)[m^2 + 2(\tau - 1)m] + c}{(\widetilde{\mu} - \mu)[3\mu + (1 - \tau)(\widetilde{\lambda} + \widetilde{\mu})]m^2 + (\mu + \widetilde{\lambda} + \widetilde{\mu})(\mu + \tau\widetilde{\mu})},$$

$$m_{1122} = |B|\frac{(\lambda + 2\mu)[(\widetilde{\mu} - \mu)(\widetilde{\lambda} - \lambda + \widetilde{\mu} - \mu)m^2 + (\widetilde{\lambda} - \lambda)(\widetilde{\mu} + \tau\mu) + (\widetilde{\mu} - \mu)^2]}{(\widetilde{\mu} - \mu)[3\mu + (1 - \tau)(\widetilde{\lambda} + \widetilde{\mu})]m^2 + (\mu + \widetilde{\lambda} + \widetilde{\mu})(\mu + \tau\widetilde{\mu})},$$

$$m_{1212} = |B|\frac{\mu(\widetilde{\mu} - \mu)(\tau + 1)}{-(\widetilde{\mu} - \mu)m^2 + \mu + \tau\widetilde{\mu}},$$

where

$$c = (\widetilde{\lambda} - \lambda + \widetilde{\mu} - \mu)(\mu + \tau\widetilde{\mu}) + (\tau - 1)(\widetilde{\mu} - \mu)(\mu + \widetilde{\lambda} + \widetilde{\mu}),$$

$m = (a - b)/(a + b)$ and $\tau = (\lambda + 3\mu)/(\lambda + \mu)$. The remaining terms are determined by the symmetry properties (11.49). If $m = 0$, *i.e.*, B is a disk, then

$$\begin{cases} m_{1122} = |B|\dfrac{(\lambda + 2\mu)[(\widetilde{\lambda} - \lambda)(\widetilde{\mu} + \tau\mu) + (\widetilde{\mu} - \mu)^2]}{(\mu + \widetilde{\lambda} + \widetilde{\mu})(\mu + \tau\widetilde{\mu})}, \\ m_{1212} = |B|\dfrac{\mu(\widetilde{\mu} - \mu)(\tau + 1)}{\mu + \tau\widetilde{\mu}}. \end{cases} \tag{11.58}$$

With notation (11.50), the EMT of a disk given by (11.58) can be rewritten as

$$\mathbb{M} = 2|B|\frac{(\lambda + 2\mu)(\widetilde{\lambda} + \widetilde{\mu} - \lambda - \mu)}{\mu + \widetilde{\lambda} + \widetilde{\mu}}\mathbb{P}_1 + 2|B|\frac{\mu(\widetilde{\mu} - \mu)(\tau + 1)}{\mu + \tau\widetilde{\mu}}\mathbb{P}_2,$$

or, equivalently,

$$\mathbb{M} = |B|m_1^{(2)}(2m_2^{(2)}\mathbb{P}_1 + 2\mathbb{P}_2) \tag{11.59}$$

with

$$m_1^{(2)} = \frac{\mu(\widetilde{\mu} - \mu)(\tau + 1)}{\mu + \tau\widetilde{\mu}},$$
$$m_2^{(2)} = \frac{(\lambda + 2\mu)(\widetilde{\lambda} + \widetilde{\mu} - \lambda - \mu)(\mu + \tau\widetilde{\mu})}{\mu(\mu + \widetilde{\lambda} + \widetilde{\mu})(\widetilde{\mu} - \mu)(\tau + 1)}. \tag{11.60}$$

Analogously, for a spherical inclusion B, $\mathbb{M}$ can be expressed as [67]

$$\mathbb{M} = |B|m_1^{(3)}(3m_2^{(3)}\mathbb{P}_1 + 2\mathbb{P}_2), \tag{11.61}$$

where

$$m_1^{(3)} = \frac{15\mu(\mu - \widetilde{\mu})(\beta - 1)}{15\mu(1 - \beta) + 2(\mu - \widetilde{\mu})(5\beta - 4)},$$

$$m_2^{(3)} = \frac{(\lambda - \widetilde{\lambda})\big(15\mu\lambda(1 - \beta) + 2\lambda(\mu - \widetilde{\mu})(5\beta - 4)\big)}{5(\mu - \widetilde{\mu})\big(3\lambda\mu(1 - \beta) - 3\mu\beta(\lambda - \widetilde{\lambda}) - \lambda(\mu - \widetilde{\mu})(1 - 2\beta)\big)} \tag{11.62}$$
$$-\frac{2(\mu - \widetilde{\mu})(\lambda(\mu - \widetilde{\mu}) - 5\mu\beta(\lambda - \widetilde{\lambda}))}{5(\mu - \widetilde{\mu})\big(3\lambda\mu(1 - \beta) - 3\mu\beta(\lambda - \widetilde{\lambda}) - \lambda(\mu - \widetilde{\mu})(1 - 2\beta)\big)},$$

and $\beta = \dfrac{\lambda}{2(\lambda + \mu)}$ denotes the Poisson ratio.

Note that from (11.59) and (11.61) it follows that the EMT $\mathbb{M}$ of a disk or a sphere is isotropic. One can write $\mathbb{M}$ as

$$\mathbb{M} = a\mathbb{I} + bI \otimes I \tag{11.63}$$

for constants a and b depending only on $\lambda, \widetilde{\lambda}, \mu, \widetilde{\mu}$ and the space dimension d, which can be easily computed. In fact, using (11.50), (11.59), and (11.61), we have

$$a = 2|B|m_1^{(d)},$$
$$b = |B|m_1^{(d)}(m_2^{(d)} - \frac{2}{d}).$$

Incompressible Limit

Let w_{jl} be the unique solution of the Stokes problem

$$\begin{cases} \mu \Delta w_{jl} + \nabla p = 0 & \text{in } \mathbb{R}^d \setminus \overline{B}, \\ \widetilde{\mu} \Delta w_{jl} + \nabla p = 0 & \text{in } B, \\ w_{jl}|_+ = w_{jl}|_- & \text{on } \partial B, \\ \left(p\nu + \mu \dfrac{\partial w_{jl}}{\partial \nu} \right)\Big|_+ = \left(p\nu + \widetilde{\mu} \dfrac{\partial w_{jl}}{\partial n} \right)\Big|_- & \text{on } \partial B, \\ w_{jl}(x) - x_j e_l + \dfrac{\delta_{jl}}{d} \displaystyle\sum_{p=1}^{d} x_p e_p = O(|x|^{1-d}) & \text{as } |m| \to +\infty, \\ p(x) = O(|x|^{-d}) & \text{as } |m| \to +\infty. \end{cases} \tag{11.64}$$

Define the tensor $\mathbb{V} = (v_{jlpq})_{j,l,p,q=1}^{d}$ by

$$v_{jlpq} := (\widetilde{\mu} - \mu) \int_B \nabla w_{jl} : \nabla^s (x_p e_q)\, dx, \quad j, l, p, q = 1, \dots, d.$$

The tensor $\mathbb{V}$, introduced in [47], is called the viscous moment tensor. Again in [47], it is proved that

$$\left\| v_{jl} - \left(w_{jl} - \frac{\delta_{jl}}{d} \sum_{p=1}^{d} w_{pp} \right) \right\|_{W(\mathbb{R}^d)} \to 0 \quad \text{as } \widetilde{\lambda}, \lambda \to +\infty, \tag{11.65}$$

where v_{jl} is defined by (11.29). Here, the limits are taken under the assumption that $\widetilde{\lambda}/\lambda = O(1)$. Therefore, one can show from (11.65) that

$$\mathbb{V} = \lim_{\widetilde{\lambda}, \lambda \to +\infty} \mathbb{P}_2 \mathbb{M} \mathbb{P}_2,$$

where $\mathbb{P}_2$, defined by (11.50), is the orthonormal projection from the space of $d \times d$ symmetric matrices onto the space of symmetric matrices of trace zero.

11.5 Asymptotic Expansions for Time-Dependent Equations

11.5.1 Asymptotic Formulas for the Wave Equation

Consider the initial boundary value problem for the (scalar) wave equation

$$\begin{cases} \partial_t^2 u - \nabla \cdot \left(\chi(\Omega \setminus \overline{D}) + k\chi(D) \right) \nabla u = 0 & \text{in } \Omega_T, \\ u(x,0) = u_0(x), \quad \partial_t u(x,0) = u_1(x) & \text{for } x \in \Omega, \\ \dfrac{\partial u}{\partial \nu} = g & \text{on } \partial \Omega_T, \end{cases} \tag{11.66}$$

where $T < +\infty$ is a final observation time, $\Omega_T = \Omega \times (0,T)$, and $\partial\Omega_T = \partial\Omega \times (0,T)$. The initial data $u_0, u_1 \in \mathcal{C}^\infty(\overline{\Omega})$, and the Neumann boundary data $g \in \mathcal{C}^\infty(0,T;\mathcal{C}^\infty(\partial\Omega))$ are subject to compatibility conditions.

Define the background solution U to be the solution of the wave equation in the absence of any anomalies. Thus U satisfies

$$
\begin{cases}
\partial_t^2 U - \Delta U = 0 \quad \text{in} \quad \Omega_T \ , \\
U(x,0) = u_0(x), \quad \partial_t U(x,0) = u_1(x) \quad \text{for} \quad x \in \Omega \ , \\
\dfrac{\partial U}{\partial \nu} = g \quad \text{on} \quad \partial\Omega_T \ .
\end{cases}
$$

For $\rho > 0$, define the operator P_ρ on tempered distributions by

$$
P_\rho[\psi](x,t) = \frac{1}{\sqrt{2\pi}} \int_{|\omega| \le \rho} e^{-i\omega t} \hat{\psi}(x,\omega) \, d\omega \ , \tag{11.67}
$$

where $\hat{\psi}(x,\omega)$ denotes the Fourier transform of $\psi(x,t)$ in the $t-$variable:

$$
\hat{\psi}(x,\omega) = \mathcal{F}_t[\psi(x,\cdot)](\omega) = \frac{1}{\sqrt{2\pi}} \int_{-\infty}^\infty \psi(x,t) e^{i\omega t} dt \ .
$$

Clearly, the operator P_ρ truncates the high-frequency component of ψ.

The following asymptotic expansion holds as $\delta \to 0$.

Theorem 11.17 (Perturbations of weighted boundary measurements)
Let $w \in \mathcal{C}^\infty(\overline{\Omega}_T)$ satisfy $(\partial_t^2 - \Delta)w(x,t) = 0$ in Ω_T with $\partial_t w(x,T) = w(x,T) = 0$ for $x \in \Omega$. Suppose that $\rho \ll 1/\sqrt{\delta}$. Define the weighted boundary measurements

$$
I_w[U,T] := \int_{\partial\Omega_T} P_\rho[u-U](x,t) \frac{\partial w}{\partial \nu}(x,t) \, d\sigma(x) \, dt \ .
$$

Then, for any fixed $T > \mathrm{diam}(\Omega)$, the following asymptotic expansion for $I_w[U,T]$ holds as $\delta \to 0$:

$$
I_w[U,T] \approx \delta^d \int_0^T \nabla P_\rho[U](z,t) M(\lambda, B) \nabla w(z,t) \, dt \ , \tag{11.68}
$$

where $M(\lambda, B)$ is defined by (11.5).

Expansion (11.68) is a weighted expansion. Pointwise expansions similar to those in Theorem 11.1 which is for the steady-state model can also be obtained.

Let $y \in \mathbb{R}^3$ be such that $|y - z| \gg \delta$. Choose $U(x,t) = U_y(x,t)$, where U_y is defined by (2.55) and consider for the sake of simplicity the wave equation in the whole three-dimensional space with appropriate initial conditions:

$$\begin{cases} \partial_t^2 u - \nabla \cdot \left(\chi(\mathbb{R}^3 \setminus \overline{D}) + k\chi(D) \right) \nabla u = \delta_{x=y}\delta_{t=0} \quad \text{in} \quad \mathbb{R}^3 \times (0, +\infty) \,, \\ u(x,0) = 0, \quad \partial_t u(x,0) = 0 \quad \text{for} \quad x \in \mathbb{R}^3, x \neq y \,. \end{cases}$$

$$(11.69)$$

The following theorem holds.

Theorem 11.18 (Pointwise perturbations) *Let u be the solution to (11.69). Set U_y to be the background solution. Suppose that $\rho \ll 1/\sqrt{\delta}$.*

(i) *The following outer expansion holds*

$$P_\rho[u - U_y](x,t) \approx -\delta^3 \int_{\mathbb{R}} \nabla P_\rho[U_z](x, t - \tau) \cdot M(\lambda, B) \nabla P_\rho[U_y](z, \tau) \, d\tau \,,$$

$$(11.70)$$

for x away from z, where $M(\lambda, B)$ is defined by (11.5) and U_y and U_z by (2.55).

(ii) *The following inner approximation holds:*

$$P_\rho[u - U_y](x,t) \approx \delta v\left(\frac{x - z}{\delta} \right) \cdot \nabla P_\rho[U_y](x,t) \quad \text{for } x \text{ near } z \,, \quad (11.71)$$

where v is given by (11.7) and U_y by (2.55).

Formula (11.70) shows that the perturbation due to the anomaly is in the time-domain a wavefront emitted by a dipolar source located at the point z.

Taking the Fourier transform of (11.70) in the time variable yields the expansions given in Theorem 11.5 for the perturbations resulting from the presence of a small anomaly for solutions to the Helmholtz equation at low frequencies (at wavelengths large compared to the size of the anomaly).

11.5.2 Asymptotic Analysis of Temperature Perturbations

Infrared thermal imaging is becoming a common screening modality in the area of breast cancer. By carefully examining aspects of temperature and blood vessels of the breasts in thermal images, signs of possible cancer or pre-cancerous cell growth may be detected up to 10 years prior to being discovered using any other procedure. This provides the earliest detection of cancer possible. Because of thermal imaging's extreme sensitivity, these temperature variations and vascular changes may be among the earliest signs of breast cancer and/or a pre-cancerous state of the breast. An abnormal infrared image of the breast is an important marker of high risk for developing breast cancer.

Suppose that the background Ω is homogeneous with thermal conductivity 1 and that the anomaly $D = \delta B + z$ has thermal conductivity $0 < k \neq 1 < +\infty$. In this section one considers the following transmission problem for the heat equation:

$$\begin{cases} \partial_t u - \nabla \cdot \left(\chi(\Omega \setminus \overline{D}) + k\chi(D) \right) \nabla u = 0 & \text{in} \quad \Omega_T \ , \\ u(x,0) = u_0(x) \quad \text{for} \quad x \in \Omega \ , \\ \dfrac{\partial u}{\partial \nu} = g \quad \text{on} \quad \partial \Omega_T \ , \end{cases} \qquad (11.72)$$

where the Neumann boundary data g and the initial data u_0 are subject to a compatibility condition. Let U be the background solution defined as the solution of

$$\begin{cases} \partial_t U - \Delta U = 0 & \text{in} \quad \Omega_T \ , \\ U(x,0) = u_0(x) \quad \text{for} \quad x \in \Omega \ , \\ \dfrac{\partial U}{\partial \nu} = g \quad \text{on} \quad \partial \Omega_T \ . \end{cases}$$

The following asymptotic expansion holds as $\delta \to 0$.

Theorem 11.19 (Perturbations of weighted boundary measurements)
Let $w \in C^\infty(\overline{\Omega}_T)$ be a solution to the adjoint problem, namely, satisfy $(\partial_t + \Delta)w(x,t) = 0$ in Ω_T with $w(x,T) = 0$ for $x \in \Omega$. Define the weighted boundary measurements

$$I_w[U,T] := \int_{\partial \Omega_T} (u - U)(x,t) \frac{\partial w}{\partial \nu}(x,t) \, d\sigma(x) \, dt \ .$$

Then, for any fixed $T > 0$, the following asymptotic expansion for $I_w[U,T]$ holds as $\delta \to 0$:

$$I_w[U,T] \approx -\delta^d \int_0^T \nabla U(z,t) \cdot M(\lambda, B) \nabla w(z,t) \, dt \ , \qquad (11.73)$$

where $M(\lambda, B)$ is defined by (11.5).

Note that (11.73) holds for any fixed positive final time T while (11.68) holds only for $T > \mathrm{diam}(\Omega)$. This difference comes from the finite speed propagation property for the wave equation compared to the infinite one for the heat equation.

Consider now the background solution to be the Green function of the heat equation at y:

$$U(x,t) := U_y(x,t) := \begin{cases} \dfrac{e^{-\frac{|x-y|^2}{4t}}}{(4\pi t)^{d/2}} & \text{for } t > 0 \ , \\ 0 & \text{for } t < 0 \ . \end{cases} \qquad (11.74)$$

Let u be the solution to the following heat equation with an appropriate initial condition:

$$\begin{cases} \partial_t u - \nabla \cdot \left(\chi(\mathbb{R}^d \setminus \overline{D}) + k\chi(D) \right) \nabla u = 0 & \text{in} \quad \mathbb{R}^d \times (0, +\infty) \ , \\ u(x,0) = U_y(x,0) \quad \text{for} \quad x \in \mathbb{R}^d. \end{cases} \qquad (11.75)$$

Proceeding as in the derivation of (11.70), one can prove that $\delta u(x, t) := u - U$ is approximated by

$$-(k-1) \int_0^t \frac{1}{(4\pi(t-\tau))^{d/2}} \int_{\partial D} e^{-\frac{|x-x'|^2}{4(t-\tau)}} \left. \frac{\partial v}{\partial \nu} \right|_- \left(\frac{x'-z}{\delta} \right) \cdot \nabla U_y(x', \tau) \, d\sigma(x') \, d\tau \,,$$

(11.76)

for x near z, where v is given by (11.1). Therefore, analogously to Theorem 11.18, the following pointwise expansion follows from the approximation (11.76).

Theorem 11.20 (Pointwise perturbations) *Let $y \in \mathbb{R}^d$ be such that $|y - z| \gg \delta$. Let u be the solution to (11.75). The following expansion holds*

$$(u-U)(x, t) \approx -\delta^d \int_0^t \nabla U_z(x, t-\tau) M(\lambda, B) \nabla U_y(z, \tau) \, d\tau \quad \text{for } |x-z| \gg O(\delta) \,,$$

(11.77)

where $M(\lambda, B)$ is defined by (11.5) and U_y and U_z by (11.74).

When comparing (11.77) and (11.70), one should point out that for the heat equation the perturbation due to the anomaly is accumulated over time.

12

Anomaly Imaging Algorithms

In this chapter we apply the accurate asymptotic formulas derived in Chapter 11 for the purpose of identifying the location and certain properties of the inclusions.

We consider conductivity, electromagnetic, and elasticity imaging and single out simple fundamental algorithms. Least-squares solutions to the imaging problems can be computed. However, the computations are done iteratively and may be difficult because of the nonlinear dependence of the data on the location, the physical parameter, the size, and the orientation of the inclusion. Moreover, there may be considerable non-uniqueness of the minimizer in the case where all parameters of the inclusions are unknown.

In this chapter we construct various direct (non-iterative) reconstruction algorithms that take advantage of the smallness of the inclusions. In particular, MUltiple Signal Classification algorithm (MUSIC), backpropagation, Kirchhoff migration, and topological derivative are investigated. We investigate their stability with respect to medium and measurement noises as well as their resolution. We also discuss multifrequency imaging. In the presence of (independent and identically distributed) measurement noise summing a given imaging functional over frequencies yields an improvement in the signal-to-noise ratio. However, if some correlation between frequency-dependent measurements exists, for example because of a medium noise, then summing an imaging functional over frequencies may not be appropriate. A single-frequency imaging functional at the frequency which maximizes the signal-to-noise ratio may give a better reconstruction.

The imaging techniques developed in this chapter could be seen as a regularizing method in comparison with iterative approaches; they reduce the set of admissible solutions. Their robustness and accuracy are related to the fact that the number of unknowns is reduced and the imaging problem is sparse. The algorithms designed for the Helmholtz equation and the time-harmonic elasticity equations use the phase information on the measured wave in an essential way. They can not be used to locate the target from intensity-only measurements.

12.1 Direct Imaging for the Conductivity Problem

In this section one applies the asymptotic formula (11.4) for the purpose of identifying the location and certain properties of the conductivity inclusions. Two simple fundamental algorithms that take advantage of the smallness of the inclusions are singled out: projection-type algorithms and MUSIC-type algorithms. These algorithms are fast, stable, and efficient.

12.1.1 Detection of a Single Inclusion: A Projection-Type Algorithm

We briefly discuss a simple algorithm for detecting a single inclusion. The projection-type location search algorithm makes use of constant current sources. Let Ω be the background medium and let U be the background solution. One wants to apply a special type of current that makes ∇U constant in the inclusion D. The injection current $g = a \cdot \nu$ for a fixed unit vector $a \in \mathbb{R}^d$ yields $\nabla U = a$ in Ω.

Let the conductivity inclusion D be of the form $z + \delta B$. Let w be a smooth harmonic function in Ω. From (11.4) it follows that the weighted boundary measurements $I_w[U]$ satisfies

$$I_w[U] := \int_{\partial\Omega} (u - U)(x)\frac{\partial w}{\partial \nu}(x)\, d\sigma(x) \approx -\delta^d \nabla U(z) \cdot M(\lambda, B)\nabla w(z) \;, \quad (12.1)$$

where $\lambda = (k + 1)/(2(k - 1))$, k being the conductivity of D.

Assume for the sake of simplicity that $d = 2$ and D is a disk. Set

$$w(x) = -(1/2\pi)\log|x - y| \quad \text{for } y \in \mathbb{R}^2 \setminus \overline{\Omega}, x \in \Omega \;.$$

Since w is harmonic in Ω, then from (11.11) and (12.1), it follows that

$$I_w[U] \approx \frac{(k - 1)|D|}{\pi(k + 1)}\frac{(y - z) \cdot a}{|y - z|^2} \;, \quad y \in \mathbb{R}^2 \setminus \overline{\Omega} \;. \qquad (12.2)$$

The first step for the reconstruction procedure is to locate the inclusion. The location search algorithm is as follows. Take two observation lines Σ_1 and Σ_2 contained in $\mathbb{R}^2 \setminus \overline{\Omega}$ given by

$$\Sigma_1 := \text{ a line parallel to } a \;,$$

$$\Sigma_2 := \text{ a line normal to } a \;.$$

Find two points $z_i^S \in \Sigma_i, i = 1, 2$, so that

$$I_w[U](z_1^S) = 0, \quad I_w[U](z_2^S) = \max_{y \in \Sigma_2} |I_w[U](y)| \;.$$

From (12.2), one can see that the intersecting point z^S of the two lines

$$\Pi_1(z_1^S) := \{y \mid a \cdot (y - z_1^S) = 0\} \,, \tag{12.3}$$

$$\Pi_2(z_2^S) := \{y \mid (y - z_2^S) \text{ is parallel to } a\} \tag{12.4}$$

is close to the center z of the inclusion D: $|z^S - z| = O(\delta^2)$.

Once one locates the inclusion, the factor $|D|(k-1)/(k+1)$ can be estimated. As it has been said before, this information is a mixture of the conductivity and the volume. A small inclusion with high conductivity and larger inclusion with lower conductivity can have the same polarization tensor.

An arbitrary shaped inclusion can be represented by means of an equivalent ellipse (ellipsoid).

12.1.2 Detection of Multiple Inclusions: A MUSIC-Type Algorithm

Consider P well-separated inclusions $D_p = \delta B_p + z_p$ (these are a fixed distance apart), with conductivities k_p, $p = 1, \ldots, P$. Suppose for the sake of simplicity that all the domains B_p are disks. Let $y_l \in \mathbb{R}^2 \setminus \Omega$ for $l = 1, \ldots, n$ denote the source points. Set

$$U_{y_l} = w_{y_l} := -(1/2\pi) \log |x - y_l| \quad \text{for } x \in \Omega, \quad l = 1, \ldots, n \,.$$

The MUSIC-type location search algorithm for detecting multiple inclusions is as follows. For $n \in \mathbb{N}$ sufficiently large, define the response matrix $A = (A_{ll'})_{l,l'=1}^n$ by

$$A_{ll'} = I_{w_{y_l}}[U_{y_{l'}}] := \int_{\partial\Omega} (u - U_{y_{l'}})(x) \frac{\partial w_{y_l}}{\partial \nu}(x)\, d\sigma(x) \,.$$

Expansion (12.1) yields

$$A_{ll'} \approx -\sum_{p=1}^P \frac{2(k_p - 1)|D_p|}{k_p + 1} \nabla U_{y_{l'}}(z_p) \cdot \nabla U_{y_l}(z_p) \,.$$

For $j = 1, 2$, introduce

$$g^{(j)}(z^S) = \left(e_j \cdot \nabla U_{y_1}(z^S), \ldots, e_j \cdot \nabla U_{y_n}(z^S) \right)^T, \quad z^S \in \Omega \,,$$

where $\{e_1, e_2\}$ is an orthonormal basis of $\mathbb{R}^2$.

Lemma 12.1 (MUSIC characterization) *There exists $n_0 > dP$ such that for any $n > n_0$ the following characterization of the location of the inclusions in terms of the range of the matrix A holds:*

$$g^{(j)}(z^S) \in \text{Range}(A) \text{ for } j = 1, 2 \text{ iff } z^S \in \{z_1, \ldots, z_P\} \,. \tag{12.5}$$

The MUSIC-type algorithm to determine the locations of the inclusions is as follows. Let $\Pi_{\mathrm{noise}} = I - \Pi$, where Π is the orthogonal projection onto the range of A. Given any point $z^S \in \Omega$, form the vector $g^{(j)}(z^S)$. The MUSIC characterization (12.5) says that the point z^S coincides with the location of an inclusion if and only if $\Pi_{\mathrm{noise}}[g^{(j)}](z^S) = 0$, $j = 1, 2$. Thus one can form an image of the inclusions by plotting, at each point z^S, the cost function

$$\mathcal{I}_{\mathrm{MU}}(z^S) = \frac{1}{\sqrt{||\Pi_{\mathrm{noise}}[g^{(1)}](z^S)||^2 + ||\Pi_{\mathrm{noise}}[g^{(2)}](z^S)||^2}} \ .$$

The resulting plot will have large peaks at the locations of the inclusions.

Once one locates the inclusions, the factors $|D_p|(k_p - 1)/(k_p + 1)$, $p = 1, \ldots, P$, can be estimated from the significant singular values of A.

12.2 Direct Imaging Algorithms for the Helmholtz Equation

12.2.1 Direct Imaging at a Fixed Frequency

In this section, we design direct imaging functionals for small inclusions at a fixed frequency ω. Consider the Helmholtz equation (11.12) with the Neumann data g in the presence of the inclusion D and let U denote the background solution.

Let w be a smooth function such that $(\Delta + k_0^2)w = 0$ in Ω with $k_0^2 = \omega^2 \mu_0 \varepsilon_0$. The weighted boundary measurements $I_w[U, \omega]$ defined by

$$I_w[U, \omega] := \int_{\partial\Omega} (u - U)(x) \frac{\partial w}{\partial \nu}(x) \, d\sigma(x) \tag{12.6}$$

satisfies

$$\begin{aligned} I_w[U, \omega] = -\delta^d \Big(\nabla U(z) \cdot M(\lambda, B) \nabla w(z) + k_0^2 (\frac{\varepsilon_\star}{\varepsilon_0} - 1)|B|U(z)w(z) \Big) \\ + o(\delta^d) \, , \end{aligned} \tag{12.7}$$

with λ given by (11.15).

We apply the asymptotic formulas (11.14) and (12.7) for the purpose of identifying the location and certain properties of the inclusions.

Consider P well-separated inclusions $D_p = z_p + \delta B_p$, $p = 1, \ldots, P$. The magnetic permeability and electric permittivity of D_p are denoted by μ_p and ε_p, respectively. Suppose that all the domains B_p are disks. In this case, we have

$$I_w[U, \omega] \approx - \sum_{p=1}^{P} |D_p| \Big(2\frac{\mu_p - \mu_0}{\mu_0 + \mu_p} \nabla U(z) \cdot \nabla w(z) + k_0^2 (\frac{\varepsilon_p}{\varepsilon_0} - 1)U(z)w(z) \Big) \ .$$

MUSIC-type Algorithm

Let $(\theta_1, \ldots, \theta_n)$ be n unit vectors in $\mathbb{R}^d$. For $\theta \in \{\theta_1, \ldots, \theta_n\}$, we assume that we are in possession of the boundary data u when the domain Ω is illuminated with the plane wave $U(x) = e^{ik_0\theta \cdot x}$. Taking the harmonic function $w(x) = e^{-ik_0\theta' \cdot x}$ for $\theta' \in \{\theta_1, \ldots, \theta_n\}$ and using (11.11) shows that the weighted boundary measurement is approximately equal to

$$I_w[U, \omega] \approx -\sum_{p=1}^{P} |D_p| k_0^2 \Big(2\frac{\mu_p - \mu_0}{\mu_0 + \mu_p} \theta \cdot \theta' + \frac{\varepsilon_p}{\varepsilon_0} - 1 \Big) e^{ik_0(\theta - \theta') \cdot z_p} .$$

Define the response matrix $A = (A_{ll'})_{l,l'=1}^n \in \mathbb{C}^{n \times n}$ by

$$A_{ll'} := I_{w_{l'}}[U_l, \omega] , \tag{12.8}$$

where $U_l(x) = e^{ik_0\theta_l \cdot x}, w_l(x) = e^{-ik_0\theta_l \cdot x}, l = 1, \ldots, n$. It is approximately given by

$$A_{ll'} \approx -\sum_{p=1}^{P} |D_p| k_0^2 \Big(2\frac{\mu_p - \mu_0}{\mu_0 + \mu_p} \theta_l \cdot \theta_{l'} + \frac{\varepsilon_p}{\varepsilon_0} - 1 \Big) e^{ik_0(\theta_l - \theta_{l'}) \cdot z_p} , \tag{12.9}$$

for $l, l' = 1, \ldots, n$. Introduce the n-dimensional vector fields $g^{(j)}(z^S)$, for $z^S \in \Omega$ and $j = 1, \ldots, d+1$, by

$$g^{(j)}(z^S) = \frac{1}{\sqrt{n}} \big(e_j \cdot \theta_1 e^{ik_0\theta_1 \cdot z^S}, \ldots, e_j \cdot \theta_n e^{ik_0\theta_n \cdot z^S} \big)^T, \quad j = 1, \ldots, d , \tag{12.10}$$

and

$$g^{(d+1)}(z^S) = \frac{1}{\sqrt{n}} \big(e^{ik_0\theta_1 \cdot z^S}, \ldots, e^{ik_0\theta_n \cdot z^S} \big)^T , \tag{12.11}$$

where $\{e_1, \ldots, e_d\}$ is an orthonormal basis of $\mathbb{R}^d$. Let $g(z^S)$ be the $n \times d$ matrix whose columns are $g^{(1)}(z^S), \ldots, g^{(d)}(z^S)$. Then (12.9) can be written as

$$A \approx -n \sum_{p=1}^{P} |D_p| k_0^2 \Big(2\frac{\mu_p - \mu_0}{\mu_0 + \mu_p} g(z_p)\overline{g(z_p)}^T + (\frac{\varepsilon_p}{\varepsilon_0} - 1) g^{(d+1)}(z_p)\overline{g^{(d+1)}(z_p)}^T \Big) .$$

Let $\Pi_{\text{noise}} = I - \Pi$, where Π is the orthogonal projection onto the range of A as before. The MUSIC-type imaging functional is defined by

$$\mathcal{I}_{\text{MU}}(z^S, \omega) := \Big(\sum_{j=1}^{d+1} \|\Pi_{\text{noise}}[g^{(j)}](z^S)\|^2 \Big)^{-1/2}. \tag{12.12}$$

This functional has large peaks only at the locations of the inclusions.

Backpropagation-type Algorithms

Let $(\theta_1, \ldots, \theta_n)$ be n unit vectors in $\mathbb{R}^d$. A backpropagation-type imaging functional at a single frequency ω is given by

$$\mathcal{I}_{\mathrm{BP}}(z^S, \omega) := \frac{1}{n} \sum_{l=1}^{n} e^{-2ik_0\theta_l \cdot z^S} I_{w_l}[U_l, \omega] , \qquad (12.13)$$

where $U_l(x) = w_l(x) = e^{ik_0\theta_l \cdot x}$, $l = 1, \ldots, n$. Suppose that $(\theta_1, \ldots, \theta_n)$ are equidistant points on the unit sphere S^{d-1}. For sufficiently large n, we have

$$\frac{1}{n} \sum_{l=1}^{n} e^{ik_0\theta_l \cdot x} \approx -4(\frac{\pi}{k_0})^{d-2} \Im m \left\{ \Gamma_{k_0}(x, 0) \right\} = \begin{cases} \mathrm{sinc}(k_0|x|) & \text{for } d = 3 , \\ J_0(k_0|x|) & \text{for } d = 2 , \end{cases}$$
$$(12.14)$$

where $\mathrm{sinc}(s) = \sin(s)/s$ is the sinc function and J_0 is the Bessel function of the first kind and of order zero.

Therefore, it follows that

$$\mathcal{I}_{\mathrm{BP}}(z^S, \omega) \approx -\sum_{p=1}^{P} |D_p| k_0^2 \left(2\frac{\mu_0 - \mu_p}{\mu_0 + \mu_p} + (\frac{\varepsilon_p}{\varepsilon_0} - 1) \right) \times \begin{cases} \mathrm{sinc}(2k_0|z^S - z_p|) & \text{for } d = 3, \\ J_0(2k_0|z^S - z_p|) & \text{for } d = 2 . \end{cases}$$

These formulas show that the resolution of the imaging functional is the standard diffraction limit. It is of the order of half the wavelength $\lambda = 2\pi/k_0$.

Note that $\mathcal{I}_{\mathrm{BP}}$ uses only the diagonal terms of the response matrix A, defined by (12.8). Using the whole matrix, we arrive at the Kirchhoff migration functional:

$$\mathcal{I}_{\mathrm{KM}}(z^S, \omega) = \sum_{j=1}^{d+1} \overline{g^{(j)}(z^S)} \cdot A g^{(j)}(z^S) , \qquad (12.15)$$

where $g^{(j)}$ are defined by (12.10) and (12.11).

Suppose for simplicity that $P = 1$ and let $(\varepsilon_\star, \mu_\star)$ denote the electromagnetic parameters of the inclusion. In the case where $\mu_\star = \mu_0$, the response matrix is

$$A = -n|D| k_0^2 (\frac{\varepsilon_\star}{\varepsilon_0} - 1) g^{(d+1)}(z) \overline{g^{(d+1)}(z)}^T$$

and we can prove that $\mathcal{I}_{\mathrm{MU}}$ is a nonlinear function of $\mathcal{I}_{\mathrm{KM}}$ [57]. In fact, we have

$$\mathcal{I}_{\mathrm{KM}}(z^S, \omega) = -n|D| k_0^2 (\frac{\varepsilon_\star}{\varepsilon_0} - 1) \left(1 - \mathcal{I}_{\mathrm{MU}}^{-2}(z^S, \omega) \right) .$$

It is worth pointing out that this transformation does not improve neither the stability nor the resolution.

Moreover, in the presence of additive measurement noise with variance $k_0^2 \sigma_{\mathrm{noise}}^2$, the response matrix can be written as

$$A = -n|D| k_0^2 (\frac{\varepsilon_\star}{\varepsilon_0} - 1) g^{(d+1)}(z) \overline{g^{(d+1)}(z)}^T + \sigma_{\mathrm{noise}} k_0 W ,$$

where W is a matrix of independent complex circularly symmetric Gaussian random variables with mean zero and variance 1.

According to [57], the Signal-to-Noise Ratio (SNR) of the imaging functional $\mathcal{I}_{\mathrm{KM}}$, defined by

$$\mathrm{SNR}(\mathcal{I}_{\mathrm{KM}}) = \frac{\mathbb{E}[\mathcal{I}_{\mathrm{KM}}(z, \omega)]}{\mathrm{Var}(\mathcal{I}_{\mathrm{KM}}(z, \omega))^{1/2}} \ ,$$

is then equal to

$$\mathrm{SNR}(\mathcal{I}_{\mathrm{KM}}) = \frac{nk_0|D|\,\big|\frac{\varepsilon_*}{\varepsilon_0} - 1\big|}{\sigma_{\mathrm{noise}}} \ . \tag{12.16}$$

For the MUSIC algorithm, the peak of $\mathcal{I}_{\mathrm{MU}}$ is affected by measurement noise. We have [170]

$$\mathcal{I}_{\mathrm{MU}}(z, \omega) = \begin{cases} \frac{n|D|k_0|\frac{\varepsilon_*}{\varepsilon_0} - 1|}{\sigma_{\mathrm{noise}}} & \text{if } n|D|k_0|\frac{\varepsilon_*}{\varepsilon_0} - 1| \gg \sigma_{\mathrm{noise}}, \\ 1 & \text{if } n|D|k_0|\frac{\varepsilon_*}{\varepsilon_0} - 1| \ll \sigma_{\mathrm{noise}} \ . \end{cases}$$

Suppose now that the medium is randomly heterogeneous around a constant background. Let $\varepsilon_\star$ be the electric permittivity of the inclusion D. The coefficient of reflection is of the form $1 + (\frac{\varepsilon_*}{\varepsilon_0} - 1)\chi(D)(x) + \nu_{\mathrm{noise}}(x)$, where 1 stands for the constant background, $(\frac{\varepsilon_*}{\varepsilon_0} - 1)\chi(D)$ stands for the localized perturbation of the coefficient of reflection due to the inclusion, and $\nu_{\mathrm{noise}}(x)$ stands for the fluctuations of the coefficient of reflection due to clutter (*i.e.*, medium noise). We assume that ν_{noise} is a random process with Gaussian statistics and mean zero, and that it is compactly supported within Ω.

If the random process ν_{noise} has a small amplitude, then the background solution U, *i.e.*, the field that would be observed without the inclusion, can be approximated by

$$U(x) \approx U^{(0)}(x) - k_0^2 \int_\Omega N_{k_0}^{(0)}(x, y)\nu_{\mathrm{noise}}(y)U^{(0)}(y)\,dy \ ,$$

where $U^{(0)}$ and $N_{k_0}^{(0)}$ are respectively the background solution and the Neumann function in the constant background case. On the other hand, in the weak fluctuation regime, the phase mismatch between $N_{k_0}(x, z)$, the Neumann function in the random background, and $N_{k_0}^{(0)}(x, z^S)$ when z^S is close to z comes from the random fluctuations of the travel time between x and z which is approximately equal to the integral of $\nu_{\mathrm{noise}}/2$ along the ray from x to z:

$$N_{k_0}(x, z) \approx N_{k_0}^{(0)}(x, z)e^{ik_0 T(x)} \ ,$$

with

$$T(x) \approx \frac{|x - z|}{2} \int_0^1 \nu_{\mathrm{noise}}\Big(z + (x - z)s\Big)\,ds \ .$$

Therefore, for any smooth function w satisfying $(\Delta + k_0^2)w = 0$ in Ω, the weighted boundary measurements $I_w[U^{(0)}, \omega]$, defined by (12.6), is approximately given by

$$I_w[U^{(0)}, \omega] \approx -|D|k_0^2(\frac{\varepsilon_\star}{\varepsilon_0} - 1)e^{-\frac{k_0^2 \text{Var}(T)}{2}}w(z)U^{(0)}(z)$$
$$-k_0^2 \int_\Omega w(y)U^{(0)}(y)\nu_{\text{noise}}(y)\, dy \,, \tag{12.17}$$

provided that the correlation length of the random process ν_{noise} is small [54]. Without the medium noise,

$$I_w[U^{(0)}, \omega] \approx -|D|k_0^2(\frac{\varepsilon_\star}{\varepsilon_0} - 1)w(z)U^{(0)}(z) \,.$$

So, expansion (12.17) shows that the medium noise reduces the height of the main peak of $\mathcal{I}_{\text{KM}}$ by the damping factor $e^{-k_0^2 \text{Var}(T)/2}$ and on the other hand it induces random fluctuations of the associated image in the form of a speckle field due to the second term on the right-hand side of (12.17).

Topological Derivative Based Imaging Functional

The topological derivative based imaging functional was introduced in [54].

Let $D' = z^S + \delta'B'$, $\mu' > \mu_0$, $\varepsilon' > \varepsilon_0$, B' be chosen a priori (usually a disk), and let δ' be small. If $\mu_\star < \mu_0$ and $\varepsilon_\star < \varepsilon_0$, then we choose $\mu' < \mu_0$ and $\varepsilon' < \varepsilon_0$.

Let w be the solution of the Helmholtz equation

$$\begin{cases} \Delta w + k_0^2 w = 0 & \text{in } \Omega \,, \\ \dfrac{\partial w}{\partial \nu} = \overline{(-\dfrac{1}{2}I + (\mathcal{K}_\Omega^{-k_0})^*)(-\dfrac{1}{2}I + \mathcal{K}_\Omega^{k_0})[U - u_{\text{meas}}]} & \text{on } \partial\Omega \,, \end{cases} \tag{12.18}$$

where u_{meas} is the boundary pressure in the presence of the inclusion. The function w is obtained by backpropagating the Neumann data

$$(-\frac{1}{2}I + (\mathcal{K}_\Omega^{k_0})^*)(-\frac{1}{2}I + \mathcal{K}_\Omega^{k_0})[U - u_{\text{meas}}]$$

inside the background medium (without any inclusion). Note that $\overline{(\mathcal{K}_\Omega^{k_0})^*} = (\mathcal{K}_\Omega^{-k_0})^*$.

The function w can be used to image the inclusion. It corresponds to backpropagating the discrepancy between the measured and the background solutions. However, we introduce here a functional that exploits better the coherence between the phases of the background and perturbed fields at the location of the inclusion. This functional turns out to be exactly the topological derivative imaging functional introduced in [54].

For a single measurement, we set

$$\mathcal{I}_{\text{TD}}[U](z^S) = \Re e \left\{ \nabla U(z^S) \cdot M(\lambda', B') \nabla w(z^S) + k_0^2(\frac{\varepsilon'}{\varepsilon_0} - 1)|B'|U(z^S)w(z^S) \right\} \,. \tag{12.19}$$

The functional $\mathcal{I}_{\mathrm{TD}}[U](z^S)$ gives, at every search point $z^S \in \Omega$, the sensitivity of the misfit function

$$\mathcal{E}[U](z^S) := \frac{1}{2}\int_{\partial\Omega}\left|(-\frac{1}{2}I + \mathcal{K}_\Omega^{k_0})[u_{z^S} - u_{\mathrm{meas}}](x)\right|^2 d\sigma(x) ,$$

where u_{z^S} is the solution of (3.62) with the inclusion $D' = z^S + \delta'B'$. The location of the maximum of $z^S \mapsto \mathcal{I}_{\mathrm{TD}}[U](z^S)$ corresponds to the point at which the insertion of an inclusion centered at that point maximally decreases the misfit function. Using the Helmholtz-Kirchhoff identity (3.80) and the relation (11.21) between the Neumann function N_{k_0}, defined by (11.20), and fundamental solution Γ_{k_0}, we can show that the functional $\mathcal{I}_{\mathrm{TD}}$ attains its maximum at $z^S = z$; see [54]. It is also shown in [54] that the postprocessing of the data set by applying the integral operator $(-\frac{1}{2}I + \mathcal{K}_\Omega^{k_0})$ is essential in order to obtain an efficient topological derivative based imaging functional, both in terms of resolution and stability. By postprocessing the data, we ensure that the topological derivative based imaging functional attains its maximum at the true location of the inclusion.

For multiple measurements, $U_l, l = 1, \ldots, n$, the topological derivative based imaging functional is simply given by

$$\mathcal{I}_{\mathrm{TD}}(z^S, \omega) := \frac{1}{n}\sum_{l=1}^n \mathcal{I}_{\mathrm{TD}}[U_l](z^S) . \tag{12.20}$$

Let, for simplicity, $(\theta_1, \ldots, \theta_n)$ be n uniformly distributed directions over the unit sphere and consider U_l to be the plane wave

$$U_l(x) = e^{ik_0\theta_l \cdot x}, \quad x \in \Omega, \quad l = 1, \ldots, n . \tag{12.21}$$

Let

$$r_{k_0}(z^S, z) := \int_{\partial\Omega}\Gamma_{k_0}(x, z^S)\overline{\Gamma_{k_0}}(x, z)\,d\sigma(x) , \tag{12.22}$$

$$R_{k_0}(z^S, z) := \int_{\partial\Omega}\nabla_z\Gamma_{k_0}(x, z^S)\nabla_z\overline{\Gamma_{k_0}}(x, z)^T\,d\sigma(x) . \tag{12.23}$$

Note that $R_{k_0}(z^S, z)$ is a $d \times d$ matrix. When $\mu_\star = \mu_0$, it is proved in [54] that

$$\mathcal{I}_{\mathrm{TD}}[U](z^S) \approx \delta^d k_0^4(\frac{\varepsilon'}{\varepsilon_0} - 1)(\frac{\varepsilon_\star}{\varepsilon_0} - 1)|B'|\Re e\left\{U(z^S)r_{k_0}(z^S, z)\overline{U}(z)\right\} , \tag{12.24}$$

where r_{k_0} is given by (12.22). Therefore, by computing the topological derivatives for the n plane waves (n sufficiently large), it follows from (12.14) together with

$$\int_{\partial\Omega}\overline{\Gamma_{k_0}}(x, z)\Gamma_{k_0}(x, z^S)\,d\sigma(x) \sim -\frac{1}{k_0}\Im m\left\{\Gamma_{k_0}(z^S, z)\right\}, \qquad d = 2, 3 , \tag{12.25}$$

where $A \sim B$ means $A \approx CB$ for some constant C independent of k_0, that

$$\frac{1}{n} \sum_{l=1}^{n} \mathcal{I}_{\mathrm{TD}}[U_l](z^S) \sim k_0^{5-d}(\Im m \left\{ \Gamma_{k_0}(z^S, z) \right\})^2 .$$

Similarly, when $\varepsilon_\star = \varepsilon_0$, by computing the topological derivatives for the n plane waves, $U_l, l = 1, \ldots, n$, given by (12.21), we obtain

$$\frac{1}{n} \sum_{l=1}^{n} \mathcal{I}_{\mathrm{TD}}[U_l](z^S) \approx$$

$$\delta^d k_0{}^2 \frac{1}{n} \sum_{l=1}^{n} \Re e \left\{ e^{ik_0\theta_l \cdot (z^S - z)} [\theta_l \cdot M(\lambda', B') R_{k_0}(z^S, z) M(\lambda, B)\theta_l] \right\} .$$

Using B' the unit disk, the polarization tensor $M(\lambda', B') = C_d I$, where C_d is a constant, is proportional to the identity; see (11.11).

If, additionally, we assume that $M(\lambda, B)$ is approximately proportional to the identity, which occurs in particular when B is a disk or a ball, then by using

$$\int_{\partial\Omega} \nabla_z \Gamma_{k_0}(x, z^S) \nabla_z \overline{\Gamma_{k_0}}(x, z)^T \, d\sigma(x)$$
$$\sim -k_0 \, \Im m \left\{ \Gamma_{k_0}(z^S, z) \right\} \left(\frac{z - z^S}{|z - z^S|} \right) \left(\frac{z - z^S}{|z - z^S|} \right)^T , \tag{12.26}$$

we arrive at

$$\frac{1}{n} \sum_{l=1}^{n} \mathcal{I}_{\mathrm{TD}}[U_l](z^S) \sim k_0^{5-d}(\Im m \left\{ \Gamma_{k_0}(z^S, z) \right\})^2 . \tag{12.27}$$

Therefore, $\mathcal{I}_{\mathrm{TD}}$ attains its maximum at z. Moreover, the resolution for the location estimation is given by the diffraction limit. We refer the reader to [54] for a detailed stability analysis of $\mathcal{I}_{\mathrm{TD}}$ with respect to both medium and measurement noises as well as its resolution. In the case of measurement noise, the SNR of $\mathcal{I}_{\mathrm{TD}}$,

$$\mathrm{SNR}(\mathcal{I}_{\mathrm{TD}}) = \frac{\mathbb{E}[\mathcal{I}_{\mathrm{TD}}(z, \omega)]}{\mathrm{Var}(\mathcal{I}_{\mathrm{TD}}(z, \omega))^{1/2}} ,$$

is equal to

$$\mathrm{SNR}(\mathcal{I}_{\mathrm{TD}}) = \frac{\sqrt{2}\pi^{1-d/2} k_0{}^{(d+1)/2} |U(z)| |(\frac{\varepsilon_\star}{\varepsilon_0} - 1)| |D|}{\sigma_{\mathrm{noise}}} .$$

In the case of medium noise, let us introduce the kernel

$$Q(z^S, z) := \Re e \left\{ U^{(0)}(z^S)\overline{U^{(0)}(z)} \int_{\partial\Omega} \Gamma_{k_0}(x, z^S)\overline{\Gamma_{k_0}(x, z)} \, d\sigma(x) \right\} .$$

We can express the topological derivative imaging functional as follows [54]:

$$
\begin{aligned}
\mathcal{I}_{\mathrm{TD}}[U^{(0)}](z^S) \approx{}& k_0{}^4(\frac{\varepsilon'}{\varepsilon_0} - 1)|B'| \int_\Omega \nu_{\mathrm{noise}}(y) Q(z^S, y)\, dy \\
&+ k_0{}^4(\frac{\varepsilon'}{\varepsilon_0} - 1)(\frac{\varepsilon_\star}{\varepsilon_0} - 1)|B'||D| Q(z^S, z) e^{-\frac{k_0{}^2 \mathrm{Var}(T)}{2}}\ ,
\end{aligned}
\tag{12.28}
$$

provided, once again, that the correlation length of the random process ν_{noise} is small and the amplitude of ν_{noise} is also small. Consequently, the topological derivative has the form of a peak centered at the location z of the inclusion (second term of the right-hand side of (12.28)) buried in a zero-mean Gaussian field or speckle pattern (first term of the right-hand side of (12.28)) that we can characterize statistically.

12.2.2 Direct Imaging at Multiple Frequencies

Let $(\theta_1, \ldots, \theta_n)$ be n uniformly distributed directions over the unit sphere. We consider plane wave illuminations at multiple frequencies, $(\omega_j)_{j=1,\ldots,m}$, instead of a fixed frequency:

$$
U_{lj}(x) := U(x, \theta_l, \omega_j) = e^{i k_j \theta_l \cdot x},
$$

where $k_j := \sqrt{\varepsilon_0 \mu_0}\,\omega_j$, and record the perturbations due to the inclusion. In this case, we can construct the topological derivative imaging functional by summing over frequencies

$$
\mathcal{I}_{\mathrm{TDF}}(z^S) := \frac{1}{m} \sum_{j=1}^m \mathcal{I}_{\mathrm{TD}}(z^S, \omega_j)\ .
\tag{12.29}
$$

Suppose for simplicity that $\mu_\star = \mu_0$. Then, (12.24) and (12.25) yield

$$
\mathcal{I}_{\mathrm{TDF}}(z^S) \sim \int_{k_0} k_0{}^{5-d} \left(\Im m \left\{ \Gamma_{k_0}(z^S, z) \right\} \right)^2 dk_0, \quad d = 2, 3\ ,
$$

and hence, $\mathcal{I}_{\mathrm{TDF}}(z^S)$ has a peak only at z. In the case where $\mu_\star \neq \mu_0$, we can use (12.26) to state the same behavior at z.

   An alternative imaging functional when searching for an inclusion using multiple frequencies is the Reverse-Time migration imaging functional [105]:

$$
\begin{aligned}
\mathcal{I}_{\mathrm{RMF}}(z^S) := {}& \frac{1}{nm} \sum_{l=1}^n \sum_{j=1}^m \overline{U}(z^S, \theta_l, \omega_j) \\
&\times \int_{\partial\Omega} (-\frac{1}{2} I + \mathcal{K}_\Omega^{k_j})[u - U](x, \theta_l, \omega_j) \overline{\Gamma_{k_j}}(x, z^S)\, d\sigma(x)\ .
\end{aligned}
\tag{12.30}
$$

In fact, when for instance $\mu_\star = \mu_0$,

$$\mathcal{I}_{\mathrm{RMF}}(z^S) \sim -\frac{1}{nm} \sum_{l=1}^{m} \sum_{j=1}^{m} \omega_j^3 U(z, \theta_l, \omega_j) \overline{U}(z^S, \theta_l, \omega_j) \Im\{\Gamma_{k_j}(z^S, z)\} \, ,$$

and therefore, it is approximately proportional to

$$- \int_S \int_{k_0} k_0{}^3 e^{ik_0\theta \cdot (z^S - z)} \Im\{\Gamma_{k_0}(z^S, z)\} dk_0 d\sigma(\theta)$$

$$\sim \int_{k_0} k_0{}^{5-d} \left(\Im\{\Gamma_{k_0}(z^S, z)\} \right)^2 dk_0 \, ,$$

where S is the unit sphere and $d = 2, 3$. Hence,

$$\mathcal{I}_{\mathrm{RMF}}(z^S) \sim \mathcal{I}_{\mathrm{TDF}}(z^S).$$

Finally, it is possible to use a backpropagation imaging functional:

$$\mathcal{I}_{\mathrm{BPF}}(z^S) := \frac{1}{m} \sum_{j=1}^{m} \mathcal{I}_{\mathrm{BP}}(z^S, \omega_j) \, ,$$

or a Kirchhoff imaging functional:

$$\mathcal{I}_{\mathrm{KMF}}(z^S) := \frac{1}{m} \sum_{j=1}^{m} \mathcal{I}_{\mathrm{KM}}(z^S, \omega_j) \, .$$

We can also use the matched field imaging functional:

$$\mathcal{I}_{\mathrm{MF}}(z^S) := \frac{1}{m} \sum_{j=1}^{m} |\mathcal{I}_{\mathrm{KM}}(z^S, \omega_j)|^2 \, ,$$

in which the phase coherence between the different frequency-dependent perturbations is not exploited. This makes sense when the different frequency-dependent perturbations are incoherent.

If the measurement noises $\nu_{\mathrm{noise}}(x, \omega_j), j = 1, \ldots, m$, are independent and identically distributed, the multiple frequencies enhance the detection performance via a higher "effective" SNR.

If some correlation between frequency-dependent perturbations exist, for example because of a medium noise, then summing over frequencies an imaging functional is not appropriate. A single-frequency imaging functional at the frequency which maximizes the SNR may give a better reconstruction.

In the presence of a medium noise, a Coherent Interferometry (CINT) procedure may be appropriate. CINT consists of backpropagating the cross correlations of the recorded signals over appropriate space-time or space-frequency windows rather than the signals themselves. Here, we provide a CINT strategy in inclusion imaging.

Following [107, 108] a CINT-like algorithm is given by

$$\mathcal{I}_{\mathrm{CINT}}(z^S) = \int_S \int_{\omega_1} \int_{\omega_2} \int_{\partial\Omega} \int_{\partial\Omega} e^{-\frac{|\omega_1-\omega_2|^2}{2\Omega_D^2}} e^{-\frac{|x_1-x_2|^2}{2X_D^2}}$$

$$(-\frac{1}{2}I + \mathcal{K}_\Omega^{k_1})[u-U](x_1,\theta,\omega_1)\overline{\Gamma_{k_1}}(x_1,z^S)\overline{U}(z^S,\theta,\omega_1)\overline{(-\frac{1}{2}I + \mathcal{K}_\Omega^{k_2})[u-U]}(x_2,\theta,\omega_2)$$

$$\Gamma_{k_2}(x_2,z^S)U(z^S,\theta,\omega_2)d\sigma(x_1)d\sigma(x_2)d\omega_1 d\omega_2 d\sigma(\theta) ,$$

$$(12.31)$$

where X_D and Ω_D are two cut-off parameters.

The purpose of the CINT-like imaging functional $\mathcal{I}_{\mathrm{CINT}}$ is to keep in (12.31) the pairs (x_1,ω_1) and (x_2,ω_2) for which the postprocessed data $(-\frac{1}{2}I + \mathcal{K}_\Omega^{k_1})[u-U](x_1,\omega_1)$ and $(-\frac{1}{2}I + \mathcal{K}_\Omega^{k_2})[u-U](x_2,\omega_2)$ are coherent, and to remove the pairs that do not bring information.

Depending on the parameters X_D, Ω_D, we get different trade-offs between resolution and stability. When X_D and Ω_D become small, $\mathcal{I}_{\mathrm{CINT}}$ presents better stability properties at the expense of a loss of resolution. In the limit $X_D \to \infty$, $\Omega_D \to \infty$, we get the square of the topological derivative functional $\mathcal{I}_{\mathrm{TDF}}$.

12.3 Direct Elasticity Imaging

In this section we present MUSIC-type location search algorithms, reverse-time migration, and Kirchhoff imaging for the detection, localization, and characterization of small elastic anomalies in dimension two.

12.3.1 A MUSIC-type Method in the Static Regime

For the sake of simplicity, we take Ω to be the unit disk centered at the origin and choose $N \gg 1$ equi-distributed points x_i along the boundary. Let the unit vectors $\theta_1,\ldots,\theta_N$ be the corresponding observation directions. Suppose that the measured $N \times 3$ matrix $A := \left((-\frac{1}{2}I + \mathcal{K}_\Omega)[u_\delta^{(l)} - u_0^{(l)}](x_j)\cdot\theta_j\right)_{j,l}$ has the spectral decomposition

$$A = \sum_{l=1}^3 \sigma_l v_l \otimes w_l,$$

where σ_l are the singular values of A and v_l and w_l are the corresponding left and right singular vectors. Let $\Pi : \mathbb{R}^N \to \mathrm{span}\{v_1, v_2, v_3\}$ be the orthogonal projector

$$\Pi = \sum_{l=1}^3 v_l \otimes v_l.$$

Let $a \in \mathbb{R}^2 \setminus \{0\}$. One can prove that for a search point $z^S \in \Omega$, the vector

$$f^{(j)}(z^S; a) := \left((W^{(j)} : \mathbb{M}\nabla_{z^S}\Gamma(x_1, z^S)) \cdot a, \dots, (W^{(j)} : \mathbb{M}\nabla_{z^S}\Gamma(x_N, z^S)) \cdot a \right)^T$$

$$(12.32)$$

in $\mathbb{R}^N$ lies in the space spanned by columns of A if and only if $z^S = z$ [41]. Let

$$g^{(j)} = (\mathbb{C}W^{(j)})n, \quad j = 1, 2, 3, \quad \text{on } \partial\Omega,$$

where

$$W^{(1)} = \begin{pmatrix} 1 & 0 \\ 0 & 1 \end{pmatrix}, \quad W^{(2)} = \begin{pmatrix} 0 & 1 \\ 1 & 0 \end{pmatrix}, \quad W^{(3)} = \begin{pmatrix} 0 & 0 \\ 0 & 1 \end{pmatrix}$$

form a basis of the space of 2×2 symmetric matrices, and let $u_\delta^{(j)}$ and $u_0^{(j)}$ be the solution of the static elastic problem (11.30) with and without inclusion, respectively. In (12.32), $\mathbb{M}$ can be estimated using the following formula:

$$\int_{\partial\Omega} (u_\delta^{(l)} - u_0^{(l)})(x) \cdot g^{(j)}(x) \, d\sigma(x) = -\delta^2 W^{(l)} : \mathbb{M}W^{(j)} + O(\delta^3), \quad j, l = 1, 2, 3.$$

$$(12.33)$$

Thus one can form an image of the elastic inclusion by plotting, at each point z^S, the MUSIC-type imaging functional

$$\mathcal{I}_{\text{MU}}(z^S) = \frac{1}{\sqrt{\sum_{j=1}^3 ||(I - \Pi)[f^{(j)}](z^S; a)||^2}},$$

where I is the $N \times N$ identity matrix. The resulting plot will have a large peak at the location of the inclusion.

12.3.2 A MUSIC-type Method in the Time-Harmonic Regime

In this subsection we extend the MUSIC algorithm to the time-harmonic regime. Let D be a small elastic inclusion (with location at z and Lamé parameters $\widetilde{\lambda}$ and $\widetilde{\mu}$). Let $x_j, j = 1, \dots, N$ be equi-distributed points along the boundary of Ω for $N \gg 1$. The array of N elements $\{x_1, \dots, x_N\}$ is used to detect the inclusion. Let $\theta_1, \dots, \theta_N$ be the corresponding unit directions of incident fields/observation directions. The array of elements $\{x_1, \dots, x_N\}$ is operating both in transmission and in reception.

We choose the background displacement to be such that

$$u_0^{(j)}(x) = \Gamma^\omega(x, x_j)\theta_j, \quad x \in \Omega. \tag{12.34}$$

From (11.42), we have

$$(-\frac{1}{2}I + \mathcal{K}_\Omega^\omega)[u_\delta^{(j)} - u_0^{(j)}](x) = -\delta^2 \Big(\nabla_z \Gamma^\omega(x, z) : \mathbb{M}\nabla_z(\Gamma^\omega(z, x_j)\theta_j)$$

$$+ \omega^2(\rho - \tilde{\rho})|B|\Gamma^\omega(x, z)\Gamma^\omega(z, x_j)\theta_j \Big) + O(\delta^3). \tag{12.35}$$

The measured data is the $N \times N$ matrix given by

$$A^\omega := \left((-\frac{1}{2}I + \mathcal{K}_\Omega)[u_\delta^{(j)} - u_0^{(j)}](x_l) \cdot \theta_l \right)_{j,l}. \qquad (12.36)$$

For any point $x \in \Omega$, let us introduce the $N \times 2$ matrix of the incident field emitted by the array of N transmitters $G(x, \omega)$, which will be called the Green matrix, and the $N \times 3$ matrix of the corresponding independent components of the stress tensors $S(x, \omega)$, which will be called the stress matrix:

$$G(x, \omega) = (\Gamma^\omega(x, x_1)\theta_1, \ldots, \Gamma^\omega(x, x_N)\theta_N)^T, \qquad (12.37)$$

$$S(x, \omega) = (s_1(x), \ldots, s_N(x))^T, \qquad (12.38)$$

where

$$s_j(x) = [\sigma_{11}^{(j)}(x), \sigma_{22}^{(j)}(x), \sigma_{12}^{(j)}(x)]^T, \quad \sigma^{(j)}(x) = \mathbb{C}\nabla^s(\Gamma^\omega(x, x_j)\theta_j).$$

One can see from (12.35) and (12.36) that the data matrix A^ω is factorized as follows:

$$A^\omega = -\delta^2 H(z, \omega) \, D(\omega) \, H^T(z, \omega), \qquad (12.39)$$

where

$$H(x, \omega) = [S(x, \omega), \, G(x, \omega)] \qquad (12.40)$$

and $D(\omega)$ is a symmetric 5×5 matrix given by

$$D(\omega) = \begin{pmatrix} \mathcal{L}[\mathbb{M}] & 0 \\ 0 & \omega^2(\rho - \tilde{\rho})|B|I \end{pmatrix} \qquad (12.41)$$

for some linear operator $\mathcal{L}$.

Consequently, the data matrix A^ω is the product of three matrices $H^T(z, \omega)$, $D(\omega)$ and $H(z, \omega)$. The physical meaning of the above factorization is the following: the matrix $H^T(z, \omega)$ is the propagation matrix from the transmitter points toward the inclusion located at the point z, the matrix $D(\omega)$ is the scattering matrix and $H(z, \omega)$ is the propagation matrix from the inclusion toward the receiver points.

Recall that MUSIC is essentially based on characterizing the range of data matrix A^ω, so-called signal space, forming projections onto its null (noise) spaces, and computing its singular value decomposition.

From the factorization (12.39) of A^ω and the fact that the scattering matrix D is nonsingular (so, it has rank 5), the standard argument from linear algebra yields that, if $N \geq 5$ and if the propagation matrix $H(z, \omega)$ has maximal rank 5 then the ranges $\mathrm{Range}(H(z, \omega))$ and $\mathrm{Range}(A)$ coincide.

The following is a MUSIC characterization of the location of the elastic inclusion and is valid if N is sufficiently large.

Proposition 12.2 *Suppose that $N \geq 5$. Let $a \in \mathbb{C}^5 \setminus \{0\}$, then*

$$H(z^S)a \in \mathrm{Range}(A^\omega) \qquad \textit{if and only if} \qquad z^S = z.$$

In other words, any linear combination of the vector columns of the propagation matrix $H(z^S, \omega)$ defined by (12.40) belongs to the range of A^ω (signal space) if and only if the points z^S and z coincide.

If the dimension of the signal space, $s\,(\leq 5)$, is known or is estimated from the singular value decomposition of A^ω, defined by $A^\omega = V\Sigma\overline{U}^T$, then the MUSIC algorithm applies. Furthermore, if v_i denote the column vectors of the matrix V then for any vector $a \in \mathbb{C}^5 \setminus \{0\}$ and for any space point z^S within the search domain, a map of the estimator $\mathcal{I}_{\mathrm{MU}}(z^S)$ defined as the inverse of the Euclidean distance from the vector $H(z^S, \omega)a$ to the signal space by

$$\mathcal{I}_{\mathrm{MU}}(z^S) = \frac{1}{\sqrt{\sum_{j=s+1}^{N} |v_j \cdot H(z^S, \omega)a|^2}} \tag{12.42}$$

peaks (to infinity, in theory) at the center z of the inclusion. The visual aspect of the peak of $\mathcal{I}_{\mathrm{MU}}$ at z depends upon the choice of the vector a. A common choice which means that we are working with all the significant singular vectors is $a = (1, 1, \ldots, 1)^T$. However, we emphasize the fact that a choice of the vector a in (12.42) with dimension (number of nonzero components) much lower than 5 still permits one to image the elastic inclusion with our MUSIC-type algorithm. See the numerical results below. It is worth mentioning that the estimator $\mathcal{I}_{\mathrm{MU}}(z^S)$ is obtained via the projection of the linear combination of the vector columns of the Green matrix $G(z^S)$ onto the noise subspace of the A^ω for a signal space of dimension l if the dimension of a is l.

Let us also point out here that the function $\mathcal{I}_{\mathrm{MU}}(z^S)$ does not contain any information about the shape and the orientation of the inclusion. Yet, if the position of the inclusion is found (approximately at least) via observation of the map of $\mathcal{I}_{\mathrm{MU}}(z^S)$, then one could attempt, using the decomposition (12.39), to retrieve the EMT of the inclusion (which is of order δ^2).

Finally, it is worth emphasizing that in dimension 3, the matrix D is 9×9 and is of rank 9. For locating the inclusion, the number N then has to be larger than 9. We also mention that the developed MUSIC algorithm applies to the crack location problem in the time-harmonic regime.

12.3.3 Reverse-Time Migration and Kirchhoff Imaging in the Time-Harmonic Regime

In this section we consider the time-harmonic regime. The perturbations of the boundary measurements due to the presence of a small inclusion are given by the asymptotic expansion (11.41).

Suppose for simplicity that a small elastic inclusion (with location at z) has only a density contrast and let the background displacement be the field

generated by a point source at $y \in \Omega$ emitting along e_j. Again, from (11.41), we have for $x, y \in \partial\Omega$:

$$(-\frac{1}{2}I + \mathcal{K}_\Omega^\omega)[u_\delta^{(j)} - u_0^{(j)}](x, y) = -\delta^2\omega^2(\rho - \tilde{\rho})|B|\Gamma^\omega(x, z)\Gamma^\omega(z, y)e_j + O(\delta^3).$$

Thus, for a search point $z^S \in \Omega$, it follows by using (3.183) that

$$\int_{\partial\Omega} \overline{\Gamma_\alpha^\omega}(z^S, x)(-\frac{1}{2}I + \mathcal{K}_\Omega^\omega)[u_\delta^{(j)} - u_0^{(j)}](x, y)d\sigma(x)$$

$$\simeq \frac{\delta^2}{c_\alpha}\omega(\rho - \tilde{\rho})|B|(\Im m\, \Gamma_\alpha^\omega(z^S, z))\Gamma^\omega(z, y)e_j.$$

We introduce the reverse-time migration imaging functional $\mathcal{I}_{\mathrm{RM},\alpha}(z^S)$ for $\alpha = p$ or s given by

$$\sum_{j=1,2} \int_{\partial\Omega} \overline{\Gamma_\alpha^\omega}(z^S, y)e_j \cdot \int_{\partial\Omega} \overline{\Gamma_\alpha^\omega}(z^S, x)(-\frac{1}{2}I + \mathcal{K}_\Omega^\omega)[u_\delta^{(j)} - u_0^{(j)}](x, y)d\sigma(x)\, d\sigma(y).$$

(12.43)

$\mathcal{I}_{\mathrm{RM},\alpha}(z^S)$ consists in backpropagating with the α-Green function the data set

$$\left\{(-\frac{1}{2}I + \mathcal{K}_\Omega^\omega)[u_\delta^{(j)} - u_0^{(j)}](x, y), y \in \partial\Omega, x \in \partial\Omega, \quad j = 1, 2\right\}$$

both from the source point y and the receiver point x.

Using (3.183) and the reciprocity property (3.177) we obtain that

$$\mathcal{I}_{\mathrm{RM},\alpha}(z^S) \simeq -\frac{\delta^2}{c_\alpha^2}(\rho - \tilde{\rho})|B||\Im m\, \Gamma_\alpha(z^S, z)|^2.$$

The imaging functional $\mathcal{I}_{\mathrm{RM},\alpha}(z^S)$ attains then its maximum (if $\rho < \tilde{\rho}$) or minimum (if $\rho > \tilde{\rho}$) at $z^S = z$.

The imaging functional $\mathcal{I}_{\mathrm{RM},\alpha}(z^S)$ can be simplified as follows to yield the Kirchhoff migration imaging functional $\mathcal{I}_{\mathrm{KM},\alpha}(z^S)$ given by

$$\sum_{j=1,2} \int_{\partial\Omega} e^{-i\kappa_\alpha|y-z^S|}e_j \cdot \int_{\partial\Omega} e^{-i\kappa_\alpha|z^S-x|}(-\frac{1}{2}I + \mathcal{K}_\Omega^\omega)[u_\delta^{(j)} - u_0^{(j)}](x)d\sigma(x)\, d\sigma(y).$$

(12.44)

The function $\mathcal{I}_{\mathrm{KM},\alpha}$ attains as well its maximum at $z^S = z$. In this simplified version, backpropagation is approximated by travel time migration.

12.4 Time-Domain Anomaly Imaging

12.4.1 Wave Imaging of Small Anomalies

To detect the anomaly from measurements of the wavefield $u - U_y$ away from the anomaly one can use a time-reversal technique in dimension three. Taking

into account the definition of the outgoing fundamental solution (2.55) to the wave equation, spatial reciprocity and time reversal invariance of the wave equation, one defines the time-reversal imaging functional W_{TR} by

$$
\begin{aligned}
W_{\mathrm{TR}}(x,t) = \int_{\mathbb{R}} \int_{S} \Bigg[& U_x(x',t-s)\frac{\partial P_\rho[u-U_y]}{\partial \nu}(x',t_0-s) \\
& - \frac{\partial U_x}{\partial \nu}(x',t-s)P_\rho[u-U_y](x',t_0-s) \Bigg] d\sigma(x')\, ds \;,
\end{aligned}
\tag{12.45}
$$

where

$$
U_x(x',t-\tau) = \frac{\delta(t-\tau-|x-x'|)}{4\pi|x-x'|} \;.
$$

The imaging functional W_{TR} corresponds to propagating inside the volume surrounded by S the time-reversed perturbation $P_\rho[u-U_y]$ and its normal derivative on S. Theorem 11.18 shows that

$$
P_\rho[u-U_y](x,t) \approx -\delta^3 \int_{\mathbb{R}} \nabla P_\rho[U_z](x,t-\tau)\cdot m(z,\tau)\, d\tau \;,
$$

where

$$
m(z,\tau) = M(\lambda,B)\nabla P_\rho[U_y](z,\tau) \;.
\tag{12.46}
$$

Therefore, since

$$
\begin{aligned}
\int_{\mathbb{R}} \int_{S} \Bigg[& U_x(x',t-s)\frac{\partial P_\rho[U_z]}{\partial \nu}(x',t_0-s-\tau) \\
& - \frac{\partial U_x}{\partial \nu}(x',t-s)P_\rho[U_z](x',t_0-s-\tau) \Bigg] d\sigma(x')\, ds \\
& = P_\rho[U_z](x,t_0-\tau-t) - P_\rho[U_z](x,t-t_0+\tau) \;,
\end{aligned}
\tag{12.47}
$$

one obtains the approximation

$$
W_{\mathrm{TR}}(x,t) \approx -\delta^3 \int_{\mathbb{R}} m(z,\tau)\cdot\nabla_z \big[P_\rho[U_z](x,t_0-\tau-t) - P_\rho[U_z](x,t-t_0+\tau)\big] d\tau \;,
$$

which can be interpreted as the superposition of incoming and outgoing waves, centered on the location z of the anomaly. Since

$$
P_\rho[U_y](x,\tau) = \frac{\sin\rho(\tau-|x-y|)}{4\pi(\tau-|x-y|)|x-y|} \;,
$$

$m(z,\tau)$ is concentrated at the travel time $\tau = T = |z-y|$. It then follows that

$$
W_{\mathrm{TR}}(x,t) \approx -\delta^3 m(z,T)\cdot\nabla_z\big[P_\rho[U_z](x,t_0-T-t) - P_\rho[U_z](x,t-t_0+T)\big] \;.
\tag{12.48}
$$

The imaging functional W_{TR} is clearly the sum of incoming and outgoing polarized spherical waves.

Approximation (12.48) has an important physical interpretation. By changing the origin of time, T can be set to 0 without loss of generality. Then by taking a Fourier transform of (12.48) over the time variable t, one obtains that

$$\widehat{W}_{\mathrm{TR}}(x,\omega) \propto \delta^3 m(z,T) \cdot \nabla \mathrm{sinc}(\omega|x-z|) \ ,$$

where ω is the wavenumber. This shows that the time-reversal perturbation W_{TR} focuses on the location z of the anomaly with a focal spot size limited to one-half the wavelength.

12.4.2 Thermal Imaging of Small Anomalies

In this subsection the formula (11.73) is applied (with an appropriate choice of test functions w and background solutions U) for the purpose of identifying the location of the anomaly D. The first algorithm makes use of constant heat flux and, not surprisingly, it is limited in its ability to effectively locate multiple anomalies.

Using many heat sources, one then describes an efficient method to locate multiple anomalies and illustrate its feasibility. For the sake of simplicity only the two-dimensional case will be considered.

Detection of a Single Anomaly

For $y \in \mathbb{R}^2 \setminus \overline{\Omega}$, let

$$w(x,t) = w_y(x,t) := \frac{1}{4\pi(T-t)} e^{-\frac{|x-y|^2}{4(T-t)}} \ . \tag{12.49}$$

The function w satisfies $(\partial_t + \Delta)w = 0$ in Ω_T and the final condition $w|_{t=T} = 0$ in Ω.

Suppose that there is only one anomaly $D = z + \delta B$ with thermal conductivity k. For simplicity assume that B is a disk. Choose the background solution $U(x,t)$ to be a harmonic (time-independent) function in Ω_T. One computes

$$\nabla w_y(z,t) = \frac{y-z}{8\pi(T-t)^2} e^{-\frac{|z-y|^2}{4(T-t)}} \ ,$$

$$M(\lambda, B)\nabla w_y(z,t) = \frac{(k-1)|B|}{k+1} \frac{y-z}{4\pi(T-t)^2} e^{-\frac{|z-y|^2}{4(T-t)}} \ ,$$

and

$$\int_0^T M(\lambda, B)\nabla w_y(z,t)\,dt = \frac{(k-1)|B|}{k+1} \frac{y-z}{4\pi} \int_0^T \frac{e^{-\frac{|z-y|^2}{4(T-t)}}}{(T-t)^2}\,dt \ .$$

But

$$\frac{d}{dt}e^{-\frac{|z-y|^2}{4(T-t)}} = \frac{-|z-y|^2}{4}\frac{e^{-\frac{|z-y|^2}{4(T-t)}}}{(T-t)^2}$$

and therefore

$$\int_0^T M(\lambda, B)\nabla w_y(z,t)\,dt = \frac{(k-1)|B|}{k+1}\frac{y-z}{\pi|z-y|^2}e^{-\frac{|z-y|^2}{4(T-t)}}\ .$$

Then the asymptotic expansion (11.73) yields

$$I_w[U,T](y) \approx \delta^2\frac{k-1}{k+1}|B|\frac{\nabla U(z)\cdot(y-z)}{\pi|y-z|^2}e^{-\frac{|y-z|^2}{4T}}\ . \qquad (12.50)$$

Now one is in a position to present the projection-type location search algorithm for detecting a single anomaly. Prescribe the initial condition $u_0(x) = a\cdot x$ for some fixed unit constant vector a and choose $g = a\cdot\nu$ as an applied time-independent heat flux on $\partial\Omega_T$, where a is taken to be a coordinate unit vector. Take two observation lines Σ_1 and Σ_2 contained in $\mathbb{R}^2\setminus\overline{\Omega}$ such that

$$\Sigma_1 := \text{a line parallel to } a, \qquad \Sigma_2 := \text{a line normal to } a\ .$$

Next find two points $P_i \in \Sigma_i$ $(i=1,2)$ so that $I_w(T)(P_1) = 0$ and

$$I_w(T)(P_2) = \begin{cases} \min_{x\in\Sigma_2} I_w(T)(x) & \text{if } k-1 < 0\ , \\ \max_{x\in\Sigma_2} I_w(T)(x) & \text{if } k-1 > 0\ . \end{cases}$$

Finally, draw the corresponding lines $\Pi_1(P_1)$ and $\Pi_2(P_2)$ given by (12.3). Then the intersecting point P of $\Pi_1(P_1)\cap\Pi_2(P_2)$ is close to the anomaly D: $|P-z| = O(\delta\,|\log\delta|)$ for δ small enough.

Detection of Multiple Anomalies: A MUSIC-type Algorithm

Consider m well-separated anomalies $D_s = \delta B_s + z_s$, $s = 1,\ldots,m$, whose heat conductivity is k_s. Choose

$$U(x,t) = U_{y'}(x,t) := \frac{1}{4\pi t}e^{-\frac{|x-y'|^2}{4t}} \quad \text{for } y'\in\mathbb{R}^2\setminus\overline{\Omega}$$

or, equivalently, g to be the heat flux corresponding to a heat source placed at the point source y' and the initial condition $u_0(x) = 0$ in Ω, to obtain that

$$I_w[U,T] \approx -\delta^2\sum_{s=1}^m\frac{(1-k_s)}{64\pi^2}(y'-z_s)M^{(s)}(y-z_s)$$

$$\times\int_0^T\frac{1}{t^2(T-t)^2}\exp\left(-\frac{|y-z_s|^2}{4(T-t)} - \frac{|y'-z_s|^2}{4t}\right)dt\ ,$$

where w is given by (12.49) and $M^{(s)}$ is the polarization tensor of D_s.

Suppose for the sake of simplicity that all the domains B_s are disks. Then it follows from (11.11) that $M^{(s)} = m^{(s)} I_2$, where $m^{(s)} = 2(k_s-1)|B_s|/(k_s+1)$ and I_2 is the 2×2 identity matrix. Let $y_l \in \mathbb{R}^2 \setminus \overline{\Omega}$ for $l \in \mathbb{N}$ be the source points. One assumes that the countable set $\{y_l\}_{l \in \mathbb{N}}$ has the property that any analytic function which vanishes in $\{y_l\}_{l \in \mathbb{N}}$ vanishes identically.

The MUSIC-type location search algorithm for detecting multiple anomalies is as follows. For $n \in \mathbb{N}$ sufficiently large, define the matrix $A = [A_{ll'}]_{l,l'=1}^n$ by

$$A_{ll'} := -\delta^2 \sum_{s=1}^m \frac{(1 - k_s)}{64\pi^2} m^{(s)} (y_{l'} - z_s) \cdot (y_l - z_s)$$

$$\times \int_0^T \frac{1}{t^2(T-t)^2} \exp\left(-\frac{|y_l - z_s|^2}{4(T-t)} - \frac{|y_{l'} - z_s|^2}{4t} \right) dt \; .$$

For $z \in \Omega$, one decomposes the symmetric real matrix C defined by

$$C := \left[\int_0^T \frac{1}{t^2(T-t)^2} \exp\left(-\frac{|y_l - z|^2}{4(T-t)} - \frac{|y_{l'} - z|^2}{4t} \right) dt \right]_{l,l'=1,\dots,n}$$

as follows:

$$C = \sum_{l=1}^p v_l(z) v_l(z)^T \tag{12.51}$$

for some $p \leq n$, where $v_l \in \mathbb{R}^n$. Define the vector $g_z^{(l)} \in \mathbb{R}^{n \times 2}$ for $z \in \Omega$ by

$$g_z^{(l)} = \left((y_1 - z) v_{l1}(z), \dots, (y_n - z) v_{ln}(z) \right)^T, \quad l = 1, \dots, p \, . \tag{12.52}$$

Here $v_{l1}, \dots, v_{ln}$ are the components of the vector v_l, $l = 1, \dots, p$. Let $y_l = (y_{lx}, y_{ly})$ for $l = 1, \dots, n$, $z = (z_x, z_y)$, and $z_s = (z_{sx}, z_{sy})$. One also introduces

$$g_{zx}^{(l)} = \left((y_{1x} - z_x) v_{l1}(z), \dots, (y_{nx} - z_x) v_{ln}(z) \right)^T$$

and

$$g_{zy}^{(l)} = \left((y_{1y} - z_y) v_{l1}(z), \dots, (y_{ny} - z_y) v_{ln}(z) \right)^T \, .$$

Lemma 12.3 (MUSIC characterization of the range of the response matrix)
The following characterization of the location of the anomalies in terms of the range of the matrix A holds:

$$g_{zx}^{(l)} \text{ and } g_{zy}^{(l)} \in \text{Range}(A) \;\; \forall l \in \{1, \dots, p\} \quad \text{if and only if} \quad z \in \{z_1, \dots, z_m\} \, . \tag{12.53}$$

Note that the smallest number n which is sufficient to efficiently recover the anomalies depends on the (unknown) number m. This is the main reason for taking n sufficiently large. As for the electrical impedance imaging, the MUSIC-type algorithm for the thermal imaging is as follows. Compute Π_{noise}, the projection onto the noise space, by the singular value decomposition of the matrix A. Compute the vectors v_l by (12.51). Form an image of the locations, $z_1, \ldots, z_m$, by plotting, at each point z, the quantity $\|g_z^{(l)} \cdot a\| / \|\Pi_{\mathrm{noise}}(g_z^{(l)} \cdot a)\|$ for $l = 1, \ldots, p$, where $g_z^{(l)}$ is given by (12.52) and a is a unit constant vector. The resulting plot will have large peaks at the locations of z_s, $s = 1, \ldots, m$.

Part IV

Multi-Wave Imaging

13

Photoacoustic Imaging

13.1 Introduction

In photoacoustic imaging, optical energy absorption causes thermoelastic expansion of the tissue, which leads to the propagation of a pressure wave. This signal is measured by transducers distributed on the boundary of the object, which in turn is used for imaging optical properties of the object. The major contribution of photoacoustic imaging is to provide images of optical contrasts (based on the optical absorption) with the resolution of ultrasound. In pure optical imaging, optical scattering in soft tissues degrades spatial resolution significantly with depth. Pure optical imaging is very sensitive to optical absorption but can only provide a spatial resolution on the order of 1 cm at cm depths. Pure conventional ultrasound imaging, which is based on the detection of mechanical properties (acoustic impedance) in biological soft tissues, can provide good spatial resolution because of its millimetric wavelength and weak scattering at MHz frequencies. The significance of photoacoustic imaging combines both approaches to provide images of optical contrasts (based on the optical absorption) with the ultrasound resolution. Because the optical absorption properties of tissue is highly related to its molecular constitution, photoacoustic images can reveal the pathological condition of the tissue and therefore, facilitate a wide-range of diagnostic tasks. Moreover, when employed with optical contrast agents, photoacoustic imaging has the potential to lead to high-resolution molecular imaging of deep structures, which cannot be achieved with pure optical methods.

In photoacoustic imaging, if the medium is acoustically homogeneous and has the same acoustic properties as the free space, then the boundary of the object plays no role and the optical properties of the medium can be extracted from measurements of the pressure wave by inverting a spherical or a circular mean Radon transform.

In some settings, the free space assumption does not hold. For example, in brain imaging, the skull plays an important acoustic role, and in small animal imaging devices, the metallic chamber may have a strong acoustic effect.

In those cases, one has to account for boundary conditions. If a boundary condition has to be imposed on the pressure field, then an explicit inversion formula no longer exists. However, using a duality approach, one can still reconstruct the optical absorption coefficient. In this chapter we investigate quantitative photoacoustic imaging in the case of a bounded medium with imposed boundary conditions and propose a geometric-control approach to deal with the case of limited view measurements. In both cases, we focus on a situation with small optical absorbers in a non-absorbing background and propose adapted algorithms to locate the absorbers and estimate their absorbed energy.

A second challenging problem in photoacoustic imaging is to take into account the issue of modelling the acoustic attenuation and its compensation. In this chapter, we propose two approaches to correct the effect of acoustic attenuation. We use a frequency power-law model for the attenuation.

A third challenging problem is to identify the locations of absorbers from limited-view data. By using the geometric control method and testing the measurements against an appropriate family of functions, we show that we can access the initial condition for the photoacoustic problem.

Another interesting problem is to correct the effect of an unknown cluttered sound speed on photoacoustic images. When the speed of sound of the medium is randomly fluctuating (around a known value), the acoustic waves undergo partial coherence loss and the designed algorithms, assuming a constant sound speed, may fail. In this chapter, by combining coherent interferometry (CINT) imaging with a spherical mean Radon inversion, we propose an efficient algorithm for photoacoustic imaging in the presence of random fluctuations of the sound speed.

The chapter is organized as follows. Section 13.2 is devoted to a mathematical formulation of the photoacoustic imaging problem. In Section 13.3 we consider the photoacoustic imaging problem in free space. We first propose an algorithm to recover the absorbing energy density from limited-view data. We then present two approaches to correct the effect of acoustic attenuation. We use a power-law model for the attenuation. We test the SVD approach proposed in [305] and provide an efficient technique based on the stationary phase theorem. The stationary phase theorem allows us to compute (approximately in terms of the attenuation coefficient) the unattenuated wave from the attenuated one. Section 13.4 is devoted to correct the effect of imposed boundary conditions. By testing our measurements against an appropriate family of functions, constructed by the geometrical control method, we show how to obtain the initial condition in the acoustic wave equation, and thus recover quantitatively the absorbing energy density. In section 13.6, we derive a quantitative photoacoustic imaging approach in the framework of small absorbers. Finally, we describe a CINT-Radon algorithm for photoacoustic imaging in acoustically inhomogeneous media. The algorithm consists in filtering the data in the same way as for the spherical mean Radon inversion

before backpropagating their local correlations. Our results in this chapter are from [31, 32, 36, 37, 39, 54].

13.2 Mathematical Formulation

In an acoustically homogeneous medium $\Omega \subseteq \mathbb{R}^d$, $d = 2, 3$, when an optical laser pulse is employed, the photoacoustic effect is described by the following wave equation:

$$\frac{\partial^2 p}{\partial t^2}(x, t) - c_0^2 \Delta p(x, t) = \gamma \frac{\partial H}{\partial t}(x, t), \quad x \in \Omega, t \in \mathbb{R},$$

where c_0 is the acoustic speed in Ω, γ is the dimensionless Grüneisen coefficient in Ω, which is assumed to be homogeneous, and H is a heat source function (absorbed energy per unit time per unit volume). The constant γ provides a measure of the conversion efficiency of heat energy to pressure.

Let $D_l, l = 1, \ldots, L$, be absorbing domains inside the nonabsorbing background Ω. Assuming the stress-confinement condition, the source term can be modeled as

$$\gamma H(x, t) = \delta_0(t) \sum_{l=1}^{L} \chi(D_l) A_l(x),$$

where δ_0 is the Dirac distribution at 0. Under this assumption, the pressure p satisfies

$$\frac{\partial^2 p}{\partial t^2}(x, t) - c_0^2 \Delta p(x, t) = 0 \quad x \in \Omega, t \in (0, T), \tag{13.1}$$

for some final observation time T, the initial conditions

$$p|_{t=0} = p_0 = \sum_{l=1}^{L} \chi(D_l) A_l(x) \quad \text{and} \quad \partial_t p|_{t=0} = 0, \tag{13.2}$$

and either the Dirichlet or the Neumann boundary condition (if Ω is bounded)

$$p = 0 \quad \text{or} \quad \frac{\partial p}{\partial \nu} = 0 \quad \text{on } \partial\Omega \times (0, T). \tag{13.3}$$

The Neumann boundary condition corresponds to the tissue/water interface while the Dirichlet boundary condition accounts for a tissue/air interface.

The inverse problem in photoacoustic imaging is to determine the supports of nonzero optical absorption, $D_l \Subset \Omega, l = 1, \ldots, L$, and the absorbed optical energy density times the Grüneisen coefficient, $A(x) = \sum_{l=1}^{L} A_l(x) \chi(D_l)$, from boundary measurements of the pressure on $\partial\Omega$ (if Ω is bounded) or measurements on the boundary of a bounded domain if $\Omega = \mathbb{R}^d$. The final observation time T is large enough that

$$T > \text{diam}(\Omega)/c_0, \tag{13.4}$$

which says that the observation time is long enough for the wave initiated inside Ω to exit the domain Ω (if Ω is bounded) or the surface where the pressure is measured. The image reconstruction problem in photoacoustic imaging can then be interpreted as an inverse source problem.

The density $A(x)$ is related to the optical absorption coefficient distribution $\mu_a(x) = \sum_{l=1}^{L} \mu_l(x)\chi(D_l)$ by the equation

$$A(x) = \gamma\mu_a(x)\Phi(x), \tag{13.5}$$

where Φ is the light fluence. The function Φ depends on the distribution of scattering and absorption within Ω, as well as the light sources. Equation (13.5) reveals that photoacoustic images are determined by the optical absorption properties of the object as well as variations in the fluence of the illuminating optical radiation.

Let μ_s denote the reduced scattering coefficient in Ω. Based on the diffusion approximation to the transport equation, the light fluence Φ satisfies

$$\left(\mu_a - \frac{1}{3}\nabla \cdot \frac{1}{\mu_a + \mu_s}\nabla\right)\Phi = 0 \quad \text{in } \Omega, \tag{13.6}$$

with the boundary condition

$$\frac{\partial\Phi}{\partial\nu} + l\Phi = g \quad \text{on } \partial\Omega. \tag{13.7}$$

Here, g denotes the light source and l a positive constant, $1/l$ being an extrapolation length.

Since A is a nonlinear function of the optical absorption coefficient distribution μ_a, the reconstruction of μ_a from A is a nontrivial task and one of considerable practical interest, since only the optical absorption properties are intrinsic to the object.

13.3 Photoacoustic Imaging in Free Space

In this section, we first formulate the imaging problem in free space and present a simulation for the reconstruction of the absorbing energy density using the spherical or circular Radon transform. Then, we provide a total variation regularization to find a satisfactory solution of the imaging problem with limited-view data. Finally, we present algorithms for compensating the effect of acoustic attenuation. The main idea is to express the effect of attenuation as a convolution operator. Attenuation correction is then achieved by inverting this operator. Two strategies are used for such deconvolution. The first one is based on the SVD of the operator and the second one uses its asymptotic expansion based on the stationary phase theorem. We compare the performances of the two approaches.

13.3.1 Full-View Setting

We consider the wave equation (13.1) in two dimensions when $c_0 = 1$ with the initial conditions (13.2). Assume that the support of p_0, the absorbing energy density, is contained in the unit disk B. Our objective in this part is to reconstruct p_0 from the measurements $g(y,t) = p(y,t)$ on $S \times (0,T)$, where S denotes the boundary of B.

The problem of reconstructing p_0 is related to the inversion formula (2.54) of the spherical mean Radon transform $\mathcal{R}$. Formula (2.54) can be rewritten as follows:

$$p_0(x) = \mathcal{R}^* \mathcal{B} \mathcal{R}[p_0](x), \tag{13.8}$$

where the backprojection operator $\mathcal{R}^*$ and the filter $\mathcal{B}$ are respectively defined by (2.61) and (2.62). We refer to (13.8) as the filtered backprojection formula for the inversion of the spherical mean Radon transform. Note that the operator $\mathcal{B}$ is symmetric and positive.

On the other hand, define the operator $\mathcal{W}$ by

$$\mathcal{W}[g](y,t) = \frac{2}{\pi} \int_0^t \frac{g(y,s)}{\sqrt{t^2 - s^2}}\, ds \tag{13.9}$$

for $g : S \times \mathbb{R}^+ \to \mathbb{R}$. Then, from the Kirchhoff formula (2.59) in two dimensions and by inverting an Abel-type equation it follows that

$$\mathcal{R}[p_0](y,t) = \mathcal{W}[p](y,t), \tag{13.10}$$

and therefore, the filtered backprojection formula (13.8) gives the initial data p_0 from measurements of the pressure p on $S \times \mathbb{R}^+$.

Let N_θ denote the number of equally spaced angles on S. Suppose that pressure signals are uniformly sampled at N time steps, and the phantom (the initial pressure distribution p_0) is sampled on a uniform Cartesian grid with $N_R \times N_R$ points. Figure 13.1 gives a numerical illustration for the reconstruction of p_0 using a discretization of (13.8).

Time-reversal imaging techniques can be applied in order to reconstruct the initial data $p_0(x)$ from measurements of $g(y,t) = \mathcal{W}[p](y,t)$ for $(y,t) \in S \times (0,T)$. Let v be defined by (7.8) and let the time-reversal imaging function $\mathcal{I}_{\mathrm{TR}}^{(1)}(x)$ be given by (7.9). Since p satisfies (7.5) with f replaced by p_0, we have

$$\mathcal{I}_{\mathrm{TR}}^{(1)}(x) = \frac{1}{2} p_0(x), \quad x \in \Omega.$$

13.3.2 Limited-View Setting

In many situations, we have only at our disposal data on $\Gamma \times (0,T)$, where $\Gamma \subset S$. Restricting the integration in formula (13.8) to Γ as follows:

$$p_0(x) \simeq \frac{1}{2\pi} \int_\Gamma \int_0^2 \left[\frac{d^2}{dt^2} \mathcal{R}[p_0](y,t) \right] \log |t^2 - |y - x|^2|\, dt\, d\sigma(y), \tag{13.11}$$
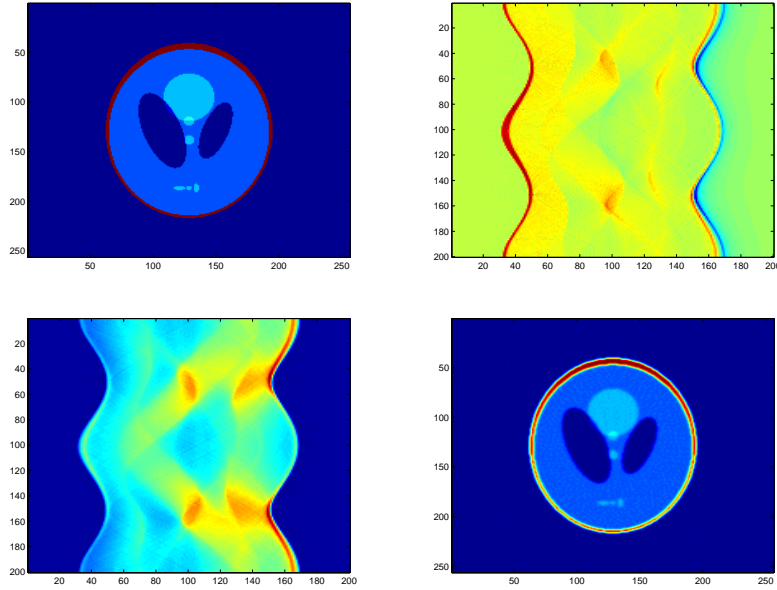
Fig. 13.1. Numerical inversion using (13.8) with $N = 256$, $N_R = 200$ and $N_\theta = 200$. Top left: p_0 ; Top right: $p(y, t)$ with $(y, t) \in S \times (0, 2)$; Bottom left: $\mathcal{R}[p_0](y, t)$ with $(y, t) \in S \times (0, 2)$; Bottom right: $\mathcal{R}^*\mathcal{B}\mathcal{R}[p_0]$.
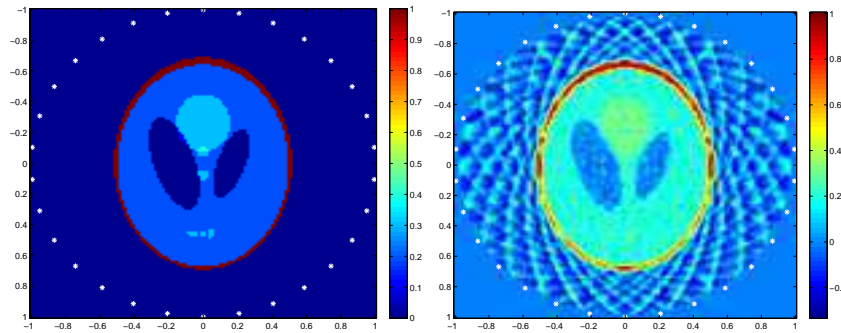

Fig. 13.2. Numerical inversion with truncated (13.8) formula with $N = 128$, $N_R = 128$, and $N_\theta = 30$. Left: p_0; Right: $\mathcal{R}^*\mathcal{B}\mathcal{R}[p_0]$.

is not stable enough to give a correct reconstruction of p_0; see Figure 13.2.

The inverse problem becomes severely ill-posed and needs to be regularized. We apply here a total variation regularization, which is well adapted to the reconstruction of smooth solutions with front discontinuities. In order to reconstruct p_0 from $g(y, t) := \mathcal{W}[p](y, t)$ for $y \in \Gamma$ and $t \in]0, 2[$, we introduce

the regularized minimization problem:

$$\min_f J_\gamma[f] := \frac{1}{2}\|\mathcal{B}^{1/2}\left[\mathcal{R}[f] - g\right]\|_{L^2(\Gamma\times(0,2))}^2 + \gamma\|\nabla f\|_{L^1(\Omega)},$$

where γ is the regularization parameter. As noted in Section 2.8.5, a direct calculation of the minimizer of J_γ is complicated, but an approximate solution can be obtained by the following algorithm.

Algorithm 13.1 Iterative shrinkage-thresholding algorithm in non-attenuated media.

1. Data g, initial set: $f_0 = x_0 = 0$, $t_0 = 1$;
2. $x_k = T_\gamma\left[f_k - \eta\mathcal{R}^*\mathcal{B}\left[\mathcal{R}[f_k] - g\right]\right]$ with T_γ being defined by (2.71) and $\eta > 0$ being the step size;
3. $f_{k+1} = x_k + \frac{t_k - 1}{t_{k+1}}(x_k - x_{k-1})$ with $t_{k+1} = \frac{1+\sqrt{1+4t_k^2}}{2}$.

Two limited-angle experiments are presented in Figure 13.3.

Test 1:

Test 2:
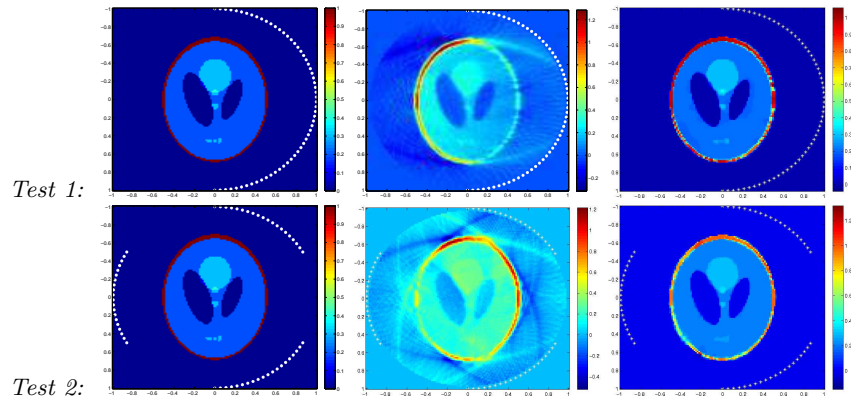
Fig. 13.3. Case of limited angle after 50 iterations, with parameters equal to $\eta = 0.01$, $N = 128$, $N_R = 128$, and $N_\theta = 64$. Left: p_0; Center: $\mathcal{R}^*\mathcal{B}\mathcal{R}[p_0]$; Right: f_{50}.

13.3.3 Compensation of the Effect of Acoustic Attenuation

Our aim in this section is to compensate for the effect of acoustic attenuation. In an attenuating medium, the pressure p_a is solution of the following wave equation:

$$\frac{1}{c_0^2}\frac{\partial^2 p_a}{\partial t^2}(x,t) - \Delta p_a(x,t) - L(t)\star p_a(x,t) = \frac{1}{c_0^2}\frac{d}{dt}\delta_0(t)p_0(x),$$

where L is defined by

$$L(t) = \frac{1}{\sqrt{2\pi}} \int_{\mathbb{R}} \left(K^2(\omega) - \frac{\omega^2}{c_0^2} \right) e^{-i\omega t} d\omega\,. \tag{13.12}$$

Many causal models exist for $K(\omega)$. Here we use the power-law model, which satisfies the Kramers-Kronig relations (2.48). Then $K(\omega)$ is the complex wave number, defined by

$$K(\omega) = \frac{\omega}{c(\omega)} + ia|\omega|^{\zeta}\,, \tag{13.13}$$

where ω is the frequency, $c(\omega)$ is the frequency dependent phase velocity and $1 \leq \zeta \leq 2$ is the power of the attenuation coefficient. The phase velocity and the attenuation coefficient are related to each other by causality; see [330]. A common model, known as the thermoviscous model, is given by

$$K(\omega) = \frac{\omega}{c_0\sqrt{1 - ia\omega c_0}} \tag{13.14}$$

and corresponds approximately to $\zeta = 2$ with $c(\omega) = c_0$.
  Our strategy is now to:

- Estimate the solution $p(y,t)$ of the non-attenuated wave equation

$$\frac{1}{c_0^2}\frac{\partial^2 p}{\partial t^2}(x,t) - \Delta p(x,t) = \frac{1}{c_0^2}\frac{d}{dt}\delta_0(t)p_0(x)\,,$$

  from $p_a(y,t)$ for all $(y,t) \in \partial\Omega \times \mathbb{R}^+$ with $\partial\Omega$ being the surface where the pressure is measured.
- Apply the inverse formula (13.8) for the spherical mean Radon transform to reconstruct p_0 from the non-attenuated data.

Relationship Between p and p_a

Recall that $\hat{p} = \mathcal{F}_t[p]$ and $\hat{p}_a == \mathcal{F}_t[p_a]$ satisfy

$$\left(\Delta + (\frac{\omega}{c_0})^2 \right) \hat{p}(x,\omega) = \frac{i\omega}{\sqrt{2\pi}c_0^2}p_0(x)$$

and

$$\left(\Delta + K(\omega)^2 \right) \hat{p_a}(x,\omega) = \frac{i\omega}{\sqrt{2\pi}c_0^2}p_0(x)\,,$$

which implies that

$$\hat{p}(x, c_0 K(\omega)) = \frac{c_0 K(\omega)}{\omega}\hat{p}_a(x,\omega).$$

The issue is to estimate p from p_a using the relationship $p_a = \mathcal{L}[p]$, where $\mathcal{L}$ is defined by

$$\mathcal{L}[\phi](s) = \frac{1}{2\pi} \int_{\mathbb{R}} \frac{\omega}{c_0 K(\omega)} e^{-i\omega s} \int_0^{\infty} \phi(t) e^{ic_0 K(\omega)t} \, dt \, d\omega \, .$$

The main difficulty is that $\mathcal{L}$ is not well conditioned. We will compare two approaches. The first one uses a regularized inverse of $\mathcal{L}$ via a singular value decomposition, which has been recently introduced in [305]. The second one is based on the asymptotic behavior of $\mathcal{L}$ as the attenuation coefficient a tends to zero.

Figure 13.4 gives some numerical illustrations of the inversion without a correction of the attenuation effect, where a thermoviscous attenuation model is used with $c_0 = 1$ and $\mathcal{W}$ defined by (13.9).
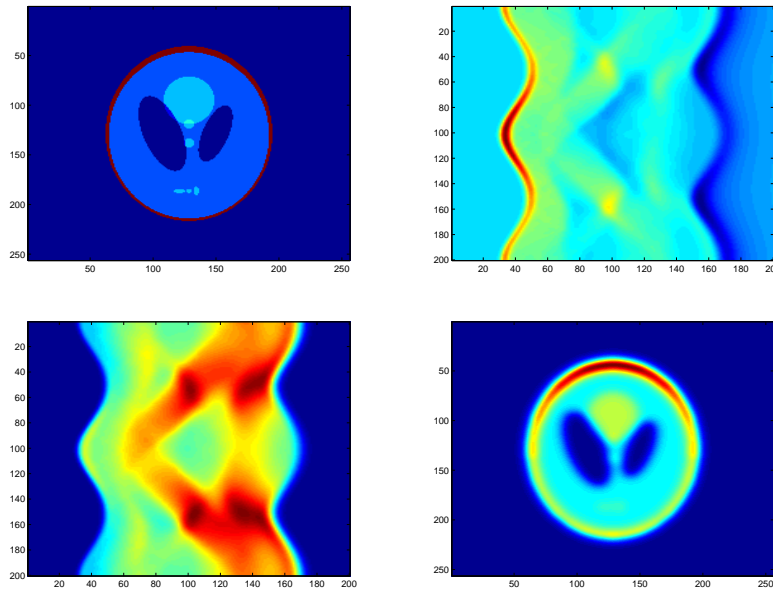
Fig. 13.4. Numerical inversion of attenuated wave equation with $K(\omega)$ given by (13.14) for $c_0 = 1$ and $a = 0.001$. Here $N = 256$, $N_R = 200$ and $N_\theta = 200$. Top left: p_0; Top right: $p_a(y,t)$ with $(y,t) \in \partial\Omega \times]0,2[$; Bottom left: $\mathcal{W}[p_a](y,t)$ with $(y,t) \in \partial\Omega \times]0,2[$; Bottom right: $\mathcal{R}^*\mathcal{B}\left[\mathcal{W}[p_a]\right](x), x \in \Omega$.

An SVD Approach

A regularized inverse of the operator $\mathcal{L}$ obtained by an SVD approach can be used [305]:

$$\mathcal{L}[\phi] = \sum_l \sigma_l (\widetilde{\psi}_l, \phi) \psi_l,$$

where $(\widetilde{\psi}_l)$ and (ψ_l) are two orthonormal bases of $L^2((0,T))$ and σ_l are positives eigenvalues such that

$$\begin{cases} \mathcal{L}^*[\phi] & = \sum_l \sigma_l (\psi_l, \phi) \widetilde{\psi}_l \,, \\ \mathcal{L}^* \mathcal{L}[\phi] & = \sum_l \sigma_l^2 (\widetilde{\psi}_l, \phi) \widetilde{\psi}_l \,, \\ \mathcal{L}\mathcal{L}^*[\phi] & = \sum_l \sigma_l^2 (\psi_l, \phi) \psi_l \,. \end{cases}$$

From (2.66), an approximate inverse of $\mathcal{L}$ is then given by

$$\mathcal{L}_{1,\gamma}^{-1}[\phi] = \sum_l \frac{\sigma_l}{\sigma_l^2 + \gamma^2} (\psi_l, \phi) \widetilde{\psi}_l \,,$$

where $\gamma > 0$ is the regularization parameter.

In Figure 13.5 we present some numerical inversions of the thermoviscous wave equation with $a = 0.0005$ and $a = 0.0025$. We first obtain the ideal measurements from the attenuated ones and then apply the inverse formula for the spherical Radon transform to reconstruct p_0 from the ideal data. We take γ respectively equal to 0.01, 0.001 and 0.0001. The operator $\mathcal{L}$ is discretized to obtain an $N_R \times N_R$ matrix to which we apply an SVD. A regularization of the SVD allows us to construct $\mathcal{L}_{1,\gamma}^{-1}$.

As expected, this algorithm corrects a part of the attenuation effect but is unstable when γ tends to zero.
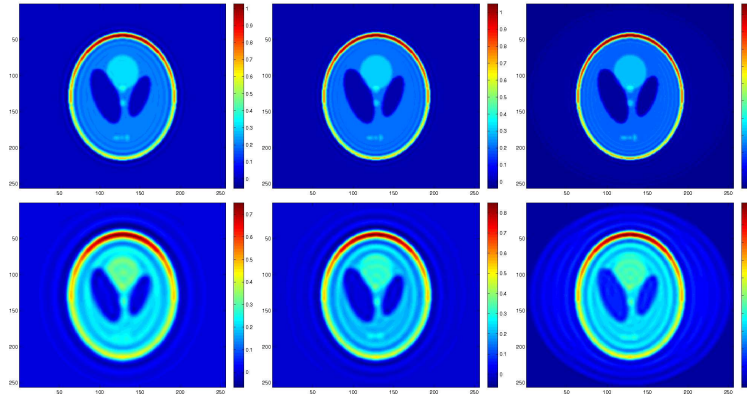
Fig. 13.5. Compensation of acoustic attenuation with SVD regularization: $N = 256$, $N_R = 200$ and $N_\theta = 200$. First line: $a = 0.0005$; second line: $a = 0.0025$. Left to right: using $\mathcal{L}_{1,\gamma}^{-1}$ respectively with $\gamma = 0.01$, $\gamma = 0.001$ and $\gamma = 0.0001$.

Asymptotics of $\mathcal{L}$

In physical situations, the coefficient of attenuation a is very small. We will take into account this phenomenon and introduce an approximation of $\mathcal{L}$ and

$\mathcal{L}^{-1}$ as a goes to zero:

$$\mathcal{L}_j[\phi] = \mathcal{L}[\phi] + o(a^{j+1}) \quad \text{and} \quad \mathcal{L}_{2,j}^{-1}[\phi] = \mathcal{L}^{-1}[\phi] + o(a^{j+1}),$$

where j represents an order of approximation.

Thermoviscous Model (13.14):

Let us consider the thermoviscous attenuation model (13.14) for $K(\omega)$. The operator $\mathcal{L}$ can be approximated as follows

$$\mathcal{L}[\phi](s) \simeq \frac{1}{2\pi} \int_0^\infty \phi(t) \int_{\mathbb{R}} \left(1 - i\frac{ac_0}{2}\omega\right) e^{-\frac{1}{2}c_0 a\omega^2 t} e^{i\omega(t-s)} \, d\omega \, dt \,.$$

Since

$$\frac{1}{\sqrt{2\pi}} \int_{\mathbb{R}} e^{-\frac{1}{2}c_0 a\omega^2 t} e^{i\omega(t-s)} d\omega = \frac{1}{\sqrt{c_0 at}} e^{-\frac{1}{2}\frac{(s-t)^2}{c_0 at}} \,,$$

and

$$\frac{i}{\sqrt{2\pi}} \int_{\mathbb{R}} \omega e^{-\frac{1}{2}c_0 a\omega^2 t} e^{i\omega(t-s)} d\omega = -\partial_s \left(\frac{1}{\sqrt{c_0 at}} e^{-\frac{1}{2}\frac{(s-t)^2}{c_0 at}}\right) \,,$$

it follows that

$$\mathcal{L}[\phi] \simeq \left(1 + \frac{ac_0}{2}\partial_s\right) \left(\frac{1}{\sqrt{2\pi}} \int_0^{+\infty} \phi(t) \frac{1}{\sqrt{c_0 at}} e^{-\frac{1}{2}\frac{(s-t)^2}{c_0 at}} \, dt\right) \,.$$

We then investigate the asymptotic behavior of $\widetilde{\mathcal{L}}$ defined by

$$\widetilde{\mathcal{L}}[\phi] = \frac{1}{\sqrt{2\pi}} \int_0^{+\infty} \phi(t) \frac{1}{\sqrt{c_0 at}} e^{-\frac{1}{2}\frac{(s-t)^2}{c_0 at}} \, dt \,. \tag{13.15}$$

Since the phase in (13.15) is quadratic and a is small, by the stationary phase theorem we can prove that

$$\widetilde{\mathcal{L}}[\phi](s) = \sum_{l=0}^j \frac{(c_0 a)^l}{2^l l!} D_l[\phi](s) + o(a^j) \,, \tag{13.16}$$

where the differential operators D_l satisfy $D_l[\phi](s) = (t^l \phi(t))^{(2l)}(s)$. We can also deduce the following approximation of order j of $\widetilde{\mathcal{L}}^{-1}$

$$\widetilde{\mathcal{L}}_j^{-1}[\psi] = \sum_{l=0}^j a^l \psi_{j,l} \,, \tag{13.17}$$

where $\psi_{j,l}$ are defined recursively by

$$\psi_{j,0} = \psi \quad \text{and} \quad \psi_{j,l} = -\sum_{n=1}^{l} \frac{c_0^n}{2^n n!} D_n[\psi_{j,l-n}], \text{ for all } n \le j.$$

Finally, we define

$$\mathcal{L}_j = \left(1 + \frac{ac_0}{2}\partial_s\right)\widetilde{\mathcal{L}}_j \quad \text{and} \quad \mathcal{L}_{2,j}^{-1} = \widetilde{\mathcal{L}}_j^{-1}\left(1 + \frac{ac_0}{2}\partial_t\right)^{-1}. \tag{13.18}$$

We can compute

$$\widetilde{\mathcal{L}}_0^{-1}[\psi] = \psi, \quad \widetilde{\mathcal{L}}_1^{-1}[\psi] = \psi - \frac{ac_0}{2}(t\psi)'',$$

and therefore,

$$\mathcal{L}[\phi] = \phi + \frac{ac_0}{2}(t\phi')' + o(a) \quad \text{and} \quad \mathcal{L}_{2,1}^{-1}[\psi] = \psi - \frac{ac_0}{2}(t\psi')'. \tag{13.19}$$

We plot in Figure 13.5 some numerical reconstructions of p_0 using a thermoviscous wave equation with $a = 0.0005$ and $a = 0.0025$. We take the value of j respectively equal to $j = 0$, $j = 1$ and $j = 8$. These reconstructions are as good as those obtained by the SVD regularization approach. Moreover, this new algorithm has better stability properties.
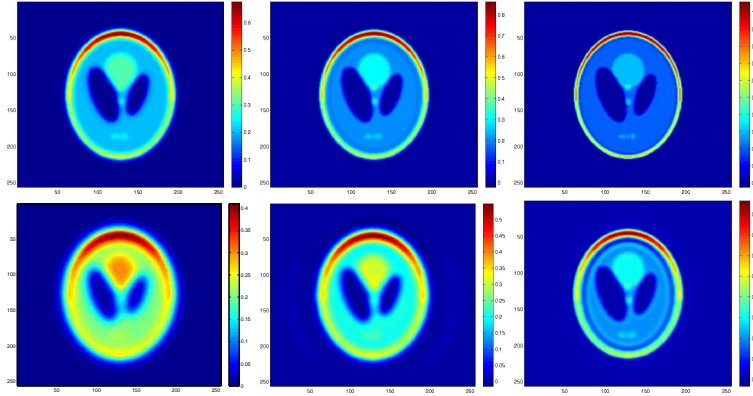
Fig. 13.6. Compensation of acoustic attenuation with formula (13.18): $N = 256$, $N_R = 200$ and $N_\theta = 200$. First line: $a = 0.0005$; second line: $a = 0.0025$. Left: $\widetilde{\mathcal{L}}_j^{-1}$ with $j = 0$; Center: $\widetilde{\mathcal{L}}_j^{-1}$ with $j = 1$; Right: $\widetilde{\mathcal{L}}_j^{-1}$ with $j = 8$.

General Case: $K(\omega) = \omega + ia|\omega|^\zeta$ with $1 \le \zeta < 2$

We now consider the attenuation model $K(\omega) = \frac{\omega}{c_0} + ia|\omega|^\zeta$ with $1 \le \zeta < 2$. We first note that this model is not causal but can be changed to a causal one.

However, since our main purpose here is to give insights for the compensation of the effect of attenuation on image reconstruction, we work with this quite general model because of its simplicity. As before, the problem can be reduced to the approximation of the operator $\widetilde{\mathcal{L}}$ defined by

$$\widetilde{\mathcal{L}}[\phi](s) = \int_0^\infty \phi(t) \int_{\mathbb{R}} e^{i\omega(t-s)} e^{-|\omega|^\zeta c_0 a t}\, d\omega dt\,.$$

It is also interesting to see that its adjoint $\widetilde{\mathcal{L}}^*$ satisfies

$$\widetilde{\mathcal{L}}^*[\phi](s) = \int_0^\infty \phi(t) \int_{\mathbb{R}} e^{i\omega(s-t)} e^{-|\omega|^\zeta c_0 a s}\, d\omega dt\,.$$

Suppose for the moment that $\zeta = 1$, and working with the adjoint operator $\mathcal{L}^*$, we see that

$$\widetilde{\mathcal{L}}^*[\phi](s) = \frac{1}{\pi} \int_0^\infty \frac{c_0 a s}{(c_0 a s)^2 + (s-t)^2} \phi(t) dt\,.$$

Invoking the dominated convergence theorem, we have

$$\lim_{a \to 0} \widetilde{\mathcal{L}}^*[\phi](s) = \lim_{a \to 0} \frac{1}{\pi} \int_{-\frac{1}{a c_0}}^\infty \frac{1}{1+y^2} \phi(s + c_0 a y s) dy = \frac{1}{\pi} \int_{-\infty}^\infty \frac{1}{1+y^2} \phi(s) dy = \phi(s)\,.$$

More precisely, introducing the fractional Laplacian $\Delta^{1/2}$ as follows

$$\Delta^{1/2} \phi(s) = \frac{1}{\pi}\, \mathrm{p.v.} \int_{-\infty}^{+\infty} \frac{\phi(t) - \phi(s)}{(t-s)^2}\, dt\,,$$

we get

$$\begin{aligned}
\frac{1}{a}\left(\widetilde{\mathcal{L}}^*[\phi](s) - \phi(s)\right) &= \frac{1}{a} \int_{-\infty}^\infty \frac{1}{\pi c_0 a s} \frac{1}{1 + \left(\frac{s-t}{c_0 a s}\right)^2} \left(\phi(t) - \phi(s)\right) dt \\
&= \int_{-\infty}^\infty \frac{1}{\pi} \frac{c_0 s}{(c_0 a s)^2 + (s-t)^2} \left(\phi(t) - \phi(s)\right) dt \\
&= \lim_{\epsilon \to 0} \int_{\mathbb{R} \setminus [s-\epsilon, s+\epsilon]} \frac{1}{\pi} \frac{c_0 s}{(c_0 a s)^2 + (s-t)^2} \left(\phi(t) - \phi(s)\right) dt \\
&\to \lim_{\epsilon \to 0} \int_{\mathbb{R} \setminus [s-\epsilon, s+\epsilon]} \frac{1}{\pi} \frac{c_0 s}{(s-t)^2} \left(\phi(t) - \phi(s)\right) dt \\
&= c_0 s \Delta^{1/2} \phi(s)\,,
\end{aligned}$$

as a tends to zero. We therefore deduce that

$$\widetilde{\mathcal{L}}^*[\phi](s) = \phi(s) + c_0 a s \Delta^{1/2}\phi(s) + o(a) \quad \text{and} \quad \widetilde{\mathcal{L}}^*[\phi](s) = \phi(s) + c_0 a \Delta^{1/2}\left(s\phi(s)\right) + o(a)\,.$$

Applying exactly the same argument for $1 < \zeta < 2$, we obtain that

$$\mathcal{L}[\phi](s) = \phi(s) + Cc_0 a \Delta^{\zeta/2}(s\phi(s)) + o(a) \,,$$

where C is a constant, depending only on ζ and $\Delta^{\zeta/2}$, defined by

$$\Delta^{\zeta/2}\phi(s) = \frac{1}{\pi}\, p.v. \int_{-\infty}^{+\infty} \frac{\phi(t) - \phi(s)}{(t-s)^{1+\zeta}}\, dt \,.$$

Iterative Shrinkage-Thresholding Algorithm with Correction of Attenuation

The previous correction of attenuation is not so efficient for a large attenuation coefficient a. In this case, to improve the reconstruction, we may use again a total variation regularization. In view of (13.10), define the attenuated spherical mean Radon transform by

$$\mathcal{R}_a[p_0] := \mathcal{W}[p_a]$$

with $\mathcal{W}$ being given by (13.9). Let $\mathcal{R}_{a,k}^{-1}$ be an approximate inverse of $\mathcal{R}_a$:

$$\mathcal{R}_{a,k}^{-1} = \mathcal{R}^* \mathcal{B} \mathcal{W} \mathcal{L}_{2,k}^{-1} \mathcal{W}^{-1} \,.$$

We consider the following algorithm, which generalizes Algorithm 13.3.2 to attenuating media.

Algorithm 13.2 Iterative shrinkage-thresholding algorithm in an attenuated medium.

---

1. Data g, initial set: $f_0 = x_0 = 0$, $t_0 = 1$;
2. $x_j = T_\gamma \left[f_j - \eta \mathcal{R}_{a,k}^{-1} \left[\mathcal{R}_a[f_j] - g \right] \right]$ with T_γ being defined by (2.71) and $\eta > 0$ being the step size;
3. $f_{j+1} = x_j + \frac{t_j - 1}{t_{j+1}}(x_j - x_{j-1})$ with $t_{j+1} = \frac{1+\sqrt{1+4t_j^2}}{2}$.

Figure 13.7 shows the efficiency of Algorithm 13.3.3.

Sources in attenuating media can be also reconstructed using a time-reversal technique. As a first-order correction of the attenuation effect, the adjoint of the attenuated wave operator can be used. Consider the thermoviscous wave model to incorporate viscosity effect in acoustic wave propagation and introduce the free space fundamental solution of the Helmholtz equation

$$\frac{\omega^2}{c_0^2}\widetilde{\Gamma}_{a,\omega}(x,y) + (1 + iac_0\omega)\Delta_x \widetilde{\Gamma}_{a,\omega}(x,y) = \delta_y(x) \quad \text{in } \mathbb{R}^2 \,.$$

The regularized time-reversal imaging function is defined by

$$\mathcal{I}_{TR}^{(\rho)}(x) = \int_{\partial\Omega} \int_0^T \frac{\partial \widetilde{\Gamma}_{a,\rho}}{\partial t}(x,y,s,T)p_a(y,T-s)\,d\sigma(y)\,ds \,,$$
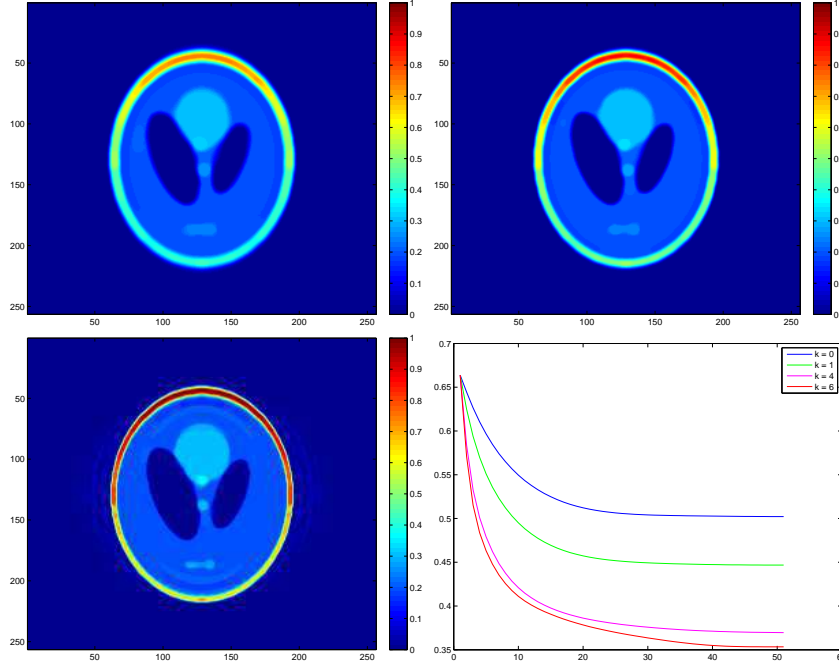
Fig. 13.7. Numerical results using iterative shrinkage-thresholding algorithm with $\eta = 0.001$ and $a = 0.0025$. Left up: f_{50} with $k = 0$; Top right: f_{50} with $k = 1$; Bottom left: f_{50} with $k = 6$; Bottom right: error $j \to \|f_j - p_0\|_{L^2(\Omega)}$ for different values of k.

where

$$\widetilde{\Gamma}_{a,\rho}(x, y, s, t) = \frac{1}{2\pi} \int_{|\omega| \leq \rho} \widetilde{\Gamma}_{a,\omega}(x, y) e^{-i\omega(t-s)} \, d\omega$$

and ρ is a regularization parameter. Hence,

$$\mathcal{I}_{\mathrm{TR}}^{(\rho)}(x) = -\frac{1}{2\pi} \int_0^T \int_{|\omega| \leq \rho} \int_{\partial\Omega} i\omega \widetilde{\Gamma}_{a,\omega}(x, y) p_a(y, T-s) \, d\sigma(y) e^{-i\omega(T-s)} \, d\omega ds \,.$$

As $a \to 0$, we can prove that

$$\mathcal{I}_{\mathrm{TR}}^{(\rho)}(x) = -\int_{\partial\Omega} \int_0^T \frac{\partial\Gamma}{\partial t}(x, y, T-s, T) \mathcal{S}_\rho[p_a(y, \cdot)] \, d\sigma(y) \, ds + o(a) \,,$$

where

$$\mathcal{S}_\rho[\phi](t) = \frac{1}{\sqrt{2\pi}} \int_{|\omega| \leq \rho} e^{-i\omega t} \mathcal{F}_{\mathrm{t}}[\phi](\omega) \, d\omega \,.$$

Finally, observe that the function $\delta_x^{(\rho)}(z)$ defined by

$$\delta_x^{(\rho)}(z) = -\frac{1}{\pi} \int_{|\omega| \leq \rho} \omega \Im \Gamma_\omega(x, z) \, d\omega \,,$$

is an approximation of the Dirac delta function $\delta_z(x)$ as $\rho \to +\infty$. This implies that

$$\mathcal{I}_{TR}^{(\rho)}(x) \approx \delta_x^{(\rho)}(z) \star p_0(z) \to p_0(x) \text{ as } \rho \to +\infty \,.$$

13.4 Photoacoustic Imaging of Small Absorbers with Imposed Boundary Conditions on the Pressure

In this section, we consider the case where a boundary condition is imposed on the pressure field. We first formulate the photoacoustic imaging problem in a bounded domain before reviewing different approaches for reconstructing small absorbing regions and absorbing energy density inside a bounded domain from boundary data. We also consider a problem of selective detection which is to locate a targeted optical absorber among several absorbers from boundary measurements of the induced acoustic signal.

13.4.1 Reconstruction Methods

Let Ω be a bounded smooth domain. We consider the wave equation (13.1) in the domain Ω with the Dirichlet (resp. the Neumann) imposed boundary conditions on $\partial\Omega \times (0, T)$. Our objective in this section is to reconstruct $p_0(x)$ from the measurements of $\dfrac{\partial p}{\partial \nu}(x, t)$ (resp. $p(x, t)$) on the boundary $\partial\Omega \times (0, T)$.

In this section, we consider a problem of identifying small absorbing regions from boundary measurements. Let $D_l, l = 1, \ldots, L$, be absorbing domains inside the nonabsorbing background Ω. We write

$$D_l = z_l + \delta B_l,$$

where z_l is the "center" of D_l, B_l contains the origin and plays a role of a reference domain, and δ is the common order of magnitude of the diameters of the D_l. Throughout this section, we assume that δ is small and z_l's are well-separated, *i.e.*,

$$|z_i - z_j| > C_0 \quad \forall i \neq j \tag{13.20}$$

for some positive constant C_0.

Spherical waves centered at some points, which we call probe waves, may serve as solutions to adjoint problems to the wave equation for the photoacoustic phenomena. By integrating the boundary measurements against a spherical wave, we can estimate the duration of the wave on the absorber. Then by choosing a few waves centered at different points and taking intersection of durations of these waves we can estimate the location and size of the absorber pretty accurately.

To fix ideas, we only consider the Dirichlet condition for the pressure p on $\partial\Omega$. The Neumann boundary condition at tissue/water interface can be treated similarly. Since p is significantly affected by the acoustic boundary conditions at the tissue/air interface, where the pressure must vanish, we cannot base photoacoustic imaging on pressure measurements made over a free surface. Instead, we propose the following algorithm.

Let v satisfy

$$\frac{1}{c_0^2}\frac{\partial^2 v}{\partial t^2} - \Delta v = 0 \quad \text{in } \mathbb{R}^d \times (0, T),\tag{13.21}$$

with the final conditions

$$v|_{t=T} = \left.\frac{\partial v}{\partial t}\right|_{t=T} = 0 \quad \text{in } \Omega.\tag{13.22}$$

We refer to v as a probe function or a probe wave.

Multiply both sides of (13.1) by v and integrate them over $\Omega \times (0, T)$. After some integrations by parts, this leads by using (13.2) to the following identity:

$$\int_0^T \int_{\partial\Omega} \frac{\partial p}{\partial \nu}(x, t) v(x, t)\, d\sigma(x)\, dt = \frac{1}{c_0^2} \sum_{l=1}^L \int_{D_l} A_l(x) \partial_t v(x, 0) dx.\tag{13.23}$$

Suppose first that $d = 3$. For $y \in \mathbb{R}^3 \setminus \overline{\Omega}$, let

$$v_y(x, t; \tau) := \frac{\delta_0\left(t + \tau - \frac{|x-y|}{c_0}\right)}{4\pi|x-y|} \quad \text{in } \Omega \times (0, T),\tag{13.24}$$

where δ is the Dirac mass at 0 and $\tau > \frac{\text{dist}(y, \partial\Omega)}{c_0}$ is a parameter. It is easy to check that v_y satisfies (13.21). It is a spherical wave emitted by a point source at y at time $-\tau$. Moreover, since

$$|x - y| \le \text{diam}(\Omega) + \text{dist}(y, \partial\Omega)$$

for all $x \in \Omega$, v_y satisfies (13.22) provided that the condition (13.4) is fulfilled.

Suppose that

$$A_l(x) = \sum_{|j|=0}^N \frac{1}{j!} a_j^{(l)}(x - z_l)^j,\tag{13.25}$$

which is reasonable as D_l is small. Here, $j = (j_1, \ldots, j_d)$, $x^j = x_1^{j_1} \ldots x_d^{j_d}$, and $j! = j_1! \ldots j_d!$. Equation (13.25) corresponds to a multipolar expansion up to order N of the optical effect of D_l.

Choosing v_y as a probe function in (13.23), we obtain the new identity

$$\frac{1}{c_0^2} \sum_{l=1}^L \sum_{|j|=0}^N \frac{1}{j!} a_j^{(l)} \int_{D_l} (x - z_l)^j \partial_t v_y(x, 0; \tau) dx = \int_0^T \int_{\partial\Omega} \frac{\partial p}{\partial \nu}(x, t) v_y(x, t; \tau)\, d\sigma(x)\, dt.$$

$$\tag{13.26}$$

Determination of location. Suppose for simplicity that there is only one absorbing object $(L = 1)$ which we denote by $D(= z + \delta B)$. Identity (13.26) shows that

$$\tau \mapsto \int_0^T \int_{\partial\Omega} \frac{\partial p}{\partial \nu}(x, t)v_y(x, t; \tau)\, d\sigma(x)\, dt \tag{13.27}$$

is nonzero only on the interval $[\tau_a, \tau_e]$, where $\tau_a = \text{dist}(y, D)/c_0$ is the first τ for which the sphere of center y and radius τ hits D and τ_e is the last τ for which such sphere hits D. This gives a simple way to detect the location (by changing the source point y and taking intersection of spheres). The quantity $\int_0^T \int_{\partial\Omega} \frac{\partial p}{\partial \nu}(x, t)v_y(x, t; \tau)\, d\sigma(x)\, dt$ can be used to probe the medium as a function of τ and y. For fixed y, it is a one-dimensional function. It is related to time-reversal in the sense that it is a convolution with a reversed wave.

Let us now compute $\int_D (x - z)^j \partial_t v_y(x, 0; \tau)dx$ for $\tau \in [\tau_a, \tau_e]$. Note that, in a distributional sense,

$$\partial_t v_y(x, 0; \tau) = \frac{\frac{d\delta_0}{dt}\left(\tau - \frac{|x-y|}{c_0}\right)}{4\pi|x - y|}. \tag{13.28}$$

Thus we have

$$\int_D (x - z)^j \partial_t v_y(x, 0; \tau)dx = \int_D \frac{(x - z)^j}{4\pi|x - y|} \frac{d\delta_0}{dt}\left(\tau - \frac{|x - y|}{c_0}\right) dx.$$

Letting $s = |x - y|$ and $\sigma = \frac{x-y}{|x-y|}$, we get by a change of variables

$$\int_D (x-z)^j \partial_t v_y(x, 0; \tau)dx = \frac{1}{4\pi} \int_0^{+\infty} s \int_S \chi(D)(s\sigma+y)(s\sigma+y-z)^j \frac{d\delta_0}{dt}(\tau-\frac{s}{c_0})\, ds\, d\sigma, \tag{13.29}$$

where S is the unit sphere.

Define for multi-indices j

$$b_j(D, t; \tau) = \int_S \chi(D)(c_0(\tau - t)\sigma + y)(c_0(\tau - t)\sigma + y - z)^j\, d\sigma.$$

Note that the function $b_j(D, t; \tau)$ is dependent on the shape of D (b_j is kind of moment of order j of the domain D). If we take D to be a sphere of radius r (its center is z), then one can compute $b_j(D, t; \tau)$ explicitly using the spherical coordinates.

Since

$$\int_0^{+\infty} s \int_S \chi(D)(s\sigma+y)(s\sigma+y-z)^j \frac{d\delta_0}{dt}(\tau-\frac{s}{c_0})\, ds\, d\sigma = -c_0^2 \frac{d}{dt}\left[(\tau-t)b_j(D, t; \tau)\right]\Big|_{t=0},$$

it follows from (13.29) that

$$\int_D (x - z)^j \partial_t v_y(x, 0; \tau)dx = \frac{c_0^2}{4\pi}(b_j(D, 0; \tau) - \tau b_j'(D, 0; \tau)),$$

where b'_j is the derivative with respect to t. We then obtain the following theorem from (13.26).

Theorem 13.1 *For $\tau \in [\tau_a, \tau_e]$,*

$$\frac{1}{4\pi} \sum_{|j|=0}^{N} \frac{a_j}{j!} (b_j(D, 0; \tau) - \tau b'_j(D, 0; \tau)) = \int_0^T \int_{\partial\Omega} \frac{\partial p}{\partial \nu}(x, t) v_y(x, t; \tau) \, d\sigma(x) \, dt \,.$$

(13.30)

If the Dirichlet boundary condition on p is replaced by the Neumann boundary condition:

$$\frac{\partial p}{\partial \nu} = 0 \quad \text{on } \partial\Omega \times (0, T) \,,$$

(13.31)

then (13.30) should be replaced by

$$\frac{1}{4\pi} \sum_{|j|=0}^{N} \frac{a_j}{j!} (b_j(D, 0; \tau) - \tau b'_j(D, 0; \tau)) = -\int_0^T \int_{\partial\Omega} \frac{\partial v_y}{\partial \nu}(x, t; \tau) p(x, t) \, d\sigma(x) \, dt \,.$$

(13.32)

Estimation of absorbing energy. Now, we show how to use formula (13.30) for estimating $a^{(j)}$ and some geometric features of D when the location z of D has been determined by the variations of the function in (13.27). Suppose that $N = 0$, *i.e.*, A is constant on D. Then (13.30) reads

$$\frac{1}{4\pi} a_0 (b_0(D, 0; \tau) - \tau b'_0(D, 0; \tau)) = \int_0^T \int_{\partial\Omega} \frac{\partial p}{\partial \nu}(x, t) v_y(x, t; \tau) \, d\sigma(x) \, dt \,.$$

Note that $\tau \mapsto b_0(D, 0; \tau) - \tau b'_0(D, 0; \tau)$ is supported in $[\tau_a, \tau_e]$. We have

$$\frac{|a_0|}{4\pi} \int_{\tau_a}^{\tau_e} \left| b_0(D, 0; \tau) - \tau b'_0(D, 0; \tau) \right| d\tau$$

$$= \int_{\tau_a}^{\tau_e} \left| \int_0^T \int_{\partial\Omega} \frac{\partial p}{\partial \nu}(x, t) v_y(x, t; \tau) \, d\sigma(x) \, dt \right| d\tau \,.$$

(13.33)

If we further assume that $D = z + \delta B$ for small δ and a sphere B of radius 1, then we can compute $b_0(D, t; \tau)$ explicitly. In fact, one can show that

$$b_0(D, t, \tau) = \begin{cases} \pi \dfrac{\delta^2 - (|z - y| - c_0|\tau - t|)^2}{c_0 |z - y| |\tau - t|} & \text{if } -\delta < |z - y| - c_0|\tau - t| < \delta \,, \\ 0 & \text{otherwise,} \end{cases}$$

(13.34)

and hence we deduce $c_0 \tau_a = |z - y| - \delta$, $c_0 \tau_e = |z - y| + \delta$, and

$$b_0(D, 0, \tau) - \tau b'_0(D, 0, \tau) = \frac{2\pi(|z - y| - c_0\tau)}{|z - y|}$$

for $\tau > 0$. Therefore, easy computations show that

$$|a_0|\delta^2 \approx c_0|z - y| \int_{\tau_a}^{\tau_e} \left| \int_0^T \int_{\partial\Omega} \frac{\partial p}{\partial\nu}(x, t)v_y(x, t; \tau) \, d\sigma(x) \, dt \right| d\tau, \qquad (13.35)$$

which gives an approximation of $|a_0|\delta^2$. Higher-order approximations can be obtained from (13.30) as well.

Suppose now $d = 2$. Due to the two-dimensional nature of the Green function, we shall rather consider a new probe wave given by

$$v_\theta(x, t; \tau) = \delta_0 \left(t + \tau - \frac{x \cdot \theta}{c_0} \right) \qquad (13.36)$$

where $|\theta| = 1$ and τ is a parameter satisfying

$$\tau > \max_{x \in \Omega} \left(\frac{x \cdot \theta}{c_0} \right).$$

We can still use the function

$$\tau \mapsto \int_0^T \int_{\partial\Omega} \frac{\partial p}{\partial\nu}(x, t)v_\theta(x, t; \tau) \, d\sigma(x) \, dt$$

to probe the medium as a function of τ. This quantity is non-zero on the interval $[\tau_a, \tau_e]$, where τ_a and τ_e are defined such that planes $x \cdot \theta = c_0\tau$ for $\tau = \tau_a$ and τ_e hit D. Changing the direction θ and intersecting stripes gives us an efficient way to reconstruct the inclusions.

By exactly the same arguments as in three dimensions, one can show that

$$\frac{1}{c_0} \sum_{|j|=0}^N \frac{a_j}{j!} b_j'(D, 0; \tau) = \int_0^T \int_{\partial\Omega} \frac{\partial p}{\partial\nu}(x, t)v_\theta(x, t; \tau) \, d\sigma(x) \, dt, \qquad (13.37)$$

where

$$b_j(D, t; \tau) := \int_{\mathbb{R}} \chi(D)(c_0(\tau - t)\theta + u\theta^\perp)(c_0(\tau - t)\theta + u\theta^\perp - z)^j \, du, \quad (13.38)$$

where $\theta^\perp$ is the unit vector obtained from θ by counterclockwise rotation by $\pi/2$.

Assuming $N = 0$ and $D = z + \delta B$, we can compute b_0 explicitly. We have

$$b_0(D, t; \tau) = \begin{cases} 2\sqrt{\delta^2 - (c_0|\tau - t| - z \cdot \theta)^2} & \text{if } -\delta < z \cdot \theta - c_0|\tau - t| < \delta, \\ 0 & \text{otherwise}. \end{cases}$$
$$(13.39)$$

Since $c_0\tau_a = z \cdot \theta - \delta$, $c_0\tau_0 = z \cdot \theta$ and $c_0\tau_b = z \cdot \theta + \delta$, we get

$$|a_0|\delta = \frac{c_0}{4} \int_{\tau_a}^{\tau_e} \left| \int_0^T \int_{\partial\Omega} \frac{\partial p}{\partial\nu}(x, t)v_\theta(x, t; \tau) \, d\sigma(x) \, dt \right| d\tau. \qquad (13.40)$$

The above formula can be used to estimate $|a_0|\delta$.

In the case when there are m inclusions, we first compute for each l the quantity

$$\theta_{l,\text{best}} = \underset{\theta \in [0,\pi]}{\operatorname{argmax}} \left(\min_{j \neq l} |(z_j - z_l) \cdot \theta| \right) \tag{13.41}$$

and then, since along the direction $\theta_{l,\text{best}}$, the inclusion D_l is well separated from all the other inclusions, we can use formula (13.40) to estimate its $|a_0|\delta$.

13.4.2 Back-Propagation of the Acoustic Signals

In this section, we show the focusing properties of the back-propagated acoustic signals.

If we separate out the time dependence of the pressure p by expanding $p(x,t)$ into a set of harmonic modes, then, for a given frequency ω, the harmonic mode $\hat{p}(x,\omega)$ satisfies the following Helmholtz equation:

$$(\omega^2 + c_0^2 \Delta)\hat{p}(x,\omega) = i\omega(\sum_{l=1}^{L} \chi(D_l)A_l(x)) \quad \text{in } \Omega, \tag{13.42}$$

with the boundary condition

$$\hat{p} = 0 \quad \text{or} \quad \frac{\partial \hat{p}}{\partial \nu} = 0 \quad \text{on } \partial\Omega.$$

Suppose that $-\omega^2/c_0^2$ is not an eigenvalue of Δ in Ω with the Dirichlet or the Neumann boundary condition. The inverse problem we consider in this section is to reconstruct $A = \sum_{l=1}^{L} \chi(D_l)A_l$ from the measurements of $\partial\hat{p}/\partial\nu$ or $\hat{p}$ on $\partial\Omega$.

Let us put $k = \frac{\omega}{c_0}$ for simplicity of notation and let $\Gamma_k(x,y) := \Gamma_k(x - y)$ be the outgoing fundamental solution of $(k^2 + \Delta)$ in $\mathbb{R}^d$ given by (3.52). Then, for $y \in \mathbb{R}^d \setminus \overline{\Omega}$, we have

$$\frac{i\omega}{c_0^2} \sum_{l=1}^{L} |D_l|A_l(z_l)\Gamma_k(z_l,y) \approx \begin{cases} \displaystyle\int_{\partial\Omega} \hat{p}(x,\omega)\frac{\partial\Gamma_k}{\partial\nu(x)}(x,y)d\sigma(x) & \text{if } \frac{\partial\hat{p}}{\partial\nu} = 0 \quad \text{on } \partial\Omega, \\ -\displaystyle\int_{\partial\Omega} \frac{\partial\hat{p}}{\partial\nu}(x,\omega)\Gamma_k(x,y)\,d\sigma(x) & \text{if } \hat{p} = 0 \quad \text{on } \partial\Omega. \end{cases} \tag{13.43}$$

For R large enough, set

$$H(y) := \frac{c_0^2}{\omega} \times \begin{cases} \displaystyle\int_{\partial\Omega} \hat{p}(x,\omega)\frac{\partial\Gamma_k}{\partial\nu}(x,y)d\sigma(x) & \text{if } \frac{\partial\hat{p}}{\partial\nu} = 0 \quad \text{on } \partial\Omega, \\ -\displaystyle\int_{\partial\Omega} \frac{\partial\hat{p}}{\partial\nu}(x,\omega)\Gamma_k(x,y)\,d\sigma(x) & \text{if } \hat{p} = 0 \quad \text{on } \partial\Omega, \end{cases} \tag{13.44}$$

and $\alpha_l = |D_l|A_l(z_l)$. Note that, for any $y \in \mathbb{R}^d \setminus \overline{\Omega}$, the function $H(y)$ can be computed from the boundary measurements of the acoustic signals.

Back-propagating the data corresponds to computing

$$W(z^S) := \int_{\partial B_R} \left[\frac{\partial \Gamma_k}{\partial \nu}(z^S, y)\overline{H}(y) - \frac{\partial \overline{H}}{\partial \nu}(y)\Gamma_k(z^S, y) \right] d\sigma(y), \quad z^S \in \Omega \,,$$

(13.45)

where H is defined in (13.44). Since from (13.43)

$$H(y) \approx i \sum_{l=1}^{L} \alpha_l \Gamma_k(z_l, y)$$

for y in a neighborhood of ∂B_R, the Helmholtz-Kirchhoff identity (3.80) yields

$$W(z^S) \approx -\sum_{l=1}^{L} i\overline{\alpha_l} \int_{\partial B_R} \left[\frac{\partial \Gamma_k}{\partial \nu}(z^S, y)\overline{\Gamma_k}(z_l, y) - \frac{\partial \overline{\Gamma_k}}{\partial \nu}(z_l, y)\Gamma_k(z^S, y) \right] d\sigma(y)$$

$$= -2\sum_{l=1}^{L} \overline{\alpha_l} \Im \, \Gamma_k(z^S, z_l) \,.$$

(13.46)

Since α_l is real and positive by (13.5), it is now easy to find the locations z_l, $l = 1, \ldots, L$, as the points where the functional W has its maxima. Equation (13.46) shows that the reversed signal focuses on the locations of the absorbers with a resolution determined by the behavior of the imaginary part of the Green function.

13.4.3 Selective Detection

We now turn our attention to the selective detection. The purpose of selective detection is to focus high-intensity ultrasound towards a targeted optical absorber in biological tissue. The main difficulty in focusing towards a targeted optical absorber is that photoacoustic waves are generated by other optical absorbers in the medium as well. In this section we propose two methods of different nature to overcome this difficulty and localize selectively the targeted absorber. The first method is based on a MUSIC type algorithm. This method works when the absorbing coefficient of the targeted absorber is in contrast with those of other absorbers. An alternative method of selective detection is based on the fact that the absorbing coefficient may vary depending on the frequencies. Some absorbers are transparent at certain frequency while they are quite absorbing at other frequencies. This phenomenon makes a multi-frequency approach work to detect a targeted absorber. We propose a detailed process of this multi-frequency approach.

Multiple Signal Classification Algorithm

Suppose that for some l_0, D_{l_0} is a targeted optical absorber and its coefficient α_{l_0} is known. However, its location z_{l_0} is not known. Suppose also that

$$|\alpha_{l_0}| \geq C, \quad |\alpha_{l_0} - \alpha_l| \geq C, \quad \forall\, l \neq l_0\,, \tag{13.47}$$

for some positive constant C. This means that α_{l_0} is significantly different from the coefficients associated with all the other absorbers in the medium. The locations and the α_l's of all the other absorbing inclusions (D_l for $l \neq l_0$) are not known.

To localize the absorbing object D_{l_0} without knowing any of the others, we compute the following quantity for $z^S \in \Omega$:

$$W_{l_0}(z^S) := \frac{1}{\overline{\alpha_{l_0}} - i4\pi \int_{\partial B_R} \Gamma_k(y, z^S)\overline{H}(y)\, d\sigma(y)}\,, \tag{13.48}$$

where H is defined by (13.44).

From (3.81), it follows that in dimension three we have for large R

$$\int_{\partial B_R} \Gamma_k(y, z^S)\overline{\Gamma_k}(y, z_l)\, d\sigma(y) \approx \frac{1}{4\pi} \frac{\sin k|z^S - z_l|}{k|z^S - z_l|}\,,$$

and hence

$$4\pi \int_{\partial B_R} \Gamma_k(y, z^S)\overline{H}(y)\, d\sigma(y) \approx i \sum_{l=1}^{L} \overline{\alpha_l} \frac{\sin k|z^S - z_l|}{k|z^S - z_l|}\,.$$

This yields

$$W_{l_0}(z^S) \approx \frac{1}{\overline{\alpha_{l_0}} - \sum_l \overline{\alpha_l} \frac{\sin k|z^S - z_l|}{k|z^S - z_l|}}\,.$$

Therefore, thanks to the assumption (13.20), we have

$$\left|W_{l_0}(z^S)\right| \approx \left|\frac{1}{\sum_{l \neq l_0} \overline{\alpha_l} \frac{\sin k|z^S - z_l|}{k|z^S - z_l|}}\right| \gg 1 \quad \text{for } z^S \text{ near } z_{l_0}\,. \tag{13.49}$$

We also have from the assumption (13.47)

$$\left|W_{l_0}(z^S)\right| \approx \left|\frac{1}{\overline{\alpha_{l_0}} - \sum_l \overline{\alpha_l} \frac{\sin k|z^S - z_l|}{k|z^S - z_l|}}\right| = O(1) \quad \text{for } z^S \text{ away from } z_{l_0}\,. \tag{13.50}$$

It then follows that z_{l_0} can be detected as the point where the functional W_{l_0} has a peak. This is a MUSIC-type algorithm for locating the anomalies.

In the two-dimensional case, we compute from (3.52) and (3.81) for large R

$$\int_{\partial B_R} \Gamma_k(y, z^S)\overline{\Gamma_k}(y, z_l)\, d\sigma(y) \approx \frac{1}{4k} J_0(k|z^S - z_l|),$$

where J_0 is the Bessel function of the first kind of order zero. It then follows that

$$4k \int_{\partial B_R} \Gamma_k(y, z^S)\overline{H}(y)\, d\sigma(y) \approx i \sum_{l=1}^{L} \overline{\alpha_l} J_0(k|z^S - z_l|)\,.$$

In two dimensions, define W_{l_0} by

$$W_{l_0}(z^S) := \frac{1}{\overline{\alpha_{l_0}} - i4k \int_{\partial B_R} \Gamma_k(y, z^S)\overline{H}(y)\, d\sigma(y)}\,.$$

As in the three-dimensional case, the behavior of the function J_0 yields

$$\left|W_{l_0}(z^S)\right| \approx \left|\frac{1}{\sum_{l \neq l_0} \overline{\alpha_l} J_0(k|z^S - z_l|)}\right| \gg 1 \quad \text{for } z^S \text{ near } z_{l_0}$$

and

$$W_{l_0}(z^S) \approx \frac{1}{\overline{\alpha_{l_0}} - \sum_l \overline{\alpha_l} J_0(k|z^S - z_l|)} = O(1) \quad \text{for } z^S \text{ away from } z_{l_0}\,.$$

Therefore, exactly as in three dimensions, z_{l_0} can be detected as the point where the functional W_{l_0} has a peak. Note that one does not need the exact value of α_{l_0}. One can get an approximation of α_{l_0} by looking numerically for the maximum of the function $F(z^S) = \int_{\partial B_R} \Gamma_k(y, z^S)\bar{H}(y) d\sigma(y)$.

Multi-Frequency Approach

An alternative method for isolating the photoacoustic signal generated by the targeted optical absorber from those generated by the others is to make use of two light pulses with slightly different excitation wavelengths, λ_1 and λ_2, tuned to the absorption spectrum of the targeted optical absorber. If the optical wavelengths are such that λ_1 corresponds to a low value (that can be neglected) of the absorption coefficient of the optical target and λ_2 to a high value of the absorption coefficient of the optical target, then the only difference in photoacoustic waves generated in the medium by the two different pulses corresponds to the photoacoustic waves generated by the light pulse selectively absorbed by the optical target. Back-propagating this signal will focus on the location of the optical target.

Suppose that there are two absorbers, say D_1 and D_2, and assume that

$$|D_2| \ll 1, \tag{13.51}$$

$$\text{dist}(D_1, D_2) \geq C > 0, \tag{13.52}$$

which means that D_2 is small and D_1 and D_2 are apart from each other.

Let Φ_1 and Φ_2 be the light fluences corresponding respectively to illuminating the medium with excitation wavelengths λ_1 and λ_2. If we take λ_2 close to λ_1, then due to the assumptions (13.51) and (13.52) we have

$$\mu_1(x, \lambda_1)\Phi_1(x) \approx \mu_1(x, \lambda_2)\Phi_2(x) \quad \text{in } D_1\,. \tag{13.53}$$

The pressures generated by the photoacoustic effect are given by

$$
\begin{cases}
\dfrac{\partial^2 p_1}{\partial t^2}(x,t) - c_0^2 \Delta p_1(x,t) = 0, & x \in \Omega, \quad t \in (0,T), \\[2mm]
p_1 = 0 \quad \text{or} \quad \dfrac{\partial p_1}{\partial \nu} = 0 \quad \text{on } \partial\Omega \times (0,T), \\[2mm]
p_1|_{t=0} = \mu_1(x,\lambda_1)\chi(D_1)\Phi_1 \quad \text{and} \quad \dfrac{\partial p_1}{\partial t}\Big|_{t=0} = 0 \quad \text{in } \Omega,
\end{cases}
$$

and

$$
\begin{cases}
\dfrac{\partial^2 p_2}{\partial t^2}(x,t) - c_0^2 \Delta p_2(x,t) = 0, & x \in \Omega, \quad t \in (0,T), \\[2mm]
p_2 = 0 \quad \text{or} \quad \dfrac{\partial p_2}{\partial \nu} = 0 \quad \text{on } \partial\Omega \times (0,T), \\[2mm]
p_2|_{t=0} = (\mu_1(x,\lambda_2)\chi(D_1) + \mu_2(x,\lambda_2)\chi(D_2))\Phi_2 \quad \text{and} \quad \dfrac{\partial p_2}{\partial t}\Big|_{t=0} = 0 \quad \text{in } \Omega.
\end{cases}
$$

For the sake of simplicity we work in the frequency domain. In view of (13.42), the difference of the generated pressures $\hat{p}_2 - \hat{p}_1$ at an acoustic frequency ω can be approximated for $x \in \Omega$ as follows:

$$
(\hat{p}_2 - \hat{p}_1)(x,\omega) \approx \frac{i\omega}{c_0^2}|D_2|\mu_2(z,\lambda_2)\Phi_2(z) \times
\begin{cases}
G_k(x,z) & \text{in the case of the} \\
& \text{Dirichlet boundary condition}, \\
N_k(x,z) & \text{in the case of the} \\
& \text{Neumann boundary condition},
\end{cases}
$$

where $k = \omega/c_0$, G_k and N_k are respectively the Dirichlet and Neumann Green functions defined by (3.70) and (3.74) with k_0 replaced by k. Here we assume that $-k^2$ is not an eigenvalue of Δ in Ω with Dirichlet or Neumann boundary condition.

Define, as in (13.44), H by

$$
H(y) := \frac{c_0^2}{\omega}
\begin{cases}
\displaystyle\int_{\partial\Omega} (\hat{p}_2 - \hat{p}_1)(x)\frac{\partial \Gamma_k}{\partial \nu}(x,y)d\sigma(x) & \text{in the case of the Neumann} \\
& \text{boundary condition}, \\[4mm]
-\displaystyle\int_{\partial\Omega} \frac{\partial(\hat{p}_2 - \hat{p}_1)}{\partial \nu}(x)\Gamma_k(x,y)\,d\sigma(x) & \text{in the case of the Dirichlet} \\
& \text{boundary condition}.
\end{cases}
$$

Back-propagating $\hat{p}_2 - \hat{p}_1$ yields

$$
2|D_2|\mu_2(z,\lambda_2)\Phi_2(z)\Im m\Gamma_k(x,z) \approx \int_{\partial B_R}\left[\frac{\partial \Gamma_k}{\partial \nu}(y,z)\overline{H}(y) - \frac{\partial\overline{H}}{\partial \nu}(y)\Gamma_k(y,z)\right]d\sigma(y),
$$

for $x \in \Omega$. Here R large enough. This equation shows that the reversed frequency-difference signal focus on the location z of the targeted optical absorber. Using the equation we can reconstruct the location z with a resolution given by the behavior of the imaginary part of the Green function and a signal-to-noise ratio function of the quantity $|D_2|\mu_2(z,\lambda_2)\Phi_2(z)$.

13.5 Imaging with Limited-View Data

In this section, we consider photoacoustic imaging from limited-view data. Our purpose is to design efficient algorithms for reconstructing the location z from boundary measurements of $\frac{\partial p}{\partial \nu}$ on $\Gamma \times (0, T)$, where $\Gamma \subset \partial \Omega$. Using as weights particular background solutions constructed by the geometrical control method, we extend the imaging algorithms developed in the previous section by appropriately averaging limited-view data. It can be shown that if one can construct accurately the geometric control, then one can perform imaging with the same resolution using limited-view as when using full-view data.

13.5.1 Geometrical Control of the Wave Equation

Suppose that T and Γ are such that they geometrically control Ω, which roughly means that every geometrical optic ray, starting at any point $x \in \Omega$, at time $t = 0$, hits Γ before time T at a nondiffractive point; see [95]. Let $\beta \in \mathcal{C}_0^\infty(\Omega)$ be a cutoff function such that $\beta(x) \equiv 1$ in a sub-domain Ω' of Ω, which contains the source point z. For any function $w \in W^{1,2}(\Omega)$, we can construct by the Hilbert Uniqueness Method (HUM) of Lions [258] a unique $g_w(x, t) \in W_0^{1,2}(0, T; L^2(\Gamma))$ in such a way that the unique weak solution $v \in \mathcal{C}^0(0, T; L^2(\Omega)) \cap \mathcal{C}^1(0, T; W^{-1,2}(\Omega))$ of the wave equation

$$
\begin{cases}
\frac{\partial^2 v}{\partial t^2} - c_0^2 \Delta v = 0 & \text{in } \Omega \times (0, T) , \\
v = 0 & \text{on } \partial \Omega \setminus \overline{\Gamma} \times (0, T) , \\
v = g_w & \text{on } \Gamma \times (0, T) , \\
v(x, 0) = c_0^2 \beta(x) w(x), \quad \partial_t v(x, 0) = 0 & \text{in } \Omega ,
\end{cases}
\tag{13.54}
$$

satisfies the final conditions

$$
v|_{t=T} = \left. \frac{\partial v}{\partial t} \right|_{t=T} = 0 \quad \text{in } \Omega .
\tag{13.55}
$$

Here $W^{-1,2}(\Omega)$ is the dual of $W_0^{1,2}(\Omega)$. The role of the cutoff function β is to have the initial condition $v|_{t=0}$ belong to $W_0^{1,2}(\Omega)$. Note that since the absorbers we are looking for are supposed to be away from the boundary, β does not play any role in the imaging procedures below. Moreover, the HUM is constructive and allows to compute the control g_w.

13.5.2 Reconstruction Procedure

Assume that measurements are only made on a part of the boundary $\Gamma \subset \partial \Omega$. Then under the geometric controllability conditions on Γ and T, existence of the probe v solution to (13.54)-(13.55) is guaranteed and we have

$$
\int_0^T \int_\Gamma \frac{\partial p}{\partial \nu}(x, t) v(x, t) d\sigma(x) dt = \int_\Omega p_0(x) \frac{\partial v}{\partial t}(x, 0) dx .
\tag{13.56}
$$

Varying our choice of $\dfrac{\partial v}{\partial t}(x, 0)$, we can adapt the imaging algorithms developed in the previous section to the case of limited view data. This approach is robust with respect to perturbations of the boundary. This is quite important in real experiments since one does not necessarily know the non-accessible part of the boundary with good accuracy.

Note also that in the full-view case ($\Gamma = \partial\Omega$), no more boundary conditions are imposed on v and consequently, there are many families of explicit functions v satisfying (13.54)-(13.55). For example, those used in the previous section as probe functions correspond to one of the following choices for w in Ω:

$$w(x) := \frac{\delta_0 \left(\tau - \frac{|x-y|}{c_0} \right)}{4\pi|x-y|} \quad \text{in three dimensions} \tag{13.57}$$

or

$$w(x) := \delta_0 \left(\tau - \frac{1}{c_0}\theta \cdot x \right) \quad \text{in two dimensions}, \tag{13.58}$$

where θ is a unit vector and τ a scalar parameter. The functions defined in (13.57) and (13.58) are respectively families of spherical and plane waves.

13.5.3 Implementation of the HUM

A systematic and constructive method for computing the control g_w such that the solution v to (13.54) satisfies the final conditions (13.55) is given by the HUM. Note that the HUM produces an ill-posed problem. If the initial datum w is highly oscillating, then the HUM can not produce a stable solution g_w.

The implementation of the HUM presented in Algorithm 13.5.3 allows us to handle general geometries and meshes. It applies a conjugate gradient algorithm as follows.

13.6 Quantitative Photoacoustic Imaging

Recall that it is the absorption coefficient, not the absorbed energy, that is a fundamental physiological parameter. The absorbed energy density is in fact the product of the optical absorption coefficient and the light fluence which depends on the distribution of scattering and absorption within the domain, as well as the light sources.

In this section, methods for reconstructing the normalized optical absorption coefficient of small absorbers from the absorbed density are proposed. Multi-wavelength acoustic measurements are combined with diffusing light measurements to separate the product of absorption coefficient and optical fluence.

Suppose that Ω contains a small absorbing object D. We write

$$D = z + \delta B,$$

Algorithm 13.3 The HUM.

1. Let $e_0, e_1 \in W_0^{1,2}(\Omega) \times L^2(\Omega)$;
2. Solve forwards on $(0, T)$ the wave equation

$$
\begin{cases}
\dfrac{\partial^2 \phi}{\partial t^2}(x, t) - c_0^2 \Delta \phi(x, t) = 0 & \text{in } \Omega \times (0, T), \\[2mm]
\phi(x, t) = 0 & \text{on } \partial\Omega \times (0, T), \\[2mm]
\phi(x, 0) = e_0(x), \qquad \dfrac{\partial \phi}{\partial t}(x, 0) = e_1(x);
\end{cases}
\tag{13.59}
$$

3. Compute $\frac{\partial \phi}{\partial \nu}(x, t)$ on $\Gamma \times (0, T)$ and solve backwards the wave equation

$$
\begin{cases}
\dfrac{\partial^2 \psi}{\partial t^2}(x, t) - c_0^2 \Delta \psi(x, t) = 0 & \text{in } \Omega \times (0, T), \\[2mm]
\psi(x, t) = \begin{cases} 0 & \text{on } \partial\Omega \backslash \bar{\Gamma} \times (0, T), \\ \frac{\partial \phi}{\partial \nu}(x, t) & \text{on } \Gamma \times (0, T), \end{cases} \\[4mm]
\psi(x, T) = 0, \qquad \dfrac{\partial \psi}{\partial t}(x, T) = 0;
\end{cases}
\tag{13.60}
$$

4. Set

$$
\Lambda(e_0, e_1) = \left(\frac{\partial \psi}{\partial t}(x, 0), -\psi(x, 0) \right);
\tag{13.61}
$$

5. The solution v of (13.54)-(13.55) can be identified with ψ when

$$
\Lambda(e_0, e_1) = \left(0, -c_0^2 \beta(x) w(x) \right)
$$

and $g_w(x, t) = \psi(x, t)$ on $\Gamma \times (0, T)$.

---

where z is the "center" of D, B is a reference domain which contains the origin, and δ is a small parameter. The main purpose is to develop, in the context of small-volume absorbers, efficient methods to recover μ_a of the absorber D from the normalized energy density $\delta^2 A$. We distinguish two cases. The first case is the one where the reduced scattering coefficient μ_s inside the background medium is known *a priori*. In this case we develop an asymptotic approach to recover the normalized absorption coefficient, $\delta^2 \mu_a$, from the normalized energy density using multiple measurements. We make use of inner expansions of the fluence distribution Φ in terms of the size of the absorber. We also provide an approximate formula to separately recover δ from μ_a. However, this requires boundary measurements of Φ.

The second case is when the reduced scattering coefficient μ_s is unknown. We use multiple optical wavelength data. We assume that the optical wavelength dependence of the scattering and absorption coefficients are known. In tissues, the wavelength-dependence of the scattering often approximates to a power law. We propose a formula to extract the absorption coefficient μ_a from multiple optical wavelength data. In fact, we combine multiple optical wavelength measurements to separate the product of absorption coefficient

and optical fluence. Note that the approximate model we use in this case for the light transport, which is based on the diffusion approximation, allows us to estimate $|D|$ independently from A and therefore, the multi-wavelength approach yields the absolute absorption coefficient.

13.6.1 Asymptotic Approach

In this section, we let $d = 3$ and consider a slightly more general equation than (13.6) and provide an asymptotic expansion of its solution as the size of the absorbing object D goes to zero. We assume that μ_s is constant.

Recall that the fluence Φ defined by (13.6) is the integral over time of the fluence rate Ψ which satisfies

$$\left(\frac{1}{c}\partial_t + \mu_a(x) - \frac{1}{3}\nabla \cdot \frac{1}{\mu_a(x) + \mu_s}\nabla \right)\Psi(x,t) = 0 \quad \text{in } \Omega \times \mathbb{R}, \qquad (13.62)$$

where c is the speed of light. Taking the Fourier transform of (13.62) yields that the Fourier transform Φ_ω of Ψ in t is the solution to

$$\left(-\frac{i\omega}{c} + \mu_a(x) - \frac{1}{3}\nabla \cdot \frac{1}{\mu_a(x) + \mu_s}\nabla \right)\Phi_\omega(x) = 0 \quad \text{in } \Omega, \qquad (13.63)$$

with the boundary condition

$$\frac{\partial \Phi_\omega}{\partial \nu} + l\Phi_\omega = g \quad \text{on } \partial\Omega. \qquad (13.64)$$

For simplicity, we assume that $l \leq C\sqrt{\mu_s}$ for some constant C, $\text{dist}(z, \partial\Omega) \geq C_0$ for some constant C_0, μ_s is a constant and known a priori and drop in the notation the dependence with respect to ω.

In what follows, we derive an asymptotic expansion of $\Phi_\omega(z)$ as δ goes to zero, where z is the location of the absorbing object D.

Define $\Phi^{(0)}$ by

$$\left(-\frac{i\omega}{c} - \frac{1}{3\mu_s}\Delta \right)\Phi^{(0)}(x) = 0 \quad \text{in } \Omega,$$

subject to the boundary condition

$$\frac{\partial \Phi^{(0)}}{\partial \nu} + l\Phi^{(0)} = g \quad \text{on } \partial\Omega,$$

where g is a bounded function on $\partial\Omega$.

Let N be the Neumann function, that is, the solution to

$$\begin{cases} \left(-\dfrac{i\omega}{c} - \dfrac{1}{3\mu_s}\Delta_x \right)N(x,y) = -\delta_y & \text{in } \Omega, \\ \dfrac{\partial N}{\partial \nu} + lN = 0 & \text{on } \partial\Omega. \end{cases} \qquad (13.65)$$

Note that N is symmetric:

$$N(x, y) = N(y, x), \quad x, y \in \Omega, \quad x \neq y. \tag{13.66}$$

Note also that

$$\Phi^{(0)}(x) = -\frac{1}{3\mu_s} \int_{\partial\Omega} g(y) N(x, y) \, d\sigma(y), \quad x \in \Omega. \tag{13.67}$$

Thus, multiplying (13.63) by N, using the symmetry property (13.66) and integrating by parts, we readily get the following representation formula of $\Phi(x)$ for $x \in \Omega$:

$$\begin{aligned}
(\Phi - \Phi^{(0)})(x) &= \mu_a \int_D \Phi(y) N(x, y) \, dy \\
&+ \frac{1}{3} \left(\frac{1}{\mu_a + \mu_s} - \frac{1}{\mu_s} \right) \int_D \nabla\Phi(y) \cdot \nabla_y N(x, y) \, dy.
\end{aligned} \tag{13.68}$$

We now derive an asymptotic expansion of $(\Phi - \Phi^{(0)})(z)$, where z is the location of D, as the size δ of D goes to zero. The asymptotic expansion also takes the smallness of μ_a/μ_s into account.

Let $\hat{N}_B$ be the Newtonian potential of B, which is given by

$$\hat{N}_B(x) := \int_B \Gamma(x - y) \, dy, \quad x \in \mathbb{R}^3, \tag{13.69}$$

and let $\mathcal{S}_B$ be the single layer potential associated to B. We have

$$(\Phi - \Phi^{(0)})(z) \approx 3\delta^2 \mu_a \mu_s \Phi^{(0)}(z) \hat{N}_B(0) - \delta \frac{\mu_a}{\mu_s} \mathcal{S}_B[\nu](0) \cdot \nabla\Phi^{(0)}(z). \tag{13.70}$$

Note that the first term in (13.70) is a point source type approximation while the second term is a dipole approximation. Formula (13.70) also shows that if $\delta\Phi^{(0)}(z)$ is of the same order as $(1/\mu_s^2(z))\nabla\Phi^{(0)}(z)$ then we have two contributions in the leading-order term of the perturbations in Φ that are due to D. The first contribution is coming from the source term $\mu_a(x, \omega)$ and the second one from the jump conditions. If $\delta\Phi^{(0)}(z)$ is much larger than $(1/\mu_s^2(z))\nabla\Phi^{(0)}(z)$ then we can neglect the second contribution. It is worth emphasizing that formula (13.70) holds for any fixed $\omega \geq 0$ as δ goes to zero.

We now turn to the reconstruction of the absorption coefficient. Given the light source g, it has been shown in this chapter that the location z and $\alpha := \delta^2 \mu_a \Phi(z)$ can be reconstructed from photoacoustic measurements. Here $\Phi = \Phi_{\omega=0}$.

Suppose that B is the unit sphere. Since $\mathcal{S}_B[\nu](0) = 0$, formula (13.70) reads

$$(\Phi - \Phi^{(0)})(z) \approx 3\delta^2 \mu_a \mu_s \Phi^{(0)}(z) \hat{N}_B(0) \approx 3\alpha \mu_s \hat{N}_B(0). \tag{13.71}$$

Thus one can easily see that

$$\delta^2 \mu_a \approx \frac{\alpha}{3\alpha\mu_s \hat{N}_B(0) + \Phi^{(0)}(z)}.$$
(13.72)

Let us see how one may separate δ from μ_a. Because of (13.67), it follows from (13.68) that

$$-\tfrac{1}{3\mu_s} \int_{\partial\Omega} g(\Phi - \Phi^{(0)})\, d\sigma \approx \mu_a \Phi(z)\Phi^{(0)}(z)|D|$$
$$+\frac{1}{3}\left(\frac{1}{\mu_s + \mu_a} - \frac{1}{\mu_s}\right)\int_D \nabla\Phi(y)\cdot\nabla\Phi^{(0)}(y)dy.$$

Thus we get from (13.70) that

$$-\frac{1}{3\mu_s}\int_{\partial\Omega} g(\Phi - \Phi^{(0)})\, d\sigma$$
$$\approx \mu_a \Phi(z)\Phi^{(0)}(z)|D| - \frac{\mu_a}{3\mu_s^2}\nabla\Phi^{(0)}(z)\cdot\left[3\delta^4 \mu_a\mu_s \Phi^{(0)}(z)\int_B \nabla\hat{N}_B(y)\, dy +\right.$$
$$\left. +\delta^3\int_B \left(I - \frac{\mu_a}{\mu_s}\nabla\mathcal{S}_B[\nu]\right)(y)\, dy\nabla\Phi^{(0)}(z)\right]$$
$$\approx \delta\alpha|B|\Phi^{(0)}(z) - \frac{\mu_a\delta^3}{3\mu_s^2}\nabla\Phi^{(0)}(z)\cdot\left[3\delta\mu_a\mu_s \Phi^{(0)}(z)\int_B \nabla\hat{N}_B(y)\, dy +\right.$$
$$\left. + \int_B \left(I - \frac{\mu_a}{\mu_s}\nabla\mathcal{S}_B[\nu]\right)(y)\, dy\nabla\Phi^{(0)}(z)\right].$$
(13.73)

One may use this approximation to separately recover δ from μ_a even in the general case, where B is not necessary a unit sphere by combining (13.73) together with (13.70). However, this approach requires boundary measurements of Φ on $\partial\Omega$.

13.6.2 Multi-Wavelength Approach

We now deal with the problem of estimating both the absorption coefficient μ_a and the reduced scattering coefficient μ_s from $A = \mu_a\Phi$ where Φ satisfies (13.63) and the boundary condition (13.64). It is known that this problem at fixed optical wavelength λ is a severely ill-posed problem. However, if the optical wavelength dependence of both the scattering and the absorption are known, then the ill-posedness of the inversion can be dramatically reduced.

Let $\mu_s(x, \lambda_j)$ and $\mu_a(x, \lambda_j)$ be the reduced scattering and absorption coefficients at the optical wavelength λ_j for $j = 1, 2$, respectively. Note that $\mu_a(\cdot, \lambda_j)$ is supported in the absorbing region D which is of the form $D = z + \delta B$ for δ of small magnitude. We assume that $\mu_s(x, \lambda)$ and $\mu_a(x, \lambda)$ depend on the wavelength in the following way:

$$\mu_s(x, \lambda) = f_s(x)g_s(\lambda),$$
(13.74)

and

$$\mu_a(x, \lambda) = f_a(x)g_a(\lambda), \tag{13.75}$$

for some functions f_a, f_s, g_a, g_s. Denote

$$C_s := \frac{\mu_s(x, \lambda_1)}{\mu_s(x, \lambda_2)} = \text{constant in the } x \text{ variable in } \Omega,$$

and

$$C_a := \frac{\mu_a(x, \lambda_1)}{\mu_a(x, \lambda_2)} = \text{constant in the } x \text{ variable in } D.$$

Assumptions (13.74) and (13.75) are physically acceptable [142].

Let A_j be the optical absorption density at $\lambda_j, j = 1, 2$. Let l_1', l_2' be two positive constants. Let Φ_j be the solution of

$$\left(\mu_a(x, \lambda_j) - \frac{1}{3} \nabla \cdot \frac{1}{\mu_s(x, \lambda_j)} \nabla \right) \Phi_j(x) = 0, \tag{13.76}$$

with the boundary condition

$$\frac{1}{\mu_s(x, \lambda_j)} \frac{\partial \Phi_j}{\partial \nu}(x) + l_j' \Phi_j(x) = g_j'(x) \quad \text{on } \partial\Omega. \tag{13.77}$$

Note that the boundary condition (13.77) is slightly different from (13.64) because μ_s is assumed variable possibly up to the boundary. Moreover, in order to simplify the derivations below we have neglected μ_a in the denominator of the second term of (13.76).

Multiplying (13.76) for $j = 1$ by Φ_2 and integrating by parts over Ω, we obtain that

$$0 = \int_\Omega \left(\mu_a(x, \lambda_1) - \frac{1}{3} \nabla \cdot \frac{1}{\mu_s(x, \lambda_1)} \nabla \right) \Phi_1(x)\Phi_2(x)dx$$

$$= \int_\Omega \mu_a(x, \lambda_1)\Phi_1\Phi_2 dx - \frac{1}{3} \int_{\partial\Omega} (g_1'\Phi_2 - l_1'\Phi_1\Phi_2) \, d\sigma$$

$$+ \frac{1}{3} \int_\Omega \frac{1}{\mu_s(x, \lambda_1)} \nabla\Phi_1(x) \cdot \nabla\Phi_2(x)dx.$$

We then replace $\mu_s(x, \lambda_1)$ by $C_s \mu_s(x, \lambda_2)$ and integrate by parts further to obtain

$$\frac{1}{3} \int_{\partial\Omega} \left(g_1'\Phi_2 - \frac{1}{C_s}g_2'\Phi_1 \right)(x) \, d\sigma(x) + \frac{1}{3} \int_{\partial\Omega} \left(\frac{l_2'}{C_s} - l_1' \right)\Phi_1(x)\Phi_2(x) \, d\sigma(x)$$

$$= \int_D \left(-\frac{\mu_a(x, \lambda_2)}{C_s} + \mu_a(x, \lambda_1) \right)\Phi_1(x)\Phi_2(x) \, dx.$$

Since $D = z + \delta B$, the following approximation holds:

$$|D|(1+o(1))\left(-\frac{1}{C_s C_a}+1\right)\frac{A_1(z)A_2(z)}{\mu_a(z,\lambda_2)} = \frac{1}{3}\int_{\partial\Omega}\left(g_1'\Phi_2 - \frac{1}{C_s}g_2'\Phi_1\right)d\sigma$$

$$+ \frac{1}{3}\int_{\partial\Omega}\left(\frac{l_2'}{C_s}-l_1'\right)\Phi_1\Phi_2\ d\sigma.$$

$$(13.78)$$

Expansion (13.78) yields approximations of $\mu_a(z,\lambda_2)$ and $\mu_a(z,\lambda_1) = C_a\mu_a(z,\lambda_2)$ from A_1 and A_2 provided that $|D|$ is known. To estimate $|D|$ one can use the following identity

$$\int_D \mu_a(x,\lambda_j)\Phi_j(x)\ dx = \frac{1}{3}\int_{\partial\Omega}\left(g_j' - l_j'\Phi_j\right)d\sigma. \qquad (13.79)$$

13.7 Coherent Interferometry Algorithms

In this chapter, we have been interested in reconstructing initial conditions for the wave equation with constant sound speed in a bounded domain. We have developed a variety of inversion approaches which can be extended to the case of variable but known sound speed and can correct for the effect of attenuation on image reconstructions. However, the situation of interest for medical applications is the case where the sound speed is perturbed by an unknown clutter noise. This means that the speed of sound of the medium is randomly fluctuating around a known value. In this situation, waves undergo partial coherence loss and the designed algorithms assuming a constant sound speed may fail.

Coherent interferometry (CINT) has been considered in Chapter 9. While classical imaging methods (time-reversal, backpropagation, Kirchhoff) back-propagate the recorded signals directly, CINT is an array imaging method that first computes cross-correlations of the recorded signals over appropriately chosen space-frequency windows and then back-propagates the local cross-correlations. It deals well with partial loss of coherence in cluttered environments.

Combining the CINT method for imaging in clutter together with a reconstruction approach by spherical mean Radon inversions, we propose CINT-Radon algorithms for photoacoustic imaging in the presence of random fluctuations of the sound speed. These algorithms provide statistically stable photoacoustic images. A detailed analysis of their stability and resolution from a simple clutter noise model is provided in [37].

Consider the wave equation

$$\begin{cases} \dfrac{\partial^2 p}{\partial t^2}(x,t) - c(x)^2 \Delta p(x,t) = 0, \\ p(x,0) = p_0(x), \qquad \dfrac{\partial p}{\partial t}(x,0) = 0, \end{cases} \qquad (13.80)$$

and assume that the pressure field p is measured at the surface of a domain Ω that contains the support of p_0. We restrict ourselves to the two-dimensional

case and assume that Ω is the unit disk with center at the origin and radius $X_0 = 1$.

We consider that the sound speed c is not perfectly known and that it fluctuates randomly around a known distribution. For simplicity, we consider the model with random fluctuations around a constant that we normalize to one:

$$\frac{1}{c(x)^2} = 1 + \sigma_c \mu\left(\frac{x}{x_c}\right), \tag{13.81}$$

where μ is a zero-mean stationary random process, x_c is the correlation length of the fluctuations of $c(x)$ and σ_c is their standard deviation.

Here and below the Fourier transform, denoted with a hat, is with respect to the time variable.

Let

$$q = \mathcal{B}\mathcal{W}[p], \tag{13.82}$$

where $\mathcal{B}$ and $\mathcal{W}$ are respectively defined by (2.62) and (13.9).

When the sound speed varies as in (13.81), the phases of the measured waves $\hat{p}(\omega, y)$ are shifted with respect to the deterministic, unperturbed phase because of the unknown clutter. When the data are numerically back-propagated in the homogeneous medium with speed of propagation equal to one, the phase terms do not compensate each other, which results in instability and loss of resolution. To correct this effect, the idea is to back-propagate the space and frequency correlations between the data:

$$\mathcal{I}_{\mathrm{CI}}(x) = \iint_{\partial\Omega \times \partial\Omega, \, |y_2 - y_1| \leq X_d} d\sigma(y_1) d\sigma(y_2) \iint_{\mathbb{R} \times \mathbb{R}, \, |\omega_2 - \omega_1| \leq \Omega_d} d\omega_1 d\omega_2$$
$$\times \hat{p}(y_1, \omega_1) e^{-i\omega_1 |x - y_1|} \overline{\hat{p}}(y_2, \omega_2) e^{i\omega_2 |x - y_2|}. \tag{13.83}$$

The cut-off parameters Ω_d and X_d play a crucial role. When one writes the CINT function in the time domain:

$$\mathcal{I}_{\mathrm{CI}}(x) = \iint_{\partial\Omega \times \partial\Omega, \, |y_2 - y_1| \leq X_d} d\sigma(y_1) d\sigma(y_2)$$
$$\times \frac{\Omega_d}{\pi} \int_{\mathbb{R}} dt \, \mathrm{sinc}(\Omega_d t) \, p(y_1, |y_1 - x| + t) p(y_2, |y_2 - x| - t),$$

it is clear that it forms the image by computing the local correlation of the recorded data in a time interval scaled by $1/\Omega_d$ and by superposing the back-propagated local correlations over pairs of receivers that are not further apart than X_d. The idea that motivates the form (13.83) of the CINT function is that, at nearby frequencies ω_1, ω_2 and nearby locations y_1, y_2 the random phase shifts of the data $\hat{p}(y_1, \omega_1), \hat{p}(y_2, \omega_2)$ are similar (say, correlated) so they cancel each other in the product $\hat{p}(y_1, \omega_1) \overline{\hat{p}}(y_2, \omega_2)$. We then say that the data $\hat{p}(y_1, \omega_1)$ and $\hat{p}(y_2, \omega_2)$ are coherent. In such a case, the back-propagation of this product in the homogeneous medium should be stable. The purpose of the CINT imaging function is to keep in (13.83) the pairs (y_1, ω_1) and (y_2, ω_2)

for which the data $\hat{p}(y_1, \omega_1)$ and $\hat{p}(y_2, \omega_2)$ are coherent and to remove the pairs that do not bring information. It then appears intuitive that the cut-off parameters X_d, resp. Ω_d, should be of the order of the spatial (resp. frequency) correlation radius of the recorded data, and we will confirm this intuition in the following.

The imaging function $\mathcal{I}_{\mathrm{CI}}$ is quite efficient in localizing point sources in cluttered media but not in finding the true value of p_0. Moreover, when the support of the initial pressure p_0 is extended, $\mathcal{I}_{\mathrm{CI}}$ may fail in recovering a good photoacoustic image. We propose two things. First, in order to avoid numerical oscillatory effects, we replace the sharp cut-offs in the integral by Gaussian convolutions. We know that the CINT function is stable when the cut-off function has a positive Fourier transform. Then instead of taking the correlations between the back-propagated raw data, we pre-process them like we do for the Radon inversion. We thus get the following CINT-Radon imaging function:

$$
\mathcal{I}_{CIR}(x) = \iint_{\partial\Omega\times\partial\Omega} d\sigma(y_1)d\sigma(y_2) \iint_{\mathbb{R}\times\mathbb{R}} d\omega_1 d\omega_2 e^{-\frac{(\omega_2-\omega_1)^2}{2\Omega_d^2}} e^{-\frac{|y_1-y_2|^2}{2X_d^2}}
$$
$$
\times \widehat{q}(y_1, \omega_1) e^{-i\omega_1|x-y_1|} \overline{\widehat{q}}(y_2, \omega_2) e^{i\omega_2|x-y_2|},
$$
$$(13.84)$$

where q is given by (13.82).

The purpose of the CINT-Radon imaging function $\mathcal{I}_{CIR}$ is to keep in (13.84) the pairs (y_1, ω_1) and (y_2, ω_2) for which the pre-processed data $\hat{q}(y_1, \omega_1)$ and $\hat{q}(y_2, \omega_2)$ are coherent and to remove the pairs that do not bring information.

Using the exact inversion formula (2.53) for the spherical mean Radon transform, the CINT-Radon algorithm can be generalized to the three-dimensional case provided that the measurements are taken on a sphere $\partial\Omega$.

13.8 Concluding Remarks

In this chapter, we have described imaging models that relate the measured photoacoustic wavefields to the sought-after absorption distribution. We have also provided methods that can compensate for boundary conditions, an object's frequency-dependent acoustic attenuation, and heterogeneous speed of sound distribution. Image reconstructions by use of algorithms that ignore this can contain artifacts and distortions.

14

Quantitative Thermoacoustic Imaging

14.1 Introduction

The aim of this chapter is to investigate quantitative thermoacoustic imaging. Given several data sets, we establish an analytical formula for reconstructing the absorption coefficient from thermal energy measurements. Since the formula involves derivatives of the given data up to the third order, it is unstable in the sense that small measurement noises may cause large errors. However, in the presence of measurement noise, the obtained formula, together with a regularization technique, provides a good initial guess for the true absorption coefficient. An optimal control problem can be used to solve the quantitative thermoacoustic imaging problem.

To describe the quantitative thermoacoustic approach, we employ several notations. Let Ω be a smooth bounded domain in $\mathbb{R}^d$, $d = 2$ or 3. Let $\partial\Omega$ denote the boundary of Ω and let ν be the outward normal at $\partial\Omega$.

Let u^k be the solution of

$$\begin{cases} \Delta u^k + (k^2 + ikq)u^k = 0 & \text{in } \Omega\,, \\ u^k = g & \text{on } \partial\Omega\,. \end{cases} \tag{14.1}$$

The thermoacoustic imaging problem can be formulated as the inverse problem of reconstructing the absorption coefficient q from thermoacoustic measurements $q|u^k|^2$ in Ω for $k \in (\underline{k}, \overline{k})$. The quantity $q|u^k|^2$ in Ω is the heat energy due to the absorption distribution q. It generates an acoustic wave propagating inside the medium. Finding the initial data in the acoustic wave from boundary measurements yields the heat energy distribution. Our aim in this chapter is to separate q from u^k. We provide an explicit formula for reconstructing q from the heat energy $q|u^k|^2$ in Ω. The formula can be used as an initial guess to achieve a resolved image of the absorption distribution in a robust way. Our results in this chapter are from [51].

14.2 Measurements

We first describe a polarization procedure to obtain more data.

Proposition 14.1 *Let $g_1, g_2 \in L^2(\partial\Omega)$. For $j = 1, 2$, and $k \in (\underline{k}, \overline{k})$, let u_j^k be the solution of*

$$\begin{cases} \Delta u_j^k + (k^2 + ikq)u_j^k = 0 & in \ \Omega, \\ u_j^k = g_j & on \ \partial\Omega. \end{cases} \tag{14.2}$$

The function $E_2^k(x) = q(x)u_2^k(x)\overline{u_1^k(x)}, x \in \Omega$ can be evaluated from the knowledge of the data

$$q|u_1^k + u_2^k|^2 \ and \ q|iu_1^k + u_2^k|^2,$$

which correspond to the use of respectively $g = g_1 + g_2$ and $g = ig_1 + g_2$ in (14.1).

Proof. It is easy to see that the data E_2^k is given by

$$E_2^k = \frac{1}{2}(q|u_1^k + u_2^k|^2 - q|u_1^k|^2 - q|u_2^k|^2) + \frac{i}{2}(q|iu_1^k + u_2^k|^2 - q|u_1^k|^2 - q|u_2^k|^2), \tag{14.3}$$

which yields the desired result. □

Let

$$(g_j)_{j=1}^{d+1} = (1, x_1, \ldots, x_d) \tag{14.4}$$

and u_j^k be the solution of (14.1) with g replaced with g_j, $j = 1, \ldots, d+1$. Due to Proposition 14.1, we are able to measure the following (polarized) data

$$\mathcal{E}^k = (E_j^k)_{j=1}^{d+1} = (qu_j^k\overline{u}_1^k)_{j=1}^{d+1} \quad \text{for all } k \in (\underline{k}, \overline{k}). \tag{14.5}$$

We will also need some property of the measured data above.

Proposition 14.2 *Assume that q is compactly supported in Ω and denote by Ω' its support. There exist $N > 1$ pairwise disjoint open subsets $B_1, B_2, \ldots, B_N$ of Ω, and N frequencies $k_1, \ldots, k_N \in (\underline{k}, \overline{k})$ such that $\overline{\Omega'} \subset \cup_{j=1}^N \overline{B}_j \subset \Omega$ and, for any $n = 1, \ldots, N$,*

(i) $|u_1^{k_n}| > 0$ in B_n;
(ii) The matrix $[u_j^{k_n}, \nabla u_j^{k_n}]_{1 \leq j \leq d+1}$ is invertible for all $x \in B_n$.

Proof. Fix an arbitrary point $z \in \Omega$, assume that $u_1^k(z) = 0$ for all $k \in (\underline{k}, \overline{k})$. Since $k \mapsto u_1^k(z)$ is analytic, $u_1^k(z) = 0$ for all $k \in \mathbb{R}$ and in particular $u_1^0(z) = 0$. However, it is easy to solve (14.1) with $k = 0$ and $g = 1$ to get $u_1^0(z) = 1$. We can conclude that for all $z \in \Omega$, there is $k_z \in (\underline{k}, \overline{k})$ such that $u_1^{k_z}(z)$ does not vanish. By the continuity of $u_1^{k_z}$, $|u_1^{k_z}| > 0$ in B_z, a small neighborhood of z in Ω. Since $\overline{\Omega}$ is compact, we can extract $B_1, \ldots, B_N$ from $\{B_z : z \in \Omega\}$ so that $\overline{B}_1, \ldots, \overline{B}_N$ cover $\overline{\Omega}$, and hence (i) holds. Item (ii) can be proved similarly using the differentiability of the determinant. □

Definition 14.3 *The set $(g_j)_{j=1}^{d+1} \subset L^2(\partial\Omega)$ is a proper set of measurements for (14.1) on an interval $(\underline{k}, \overline{k})$ if and only if the corresponding (u_j^k), $j = 1, \ldots, d+1$, $k \in (\underline{k}, \overline{k})$ satisfy the assertion of Proposition 14.2.*

14.3 Exact Formula

The aim of this section is to reconstruct q when a proper set of measurements $(g_j)_{j=1}^{d+1}$, as the one in (14.4) is used, and the data $\mathcal{E}^k$, defined in (14.5), are given.

Recall $N, k_1, \ldots, k_N, B_1, \ldots, B_N$ as in Proposition 14.2. Fix $n \in \{1, \ldots, N\}$. Let

$$\alpha_j^{k_l} = \frac{E_j^{k_l}}{E_1^{k_l}}, \quad 2 \leq j \leq d+1, \quad 1 \leq l \leq N \tag{14.6}$$

in B_n. Then it is not hard to see that

$$u_j^{k_l} = \alpha_j^{k_l} u_1^{k_l},$$

for $2 \leq j \leq d+1$ and $1 \leq l \leq N$. We have the following lemma.

Lemma 14.4 *Let $\beta^{k_l} = \Im(\overline{u}_1^{k_l} \nabla u_1^{k_l})$. Then*

$$-\nabla \cdot \beta^{k_l} = k_l E_1^{k_l} \quad in \ B_n. \tag{14.7}$$

Proof. Let $\varphi \in \mathcal{C}_c^\infty(B_n, \mathbb{R})$ be an arbitrary function. Then using $\varphi u_1 \in W_0^{1,2}(B_n)$ as a test function in

$$-\Delta u_1^{k_l} = (k_l^2 + ik_l q) u_1^{k_l}$$

yields

$$\int_\Omega \varphi |\nabla u_1^{k_l}|^2 dx + \int_\Omega \overline{u_1^{k_l}} \nabla u_1^{k_l} \cdot \nabla \varphi dx = \int_\Omega (k_l^2 + ik_l q) |u_1^{k_l}|^2 \varphi dx.$$

Taking the imaginary part of the equation above gives

$$-\int_\Omega \nabla \cdot (\Im \overline{u_1^{k_l}} \nabla u_1^{k_l}) \varphi dx = \int_\Omega k_l q |u_1^{k_l}|^2 \varphi dx = \int_\Omega k_l E_1^{k_l} \varphi dx,$$

and (14.7) follows. $\square$

The following lemma plays an important role in the derivation of an exact inversion formula for q.

Lemma 14.5 *For all $2 \leq j \leq d+1$ and $1 \leq l \leq N$,*

$$\nabla \alpha_j^{k_l} \cdot \left(\nabla \log \frac{q}{E_1^{k_l}} - \frac{2iq\beta^{k_l}}{E_1^{k_l}} \right) = \Delta \alpha_j^{k_l} \tag{14.8}$$

in B_n.

Proof. Let us fix $j \in \{2, \ldots, d+1\}$. Since $u_j^{k_l}$ is a solution of the Helmholtz equation under consideration,

$$
\begin{aligned}
(k_l^2 + ik_l q)\alpha_j^{k_l} u_1^{k_l} &= -\Delta\big(\alpha_j^{k_l} u_1^{k_l}\big) \\
&= -\alpha_j^{k_l}\Delta u_1 - u_1 \Delta\alpha_j^{k_l} - 2\nabla u_1^{k_l}\cdot\nabla\alpha_j^{k_l} \\
&= (k_l^2 + ikq)\alpha_j^{k_l} u_1^{k_l} - u_1^{k_l}\Delta\alpha_j^{k_l} - 2\nabla u_1^{k_l}\cdot\nabla\alpha_j^{k_l}.
\end{aligned}
$$

Therefore,

$$
\begin{aligned}
-E_1^{k_l}\Delta\alpha_j^{k_l} &= 2q\overline{u_1^{k_l}}\nabla u_1^{k_l}\cdot\nabla\alpha_j^{k_l} \\
&= 2q\left(\Re\overline{u_1^{k_l}}\nabla u_1^{k_l} + i\Im\overline{u_1^{k_l}}\nabla u_1^{k_l}\right)\cdot\nabla\alpha_j^{k_l} \\
&= q\left(\nabla|u_1^{k_l}|^2 + 2i\Im\overline{u_1^{k_l}}\nabla u_1^{k_l}\right)\cdot\nabla\alpha_j^{k_l}.
\end{aligned}
$$

We have proved that

$$
-E_1^{k_l}\Delta\alpha_j^{k_l} = q\left(\nabla|u_1^{k_l}|^2 + 2i\beta^{k_l}\right)\cdot\nabla\alpha_j^{k_l},
$$

or equivalently,

$$
q\nabla|u_1^{k_l}|^2\cdot\nabla\alpha_j^{k_l} = -E_1^{k_l}\Delta\alpha_j^{k_l} - 2iq\beta^{k_l}\cdot\nabla\alpha_j^{k_l}. \tag{14.9}
$$

On the other hand, differentiating the equation $E_1^{k_l} = q|u_1^{k_l}|^2$ gives

$$
\nabla E_1^{k_l} = q\nabla|u_1^{k_l}|^2 + E_1^{k_l}\nabla\log q.
$$

This, together with (14.9), implies

$$
(\nabla E_1^{k_l} - E_1^{k_l}\nabla\log q)\cdot\nabla\alpha_j^{k_l} = -E_1^{k_l}\Delta\alpha_j^{k_l} - 2iq\beta^{k_l}\cdot\nabla\alpha_j^{k_l},
$$

and (14.8), therefore, holds.   □

We claim that the set

$$
\{\nabla\alpha_j^{k_l}\}_{2\leq j\leq d+1}
$$

is linearly independent for all $x \in \overline{\Omega}$, where $\alpha_j^{k_l}$ was defined in (14.6). We only prove this when $d = 2$. The proof when d is larger than 2 can be done in the same manner. In fact, the linear independence of $\{\nabla\alpha_2^{k_l}, \nabla\alpha_3^{k_l}\}$ comes from the following calculation:

$$\det\begin{bmatrix}\nabla\alpha_2^{k_l}\\\nabla\alpha_3^{k_l}\end{bmatrix}=\frac{1}{(u_1^{k_l})^4}\det\begin{bmatrix}u_1^{k_l}\nabla u_2^{k_l}-u_2^{k_l}\nabla u_1^{k_l}\\u_1^{k_l}\nabla u_3^{k_l}-u_3^{k_l}\nabla u_1^{k_l}\end{bmatrix}$$

$$=\frac{1}{(u_1^{k_l})^4}\left(\det\begin{bmatrix}u_1^{k_l}\nabla u_2^{k_l}\\u_1^{k_l}\nabla u_3^{k_l}-u_3^{k_l}\nabla u_1^{k_l}\end{bmatrix}\right.$$

$$\left.-u_2^{k_l}\det\begin{bmatrix}\nabla u_1^{k_l}\\u_1^{k_l}\nabla u_3^{k_l}-u_3^{k_l}\nabla u_1^{k_l}\end{bmatrix}\right)$$

$$=\frac{1}{(u_1^{k_l})^3}\left(u_1^{k_l}\det\begin{bmatrix}\nabla u_2^{k_l}\\\nabla u_3^{k_l}\end{bmatrix}+u_3^{k_l}\det\begin{bmatrix}\nabla u_1^{k_l}\\\nabla u_2^{k_l}\end{bmatrix}\right.$$

$$\left.-u_2^{k_l}\det\begin{bmatrix}\nabla u_1^{k_l}\\\nabla u_3^{k_l}\end{bmatrix}\right)$$

$$=\frac{1}{(u_1^{k_l})^3}\det\begin{bmatrix}u_1^{k_l}&\nabla u_1^{k_l}\\u_2^{k_l}&\nabla u_2^{k_l}\\u_3^{k_l}&\nabla u_3^{k_l}\end{bmatrix}\neq0\,.$$

Here, part (ii) in Proposition 14.2 has been used. Since the $d\times d$ matrix

$$A^{k_l}=[\nabla\alpha_{j+1}^{k_l}]_{1\leq j\leq d}\tag{14.10}$$

is invertible in B_n, we can solve system (14.8) to get

$$\nabla\log\frac{q}{E_1^{k_l}}-\frac{2iq\beta^{k_l}}{E_1^{k_l}}=a^{k_l}\,,\tag{14.11}$$

where a^{k_l} is the vector $(A^{k_l*}A^{k_l})^{-1}[A^{k_l*}(\nabla\cdot A^{k_l})]$.

We are now ready to evaluate q. We first split the real and the imaginary parts of (14.11) to get

$$\nabla\log\frac{q}{E_1^{k_l}}=\frac{\nabla q}{q}-\nabla\log E_1^{k_l}=\Re(a^{k_l})\tag{14.12}$$

and

$$\beta^{k_l}=-\frac{E_1^{k_l}\Im(a^{k_l})}{2q}\,.\tag{14.13}$$

Then, differentiating (14.13), we have

$$\nabla\cdot\beta^{k_l}=\frac{E_1^{k_l}\Im(a^{k_l})\cdot\nabla q}{2q^2}-\frac{\nabla\cdot(E_1^{k_l}\Im(a^{k_l}))}{2q}\,.$$

This, together with (14.7) and (14.12), implies

$$q=-\frac{E_1^{k_l}(\Re(a^{k_l})+\nabla\log E_1^{k_l})\cdot\Im(a^{k_l})-\nabla\cdot(E_1^{k_l}\Im(a^{k_l}))}{2k_lE_1^{k_l}}$$

$$=-\frac{E_1^{k_l}\Re(a^{k_l})\cdot\Im(a^{k_l})+\nabla E_1^{k_l}\cdot\Im(a^{k_l})}{2k_lE_1^{k_l}}+\frac{E_1\nabla\cdot\Im(a^{k_l})+\nabla E_1^{k_l}\cdot\Im(a)}{2k_lE_1^{k_l}}$$

$$=-\frac{\Re(a^{k_l})\cdot\Im(a^{k_l})-\nabla\cdot\Im(a^{k_l})}{2k_l}\,.$$

The results above are summarized in the following theorem.

Theorem 14.6 *Let A^k be defined as*

$$A^k = [\nabla \alpha_{j+1}^k]_{j=1}^d \,,$$

where

$$\alpha_j^k = \frac{E_j^k}{E_1^k}$$

and the data $(E_j)_{j=1}^{d+1}$ is given by the proper set of measurements $\{1, x_1, \ldots, x_d\}$. We have

$$q(x) = \frac{-\Re(a^k) \cdot \Im(a^k) + \nabla \cdot \Im(a^k)}{2k} \,, \tag{14.14}$$

where

$$a^k = ((A^k)^* A^k)^{-1}[(A^k)^* \nabla \cdot A^k] \,. \tag{14.15}$$

Remark 14.7 *In practice, the vector a^k in (14.15) can be found as the least square solution of*

$$\min \int_\Omega \left| A^{k*} A^k a^k - A^{k*} \nabla \cdot A^k \right|^2 dx$$

and q is given by

$$q = \frac{1}{\overline{k} - \underline{k}} \int_{\underline{k}}^{\overline{k}} \frac{-\Re(a^k) \cdot \Im(a^k) + \nabla \cdot \Im(a^k)}{2k} dk \,. \tag{14.16}$$

Remark 14.8 *Formula (14.16) is unstable in the sense that if there are some noises occurring when we measure the data E_j^k, $1 \le j \le d+1$, then q, given by (14.16), might be far away from the actual q since the right-hand side of (14.16) depends on the derivatives of the noise (up to the third order).*

14.4 Optimal Control Approach

Due to Remark 14.8, we need to correct the errors caused from noises in measurements to obtain the actual q. To do so, we minimize

$$J[q] = \frac{1}{2} \int_{\underline{k}}^{\overline{k}} \int_\Omega \left| q|u^k|^2 - E^k \right|^2 dx dk \tag{14.17}$$

with the initial guess q_I given by (14.16). Here, u^k is the solution of (14.1) when $g = 1$.

14.4.1 The Differentiability of the Data Map and Its Inverse

Let $0 < \underline{q} < \overline{q}$. Let

$$L^\infty_+(\Omega) = \left\{ p \in L^\infty(\Omega) : \underline{q} < p < \overline{q} \text{ in } \Omega \right\} .$$

Then, $L^\infty_+(\Omega)$ is an open set in $L^\infty(\Omega)$.

Fix $k \in (\underline{k}, \overline{k})$. We define the solution and the data map as

$$\begin{aligned} u^k : L^\infty_+(\Omega) &\to W^{1,2}(\Omega) \\ q &\mapsto u^k[q] \end{aligned} \tag{14.18}$$

and

$$\begin{aligned} F^k : L^\infty_+(\Omega) &\to L^2(\Omega) \\ q &\mapsto F^k[q] = q|u^k[q]|^2 \, , \end{aligned} \tag{14.19}$$

where $u^k[q]$ is the solution of

$$\begin{cases} \Delta u^k + (k^2 + ikq)u^k = 0 & \text{in } \Omega \, , \\ u^k = 1 & \text{on } \partial\Omega \, . \end{cases} \tag{14.20}$$

The map F^k is well-defined because of regularity results guaranteeing $u^k \in \mathcal{C}^1(\overline{\Omega})$.

The main purpose of this subsection is to study the derivative operator of F^k.

Lemma 14.9 *For any $k > 0$, the map u^k, defined in (14.18), is Fréchet differentiable in $L^\infty_+(\Omega)$. Its derivative at the function q is given by*

$$du^k[q](\rho) = v^k(\rho), \quad \forall \rho \in B_q \, , \tag{14.21}$$

where $B_q \subset L^\infty_+(\Omega)$ is an open neighborhood of 0 (that depends on q) in $L^\infty(\Omega)$ and $v^k(\rho)$ is the solution of

$$\begin{cases} \Delta v^k + (k^2 + ikq)v^k = -ik\rho u^k[q] & \text{in } \Omega \, , \\ v^k = 0 & \text{on } \partial\Omega \, . \end{cases} \tag{14.22}$$

In addition,

(i) F^k is also Fréchet differentiable and

$$dF^k[q](\rho) = \rho|u^k[q]|^2 + 2q\Re(u^k[q]\overline{v}^k(\rho)), \quad \forall q \in L^\infty_+(\Omega), \rho \in B_q \, . \tag{14.23}$$

(ii) The dual of dF^k, dF^{k*}, is given by

$$(\rho, dF^{k*}[q](h)) = \Re \int_\Omega \left(q|u^k[q]|^2 h + iku^k[q]\overline{p}^k(h) \right) \rho dx \, , \tag{14.24}$$

where $p^k(h)$ is the solution of

$$\begin{cases} \Delta p^k + (k^2 + ikq)p^k = 2qu^k[q]h \; in \; \Omega \,, \\ \qquad\qquad\qquad\quad p^k = 0 \qquad\quad on \; \partial\Omega \,. \end{cases}$$

(14.25)

(iii) There exists $c > 0$ such that for all $\rho \in L^2(\Omega)$

$$\int_{\underline{k}}^{\overline{k}} \|dF^k[q](\rho)\|_{L^2(\Omega)} dk \geq c\|\rho\|_{L^2(\Omega)} \,.$$

(14.26)

Proof. It is sufficient to show that

$$\lim_{\|\rho\|_{L^\infty(\Omega)} \to 0} h(\rho) = 0 \,,$$

(14.27)

where

$$h(\rho) = \frac{\|u^k[q+\rho] - u^k[q] - v^k(\rho)\|_{L^2(\Omega)}}{\|\rho\|_{L^\infty(\Omega)}} \,.$$

In fact, since $u^k[q+\rho] - u^k[q] - v^k(\rho)$ solves the problem

$$\begin{cases} (\Delta + k^2 + ikq)(u^k[q+\rho] - u^k[q] - v^k(\rho)) = -ik\rho(u^k[q+\rho] - u^k[q]) \; in \; \Omega \,, \\ \qquad\qquad u^k[q+\rho] - u^k[q] - v^k(\rho) = 0 \qquad\qquad\qquad\qquad on \; \partial\Omega \,, \end{cases}$$

we can obtain

$$\|u^k[q+\rho] - u^k[q] - v^k(\rho)\|_{L^2(\Omega)} \leq \frac{\|\rho\|_{L^\infty(\Omega)}\|(u^k[q+\rho] - u^k[q])\|_{L^2(\Omega)}}{\inf q} \,.$$

(14.28)

On the other hand, since $u^k[q+\rho] - u^k[q]$ satisfies

$$\begin{cases} \Delta(u^k[q+\rho] - u^k[q]) + (k^2 + ik(q+\rho))(u^k[q+\rho] - u^k[q]) = -ik\rho u^k[q] \; in \; \Omega \,, \\ \qquad\qquad\qquad\qquad\qquad u^k[q+\rho] - u^k[q] = 0 \qquad\qquad on \; \partial\Omega \,, \end{cases}$$

we have

$$\|u^k[q+\rho] - u^k[q]\|_{L^2(\Omega)} \leq \frac{\|\rho\|_{L^\infty(\Omega)}\|u^k[q]\|_{L^2(\Omega)}}{\inf(q+\rho)} \,.$$

(14.29)

Combining (14.28) and (14.29) yields (14.27). Using the chain rule in differentiation, we readily get (14.23). Formula (14.24) can be obtained by integration by parts.

We next prove the last part of the lemma. Since $dF^k[q]$ takes the form $|u^k[q]|^2(I + \text{compact})$, it is sufficient to prove that

$$\cap_{k \in (\underline{k}, \overline{k})} \text{Ker} dF^k[q] = \{0\}$$

and then apply the Fredholm alternative. Assume there exists $\rho \in L^2(\Omega) \setminus \{0\}$ such that

$$dF^k[q](\rho) = 0$$

for all $k \in (\underline{k}, \overline{k})$. By analyticity, it follows that $dF^0[q](\rho) = 0$. This is not a true fact because $v^0(\rho) = 0$ and $u^0[q] = 1$. $\square$

Using regularity theory, we see that $u^k[q]$ belongs to $L^\infty(\Omega)$. Hence, $dF^k[q]$ can be extended so that its domain is $L^2(\Omega)$. By abuse of notation, we denote the extended operator still by $dF^k[q]$.

14.4.2 Landweber's Iteration

Lemma 14.10 *The map J defined in (14.17) is Fréchet differentiable in q. Moreover, for all $q \in L_+^\infty(\Omega)$,*

$$dJ[q](\rho) = \int_{\underline{k}}^{\overline{k}} \int_\Omega \rho \left(|u^k[q]|^2 (q|u^k|^2 - E^k) + \Re i k p^k \overline{u}^k[q] \right) dx dk, \qquad (14.30)$$

where p^k is the solution of (14.25) with $h = (q|u^k|^2 - E^k)$.

Now we can apply the gradient descent method to minimize J and arrive at the iteration

$$q^{(n+1)} = Tq^{(n)} - \eta dJ[Tq^{(n)}], \qquad (14.31)$$

where $\eta > 0$ is the step size,

$$Tf = \max\{\underline{q}, \min\{\overline{q}, f\}\}. \qquad (14.32)$$

Here, $dJ[Tq^{(n)}]$ is computed using (14.30). Moreover, the presence of T in (14.31) improves the rate of convergence because $Tq^{(n)}$ is closer to the true coefficient q_* than $q^{(n)}$ and is necessary because $J[q^{(n)}]$ might not be well-defined. Using (14.24) we can show that this optimal control problem is nothing else than the Landweber scheme:

$$q^{(n+1)} = Tq^{(n)} - \eta \int_{\underline{\omega}}^{\overline{\omega}} \left[dF^*[Tq^{(n)}] \left(F^k(Tq^{(n)}) - E^k \right) \right] dk.$$

Using (14.26) it follows that there exists $\eta > 0$ sufficiently small such that the Landweber scheme or equivalently the optimal control approach converges to q_*.

15

Ultrasonically-Induced Lorentz Force Electrical Impedance Tomography

15.1 Introduction

In ultrasonically-induced Lorentz force method (experimental apparatus presented in Figure 15.1) an ultrasound pulse propagates through the medium to be imaged in the presence of a static magnetic field. The ultrasonic wave induces Lorentz' force on ions in the medium, causing the negatively and positively charged ions to separate. This separation of charges acts as a source of electrical current and potential. Measurements of the induced current give information on the conductivity in the medium. A 1 *Tesla* magnetic field and a 1 *MPa* ultrasonic pulse induce current at the *nanoampere* scale. Stronger magnetic fields and ultrasonic beams can be used to enhance the signal-to-noise ratio.

   This chapter provides a rigorous mathematical and numerical framework for ultrasonically-induced Lorentz force electrical impedance tomography. Ultrasonic vibration of a tissue in the presence of a static magnetic field induces an electrical current by the Lorentz force. This current can be detected by electrodes placed around the tissue; it is proportional to the velocity of the ultrasonic pulse, but depends nonlinearly on the conductivity distribution. The imaging problem is to reconstruct the conductivity distribution from measurements of the induced current. To solve this nonlinear inverse problem, we first make use of a virtual potential to relate explicitly the current measurements to the conductivity distribution and the velocity of the ultrasonic pulse. Then, by applying a Wiener filter to the measured data, we reduce the problem to imaging the conductivity from an internal electric current density. We first introduce an optimal control method for solving such a problem. A direct reconstruction scheme involving a partial differential equation is then proposed based on viscosity-type regularization to a transport equation satisfied by the current density field. We prove that solving such an equation yields the true conductivity distribution as the regularization parameter approaches zero. We also test both schemes numerically in the presence of measurement noise, quantify their stability and resolution, and compare their performance.

The chapter is organized as follows. We start by describing a model for the electrical conductivity in electrolytic media. From this model we derive the current density induced by an ultrasonic pulse in the presence of a static magnetic field. We then find an expression of the measured current. The inverse problem is to image the conductivity distribution from such measurements corresponding to different pulse sources and directions. A virtual potential used with simple integrations by parts can relate the measured current to the conductivity distribution and the velocity of the ultrasonic pulse. A Wiener deconvolution filter can then reduce the problem to imaging the conductivity from the internal electric current density. The internal electric current density corresponds to that which would be induced by a constant voltage difference between one electrode and another with zero potential. We introduce two reconstruction schemes for solving the imaging problem from the internal data. The first is an optimal control method; we also propose an alternative to this scheme via the use of a transport equation satisfied by the internal current density. The second algorithm is direct and can be viewed as a PDE-based reconstruction scheme. We prove that solving such a PDE yields to the true conductivity distribution as the regularization parameter tends to zero. In doing so, we prove the existence of the characteristic lines for the transport equation under some conditions on the conductivity distribution. We finally test numerically the two proposed schemes in the presence of measurement noise, and also quantify their stability and resolution. Our results in this chapter are from [60].
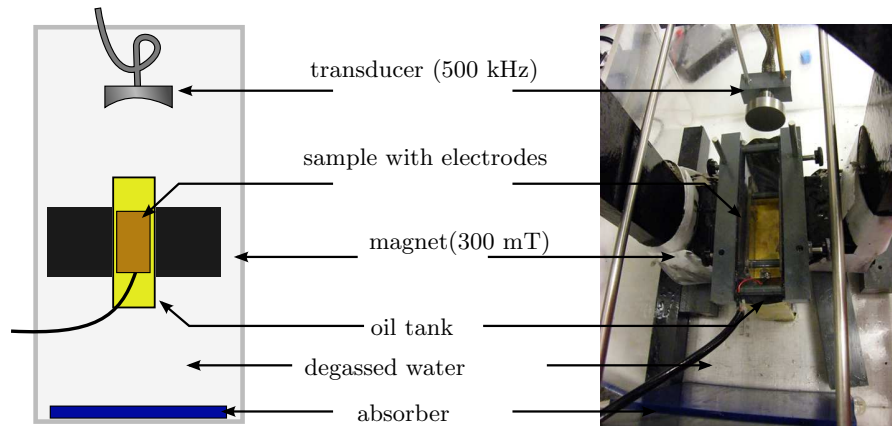
Fig. 15.1. Example of the imaging device. The transducer is emitting ultrasound in a sample placed in a constant magnetic field. An induced electrical current is collected by two electrodes.

15.2 Electric Measurements From Acousto-Magnetic Coupling

Let a physical object to be imaged occupy a three-dimensional domain Ω with a smooth boundary $\partial\Omega$. Assume that this body is placed in a constant magnetic field B in the direction e_3 where $\{e_1, e_2, e_3\}$ denotes the standard orthonormal basis of $\mathbb{R}^3$. We are interested in recovering the electrical conductivity of this body $\sigma \in L^\infty(\Omega)$ with the known lower and upper bounds:

$$0 < \underline{\sigma} \leq \sigma \leq \overline{\sigma} < \infty\,.$$

An acoustic transducer sends a short acoustic pulse from $y \in \mathbb{R}^3$ in the direction $\xi \in S$, with S being the unit sphere, such that $\xi \cdot e_3 = 0$. This pulse generates the velocity field $v(x,t)\xi$ with $v(x,t)$ taking the following form:

$$v(x,t) = w(z - ct)\ A(z, |r|), \tag{15.1}$$

where

$$z = (x - y) \cdot \xi \quad \text{and} \quad r = x - y - z\xi\ \in \Upsilon_\xi := \{\zeta \in \mathbb{R}^3\ :\ \zeta \cdot \xi = 0\}\,. \tag{15.2}$$

Here, $w \in \mathcal{C}_c^\infty(\mathbb{R})$, supported in $(-\eta, 0)$, is the ultrasonic pulse profile; $A \in \mathcal{C}^\infty(\mathbb{R} \times \mathbb{R}^+)$, supported in $\mathbb{R}^+ \times [0, R]$, is the cylindrical profile distribution of the wave corresponding to the focus of the acoustic transducer; and R is the maximal radius of the acoustic beam.

15.2.1 Electrical Conductivity in Electrolytes

We describe here the electrical behavior of the medium as an electrolytic tissue composed of ions capable of motion in an aqueous tissue. We consider k types of ions in the medium with charges of q_i, $i \in \{1, \ldots, k\}$. The corresponding volumetric density n_i is assumed to be constant. Neutrality in the medium is described as

$$\sum_i q_i n_i = 0\,. \tag{15.3}$$

Kohlrausch's law [86] defines the conductivity of such a medium as a linear combination of the ionic concentrations

$$\sigma = e^+ \sum_i \mu_i q_i n_i, \tag{15.4}$$

where e^+ is the elementary charge, and the coefficients μ_i denote the ionic mobility of each ion i.

15.2.2 Ion Deviation by Lorentz Force

We embed the medium in a constant magnetic field with direction e_3, Be_3, and perturb it mechanically using the short, focused, ultrasonic pulses v defined in (15.1). The motion of the charged particle i inside the medium is deviated by the Lorentz force

$$F_i = q_i v B \xi \times e_3 \,. \qquad (15.5)$$

This force accelerates the ion in the orthogonal direction

$$\tau(\xi) = \xi \times e_3 \,. \qquad (15.6)$$

Then, almost immediately, the ion reaches a constant speed given by

$$v_{\tau,i} = \mu_i B v$$

at the first order. Finally, the ion i has a total velocity

$$v_i = v\xi + \mu_i B v \tau \,.$$

The current density generated by the displacement of charges can be described as follows:

$$j_S = \sum_i n_i q_i v_i = \left(\sum_i n_i q_i \right) v\xi + \left(\sum_i n_i \mu_i q_i \right) B v \tau \,.$$

Using the neutrality condition (15.3) and the definition of σ in (15.4), we get the following simple formula for j_S:

$$j_S = \frac{1}{e^+} B \sigma v \tau \,. \qquad (15.7)$$

This electrolytic description of the tissue characterizes the interaction between the ultrasonic pulse and the magnetic field through a small deviation of the charged particles embedded in the tissue. This deviation generates a current density j_S orthogonal to ξ and to B, locally supported inside the domain. At a fixed time t, j_S is supported in the support of $x \mapsto v(x,t)$. This current is proportional to σ, and is the source of the current that we measure on the electrodes placed at $\partial\Omega$. In the next section, a formal link is substantiated between j_S and the measured current I.

15.2.3 Internal Electrical Potential

Because the characteristic time of the acoustic propagation is very long compared with the electromagnetic wave propagation characteristic time, we can adopt the electrostatic frame. Consequently, the total current j in Ω at a fixed time t can be formulated as

$$j(x,t) = j_S(x,t) + \sigma(x)\nabla_x u(x,t) \,, \qquad (15.8)$$

where u is the electrical potential. It satisfies

$$\nabla_x \cdot (j_S(x,t) + \sigma(x)\nabla_x u(x,t)) = \nabla \cdot j(x,t) = 0 \,. \qquad (15.9)$$

Figure 15.2 shows the configuration under consideration. Let Γ_1 and Γ_2 be portions of the boundary $\partial\Omega$ where two planar electrodes are placed. Denote $\Gamma_0 = \partial\Omega \setminus (\Gamma_1 \cup \Gamma_2)$.
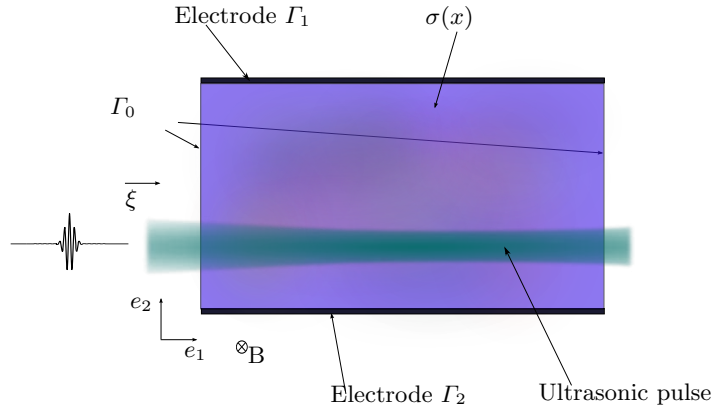
Fig. 15.2. Imaging system configuration. An ultrasonic wave propagates in a medium of electrical conductivity σ comprised between electrodes Γ_1 and Γ_2.

As we measure the current between the two electrodes Γ_1 and Γ_2, the electrical potential is the same on both electrodes, and can be fixed to zero without loss of generality. Further, it is assumed that no current can leave from Γ_0. The potential $u(\cdot, t)$ can then be defined as the unique solution in $W^{1,2}(\Omega)$ of the elliptic system

$$\begin{cases} -\nabla_x \cdot (\sigma(x)\nabla_x u(x,t)) = \nabla_x \cdot j_S(x,t) & \text{in } \Omega \,, \\[2mm] u(x,t) = 0 & \text{on } \Gamma_1 \cup \Gamma_2 \,, \\[2mm] \dfrac{\partial u}{\partial \nu}(x,t) = 0 & \text{on } \Gamma_0 \,. \end{cases} \qquad (15.10)$$

Note that the source term j_S depends on the time $t > 0$, the longitudinal axis $\xi \in S$ and the profile of the acoustic pulse. The electrical potential u also depends on these variables.

The measurable intensity I is the current flow through the electrodes. Integrating (15.10) by parts gives

$$\int_{\Gamma_1} \sigma \frac{\partial u}{\partial \nu} + \int_{\Gamma_2} \sigma \frac{\partial u}{\partial \nu} = 0\,,$$

which is the expression of current flow conservation. We define the intensity I by

$$I(t) = \int_{\Gamma_2} \sigma(x) \frac{\partial u}{\partial \nu}(x,t)\, ds(x)\,. \tag{15.11}$$

15.2.4 Virtual Potential

In order to link I to σ, we introduce a virtual potential $U \in W^{1,2}(\Omega)$ defined as the unique solution of

$$\begin{cases} -\nabla \cdot (\sigma \nabla U) = 0 & \text{in } \Omega\,, \\ \qquad\qquad U = 0 & \text{on } \Gamma_1\,, \\ \qquad\qquad U = 1 & \text{on } \Gamma_2\,, \\ \qquad \dfrac{\partial U}{\partial \nu} = 0 & \text{on } \Gamma_0\,. \end{cases} \tag{15.12}$$

Then we multiply (15.10) by U and integrate by parts. Assuming that the support of v does not intersect the electrodes Γ_1 and Γ_2, we obtain

$$-\int_{\Omega} \sigma \nabla u \cdot \nabla U + \int_{\Gamma_2} \sigma \frac{\partial u}{\partial \nu} = \int_{\Omega} j_S \cdot \nabla U\,.$$

From the property of U in (15.12) and the definition of I in (15.11), the above identity becomes

$$I = \int_{\Omega} j_S \cdot \nabla U\,.$$

The above identity links the measured intensity I to an internal information of σ using the expression of j_S in (15.7):

$$I = \frac{B}{e^+} \int_{\Omega} v(x,t)\sigma(x)\nabla U(x)dx \cdot \tau\,.$$

According to (15.1), v depends on y, ξ, and t, so does I. We define the measurement function as

$$M(y,\xi,z) = \int_{\Omega} v(x,z/c)\sigma(x)\nabla U(x)dx \cdot \tau(\xi) \tag{15.13}$$

for any $y \in \mathbb{R}^3$, $\xi \in S$ and $z > 0$. We assume the knowledge of this function in a certain subset of $\mathbb{R}^3 \times S \times \mathbb{R}^+$ denoted by $Y \times \mathfrak{S} \times (0, z_{max})$. We will discuss later the assumptions we have to impose on this subset in order to make the reconstruction accurate and stable.

15.3 Construction of the Virtual Current

For simplicity, let us restrict ourselves to the two dimensional case where both the conductivity σ and the virtual potential U do not change in e_3-direction. For convenience, the same notations will be used as in the three dimensional case.

In order to obtain the information of σ contained in M, we need to separate the contribution of the displacement term v from this measurement function. Using the cylindrical symmetry of this integration we write for any $z \in (0, z_{max})$,

$$
\begin{aligned}
M(y, \xi, z) &= \int_{\mathbb{R}} \int_{\Upsilon_\xi} w(z - z')(\sigma \nabla U)(y + z'\xi + r) A(z', |r|) dr dz' \cdot \tau(\xi) \\
&= \int_{\mathbb{R}} w(z - z') \int_{\Upsilon_\xi} (\sigma \nabla U)(y + z'\xi + r) A(z', |r|) dr dz' \cdot \tau(\xi) \\
&= (W \star \Phi_{y, \xi})(z) \cdot \tau(\xi),
\end{aligned}
$$

(15.14)

where Υ_ξ is defined by (15.2), $\tau(\xi)$ by (15.6), $W(z) = w(-z)$, $\star$ denotes the convolution product, and

$$
\Phi_{y, \xi}(z) = \int_{\Upsilon_\xi} \sigma(y + z\xi + r) A(z, |r|) \nabla U(y + z\xi + r) dr.
$$

As will be shown in section 15.6, through a one dimensional deconvolution problem that can be stably solved using, for instance, a Wiener-type filtering method, we get access to the function $\Phi_{y, \xi} \cdot \tau(\xi)$. Now the question is about the reconstruction of σ from $\Phi_{y, \xi} \cdot \tau(\xi)$. We can notice that $\Phi_{y, \xi}$ is a weighted Radon transform applied to the virtual current field $\sigma \nabla U$. The weight $A(z, |r|)$ is critical for the choice of the method that we can use. Closer this weight is to a Dirac mass function, better is the stability of the reconstruction. In this case, if the field $\sigma \nabla U$ does not have too large variations, we can recover a first-order approximation, as discussed in the rest of this section.

In order to make the reconstruction accurate and stable, we make two assumptions on the set of parameters $Y \times \mathfrak{S} \times (0, z_{max})$. For any $x \in \Omega$, we define

$$
\mathfrak{S}_x = \left\{ \xi \in \mathfrak{S} \ : \ \xi = \frac{x - y}{|x - y|} \ \text{ for some } \ y \in Y \right\}.
$$

The first assumption is

$$
\text{(H1)} \quad \forall x \in \Omega, \ \exists \, \xi_1, \xi_2 \in \mathfrak{S}_x \quad \text{s.t.} \quad |\xi_1 \times \xi_2| \neq 0,
$$

and the second one reads

$$
\text{(H2)} \quad \forall x \in \Omega, \ \forall \xi \in \mathfrak{S}_x, \ \exists \, \text{unique} \ y \in Y \quad \text{s.t.} \quad \xi = \frac{x - y}{|x - y|}.
$$

From the assumption (H2), we can define a distance map $|x - y|$ as a function of x and ξ. We will denote $d_Y(x, \xi) = |x - y|$. By a change of variables, we rename our data function as

$$\psi(x, \xi) = \Phi_{y, \xi}\big(d_Y(x, \xi)\big) \cdot \tau(\xi)$$
$$= \int_{\Upsilon_\xi} (\sigma \nabla U)(x + r) A\big(d_Y(x, \xi), |r|\big) dr \cdot \tau(\xi). \tag{15.15}$$

Now if we denote by

$$\gamma(x, \xi) = \int_{\Upsilon_\xi} A\big(d_Y(x, \xi), |r|\big) dr \; \tau(\xi), \tag{15.16}$$

then we expect that

$$\psi(x, \xi) \approx (\sigma \nabla U)(x) \cdot \gamma(x, \xi),$$

provided the supp(A) is small enough and $\sigma \nabla U$ does not vary too much. The following lemma makes this statement precise.

Lemma 15.1 *Consider a fixed direction $\xi \in \mathfrak{S}$ and consider the domain covered by the pulses of direction ξ defined by $\Omega_\xi = \{x \in \Omega \; : \; \xi \in \mathfrak{S}_x\}$. Suppose that the virtual current $\sigma \nabla U$ has bounded variations, then*

$$\|\psi(\cdot, \xi) - \sigma \nabla U \cdot \gamma(\cdot, \xi)\|_{L^1(\Omega_\xi)} \leq cR \big|\sigma \nabla U\big|_{TV(\Omega)},$$

where R is the maximum radius of the cylindrical support of the envelope A and $c > 0$ depends on the shape of A. Here, $\big|\; \big|_{TV(\Omega)}$ denotes the total variation semi-norm.

Proof. For a.e. $x \in \Omega_\xi$, we have

$$|\psi(x, \xi) - (\sigma \nabla U)(x) \cdot \gamma(x, \xi)| \leq$$
$$\int_{\Upsilon_\xi} |(\sigma \nabla U)(x + r) - (\sigma \nabla U)(x)| \, A\big(d_Y(x, \xi), |r|\big) dr,$$

and so

$$\|\psi(\cdot, \xi) - \sigma \nabla U \cdot \gamma(\cdot, \xi)\|_{L^1(\Omega_\xi)}$$
$$\leq \int_{\Upsilon_\xi} \int_{\Omega_\xi} |(\sigma \nabla U)(x + r) - (\sigma \nabla U)(x)| \, A\big(d_Y(x, \xi), |r|\big) dx dr$$
$$\leq \big|\sigma \nabla U\big|_{TV(\Omega)} \int_{\Upsilon_\xi} |r| \sup_{0 < z < z_{max}} A(z, |r|) dr$$
$$\leq 2\pi R \big|\sigma \nabla U\big|_{TV(\Omega)} \int_{\mathbb{R}_+} \sup_{0 < z < z_{max}} A(z, \rho) d\rho,$$

which completes the proof. $\square$

Note that in the most interesting cases, $\sigma\nabla U$ has bounded variations. For example, if σ has a piecewise $W^{1,\infty}$ smoothness on smooth inclusions, then $\sigma\nabla U$ has bounded variations. This also holds true for σ in some subclasses of functions of bounded variations. In the following, we make the assumption, as in Lemma 15.1, that $\sigma\nabla U$ has bounded variations.

In conclusion, our data approximates the quantity $(\sigma\nabla U)(x) \cdot \gamma(x, \xi)$ for any $x \in \Omega$, $\xi \in \mathfrak{S}_x$ where the vector $\gamma(x, \xi)$ is supposed to be known. To get the current $(\sigma\nabla U)(x)$, we simply consider data from two linearly independent directions. Using assumption (H1), for a fixed $x \in \Omega$, there exist $\xi_1, \xi_2 \in \mathfrak{S}_x$ such that $\det(\xi_1, \xi_2) \neq 0$. We construct the 2×2 invertible matrix

$$\Gamma(x, \xi_1, \xi_2) = \begin{bmatrix} \gamma(x, \xi_1)^\perp \\ \gamma(x, \xi_2)^\perp \end{bmatrix},$$

and the data column vector

$$\Psi(x, \xi_1, \xi_2) = \begin{bmatrix} \psi(x, \xi_1) \\ \psi(x, \xi_2) \end{bmatrix}.$$

We approximate the current $\sigma\nabla U(x)$ by the vector field

$$V(x, \xi_1, \xi_2) = \Gamma(x, \xi_1, \xi_2)^{-1}\Psi(x, \xi_1, \xi_2).$$

Indeed, for any open set $\widetilde{\Omega} \subset \Omega_{\xi_1} \cap \Omega_{\xi_2}$, the following estimate holds:

$$\|V(\cdot, \xi_1, \xi_2) - \sigma\nabla U\|_{L^1(\widetilde{\Omega})}$$

$$\leq \sup_{x \in \widetilde{\Omega}} \left\|\Gamma(x, \xi_1, \xi_2)^{-1}\right\|_{\mathcal{L}(\mathbb{R}^2)} \left(\sum_{i=1}^{2} \|\psi(\cdot, \xi_i) - \sigma\nabla U \cdot \gamma(\cdot, \xi_i)\|_{L^1(\Omega_{\xi_i})}\right)^{1/2}$$

$$\leq cR\big|\sigma\nabla U\big|_{TV(\Omega)}.$$

It is worth mentioning that if more directions are available, then we can use them to enhance the stability of the reconstruction. The linear system becomes over-determined and we can get the optimal approximation by using a least-squares method.

15.4 Recovering the Conductivity by Optimal Control

In this section we assume that, according to the previous one, we are in the situation where we know a good approximation of the virtual current $D := \sigma\nabla U$ in the sense of $L^1(\Omega)$. The objective here is to provide efficient methods for separating σ from D.

For $a < b$, let us denote by $L^\infty_{a,b}(\Omega) := \{f \in L^\infty(\Omega) : a < f < b\}$ and define the operator $\mathcal{F} : L^\infty_{\underline{\sigma}, \overline{\sigma}}(\Omega) \longrightarrow W^{1,2}(\Omega)$ by

$$\mathcal{F}[\sigma] = U: \begin{cases} \nabla \cdot (\sigma \nabla U) = 0 & \text{in } \Omega\,, \\ U = 0 & \text{on } \Gamma_1\,, \\ U = 1 & \text{on } \Gamma_2\,, \\ \dfrac{\partial U}{\partial \nu} = 0 & \text{on } \Gamma_0\,. \end{cases} \qquad (15.17)$$

The following lemma holds.

Lemma 15.2 *Let $d\mathcal{F}$ be the Fréchet derivative of $\mathcal{F}$. For any $\sigma \in L^\infty_{\underline{\sigma},\overline{\sigma}}(\Omega)$ and $h \in L^\infty(\Omega)$ such that $\sigma + h \in L^\infty_{\underline{\sigma},\overline{\sigma}}(\Omega)$ we have*

$$d\mathcal{F}[\sigma](h) = v: \begin{cases} \nabla \cdot (\sigma \nabla v) = -\nabla \cdot (h \nabla \mathcal{F}[\sigma]) & \text{in } \Omega\,, \\ v = 0 & \text{on } \Gamma_1 \cup \Gamma_2\,, \\ \dfrac{\partial v}{\partial \nu} = 0 & \text{on } \Gamma_0\,. \end{cases} \qquad (15.18)$$

Proof. Let us denote by $w = \mathcal{F}[\sigma + h] - \mathcal{F}[\sigma] - v$. This function is in $W^{1,2}(\Omega)$ and satisfies the equation

$$\nabla \cdot (\sigma \nabla w) = -\nabla \cdot (h \nabla (\mathcal{F}[\sigma + h] - \mathcal{F}[\sigma]))$$

with the same boundary conditions as v. We have the elliptic global control:

$$\|\nabla w\|_{L^2(\Omega)} \le \frac{1}{\underline{\sigma}} \|h\|_{L^\infty(\Omega)} \|\nabla(\mathcal{F}[\sigma + h] - \mathcal{F}[\sigma])\|_{L^2(\Omega)}\,.$$

Since

$$\nabla \cdot (\sigma \nabla(\mathcal{F}[\sigma + h] - \mathcal{F}[\sigma])) = -\nabla \cdot (h \nabla \mathcal{F}[\sigma + h])\,,$$

we can also control $\mathcal{F}[\sigma + h] - \mathcal{F}[\sigma]$ with

$$\|\nabla(\mathcal{F}[\sigma + h] - \mathcal{F}[\sigma])\|_{L^2(\Omega)} \le \frac{1}{\sqrt{\underline{\sigma}}} \|h\|_{L^\infty(\Omega)} \|\nabla \mathcal{F}[\sigma + h]\|_{L^2(\Omega)}\,.$$

Then, there is a positive constant C depending only on Ω such that

$$\|\nabla \mathcal{F}[\sigma + h]\|_{L^2(\Omega)} \le C \sqrt{\frac{\overline{\sigma}}{\underline{\sigma}}}\,.$$

Finally, we obtain

$$\|\nabla w\|_{L^2(\Omega)} \le C \frac{\sqrt{\overline{\sigma}}}{\underline{\sigma}^2} \|h\|^2_{L^\infty(\Omega)}\,,$$

and the proof is complete. $\square$

We look for the minimizer of the functional

$$J[\sigma] = \frac{1}{2} \int_\Omega |\sigma \nabla \mathcal{F}[\sigma] - D|^2\,. \qquad (15.19)$$

In order to do so, we compute its gradient. The following lemma holds.

Lemma 15.3 *For any $\sigma \in L^\infty_{\underline{\sigma},\overline{\sigma}}(\Omega)$ and $h \in L^\infty(\Omega)$ such that $\sigma + h \in L^\infty_{\underline{\sigma},\overline{\sigma}}(\Omega)$,*

$$dJ[\sigma](h) = -\int_\Omega h\left((\sigma\nabla\mathcal{F}[\sigma] - D - \nabla p) \cdot \nabla\mathcal{F}[\sigma] \right),$$

where p is defined as the solution to the adjoint problem:

$$\begin{cases} \nabla \cdot (\sigma\nabla p) = \nabla \cdot (\sigma^2\nabla\mathcal{F}[\sigma] - \sigma D) & in \ \Omega\,, \\ \quad\quad p = 0 & on \ \Gamma_1 \cup \Gamma_2\,, \\ \quad\dfrac{\partial p}{\partial \nu} = 0 & on \ \Gamma_0\,. \end{cases} \quad (15.20)$$

Proof. As $\mathcal{F}$ is Fréchet differentiable, so is J. For $\sigma \in L^\infty_{\underline{\sigma},\overline{\sigma}}(\Omega)$ and $h \in L^\infty(\Omega)$ such that $\sigma + h \in L^\infty_{\underline{\sigma},\overline{\sigma}}(\Omega)$, we have

$$dJ[\sigma](h) = \int_\Omega (\sigma\nabla\mathcal{F}[\sigma] - D) \cdot (h\nabla\mathcal{F}[\sigma] + \sigma\nabla d\mathcal{F}[\sigma](h))\,.$$

Now, multiplying (15.20) by $d\mathcal{F}[\sigma](h)$, we get

$$\int_\Omega \sigma\nabla p \cdot \nabla d\mathcal{F}[\sigma](h) = \int_\Omega (\sigma^2\nabla\mathcal{F}[\sigma] - \sigma D) \cdot \nabla d\mathcal{F}[\sigma](h)\,.$$

On the other hand, multiplying (15.18) by p we arrive at

$$\int_\Omega \sigma\nabla p \cdot \nabla d\mathcal{F}[\sigma](h) = -\int_\Omega h\nabla\mathcal{F}[\sigma] \cdot \nabla p\,,$$

and therefore,

$$dJ[\sigma](h) = \int_\Omega h(\sigma\nabla\mathcal{F}[\sigma] - D - \nabla p) \cdot \nabla\mathcal{F}[\sigma]\,,$$

which completes the proof. $\square$

Lemma 15.3 allows us to implement a numerical gradient descent method in order to find σ. A regularization term can also be added to $J[\sigma]$ in order to avoid instability. As we are seeking discontinuous σ with smooth variations out of the discontinuity set, a good choice would be the minimization of the regularized functional:

$$J_\varepsilon[\sigma] = \frac{1}{2}\int_\Omega |\sigma\nabla\mathcal{F}[\sigma] - D|^2 + \varepsilon|\sigma|_{TV(\Omega)}\,, \quad\quad (15.21)$$

where $\varepsilon > 0$ is the regularization parameter.

15.5 The Orthogonal Field Method

In this section, we present an alternative direct method to optimal control for reconstructing the conductivity σ from the internal data $\sigma \nabla U$. It is based on solving a transport equation. The following approach may be extended to the three dimensional case. However, several proofs would need to be revisited.

Given a vector field $D = \sigma \nabla U$ which is parallel to ∇U everywhere, we may construct the vectorial field $F = (\sigma \nabla U)^\perp = (D_2, -D_1)$ which is everywhere orthogonal to D. The flow of F may define the level sets of U. Assuming that the variations of the conductivity σ are far enough from Γ_0, we can assume that $U(x) = x_2$ on this boundary part. Then U is a solution of the following transport equation:

$$\begin{cases} F \cdot \nabla U = 0 & \text{in } \Omega \,, \\ \qquad U = x_2 & \text{on } \partial \Omega \,. \end{cases} \tag{15.22}$$

In the case where (15.22) is well posed and can be solved, we can reconstruct the virtual potential U. The conductivity σ is deduced from U and D by the following identity

$$\frac{1}{\sigma} = \frac{D \cdot \nabla U}{|D|^2} \,. \tag{15.23}$$

Despite to its very simple form, this first-order equation is really tricky. Existence and uniqueness are both difficult challenges in the general case. Our main difficulty here is due to the fact that F is discontinuous. As the function U that we are looking for is a natural solution of this equation, we are only concerned here with the uniqueness of a solution to (15.22).

15.5.1 Uniqueness Result for the Transport Equation

The uniqueness of a solution to (15.22) is directly linked to the existence of outgoing characteristic lines defined by the dynamic system [114]:

$$\begin{cases} X'(t) = F(X(t)), \ t \ge 0 \,, \\ X(0) = x, \ x \in \Omega \,, \end{cases} \tag{15.24}$$

which usually needs the continuity of F. As σ is in general not continuous, F is not continuous, which makes the classical existence results useless. Nevertheless, under some assumptions on σ, we can insure the existence of the characteristic lines.

Definition 15.4 *For any $k \in \mathbb{N}$, $\alpha \in (0,1)$, for any simple closed curve $\mathcal{C}$ of class $\mathcal{C}^{1,\alpha}$ such that $\Omega \setminus \mathcal{C}$ is a union of connected domains $\Omega_i, i = 1, 2, \ldots, n$, we define $C_{\mathcal{C}}^{k,\alpha}\left(\overline{\Omega}\right)$ to be the class of functions $f : \Omega \longrightarrow \mathbb{R}$ satisfying*

$$f|_{\Omega_i} \in \mathcal{C}^{k,\alpha}\left(\overline{\Omega_i}\right) \quad \forall i = 1, \ldots, n \,.$$

Definition 15.5 *A conductivity σ is said to be admissible if there exists a constant $\alpha \in (0,1)$ and a curve $\mathcal{C}$ of class $\mathcal{C}^{1,\alpha}$ such that $\sigma \in C_{\mathcal{C}}^{0,\alpha}\left(\overline{\Omega}\right) \cap L_{\underline{\sigma},\overline{\sigma}}^{\infty}(\Omega)$ and*

$$\inf_{\Omega \backslash \mathcal{C}} \sigma \nabla \mathcal{F}[\sigma] \cdot e_2 \; > \; 0 \, .$$

If σ is admissible and belongs to $C_{\mathcal{C}}^{0,\alpha}\left(\overline{\Omega}\right)$, then the solution U of (15.12) belongs to $C_{\mathcal{C}}^{1,\alpha}\left(\overline{\Omega}\right)$ and the field $F = (\sigma \nabla U)^{\perp}$ satisfies

$$F \in C_{\mathcal{C}}^{0,\alpha}\left(\overline{\Omega}\right) \quad \text{and} \quad \inf_{\Omega \backslash \mathcal{C}} F \cdot e_1 \; > \; 0 \, .$$

Moreover, as F is orthogonal to $\sigma \nabla U$, we can describe the jump of F at the curve $\mathcal{C}$. Defining the normal and tangential unit vectors ν and τ and also the local sides (+) and (-) with respect to ν, we can write F on both sides as

$$F^+ = \sigma^+ \frac{\partial U^+}{\partial \nu} \tau + \sigma^+ \frac{\partial U^+}{\partial \tau} \nu \, ,$$

$$F^- = \sigma^- \frac{\partial U^-}{\partial \nu} \tau + \sigma^- \frac{\partial U^-}{\partial \tau} \nu \, ,$$

with the transmission conditions, $\sigma^+ \partial U^+ / \partial \nu = \sigma^- \partial U^- / \partial \nu$ and $\partial U^+ / \partial \tau = \partial U^- / \partial \tau$. Finally, we characterize the discontinuity of F by

$$[F] = [\sigma] \frac{\partial U}{\partial \tau} \nu,$$

where $[\,]$ denotes the jump across $\mathcal{C}$.

With all of these properties for the field F, we can prove the existence of the characteristic lines for (15.24).

Theorem 15.6 *(Local existence of characteristics) Assume that $F \in C_{\mathcal{C}}^{0,\alpha}\left(\overline{\Omega}\right)$ with $\mathcal{C}$ of class $\mathcal{C}^{1,\alpha}$ for $\alpha \in (0,1)$. Assume that the discontinuity of F on $\mathcal{C}$ satisfies*

$$F^+ = f\tau + \sigma^+ g\nu \, ,$$

$$F^- = f\tau + \sigma^- g\nu \, ,$$

with $f, g, \sigma^+, \sigma^- \in \mathcal{C}^{0,\alpha}(\mathcal{C})$ where σ^+, σ^- are positive and g is locally signed. Then, for any $x_0 \in \Omega$, there exists $T > 0$ and $X \in \mathcal{C}^1\left([0,T[,\Omega\right)$ such that $t \mapsto F(X(t))$ is measurable and

$$X(t) = x_0 + \int_0^t F(X(s))ds, \quad \forall t \in [0,T[\, .$$

Proof. If $x_0 \notin \mathcal{C}$, then F is continuous in a neighborhood of x_0 and the Cauchy-Peano theorem can be applied.

If $x_0 \in \mathcal{C}$, then we choose a disk $B \subset \Omega$ centered at x_0. The oriented line $\mathcal{C}$ separates B in two simply connected open domains called B^+ and B^-. For

ease of explanation, we may assume that $\mathcal{C} \cap B$ is straight line (since we can flatten the curve using a proper $\mathcal{C}^{0,\alpha}$-diffeomorphism).

Assume that $g(x_0) > 0$. Up to rescaling B, we can assume that $g(x) > 0$ for all $x \in \mathcal{C} \cap B$. We extend $F|_{B^+}$ to a continuous field $\tilde{F} \in \mathcal{C}^0(B)$ by even reflection. The Cauchy-Peano theorem insures the existence of $T > 0$ and $X \in \mathcal{C}^1\big([0, T[, \Omega\big)$ such that $X(0) = x_0$ and $X'(t) = \tilde{F}(X(t))$ for all $t \in [0, T[$. As $g(x_0) > 0$, we have $X'(0) \cdot \nu(x_0) > 0$ and $X(t) \in \overline{B^+}$ in a neighborhood of 0. Thus, for a small enough t, $X'(t) = F(X(t))$. If $g(x_0) < 0$, then we apply the same argument by interchanging B^- and B^+.

Suppose now that $g(x_0) = 0$. The field F is now tangent to the discontinuity line. If $f(x_0) = 0$, then $X(t) = x_0$ is a solution. We assume here that $f(x_0) > 0$. As g is assumed to be locally signed, we can suppose that $g \geq 0$ in a small sub-curve of $\mathcal{C}$ satisfying $(x - x_0) \cdot \tau(x_0) > 0$. Again, we extend $F|_{B^+}$ to a continuous field $\tilde{F} \in \mathcal{C}^0(B)$ by even reflection and use the Cauchy-Peano theorem to show that there exists $T > 0$ and $X \in \mathcal{C}^1\big([0, T[, \Omega\big)$ such that $X(0) = x_0$ and $X'(t) = \tilde{F}(X(t))$ for all $t \in [0, T[$. In order to complete the proof, we should show that $X(t)$ belongs to $\overline{B^+}$ for t small enough. If not, there exists a sequence $t_n \searrow 0$ such that $X(t_n) \in B^-$. By the mean value theorem, there exists $\tilde{t}_n \in (0, t_n)$ such that $F(X(\tilde{t}_n)) \cdot \nu(x_0) = X'(\tilde{t}_n) \cdot \nu(x_0) < 0$. Thus, $X(t)$ belongs to $\overline{B^+}$ and $X'(t) = F(X(t))$ for t small enough.

Note that the local monotony of g is satisfied in many cases. For instance if $\mathcal{C}$ is analytic and σ is piecewise constant, then ∇U is analytic on $\mathcal{C}$ and hence, g is locally signed. $\square$

It is worth mentioning that existence of a solution for the Cauchy problem (15.24) has been proved in [114] provided that $F \cdot \nu > 0$ on $\mathcal{C}$. Here, we have made a weaker assumption. In fact, we only need that $F \cdot \nu$ is locally signed.

Corollary 15.7 *(Existence of outgoing characteristics) Consider $F \in C_{\mathcal{C}}^{0,\alpha}(\Omega)$ satisfying the same conditions as in Theorem 15.6 and the condition*

$$\inf_{\Omega \setminus \mathcal{C}} F \cdot e_1 \geq c \,,$$

where c is a positive constant. Then for any $x_0 \in \Omega$ there exists $0 < T < T_{\max}$ where $T_{\max} = \dfrac{1}{c} diam(\Omega)$ and $X \in \mathcal{C}^0\big([0, T[, \Omega\big)$ satisfying

$$X(t) = x_0 + \int_0^t F(X(s))ds, \quad \forall t \in [0, T[\,,$$

$$\lim_{t \to T} X(t) \in \partial \Omega \,.$$

This result means that from any point $x_0 \in \Omega$, the characteristic line reaches $\partial \Omega$ in a finite time.

Proof. Let $x_0 \in \Omega$ and $X \in \mathcal{C}^0\big([0, T[, \Omega\big)$ a maximal solution of (15.24). Using $F \cdot e_1 \geq c$ we have that $X'(t) \cdot e_1 \geq c$ and so $X(t) \cdot e_1 \geq x_0 \cdot e_1 + ct$ and as $X(t) \in \Omega$ for all $t \in [0, T[$, it is necessary that $T < T_{\max}$. As $F \in \mathcal{C}_{\mathcal{C}}^{0,\alpha}(\Omega)$, F is

bounded, X is Lipschitz, and the limit of $X(t)$ when t goes to T exists in $\overline{\Omega}$ and is called $X(T)$. Let us show that $X(T) \in \partial\Omega$. Suppose that $X(T) \in \Omega$, then applying Theorem 15.6 at $X(T)$, we can continuously extend X on $[T, T + \varepsilon[$ for some positive ε which contradicts the fact that X is a maximal solution. $\square$

Corollary 15.8 *[Uniqueness for the transport problem] Consider $F \in C_{\mathcal{C}}^{0,\alpha}(\Omega)$ satisfying the same conditions as in Corollary 15.7 and consider $u \in \mathcal{C}^0(\overline{\Omega}) \cap \mathcal{C}_{\mathcal{C}}^1(\overline{\Omega})$. If u is a solution of the system*

$$\begin{cases} F \cdot \nabla u = 0 & in \ \Omega \,, \\ u = 0 & on \ \partial\Omega \,, \end{cases} \tag{15.25}$$

then $u = 0$ in Ω.

Proof. Consider $x_0 \in \Omega$ and a characteristic $X \in \mathcal{C}^0([0, T[, \Omega)$ satisfying

$$X(t) = x_0 + \int_0^t F(X(s))ds, \quad \forall t \in [0, T[\,,$$

$$\lim_{t \to T} X(t) \in \partial\Omega \,.$$

We define $f \in \mathcal{C}^0([0, T], \mathbb{R})$ by $f(t) = u(X(t))$. We show that f is constant. Let us define $I = X^{-1}(\mathcal{C})$ then f is differentiable in $[0, T] \setminus I$ and $f'(t) = \nabla u(X(t)) \cdot F(X(t)) = 0$. Let us take $t \in I$. If t is not isolated in I, using the fact that $\partial_\tau u^+$ and $\partial_\tau u^-$ are locally signed, $F(X(t))$ is parallel to $\mathcal{C}$ and for an $\varepsilon > 0$, $X(s) \in \overline{B^+}$ (or $\overline{B^-}$) for $s \in [t, t + \varepsilon[$. Then, $f(s) = u(x(s))$ is differentiable on $[t, t + \varepsilon[$ with $f'(s) = \nabla u^+(X(s)) \cdot F(X(s))$. This proves that f is right differentiable at t and $(f')^+(t) = 0$. By the same argument, f is left differentiable at t and $(f')^-(t) = 0$ and so f is differentiable at t with $f'(t) = 0$. Finally, except for a zero measure set of isolated points, f is differentiable on $[0, T]$ and $f' = 0$ almost everywhere. This is not enough to conclude because there exists continuous increasing functions whose derivative is zero almost everywhere. Since for all $t, s \in [0, T]$,

$$|f(t) - f(s)| \leq \sup_{x \in \Omega} |\nabla u| |X(t) - X(s)| \leq \sup_{x \in \Omega} |\nabla u| \sup_{x \in \Omega} |F| |t - s|,$$

f is Lipschitz and thus absolutely continuous which implies, since $f' = 0$ a.e., that f is constant on $[0, T]$. We finally have $u(x_0) = f(0) = f(T) = u(X(T)) = 0$. $\square$

Hence we conclude that if σ is admissible, then U is the unique solution to (15.22) and we can recover σ by (15.23).

Remark 15.9 *The characteristic method can be used to solve the transport problem. However, it suffers from poor numerical stability which is exponentially growing with the distance to the boundary. To avoid this delicate numerical issue, we propose a regularized approach for solving (15.22). Our approach*

*consists in forming from (15.22) a second-order PDE and adding to this PDE
a small elliptic term of order two.*

15.5.2 The Viscosity-Type Regularization

In this subsection we introduce a viscosity approximation to (15.22). Let $\eta > 0$. We regularize the transport equation (15.22) by considering the well-posed elliptic problem

$$\begin{cases} \nabla \cdot \left[\left(\eta I + FF^T \right) \nabla U_\eta \right] = 0 & \text{in } \Omega\,, \\ \qquad\qquad\quad U_\eta = x_2 & \text{on } \partial\Omega\,, \end{cases} \tag{15.26}$$

where I is the identity matrix. The main question is to understand the behavior of U_η when $\eta \to 0$. Or more precisely, whether U_η converges to the solution U of the transport equation (15.22) for a certain topology. The following result holds.

Theorem 15.10 *The sequence* $(U_\eta - U)_{\eta>0}$ *converges strongly to zero in* $W_0^{1,2}(\Omega)$.

Proof. We first prove that the sequence $(U_\eta - U)_{\eta>0}$ converges weakly to zero in $W_0^{1,2}(\Omega)$ when η goes to zero. For any $\eta > 0$, $\tilde{U}_\eta := U_\eta - U$ is in $W_0^{1,2}(\Omega)$ and satisfies

$$\nabla \cdot \left[\left(\eta I + FF^T \right) \nabla \tilde{U}_\eta \right] = -\eta \triangle U \quad \text{in } \Omega\,. \tag{15.27}$$

Multiplying this equation by $\tilde{U}_\eta$ and integrating by parts over Ω, we obtain

$$\eta \int_\Omega |\nabla \tilde{U}_\eta|^2 + \int_\Omega |F \cdot \nabla \tilde{U}_\eta|^2 = -\eta \int_\Omega \nabla U \cdot \nabla \tilde{U}_\eta\,, \tag{15.28}$$

and so,

$$\left\| \tilde{U}_\eta \right\|_{W_0^{1,2}(\Omega)}^2 \leq \int_\Omega |\nabla U \cdot \nabla \tilde{U}_\eta| \leq \|U\|_{W^{1,2}(\Omega)} \left\| \tilde{U}_\eta \right\|_{W_0^{1,2}(\Omega)}\,.$$

Then $\left\| \tilde{U}_\eta \right\|_{W_0^{1,2}(\Omega)} \leq \|U\|_{W^{1,2}(\Omega)}$. The sequence $(\tilde{U}_\eta)_{\eta>0}$ is bounded in $W_0^{1,2}(\Omega)$ and so by Banach-Alaoglu's theorem, we can extract a subsequence which converges weakly to U^* in $W_0^{1,2}(\Omega)$. Multiplying (15.27) by U^* and integrating by parts, we get

$$\int_\Omega \left(F \cdot \nabla \tilde{U}_\eta \right) \left(F \cdot \nabla U^* \right) = -\eta \int_\Omega \nabla U \cdot \nabla U^* - \eta \int_\Omega \nabla \tilde{U}_\eta \cdot \nabla U^*\,.$$

Taking the limit when η goes to zero,

$$\|F \cdot \nabla U^*\|_{L^2(\Omega)} = 0\,.$$

So U^* is a solution of the transport equation (15.25), and by Corollary 15.8, $U^* = 0$ in Ω. Since the limit U^* is independent of the subsequence, the convergence holds for $\tilde{U}_\eta$.

Now, we are ready to prove the strong convergence. From (15.28) we get that

$$\int_\Omega |\nabla \tilde{U}_\eta|^2 \leq -\int_\Omega \nabla U \cdot \nabla \tilde{U}_\eta\,,$$

and as $\tilde{U}_\eta \rightharpoonup 0$ in $W_0^{1,2}(\Omega)$, the term in the right-hand side goes to zero when η goes to zero. Hence, $\left\|\tilde{U}_\eta\right\|_{W_0^{1,2}(\Omega)} \to 0$.   □

Finally, using Theorem 15.10 we define the approximate resistivity by

$$\frac{1}{\sigma_\eta} = \frac{D \cdot \nabla U_\eta}{|D|^2}\,,$$

which strongly converges to $\dfrac{1}{\sigma_*}$ in $L^2(\Omega)$, where σ_* is the true conductivity.

15.6 Numerical Illustrations

In this section we first discuss the deconvolution step. Then we test both the optimal control and the orthogonal field reconstruction schemes.

15.6.1 Deconvolution

In this subsection, we consider the problem of recovering $\Phi_{y,\xi}$ from the measurements $M(y, \xi, \cdot)$ in the presence of noise. From (15.14), it is easy to see that this can be done by deconvolution. However, deconvolution is a numerically very unstable process. In order to render stability we use a Wiener-type filter. We assume that the signal $M(y, \xi, \cdot)$ is perturbed by a random white noise:

$$\widetilde{M}(y, \xi, z) = M(y, \xi, z) + \mu(z), \tag{15.29}$$

where μ is a white Gaussian noise with variance ν^2 such that

$$\mathbb{E}[\mu(z)\mu(z')] = \nu^2 \delta_0(z - z')$$

and

$$\mathbb{E}[\mathcal{F}(\mu)(k)\overline{\mathcal{F}(\mu)(k')}] = \nu^2 \delta_0(k - k')\,,$$

where

$$\mathcal{F}[\mu](k) = \frac{1}{\sqrt{2\pi}} \int \mu(z)e^{-ikz}dz\,.$$

Equation (15.29) can be written as

$$\widetilde{M}_{y,\xi}(z) = \left(W \star \Psi_{y,\xi}\right)(z) + \mu(z),$$

where $\Psi_{y,\xi}(z) = \Phi_{y,\xi}(z) \cdot \tau(\xi)$. Denote by $S(\Psi_{y,\xi}) = \int_{\mathbb{R}} |\mathcal{F}(\Psi_{y,\xi})(k)|^2 dk$ the spectral density of $\Psi_{y,\xi}$, where $\mathcal{F}$ is the Fourier transform. We introduce a Wiener deconvolution filter in the frequency domain:

$$\widehat{L}(k) = \frac{\overline{\mathcal{F}(W)}(k)}{|\mathcal{F}(W)|^2(k) + \frac{\nu^2}{S(\Psi_{y,\xi})}}.$$

The quotient $\nu^2/S(\Psi_{y,\xi})$ is the signal-to-noise ratio. So, in order to use the filter, we need to have an a priori estimate of the signal-to-noise ratio. We then recover $\Psi_{y,\xi}$ up to a small error by

$$\widetilde{\Psi}_{y,\xi} = \mathcal{F}^{-1}\left(\mathcal{F}(\widetilde{M})\widehat{L}\right).$$
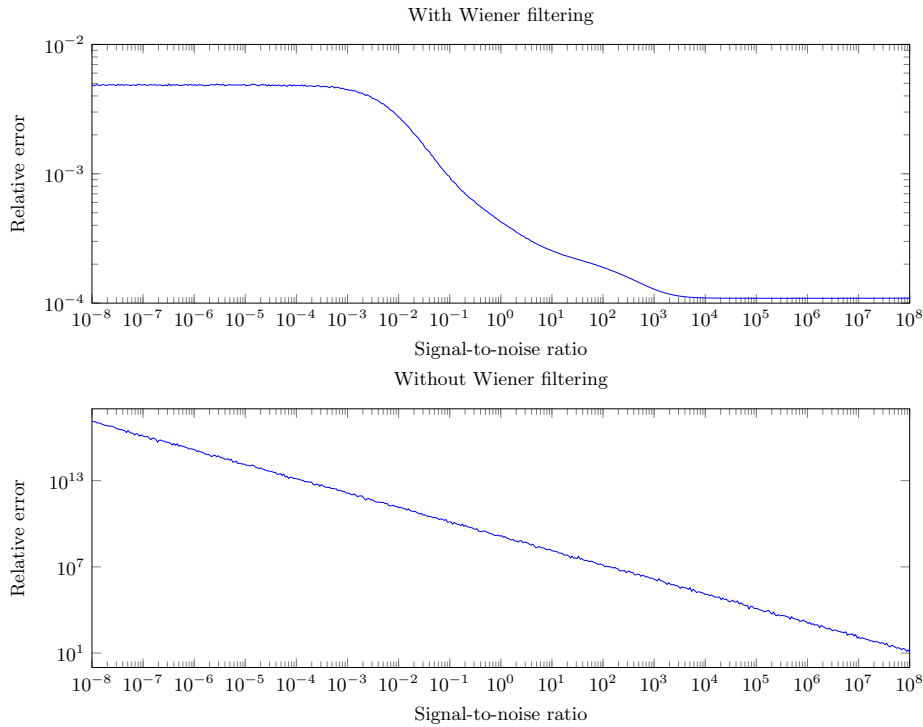
Fig. 15.3. L^2 norm of the relative error $\frac{\|\Psi_{y,\xi} - \widetilde{\Psi}_{y,\xi}\|_2}{\|\Sigma\|_2}$ with respect to the signal-to-noise ratio.

15.6.2 Conductivity Reconstructions

In the numerical simulations, we choose $\Omega = (0, 2) \times (0, 1)$. Figure 15.4 shows the true conductivity map in the medium. The simulations are done using a PDE solver. The data is simulated numerically on a fine mesh. For the orthogonal field method, in order to solve (15.26), we use a coarse mesh. Then we reconstruct an initial image of the conductivity. Based on the initial image, an adaptive mesh refinement for solving (15.26) yields a conductivity image of a better quality.
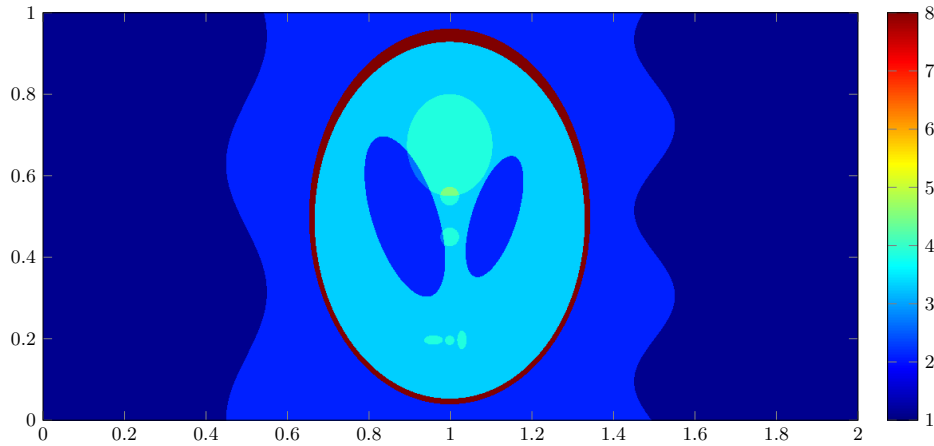
Fig. 15.4. Conductivity map to be reconstructed.

Optimal Control Algorithm

The minimization procedure gives a decent qualitative reconstruction. The main interfaces are easy to see, yet this method, due to its regularizing effect, fails to show details in weaker contrasts zones. Figures 15.5, 15.6, and 15.7 show the reconstruction obtained with different measurement noise levels.

Orthogonal Field Method

To find the solution of problem (15.26), we fix $\eta = 10^{-3}$, and solve the equation on a uniform mesh on Ω. We reconstruct an approximation of σ, and adapt the mesh to this first reconstruction. We do this procedure a couple of times in order to get refined mesh near the conductivity jumps. We can see that besides being computationally lighter than the minimization method, the orthogonal field method allows a quantitative reconstruction of σ and shows details even
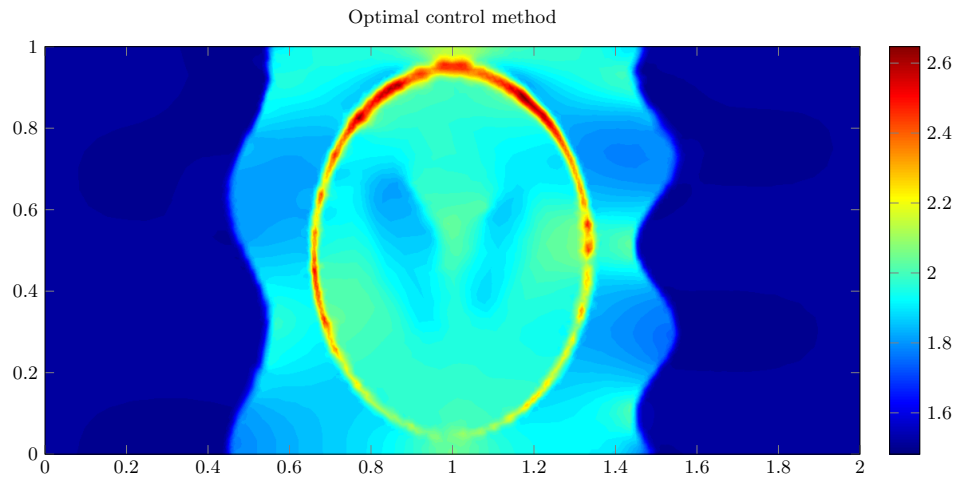
Fig. 15.5. Reconstructed image without measurement noise.
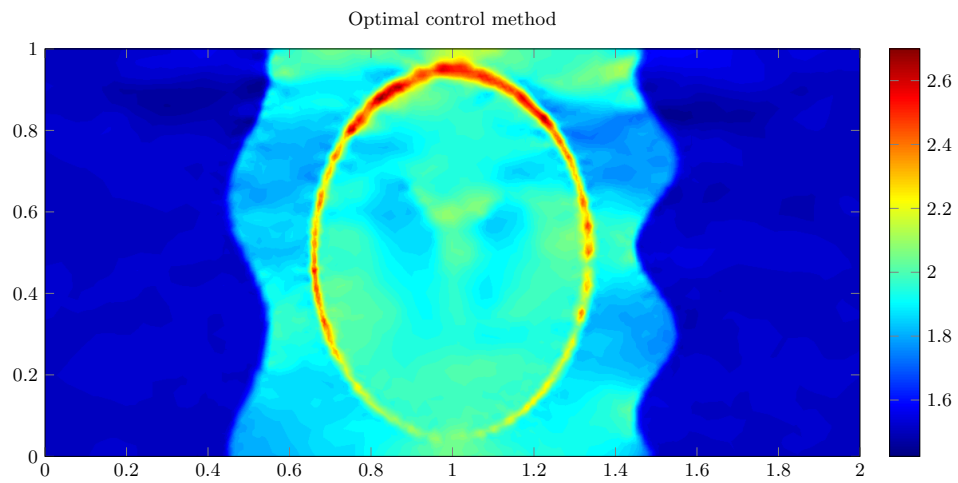
Fig. 15.6. Reconstructed image with 2% measurement noise (each measurement is perturbed by an additive Gaussian random variable with mean zero and standard deviation equal to 2% of the maximal absolute value of the unperturbed measurements).

Optimal control method
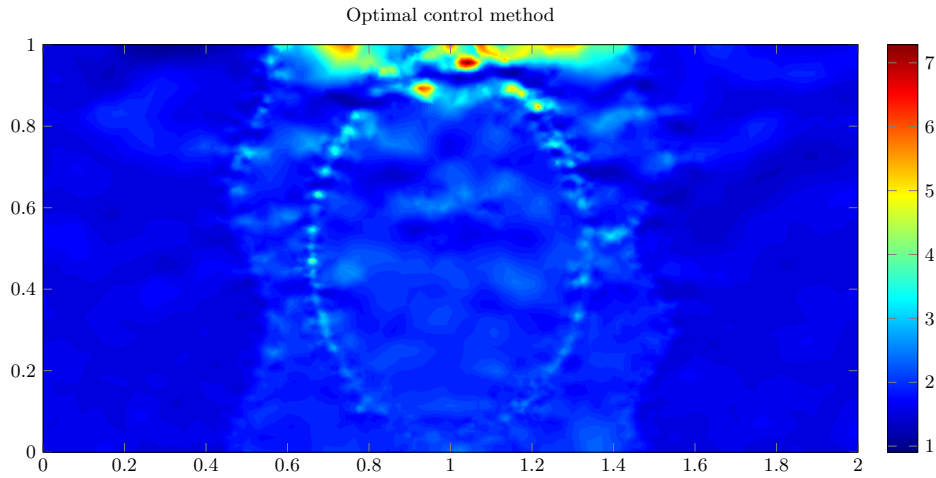
Fig. 15.7. Reconstructed image with 20% measurement noise.

in the low contrast zones. It is relatively stable with respect to measurement noise. Figures 15.8, 15.9, and 15.10 show the reconstruction with different measurement noise levels.

Orthogonal field method
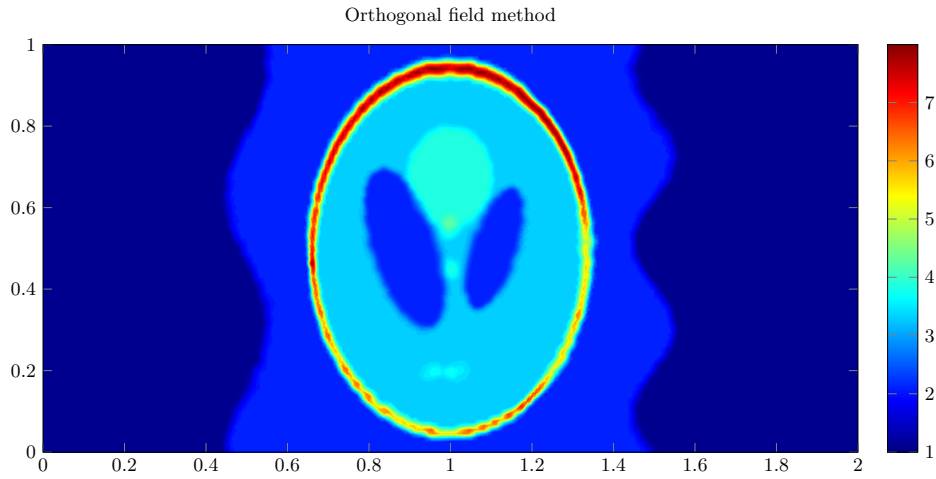
Fig. 15.8. Reconstructed image without measurement noise.

Orthogonal field method
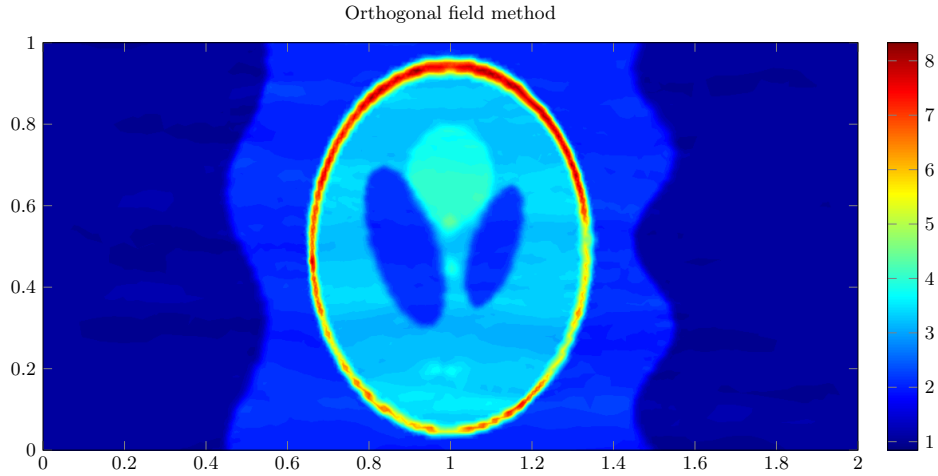
Fig. 15.9. Reconstructed image with 2% measurement noise.

Orthogonal field method
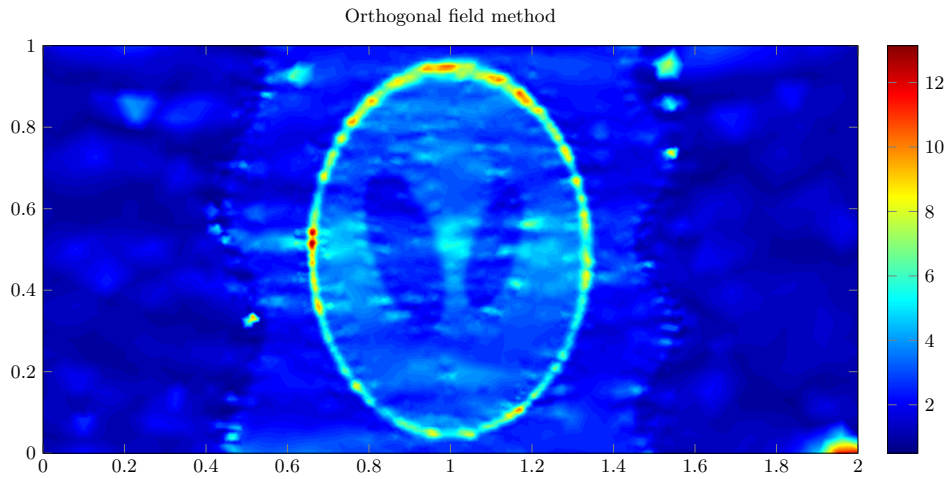
Fig. 15.10. Reconstructed image with 20% measurement noise.

15.7 Concluding Remarks

In this chapter we have provided the mathematical basis of ultrasonically-induced Lorentz force electrical impedance tomography. We have designed two efficient algorithms and tested them numerically. The resolution of the reconstructed images is fixed by the ultrasound wavelength and the width of the ultrasonic beam. The orthogonal field method performs much better than the optimization scheme in terms of both computational time and accuracy.

16

Magnetoacoustic Tomography With Magnetic Induction

16.1 Introduction

Electrical conductivity varies widely among soft tissue types and pathological states and its measurement can provide information about the physiological and pathological conditions of tissue.

Acousto-magnetic tomographic techniques have the potential to detect small conductivity inhomogeneities, enabling them to diagnose pathologies such as cancer by detecting tumorous tissues when other conductivity imaging techniques fail to do so.

In magnetoacoustic imaging with magnetic induction, magnetic fields are used to induce currents in the tissue. Ultrasound is generated by placing the tissue in a dynamic and static magnetic field. The dynamic field induces eddy currents and the static field leads to generation of acoustic vibration from Lorentz force on the induced currents. The divergence of the Lorentz force acts as acoustic source of propagating ultrasound waves that can be sensed by ultrasonic transducers placed around the tissue. The imaging problem is to obtain the conductivity distribution of the tissue from the acoustic source map.

In this chapter we provide a mathematical analysis and a numerical framework for magnetoacoustic tomography with magnetic induction. The imaging problem is to reconstruct the conductivity distribution of biological tissue from measurements of the Lorentz force induced tissue vibration. We begin with reconstructing from the acoustic measurements the divergence of the Lorentz force, which is acting as the source term in the acoustic wave equation. Then we recover the electric current density from the divergence of the Lorentz force. To solve the nonlinear inverse conductivity problem, we introduce an optimal control method for reconstructing the conductivity from the electric current density. We prove its convergence and stability. We also present a point fixed approach and prove its convergence to the true solution. A direct reconstruction scheme involving a partial differential equation is then proposed based on viscosity-type regularization to a transport equation satisfied by the electric

current density field. We show that solving such an equation yields the true conductivity distribution as the regularization parameter approaches zero.

The chapter is organized as follows. We start by describing the forward problem. Then we reconstruct from the acoustic measurements the divergence of the Lorentz force, which is acting as the source term in the acoustic wave equation. We recover the electric current density from the divergence of the Lorentz force, which reduces the problem to imaging the conductivity from the internal electric current density. We introduce three reconstruction schemes for solving the conductivity imaging problem from the internal electric current density. The first is an optimal control method. One of the contributions of this chapter is the proof of convergence and stability of the optimal control approach provided that two magnetic excitations leading to nonparallel current densities are employed. Then we present a point fixed approach and prove that it converges to the true conductivity image. Finally, we propose an alternative to these iterative schemes via the use of a transport equation satisfied by the internal electric current density. Our third algorithm is direct and can be viewed as a PDE-based reconstruction scheme. We test numerically the three proposed schemes in the presence of measurement noise, and also quantify their stability and resolution.

The feasibility of imaging of Lorentz-force-induced motion in conductive samples was shown in [96]. The magnetoacoustic tomography with magnetic induction investigated here was experimentally tested in [263, 264], and was reported to produce conductivity images of quality comparable to that of ultrasound images taken under similar conditions. Our results in this chapter are from [35].

16.2 Forward Problem Description

16.2.1 Time Scales Involved

The forward problem in magnetoacoustic tomography with magnetic induction (MAT-MI) is multiscale in nature. The different phenomena involved in the experiment evolve on very different time scales. Precisely, there are three typical times that appear in the mathematical model for MAT-MI.

- The first one is the time needed for an electromagnetic wave to propagate in the medium and is denoted by τ_{em}. Typically, if the medium has a diameter of $1cm$, we have $\tau_{em} \sim 10^{-11}s$.
- The second characteristic time, denoted by τ_{pulse} is the time width of the magnetic pulse sent into the medium. Since the time-varying magnetic field is generated by discharging a capacitor, τ_{pulse} is in fact the time needed to discharge the capacitor such that $\tau_{pulse} \sim 1\mu s$ [346].
- The third characteristic time, τ_{sound}, is the time consumed by the acoustic wave to propagate through the medium. The speed of sound is about $1.5 \cdot 10^3 m.s^{-1}$ so $\tau_{sound} \sim 6\mu s$ for a medium of $1cm$ diameter.

16.2.2 Electromagnetic Model

Let $(e_i)_{i=1,2,3}$ be an orthonormal basis of $\mathbb{R}^3$. Let Ω be a three-dimensional bounded $\mathcal{C}^1$ convex domain. The medium is assumed to be non magnetic, and its conductivity is given by σ (the question of the regularity of σ will arise later). Assume that the medium Ω is placed in a uniform, static magnetic field $B_0 = B_0 e_3$.

Magnetoquasistatic Regime

At time $t = 0$ a second time varying magnetic field is applied in the medium. The time varying magnetic field has the form $B_1(x,t) = B_1(x)w(t)e_3$. B_1 is assumed to be a known smooth function and w is the shape of the stimulating pulse. The typical width of the pulse is about $1\mu s$ so we are in presence of a slowly varying magnetic-field. This regime can be described by the magnetoquasistatic equations, where the propagation of the electrical currents is considered as instantaneous, but, the induction effects are not neglected. These governing equations in $\Omega \times \mathbb{R}_+$ are

$$\nabla \cdot B = 0, \tag{16.1}$$

$$\nabla \times E = -\frac{\partial B}{\partial t}, \tag{16.2}$$

and

$$\nabla \cdot J = 0, \tag{16.3}$$

where B is the total magnetic field in the medium and E is the total electric field in the medium. Ohm's law is valid and is expressed as

$$J = \sigma E \quad \text{in } \Omega \times \mathbb{R}_+, \tag{16.4}$$

where σ is the electrical conductivity of the medium. From now on, we assume that $\sigma \in L^\infty_{\underline{\sigma},\overline{\sigma}}(\Omega)$, where

$$L^\infty_{\underline{\sigma},\overline{\sigma}}(\Omega) := \{f \in L^\infty(\Omega') : \underline{\sigma} < f < \overline{\sigma} \text{ in } \Omega', \quad f \equiv \sigma_0 \text{ in } \Omega \setminus \overline{\Omega'}\}$$

with $\sigma_0, \underline{\sigma}$, and $\overline{\sigma}$ being three given positive constants, $0 < \underline{\sigma} < \overline{\sigma}$, and $\Omega' \Subset \Omega$.

We use the Coulomb gauge ($\nabla \cdot A = 0$) to express the potential representation of the fields B and E. The magnetic field B is written as

$$B = \nabla \times A, \tag{16.5}$$

and the electric field E is then of the form

$$E = -\nabla \widetilde{V} - \frac{\partial A}{\partial t} \quad \text{in } \Omega \times \mathbb{R}_+, \tag{16.6}$$

where $\widetilde{V}$ is the electric potential. Writing A as follows:

$$A(x,t) = A_0(x) + A_1(x)w(t)\,,$$

where A_0 and A_1 are assumed to be smooth. In view of (16.3) and (16.6), we look for $\widetilde{V}(x,t)$ of the form $\widetilde{V}(x,t) = V(x)w'(t)$ with V satisfying

$$\nabla \cdot \sigma \nabla V = -\nabla \cdot \sigma A_1 \quad \text{in } \Omega \times \mathbb{R}_+\,.$$

The boundary condition on V can be set as a Neumann boundary condition. Since the medium Ω is usually embedded in a non-conductive medium (air), no currents leave the medium, *i.e.*, $J \cdot \nu = 0$ on $\partial\Omega$, where ν is the outward normal at $\partial\Omega$. To make sure that the boundary-value problem satisfied by V is well posed, we add the condition $\int_\Omega V = 0$. We have the following boundary value problem for V:

$$\begin{cases} \nabla \cdot \sigma \nabla V = -\,\nabla \cdot \sigma A_1 & \text{in } \Omega\,, \\[2mm] \sigma \dfrac{\partial V}{\partial \nu} = -\,\sigma A_1 \cdot \nu & \text{on } \partial\Omega\,, \\[2mm] \displaystyle\int_\Omega V = 0\,. \end{cases} \qquad (16.7)$$

16.2.3 Acoustic Problem

Elasticity Formulation

The eddy currents induced in the medium, combined with the magnetic field, create a Lorentz force based stress in the medium. The Lorentz force F is determined as

$$F = J \times B \quad \text{in } \Omega \times \mathbb{R}_+\,. \qquad (16.8)$$

Since the duration and the amplitude of the stimulation are both small, we assume that we can use the linear elasticity model. The displacements inside the medium can be described by the initial boundary-value problem for the Lamé system of equations

$$\begin{cases} \rho \partial_t^2 u - \nabla \lambda \nabla \cdot u - \nabla \cdot \mu \nabla^s u = J \times B & \text{in } \Omega \times \mathbb{R}_+\,, \\[2mm] \dfrac{\partial u}{\partial n} = 0 & \text{on } \partial\Omega \times \mathbb{R}_+\,, \\[2mm] u(x,0) = \dfrac{\partial u}{\partial t}(x,0) = 0 & \text{in } \Omega\,, \end{cases} \qquad (16.9)$$

where λ and μ are the Lamé coefficients, ρ is the density of the medium at rest, and ∇^s is the symmetric gradient defined by (3.124). Here, $\partial/\partial n$ denotes the co-normal derivative defined by

$$\frac{\partial u}{\partial n} = \lambda(\nabla \cdot u)\nu + 2\mu \nabla^s u\,\nu \quad \text{on } \partial\Omega\,,$$

where ν is the outward normal at $\partial\Omega$. The functions λ, μ, and ρ are assumed to be positive, smooth functions on $\overline{\Omega}$.

The Neumann boundary condition, $\partial u/\partial n = 0$ on $\partial\Omega$, comes from the fact that the sample is embedded in air and can move freely at the boundary.

Acoustic Wave Equation

Under some physical assumptions, the Lamé system of equations (16.9) can be reduced to an acoustic wave equation. For doing so, we neglect the shear effects in the medium by taking $\mu = 0$. The acoustic approximation says that the dominant wave type is a compressional wave. Equation (16.9) becomes

$$
\begin{cases}
\rho \partial_t^2 u - \nabla \lambda \nabla \cdot u = J \times B & \text{in } \Omega \times \mathbb{R}_+ , \\
\dfrac{\partial u}{\partial n} = 0 & \text{on } \partial\Omega \times \mathbb{R}_+ , \\
u(x,0) = \dfrac{\partial u}{\partial t}(x,0) = 0 & \text{in } \Omega .
\end{cases}
\tag{16.10}
$$

Introduce the pressure

$$
p = \lambda \nabla \cdot u \quad \text{in } \Omega \times \mathbb{R}_+ .
$$

Taking the divergence of (16.10) yields the acoustic wave equation

$$
\begin{cases}
\dfrac{1}{\lambda} \dfrac{\partial^2 p}{\partial t^2} - \nabla \cdot \dfrac{1}{\rho} \nabla p = \nabla \cdot \dfrac{1}{\rho}(J \times B) & \text{in } \Omega \times \mathbb{R}_+ , \\
p = 0 & \text{on } \partial\Omega \times \mathbb{R}_+ , \\
p(x,0) = \dfrac{\partial p}{\partial t}(x,0) = 0 & \text{in } \Omega .
\end{cases}
\tag{16.11}
$$

We assume that the duration τ_{pulse} of the electrical pulse sent into the medium is short enough so that p is the solution to

$$
\begin{cases}
\dfrac{1}{\lambda} \dfrac{\partial^2 p}{\partial t^2}(x,t) - \nabla \cdot \dfrac{1}{\rho} \nabla p(x,t) = -f(x)\delta_0 & \text{in } \Omega \times \mathbb{R}_+ , \\
p = 0 & \text{on } \partial\Omega \times \mathbb{R}_+ , \\
p(x,0) = \dfrac{\partial p}{\partial t}(x,0) = 0 & \text{in } \Omega ,
\end{cases}
\tag{16.12}
$$

where

$$
f(x) = - \int_0^{\tau_{\text{pulse}}} \nabla \cdot (\dfrac{1}{\rho} J(x,t) \times B(x,t)) dt .
\tag{16.13}
$$

Recall that acoustic wave reflection in soft tissue by an interface with air can be modeled well by a homogeneous Dirichlet boundary condition.

Let

$$
g(x,t) = \dfrac{\partial p}{\partial \nu}(x,t), \quad \forall (x,t) \in \partial\Omega \times \mathbb{R}_+ .
$$

In the next section, we aim at reconstructing the source term f from the data g.

16.3 Reconstruction of the Acoustic Source

In this subsection, we assume that $\lambda = \lambda_0 + \delta\lambda$ and $\rho = \rho_0 + \delta\rho$, where the functions $\delta\lambda$ and $\delta\rho$ are such that $||\delta\lambda||_{L^\infty(\Omega)} \ll \lambda_0$ and $||\delta\rho||_{L^\infty(\Omega)} \ll \rho_0$. We assume that λ, λ_0, ρ, and ρ_0 are known and denote by $c_0 = \sqrt{\frac{\lambda_0}{\rho_0}}$ the background acoustic speed. Based on the Born approximation, we image the source term f. Let $k_0 = \omega/c_0$. Let Γ_{k_0} be the outgoing fundamental solution to $\Delta + k_0^2$ and let G_{k_0} be the Dirichlet Green function for $\Delta + k_0^2$ in Ω, *i.e.*, for each $y \in \Omega$, $G_{k_0}(x, y)$ is the solution to (3.70).

Let $\hat{p}$ denote the Fourier transform of the pressure p and $\hat{g}$ the Fourier transform of g. The function $\hat{p}$ is the solution to the Helmholtz equation:

$$
\begin{cases}
\dfrac{\omega^2}{\lambda(x)}\hat{p}(x,\omega) + \nabla \cdot \dfrac{1}{\rho(x)}\nabla\hat{p}(x,\omega) = f(x), & x \in \Omega\,, \\[2ex]
\hat{p}(x,\omega) = 0, & x \in \partial\Omega\,.
\end{cases}
$$

Note that f is a real-valued function.

The Lippmann-Schwinger representation formula (3.78) shows that

$$
\hat{p}(x,\omega) = \int_\Omega (\frac{\rho_0}{\rho(y)} - 1)\nabla\hat{p}(y,\omega) \cdot \nabla G_{k_0}(x,y)\,dy
$$
$$
-\omega^2 \int_\Omega (\frac{\rho_0}{\lambda(y)} - \frac{\rho_0}{\lambda_0})\hat{p}(y,\omega)G_{k_0}(x,y)\,dy + \rho_0 \int_\Omega f(y)G_{k_0}(x,y)\,dy\,.
$$

Using the Born approximation (3.79), we obtain

$$
\hat{p}(x,\omega) \approx -\frac{1}{\rho_0}\int_\Omega \delta\rho(y)\nabla\hat{p}_0(y,\omega) \cdot \nabla G_{k_0}(x,y)\,dy + \frac{\omega^2}{c_0^2}\int_\Omega \frac{\delta\lambda(y)}{\lambda_0}\hat{p}_0(y,\omega)G_{k_0}(x,y)\,dy
$$
$$
+\rho_0 \int_\Omega f(y)G_{k_0}(x,y)\,dy
$$

for $x \in \Omega$, where

$$
\hat{p}_0(x,\omega) := \rho_0 \int_\Omega f(y)G_{k_0}(x,y)\,dy, \quad x \in \Omega\,.
$$

Therefore, from identity (3.73), it follows that

$$
(\frac{1}{2}I + (\mathcal{K}_\Omega^{k_0})^*)[\hat{g}](x,\omega) \approx -\frac{1}{\rho_0}\int_\Omega \delta\rho(y)\nabla\hat{p}_0(y,\omega) \cdot \nabla\frac{\partial\Gamma_{k_0}(x,y)}{\partial\nu(x)}\,dy
$$
$$
+k_0^2 \int_\Omega \frac{\delta\lambda(y)}{\lambda_0}\hat{p}_0(y,\omega)\frac{\partial\Gamma_{k_0}(x,y)}{\partial\nu(x)}\,dy + \rho_0 \int_\Omega f(y)\frac{\partial\Gamma_{k_0}(x,y)}{\partial\nu(x)}\,dy
$$

for $x \in \partial\Omega$.

Introduce

$$I(z,\omega) := \int_{\partial\Omega}\left[\overline{\Gamma_{k_0}}(x,z)(\tfrac{1}{2}I+(\mathcal{K}_\Omega^{k_0})^*)[\hat{g}](x,\omega)-\Gamma_{k_0}(x,z)\overline{(\tfrac{1}{2}I+(\mathcal{K}_\Omega^{k_0})^*)[\hat{g}]}(x,\omega)\right]d\sigma(x)$$

for $z \in \Omega$.

Recall that f is real-valued and write $f \approx f^{(0)} + \delta f$. In view of the Helmholtz-Kirchhoff identity (3.80), given $I(z,\omega)$ we solve the deconvolution problem

$$2i\rho_0 \int_\Omega \Im\Gamma_{k_0}(z,y)f^{(0)}(y)\,dy = I(z,\omega)\,,\quad z \in \Omega, \qquad (16.14)$$

in order to reconstruct $f^{(0)}$ with a resolution limit determined by the diffraction limit. Once $f^{(0)}$ is determined, we solve the second deconvolution problem (16.15)

$$2i\rho_0 \int_\Omega \Im\Gamma_{k_0}(z,y)\delta f(y)\,dy = \delta I(z,\omega)\,,\quad z \in \Omega, \qquad (16.15)$$

to find the correction δf. Here,

$$\delta I(z,\omega) := \int_{\partial\Omega}\left[\overline{\Gamma_{k_0}}(x,z)\delta\hat{g}(x,\omega) - \Gamma_{k_0}(x,z)\overline{\delta\hat{g}}(x,\omega)\right]d\sigma(x)$$

with

$$\delta\hat{g}(x,\omega) = \frac{1}{\rho_0}\int_\Omega \delta\rho(y)\nabla\hat{p}^{(0)}(y,\omega)\cdot\nabla\frac{\partial\Gamma_{k_0}(x,y)}{\partial\nu(x)}\,dy + k_0^2\int_\Omega \frac{\delta\lambda(y)}{\lambda_0}\hat{p}^{(0)}(y,\omega)\frac{\partial\Gamma_{k_0}(x,y)}{\partial\nu(x)}\,dy\,,$$

and

$$\hat{p}^{(0)}(x,\omega) := \rho_0\int_\Omega f^{(0)}(y)G_{k_0}(x,y)\,dy\,,\quad x \in \Omega\,.$$

Since by Fourier transform, $\hat{g}$ is known for all $\omega \in \mathbb{R}_+$, $I(z,\omega)$ can be computed for all $\omega \in \mathbb{R}_+$. Then recall identity (7.14)

$$\frac{2}{\pi}\int_{\mathbb{R}_+} k\Im\Gamma_k(x,z)\,dk = -\delta_z(x)\,,$$

where δ_z is the Dirac mass at z, it follows that

$$f^{(0)}(z) = -\frac{1}{i\pi\rho_0 c_0^2}\int_{\mathbb{R}_+}\omega I(z,\omega)\,d\omega \quad \text{and} \quad \delta f(z) = -\frac{1}{i\pi\rho_0 c_0^2}\int_{\mathbb{R}_+}\omega\delta I(z,\omega)\,d\omega\,.$$

16.4 Reconstruction of the Conductivity

We assume that we have reconstructed the pressure source f given by (16.13). We also assume that the sample Ω is thin and hence can be assimilated to a two dimensional domain. Further, we suppose that $\Omega \subset \text{vect}\,(e_1, e_2)$. Here, vect (e_1, e_2) denotes the vector space spanned by e_1 and e_2. Recall that the magnetic fields B_0 and B_1 are parallel to e_3. We write $J(x,t) = J(x)w'(t)$. In order to recover the conductivity distribution, we start by reconstructing the vector field $J(x)$ in Ω.

16.4.1 Reconstruction of the Electric Current Density

Helmholtz Decomposition

We need the following two classical results.

Lemma 16.1 *If $\sigma \in L^{\infty}_{\underline{\sigma},\overline{\sigma}}(\Omega)$ then the solution V of (16.7) belongs to $W^{1,2}(\Omega)$ and hence, the electric current density J belongs to $L^2(\Omega)$.*

The following Helmholtz decomposition in two dimensions holds [327].

Lemma 16.2 *If f is a vector field in $L^2(\Omega)$, then there exist two scalar functions $v, \phi \in W^{1,2}(\Omega)$ such that*

$$f = \nabla v + \mathrm{curl}\varphi. \tag{16.16}$$

The differential operator curl *of a scalar function is defined by* $\mathrm{curl}\varphi = (-\partial_2\varphi, \partial_1\varphi)$. *Furthermore, if* $\nabla \cdot f \in L^2(\Omega)$, *then the potential v is a solution to*

$$\begin{cases} \Delta v = \nabla \cdot f & in \ \Omega, \\ \dfrac{\partial v}{\partial \nu} = f \cdot \nu & on \ \partial\Omega. \end{cases} \tag{16.17}$$

Let the curl of a vector function f be defined by $\mathrm{curl} f = -\partial_2 f_1 + \partial_1 f_2$. We apply the Helmholtz decomposition (16.16) to the vector field $J \in L^2(\Omega)$ and get the following proposition.

Proposition 16.3 *There exists a function $\varphi \in W_0^{1,2}(\Omega)$ such that*

$$J = \mathrm{curl}\varphi, \tag{16.18}$$

and φ is the unique solution of

$$\begin{cases} -\Delta\varphi = \mathrm{curl} J & in \ \Omega, \\ \varphi = 0 & on \ \partial\Omega. \end{cases} \tag{16.19}$$

Recall (16.3) together with the fact that no current leaves the medium

$$J \cdot \nu = 0 \quad on \ \partial\Omega.$$

Since v is a solution to (16.7), v has to be constant. So, in order to reconstruct J one only needs to reconstruct φ.

Recovery of J

Under the assumption $|B_1| \ll |B_0|$ in $\Omega \times \mathbb{R}_+$ and $|\delta\rho| \ll \rho_0$ in Ω, the pressure source term f defined by (16.13) can be approximated as follows:

$$f(x) \approx -\frac{1}{\rho_0}\nabla \cdot (J(x) \times B_0)(w(\tau_{\mathrm{pulse}}) - w(0)),$$

where we have used that $J(x,t) = J(x)w'(t)$.

Since B_0 is constant we get

$$\nabla \cdot (J(x) \times B_0) = (\nabla \times J) \cdot B_0 = |B_0|\mathrm{curl}J \,.$$

Now, since B_0 is known, we can compute φ as the unique solution of

$$\begin{cases} \Delta\varphi = \dfrac{\rho_0 f}{|B_0|(w(\tau_{\mathrm{pulse}}) - w(0))} & \text{in } \Omega\,, \\[2mm] \qquad\qquad\qquad\qquad \varphi = 0 & \text{on } \partial\Omega\,, \end{cases} \tag{16.20}$$

and then, by Proposition 16.3, compute J by $J = \mathrm{curl}\varphi$.

Note that since the problem is reduced to the two dimensional case, J is then contained in the plane $B_0^\perp$ with $\perp$ denoting the orthogonal.

16.4.2 Recovery of the Conductivity from Internal Electric Current Density

In this subsection we denote by σ_* the true conductivity of the medium, and we assume that $\sigma_* \in L^\infty_{\underline{\sigma},\overline{\sigma}}(\Omega)$ with $0 < \underline{\sigma} < \overline{\sigma}$, *i.e.*, it is bounded from below and above by positive known constants and is equal to some given positive constant σ_0 in a neighborhood of $\partial\Omega$.

Optimal Control Algorithm

Recall that A_1 is defined by $\nabla \cdot A_1 = 0, B_1(x)e_3 = \nabla \times A_1(x)$. Define the following operator $\mathcal{F}$:

$$L^\infty_{\underline{\sigma},\overline{\sigma}}(\Omega) \longrightarrow W^{1,2}(\Omega)$$

$$\sigma \longmapsto \mathcal{F}[\sigma] := U$$

with

$$\begin{cases} \nabla \cdot \sigma\nabla U = -\nabla \cdot \sigma A_1 & \text{in } \Omega\,, \\[2mm] \sigma\dfrac{\partial U}{\partial\nu} = -\sigma A_1 \cdot \nu & \text{on } \partial\Omega\,, \\[2mm] \displaystyle\int_\Omega U = 0\,. \end{cases} \tag{16.21}$$

The following lemma holds.

Lemma 16.4 *The operator $\mathcal{F}$ is Fréchet differentiable. For any $\sigma \in L^\infty_{\underline{\sigma},\overline{\sigma}}(\Omega)$ and h such that $\sigma + h \in L^\infty_{\underline{\sigma},\overline{\sigma}}(\Omega)$, we have*

$$d\mathcal{F}[\sigma](h) := q \quad s.t. \quad \begin{cases} \nabla \cdot \sigma\nabla q = -\nabla \cdot hA_1 - \nabla \cdot h\nabla\mathcal{F}[\sigma] & \text{in } \Omega\,, \\[2mm] \sigma\dfrac{\partial q}{\partial\nu} = 0 & \text{on } \partial\Omega\,, \\[2mm] \displaystyle\int_\Omega q = 0\,. \end{cases}$$

$$\tag{16.22}$$

Proof. Denote by r the function $\mathcal{F}[\sigma + h] - \mathcal{F}[\sigma] - q$. The function r belongs to $W^{1,2}(\Omega)$ and satisfies the following equation in Ω:

$$\nabla \cdot \sigma \nabla r = \nabla \cdot h \nabla \left(\mathcal{F}[\sigma] - \mathcal{F}[\sigma + h] \right) ,$$

together with the boundary condition

$$\frac{\partial r}{\partial \nu} = 0 \quad \text{on } \partial\Omega ,$$

and the zero mean condition $\int_\Omega r = 0$. We have the following estimate:

$$\|\nabla r\|_{L^2(\Omega)} \leq \frac{1}{a} \|h\|_{L^\infty(\Omega)} \|\nabla \left(\mathcal{F}[\sigma] - \mathcal{F}[\sigma + h] \right) \|_{L^2(\Omega)} .$$

Since $\mathcal{F}[\sigma] - \mathcal{F}[\sigma + h]$ satisfies

$$\nabla \cdot \left(\sigma \nabla \left(\mathcal{F}[\sigma] - \mathcal{F}[\sigma + h] \right) \right) = -\nabla \cdot \left(h \nabla \mathcal{F}[\sigma + h] \right) + \nabla \cdot (h A_1)$$

with the boundary condition

$$\frac{\partial}{\partial \nu} \left(\mathcal{F}[\sigma + h] - \mathcal{F}[\sigma] \right) = 0,$$

and the zero mean condition $\int_\Omega \left(\mathcal{F}[\sigma + h] - \mathcal{F}[\sigma] \right) = 0$. We can also estimate the L^2-norm of $\nabla \left(\mathcal{F}[\sigma + h] - \mathcal{F}[\sigma] \right)$ as follows:

$$\|\nabla \left(\mathcal{F}[\sigma + h] - \mathcal{F}[\sigma] \right) \|_{L^2(\Omega)} \leq \frac{1}{a} \|h\|_{L^\infty(\Omega)} \left(\|\nabla \mathcal{F}[\sigma + h]\|_{L^2(\Omega)} + \|A_1\|_{L^2(\Omega)} \right) .$$

Therefore, we can bound the $W^{1,2}$-norm of $\mathcal{F}[\sigma + h]$ independently of σ and h for $\|h\|_{L^\infty}$ small enough. There exists a constant C, depending only on Ω, a, b, and A_1, such that

$$\|\nabla \mathcal{F}[\sigma + h]\|_{L^2(\Omega)} \leq C .$$

Hence, we get

$$\|\nabla \left(\mathcal{F}[\sigma + h] - \mathcal{F}[\sigma] \right) \|_{L^2(\Omega)} \leq \frac{1}{a} \|h\|_{L^\infty(\Omega)} \left(C + \|A_1\|_{L^2(\Omega)} \right) ,$$

and therefore,

$$\|\nabla r\|_{L^2(\Omega)} \leq \widetilde{C} \|h\|_{L^\infty(\Omega)}^2 ,$$

which shows the Fréchet differentiability of $\mathcal{F}$. $\square$

Now, we introduce the misfit functional:

$$
\begin{aligned}
L^\infty_{\underline{\sigma}, \overline{\sigma}} &\longrightarrow \mathbb{R} \\
\sigma &\longmapsto \mathcal{J}[\sigma] = \frac{1}{2} \int_\Omega \left| \sigma \left(\nabla \mathcal{F}[\sigma] + A_1 \right) - J \right|^2 .
\end{aligned}
\tag{16.23}
$$

Lemma 16.5 *The misfit functional $\mathcal{J}$ is Fréchet-differentiable. For any $\sigma \in L^\infty_{\underline{\sigma},\overline{\sigma}}(\Omega)$, we have*

$$d\mathcal{J}[\sigma] = (\sigma \nabla \mathcal{F}[\sigma] + \sigma A_1 - J) \cdot (\nabla \mathcal{F}[\sigma] + A_1) + \nabla s \cdot (A_1 + \nabla \mathcal{F}[\sigma]) \,,$$

where s is defined as the solution to the adjoint problem:

$$\begin{cases} \nabla \cdot \sigma \nabla s = \nabla \cdot \left(\sigma^2 \nabla \mathcal{F}[\sigma] + \sigma^2 A_1 - \sigma J \right) & in \ \Omega \,, \\[2mm] \sigma \dfrac{\partial s}{\partial \nu} = 0 & on \ \partial \Omega \,, \\[2mm] \displaystyle\int_\Omega s = 0 \,. \end{cases} \qquad (16.24)$$

Proof. Since $\mathcal{F}$ is Fréchet-differentiable, so is $\mathcal{J}$. For any $\sigma \in L^\infty_{\underline{\sigma},\overline{\sigma}}(\Omega)$ and h such that $\sigma + h \in L^\infty_{\underline{\sigma},\overline{\sigma}}(\Omega)$, we have

$$d\mathcal{J}[\sigma](h) = \int_\Omega (\sigma \nabla \mathcal{F}[\sigma] + \sigma A_1 - J) \cdot (h \nabla (\mathcal{F}[\sigma] + A_1) + \sigma \nabla (d\mathcal{F}[\sigma](h))) \,.$$

Multiplying (16.24) by $d\mathcal{F}[\sigma](h)$ we get

$$\int_\Omega \sigma \left(\sigma \nabla \mathcal{F}[\sigma] + \sigma A_1 - J \right) \cdot \nabla d\mathcal{F}[\sigma](h) = \int_\Omega \sigma \nabla s \cdot \nabla d\mathcal{F}[\sigma](h) \,.$$

On the other hand, multiplying (16.22) by s we obtain

$$\int_\Omega \sigma \nabla s \cdot \nabla d\mathcal{F}[\sigma](h) = \int_\Omega h \nabla s \cdot (A_1 + \nabla \mathcal{F}[\sigma]) \,.$$

So we have

$$d\mathcal{J}[\sigma](h) = \int_\Omega h \left[(\sigma \nabla \mathcal{F}[\sigma] + \sigma A_1 - J) \cdot (\nabla \mathcal{F}[\sigma] + A_1) + \nabla s \cdot (A_1 + \nabla \mathcal{F}[\sigma]) \right],$$

and the proof is complete. $\quad\square$

Lemma 16.5 allows us to apply the gradient descent method in order to minimize the discrepancy functional $\mathcal{J}$. Let $\sigma^{(0)}$ be an initial guess in $L^\infty_{\underline{\sigma},\overline{\sigma}}(\Omega)$. We compute the iterates

$$\sigma^{(n+1)} = T[\sigma^{(n)}] - \eta d\mathcal{J}[T[\sigma^{(n)}]] \,, \quad \forall n \in \mathbb{N}, \qquad (16.25)$$

where $\eta > 0$ is the step size and $T[f] = \min\{\max\{f, \underline{\sigma}\}, \overline{\sigma}\}$.

In what follows, we prove the convergence of (16.25) with two excitations. Let $J^{(1)}$ and $J^{(2)}$ correspond to two different excitations $A_1^{(1)}$ and $A_1^{(2)}$. Assume that $J^{(1)} \times J^{(2)} \neq 0$ in Ω. Let $\mathcal{G}^{(i)} : \sigma \mapsto \sigma \nabla \left(\mathcal{F}^{(i)}[\sigma] + A_1^{(i)} \right) - J_i$, where $\mathcal{F}^{(i)}$ is defined by (16.22) with $A_1 = A_1^{(i)}$ for $i = 1, 2$. The optimal

control algorithm (16.25) with two excitations is equivalent to the following Landweber scheme given by

$$\sigma^{(n+1)} = T[\sigma^{(n)}] - \eta d\mathcal{G}^*[\mathcal{G}[T[\sigma^{(n)}]]], \quad \forall n \in \mathbb{N}, \qquad (16.26)$$

where $\mathcal{G}[\sigma] = (\mathcal{G}^{(1)}[\sigma], \mathcal{G}^{(2)}[\sigma])^T$.

We now prove the convergence and stability of (16.26) provided that two magnetic excitations leading to nonparallel current densities are employed.

Proposition 16.6 *Let $J^{(1)}$ and $J^{(2)}$ correspond to two different excitations. Assume that $J^{(1)} \times J^{(2)} \neq 0$ in Ω. Then there exists $\eta > 0$ such that if $||\sigma^{(0)} - \sigma_*||_{W_0^{1,2}(\Omega)} \leq \eta$, then $||\sigma^{(n)} - \sigma_*||_{W_0^{1,2}(\Omega)} \to 0$ as $n \to +\infty$.*

Proof. It suffices to prove that there exists a positive constant C such that

$$||d\mathcal{G}[\sigma](h)||_{W^{1,2}(\Omega)} \geq C||h||_{W_0^{1,2}(\Omega)} \qquad (16.27)$$

for all $h \in W_0^{1,2}(\Omega)$ such that $\sigma + h \in L_{\underline{\sigma},\overline{\sigma}}^\infty(\Omega)$. We have

$$d\mathcal{G}^{(i)}[\sigma](h) = hJ^{(i)} + \sigma\nabla d\mathcal{F}^{(i)}[\sigma](h).$$

Therefore,

$$\nabla \cdot d\mathcal{G}^{(i)}[\sigma](h) = 0, \quad d\mathcal{G}^{(i)}[\sigma](h) \cdot \nu = 0,$$

and

$$\nabla \times (\frac{1}{\sigma}d\mathcal{G}^{(i)}[\sigma](h)) = h\nabla \times (\frac{1}{\sigma}J^{(i)}) + \sigma\nabla h \times J^{(i)}.$$

Since $\nabla \times (\frac{1}{\sigma}J^{(i)}) \times e_3 = 0$ and $J^{(1)} \times J^{(2)} \neq 0$, it follows that

$$||h||_{W_0^{1,2}(\Omega)} \leq C\sum_{i=1}^{2} ||d\mathcal{G}^{(i)}[\sigma](h)||_{W_0^{1,2}(\Omega)},$$

which completes the proof. $\square$

Let $\mathcal{F}[\sigma] = (\mathcal{F}^{(1)}[\sigma], \mathcal{F}^{(2)}[\sigma])^T$. Note that analogously to (16.27) there exists a positive constant C such that

$$||d\mathcal{F}[\sigma](h)||_{W_0^{1,2}(\Omega)} \geq C||h||_{W_0^{1,2}(\Omega)}$$

for all $h \in W_0^{1,2}(\Omega)$ such that $\sigma + h \in L_{\underline{\sigma},\overline{\sigma}}^\infty(\Omega)$, provided that $J^{(1)} \times J^{(2)} \neq 0$ in Ω.

Fixed Point Algorithm

In this subsection, we denote by σ_* the true conductivity inside the domain Ω. We also make the following assumptions:

- $\exists c > 0,$ such that $|B_1| > c$ in Ω;
- $\sigma \in \mathcal{C}^{0,\alpha}(\overline{\Omega}),$ $\alpha \in (0,1)$;
- $\sigma_* = \sigma_0$ in an open neighborhood of $\partial\Omega$.

From the unique continuation principle, the following lemma holds.

Lemma 16.7 *The set $\{x \in \Omega, J(x) = 0\}$ is nowhere dense.*

The interior data is $J = \sigma_* \left[\nabla \mathcal{F}[\sigma_*] + A_1\right]$. One can only hope to recover σ_* at the points where $J \neq 0$. Even then, we can expect any type of reconstruction to be numerically unstable in sets where J is very small. Assume that J is continuous and let $\varepsilon > 0$ and x_0 be such that $|J(x_0)| > 2\varepsilon$. We define Ω_ε to be a neighborhood of x_0 such that for any $x \in \Omega_\varepsilon$, $|J(x)| > \varepsilon$. One can assume that Ω_ε is a $\mathcal{C}^1$ domain without loosing generality. Now, introduce the operator $\mathcal{F}_\varepsilon$ as follows:

$$L^\infty_{\underline{\sigma},\overline{\sigma}}(\Omega_\varepsilon) \longrightarrow W^{1,2}(\Omega_\varepsilon)$$
$$\sigma \longmapsto \mathcal{F}_\varepsilon[\sigma] := V_\varepsilon \,,$$

where V_ε satisfies the following equation:

$$\begin{cases} \nabla \cdot \sigma \nabla V_\varepsilon = -\nabla \cdot (\sigma A_1) & \text{in } \Omega_\varepsilon \,, \\ \sigma \dfrac{\partial V_\varepsilon}{\partial \nu} = -\sigma A_1 \cdot \nu + J \cdot \nu & \text{on } \partial\Omega_\varepsilon \,, \\ \displaystyle\int_{\Omega_\varepsilon} V_\varepsilon = 0 \,, \end{cases} \tag{16.28}$$

where ν denotes the outward normal to $\partial\Omega_\varepsilon$. Note that $\int_{\partial\Omega_\varepsilon} J \cdot \nu = 0$ since $\nabla \cdot J = 0$ in Ω_ε.

We also define the nonlinear operator $\mathcal{G}_\varepsilon$ by

$$L^\infty_{\underline{\sigma},\overline{\sigma}}(\Omega_\varepsilon) \longrightarrow L^\infty(\Omega_\varepsilon)$$
$$\sigma \longmapsto \mathcal{G}_\varepsilon[\sigma] := \sigma \frac{(\sigma\nabla V_\varepsilon[\sigma] + \sigma A_1) \cdot J}{|J|^2} \,. \tag{16.29}$$

Lemma 16.8 *The restriction of σ_* on Ω_ε is a fixed point for the operator $\mathcal{G}_\varepsilon$.*

Proof. For the existence it suffices to prove that $\mathcal{F}_\varepsilon \left[\sigma_*|_{\Omega_\varepsilon}\right] = \mathcal{F}[\sigma_*]\big|_{\Omega_\varepsilon}$. Denote by $V_* = \mathcal{F}[\sigma_*]$. We can see that V_* satisfies

$$\nabla \cdot \sigma_* \nabla V_* = -\nabla \cdot (\sigma A_1) \quad \text{in } \Omega_\varepsilon \,.$$

Taking the normal derivative along the boundary of Ω_ε, we get

$$\sigma \frac{\partial V_*}{\partial \nu} = -\sigma A_1 \cdot \nu + J \cdot \nu \quad \text{on } \partial\Omega_\varepsilon \,.$$

From the well posedness of (16.28), it follows that

$$V_*\big|_{\Omega_\varepsilon} = \mathcal{F}_\varepsilon[\sigma_*\big|_{\Omega_\varepsilon}] + c, \quad c \in \mathbb{R}.$$

So, we arrive at

$$\mathcal{G}_\varepsilon\left[\sigma_*\big|_{\Omega_\varepsilon}\right] = \sigma_*\big|_{\Omega_\varepsilon}.$$

We need the following lemma. We refer to [327] for its proof.

Lemma 16.9 *Let $\Omega \subset \mathbb{R}^2$ be a bounded domain with Lipschitz boundary. For each $g \in W^{-1,2}(\Omega)$ there exists at least one $v \in L^2(\Omega)$ with $\nabla \cdot v = g$ in the sense of the distributions and*

$$\|v\|_{L^2(\Omega)} \leq C\|g\|_{W^{-1,2}(\Omega)}$$

with the constant C depending only on Ω.

The following result holds.

Lemma 16.10 *If $\|A_1\|_{L^2(\Omega_\varepsilon)}$ is small enough, then the operator $\mathcal{G}_\varepsilon$ is a contraction.*

Proof. Take σ_1 and σ_2 in $L^\infty_{\underline{\sigma},\overline{\sigma}}(\Omega)$. We have

$$|\mathcal{G}_\varepsilon[\sigma_1](x) - \mathcal{G}_\varepsilon[\sigma_2](x)| = \frac{1}{|J(x)|^2}$$
$$\times \left|\left(\sigma_1^2(x)\nabla V_\varepsilon[\sigma_1](x) - \sigma_2^2(x)\nabla V_\varepsilon[\sigma_2](x) + \left(\sigma_1^2(x) - \sigma_2^2(x)\right)A_1(x)\right) \cdot J(x)\right|,$$

which gives, using the Cauchy–Schwarz inequality:

$$|\mathcal{G}_\varepsilon[\sigma_1](x) - \mathcal{G}_\varepsilon[\sigma_2](x)| \leq \frac{1}{\varepsilon}$$
$$\times \left|\left(\sigma_1^2(x)\nabla V_\varepsilon[\sigma_1](x) - \sigma_2^2(x)\nabla V_\varepsilon[\sigma_2](x) + \left(\sigma_1^2(x) - \sigma_2^2(x)\right)A_1(x)\right)\right|.$$

The right-hand side can be rewritten using the fact that $|\sigma_i(x)| \leq b$ for $i = 1, 2$, and hence,

$$|\mathcal{G}_\varepsilon[\sigma_1](x) - \mathcal{G}_\varepsilon[\sigma_2](x)| \leq \frac{b}{\varepsilon}$$
$$\times \left[|\sigma_1(x)\nabla V_\varepsilon[\sigma_1](x) - \sigma_2(x)\nabla V_\varepsilon[\sigma_2](x)| + |(\sigma_1(x) - \sigma_2(x))A_1(x)|\right].$$
$$(16.30)$$

Now, consider the function $v = \sigma_1 \nabla V_\varepsilon[\sigma_1] - \sigma_2 \nabla V_\varepsilon[\sigma_2]$. We get

$$\nabla \cdot v = -\nabla \cdot [(\sigma_1 - \sigma_2)A_1] \quad \text{in } \partial\Omega_\varepsilon,$$

along with the boundary condition $v \cdot \nu = 0$ on $\partial\Omega_\varepsilon$. Using Lemma 16.9, there exists a constant C depending only on Ω_ε such that

$$\|v\|_{L^2(\Omega_\varepsilon)} \le C \|\nabla \cdot [(\sigma_1 - \sigma_2) A_1]\|_{W^{1,2}(\Omega_\varepsilon)},$$

which shows that

$$\|v\|_{L^2(\Omega_\varepsilon)} \le C \|(\sigma_1 - \sigma_2) A_1\|_{L^2(\Omega_\varepsilon)}.$$

Using the Cauchy–Schwarz inequality:

$$\|v\|_{L^2(\Omega_\varepsilon)} \le C \|\sigma_1 - \sigma_2\|_{L^2(\Omega_\varepsilon)} \|A_1\|_{L^2(\Omega_\varepsilon)}. \tag{16.31}$$

Putting together (16.30) with (16.31), we arrive at

$$\|\mathcal{G}_\varepsilon[\sigma_1] - \mathcal{G}_\varepsilon[\sigma_2]\|_{L^2(\Omega_\varepsilon)} \le (C+1) \frac{b}{\varepsilon} \|A_1\|_{L^2(\Omega_\varepsilon)} \|\sigma_1 - \sigma_2\|_{L^2(\Omega_\varepsilon)}.$$

The proof is then complete. $\square$

The following proposition shows the convergence of the fixed point reconstruction algorithm.

Proposition 16.11 *Let $\sigma^{(n)} \in \left(L^2(\Omega_\varepsilon)\right)^{\mathbb{N}}$ be the sequence defined by*

$$
\begin{aligned}
\sigma^{(0)} &= 1, \\
\sigma^{(n+1)} &= \max\left(\min\left(\mathcal{G}_\varepsilon[\sigma^{(n)}], \overline{\sigma}\right), \underline{\sigma}\right), \quad \forall n \in \mathbb{N}.
\end{aligned} \tag{16.32}
$$

If $\|A_1\|_{L^2(\Omega_\varepsilon)}$ is small enough, then the sequence is well defined and $\sigma^{(n)}$ converges to $\sigma_*\big|_{\Omega_\varepsilon}$ in $L^2(\Omega_\varepsilon)$.

Proof. Let $(X, d) = \left(L^\infty_{\underline{\sigma},\overline{\sigma}}(\Omega_\varepsilon), \|\cdot\|_{L^2(\Omega_\varepsilon)}\right)$. Then, (X, d) is a complete, non empty metric space. Let T_ε be the map defined by

$$
\begin{aligned}
L^\infty_{\underline{\sigma},\overline{\sigma}}(\Omega_\varepsilon) &\longrightarrow L^\infty_{\underline{\sigma},\overline{\sigma}}(\Omega_\varepsilon) \\
\sigma &\longmapsto T_\varepsilon[\sigma] := \max\left(\min\left(\mathcal{G}_\varepsilon[\sigma], b\right), a\right).
\end{aligned}
$$

Using Lemma 16.10, we get that T_ε is a contraction, provided that $\|A_1\|_{L^2(\Omega_\varepsilon)}$ is small enough. We already have the existence of a fixed point given by Lemma 16.8, and therefore, Banach's fixed point theorem gives the convergence of the sequence for the L^2 norm over Ω_ε, and the uniqueness of the fixed point. $\square$

Orthogonal Field Method

In this section we present a non-iterative method to reconstruct the electrical conductivity from the electric current density. We assume that $\sigma_* \in \mathcal{C}^{0,\alpha}(\overline{\Omega})$, $\alpha \in (0, 1]$. The fields $J = (J_1, J_2)$ and A_1 are assumed to be known in Ω. Our goal is to reconstruct V_* the solution of (16.7) in $W^{1,2}(\Omega)$. Then, computing $\frac{|\nabla V_* + A_1|}{|J|}$ for $|J|$ nonzero will give us $\frac{1}{\sigma_*}$. Recall that $J = \text{curl} w$

where w is defined by equation (16.20). We say that the data f on the right hand side of (16.20) is admissible if $f > 0$ or $f < 0$ in Ω and if the critical points of w are isolated.

Introduce $F = (-J_2, J_1)^T$ the rotation of J by $\frac{\pi}{2}$. It is worth noticing that the true electrical potential V_* is a solution of

$$\begin{cases} F \cdot \nabla V_* = -F \cdot A_1 & \text{in } \Omega\,, \\ \dfrac{\partial V_*}{\partial \nu} = -A_1 \cdot \nu & \text{on } \partial\Omega\,, \\ \displaystyle\int_\Omega V_* = 0\,. \end{cases} \tag{16.33}$$

Equation (16.33) has a unique solution in $W^{1,2}(\Omega)$, and this solution is the true potential V_*.

As in Chapter 15, by using the method of characteristics, we can prove that the following uniqueness result holds.

Proposition 16.12 *If $U \in W^{1,2}(\Omega)$ is a solution of*

$$\begin{cases} F \cdot \nabla U = 0 & \text{in } \Omega\,, \\ \dfrac{\partial U}{\partial \nu} = 0 & \text{on } \partial\Omega\,, \\ \displaystyle\int_\Omega U = 0\,, \end{cases} \tag{16.34}$$

then $U = 0$ in Ω.

In order to solve numerically (16.33), we use the method of viscosity regularization introduced in Subsection 15.5.2. The field A_1 is known and we can solve uniquely the following problem:

$$\begin{cases} \nabla \cdot \left[\left(\eta I + F F^T \right) \nabla U_\eta \right] = -\nabla \cdot F F^T A_1 & \text{in } \Omega\,, \\ \dfrac{\partial U_\eta}{\partial \nu} = -A_1 \cdot \nu & \text{on } \partial\Omega\,, \\ \displaystyle\int_\Omega U_\eta = 0\,, \end{cases} \tag{16.35}$$

for some small $\eta > 0$. Here, I denotes the 2×2 identity matrix.

Proposition 16.13 *Let σ_* be the true conductivity. Let V_* be the solution to (16.21) with $\sigma = \sigma_*$. The solution U_η of (16.35) converges strongly to V_* in $W^{1,2}(\Omega)$ when η goes to zero.*

Proof. We can easily see that $\widetilde{U}_\eta = U_\eta - V_*$ is the solution to

$$\begin{cases} \nabla \cdot \left[\left(\eta I + F F^T \right) \nabla \widetilde{U}_\eta \right] = -\eta \Delta V_* & \text{in } \Omega\,, \\ \dfrac{\partial \widetilde{U}_\eta}{\partial \nu} = 0 & \text{on } \partial\Omega\,, \\ \displaystyle\int_\Omega \widetilde{U}_\eta = 0\,. \end{cases} \tag{16.36}$$

Multiplying (16.36) by $\widetilde{U}_\eta$ and integrating by parts over Ω, we find that

$$\eta \int_\Omega |\nabla \widetilde{U}_\eta|^2 + \int_\Omega |F \cdot \nabla \widetilde{U}_\eta|^2 = \eta \int_\Omega \nabla \widetilde{U}_\eta \cdot \nabla V_* + \eta \int_{\partial\Omega} \widetilde{U}_\eta A_1 \cdot \nu, \quad (16.37)$$

since $\dfrac{\partial \widetilde{U}_\eta}{\partial \nu} = 0$ and $\dfrac{\partial V_*}{\partial \nu} = -A_1 \cdot \nu$. Therefore, we have

$$\|\widetilde{U}_\eta\|^2_{W^{1,2}(\Omega)} \leq \|\widetilde{U}_\eta\|_{W^{1,2}(\Omega)} \|V_*\|_{W^{1,2}(\Omega)} + C\|\widetilde{U}_\eta\|_{W^{1,2}(\Omega)},$$

where C depends only on Ω and A_1. This shows that the sequence $(\widetilde{U}_\eta)_{\eta>0}$ is bounded in $W^{1,2}(\Omega)$. Using Banach-Alaoglu's theorem we can extract a subsequence which converges weakly to some u^* in $W^{1,2}(\Omega)$. We multiply (16.36) by u^* and integrate by parts over Ω to obtain

$$\int_\Omega \left(F \cdot \nabla \widetilde{U}_\eta\right)\left(F \cdot \nabla u^*\right) = \eta \left[\int_\Omega \nabla V_* \cdot \nabla u^* - \int_\Omega \nabla \widetilde{U}_\eta \cdot \nabla u^* + \int_{\partial\Omega} u^* A_1 \cdot \nu\right].$$

Taking the limit when η goes to zero yields

$$\|F \cdot \nabla u^*\|_{L^2(\Omega)} = 0.$$

Using Proposition 16.12, we have

$$u^* = 0 \text{ in } \Omega,$$

since u^* is a solution to (16.34).

Actually, we can see that there is no need for an extraction, since 0 is the only accumulation point for $\widetilde{U}_\eta$ with respect to the weak topology. If we consider a subsequence $\widetilde{U}^{(\phi(\eta))}$, it is still bounded in $W^{1,2}(\Omega)$ and therefore, using the same argument as above, zero is an accumulation point of this subsequence. For the strong convergence, we use (16.37) to get

$$\int_\Omega |\nabla \widetilde{U}_\eta|^2 \leq \int_\Omega \nabla \widetilde{U}_\eta \cdot \nabla V_* + \int_{\partial\Omega} \widetilde{U}_\eta A_1 \cdot \nu. \quad (16.38)$$

Since $\widetilde{U}_\eta \rightharpoonup 0$, the right-hand side of (16.38) goes to zero when η goes to zero. Hence,

$$\|\widetilde{U}_\eta\|_{W^{1,2}(\Omega)} \longrightarrow 0 \quad \text{as } \eta \to 0,$$

and the proof is complete. $\square$

Now, we take U_η to be the solution of (16.35) and define the approximated resistivity (inverse of the conductivity) by

$$\frac{1}{\sigma_\eta} = \frac{|\nabla U_\eta + A_1|}{|J|}. \quad (16.39)$$

Since

$$\frac{1}{\sigma_*} = \frac{|\nabla V_* + A_1|}{|J|}\,,$$

Proposition 16.13 shows that $\dfrac{1}{\sigma_\eta}$ is a good approximation for $\dfrac{1}{\sigma_*}$ in the L^2-sense.

Proposition 16.14 *Let σ_* be the true conductivity and let σ_η be defined by (16.39). We have*

$$\left\|\frac{1}{\sigma_\eta} - \frac{1}{\sigma_*}\right\|_{L^2(\Omega)} \longrightarrow 0 \quad as\ \eta \to 0\,.$$

16.5 Numerical Illustrations

We set $\Omega = \left\{(x,y) \in \mathbb{R}^2,\ \left(\dfrac{x}{2}\right)^2 + y^2 < 1\right\}$. We take a conductivity $\sigma \in \mathcal{C}^{0,\alpha}(\Omega)$ as represented on Figure 16.1. The potential A_1 is chosen as

$$A_1(x) = 10^{-2}\left(\frac{y}{2} + 1; -\frac{x}{2} + 1\right),$$

so that B_1 is constant in space.

16.5.1 Optimal Control

We use the algorithm presented in section 16.4.2. We set a step size equal to $8 \cdot 10^{-7}$ and $\sigma^{(0)} = 3$ as an initial guess. After 50 iterations, we get the reconstruction shown in Figure 16.2. The general shape of the conductivity as well as the conductivity contrast are quite well recovered. However, the convergence is quite slow. It is worth mentioning that using two nonparallel electric current densities does not improve significantly the quality of the reconstruction.
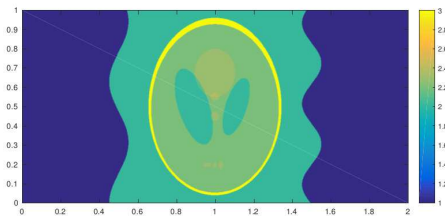
Fig. 16.1. Conductivity to be reconstructed.
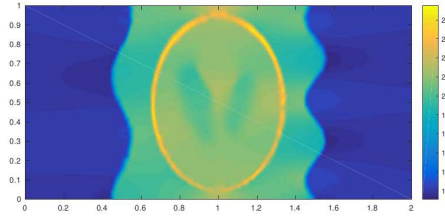
Fig. 16.2. Conductivity reconstructed by the optimal control method after 50 iterations.

16.5.2 Fixed Point Method

We use the algorithm described in section 16.4.2, but slightly modified. The operator $\mathcal{G}$ defined by

$$\mathcal{G}[\sigma] := \sigma \frac{(\sigma \nabla V[\sigma] + \sigma A_1) \cdot J}{|J|^2}$$

is replaced by

$$\widetilde{\mathcal{G}}[\sigma] := \frac{(\nabla V[\sigma] + A_1) \cdot J}{|\nabla V[\sigma] + A_1|^2} \, ,$$

which is analytically the same but numerically is more stable. Since the term $|\nabla V[\sigma] + A_1|^2$ can be small, we smooth out the reconstructed conductivity $\sigma^{(n)}$ at each step by convolving it with a Gaussian kernel. This makes the algorithm less unstable. The result after 9 iterations is shown in Figure 16.3. The convergence is faster than the gradient descent, but the algorithm still fails at recovering the exact values of the true conductivity.

16.5.3 Orthogonal Field Method

We set $\eta = 5 \cdot 10^{-4}$ and perform the computation described in section 16.4.2. The result we get is shown in Figure 16.4. It is a scaled version of the true conductivity σ_*, which means that the contrast is recovered. So assuming we know the conductivity in a small region of Ω (or near the boundary $\partial\Omega$) we can re-scale the result, as shown in Figure 16.5. When η goes to zero, the solution of (16.35) converges to the true potential V_* up to a scaling factor which goes to infinity. When η is large, the scaling factor goes to one but the solution U_η becomes a "smoothed out" version of V_*. This method allows an accurate reconstruction of the conductivity by solving only one partial differential equation. It covers the contrast accurately, provided we have a little bit of a prior information on σ_*.

Finally, we study the numerical stability with respect to measurement noise of the orthogonal field method. We compute the relative error defined by
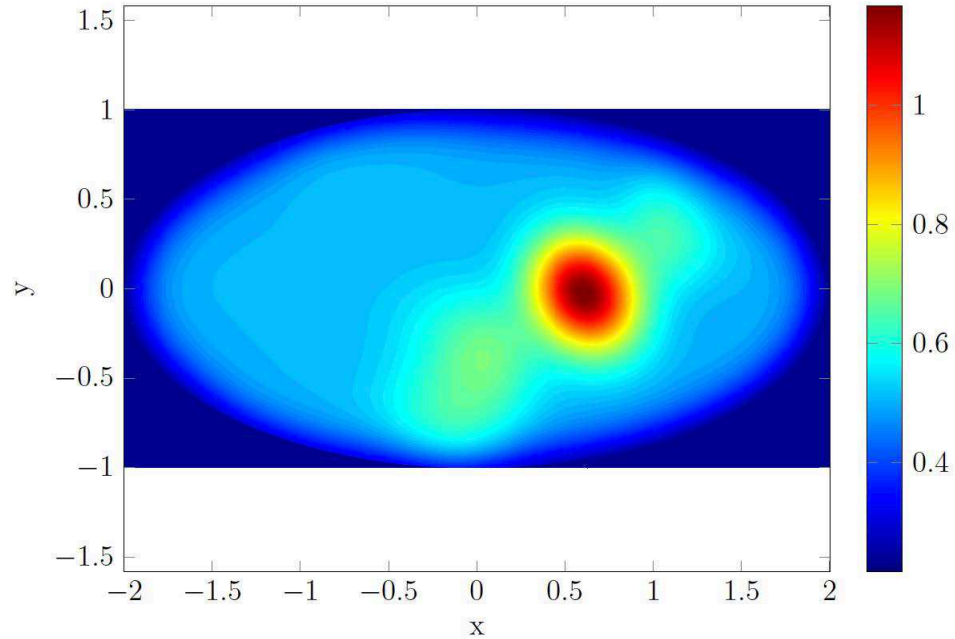
Fig. 16.3. Conductivity reconstructed by the fixed point method.

$$e := \frac{\|\sigma_\eta - \sigma_*\|_{L^2}}{\|\sigma_*\|_{L^2}},$$

averaged over 150 different realizations of measurement noise on J. The results are shown in Figure 16.6. We show the results of a reconstruction with noise level of 2% (resp. 10%) in Figure 16.7 (resp. Figure 16.8). Clearly, the orthogonal method is quite robust with respect to measurement noise.

16.6 Concluding Remarks

In this chapter we have presented a mathematical and numerical framework for conductivity imaging using magnetoacoustic tomography with magnetic induction. We have developed three different algorithms for conductivity imaging from boundary measurements of the Lorentz force induced tissue vibration. We have proved convergence and stability properties of the three algorithms and compared their performance. The orthogonal field method performs much better than the optimization scheme and the fixed-point method in terms of both computational time and accuracy. Indeed, it is robust with respect to measurement noise.
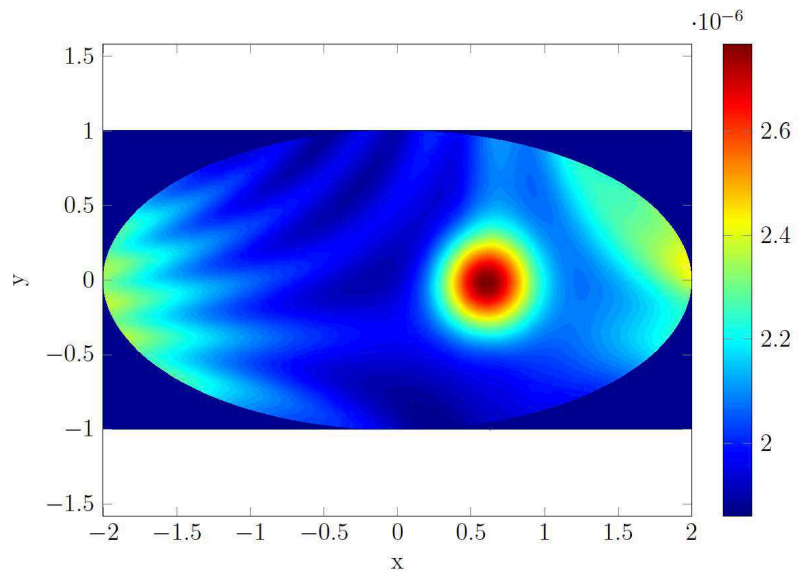
Fig. 16.4. Conductivity recovered by the orthogonal field method before scaling.
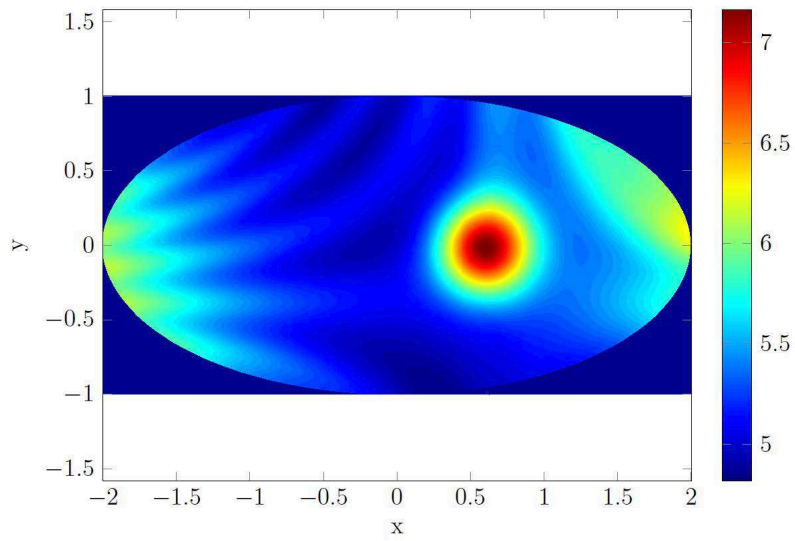
Fig. 16.5. Conductivity recovered by the orthogonal field method after scaling.
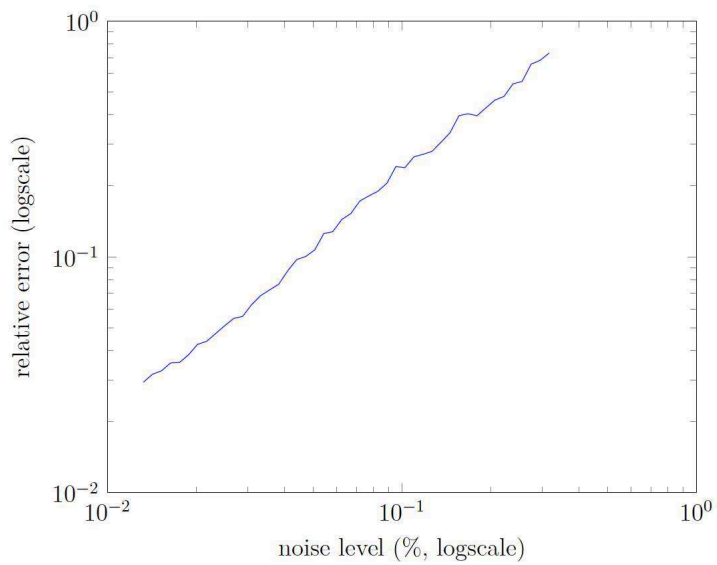
Fig. 16.6. Relative error with respect to measurement noise.
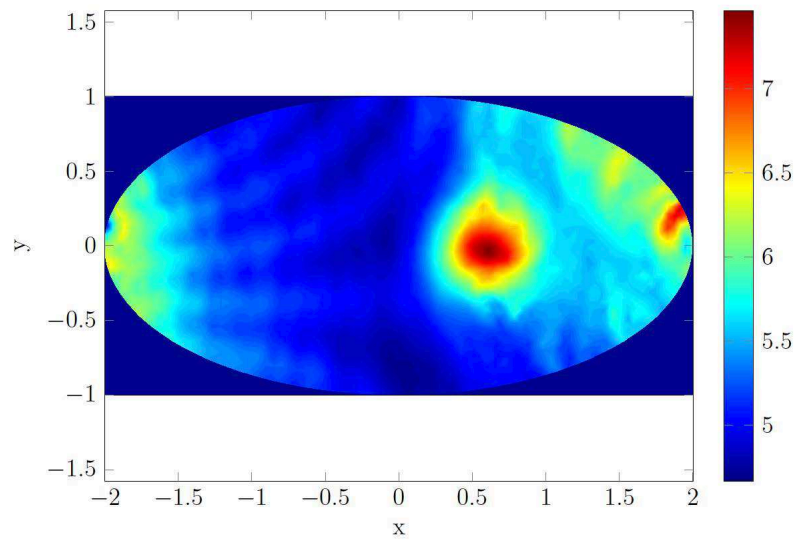
Fig. 16.7. Reconstruction with the orthogonal field method with measurement noise level of 2%.
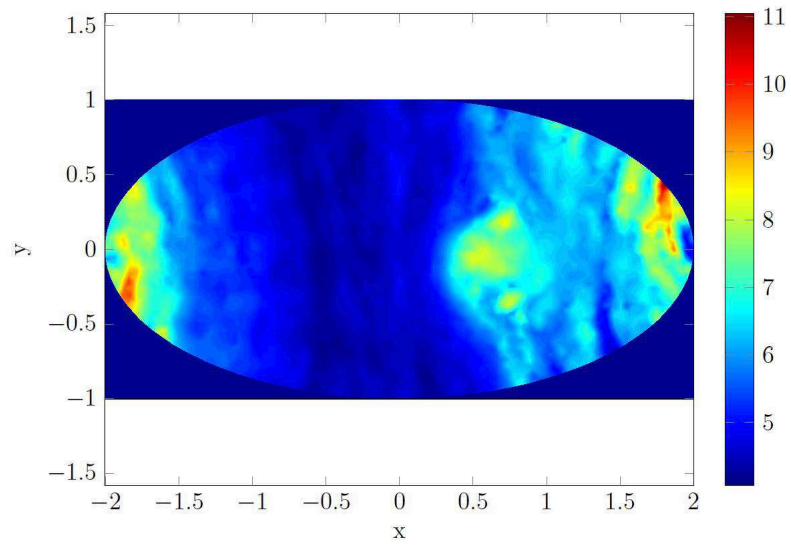
Fig. 16.8. Reconstruction with the orthogonal field method with measurement noise level of 10%.

17

Impediography

17.1 Introduction

In this chapter we introduce a mathematical and numerical framework for impediography. Impediography is an emerging hybrid approach for conductivity imaging. It keeps the most important merits of electrical impedance tomography (real time imaging, low cost, portability). Its core idea is to couple electric measurements to localized elastic perturbations. A body is electrically probed: one or several currents are imposed on the surface and the induced potentials are measured on the boundary. At the same time, a circular region of a few millimeters in the interior of the body is mechanically excited by ultrasonic waves. The measurements are made as the focus of the ultrasounds scans the entire domain. Several sets of measurements can be obtained by varying amplitudes of the ultrasound waves and the applied currents. The focused acoustic waves are used to generate localized electrical conductivity perturbations that allow a drastic improvement in the conditioning of the inverse conductivity problem. This is based the acousto-electric effect in order to achieve super-resolution conductivity imaging. The intrinsic resolution of impediography depends on the size of the focal spot of the acoustic perturbation, and thus it may provide high resolution images. The acousto-electric effect describes the phenomenon of conductivity modulation by ultrasound. For an electric and acoustic media, using the acousto-electric effect, the temporal change $\delta\sigma(x, t)$ in electrical conductivity $\sigma(x)$ due to an ultrasound pressure wave $p(x, t)$ can be written as

$$\delta\sigma(x, t) = K\sigma(x)p(x, t), \qquad (17.1)$$

where K is an interaction constant. The ultrasound pressure as a spatial and temporal function can be expressed as

$$p(x, t) = p_0 b(x)a(t), \qquad (17.2)$$

where p_0 is the amplitude of ultrasound pressure, b is the beam pattern, and $a(t)$ describes the ultrasound waveform. In the focal zone, the ultrasonic

strength varies slowly along the beam axis. The acousto-electric effect is a volume integration. If the waveform $a(t)$ is an oscillatory bipolar pulse, the integration and therefore the acousto-electric effect will be very small. In order to enhance the acousto-electric effect, it is therefore desirable to use unipolar ultrasonic pulse. Ultrasonic waves can be focused in very small regions deep inside the tissues. The support of the focal spot is better represented by an ellipsoid, but locus the most intense area can, in a first approximation, be represented by a sphere. The experiment is successful if for each focal point, a difference in the boundary voltage potential can be measured between the potential corresponding to the unperturbed medium and the potential corresponding to the perturbed one.

In this chapter, we first introduce a mathematical formulation for impediography. Then we describe a substitution algorithm based on a non-linear PDE, denominated the 0–Laplacian and an optimal control approach for solving the inverse problem in impediography. This uses internal electrical energy densities that are quantities estimated from boundary voltage measurements. Finally, we discuss stability and resolution properties of the reconstructed conductivity distributions from impediographic measurements and compare between the proposed approaches in terms of accuracy of the reconstructed electrical conductivity and their ability to deal with limited perturbation data. Our results in this chapter are from [28, 49].

17.2 Mathematical Model

Similar to the formulation of the electrical impedance tomography in Chapter 6, the forward problem for impediography is based on the solution of Maxwell's equations. A low-frequency current is used to probe the domain. For a two-dimensional domain Ω with a boundary $\partial\Omega$, the voltage potential induced by a current $g \in L_0^2(\partial\Omega)$, in the absence of ultrasonic perturbations is given by

$$\begin{cases} \nabla \cdot (\sigma(x)\nabla u) = 0 & \text{in } \Omega , \\ \sigma\dfrac{\partial u}{\partial \nu} = g & \text{on } \partial\Omega , \end{cases} \tag{17.3}$$

with the convention that $\int_{\partial\Omega} u = 0$. One supposes that the conductivity σ of the region close to the boundary of the domain is known, so that ultrasonic probing is limited to interior points. One denotes the region (open set) by Ω'.

To model the effect of the pressure wave, we assume that within each disk of (small) area, the conductivity is constant per area unit. When an acoustic wave is focused at $x \in \Omega$, the perturbed electrical conductivity $\sigma + \delta\sigma$ within the disk-shaped zone D deformed by the ultrasound wave satisfies

$$\forall\, x \in \Omega, \quad (\sigma + \delta\sigma)(x) = \sigma(x)\eta(x) ,$$

where $\eta(x)$ is a known function and

$$\forall x \in \Omega, \ \eta(x) > 1, \ \frac{\eta(x) - 1}{\eta(x) + 1} \geq C \,, \tag{17.4}$$

for some positive constant C.

In order to solve the impediographic imaging problem we need to introduce the notion of proper set of measurements for (17.3).

Let $g_j \in L_0^2(\partial\Omega)$, $j = 1, 2$ and let $u^{(j)}$ be the voltage potential induced by g_j, in the absence of ultrasonic perturbations, that is,

$$\begin{cases} \nabla \cdot \big(\sigma(x)\nabla u^{(j)}\big) = 0 & \text{in } \Omega \,, \\ \quad \sigma \dfrac{\partial u^{(j)}}{\partial \nu} = g_j & \text{on } \partial\Omega \,, \end{cases} \tag{17.5}$$

with the convention that $\int_{\partial\Omega} u^{(j)} = 0$. Let

$$\mathcal{E}_{jl}[\sigma](z) := \sigma(z)\nabla u^{(j)}(z)\nabla u^{(l)}(z), \quad j, l = 1, 2 \,,$$

and

$$\mathcal{E}[\sigma] := (\mathcal{E}_{jl}[\sigma])_{j,l=1,2} \,.$$

Definition 17.1 *The pair of currents (g_1, g_2) is a proper set of measurements if*

(i) $|\nabla u^{(j)}| > 0$ in Ω_1;

(ii) The matrix $\mathcal{E}[\sigma]$ is invertible (or equivalently, $|\det \mathcal{E}[\sigma]| > 0$) for all $x \in \Omega_1$.

We now give an evidence of the possibility of constructing proper sets of measurements [222].

Lemma 17.2 *Let f be a smooth function on $\partial\Omega$ such that there exist P and Q on $\partial\Omega$ such that $f|_{\Gamma_1}$ and $f|_{\Gamma_2}$ are one-to-one, where Γ_1 and Γ_2 are two parts of $\partial\Omega$, connecting P and Q. We have, for all positive and smooth function σ, $\nabla v \neq 0$ in Ω where v is the solution of*

$$\begin{cases} \nabla \cdot \sigma \nabla v = 0 \ \text{in } \Omega \,, \\ \qquad v = f \ \text{on } \partial\Omega \,. \end{cases} \tag{17.6}$$

Proof. Fix $x_0 \in \Omega$. Let $X \in \Gamma_1$ and $Y \in \Gamma_2$ be such that

$$f(X) = f(Y) = v(x_0).$$

Note that such a pair is unique due to the one-to-one property of f on Γ_1 and Γ_2. Since v is continuous and v does not attain local extreme value in Ω, the level set $\{x : v(x) = x_0\}$ is a curve connecting X and Y. This curve divides Ω into two subdomains $\Omega^\pm$. On Ω^+, $v > v(x_0)$ and on Ω^-, $v < v(x_0)$. We now can employ Hopf's lemma to see that $\nabla v(x) \neq 0$. $\square$

Employing Lemma 17.2, we simply take any $g_j = \partial v_j / \partial \nu, j = 1, 2$, with f_1 and f_2 satisfying: for all $\alpha \in \mathbb{R}$, there exist P and Q in $\partial \Omega$ such that the function $f_1 - \alpha f_2$ is one-to-one on each of two curves along $\partial \Omega$ connecting P and Q. For example, if $\partial \Omega$ does not contain any line segment, then we can choose $f_1 = x_1 + M$ and $f_2 = x_2 + M$ for a sufficiently large number M.

Let the pair of currents (g_1, g_2) be a proper set of measurements and let $u^{(j)}$, $j = 1, 2$, be the induced voltage potentials in the absence of ultrasonic perturbations. Let $u_\delta^{(j)}$ be the voltage potential induced by the current g_j, in the presence of ultrasonic perturbations localized in a disk-shaped domain $D := z + \delta B$ of volume $|D| = O(\delta^2)$. The voltage potential u_δ is a solution to

$$\begin{cases} \nabla \cdot \left(\sigma_\delta(x) \nabla u_\delta^{(j)}(x) \right) = 0 & \text{in } \Omega, \\ \qquad\qquad \sigma \dfrac{\partial u_\delta^{(j)}}{\partial \nu} = g_j & \text{on } \partial \Omega, \end{cases} \tag{17.7}$$

with the notation

$$\sigma_\delta(x) = \sigma(x) \left[1 + \chi(D)(x)\,(\eta(x) - 1) \right].$$

As the zone deformed by the ultrasound wave is small, one can view it as a small volume perturbation of the background conductivity σ, and seek an asymptotic expansion of the boundary values of $u_\delta^{(j)} - u^{(j)}, j = 1, 2$. The method of small-volume expansions shows that comparing $u_\delta^{(j)}$ and $u^{(j)}$ on $\partial \Omega$ provides information about the conductivity. Indeed, analogously to (11.6), one can prove that, for $j, l = 1, 2$,

$$\int_{\partial \Omega} (u_\delta^{(j)} - u^{j)}) g_l \, d\sigma = \int_D \sigma(x) \frac{2\,(\eta(x) - 1)}{\eta(x) + 1} \nabla u^{(j)} \cdot \nabla u^{(l)} \, dx + o(|D|)$$

$$= \sigma(z) \nabla u^{(j)}(z) \cdot \nabla u^{(l)}(z) \int_D \frac{2\,(\eta(x) - 1)}{\eta(x) + 1} \, dx + o(|D|) .$$

Note that because of assumption (17.4), it follows that

$$\int_D \frac{(\eta(x) - 1)}{\eta(x) + 1} \, dx \geq C|D| .$$

Therefore, one has

$$\mathcal{E}_{jl}[\sigma](z) = \left(\int_D \frac{2\,(\eta(x) - 1)}{\eta(x) + 1} dx \right)^{-1} \int_{\partial \Omega} (u_\delta^{(j)} - u^{(j)}) g_l \, d\sigma + o(1) . \tag{17.8}$$

Note that

$$\int_D \frac{2\,(\eta(x) - 1)}{\eta(x) + 1} dx \approx \frac{2 \frac{\delta \sigma(z)}{\sigma(z)}}{2 + \frac{\delta \sigma(z)}{\sigma(z)}} |D| ,$$

which is nothing else than the polarization tensor (11.5) associated with the disk D of conductivity $\delta\sigma(z) + \sigma(z)$ inside a background of constant conductivity $\sigma(z)$.

By scanning the interior of the body with ultrasound waves, given applied currents g_j, one then obtains data from which one can (approximately) compute $(\mathcal{E}_{jl}[\sigma])_{j,l=1,2}$ in an interior subregion of Ω. The new inverse problem is now to reconstruct σ knowing the data matrix $\mathcal{E}[\sigma]$.

17.3 Substitution Algorithm

Let (g_1, g_2) be a proper set of measurements. The use of the electrical energy densities $\mathcal{E}_{jj}$, $j = 1, 2$, leads one to transform (17.5), having two unknowns σ and $u^{(j)}$ with highly nonlinear dependency on σ, into the following nonlinear PDE (the 0–Laplacian)

$$\begin{cases} \nabla_x \cdot \left(\dfrac{\mathcal{E}_{jj}}{\left|\nabla u^{(j)}\right|^2} \nabla u^{(j)} \right) = 0 & \text{in } \Omega , \\[2mm] \dfrac{\mathcal{E}_{jj}}{\left|\nabla u^{(j)}\right|^2} \dfrac{\partial u^{(j)}}{\partial \nu} = g_j & \text{on } \partial\Omega . \end{cases} \tag{17.9}$$

It is worth emphasizing that $\mathcal{E}_{jj}$ is a known function, constructed from the measured data (17.8). Consequently, all the parameters entering in equation (17.9) are known. Thus, the ill-posed inverse problem in electrical impedance tomography is converted into a less complicated direct problem (17.9).

The substitution algorithm is based on an approximation of a linearized version of problem (17.9).

Suppose that σ is a small perturbation of conductivity profile σ_0: $\sigma = \sigma_0 + \delta\sigma$. Let $u_0^{(j)}$ and $u^{(j)} = u_0^{(j)} + \delta u^{(j)}$ denote the potentials corresponding to σ_0 and σ with the same Neumann boundary data g_j. It is easily seen that $\delta u^{(j)}$ satisfies $\nabla \cdot \left(\sigma \nabla \delta u^{(j)} \right) = -\nabla \cdot (\delta\sigma \nabla u_0^{(j)})$ in Ω with the homogeneous Dirichlet boundary condition. Moreover, from

$$\mathcal{E}_{jj} = (\sigma_0 + \delta\sigma)|\nabla(u_0^{(j)} + \delta u^{(j)})|^2 \approx \sigma_0 |\nabla u_0^{(j)}|^2 + \delta\sigma |\nabla u_0^{(j)}|^2 + 2\sigma_0 \nabla u_0^{(j)} \cdot \nabla \delta u^{(j)} ,$$

after neglecting the terms $\delta\sigma \nabla u_0^{(j)} \cdot \nabla \delta u^{(j)}$ and $\delta\sigma |\nabla \delta u^{(j)}|^2$, it follows that

$$\delta\sigma \approx \frac{\mathcal{E}_{jj}}{\left|\nabla u_0^{(j)}\right|^2} - \sigma_0 - 2\sigma_0 \frac{\nabla \delta u^{(j)} \cdot \nabla u_0^{(j)}}{\left|\nabla u_0^{(j)}\right|^2} .$$

The substitution algorithm is as follows.

Algorithm 17.1 Substitution algorithm.

1. Start from an initial guess for the conductivity σ;
2. Solve the corresponding Dirichlet conductivity problem

$$\begin{cases} \nabla \cdot (\sigma \nabla u_0) = 0 & \text{in } \Omega \,, \\ \qquad\quad u_0 = \psi & \text{on } \partial\Omega \,. \end{cases}$$

The data ψ is the Dirichlet data measured as a response to the current $g = g_1$ in absence of elastic deformation;

3. Define the discrepancy between the data and the guessed solution by

$$\epsilon_0 := \frac{\mathcal{E}_{11}}{|\nabla u_0|^2} - \sigma \,. \tag{17.10}$$

4. Introduce the corrector, δu, computed as the solution to

$$\begin{cases} \nabla \cdot (\sigma \nabla \delta u) = -\nabla \cdot (\varepsilon_0 \nabla u_0) & \text{in } \Omega \,, \\ \qquad\qquad\quad\, \delta u = 0 & \text{on } \partial\Omega \,; \end{cases}$$

5. Update the conductivity

$$\sigma := \frac{\mathcal{E}_{11} - 2\sigma \nabla \delta u \cdot \nabla u_0}{|\nabla u_0|^2} \,;$$

6. Iteratively update the conductivity, alternating directions of currents (*i.e.*, with $g = g_2$ and $\mathcal{E}_{11}$ replaced with $\mathcal{E}_{22}$ in (17.10)).

17.4 Optimal Control Algorithm

Let (g_1, g_2) be a proper set of measurements. Let σ and $\tilde{\sigma}$ be two $\mathcal{C}^1$-conductivities with $\sigma(x_0) = \tilde{\sigma}(x_0)$ for some $x_0 \in \overline{\Omega}$. Then, the following stability estimate holds [92]:

$$\| \log \sigma - \log \tilde{\sigma} \|_{W^{1,\infty}(\Omega)} \le C \| \mathcal{E}[\sigma] - \mathcal{E}[\tilde{\sigma}] \|_{W^{1,\infty}(\Omega)} \,. \tag{17.11}$$

We will prove later that $\sigma \mapsto \mathcal{E}[\sigma]$ is Fréchet differentiable. A direct consequence of (17.11) is

$$\mathrm{Ker}(d\mathcal{E}[\sigma])|_{W_0^{1,\infty}(\Omega)} = \{0\} \,, \tag{17.12}$$

provided that $\sigma > c_0 > 0$ for some constant c_0. In fact, for all $h \in W_0^{1,\infty}(\Omega)$, we have

$$\begin{aligned} \| d\mathcal{E}[\sigma](h) \|_{W_0^{1,\infty}(\Omega)} &= \lim_{t \to 0} \frac{\| \mathcal{E}[\sigma + th] - \mathcal{E}[\sigma] \|_{W_0^{1,\infty}(\Omega)}}{|t|} \\ &\ge \frac{1}{C} \lim_{t \to 0} \frac{\| \log(\sigma + th) - \log \sigma \|_{W_0^{1,\infty}(\Omega)}}{|t|} \\ &= \frac{1}{C\sigma} \| h \|_{W_0^{1,\infty}(\Omega)} \,. \end{aligned}$$

Let A be the following admissible set of conductivities:

$$A = \{\sigma \in W^{1,2}(\Omega) : c_0 < \sigma < C_0, |\nabla\sigma| < C_1\}, \qquad (17.13)$$

which is an open subset of $W^{1,\infty}(\Omega)$.

Lemma 17.3 *For $j, l = 1, 2$, the map $\sigma \mapsto \mathcal{E}_{jl}[\sigma]$ is Fréchet differentiable. Moreover, for $h \in W_0^{1,2}(\Omega)$ such that $\sigma + h \in A$, we have*

$$d\mathcal{E}_{jl}[\sigma]h = h\nabla u^{(j)} \cdot \nabla u^{(l)} + \sigma\left[\nabla u^{(j)} \cdot \nabla v^{(l)} + \nabla u^{(l)} \cdot \nabla v^{(j)}\right], \qquad (17.14)$$

where $v^{(j)}$ is the solution of

$$\begin{cases} \nabla \cdot \sigma\nabla v^{(j)} = -\nabla \cdot h\nabla u^{(j)} & in\ \Omega, \\ \sigma\dfrac{\partial v^{(j)}}{\partial \nu} = 0 & on\ \partial\Omega, \\ \displaystyle\int_{\partial\Omega} v^{(j)} = 0. \end{cases} \qquad (17.15)$$

Introduce the minimization problem

$$\min_{\sigma \in A} J[\sigma] := \frac{1}{2}\sum_{j,l=1}^{2}\int_{\Omega}\left|\mathcal{E}_{jl}[\sigma] - \mathcal{E}_{jl}^{(m)}\right|^2 dx, \qquad (17.16)$$

where $\mathcal{E}_{jl}^{(m)}$ are obtained from measurements. The Fréchet derivative of the discrepancy functional $J[\sigma]$ is given by

$$\begin{aligned}
dJ[\sigma] &= \sum_{j,l=1}^{2} d\mathcal{E}_{jl}[\sigma]^*(\mathcal{E}_{jl}[\sigma] - \mathcal{E}_{jl}^{(m)}) \\
&= \frac{1}{2}\sum_{j,l=1}^{2}(\mathcal{E}_{jl}[\sigma] - \mathcal{E}_{jl}^{(m)})\nabla u^{(j)} \cdot \nabla u^{(l)} + \sum_{j,l=1}^{2}\nabla u^{(j)} \cdot \nabla p^{(j,l)},
\end{aligned} \qquad (17.17)$$

where $p^{(j,l)}$ is the solution of the adjoint problem

$$\begin{cases} \nabla \cdot \sigma\nabla p^{(j,l)} = -\nabla \cdot (\mathcal{E}_{jl}[\sigma] - \mathcal{E}_{jl}^{(m)})\sigma\nabla u^{(l)} & in\ \Omega, \\ \sigma\frac{\partial p^{(j,l)}}{\partial \nu} = 0 & on\ \partial\Omega, \\ \displaystyle\int_{\partial\Omega} p^{(j,l)} = 0. \end{cases} \qquad (17.18)$$

The following results hold.

Lemma 17.4 *Let $\sigma \in A$. The following assertions hold:*

1. The map $h \mapsto \nabla v^{(j)}$ from $W_0^{1,2}(\Omega)$ into $L^2(\Omega)$ is compact.

2. *The map $d\mathcal{E}_{jl}$ takes the form $I +$ compact, up to a multiplication by a continuous function.*

Proof. Let $h \in W_0^{1,2}(\Omega)$. The function $v^{(j)}$ satisfies

$$-\sigma \Delta v^{(j)} = \nabla \sigma \cdot \nabla v^{(j)} + \nabla \cdot h \nabla u^{(j)},$$
$$= \nabla \sigma \cdot \nabla v^{(j)} + h \Delta u^{(j)} + \nabla h \cdot \nabla u^{(j)},$$
$$= \nabla \sigma \cdot \nabla v^{(j)} - h \frac{\nabla \sigma \cdot \nabla u^{(j)}}{\sigma} + \nabla h \cdot \nabla u^{(j)},$$

which is in $L^2(\Omega)$. As a result, $v^{(j)} \in W^{2,2}(\Omega)$ and its $W^{2,2}$-norm is bounded by $\|h\|_{W_0^{1,2}(\Omega)}$. The first part of this lemma is proved by using the compact embeddings

$$W^{2,2}(\Omega) \hookrightarrow W^{1,2}(\Omega) \hookrightarrow L^2(\Omega). \tag{17.19}$$

From (17.14), it follows that $\mathcal{E}[\sigma]^{-1} d\mathcal{E}[\sigma] = I +$ compact operator, and consequently, the second item holds. $\square$

Applying (17.12) and Lemma 17.4, we can deduce from the Fredholm alternative that

$$\|d\mathcal{E}[\sigma]\|_{\mathcal{L}(W_0^{1,2}(\Omega), L^2(\Omega))} \geq C. \tag{17.20}$$

Proposition 2.5 yields the following convergence result of the Landweber iteration scheme.

Theorem 17.5 *Assume that $\sigma^{(0)}$ is a good initial guess for σ_*. As $n \to +\infty$, the sequence*

$$\sigma^{(n+1)} = T\sigma^{(n)} - \eta d\mathcal{E}^*[T\sigma^{(n)}](\mathcal{E}[\sigma^{(n)}] - \mathcal{E}^{(m)}) \tag{17.21}$$

converges to σ_*, where T is the Hilbert projection of $W^{1,2}(\Omega)$ onto A, σ_* is the true conductivity distribution, η is the step size, and $\mathcal{E}^{(m)} = (\mathcal{E}_{jl}^{(m)})_{j,l=1,2}$.

17.5 Concluding Remarks

In this chapter, we have presented a mathematical and numerical framework for impediography. This approach relies on the acousto-electric effect. It generates high sensitivity and high resolution maps of the internal electrical conductivity distribution. Evidence of resolution enhancement and a stability analysis have been given in [49]. In the case of incomplete data, that is, if the matrix $\mathcal{E}$ is only known on a subset of the domain, one can follow the optimal control approach, which allows better flexibility than the substitution scheme.

18

Microwave Imaging by Elastic Deformation

18.1 Introduction

Let $a \in \mathcal{C}^1(\overline{\Omega})$ and $q \in \mathcal{C}^0(\overline{\Omega})$ be two scalar real-valued functions in two dimensions. We also assume that a and q are such that $0 < c_0 < a, q < C_0$. For smooth (real-valued) function φ, let $u[k, \varphi] \in W^{1,2}(\Omega)$ be such that

$$\begin{cases} \nabla \cdot (a\nabla u[k, \varphi]) + k^2 qu[k, \varphi] = 0 & \text{in } \Omega, \\ u[k, \varphi] = \varphi & \text{on } \partial\Omega. \end{cases} \tag{18.1}$$

Here k is the angular frequency and a and q are the electromagnetic parameters. In the transverse magnetic case, Maxwell's equations can be reduced to (18.1) with u being the electric field, q the electric permittivity and a the inverse of the magnetic permeability. The well-posedness of problem (18.1) requires that k^2 must not be an eigenvalue of the problem

$$\begin{cases} -\nabla \cdot (a\nabla u) = k^2 qu & \text{in } \Omega, \\ u = 0 & \text{on } \partial\Omega. \end{cases} \tag{18.2}$$

It is well known that this problem admits a countable number of eigenvalues with no accumulation point and that each eigenvalue has a finite multiplicity. We will assume that k does not correspond to any eigenvalue of (18.2).

The aim of this chapter is to generalize impediography to the electromagnetic case. A frequency k and a source field pattern φ being fixed, we measure the field $u[k, \varphi]$, solution of (18.1), on $\partial\Omega$.

Assume now that ultrasonic waves are focalized around a point $z \in \Omega$, creating a local change in the physical parameters of the medium. Suppose that this deformation affects a and q linearly with respect to the amplitude of the ultrasonic signal. Such an assumption is reasonable if the amplitude is not too large. Thus, when the electric potential is measured while the ultrasonic perturbation is enforced, the equation for the electric field is

$$\begin{cases} \nabla \cdot (a_\delta \nabla u_\delta) + k^2 q_\delta u_\delta = 0 & \text{in } \Omega, \\ u_\delta = \varphi & \text{on } \partial\Omega, \end{cases}$$

with

$$\begin{cases} a_\delta = a + (a_1\alpha - a)\chi(D)\,, \\ q_\delta = q + (q_1\alpha - q)\chi(D)\,, \end{cases}$$

where α is the amplitude of the ultrasonic perturbation, a_1 and q_1 are unknown functions, and D is a small zone where the perturbation is focalized.

As in the previous chapter, the signature of the perturbations on boundary measurements can be measured by the change of energy on the boundary, namely

$$\int_{\partial\Omega} \frac{\partial}{\partial\nu}(u_\delta[k,\varphi] - u\,[k,\varphi])\varphi d\sigma$$

$$= M\big(\frac{\alpha a_1(z)}{a(z)}, D\big)(\alpha a_1(z) - a(z))\nabla u\,[k,\varphi]\,(z) \cdot \nabla u[k,\varphi](z)$$

$$+ k^2|D|(\alpha q_1(z) - q(z))(u\,[k,\varphi]\,(z))^2 + o\big(|D|\big)\,, \quad (18.3)$$

where z is the center of D and M is the polarization tensor associated with D and the contrast $\alpha a_1(z)/a(z)$. It is given by (11.5). Assuming the perturbed region D to be a disk, the polarization tensor is given by

$$M\big(\frac{\alpha a_1(z)}{a(z)}, D\big) = |D|\frac{2a(z)}{\alpha a_1(z) + a(z)}I\,.$$

Therefore, for a localized perturbation focused at a point z, we read the following data (rescaled by the volume $|D|$)

$$D_z(\alpha) = 2a|\nabla u\,[k,\varphi]\,(z)|^2 \frac{\alpha\frac{a_1(z)}{a(z)} - 1}{\alpha\frac{a_1(z)}{a(z)} + 1} + k^2 q(z)(u\,[k,\varphi]\,(z))^2(\alpha\frac{q_1(z)}{q(z)} - 1)\,.$$

$$(18.4)$$

The parameters $(a_1/a)(z)$ and $(q_1/q)(z)$ are unknown, but the amplitude α is known. By linear algebra, one can prove from (18.4) that if $|\nabla u\,[k,\varphi]\,(z)| \gg |D|$ and $|u\,[k,\varphi]\,(z)| \gg |D|$ and the data D_z is known for 4 distinct values of α, chosen independently of a and q, then, one can recover the electromagnetic energies

$$E\,[k,\varphi]\,(z) := a(z)|\nabla u\,[k,\varphi]\,(z)|^2\,,$$

and

$$e\,[k,\varphi]\,(z) := q(z)(u\,[k,\varphi]\,(z))^2\,.$$

At this point, one can respectively substitute a and q by $E\,[k,\varphi]\,/|\nabla u\,[k,\varphi]\,|^2$ and $e\,[k,\varphi]\,/|u\,[k,\varphi]\,|^2$ to arrive at the nonlinear partial differential equation

$$\begin{cases} \nabla \cdot \left(\frac{E\,[k,\varphi]}{|\nabla u\,[k,\varphi]\,|^2}\nabla u\,[k,\varphi]\right) + k^2\frac{e\,[k,\varphi]}{(u\,[k,\varphi])^2}u\,[k,\varphi] = 0 \quad \text{in } \Omega\,, \\ u = \varphi \quad \text{on } \partial\Omega\,. \end{cases} \quad (18.5)$$

Based on the nonlinear direct formulation (18.5), an iterative scheme similar to the one introduced in Section 17.3 can be derived. However, an optimal

control approach is more efficient for reconstructing the parameters than the nonlinear based direct formulation (18.5), specially when the data is available only on a subset of the background medium Ω. Our results in this chapter are from [42].

18.2 Exact Reconstruction Formulas

In this section, we first construct a proper set of measurements for the Helmholtz equation

$$\nabla \cdot a\nabla u + k^2 qu = 0 \,, \tag{18.6}$$

where k belongs to a fixed and known interval $(\underline{k}, \overline{k})$. For all $g \in W^2_{1/2}(\partial\Omega)$, let $u[k, g]$ be the solution of (18.6) with $u[k, g]|_{\partial\Omega} = g$. Note that $u[k, g]$ is uniquely determined when k is such that k^2 is not an eigenvalue of

$$\begin{cases} -\nabla \cdot a\nabla u = k^2 qu \text{ in } \Omega \,, \\ \qquad\quad u = 0 \quad \text{ on } \partial\Omega \,. \end{cases}$$

Denote by $\mathcal{K}$ the domain of the map $u[\cdot, g]$. It is obvious that for all a and q, $\mathcal{K}$ is an open set of $\mathbb{C}$ containing 0. We have the definition.

Definition 18.1 *A set of 3 smooth functions $(g_j)^3_{j=1}$ is called a proper set of measurements for (18.6) if there exists $N \geq 1$, $k_1, \ldots, k_N \in (\underline{k}, \overline{k})$ and $B_1, \ldots, B_N \subset \Omega$ such that*

1. $\cup^N_{j=1}\overline{B}_j = \overline{\Omega}$;
2. for all $z \in B_j$, $j = 1, \ldots, N$, $l = 1, 2, 3$,

$$|u[k_j, g_l](z)| > 0 \,;$$

3. for all $z \in B_j$, $j = 1, \ldots, N$,

$$\left| \det\left(\nabla u\left[k_j, g_l\right](z)\right)^3_{l=2} \right| > 0 \,,$$

   where det *denotes the determinant;*
4. for all $z \in B_j$, $j = 1, \ldots, N$,

$$\left| \det(u[k_j, g_l](z), \nabla u[k_j, g_l](z))^3_{l=1} \right| > 0 \,.$$

The following lemma is useful in the construction of a simple proper set of measurements for (18.6).

Lemma 18.2 *Let $g \in \mathcal{C}^1(\partial\Omega)$. The map*

$$\mathcal{K} \ni k \mapsto u[k, g] \in \mathcal{C}^1(\overline{\Omega})$$

is analytic.

Proof. Fix $k \in \mathcal{K}$. Let $k' \in \mathbb{C}$ be close to k. We have that $u[k', g]$ is well-defined. The difference $u[k', g] - u[k, g]$ is the solution of

$$\begin{cases} \nabla \cdot a\nabla U + (k')^2 qU = [k^2 - (k')^2]qu[k, g] \ \text{in}\, \Omega\,, \\ \qquad\qquad\qquad U = 0 \qquad\qquad \text{on} \quad \partial\Omega\,. \end{cases} \tag{18.7}$$

As a result,

$$\|u[k', g] - u[k, g]\|_{\mathcal{C}^1(\overline{\Omega})} \le O(|(k')^2 - (k)^2|) \le O(|k' - k|)\,. \tag{18.8}$$

Here, we have used the fact that a is a smooth and strictly positive function for the $\mathcal{C}^1$ estimate above. On the other hand, letting v^k be the solution of

$$\begin{cases} \nabla \cdot a\nabla v^k + k^2 q v^k = -2kqu^k \ \text{in}\, \Omega\,, \\ \quad u[k', g] - u[k, g] = 0 \qquad \text{on} \quad \partial\Omega\,, \end{cases} \tag{18.9}$$

we can see that

$$\left\| \frac{u^{k'} - u^k}{k' - k} - v^k \right\|_{\mathcal{C}^1(\overline{\Omega})} \le O(|k' - k|)\,.$$

The proof is complete. $\square$

We are now at the position to find a proper set of measurements for (18.6) [9].

Proposition 18.3 *A proper set of measurements for (17.5) is also a proper set of measurements for* (18.6).

Proof. Fix an arbitrary point $z \in \Omega$ and $j \in \{1, \ldots, 3\}$. Assume that $u[k, g_j](z) = 0$ for all $k \in (\underline{k}, \overline{k})$. It follows from Lemma 18.2 that $k \mapsto u[k, g_j]$ is analytic with respect to k. Hence, $u[k, g_j](z) = 0$ for all $k \in \mathcal{U}$ and in particular $u[0, g_j](z) = 0$. However, $u[0, g_j](x) \ne 0$. We can conclude that for all $z \in \Omega$, there is $k_z \in (\underline{k}, \overline{k})$ such that $u[k_z, g_1](z)$ does not vanish. By the continuity of $u[k_z, g_j]$, $|u[k_z, g_j]| > 0$ in B_z, a small neighborhood of z in Ω. Since $\overline{\Omega}$ is compact, we can extract $B_1, \ldots, B_N$ from $\{B_z : z \in \Omega\}$ so that $\overline{B}_1, \ldots, \overline{B}_N$ cover $\overline{\Omega}$. Refining $\{B_1, \ldots, B_N\}$, we have the first part of Definition 18.1. The proof for other parts of Definition 18.1 can be done similarly using Lemma 18.2 and the differentiability of the determinant. $\square$

We now assume that $(\varphi_j)_{j=1}^3$ is a proper set of measurements for

$$\nabla \cdot a\nabla u + k^2 qu = 0$$

on an interval $(\underline{k}, \overline{k})$ and the matrix-valued functions e^k and E^k, given by

$$E_{ij}^k(z) = a(z)\nabla u\,[k, \varphi_i] \cdot \nabla u\,[k, \varphi_j]\,, \tag{18.10}$$

and

$$e_{ij}^k(z) = q(z)u\,[k, \varphi_i] \cdot u\,[k, \varphi_j]\,, \tag{18.11}$$

are known for all $k \in (\underline{k}, \overline{k})$. Our aim is to find a and q in D.

Theorem 18.4 *Note that using (18.3) and (18.4) the 'polarized' data E_{ij} and e_{ij} for $i \neq j$ is available without additional measurements, thanks to the bilinear structure of the asymptotic formula (18.3). In fact, we have*

$$\int_{\partial\Omega} \frac{\partial}{\partial\nu}(u_\delta[k,\varphi] - u[k,\varphi])\psi d\sigma$$

$$= M\big(\frac{\alpha a_1(z)}{a(z)}, D\big)(\alpha a_1(z) - a(z))\nabla u[k,\varphi](z) \cdot \nabla u[k,\psi](z)$$

$$+ k^2|D|(\alpha q_1(z) - q(z))u[k,\varphi](z)u[k,\psi](z) + o(|D|).$$

Let

$$P_{ij}^k = \frac{e_{ij}^k}{\text{trace}(e^k)} = U_i U_j, \quad k \in (\underline{k}, \overline{k}), \tag{18.12}$$

where

$$U_i = \frac{u[k,\varphi_i]}{\sqrt{\sum_{m=1}^3 |u[k,\varphi_m]|^2}}, \quad i = 1, 2, 3.$$

We claim that $P^k(z)$ is well-defined except at a finite number of k for each $z \in \Omega$. In fact, if there exists an infinite sequence $\{k_n\} \subset (\underline{k}, \overline{k})$ such that $\text{trace}(e^{k_n})(z) = 0$ for all n. Then, by Lemma 18.2, $\text{trace}(e^0)(z) = 0$, which contradicts to our choice of boundary conditions. By the smoothness of $u[k,\varphi_j]$, assume that P^k and hence ∇P^k is well-defined except at a finite number of k in a small neighborhood of z. We also assume that

$$\nabla P^k(z) \neq 0 \tag{18.13}$$

because it implies the determinant in item 4 of Definition 18.1 vanishes.

Fix k such that P^k and ∇P^k is well-defined. Differentiating formula (18.12), we obtain

$$\frac{1}{2}\left|\nabla P^k\right|_2^2 = |\nabla U|_2^2 |U|_2^2 + \left|\sum_{i=1}^N U_i \nabla U_i\right|^2 = |\nabla U|_2^2, \tag{18.14}$$

since $\sum_{i=1}^N U_i^2 = 1$. We compute that

$$\left(\sum_{n=1}^N u[k,\varphi_n]^2\right)^2 |\nabla U|_2^2 = \left(\sum_{n=1}^N u[k,\varphi_n]^2\right)\sum_{p=1}^N |\nabla u[k_p,\varphi_p]|^2$$

$$- \sum_{p=1}^N \sum_{n=1}^N \nabla u[k,\varphi_n] \cdot \nabla u[k,\varphi_p] u[k,\varphi_n] u[k_p,\varphi_p],$$

which, together with (18.14), gives

$$\frac{a}{q}\left|\nabla P^k\right|_2^2 = \frac{1}{\text{trace}(e^k)}\left(\text{trace}(E^k) - \text{trace}(P^k E^k)\right).$$

We now have the knowledge of $\dfrac{a}{q}$ thanks to (18.13). In practice, we can evaluate $\dfrac{a}{q}$ by the following proposition.

Proposition 18.5 *Let P^k as in (18.12). For all $z \in \Omega$,*

$$\frac{a}{q} = \frac{2}{\overline{k} - \underline{k}} \int_{\underline{k}}^{\overline{k}} \frac{\text{trace}(E^k - P^k E^k)}{|\nabla P^k|^2 \text{trace}(e^k)} \, dk \, .$$
(18.15)

Moreover, the following Proposition gives an explicit formula to determine q up to a multiplicative constant.

Proposition 18.6 *Suppose that $\text{trace}(e^k) \in W^{1,\infty}(\Omega)$ for all $k \in (\underline{k}, \overline{k})$. We have*

$$\frac{\partial_{x_l} q}{q} = \frac{1}{\overline{k} - \underline{k}} \int_{\underline{k}}^{\overline{k}} \left(\frac{\partial_{x_l} \text{trace}(e^k)}{\text{trace}(e^k)} - 2\lambda_l^k \right) dk, \quad l = 1, 2 \, ,$$
(18.16)

where λ_1^k and λ_2^k satisfy

$$\lambda_1^{k\,2} + \lambda_2^{k\,2} = \frac{q}{a} \frac{\text{trace}(P^k E^k)}{\text{trace}(e^k)} \, ,$$
(18.17)

and are determined by the linear system

$$M^k \begin{pmatrix} \lambda_1^k \\ \lambda_2^k \end{pmatrix} = B^k$$
(18.18)

with

$$M^k = \begin{pmatrix} |\partial_{x_1} U^k|^2 & \partial_{x_1} U^k \cdot \partial_{x_2} U^k \\ \partial_{x_1} U^k \cdot \partial_{x_2} U^k & |\partial_{x_2} U^k|^2 \end{pmatrix} \quad \text{and} \quad B^k = \frac{q}{a\,\text{trace}(e^k)} \begin{pmatrix} E^k U^k \cdot \partial_{x_1} U^k \\ E^k U^k \cdot \partial_{x_2} U^k \end{pmatrix} \, .$$
(18.19)

Remark 18.7 *As in the proof of Proposition 18.5, the integral in (18.16) is well-defined because $\text{trace}(e^k)$ does not vanish except at a finite number of frequencies k. Since M^0 is invertible, so is M^k by a similar argument.*

Remark 18.8 *Finally, we shall note that the exact reconstruction formulas given in Propositions 18.5 and 18.6 are not valid when a and/or q are complex.*

Proof of Proposition 18.6. Without loss of generality, assume that $\text{trace}(e^k) \neq 0$ for all $z \in \Omega$ by Remark 18.7. Differentiating the formula for $\text{trace}(e^k)$, we obtain

$$\frac{\partial_{x_l} \text{trace}(e^k)}{\text{trace}(e^k)} = \frac{\partial_{x_l} q}{q} + 2\lambda_l^k, \quad l = 1, 2 \, ,$$

where,

$$\lambda_l^k = \frac{1}{\sum_{i=1}^N u\,[k_i,\varphi_i]^2} \sum_{n=1}^N u\,[k,\varphi_n]\,\partial_{x_l} u\,[k,\varphi_n] = \frac{n_l}{n_0} U^k \cdot \widetilde{U}_l^k\,,$$

with the notations

$$n_0^k := \sqrt{\sum_{n=1}^N \left(u\,[k,\varphi_n]\right)^2},$$

$$n_l^k := \sqrt{\sum_{n=1}^N \left(\partial_{x_l} u\,[k,\varphi_n]\right)^2}, \quad \text{for } l = 1,2,$$

$$(\widetilde{U}_l^k)_j := \frac{\partial_{x_l} u[k,\varphi_j]}{n_l^k}, \quad \text{for } l = 1,2\,.$$

Differentiating U^k, we find

$$\partial_{x_l} U^k = \frac{n_l^k}{n_0^k}\left(I - P^k\right) \widetilde{U}_l^k\,. \tag{18.20}$$

Write the matrix E^k in the form

$$E^k = \mathrm{trace}(E^k) \sum_{l=1}^2 \frac{\left(n_l^k\right)^2}{\left(n_1^k\right)^2 + \left(n_2^k\right)^2} P_{\widetilde{U}_l^k}\,,$$

where $P_{\widetilde{U}_l^k}$ is the orthogonal projection onto the vector $\widetilde{U}_l^k$. We compute that

$$E^k U^k = \mathrm{trace}(E^k) \sum_{l=1}^2 \frac{\left(n_l^k\right)^2}{\left(n_1^k\right)^2 + \left(n_2^k\right)^2}(\widetilde{U}_l^k \cdot U^k)\widetilde{U}_l^k = a\sum_{l=1}^2 n_l^k n_0^k \lambda_l^k \widetilde{U}_l^k\,. \tag{18.21}$$

Testing (18.21) against U^k, we obtain

$$E^k U^k \cdot U^k = a \sum_{l=1}^2 n_l^k n_0^k \lambda_l^k \widetilde{U}_l^k \cdot u = a \sum_{l=1}^2 \left(n_0^k\right)^2 (\lambda_l^k)^2\,,$$

which is (18.17). Alternatively, testing (18.21) against $\partial_{x_{l'}} U^k$ gives, using (18.20),

$$E^k U^k \cdot \partial_{x_{l'}} U^k = a \sum_{l=1}^{2} n_l^k n_{l'}^k \lambda_l^k \widetilde{U}_l^k \cdot \left(I - P^k\right) \widetilde{U}_{l'}^k$$

$$= a \sum_{l=1}^{2} n_l^k n_{l'}^k \lambda_l^k \left(I - P^k\right) \widetilde{U}_l^k \cdot \left(I - P^k\right) \widetilde{U}_{l'}^k$$

$$= a \sum_{l=1}^{2} \left(n_0^k\right)^2 \lambda_l^k \partial_{x_l} U^k \cdot \partial_{x_{l'}} U^k$$

$$= \frac{a}{q} \mathrm{trace}(e^k) \sum_{l=1}^{2} \lambda_l^k \partial_{x_l} U^k \cdot \partial_{x_{l'}} U^k \,,$$

which is the desired 2×2 system given by (18.18). Note that since $|U^k|_2^2 = 1$, we have $\partial_{x_1} U^k \cdot U^k = 0$. Therefore, if U^k has only two components, $\partial_{x_1} U^k$ and $\partial_{x_2} U^k$ are necessarily colinear, and system (18.18) is degenerate.

However, it is never a zero matrix. Indeed,

$$|\nabla U^k|_2^2 = \frac{1}{2} |\nabla P^k|_2^2 \neq 0,$$

thanks to (18.15).

18.3 The Forward Problem and the Differentiabillity of the Data at a Fixed Frequency

The forward problem is formulated as follows. Given a and q, at a fixed k, we are able to solve

$$\begin{cases} \nabla \cdot a \nabla u + k^2 q u = 0 & \text{in } \Omega , \\ \qquad\qquad\qquad u = \varphi_i & \text{on } \partial\Omega , \end{cases} \tag{18.22}$$

to get $u_i(a, q)$ for $i = 1, 2, 3$. The data maps are given by

$$E_i = a |\nabla u_i(a, q)|^2, e_i = q |u_i(a, q)|^2, \quad i = 1, 2, 3 . \tag{18.23}$$

The main purpose of this section is to study the differentiability of the maps E_i and e_i in (18.23). Assume that a and q belong to

$$A = \{\gamma \in W^{1,2}(\Omega) : c_0 < \gamma < C_0, |\nabla\gamma| < C_1\} \tag{18.24}$$

and

$$Q = \{\gamma \in L^2(\overline{\Omega}) : c_0 < \gamma < C_0\} , \tag{18.25}$$

where c_0, C_0 and C_1 are given positive numbers. Note that A stands for an admissible set for the true a and Q does for the true q. They are open in $W^{1,\infty}(\Omega)$ and $L^\infty(\Omega)$, respectively. The following lemma holds.

Lemma 18.9 *Let $f \in W^{-1,2}(\Omega)$, $g \in W^2_{1/2}(\partial\Omega)$, a be in A and q belong to Q. Assume that f and g are real-valued and k^2 is not a Dirichlet eigenvalue of $-\frac{\nabla \cdot a\nabla}{q}$ and u is the unique solution of*

$$\begin{cases} \nabla \cdot a\nabla u + k^2 qu = f \ in \ \Omega \,, \\ \qquad\qquad\quad u = g \ on \ \partial\Omega \,. \end{cases} \tag{18.26}$$

Then there exists C, only depending on k, a, q, such that

$$\|u\|_{W^{1,2}(\Omega)} \leq C(\|f\|_{W^{-1,2}(\Omega)} + \|g\|_{W^2_{1/2}(\partial\Omega)}) \,. \tag{18.27}$$

Proof. Assume for a moment that $g = 0$. We claim that

$$\|u\|_{L^2(\Omega)} \leq C\|f\|_{W^{-1,2}(\Omega)} \,. \tag{18.28}$$

If this is not true, for all $n \geq 1$, there exists $f_n \in W^{-1,2}(\Omega)$ such that

$$\|u_n\|_{L^2(\Omega)} \geq n\|f_n\|_{W^{-1,2}(\Omega)} \,, \tag{18.29}$$

where u_n solves

$$\begin{cases} \nabla \cdot a\nabla u_n + k^2 qu_n = f_n \ in \ \Omega \,, \\ \qquad\qquad\qquad u_n = 0 \ \ on \ \partial\Omega \,. \end{cases} \tag{18.30}$$

Define

$$v_n = \frac{u_n}{\|u_n\|_{L^2(\Omega)}} \,. \tag{18.31}$$

We have that v_n solves

$$\begin{cases} \nabla \cdot a\nabla v_n + k^2 qv_n = \frac{f_n}{\|u_n\|_{L^2(\Omega)}} \ in \ \Omega \,, \\ \qquad\qquad\qquad u_n = 0 \qquad\qquad on \ \partial\Omega \,. \end{cases} \tag{18.32}$$

Therefore,

$$\int_\Omega a|\nabla v_n|^2 dx = \int_\Omega k^2 q(v_n)^2 dx - \int_\Omega \frac{f_n v_n}{\|u_n\|_{L^2(\Omega)}} dx \,, \tag{18.33}$$

which gives the boundedness of (v_n). From (18.32) and the assumption that k^2 is not a Dirichlet eigenvalue of $-\frac{\nabla \cdot a\nabla}{q}$, it is not hard to verify that (v_n) has a subsequence weakly converging in $W^{1,2}(\Omega)$ to 0. This contradicts to (18.31), which implies $\|v_n\|_{L^2(\Omega)} = 1$ for all n. Taking u as the test function for (18.26) and using (18.28), we obtain (18.27).

In the case when $g \neq 0$, let v be the solution of

$$\begin{cases} \nabla \cdot a\nabla v + k^2 qv = 0 \ in \ \Omega \,, \\ \qquad\qquad\quad v = g \ on \ \partial\Omega \,. \end{cases} \tag{18.34}$$

and then apply the result when $g = 0$ for $w = u - v$. □

Remark 18.10 *In the particular case when $f = 0$ and g is smooth enough. Then $u \in W^{2,2}(\Omega) \cap \mathcal{C}^1(\overline{\Omega})$ and there exists C, only depending on k, a, q, such that*

$$\|u\|_{W^{2,2}(\Omega)} + \|u\|_{\mathcal{C}^1(\overline{\Omega})} \leq C\|g\|. \tag{18.35}$$

Proof. The Helmholtz equation in (18.26) can be rewritten as

$$-\Delta u = \frac{\nabla a \nabla u + k^2 q u}{a}, \tag{18.36}$$

whose right hand side is in $L^2(\Omega)$. By regularity, u is in $W^{2,2}(\Omega) \cap \mathcal{C}^1(\overline{\Omega})$. Its $\mathcal{C}^1$ and $W^{2,2}$ norms are bounded by its norm in $W^{1,2}(\Omega)$ and hence by $\|g\|$ because $a \in A$ and $q \in Q$. □

We next study the differentiability of the forward problem.

Proposition 18.11 *For $i = 1, 2, 3$, the map u_i that sends $(a, q) \in A \times Q$ to the solution of (18.22) is Fréchet differentiable. Its derivative $du_i(a, q)(h_a, h_q)$ is given by the solution of*

$$\begin{cases} \nabla \cdot a \nabla v_i + k^2 q v_i = -\nabla \cdot h_a \nabla u_i(a, q) - k^2 h_q u_i(a, q) & \text{in } \Omega, \\ \qquad\qquad v_i = 0 & \text{on } \partial\Omega, \end{cases} \tag{18.37}$$

for all $(h_a, h_q) \in W_0^{1,\infty}(\Omega) \times L^\infty(\Omega)$. As a result, E_i and e_i are also Fréchet differentiable and

$$dE_i(a, q)(h_a, h_q) = h_a |\nabla u_i(a, q)|^2 + 2a \nabla u_i(a, q) \cdot \nabla v_i \tag{18.38}$$

and

$$de_i(a, q)(h_a, h_q) = h_q (u_i(a, q))^2 + 2q u_i(a, q) v_i. \tag{18.39}$$

These maps can be continuously extended into $W_0^{1,2}(\Omega) \times L^2(\Omega)$ by the same formulas (18.38) and (18.39).

Proof. The proof is similar to that of Lemma 18.2. □

Lemma 18.12 *Let $a \in A$ and $q \in Q$. The followings are true.*

1. *The maps $du_i(a, q)(h_a, h_q) \mapsto \nabla v_i$ and $du_i(a, q)(h_a, h_q) \mapsto v_i$, $i = 1, 2, 3$, defined in (18.37), can be continuously extended to compact maps $W_0^{1,2}(\Omega)^2 \times L^2(\Omega) \to L^2(\Omega)^3$ and $W_0^{1,2}(\Omega)^2 \times L^2(\Omega) \to L^2(\Omega)$ respectively.*
2. *The maps $dE(a, q)$ and $de(a, q)$ takes the form $I + $ compact multiplied by a continuous function.*

Proof. Assume that (h_a, h_q) is in $W_0^{1,2}(\Omega) \times L^2(\Omega)$. For $i \in \{1, 2, 3\}$, the function $v_i \in W_0^{1,0}(\Omega)$ is the solution of

$$-a\Delta v_i = \nabla a \nabla v_i + k^2 q v_i + \nabla \cdot h_a \nabla u_i(a,q) + k^2 h_q u_i(a,q)$$
$$= \nabla a \nabla v_i + k^2 q v_i + h_a \Delta u_i(a,q) + \nabla h_a \nabla u_i(a,q) + k^2 h_q u_i(a,q)\,,$$
$$= \nabla a \nabla v_i + k^2 q v_i - h_a \frac{\nabla a \nabla u + k^2 q u}{a} + \nabla h_a \nabla u_i(a,q) + k^2 h_q u_i(a,q)\,,$$

which is in $L^2(\Omega)$. As a result, $v_i \in W^{2,2}(\Omega)$ and its $W^{2,2}$-norm is bounded by $\|(h_a, h_q)\|_{W_0^{1,2}(\Omega) \times L^2(\Omega)}$. The first part of this lemma is proved by (17.19). Consequently, the second one is true. $\square$

18.4 Optimal Control Algorithm

In this section, we discuss how the scalar coefficients a_* and q_* can be recovered in practice from multiple-frequency measurements

$$E_{i\,*}^k = a_* |\nabla u_i^k(a_*, q_*)|^2, \quad e_{i\,*}^k = q_* (u_i^k(a_*, q_*))^2\,, \tag{18.40}$$

$i = 1, 2, 3$. Here, we add the superscript ^{k} to indicate that the data are measured at the frequency k.

It is natural to think of a minimization approach, namely,

$$\text{minimize } J[a,q] := \frac{1}{2} \sum_{i=1}^{3} \int_{\underline{k}}^{\overline{k}} \int_{\Omega} \left| (E_i^k(a,q) - E_{i\,*}^k)^2 + (e_i^k(a,q) - e_{i\,*}^k)^2 \right|^2 dx dk\,, \tag{18.41}$$

where the data maps are defined in (18.23) with

$$(\varphi_1, \varphi_2, \varphi_3) = (1, x_1, x_2)$$

being a proper set of measurements. Here, the admissible sets for a and q are respectively A in (18.24) and Q in (18.25).

Our resolution method contains therefore two parts. First, we compute a_I and q_I following Propositions 18.5 and 18.6. Note that a_I/q_I is given by (18.15) and $\nabla \log q_I$ is the solution of

$$\begin{cases} \Delta v = \dfrac{1}{\overline{k} - \underline{k}} \displaystyle\int_{\underline{k}}^{\overline{k}} \nabla \cdot \left(\dfrac{\partial_{x_1} \text{trace}(e^k)}{\text{trace}(e^k)} - 2\lambda_1^k, \dfrac{\partial_{x_2} \text{trace}(e^k)}{\text{trace}(e^k)} - 2\lambda_2^k \right) dk \text{ in } \Omega\,, \\ v = \log q_0 \hspace{6cm} \text{on } \partial\Omega\,, \end{cases} \tag{18.42}$$

because of (18.16) where $q_0 = q_*|_{\partial\Omega}$ is known. We perform a gradient descent on J to improve this initial guess. Note that J is Fréchet differentiable and its derivative can be evaluated as follows: for all $h_a, h_q \in W_0^{1,2}(\Omega) \times L^2(\Omega)$

$$dJ[a,q](h_a,h_q) = \frac{1}{2}\sum_{i=1}^{3}\int_{\underline{k}}^{\overline{k}}\int_{\Omega}\left(h_a\delta_i^k|\nabla u_i^k|^2 + h_q\epsilon_i^k(u_i^k)^2\right)dxdk$$

$$+2\sum_{i=1}^{3}\int_{\underline{k}}^{\overline{k}}\int_{\Omega}\left(a\delta_i^k\nabla u_i^k\nabla v_i^k + q\epsilon_i^k u_i^k v_i^k\right)dxdk$$

$$=\sum_{i=1}^{3}\int_{\underline{k}}^{\overline{k}}\int_{\Omega}\left(h_a\delta_i^k|\nabla u_i^k|^2 + h_q\epsilon_i^k(u_i^k)^2\right)dxdk$$

$$+2\sum_{i=1}^{3}\int_{\underline{k}}^{\overline{k}}\int_{\Omega}\left(h_a\nabla u_i^k\nabla p_i^k - k^2 h_q u_i^k p_i^k\right)dxdk \tag{18.43}$$

where

$$\delta_i^k = a|\nabla u_i^k|^2 - E_{i\,*}^k, \quad\text{and}\quad \epsilon_i^k = q(u_i^k)^2 - e_{i\,*}^k \tag{18.44}$$

and p_i^k is the solution of

$$\begin{cases} \nabla\cdot(a\nabla p_i^k) + k_i^2 qp_i^k = -\nabla\cdot(\delta_i^k a\nabla u_i^k) + 2\epsilon_i^k qu_i^k & \text{in } \Omega\,, \\ \qquad\qquad p_i^k = 0 \quad\text{on } \partial\Omega\,. \end{cases} \tag{18.45}$$

It follows from (18.43) and the Riesz representation theorem that

$$(dE_i^k(a,q)(\delta_i^k,\epsilon_i^k), de_i^k(a,q)(\delta_i^k,\epsilon_i^k))^* = (\delta_i^k|\nabla u_i^k|^2 + \nabla u_i^k\nabla p_i^k, \epsilon_i^k(u_i^k)^2 - k^2 u_i^k p_i^k)\,. \tag{18.46}$$

Note that the differentiability of J on $A\times Q$ holds for any positive constants c_0, C_0, and C_1 such that $c_0 < C_0$.

Theorem 18.13 *Assume that a_* and q_* are in A and Q respectively and assume that we have the initial guess a_I, q_I with $a_I = a^{(0)}$ and $q_I = q^{(0)}$ on $\partial\Omega$ in hand. If $\|a_I - a_*\|_{W^{1,2}}$ and $\|q_I - q_*\|_{L^2}$ are small enough, then the sequence*

$$(a^{(n+1)}, q^{(n+1)}) = T(a^{(n)}, q^{(n)})$$

$$-\sum_{i=1}^{3}\int_{\underline{k}}^{\overline{k}}(dE_i^k(T(a^{(n)},q^{(n)}))^*(\delta_i^k,\epsilon_i^k), de_i^k(T(a^{(n)},q^{(n)})^*(\delta_i^k,\epsilon_i^k))$$

converges to (a_*,q_*) in $L^2(D)^2$. Here, T is the Hilbert projection of $W^{1,2}(\Omega)\times L^2(\Omega)$ onto $A\times Q$.

Proof. We first prove that

$$\bigcap_{k\in(\underline{k},\overline{k})} (dE^k(a,q), de^k(a,q))|_{L^2(\Omega)\times L^2(\Omega)} = \{0\}\,. \tag{18.47}$$

In fact, let $(h_a, h_q) \in L^2(\Omega)\times L^2(\Omega)$ such that

$$(dE^k(a,q)(h_a,h_q), de^k(a,q)(h_a,h_q)) = 0$$

for all $k \in (\underline{k}, \overline{k})$. Applying Lemma 18.2, we have

$$dE^0(a,q)(h_a,h_q) = 0, \quad \text{and} \quad de^0(a,q)(h_a,h_q) = 0. \tag{18.48}$$

Applying (17.12), we see that $h_a = 0$ in Ω. Thus $v_i^0 = 0$ and $h_q = 0$. It follows from Lemma 18.12 and Fredholm alternative with the note that $de^k(a,q)$ and $dE^k(a,q)$ takes the form $(u^k)^2(I + \text{compact})$ and $|\nabla u^k|^2(I + \text{compact})$ that

$$\|(dE^k(a,q), de^k(a,q))\|_{\mathcal{L}(W_0^{1,2}(\Omega) \times L^2(\Omega), L^2(\Omega) \times L^2(\Omega))} \geq C \tag{18.49}$$

for some positive constant C. The theorem follows from Proposition 2.5. $\quad\square$

19

Ultrasound-Modulated Optical Tomography

19.1 Introduction

The aim of this chapter is to develop an efficient reconstruction algorithm for ultrasound-modulated diffuse optical tomography. In diffuse optical imaging, the resolution is in general low. By mechanically perturbing the medium, we show that it is possible to achieve a significant resolution enhancement. When a spherical acoustic wave is propagating inside the medium, the optical parameter of the medium is perturbed. Using cross-correlations of the boundary measurements of the intensity of the light propagating in the perturbed medium and in the unperturbed one, we provide two iterative algorithms for reconstructing the optical absorption coefficient. Using a spherical Radon transform inversion, we first establish an equation that the optical absorption satisfies. This equation together with the diffusion model constitutes a nonlinear system. Then, solving iteratively such a nonlinear coupled system, we obtain the true absorption parameter. We prove the convergence of the proposed algorithms and present numerical results to illustrate their resolution and stability performances.

Let Ω be a smooth bounded domain of $\mathbb{R}^d$, for $d = 2, 3$, satisfying the interior ball condition. Let ν denote the unit normal outward vector on $\partial\Omega$ and let $\partial/\partial\nu$ denote the normal derivative at $\partial\Omega$. When a laser beam is applied at a point x_0 on $\partial\Omega$, the energy density φ_* is governed by the diffusion equation

$$\begin{cases} -\Delta\varphi_* + q_*\varphi_* = 0 \text{ in } \Omega \,, \\ \quad l\frac{\partial\varphi_*}{\partial\nu} + \varphi_* = g \text{ on } \partial\Omega \,, \end{cases} \tag{19.1}$$

where q_* is the (spatially-varying) optical absorption coefficient and $g \geq 0$ is a smooth approximation of the Dirac function at x_0. Note that in the Robin type boundary condition in (19.1), l is the extrapolation length. Throughout this chapter we will assume for simplicity that $l = 1$.

Using boundary measurements of the normal derivative of the solution to the diffusion equation (19.1) corresponding to many g, it is possible to

determine the optical coefficient q_*. Direct reconstruction methods can be designed in the linearized case under the Born assumption and for particular experimental geometries. Nevertheless, the resolution of the reconstruction is usually low due to the inherent severely ill-posed character of diffuse optical imaging.

Based on the use of mechanical perturbations of the medium, the optical coefficient can be reconstructed with high resolution. The idea behind the method is to perturb the medium by a propagating acoustic wave while taking the boundary measurements of the normal derivative of the energy density corresponding to g. Let $y \in \Omega \setminus \overline{D}$. Consider a displacement field u_y generated at the source point y such that its support is a thin spherical shell growing at a constant speed c. Denote $q_*(x + u_y(x,t))$ by $q_u(x,y,t)$, $x \in \Omega$, $t > 0$, and the corresponding energy density by $\varphi_u(x,y,t)$. The presence of the propagating acoustic wave generated at the source point y changes the medium and yields the perturbed diffusion equation

$$\begin{cases} -\Delta\varphi_u + q_u\varphi_u = 0 \text{ in } \Omega\,, \\ \quad \partial_\nu\varphi_u + \varphi_u = g \text{ on } \partial\Omega\,. \end{cases} \tag{19.2}$$

Then, in order to reconstruct q_*, we cross-correlate the boundary values of the intensity of the light propagating in the medium changed by the propagation of the acoustic wave and those corresponding to the unperturbed one. We compute the quantity

$$\int_{\partial\Omega} g\left(\frac{\partial\varphi_*}{\partial\nu} - \frac{\partial\varphi_u}{\partial\nu}\right) d\sigma\,. \tag{19.3}$$

Assume that y moves along a circle or a sphere. Then the use of a Helmholtz decomposition yields (19.18) for q_* where the source term is obtained from the data given by (19.3) by using a circular or a spherical Radon transform inversion. Hence the functions q_* and φ_* satisfy the coupled system of equations (19.1) and (19.18). This nonlinear coupling suggests two iterative approaches for reconstructing q_*. The first approach is a fixed point scheme and the second one is an optimal control algorithm. We prove the convergence of the iterative fixed point scheme to the true image of q_* using the contraction fixed point theorem and illustrate it numerically. Using Proposition 2.5, the convergence of the optimal control algorithm is also shown. Moreover, the high resolution and the good stability properties of the reconstructed images are shown under different conditions.

The chapter is organized as follows. In Section 19.2, we introduce some preliminary results. In Section 19.3, we present our reconstruction algorithms and provide proofs of their convergence. In Section 19.4 we illustrate the performance of the proposed algorithm in terms of resolution and stability. Throughout the chapter, C is an universal constant depending only on known quantities and functions. Our results in this chapter are from [29, 30, 56, 74].

19.2 Preliminaries

19.2.1 Acoustic Wave

In this section we first see how the displacement field u can be created by a short spherical acoustic wave and what its typical form is.

The acoustic wave equations are obtained by linearizing the fluid dynamics equations for small disturbances around a fluid at rest. The state of a fluid is characterized by macroscopic quantities such as the density, the fluid velocity, the pressure, and the temperature.

We consider the three-dimensional case. We denote by p_0 and ρ_0 the unperturbed pressure and density, with the unperturbed velocity equal to 0, and we consider small perturbations of the pressure and velocity, denoted by p and v. Doing so, we obtain the acoustic wave equations

$$
\begin{cases}
\dfrac{1}{K_0}\dfrac{\partial p}{\partial t} + \nabla \cdot v = 0\,, \\[2mm]
\rho_0 \dfrac{\partial v}{\partial t} + \nabla p \quad = 0\,.
\end{cases}
$$

We assume initial conditions of the form

$$
v(x,t=0) = 0, \qquad p(x,t=0) = p_0(x) = \frac{1}{\eta}f_0\Big(\frac{|x|^2}{\eta^2}\Big), \tag{19.4}
$$

where f_0 is a smooth function compactly supported in $[0,1]$ and η is the radius of the support of the initial condition (that will be taken small at the end of the analysis). The solution of the acoustic wave equations has the form

$$
p(x,t) = \frac{\partial}{\partial t}\Big[\frac{t}{4\pi}\int_{\partial B} p_0(x_0 + cts)d\sigma(s)\Big]\,,
$$

$$
v(x,t) = -\frac{1}{\rho_0}\nabla\Big[\frac{t}{4\pi}\int_{\partial B} p_0(x_0 + cts)d\sigma(s)\Big]\,,
$$

where B is the ball centered at 0 and with radius 1 and c is the speed of sound defined by $c = \sqrt{K_0/\rho_0}$. We have

$$
\int_{\partial B} p_0(x_0 + cts)d\sigma(s) = \frac{2\pi}{\eta}\int_0^2 f_0\Big(\frac{(|x|-ct)^2}{\eta^2} + \frac{2ct|x|}{\eta^2}r\Big)dr\,.
$$

As soon as $ct > \eta$, this can be rewritten as follows:

$$
\int_{\partial B} p_0(x_0 + cts)d\sigma(s) = \frac{\pi\eta}{ct|x|}F_0\Big(\frac{(|x|-ct)^2}{\eta^2}\Big)\,,
$$

where

$$
F_0(r) = \int_r^\infty f_0(r')dr'\,.
$$

Note that F_0 is a smooth function compactly supported in $[0, 1]$. Therefore, we find that the velocity field is given by

$$v(x, t) = \frac{1}{4\rho_0 c} \frac{x}{|x|} \left[\frac{2}{\eta} \frac{|x| - ct}{|x|} f_0 \left(\frac{(|x| - ct)^2}{\eta^2} \right) + \frac{\eta}{|x|^2} F_0 \left(\frac{(|x| - ct)^2}{\eta^2} \right) \right].$$

When $ct \gg \eta$, this becomes

$$v(x, t) \approx \frac{1}{2\eta\rho_0 c} \frac{x}{|x|} \frac{|x| - ct}{|x|} f_0 \left(\frac{(|x| - ct)^2}{\eta^2} \right),$$

up to a term of relative order $\eta^2/(ct)^2$.

Remember that $v(x, t)$ is the fluid velocity at position x. If a particle is at x at time 0, then its position $P(x, t)$ at time t satisfies

$$\frac{\partial P(x, t)}{\partial t} = v\big(P(x, t), t\big), \qquad P(x, 0) = x.$$

Using the assumption that the amplitude of the displacement is small we can linearize around the original position and obtain that the position satisfies

$$\frac{\partial P(x, t)}{\partial t} = v(x, t) \quad \text{or} \quad P(x, t) = x + \int_0^t v(x, t') dt',$$

and it is therefore given by

$$P(x, t) = x + \frac{\eta}{4\rho_0 c^2} \frac{x}{|x|} F_0 \left(\frac{(|x| - ct)^2}{\eta^2} \right).$$

The displacement field $x \to x + u(x, t)$ is the inverse function of the position $x \to P(x, t)$. Using again the small displacement assumption which allows us to linearize around the initial position, we find

$$u(x, t) = -\frac{\eta}{4\rho_0 c^2} \frac{x}{|x|} F_0 \left(\frac{(|x| - ct)^2}{\eta^2} \right).$$

In the previous analysis the initial condition p_0 was chosen to be centered at 0. If p_0 is nonnegative-valued, $y \in \Omega$ is the center, then the displacement field is given by

$$u_y(x, t) = -\frac{\eta}{|x - y|} w \left(\frac{|x - y| - ct}{\eta} \right) \frac{x - y}{|x - y|}$$

and defined for $x \in \Omega \backslash \{y\}$ and $t \gg \eta/c$. The support of the displacement field can be seen as a thin spherical shell growing at the constant speed c. This can be approximated up to a term of order $\eta/(ct)$ by

$$u_y(x, t) = -\frac{\eta}{ct} w \left(\frac{|x - y| - ct}{\eta} \right) \frac{x - y}{|x - y|}. \tag{19.5}$$

In this formulation, w is the shape function and is such that $w \in \mathcal{C}^\infty(\mathbb{R}, \mathbb{R}^+)$ and $\operatorname{supp}(w) \subset [-1, 1]$. Here, η is a positive parameter representing the thickness of the wavefront. Note that, in order to have a wavefront with nonzero thickness, initial conditions of the form (19.4) are required.

Although the derivations in this section are in three-dimensions, we will use for the sake of simplicity the same form of the displacement field in the numerical experiments carried out in two dimensions.

19.2.2 Regularity Results

In this section, we recall two consequences of well-known regularity results [242, 254]. These results will be used for proving the convergence of the fixed point scheme and the optimal control approach.

Proposition 19.1 *Suppose that Ω is smooth. If $p \in L^\infty(\Omega)$, then any weak and bounded solution φ of the equation*

$$-\Delta\varphi + p\varphi = 0, \quad \text{with } \|\varphi\|_{L^\infty(\Omega)} \leq M, \tag{19.6}$$

is in $\mathcal{C}^1(\Omega)$ and

$$\|\varphi\|_{\mathcal{C}^1(\overline{\Omega'})} \leq c_1(M, \|p\|_{L^\infty(\Omega)}, \operatorname{dist}(\Omega', \partial\Omega))$$

for all $\Omega' \Subset \Omega$.

The following proposition is from [182, 253].

Proposition 19.2 *Let D be a bounded smooth domain and $\lambda < \Lambda, M$ be positive constants. If $\varphi \in L^\infty(D)$ is such that*

$$0 < \lambda \leq \varphi \leq \Lambda \quad \text{in } D$$

and if $f \in L^\infty(D)$ is such that $\|f\|_{L^\infty(D)} \leq M$, then the solution q of

$$\begin{cases} \nabla \cdot (\varphi^2 \nabla q) = f \text{ in } D, \\ \qquad\quad q = 0 \text{ on } \partial D \end{cases} \tag{19.7}$$

is in $\mathcal{C}^1(\overline{D})$ with

$$\|q\|_{\mathcal{C}^1(\overline{D})} \leq c_2(\lambda, \Lambda, M). \tag{19.8}$$

Remark 19.3 *Assume that the constant c_2 in (19.8) is optimal; i.e., c_2 is the infimum of all of its possible values. Then,*

$$c_2(\lambda, \Lambda, \delta M) \leq \delta c_2(\lambda, \Lambda, M) \tag{19.9}$$

for all $0 < \delta < 1$. This can be seen by multiplying both sides of (19.7) by δ.

We next recall the weak comparison principle and the strong maximum principle for Laplace equations with the Robin boundary condition [286].

Proposition 19.4 (weak comparison principle) *Let p be a nonnegative measurable function and assume that $\varphi \in W^{1,2}(\Omega)$ satisfies*

$$\begin{cases} -\Delta\varphi + p\varphi \geq 0 \ in \ \Omega\,, \\ \quad \partial_\nu\varphi + \varphi \geq 0 \ on \ \partial\Omega\,. \end{cases} \tag{19.10}$$

We have $\varphi \geq 0$ a.e. in Ω.

Proof. Using $\varphi^- = \max\{0, -\varphi\} \geq 0$ as a real-valued test function in the variational formulation of (19.10) gives

$$0 \leq \int_\Omega \nabla\varphi \cdot \nabla\varphi^- dx - \int_{\partial B} \frac{\partial\varphi}{\partial\nu}\varphi^- d\sigma + \int_\Omega p\varphi\varphi^- dx$$

$$\leq \int_\Omega \nabla\varphi \cdot \nabla\varphi^- dx + \int_{\partial B} \varphi\varphi^- d\sigma + \int_\Omega p\varphi\varphi^- dx$$

$$= -\int_\Omega |\nabla\varphi^-|^2 dx - \int_{\partial B} |\varphi^-|^2 d\sigma - \int_\Omega p|\varphi^-|^2 dx\,.$$

It follows that $\varphi^- = 0$. Note that φ^- is admissible to be a test function because it belongs to $W^{1,2}(\Omega)$ (see [184]). □

We need the following lemma to prove this strong maximum principle [300].

Lemma 19.5 (Hopf lemma) *Let $\varphi \in \mathcal{C}^1\left(\overline{\Omega}\right) \cap \mathcal{C}^2\left(\Omega\right)$ satisfy*

$$-\Delta\varphi + c\varphi \geq 0$$

on Ω where c is a nonnegative constant. If there exists $x_0 \in \partial\Omega$ such that $\varphi(x_0) \leq 0$ and $\varphi(x) > \varphi(x_0)$ for all $x \in \Omega$, then

$$\partial_\nu\varphi(x_0) < 0.$$

Proposition 19.6 (strong maximum principle) *Let $g \not\equiv 0$ be a nonnegative smooth function defined on $\partial\Omega$. Let $D \Subset \Omega$ be smooth. For all $c > 0$, the solution φ_c of*

$$\begin{cases} -\Delta\varphi_c + c\varphi_c = 0 \ in \ \Omega\,, \\ \quad \partial_\nu\varphi_c + \varphi_c = g \ on \ \partial\Omega \end{cases} \tag{19.11}$$

is bounded and positive in D.

Proof. Since g is nonnegative, so is φ_c because of Proposition 19.4. On the other hand, applying Proposition 19.4 again for $\|g\|_{L^\infty(\partial\Omega)} - \varphi$, we can see that $\varphi \leq \|g\|_{L^\infty(\partial\Omega)}$. The boundedness of φ_c in Ω, and hence D, has been

verified. In order to use the Hopf lemma, we show that $\varphi_c \in \mathcal{C}^2(\Omega)$. In fact, for all $x_0 \in \Omega$, let D_1 and D_2 satisfying

$$D_1 \Subset D_2 \Subset \Omega$$

be two open neighbourhoods of x_0. The boundedness of φ_c in the previous paragraph and Proposition 19.1 imply that φ_c belongs to $\mathcal{C}^1(\overline{D}_2)$. On the other hand, [184, Theorem 8.8] helps us to see that $\varphi_c \in W^{2,2}(D_2)$. Hence, $\partial_{x_i}\varphi_c$, $i = 1, \ldots, d$, is in $W^{1,2}(D_2)$. It also satisfies the equation

$$-\Delta\partial_{x_i}\varphi_c + c\partial_{x_i}\varphi_c = 0\,.$$

Hence, $\partial_{x_i}\varphi_c$ belongs to $\mathcal{C}^1(\overline{D}_1)$ by Proposition 19.1. In other words, $\varphi_c \in \mathcal{C}^2(\overline{D}_1)$.

We claim that $\varphi_c > 0$ not only in $\overline{D}$ but also in Ω. Assume that $\varphi_c(x_0) = 0$ for some $x_0 \in \Omega$. Since g is not identically zero, neither is φ_c. Thus, we can find a point $x_1 \in \Omega$ such that $\varphi_c(x_1) > 0$. Without loss of generality, we can suppose that $B(x_1, r) \subset \Omega$ with $r = |x_1 - x_0|$ and $\varphi_c(x) > 0$ for all $x \in B(x_1, r)$. Since $\varphi_c \in \mathcal{C}^2(\Omega)$, φ_c belongs to $\mathcal{C}^1(\overline{B(x_1, r)}) \cap \mathcal{C}^2(B(x_1, r))$. We can apply the Hopf lemma for φ_c in $B(x_1, r)$ to get

$$\nabla\varphi_c(x_0) \cdot (x_1 - x_0) < 0\,.$$

This is a contradiction because φ_c attains its minimum value at x_0 and $\nabla\varphi_c(x_0) = 0$. $\square$

19.3 Reconstruction Algorithms

In order to achieve a resolution enhancement ultrasound-modulated optical tomography can be used. Its basic principles are as follows. We generate a spherical acoustic wave inside the medium. The propagation of the acoustic wave changes the absorption parameter of the medium. During the propagation of the wave we measure the light intensity on $\partial\Omega$. The aim is now to reconstruct the optical absorption coefficient from such set of measurements with a better resolution and stability than using pure optical tomography.

In the previous section, we have shown that the displacement function u at x caused by a short diverging spherical acoustic wave generated at $y \in \mathbb{R}^d \setminus \overline{D}$ is of the form

$$u(x) = u_y(x, t) = -\frac{\eta}{ct}w\left(\frac{|x - y| - ct}{\eta}\right)\frac{x - y}{|x - y|}, \quad x \in \Omega, \qquad (19.12)$$

where the constant c is the acoustic wave speed, $w \in \mathcal{C}^\infty(\mathbb{R}, \mathbb{R}^+)$ (called the shape function) is with support contained in $[-1, 1]$, η is a positive parameter representing the thickness of the wavefront, *i.e.*, the thickness of the support of the displacement field u, and t is understood as the time parameter.

Now, from (19.1) and (19.2), it follows that

$$\|\varphi_u - \varphi_*\|_{W^{1,2}(\Omega)} \leq c\|q_u - q_*\|_{L^2(\Omega)} \,,$$

for some positive constant c.

Multiplying (19.2) by φ_*, integrating by parts, and using (19.1), we obtain the cross-correlation formula

$$\int_{\partial\Omega} g\left(\frac{\partial\varphi_*}{\partial\nu} - \frac{\partial\varphi_u}{\partial\nu}\right) d\sigma \,. \tag{19.13}$$

The main idea for recovering q_* is to notice that

$$\int_{\partial\Omega} g\left(\frac{\partial\varphi_*}{\partial\nu} - \frac{\partial\varphi_u}{\partial\nu}\right) d\sigma \approx -\int_{\Omega} \varphi_*^2 \nabla q_* \cdot u \, dx \,, \tag{19.14}$$

which follows from a Taylor expansion of q_* and a Born approximation for φ_u.

Since $\partial\varphi_*/\partial\nu$ and $\partial\varphi_u/\partial\nu$ can be measured on $\partial\Omega$, it is possible to evaluate the quantity

$$\int_{\partial\Omega} g\left(\frac{\partial\varphi_*}{\partial\nu} - \frac{\partial\varphi_u}{\partial\nu}\right) d\sigma$$

for all y, t. This quantity is nothing other than the cross-correlations between the boundary measurements in the perturbed and unperturbed media.

Next, from (19.14) we establish an equation for q_*. Using Helmholtz decomposition, we write

$$\varphi_*^2 \nabla q_* = -\nabla\psi + \nabla \times \Psi \,. \tag{19.15}$$

Here, in order to insure the uniqueness of ψ and Ψ we assume that Ω is simply connected, Ψ is such that $\nabla \cdot \Psi = 0$, and we supply the boundary conditions

$$\frac{\partial\psi}{\partial\nu} = -\varphi_*^2 \frac{\partial q_*}{\partial\nu}$$

and $\Psi \times \nu = 0$ on $\partial\Omega$.

Since u takes the radial form (19.12), integration by parts yields

$$\int_{\Omega} \nabla \times \Psi \cdot u \, dx = 0 \,,$$

and so (19.14) can be rewritten as

$$\int_{\partial\Omega} g\left(\frac{\partial\varphi_*}{\partial\nu} - \frac{\partial\varphi_u}{\partial\nu}\right) d\sigma \approx \int_{\Omega} \nabla\psi \cdot u \, dx \,.$$

Hence, ψ can be constructed and considered as the given data by employing the spherical mean Radon transform.

Let

$$N_u(y, r) := \int_{\partial\Omega} g(x) \left(\frac{\partial\varphi_*}{\partial\nu}(x) - \frac{\partial\varphi_u}{\partial\nu}(x, y, r/c) \right) d\sigma(x) , \qquad (19.16)$$

where u_y is given by (19.12).

For $f \in C^0(\mathbb{R}^d)$ and $E \subset \mathbb{R}^d$, recall that the spherical mean Radon transform of f over E, $\mathcal{R}[f]$, is defined by (2.52).

The following lemma holds.

Lemma 19.7 *Fix $y \in \Omega \setminus \overline{D}$ and let $r_0 > 0$. Suppose that $q_*(x) = q_0$ for $x \in B(y, r_0)$, where B is the ball of center y and radius r_0. Suppose also that $q_* \in C^{1,\beta}(\overline{\Omega})$ and η is small enough. Then, for all $r > r_0$ and $\eta \ll r$, we have*

$$\mathcal{R}[\psi](y, r) \approx -\frac{1}{\eta^2 \|w\|_{L^1}|S|} \int_{r_0}^{r} \frac{N_u(y, \rho)}{\rho^{d-2}} d\rho , \qquad (19.17)$$

where $|S|$ is the surface of the unit sphere S.

Having in hand ψ from the cross-correlations between boundary measurements using the filtered backprojection formula (13.8), we take the divergence of (19.15) to arrive at

$$-\nabla \cdot (\varphi_*^2 \nabla q_*) = \Delta\psi . \qquad (19.18)$$

Assume that q_* is bounded from below and above by two known positive constants $\underline{q}$ and $\overline{q}$, respectively. Since φ_* solves problem (19.6) with q_* replacing p and $\overline{\Lambda}$, which will be defined later in Lemma 14.9, replacing M, its $C^1(\overline{D})$ norm is bounded. The analysis allows us to recover q_* in D by solving the system of equations for the two unknowns φ and q:

$$\begin{cases} -\Delta\varphi + q\varphi = 0 \text{ in } \Omega , \\ \partial_\nu\varphi + \varphi = g \text{ on } \partial\Omega , \end{cases} \qquad (19.19)$$

and

$$\begin{cases} -\nabla \cdot (\varphi^2 \nabla q) = \Delta\psi \text{ in } D , \\ q = q_0 \quad \text{ on } \partial D . \end{cases} \qquad (19.20)$$

19.3.1 Fixed Point Algorithm

The system of equations (19.19)–(19.20) suggests Algorithm 19.1.

Remark 19.8 *Consider the Born assumption*

$$q_* = q_0(1 + \delta s_*) , \qquad (19.24)$$

where δ is a small constant and s_* is a smooth function supported in $D \Subset \Omega$, with known bound on its $C^2(D)$ norm. We have

$$-\Delta\psi = \delta q_0 \nabla \cdot (\varphi_*^2 \nabla s_*) , \qquad (19.25)$$

and therefore,

$$\|\Delta\psi\|_{L^\infty(\Omega)} = O(\delta) \quad as \ \delta \ll 1 .$$

Algorithm 19.1 Fixed point algorithm

---

1. Define the initial guess $q^{(0)} = q_0$.
2. For $n \geq 1$, solve

$$\begin{cases} -\Delta\varphi^{(n)} + Tq^{(n-1)}\varphi^{(n)} = 0 \text{ in } \Omega\,, \\ \qquad\qquad \partial_\nu\varphi^{(n)} + \varphi^{(n)} = g \text{ on } \partial\Omega\,, \end{cases} \tag{19.21}$$

where

$$Tp := \min\{\max\{p, \underline{q}\}, \overline{q}\}\,. \tag{19.22}$$

3. Find $q^{(n)}$ by solving

$$\begin{cases} -\nabla \cdot ((\varphi^{(n)})^2 \nabla q^{(n)}) = \Delta\psi \text{ in } D\,, \\ \qquad\qquad\qquad q^{(n)} = q_0 \quad \text{on } \partial D\,. \end{cases} \tag{19.23}$$

and defining $q^{(n)} = q_0$ in $\Omega \setminus D$.
4. For $\|\Delta\psi\|_{L^\infty(\Omega)}$ small enough, the convergent function of $\{q^{(n)}\}$ is the true optical absorption coefficient q_*.

Remark 19.9 *The convergence of $\{q^{(n)}\}$, mentioned in Step 4, will be shown below by the Banach fixed point theorem. This also implies the well-posedness of the system constituted by (19.19) and (19.20).*

Remark 19.10 *Problem (19.21) is uniquely solvable because we are able to avoid the case that $(\varphi^{(n)})^2$ approaches 0 or ∞ somewhere inside D.*

Remark 19.11 *We modify $q^{(n-1)}$ by $Tq^{(n-1)}$ in (19.21) because of the obvious inequality*

$$|Tp - q_*| \leq |p - q_*|,$$

which makes the proof of the algorithm easier and may increase the rate of convergence.

In order to prove the convergence of $\{q^{(n)}\}$, we define the open set of $L^\infty(\Omega)$

$$\mathcal{Q} = \{p \in L^\infty(\Omega) : \underline{q} < p < \overline{q}\}\,, \tag{19.26}$$

and the map

$$\begin{aligned} F_1 : \mathcal{Q} &\to W^{1,2}(\Omega) \\ q &\mapsto F_1[q] = \varphi, \text{where } \varphi \text{ is the solution of (19.19)}\,. \end{aligned} \tag{19.27}$$

We have the following result.

Lemma 19.12 *For all $q \in \mathcal{Q}$, $F_1[q]$ is in $L^\infty(\Omega)$. There exists a positive constant $\Lambda(\underline{q}, \overline{q})$ such that*

$$\big|F_1[q](x)\big| \leq \Lambda, \quad \forall\, x \in \Omega. \tag{19.28}$$

Moreover, for any $D \Subset \Omega$, there exists a positive constant $\lambda(D, \underline{q}, \overline{q})$ such that

$$\lambda \leq F_1[q](x), \quad \forall x \in D. \tag{19.29}$$

Proof. Let $\varphi_{\underline{q}}$ and $\varphi_{\overline{q}}$ be the solutions of (19.11) with c replaced by $\underline{q}$ and $\overline{q}$, respectively. It follows by Proposition 19.4 that

$$\varphi_{\overline{q}} \leq \varphi \leq \varphi_{\underline{q}} \quad \text{in } \Omega.$$

On the other hand, we can apply Proposition 19.6 to see that

$$\varphi_{\overline{q}} > 0 \quad \text{in } D.$$

The lemma is proved by letting $\lambda = \inf_D \varphi_{\overline{q}}$ and $\Lambda = \sup_\Omega \varphi_{\underline{q}}$. $\quad\square$

Lemma 19.13 *The map F_1 is Fréchet differentiable. Its derivative at q is given by*

$$dF_1[q](h) = \phi, \tag{19.30}$$

for $h \in L^\infty(\Omega)$, where ϕ solves

$$\begin{cases} -\Delta\phi + q\phi = -h\varphi \text{ in } \Omega, \\ \quad \partial_\nu\phi + \phi = 0 \quad \text{on } \partial\Omega \end{cases} \tag{19.31}$$

with $\varphi = F_1[q]$. Moreover, $dF_1[q]$ can be continuously extended to the whole $L^2(\Omega)$ by the same formula in (19.31) with

$$\|dF_1[q]\|_{\mathcal{L}(L^2(\Omega), W^{1,2}(\Omega))} \leq C\Lambda, \tag{19.32}$$

where Λ is defined in Lemma 19.12.

Proof. Let φ' be the solution of (19.19) with $q + h$ replacing q, assuming $\|h\|_{L^\infty(\Omega)} \ll 1$ so that $q + h \in \mathcal{Q}$ a.e. in Ω. Note that $\varphi' - \varphi$ solves

$$\begin{cases} -\Delta(\varphi' - \varphi) + (q + h)(\varphi' - \varphi) = -h\varphi \text{ in } \Omega, \\ \quad\quad \partial_\nu(\varphi' - \varphi) + (\varphi' - \varphi) = 0 \quad \text{on } \partial\Omega. \end{cases}$$

Using $\varphi' - \varphi$ as a test function in the variational formulation of the problem above gives

$$\|\varphi' - \varphi\|_{W^{1,2}(\Omega)} \leq C\|h\|_{L^\infty(\Omega)}\|\varphi\|_{L^2(\Omega)}. \tag{19.33}$$

On the other hand, since $\varphi' - \varphi - \phi$ solves

$$\begin{cases} -\Delta(\varphi' - \varphi - \phi) + q(\varphi' - \varphi - \phi) = -h(\varphi' - \varphi) \text{ in } \Omega, \\ \quad \partial_\nu(\varphi' - \varphi - \phi) + (\varphi' - \varphi - \phi) = 0 \quad\quad\quad \text{on } \partial\Omega, \end{cases}$$

we can apply the argument above to obtain

$$\|\varphi' - \varphi - \phi\|_{W^{1,2}(\Omega)} \leq C\|h\|_{L^\infty(\Omega)}\|\varphi' - \varphi\|_{L^2(\Omega)}. \tag{19.34}$$

Combining (19.33) and (19.34) shows that

$$\|\varphi' - \varphi - \phi\|_{W^{1,2}(\Omega)} \leq C\|h\|^2_{L^\infty(\Omega)}\|\varphi\|_{L^2(\Omega)},$$

which implies

$$\lim_{\|h\|_{L^\infty(\Omega)}\to 0} \frac{\|\varphi' - \varphi - \phi\|_{W^{1,2}(\Omega)}}{\|h\|_{L^\infty(\Omega)}} = 0.$$

The first part of the lemma follows.

Because of Lemma 19.12 and Proposition 19.4, which shows that $\varphi \in L^\infty(\Omega)$, problem (19.31) is uniquely solvable for all $h \in L^2(\Omega)$, and therefore the extension $dF_1[q] : L^2(\Omega) \to W^{1,2}(\Omega)$ is well-defined. Its continuity and (19.32) can be deduced, using ϕ as a test function in the variational formulation of (19.31) and applying Lemma 19.12:

$$\|\phi\|_{W^{1,2}(\Omega)} \leq C\|h\|_{L^2(\Omega)}\|\varphi\|_{L^\infty(\Omega)}.$$

The proof is then complete. $\square$

Note that the differentiability of F_1 on $\mathcal{Q}$ holds for any positive constants $\underline{q}$ and $\overline{q}$ such that $\underline{q} < \overline{q}$.

We next introduce another open set of $L^\infty(\Omega)$:

$$\mathcal{P} = \left\{\rho \in L^\infty(\Omega) : \frac{\lambda}{2} < \rho < 2\Lambda \text{ in } D\right\}. \tag{19.35}$$

Let

$F_2 : \mathcal{P} \to W^{1,2}(\Omega)$

$\quad \varphi \mapsto F_2[\varphi] = q$, where q is the solution of (19.20) in D and $q = q_0$ in $\Omega \setminus D$.

The following lemma can be proved in the same manner as Lemma 19.13.

Lemma 19.14 *The map F_2 is Fréchet differentiable. Its derivative at φ is given by*

$$dF_2[\varphi](h) = Q, \tag{19.36}$$

for $h \in L^\infty(\Omega)$, where Q solves

$$\begin{cases} -\nabla \cdot (\varphi^2 \nabla Q) = \nabla \cdot (2\varphi h \nabla q) \text{ in } D, \\ \qquad\qquad Q = 0 \qquad\qquad \text{ on } \partial D \end{cases} \tag{19.37}$$

with $q = F_2[\varphi]$ being the solution of (19.20) and $Q = 0$ in $\Omega \setminus D$. Moreover, $dF_2[\varphi]$ can be extended continuously to $L^2(\Omega)$ and

$$\|dF_2[\varphi]\|_{\mathcal{L}(L^2(\Omega), W^{1,2}(\Omega))} \leq \frac{2\Lambda}{\lambda^2} c_2(\lambda, \Lambda, M), \tag{19.38}$$

where M is an upper bound of $\|\nabla \cdot (\varphi \nabla q)\|_{L^\infty(D)}$.

Proof. Since evaluating the derivative of F_2 at φ is similar to doing so in Lemma 19.13, we only verify the well-definedness of the extension of $dF_2[\varphi]$ and (19.38). Since $\varphi \in \mathcal{P}$, we can apply Proposition 19.2 to see that the solution q of (19.20) is in $\mathcal{C}^1(\overline{D})$ and

$$\|q - q_0\|_{\mathcal{C}^1(\overline{D})} \le c_2(\lambda, \Lambda, M).$$

As a consequence, since $q = q_0$ on $\Omega \setminus D$, we deduce that

$$\|\nabla q\|_{L^\infty(\Omega)} \le c_2(\lambda, \Lambda, \delta M).\tag{19.39}$$

Thus, (19.37) is uniquely solvable if $h \in L^2(\Omega)$. This shows how to extend $dF_2[\varphi]$ to $L^2(\Omega)$.

In order to prove (19.38), we use Q as a test function in the variational formulation of (19.37) and employ (19.39) to get

$$\lambda^2 \int_D |\nabla Q|^2 dx \le \int_D \varphi^2 |\nabla Q|^2 dx$$

$$\le 2\Lambda \|\nabla q\|_{L^\infty(D)} \int_D |h||\nabla Q| dx$$

$$\le 2\Lambda c_2(\lambda, \Lambda, M)\|h\|_{L^2(D)}\|\nabla Q\|_{L^2(D)}.$$

Therefore,

$$\|Q\|_{W_0^{1,2}(D)} \le \frac{2\Lambda}{\lambda^2} c_2(\lambda, \Lambda, M),$$

and the proof is complete. □

Our main result in this section is the following.

Theorem 19.15 *Assume that $\underline{q}$, $\overline{q}$, and M are given. If $\|\Delta \psi\|_{L^\infty(\Omega)}$ is sufficiently small, then the iteration sequence in the algorithm converges in $L^2(\Omega)$ to q_*, the unique solution of (19.19) and (19.20).*

Proof. Introduce the map

$$F[q] = F_2 \circ F_1[q]$$

defined on $\mathcal{Q}$ given by (19.26). Thanks to (19.28) and (19.29), the range of F_1 is contained in the domain of F_2. This shows how the definition above makes sense. Considering F as the map $\mathcal{P} \to L^2(\Omega)$, using the standard chain rule in differentiation and the fact that $W^{1,2}(\Omega) \subset L^2(\Omega)$, we have

$$dF[q] : L^\infty(\Omega) \to L^2(\Omega)$$

given by

$$dF[q](h) = dF_2[F_1[q]](dF_1[q](h))\tag{19.40}$$

is the Fréchet derivative of F. Moreover, by Lemmas 19.13 and 19.14, $dF[q]$ can be extended continuously to $L^2(\Omega)$ with

$$\|dF[q]\|_{\mathcal{L}(L^2(\Omega),L^2(\Omega))} \leq \|dF_1[q]\|_{\mathcal{L}(L^2(\Omega),W^{1,2}(\Omega))}\|dF_2[q]\|_{\mathcal{L}(L^2(\Omega),W^{1,2}(\Omega))}$$
$$\leq C\|\Delta\psi\|_{L^\infty(\Omega)}.$$

Recall from the algorithm that $q^{(0)} = q_0$ is the initial guess for the true coefficient q_* and for $n \geq 1$, define

$$q^{(n)} = F[Tq^{(n-1)}] \quad n \geq 1,$$

where $Tp = \min\{\max\{p, \underline{q}\}, \overline{q}\}$. Note that for all $m, n \geq 1$,

$$\|F[Tq^{(n)}] - F[Tq^{(m)}]\|_{L^2(\Omega)} = \left\|\int_0^1 dF[(1-t)Tq^{(n)} + tTq^{(m)}](q^{(m)} - q^{(n)})dt\right\|_{L^2(\Omega)}$$
$$\leq C\|\Delta\psi\|_{L^\infty(\Omega)}\|q^{(m)} - q^{(n)}\|_{L^2(\Omega)}.$$

Thus, if $\|\Delta\psi\|_{L^\infty(\Omega)}$ is small enough, then

$$F \circ T : L^2(\Omega) \to L^2(\Omega)$$

is a contraction map. Let q^* denote the fixed point of $F \circ T$ and hence the convergent point of $q^{(n)}$. Since q_*, the true absorption coefficient, is a fixed point of F and is in the interval $[\underline{q}, \overline{q}]$, it is the fixed point of $F \circ T$. Therefore, $q^* = q_*$ and the proof is complete. $\square$

19.3.2 Optimal Control Algorithm

Let

$$K := \{q - q_0 \in W_0^{1,4}(\Omega) : \underline{q} \leq q \leq \overline{q} \text{ and } \|\nabla q\|_{L^4(\Omega)} \leq \theta\}, \qquad (19.41)$$

where θ will be determined later in (19.44). It is obvious that K is closed and convex in $W_0^{1,2}(\Omega)$.

Now, let the map $F : K \to W^{-1,2}(\Omega)$. For all $q \in K$, let

$$F[q](v) = \int_\Omega F_1[q]^2 \nabla q \cdot \nabla v \qquad \text{for all } v \in W_0^{1,2}(\Omega). \qquad (19.42)$$

We call F the *internal data* map.

Theorem 19.16 *The map F is Fréchet differentiable in K and*

$$dF[q](h, v) = \int_\Omega (2F_1[q]dF_1[q](h)\nabla q + F_1[q]^2\nabla h) \cdot \nabla v\, dx \qquad (19.43)$$

for all $q \in K$, $h \in W_0^{1,4}(\Omega) \cap L^\infty(\Omega)$ and $v \in W_0^{1,2}(\Omega)$. Assume further

$$0 < \theta < \frac{C_\Omega\lambda^2}{\Lambda^2}, \qquad (19.44)$$

where C_Ω is the norm of the embedding map of $W^{1,2}(\Omega)$ into $L^4(\Omega)$, multiplied with the constant in (19.32). Then, $dF[q]$ is well-defined on $W_0^{1,2}(\Omega)$ and there exists a positive constant C such that for all $h \in W_0^{1,2}(\Omega)$,

$$\|dF[q](h)\|_{W^{-1,2}(\Omega)} \geq C\|h\|_{W_0^{1,2}(\Omega)}. \tag{19.45}$$

Here, $dF[q](h) : v \in W_0^{1,2}(\Omega) \mapsto dF[q](h, v)$.

Proof. The Fréchet differentiability of F and the expression (19.43) of dF can be deduced from Lemma 19.13 and the standard rules in differentiation. We only prove (19.45). In fact, for all $h \in W_0^{1,2}(\Omega)$,

$$
\begin{aligned}
dF[q](h, h) &= \big(F_1[q]^2|\nabla h|^2 + 2F_1[q]dF_1[q](h)\nabla q\nabla h\big)\, dx \\
&\geq \int_\Omega \big(F_1[q]^2|\nabla h|^2\big)\, dx - \int_\Omega |2F_1[q]dF_1[q](h)\nabla q\nabla h|dx \\
&\geq \lambda^2 \left(\|h\|_{W_0^{1,2}(\Omega)} - \frac{\Lambda}{\lambda^2}\|dF_1[q](h)\|_{L^4(\Omega)}\|\nabla q\|_{L^4(\Omega)}\|\nabla h\|_{L^2(\Omega)} \right).
\end{aligned}
$$

It follows from the continuous embedding of $W^{1,2}(\Omega)$ into $L^4(\Omega)$ and (19.32) that

$$dF[q](h, h) \geq \lambda^2 \left(1 - \frac{C_\Omega\Lambda^2\theta}{\lambda^2} \right) \|h\|_{W_0^{1,2}(\Omega)}.$$

Therefore, the bilinear form $dF[q] : (h, v) \in W_0^{1,2}(\Omega) \times W_0^{1,2}(\Omega) \mapsto dF[q](h, v)$ is coercive, which shows that inequality (19.45) holds true with $C = \lambda^2(1 - \frac{C_\Omega\Lambda^2\theta}{\lambda^2})$. □

We now make use of Theorem 19.16 in order to prove a local Landweber condition which guarantees the convergence of the reconstruction algorithm.

Let q and q' be in K. We can find $t \in [0, 1]$ such that

$$\|F[q] - F[q']\|_{W^{-1,2}(\Omega)} = \|dF[tq+(1-t)q'](q-q')\|_{W^{-1,2}(\Omega)} \geq C\|q-q'\|_{W_0^{1,2}(\Omega)} \tag{19.46}$$

by (19.45). Hence, if $\|q - q'\|_{W_0^{1,2}(\Omega)}$ is small enough, then F satisfies the local Landweber condition:

$$\|F[q] - F[q'] - dF[q](q - q')\|_{W^{-1,2}(\Omega)} \leq \eta\|F[q] - F[q']\|_{W^{-1,2}(\Omega)} \tag{19.47}$$

for some $\eta < \frac{1}{2}$.

Consider $\Delta\psi$ as an element of $W^{-1,2}(\Omega)$ and rewrite

$$\nabla \cdot F_1[q]^2\nabla q = \Delta\psi\,,$$

in the sense of distributions, as

$$F[q] = \Delta\psi\,. \tag{19.48}$$

Recalling that K is closed and convex in $W_0^{1,2}(\Omega)$, we can employ the classical Hilbert projection theorem to define the projection T from $W_0^{1,2}(\Omega)$ onto K.

The optimal control algorithm is to minimize the discrepancy between $F[q]$ and $\Delta\psi$:

$$\min_{q\in K} J[q] := \frac{1}{2}\|F[q] - \Delta\psi\|^2_{W^{-1,2}(\Omega)}. \qquad (19.49)$$

It reads as follows.

Algorithm 19.2 Optimal control algorithm

---

1. Define the initial guess $q^{(0)} = q_0$.
2. For $n \geq 1$,

$$q^{(n+1)} = Tq^{(n)} - \eta dF[Tq^{(n)}]^*(F[Tq^{(n)}] - \Delta\psi), \qquad (19.50)$$

where η is the step size and T is defined by (19.22).
3. For $\|q_0 - q_*\|_{W_0^{1,2}(\Omega)}$ small enough, the convergent function of $\{q^{(n)}\}$ is the true optical absorption coefficient q_*.

The following convergence result for Algorithm 19.2 follows from Proposition 2.5.

Theorem 19.17 *Suppose that the true optical distribution q_* belongs to K and μ is sufficiently small. Let $q^{(n)}$ be defined by (19.50) with $q^{(0)}$ being the initial. Then the sequence $q^{(n)}$ converges in $W_0^{1,2}(\Omega)$ to q_* as $n \to \infty$.*

19.4 Numerical Illustrations

As a test case, we consider $\Omega = (-1,1)^2$ and $q_0 = 1$. We set

$$q_*(x) = 1 + (q_i - 1)\chi(\Omega_i)(x),$$

with $\Omega_i \Subset \Omega$ and $q_i > 1$ a constant. We take the dimensionless shape function w in (19.12) as follows:

$$w(\alpha) = e^{1/(\alpha^2-1)}, \quad \alpha \in [-1,1].$$

We generate the cross-correlation between boundary measurements N_u given by (19.16), with $u = u_y$ for sampling points y (such that $q_*(y) = q_0$) on the unit circle and sampling radii $r \in (0,2)$. Then, using Lemma 19.7 and adopting the same numerical approach as in Chapter 13, we generate the data Ψ by inverting the spherical mean Radon transform. In the case where the number of sampling points y is small, the total variation regularization method developed in Chapter 13 can be used. Problems (19.21) and (19.23)

are solved iteratively using a finite element code. We use a structured mesh with 10^4 vertices and $P1$ finite elements.

In order to measure the quality of the reconstruction, we introduce two indicators of the errors made in the image. Let $m = \min(q_{\mathrm{mes}})$ and $M = \max(q_{\mathrm{mes}})$. We compute the support of $q_{\mathrm{mes}} - q_0$ by

$$\Omega_{i,\mathrm{mes}} = \left\{ q_{\mathrm{mes}} - 1 > \frac{M - m}{2} \right\}$$

and define a position error by

$$E_{\mathrm{pos}} = \frac{|\Omega_i \triangle \Omega_{i,\mathrm{mes}}|}{2|\Omega_i|}$$

with Ω_i being the correct support of $q_* - q_0$. Here, $|\Omega_i \triangle \Omega_{i,\mathrm{mes}}|$ denotes the symmetric difference between Ω_i and $\Omega_{i,\mathrm{mes}}$. The second quantity we have to recover is q_i, the correct value of q_* in the inclusion. For doing so, let us define an estimation of q_i by

$$q_{i,\mathrm{mes}} = \frac{1}{|\Omega_{i,\mathrm{mes}}|} \int_{\Omega_{i,\mathrm{mes}}} q_{\mathrm{mes}}$$

and introduce the relative error for this estimation as follows:

$$E_{\mathrm{val}} = \frac{|q_{i,\mathrm{mes}} - q_i|}{|q_i - 1|}.$$

Finally, we introduce the relative L^2-error,

$$\|\varphi^{(n)} - \varphi_*\|_{L^2(\Omega)} / \|\varphi_*\|_{L^2(\Omega)},$$

where n is the number of iterations and φ_* is the true energy density.

As illustrated in Figure 19.1, if $|q_i - 1||\Omega_i| \ll |\Omega|$, then one iteration could be enough to obtain a quite resolved image (*i.e.*, with high resolution) since the relative L^2-error $\|\varphi^{(1)} - \varphi_*\|_{L^2(\Omega)} / \|\varphi_*\|_{L^2(\Omega)}$ is very small (of order 10^{-10} in the example in Figure 19.1).

In Figure 19.2 we consider the same example as in Figure 19.1. We plot the behaviors of E_{val} and E_{pos} as functions of η. It can be seen that the smaller η is, the better the reconstruction. However, there is a saturation effect for very small η due to the finite element discretization.

Next, we show in Figure 19.3 that a few iterations are necessary to reconstruct a resolved image if $|q_i - 1||\Omega_i|/|\Omega|$ is not too small. In Figure 19.3, the reconstructed images after one, two, and three iterations are given. In Figure 19.4 it can be seen that while the support of the inclusion is quite well reconstructed at the first iteration (it is in fact the support of the data Ψ), a few iterations are needed in order to find a good approximation of the value of the optical absorption parameter.
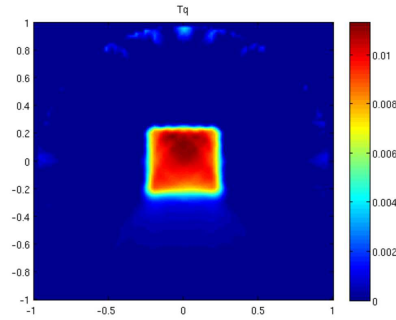
Fig. 19.1. Reconstruction after one iteration with $\eta = 0.02$, $q_i = 1.01$, $\Omega_i = (-0.25, 0.25)^2$, and the measurements N_u are for 50 sources on the unit circle and for $r \in (0, 2)$.
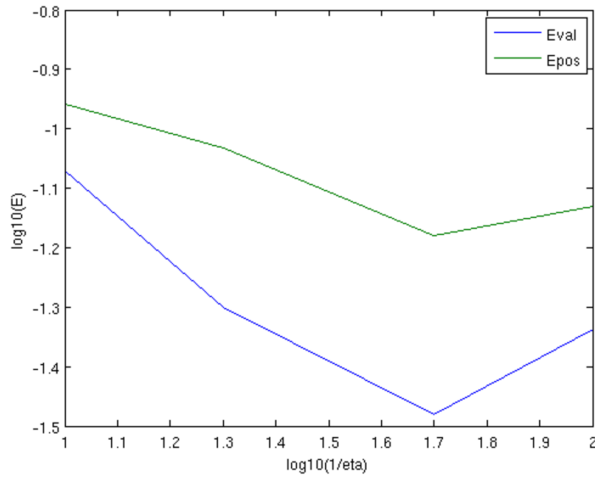
Fig. 19.2. Reconstruction errors E_{val} and E_{pos} as functions of η.

Finally, we illustrate the stability of the proposed algorithm. For doing so, we add to the measurements a discrete Gaussian white noise with standard deviation ranging from 0 to 10% of the L^∞-norm of N_u and compute the root mean square errors of the optical absorption parameter, $\mathbb{E}(E_{\mathrm{val}}^2)^{1/2}$, and the position, $\mathbb{E}(E_{\mathrm{pos}}^2)^{1/2}$, as functions of the noise level. Here $\mathbb{E}$ stands for the expectation. In Figure 19.5, we compute 100 realizations of the measurement noise and apply the fixed point algorithm for estimating both the shape and the optical absorption of the inclusion. Figure 19.5 gives, for $\eta = 0.02$, $\mathbb{E}(E_{\mathrm{val}}^2)^{1/2}$ and $\mathbb{E}(E_{\mathrm{pos}}^2)^{1/2}$, as functions of the noise level. It shows the ro-
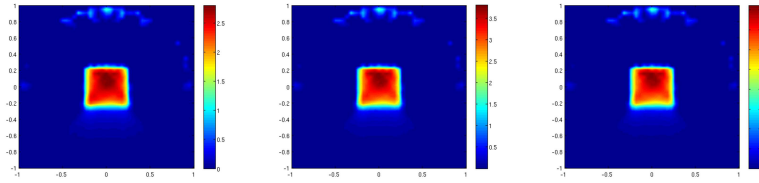
Fig. 19.3. Reconstruction after (from left to right) one, two, and three iterations with $\eta = 0.02$, $q_i = 3$ and $\Omega_i = (-0.25, 0.25)^2$, and the measurements N_u are for 50 sources on the unit circle and for $r \in (0, 2)$.
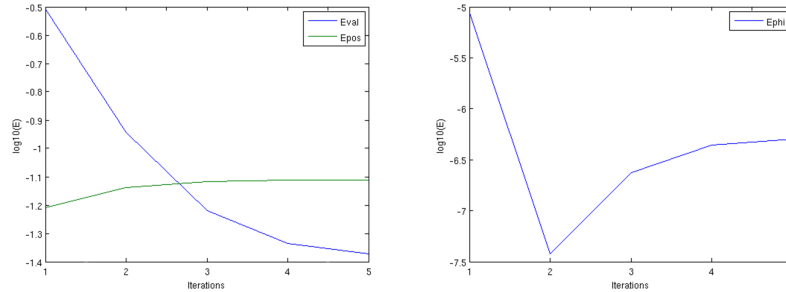
Fig. 19.4. Left: Reconstruction errors E_{val} and E_{pos} as functions of the number of iterations. Right: Relative L^2-error on $\varphi^{(n)}$, where n is the number of iterations.

bustness of the proposed approach. It also shows that finding the value of the optical absorption parameter is more stable than locating the inclusion. This seems to be due to the diffusion character of the problem satisfied by the optical absorption distribution.

19.4.1 Concluding Remarks

In this chapter we have presented efficient algorithms for ultrasound-modulated optical diffuse tomography. The modulation of light is due to the propagation of spherical acoustic waves. It leads to a coupled system of equations. Solving iteratively such a system yields a resolved image for the optical absorption coefficient under the assumption that $\|\Delta\psi\|_{L^\infty}$ is small enough. The proposed fixed point algorithm has good stability properties. Its performance depends on the boundary data. In order to obtain optimal images in the sense of resolution and stability, the boundary data has to be chosen in such a way that the interior of the domain is illuminated. In the case when $\|\Delta\psi\|_{L^\infty}$ is not small, an optimal control approach has been designed and its convergence proved provided that the initial guess is close enough to the true solution.
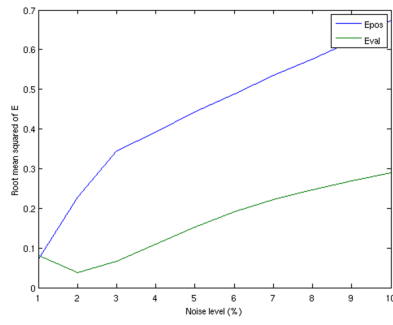
Fig. 19.5. Root mean square errors of the position and the value of q_{meas} for a noise level from 0% to 10%.

Mechanical Vibration-Assisted Conductivity Imaging

20.1 Introduction

This chapter aims at mathematically modeling a multi-physics conductivity imaging system incorporating mechanical vibrations simultaneously applied to an imaging object together with current injections. We perturb the internal conductivity distribution by applying time-harmonic mechanical vibrations on the boundary. This enhances the effects of any conductivity discontinuity on the induced internal current density distribution. Unlike other conductivity contrast enhancing frameworks, it does not require a prior knowledge of a reference data. In this chapter, we provide a mathematical framework for this emerging imaging modality. As an application of the vibration-assisted impedance imaging framework, we investigate a conductivity anomaly detection problem and provide an efficient location search algorithm. We show both theoretically and numerically that the applied mechanical vibration increases the data sensitivity to the conductivity contrast and enhances the quality of anomaly detection results.

In this chapter, we first describe the mathematical framework of the vibration-difference method in EIT. Emphasizing the sensitivity improvement by the conductivity modulation through a mechanical vibration, we adopt this approach to anomaly detection. We carry out the derivations of the vibration-difference method for anomaly detection and show its performance and feasibility through numerical experiments. Our results in this chapter are from [72].

20.2 Mathematical Modeling

In this section, we provide a mathematical model for a mechanical vibration assisted conductivity imaging and its theoretical ground. We set Ω to be a bounded domain with a boundary $\partial\Omega$ of class $\mathcal{C}^2$ in $\mathbb{R}^3$. We assume that the electrical conductivity σ of Ω is of class $\mathcal{C}^2(\overline{\Omega})$. Moreover, there exist $\underline{\sigma}$ and

$\overline{\sigma}$ such that $0 < \underline{\sigma} < \sigma < \overline{\sigma} < \infty$. Furthermore, we suppose that σ is constant on a neighborhood of the boundary $\partial\Omega$.

As seen in Chapter 6, when we inject a current $q \in \mathcal{C}^{1,\alpha}(\partial\Omega)$ for some $0 < \alpha < 1$ with its mean-value of zero, $\int_{\partial\Omega} q = 0$, the resulting electrical potential v is governed by the following conductivity equation:

$$\begin{cases} \nabla \cdot (\sigma\nabla v) = 0 \text{ in } \Omega\,, \\ \sigma\frac{\partial v}{\partial\nu} = q \text{ on } \partial\Omega\,, \\ \int_{\partial\Omega} v = 0\,, \end{cases} \tag{20.1}$$

where $\sigma\partial v/\partial\nu = \nu \cdot (\sigma\nabla)$ with ν being the outward unit normal vector at $\partial\Omega$.

To perturb the conductivity distribution σ, we attach a mechanical vibrator on the boundary $\partial\Omega$ and apply a time-harmonic vibration. We assume that Ω is composed of a linearly elastic, isotropic, and incompressible material of density equal to 1. We let μ be the shear modulus of Ω. We assume that μ belongs to $\mathcal{C}^{0,\alpha}(\overline{\Omega})$ and there exist $\underline{\mu}$ and $\overline{\mu}$ such that $0 < \underline{\mu} < \mu < \overline{\mu} < \infty$. If ω is the operating angular frequency, the resulting time-harmonic elastic displacement is denoted as $\underline{u}(x,t) = \Re\{e^{i\omega t}u(x)\}$ for $x \in \Omega$ and $t \in \mathbb{R}^+$, where u satisfies the Stokes system

$$\begin{cases} \omega^2 u + \nabla \cdot (\mu(\nabla u + \nabla u^T)) + \nabla p = 0 \text{ in } \Omega\,, \\ \nabla \cdot u = 0 \text{ in } \Omega\,, \\ u = g \text{ on } \partial\Omega\,. \end{cases} \tag{20.2}$$

Here, $g \in \mathcal{C}^{1,\alpha}(\partial\Omega)$ is such that the compatibility condition $\int_{\partial\Omega} g \cdot \nu = 0$ holds.

In what follows, we assume that $-\omega^2$ is not a Dirichlet eigenvalue of the Stokes system on Ω. We also recall that the analytical continuation principle holds true for the Stokes system. In fact, it can be proved that if u is zero in a ball inside Ω, then u is identically zero everywhere in Ω provided that $\mu \in \mathcal{C}^{0,1}(\overline{\Omega})$. Moreover, from [183], $u \in \mathcal{C}^{1,\alpha}(\overline{\Omega})$ and there exists a positive constant C depending only on μ, ω, and Ω such that

$$\|u\|_{\mathcal{C}^{1,\alpha}(\overline{\Omega})} \leq C\|g\|_{\mathcal{C}^{1,\alpha}(\partial\Omega)}\,.$$

The displacement $\underline{u}$ causes the perturbation of the conductivity distribution, $\sigma^\diamond$, which can be described as, for a time $t \in \mathbb{R}^+$,

$$\sigma^\diamond(x + \underline{u}(x,t), t) = \sigma(x), \quad \forall x \in \Omega\,. \tag{20.3}$$

It induces $u \cdot \nabla\sigma$, which can be captured by various electrical impedance imaging techniques. To show this, we let $\Omega^\diamond = \{x + \underline{u}(x,t) \mid x \in \Omega$, for a time $t \in \mathbb{R}^+\}$. We can rewrite the relation (20.3) as

$$\sigma^\diamond = \sigma \circ (I + \underline{u})^{-1}\,, \quad \sigma = \sigma^\diamond \circ (I + \underline{u}), \quad x \in \Omega', t \in \mathbb{R}^+\,, \tag{20.4}$$

where $I + \underline{u}$ is a map such that, for a time $t \in \mathbb{R}^+$,

$$I + \underline{u}(\cdot, t) : x \mapsto (x + u(x,t), t)$$

and $\Omega' \Subset (\Omega \cap \Omega^\diamond)$ is any smooth simply connected domain.

Assuming that $\mu \in \mathcal{C}^{0,\alpha}(\overline{\Omega})$, $\|u\|_{L^\infty(\Omega)} \ll 1$ and $\sigma \in \mathcal{C}^2(\overline{\Omega})$, the perturbed conductivity can be approximated as

$$\sigma^\diamond(x,t) \approx \sigma((I - \underline{u}(\cdot,t))(x)) = \sigma(x) - \underline{u}(x,t) \cdot \nabla\sigma(x) + O(|\underline{u}|^2)$$
$$\approx \sigma(x) - \underline{u}(x,t) \cdot \nabla\sigma(x), \quad x \in \Omega', \ t \in \mathbb{R}^+, \tag{20.5}$$

since σ is assumed to be constant on a neighborhood of the boundary $\partial\Omega$. Let $\underline{v}^\diamond$ denote the electrical potential of (20.1) with the conductivity distribution $\sigma^\diamond$ in place of σ. The potential $\underline{v}^\diamond$ varies with the time-change of $\sigma^\diamond$:

$$\nabla \cdot ((\sigma(x) - \underline{u}(x,t) \cdot \nabla\sigma(x))\nabla\underline{v}^\diamond(x,t)) \approx 0 \quad \text{for } x \in \Omega, t \in \mathbb{R}^+. \tag{20.6}$$

Denoting $\underline{v_1}(x,t) := \underline{v}^\diamond(x,t) - v(x)$, we have

$$\nabla \cdot (\sigma(x)\nabla\underline{v_1}(x,t)) = \nabla \cdot (\underline{u}(x,t) \cdot \nabla\sigma(x) \ \nabla v(x)) + \nabla \cdot \left(\underline{u}(x,t) \cdot \nabla\sigma(x) \ \nabla\underline{v_1}(x,t)\right)$$
$$\approx \nabla \cdot (\underline{u}(x,t) \cdot \nabla\sigma(x) \ \nabla v(x)) . \tag{20.7}$$

In the last approximation, we dropped $\nabla\cdot\left(\underline{u}(x,t) \cdot \nabla\sigma(x)\nabla\underline{v_1}(x,t)\right)$ since both $\underline{u}$ and $\underline{v_1}$ are small.

From (20.1), by virtue of the approximation (20.7), it follows that $\underline{v_1}(x,t)$ satisfies

$$\begin{cases} \nabla \cdot (\sigma(x)\nabla\underline{v_1}(x,t)) = \Re\{e^{i\omega t}\nabla \cdot (u(x) \cdot \nabla\sigma(x) \ \nabla v(x))\} \text{ for } (x,t) \in \Omega \times \mathbb{R}^+, \\ \sigma\frac{\partial \underline{v_1}}{\partial\nu} = 0 \qquad\qquad\qquad\qquad\qquad\qquad \text{on } \partial\Omega \times \mathbb{R}^+. \end{cases} \tag{20.8}$$

Therefore, we can express $\underline{v_1}$ as

$$\underline{v_1}(x,t) = \Re\{e^{i\omega t}v_1(x)\},$$

where v_1 is the solution to the following conductivity equation:

$$\begin{cases} \nabla \cdot (\sigma\nabla v_1) = \nabla \cdot ((u \cdot \nabla\sigma)\nabla v) \text{ in } \Omega, \\ \sigma\frac{\partial v_1}{\partial\nu} = 0 \qquad\qquad\qquad \text{on } \partial\Omega. \end{cases} \tag{20.9}$$

Finally, we arrive at

$$\underline{v}^\diamond(x,t) \approx v(x) + \Re\{e^{i\omega t}v_1(x)\}, \quad x \in \Omega, t \in \mathbb{R}^+, \tag{20.10}$$

where v_1 is the solution to (20.9). Note that the measured data over time yields the knowledge of v_1, which is (approximately) the difference between v and $\underline{v}^\diamond$ measured without and with the mechanical vibration, respectively. Equation (20.9) clearly shows that v_1 carries information of $u\cdot\nabla\sigma$. The major advantage of the proposed method is then to extract the additional information of $u\cdot\nabla\sigma$ from the boundary current-voltage relation.

In the following sections, we will deal with the anomaly imaging problem. Based on the approximation (20.10), we will provide a reconstruction method. We will extend the approximation (20.10) to piecewise constant conductivity distributions.

20.3 Vibration-Assisted Anomaly Identification

As seen in Chapter 6, the static EIT imaging has a fundamental drawback due to the technical difficulties in handling forward modeling errors including the boundary geometry, electrode positions, and other systematic artifacts. Hence, in the anomaly identification problem using EIT, a reference current-voltage data (Neumann-to-Dirichlet data) is required to cancel out these common errors by a data subtraction method. Since we can repeat the measurements without and with the mechanical vibration, we can extract the effects of the vibration by taking the difference between two sets of the measured data. In this section, we consider a piecewise constant conductivity distribution and present an anomaly location search and parameter estimation algorithm based on the vibration-difference approach.

Let $D = z_* + \delta B$ be an anomaly compactly embedded in Ω, where z_* is a gravitational center of D, B is a $\mathcal{C}^2$-bounded domain containing the origin and δ is a small positive parameter representing the order of magnitude of the anomaly size. We suppose that σ is locally homogeneous and σ changes abruptly across the boundary of the anomaly D.

We also suppose that the shear modulus μ is piecewise constant such as

$$\mu = \begin{cases} \mu_- \text{ in } \Omega \backslash \overline{D}, \\ \mu_+ \text{ in } D. \end{cases}$$

Then the displacement field u satisfies

$$\begin{cases} \omega^2 u + \mu_- \Delta u + \nabla p = 0 \text{ in } \Omega \backslash \overline{D}, \\ \omega^2 u + \mu_+ \Delta u + \nabla p = 0 \text{ in } D, \\ \nabla \cdot u = 0 \text{ in } \Omega, \\ u|_- - u|_+ = 0 \text{ on } \partial D, \\ \left(\mu_- \frac{\partial u}{\partial \nu} + p\nu \right) \Big|_- - \left(\mu_+ \frac{\partial u}{\partial \nu} + p\nu \right) \Big|_+ = 0 \text{ on } \partial D, \\ u = g \text{ on } \partial \Omega, \end{cases} \quad (20.11)$$

where $\pm$ denotes the limit from outside and inside of D, respectively.

Let τ_1, τ_2 be the tangent vectors at ∂D such that $\{\tau_1, \tau_2, \nu\}$ is an orthonormal basis of $\mathbb{R}^3$. Our first goal is to provide a representation of v_1 in the case of piecewise constant conductivity distributions. This can be achieved using layer potential techniques. Integration by parts yield, for $x \in \Omega \setminus \overline{D}$,

$$v_1(x) = \sigma_+ \int_{\partial D} u \cdot \nu \left[\left(1 - \frac{\sigma_+}{\sigma_-} \right) \frac{\partial v}{\partial \nu} \Big|_+ \frac{\partial N}{\partial \nu} \Big|_+ + \left(1 - \frac{\sigma_-}{\sigma_+} \right) \sum_{j=1}^{2} \frac{\partial v}{\partial \tau_j} \frac{\partial N}{\partial \tau_j} \right] ds,$$

$$(20.12)$$

where N is the Neumann function given by

$$\begin{cases} \nabla \cdot (\sigma \nabla N) = -\delta_y \text{ in } \Omega, \\ \sigma \frac{\partial N}{\partial \nu} = -\frac{1}{|\partial \Omega|} \text{ on } \partial \Omega, \\ \int_{\partial \Omega} N = 0 \end{cases}$$

with $|\partial\Omega|$ being the measure of $\partial\Omega$.

Now, let $w \in W^{1,2}(\Omega)$ satisfy $\nabla \cdot (\sigma\nabla w) = 0$ and let h be defined by

$$h = \sigma_+ \left[\left(1 - \frac{\sigma_+}{\sigma_-}\right) \frac{\partial v}{\partial\nu}\Big|_+ \frac{\partial w}{\partial\nu}\Big|_+ + \left(1 - \frac{\sigma_-}{\sigma_+}\right) \sum_{j=1}^{2} \frac{\partial v}{\partial\tau_j} \frac{\partial w}{\partial\tau_j} \right] \quad \text{on } \partial D. \quad (20.13)$$

Note that since the restrictions to D of the solutions to the conductivity equation $\nabla \cdot (\sigma\nabla w) = 0$ in Ω are in $\mathcal{C}^{1,\alpha}(\overline{D})$, then $h \in L^2(\partial D)$. In order to emphasize the dependence of v_1 on u, we denote it by $v_1^u = v_1$.

The next proposition follows from (20.12) by integration by parts. It gives the relation between measurable boundary data and interior information of anomaly D.

Proposition 20.1 *For $w \in W^{1,2}(\Omega)$ satisfying $\nabla \cdot (\sigma\nabla w) = 0$, we have*

$$\int_{\partial\Omega} v_1^u \, \sigma \frac{\partial w}{\partial\nu} \, ds = \int_{\partial D} u \cdot \nu \, h \, ds, \quad (20.14)$$

where $h \in L^2(\partial D)$ is defined by (20.13).

In what follows, we set

$$\eta(u) := \int_{\partial\Omega} v_1^u \, \sigma \frac{\partial w}{\partial\nu} \, ds. \quad (20.15)$$

The imaging problem is then to locate the anomaly D and to reconstruct its size, its conductivity, and its shear modulus from $\eta(u)$.

20.3.1 Location Search Method and Asymptotic Expansion

In order to have further analysis regarding $\eta(u)$ in (20.15), we write the inner expansion of the solution u of (20.11) as follows

$$u(x) = u_0(x) + \delta v_* \left(\frac{x - z_*}{\delta}\right) + O(\delta^2), \quad (20.16)$$

where u_0 is the background displacement field (in the absence of any anomaly)

$$\begin{cases} \omega^2 u_0 + \mu_- \triangle u_0 + \nabla p_0 = 0 \text{ in } \Omega, \\ \nabla \cdot u_0 = 0 \text{ in } \Omega, \\ u_0 = g \text{ on } \partial\Omega, \end{cases} \quad (20.17)$$

and v_* is the solution of

$$\begin{cases} \mu_- \triangle v_* + \nabla q = 0 & \text{in } \mathbb{R}^3 \backslash \overline{D}, \\ \mu_+ \triangle v_* + \nabla q = 0 & \text{in } D, \\ \nabla \cdot v_* = 0 & \text{in } \mathbb{R}^3, \\ v_*|_- - v_*|_+ = 0 & \text{on } \partial D, \\ \left(\mu_- \frac{\partial v_*}{\partial\nu} + q\nu\right)\Big|_- - \left(\mu_+ \frac{\partial v_*}{\partial\nu} + q\nu\right)\Big|_+ = (\mu_- - \mu_+)(\nabla u_0 + \nabla u_0^T)\nu & \text{on } \partial D, \\ v_*(x) \to 0 & \text{as } |x| \to +\infty, \\ q(x) \to 0 & \text{as } |x| \to +\infty. \end{cases}$$

$$(20.18)$$

For explicit representations of u_0 and v_*, let us introduce the fundamental tensor solution $\Gamma = (\Gamma_{jk})_{j,k=1}^3$ and $\mathcal{F} = (F_1, F_2, F_3)$ corresponding to the equation

$$\left(\Delta + \frac{\omega^2}{\mu_-}\right)\Gamma_{jk}(x) + \partial_k F_j(x) = \delta_{jk}\delta(x) \quad \text{in } \mathbb{R}^3$$

and $\nabla \cdot \Gamma = 0$ in $\mathbb{R}^3$, where

$$\Gamma_{jk}(x) = -\frac{\delta_{jk}}{4\pi}\frac{e^{i\omega|x|/\sqrt{\mu_-}}}{|x|} - \frac{\mu_-}{4\pi\omega^2}\partial_j\partial_k\frac{e^{i\omega|x|/\sqrt{\mu_-}} - 1}{|x|} \qquad (20.19)$$

$$F_j(x) = \frac{1}{4\pi}\frac{x_j}{|x|^3}.$$

Here, δ_{jk} is the Kronecker delta. Define $B_R = \{y : |y| \le R, \ R \text{ sufficiently large}\}$ such that $\overline{\Omega} \subset B_R$. If $g(x) = \Gamma(x - \bar{y})q$ with direction of the wave q for a point source $\bar{y} \in \partial B_R$, then we have $p_0(x) = \mathcal{F}(x - \bar{y}) \cdot q$ and

$$u_0(x) = \tfrac{1}{\mu_-}\Gamma(x - \bar{y})\, q,$$

$$v_*\left(\tfrac{x-z_*}{\delta}\right) = \mathcal{S}_B^0\left(-\tfrac{\mu_- + \mu_+}{2(\mu_- - \mu_+)}I + \left(\mathcal{K}_B^0\right)^*\right)^{-1}\left[\tfrac{\partial u_0}{\partial \nu}(z_*)\right]\left(\tfrac{x-z_*}{\delta}\right),$$

where $\mathcal{S}_B^0$ is a single layer potential for the Stokes system, $\mathcal{K}_B^0$ is the Neumann-Poincaré operator associated with the fundamental tensor solution Γ and $(\mathcal{K}_B^0)^*$ is the L^2-adjoint operator of $\mathcal{K}_B^0$ with superscript 0 standing for the static case $\omega = 0$.

Noting that u is depending on q and the point source $\bar{y}$, we can denote u by $u_{q,\bar{y}}$.

Define $J : \Omega \to \mathbb{R}$ by

$$J(z^S) := \sum_{j=1}^{3}\int_{\partial B_R} k^T\, \Gamma(z^S - \bar{y})\, q_j\, \overline{\eta(u_{q_j,\bar{y}})}\, ds(\bar{y}) \qquad (20.20)$$

for three orthonormal vectors q_j $(j = 1, 2, 3)$, $z^S \in \Omega$ and a constant unit vector k. Here, z^S is considered as a searching point in Ω.

The following lemma follows from the Helmholtz-Kirchhoff identity for the fundamental tensor solution Γ.

Lemma 20.2 *The functional $J(z^S)$ can be estimated by*

$$J(z^S) = k^T\,\Im(\Gamma(z^S - z_*))\left(\frac{1}{\mu_-}\int_{\partial D} h\,\nu\,ds\right) + O(\delta^3(\omega^2 + 1 + R^{-1})). \quad (20.21)$$

Proof. Using (20.16) and the above representations, the functional $\eta(u)$ can be written as

$$\eta(u) = \int_{\partial D} u(x) \cdot \nu\, h(x)\, ds(x) = \int_{\partial D} u_0(x) \cdot \nu\, h(x)\, ds(x) + O\left(\frac{\delta^3(\omega^2 + 1)}{R^2}\right).$$

Then we can write $J(z^S)$ as

$$J(z^S) = \sum_{j=1}^{3} \int_{\partial B_R} k^T \Gamma(z^S - y) q_j \; \overline{\eta(u_{q_j,y})} \, ds(y)$$

$$= \sum_{j=1}^{3} \int_{\partial B_R} k^T \Gamma(z^S - y) q_j \; \overline{\int_{\partial D} u_{q_j,y} \cdot \nu \, h \, ds} \, ds(y)$$

$$= \frac{1}{\mu_-} \int_{\partial D} k^T \left[\int_{\partial B_R} \Gamma(z^S - y) \overline{\Gamma(z_* - y)} \, ds(y) \right] \nu \, h(x) \, ds(x) + O(\delta^3(\omega^2 + 1)).$$

From the Sommerfeld radiation condition satisfied by Γ, we have

$$\int_{\partial B_R} \Gamma(z^S - y) \overline{\Gamma(z_* - y)} \, ds(y)$$

$$= \int_{\partial B_R} \left(\frac{\partial}{\partial \nu} \Gamma(z^S - y) \overline{\Gamma(z_* - y)} - \Gamma(z^S - y) \frac{\partial}{\partial \nu} \overline{\Gamma(z_* - y)} \right) ds(y) + O\left(\frac{1}{R} \right).$$

Since $|z^S|$, $|z_*| < R$, the property of fundamental solution and Green's identity imply

$$\int_{\partial B_R} \left(\frac{\partial}{\partial \nu} \Gamma(z^S - y) \overline{\Gamma(z_* - y)} - \Gamma(z^S - y) \frac{\partial}{\partial \nu} \overline{\Gamma(z_* - y)} \right) ds(y) = 2i \, \Im \Gamma(z^S - z_*).$$

Hence we have

$$J(z^S) = \frac{1}{\mu_-} k^T \Im \Gamma(z^S - z_*) \int_{\partial D} h \, \nu \, ds + O\left(\delta^3 R^{-1} \right) + O(\delta^3(\omega^2 + 1)),$$

which completes the proof. $\square$

Since $\Im \Gamma(z^S - z_*)$ has a sinc function as a component, J has its maximum at $z^S = z_*$. In J, the fundamental tensor of the Stokes problem, Γ, can be replaced by a simple exponential function. Using that the following proposition proposes an approximation of $J(z^S)$ which is more practical for finding the maximum and hence locating the anomaly.

Proposition 20.3 *Define $\widetilde{J}$ by*

$$\widetilde{J}(z^S) := \int_{\partial B_R} e^{i\omega|z^S - y|/\sqrt{\mu_-}} \overline{\eta(u_{q,y})} \, ds(y) . \tag{20.22}$$

Then the point $z^S \in \Omega$ satisfying $z^S = \arg\max_{z \in \Omega} \widetilde{J}(z)$ is the center position of D.

Proof. From the definition of Γ in (20.19), we have

$$-4\pi \Gamma_{jk}(x) = \delta_{jk} \frac{e^{i\omega|x|/\sqrt{\mu_-}}}{|x|} + \frac{\mu_-}{\omega^2} \partial_j \partial_k \frac{e^{i\omega|x|/\sqrt{\mu_-}} - 1}{|x|} = \delta_{jk} \frac{e^{i\omega|x|/\sqrt{\mu_-}}}{|x|} + O(|x|^{-3}).$$

If $|z^S - y| \to \infty$, then the following approximation holds

$$\Gamma(z^S - y) \approx -\frac{1}{4\pi} \frac{e^{i\omega|z^S-y|/\sqrt{\mu_-}}}{|z^S - y|} I$$

with I the identity matrix. Here, the phase terms of J and $\widetilde{J}$ are the same for the identity matrix I. In fact, the phase term of $\widetilde{J}$ is

$$\int_{\partial D} \int_{\partial B_R} e^{i\omega|z^S-y|/\sqrt{\mu_-}} \overline{e^{i\omega|z_*-y|/\sqrt{\mu_-}}} ds(y) ds(x)$$

$$\approx \int_{\partial D} \int_{\partial \Omega} e^{i\omega\left(|y| - \frac{z^S \cdot y}{|y|}\right)/\sqrt{\mu_-}} e^{-i\omega\left(|y| - \frac{z_* \cdot y}{|y|}\right)/\sqrt{\mu_-}} ds(y) ds(x)$$

$$= \int_{\partial D} \int_{\partial B_R} e^{i\omega\left(\frac{(z_* - z^S) \cdot y}{|y|}\right)/\sqrt{\mu_-}} ds(y) ds(x) = \int_{\partial D} \int_{\partial B_1} e^{i\omega(z_* - z^S) \cdot \hat{y}/\sqrt{\mu_-}} ds(\hat{y}) ds(x)$$

$$\approx \int_{\partial D} \frac{\sqrt{\mu_-}}{\omega} \frac{\sin\left(\frac{\omega|z_*-z^S|}{\sqrt{\mu_-}}\right)}{|z_* - z^S|} ds(x),$$

in which the first approximation holds because $|y|, |y - z^S|, |y - z_*| \gg 1$ imply that the angles between them are close to 0. Therefore, it has its maximum at $|z_* - z^S| = 0$. $\square$

Proposition 20.3 shows that the conductivity anomaly can be detected with a resolution of the order of half the elastic wavelength.

20.3.2 Size Estimation and Reconstruction of the Material Parameters

In the previous subsection, a formula to find the center position z_* of D has been derived. Here, we present a method to estimate the size δ, the conductivity σ_+, and the shear modulus μ_+ of the anomaly D. For computational simplicity, we assume that D is a sphere and that the background conductivity, σ_-, and shear modulus, μ_-, are known.

Using a broadband frequency range for elastic vibrations, we can acquire time-domain data corresponding to $g(x, t) = \check{\Gamma}(x - y, t)q$ for $y \in \partial \Omega$. Here, $\check{\Gamma}$ is the inverse Fourier transform taken in ω variable of the fundamental solution Γ to the Stokes system. Take $w = v$ in (20.15) and rewrite η as a function of time t. It follows that

$$\eta(t) = \int_{\partial D} u(x, t) \cdot \nu(x) \, h(x) \, ds(x), \tag{20.23}$$

where $h = \sigma_+\left[\left(1 - \frac{\sigma_+}{\sigma_-}\right)\left(\frac{\partial v}{\partial \nu}\big|_+\right)^2 + (1 - \frac{\sigma_-}{\sigma_+})\sum_{j=1}^2 \left(\frac{\partial v}{\partial \tau_j}\right)^2\right]$. Define t_y^a and t_y^b by

$t_y^a :=$ the first t such that $\eta(t) \neq 0$

    $=$ the first t such that a sphere of center y and growing radius hits ∂D, say z_a

    $= |z_a - y|/\sqrt{\mu_-}$

$t_y^b :=$ the last t such that $\eta(t) \neq 0$

    $=$ the last t such that a sphere of center y and growing radius hits ∂D, say z_b

    $= |z_b - y|/\sqrt{\mu_-}$.

Then the radius, δ, of D can be estimated by

$$2\delta \approx \sqrt{\mu_+} \left(t_y^b - t_y^a \right) . \tag{20.24}$$

If we know the size of D, then we can extract μ_+ information. If not, we can minimize over μ_+ and σ^+ the following discrepancy functional:

$$\int_{t_y a}^{t_y b} \left| \eta(t) - \check{\Gamma}(x - z_*, t) q \cdot \int_{\partial D} \nu\, h\, ds \right|^2 .$$

To compute v we use relation (20.24) and the fact that $D = z_* + \delta B$ with B being the unit sphere centered at the origin.

20.4 Numerical Illustrations

First, we will present numerical simulation results showing voltage differences when the mechanical vibration is applied. Then, we will show a numerical evidence of the position finding formula proposed in Subsection 20.3.1.

20.4.1 Simulations of the Voltage Difference Map

We present two results of numerical simulations to show the voltage difference map of v_1 before and after the applied mechanical vibration. We consider a cubic container as shown in Figure 20.1. The sensing (measuring) electrodes are placed at the bottom of the container and the sinusoidal mechanical vibration is applied through the top surface, which is also the current driving electrode. In the second numerical test, the mechanical vibration is applied through the lateral surface. Two anomalies, a small spherical anomaly and a large cylindrical anomaly, are placed in the container with different material properties shown in Table 20.1.

	Background	Anomalies
Shear modulus	0.266	2.99

Table 20.1. Shear modulus values used in numerical simulations.

Figures 20.2 presents the measured voltage difference v_1 at the bottom surface. It clearly shows the perturbation of the conductivity distribution inside Ω caused by the mechanical vibration.
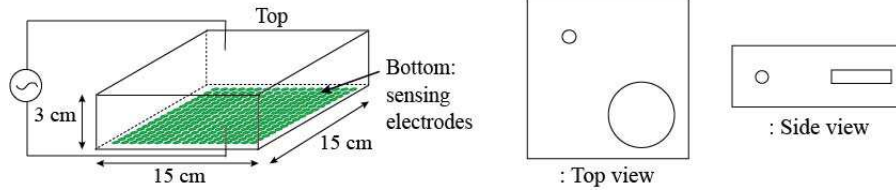
Fig. 20.1. Model for numerical simulations.
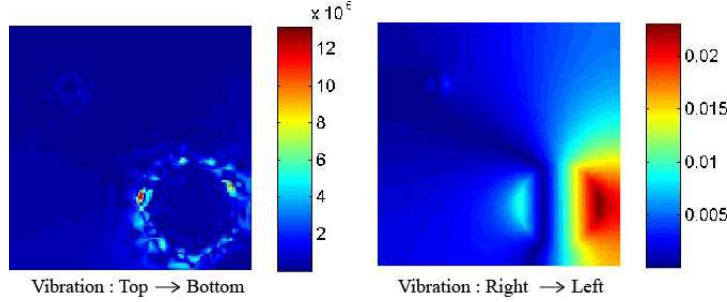
Fig. 20.2. Maps of the voltage difference v_1 on the bottom surface subject to two different mechanical vibrations.

20.4.2 Anomaly Location

In Subsection 20.3.1, formula (20.21) and Proposition 20.3 suggest seeking the maximizer of J or $\widetilde{J}$ to locate the center position of anomaly. To verify Proposition 20.3, we consider a cylindrical domain Ω centered at $(0,0,1.5)$ with radius 7.5 cm and height 3 cm. Let the anomaly D be a sphere with radius 0.25 cm, centered at $z_* = (3.75, 0, 1.5)$. As shown in Subsection 20.3.1, the displacement u depends on q and the point source y. Here, q is set to $(1,0,0)$, $(0,1,0)$ and $(0,0,1)$ and the point source y_k is chosen for $k = 1, \ldots, 1940$, which are uniformly distributed on B_R, a sphere centered at $(0,0,1.5)$ with radius 37.5 cm so that $\overline{\Omega} \subset B_R$. Figure 20.3 shows the computed discrete version of $\widetilde{J}(z^S)$ for each $z^S = (x, y, 1.5)$ as follows:

$$\widetilde{J}(z^S) := \int_{\partial B_R} e^{i\omega|z^S - y|/\sqrt{\mu_-}} \overline{\eta(u_{q,y})} \, ds(y) \approx \sum_{k=1}^{1940} e^{i\omega|z^S - y_k|/\sqrt{\mu_-}} \overline{\eta(u_{q,y_k})},$$

where $\mu_- = 1$ and $\omega = 200 \times \pi$.

Figure 20.3 shows that the formula proposed in Proposition 20.3 finds the center position of anomaly D under an ideal circumstance such that no noise is added and all mathematical assumptions are satisfied. An analysis of the statistical stability with respect to measurement and medium noises of the localization algorithm can be performed.
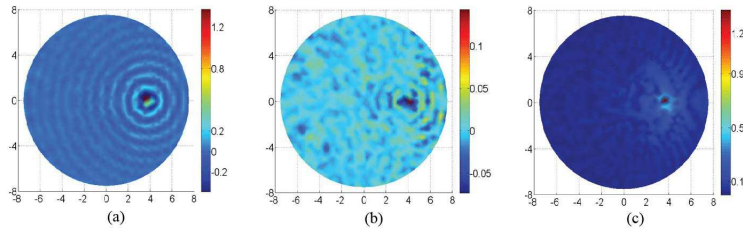
Fig. 20.3. $\widetilde{J}(z^S)$ when $z^S = (x, y, 1.5)$: The maximum point is the center position of D which is $(3.75, 0, 1.5)$: (a) $\Re J(z^S)$, (b) $\Im J(z^S)$, and (c) $|J(z^S)|$.

20.5 Concluding Remarks

In this chapter, we have investigated a multi-physics electrical impedance imaging approach using mechanical vibrations simultaneously applied to an imaging object together with current injections. We have provided the mathematical framework for the proposed approach and presented a few numerical simulation results to illustrate its resolution and stability.

It is worth mentioning that the proposed approach can also be used to measure the elasticity of an internal object with known electrical conductivity values. Using the electrical conductivity image, one can reconstruct the displacement field at the scale of the changes of the conductivity and then, recover the shear modulus using our approach in the next chapter. This approach will be applied for optical coherence tomography in Chapter 22.

Viscoelastic Modulus Reconstruction

21.1 Introduction

Elastography aims at providing a quantitative visualization of the mechanical properties of human tissues by using the relation between the wave propagation velocity and the mechanical properties of the tissues. During the last three decades, elastography led to significant improvements in the quantitative evaluation of tissue stiffness. The two major elastographic techniques are based on ultrasound and on magnetic resonance imaging. GE Healthcare has recently commercialized magnetic resonance elastography (MRE). Its main use is to assess mechanical changes in liver tissue. The mechanical properties of tissue include the shear modulus, shear viscosity, and compression modulus. Quantification of the tissue shear modulus *in vivo* can provide evidence of the manifestation of tissue diseases.

This chapter focuses on the image reconstruction methods for tissue viscoelasticity imaging. It presents an iterative reconstruction approach to provide high-resolution images of shear modulus and viscosity using the internal measurements of displacement field. To simplify the underlying inverse problem, the reconstruction of both the shear modulus and shear viscosity are considered under the assumption of isotropic elastic moduli.

We consider the inverse problem of recovering the distribution of the shear modulus (μ) and shear viscosity (η) from the internal measurement of the time-harmonic mechanical displacement field u produced by the application of an external time harmonic excitation at frequency $\omega/2\pi$ in the range $50 \sim 200$Hz through the surface of the subject. Modeling soft tissue as being linearly viscoelastic and nearly incompressible, the displacement is of the form $\Re(u(x)e^{i\omega t})$ where the complex-valued field u satisfies the elasticity equation

$$\nabla \cdot \left((\mu + i\omega\eta)(\nabla u + \nabla u^T)\right) + \nabla((\lambda + i\omega\eta_\lambda)\nabla \cdot u) + \rho\omega^2 u = 0, \qquad (21.1)$$

where ρ denotes the density of the medium, ∇u^T is the transpose of the matrix ∇u, λ is the compression modulus and η_λ is the compression viscosity.

The most widely used reconstruction method is the algebraic inversion method [262]: For any non-zero constant vector a,

$$\mu + i\omega\eta = -\frac{\rho\omega^2(a \cdot u)}{\nabla \cdot \nabla(a \cdot u)}, \qquad (21.2)$$

which requires the strong assumptions of $\nabla(\mu + i\omega\eta) \approx 0$ (local homogeneity) and $(\lambda + i\omega\eta_\lambda)\nabla \cdot u \approx 0$ (negligible pressure).

The algebraic formula (21.2) ignores reflection effects of the propagating wave due to abrupt changes of $\mu + i\omega\eta$, so that the method cannot measure any change of $\mu + i\omega\eta$ in the direction of a.

To deal with these fundamental drawbacks in the algebraic inversion method, we consider the full elasticity model and introduce a method based on the minimization of a misfit functional involving the discrepancy between the measured and fitted data. The minimization approach does not require any derivative of u. The Fréchet derivatives of the functional with respect to μ and η are then computed by introducing an adjoint problem. This Fréchet derivatives based-iterative scheme requires a well-matched initial guess, because the minimization problem is highly nonlinear and may have multiple local minima. We find a well-matched initial guess that captures the edges of the image of the shear viscoelasticity. The numerical results presented herein demonstrate the viability and efficiency of the proposed minimization method. Our results in this chapter are from [47, 38, 77].

21.2 Reconstruction Methods

21.2.1 Viscoelasticity Model

Let an elastic body occupy the smooth domain $\Omega \subset \mathbb{R}^d, d = 2, 3$ with boundary $\partial\Omega$. To evaluate the viscoelastic tissue properties, we create an internal time-harmonic displacement in the tissue by applying a time-harmonic excitation through the surface of the object. Under the assumptions of mechanical isotropy and incompressibility in the tissue, the induced time-harmonic displacement at angular frequency ω, denoted by u, is then governed by the full elasticity equation

$$2\nabla \cdot ((\mu + i\omega\eta)\nabla^s u) + \nabla((\lambda + i\omega\eta_\lambda)\nabla \cdot u) + \rho\omega^2 u = 0 \quad \text{in } \Omega, \qquad (21.3)$$

where $\nabla^s u = \frac{1}{2}(\nabla u + \nabla u^T)$ is the strain tensor with ∇u^T denoting the transpose of the matrix ∇u; ρ is the density of the medium; the complex quantity $\mu + i\omega\eta$ is the shear modulus, with μ indicating the storage modulus and η indicating the loss modulus reflecting the attenuation of a viscoelastic medium; λ and η_λ are the compression modulus and compression viscosity, respectively. We assume that these heterogeneous parameters satisfy:

$$\mu > 0, \quad \eta > 0, \quad \eta_\lambda > 0, \quad d\lambda + 2\mu > 0.$$

For a fixed $\epsilon > 0$, denote $\Omega' := \{x \in \Omega \mid \text{dist}(x, \partial\Omega) > \epsilon\}$ and $\mathcal{E} := \Omega \backslash \overline{\Omega'}$. Throughout this paper, we assume that μ and η are contained in the following set

$$\widetilde{S} := \{(\mu_0, \eta_0) + (\phi_1, \phi_2) \mid (\phi_1, \phi_2) \in S\}$$

where positive constants μ_0 and η_0 are respectively known shear modulus and shear viscosity in $\mathcal{E}$. And S is given by

$$S := \big\{(\phi_1, \phi_2) \in W_0^{2,2}(\Omega) \times W_0^{2,2}(\Omega) : \ c_1 < \phi_1 + \mu_0 < c_2, c_1 < \phi_2 + \eta_0 < c_2,$$
$$\|\phi_j\|_{W^{2,2}(\Omega)} \leq c_3, \ \text{supp } \phi_j \subset \Omega' \text{ for } j = 1, 2\big\},$$

with c_1, c_2, c_3 being positive constants. Hence, $\tilde{S}$ can be viewed as $\tilde{S} = (\mu_0, \eta_0) + S$.
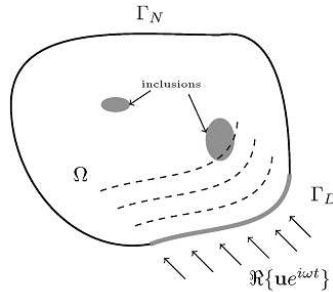
Fig. 21.1. Illustration of the domain and boundary portions.

To impose boundary conditions, let us take Γ_D and Γ_N such that $\overline{\Gamma_D \cup \Gamma_N} = \partial\Omega$ and $\Gamma_D \cap \Gamma_N = \emptyset$. Typically, we use an acoustic speaker system to generate harmonic vibration. If the acoustic speaker is placed on the portion Γ_D of the boundary $\partial\Omega$, then the boundary conditions for u can be expressed approximately by

$$u = g \qquad\qquad \text{on } \Gamma_D \,,$$
$$2(\mu + i\omega\eta)\nabla^s u \,\nu + (\lambda + i\omega\eta_\lambda)(\nabla \cdot u)\nu = 0 \quad \text{on } \Gamma_N \,,$$

where ν is the outward unit normal vector to the boundary.

It is known that soft tissues are nearly incompressible and the compression modulus λ fulfills $\lambda \approx \infty$. Therefore, the displacement field u satisfies $\nabla \cdot u \approx 0$. It is shown in Theorem 3.53 that the term $(\lambda + i\omega\eta_\lambda)\nabla \cdot u$ in (21.3) is not negligible because $\nabla \cdot u$ and λ could balance each other out. Let us impose the incompressibility condition $\nabla \cdot u = 0$. This introduce the internal pressure $p = \lambda \nabla \cdot u$ which can be understood as a limit of $\lambda \nabla \cdot u$ as λ goes to infinity and $\nabla \cdot u$ goes to zero. Then, the time harmonic displacement u satisfies (approximately) the following quasi-incompressible viscoelasticity model:

$$\begin{cases} 2\nabla \cdot ((\mu + i\omega\eta)\nabla^s u) + \nabla p + \rho\omega^2 u = 0 & \text{in } \Omega\,, \\ \nabla \cdot u = 0 & \text{in } \Omega\,, \\ u = g & \text{on } \Gamma_D\,, \\ 2(\mu + i\omega\eta)\nabla^s u\,\nu + p\nu = 0 & \text{on } \Gamma_N\,. \end{cases} \tag{21.4}$$

Note that if $\Gamma_D = \partial\Omega$ ($\Gamma_N = \emptyset$), then g should satisfy the compatibility condition $\int_{\partial\Omega} g \cdot \nu\, ds = 0$. It is worth noticing that p can be regarded as a Lagrange multiplier to enforce the incompressibility condition.

Let $u^{(m)}$ denote the displacement data that is measured in Ω. Then, the inverse problem is to reconstruct the distribution of μ and η from the measured data $u^{(m)}$.

21.2.2 Optimal Control Algorithm

Define the misfit (or discrepancy) functional $J[\mu, \eta]$ in terms of μ and η by the L^2-norm in Ω of the difference between the numerical solution $u[\mu, \eta]$ of the forward problem (21.4) and the measured displacement data $u^{(m)} = u^{(m)}[\mu_*, \eta_*]$:

$$J[\mu, \eta] = \frac{1}{2}\int_\Omega |u[\mu, \eta] - u^{(m)}|^2 dx\,. \tag{21.5}$$

where μ_* and η_* are true distributions of shear elasticity and viscosity, respectively. The reconstruction of the unknowns μ and η can be obtained by minimizing the misfit functional $J[\mu, \eta]$ with respect to μ and η.

In order to construct a minimizing sequence of $J[\mu, \eta]$, we need to compute the Fréchet derivatives of $J[\mu, \eta]$ with respect to μ and η. Assume that δ_μ and δ_η are small perturbations of μ and η, respectively, by regarding $\frac{\delta_\mu + i\omega\delta_\eta}{\mu + i\omega\eta} \approx 0$. For notational simplicity, we denote $u_0 := u[\mu, \eta]$, $p_0 :=$ the pressure corresponding to u_0 and $p_0 + p_1 :=$ the pressure corresponding to $u[\mu + \delta_\mu, \eta + \delta_\eta]$. Denoting the perturbation of displacement field by

$$\delta u := u[\mu + \delta_\mu, \eta + \delta_\eta] - u_0\,, \tag{21.6}$$

it follows from (21.4) that

$$2\nabla \cdot ((\mu + i\omega\eta)\nabla^s \delta u) + \nabla p_1 + \rho\omega^2 \delta u = -2\nabla \cdot ((\delta_\mu + i\omega\delta_\eta)\nabla^s u_0)$$
$$- 2\nabla \cdot ((\delta_\mu + i\omega\delta_\eta)\nabla^s \delta u) \quad \text{in} \quad \Omega\,. \tag{21.7}$$

Let u_1 be the solution of the following problem

$$\begin{cases} 2\nabla \cdot ((\mu + i\omega\eta)\nabla^s u_1) + \nabla p_1 + \rho\omega^2 u_1 = \\ \qquad\qquad -2\nabla \cdot ((\delta_\mu + i\omega\delta_\eta)\nabla^s u_0) & \text{in } \Omega, \\ \nabla \cdot u_1 = 0 & \text{in } \Omega\,, \\ u_1 = 0 & \text{on } \Gamma_D\,, \\ 2(\mu + i\omega\eta)\nabla^s u_1\nu + p_1\nu = 0 & \text{on } \Gamma_N\,. \end{cases} \tag{21.8}$$

Now we are ready to state two main theorems in this section which give the Fréchet derivatives of $J[\mu, \eta]$ with respect to μ and η. Denote $A : B = \sum_{i,j} A_{ij} B_{ij}$ for two matrices $A = (A_{ij})$ and $B = (B_{ij})$.

Theorem 21.1 *For $(\delta\mu + \mu, \delta\eta + \eta) \in \widetilde{S}$, if u_1 is defined by (21.8), then we have*

$$\Re \int_{\Omega} u_1 \overline{(u_0 - u^{(m)})} \, dx = \Re \int_{\Omega} 2(\delta_{\mu} + i\omega\delta_{\eta}) \nabla^s u_0 : \nabla^s \bar{v} \, dx \,. \qquad (21.9)$$

Furthermore, the Fréchet derivatives of $J[\mu, \eta]$ with respect to μ and η are given by

$$\frac{\partial}{\partial \mu} J[\mu, \eta] = \Re \left[2\nabla^s u_0 : \nabla^s \bar{v} \right], \; \frac{\partial}{\partial \eta} J[\mu, \eta] = \Re \left[2(i\omega\nabla^s u_0) : \nabla^s \bar{v} \right], \qquad (21.10)$$

where v is the $W^{1,2}$ solution of the following adjoint problem:

$$\begin{cases} 2\nabla \cdot ((\mu - i\omega\eta)\nabla^s v) + \nabla q + \rho\omega^2 v = (u_0 - u^{(m)}) & in \; \Omega \,, \\ \nabla \cdot v = 0 & in \; \Omega \,, \\ v = 0 & on \; \Gamma_D \,, \\ 2(\mu - i\omega\eta)\nabla^s v \, \nu + q\nu = 0 & on \; \Gamma_N \,. \end{cases} \qquad (21.11)$$

The next theorem shows the differentiability of $J[\mu, \eta]$.

Theorem 21.2 *The misfit functional $J[\mu, \eta]$ is Fréchet differentiable for $(\mu, \eta) \in \widetilde{S}$. More precisely, if $u_1 \in W^{1,2}(\Omega)$ is the weak solution to (21.8), as the perturbations $\delta_{\mu}, \delta_{\eta} \to 0$, we have the following formula:*

$$\left| J[\mu + \delta_{\mu}, \eta + \delta_{\eta}] - J[\mu, \eta] - \Re \int_{\Omega} u_1 \overline{(u_0 - u^{(m)})} dx \right|$$
$$= O\left((||\delta_{\mu}||_{W^{2,2}(\Omega)} + ||\delta_{\eta}||_{W^{2,2}(\Omega)})^2 \right) \,.$$

To prove the Fréchet differentiability Theorem 21.2 and the main Theorem 21.1, we need the following preliminary results.

Firstly, we state an interior estimate for the solution of (21.4) whose proof basically follows from [183] by observing $2\nabla \cdot \nabla^s w = \Delta w$ for w satisfying $\nabla \cdot w = 0$.

Lemma 21.3 *For $F \in L^2(\Omega)$ and $(\mu, \eta) \in \widetilde{S}$, let $w \in W^{1,2}(\Omega)$ be a weak solution of the following problem:*

$$\begin{cases} 2\nabla \cdot (\mu + i\omega\eta)\nabla^s w + \nabla p + \rho\omega^2 w = F & in \; \Omega \,, \\ \nabla \cdot w = 0 & in \; \Omega \,, \\ w = 0 & on \; \partial\Omega \,. \end{cases}$$

Then, $w \in W^{2,2}(\Omega)$ and

$$||w||_{W^{2,2}(\Omega)} \le C||F||_{L^2(\Omega)} \,, \qquad (21.12)$$

where C is positive constant independent of F.

The following estimate for δu holds.

Proposition 21.1. *The perturbation of displacement field $\delta u \in W^{1,2}(\Omega)$ satisfies the following estimate:*

$$||\delta u||_{W^{2,2}(\Omega)} \leq C(||\delta_\mu||_{W^{2,2}(\Omega)} + ||\delta_\eta||_{W^{2,2}(\Omega)})||u_0||_{W^{2,2}(\Omega)},$$

where C is positive constant independent of δ_μ and δ_η.

Proof.   From (21.7), δu satisfies

$$2\nabla \cdot ((\mu + \delta_\mu + i\omega(\delta_\eta + \eta))\nabla^s \delta u) + \nabla p_1 + \rho\omega^2 \delta u$$
$$= -2\nabla \cdot ((\delta_\mu + i\omega\delta_\eta)\nabla^s u_0) \quad \text{in} \quad \Omega. \qquad (21.13)$$

Applying the interior estimate (21.12) to (21.13) and using Hölder's inequality and Sobolev embedding theorem, we arrive at

$$||\delta u||_{W^{2,2}(\Omega)} \leq C||\nabla \cdot ((\delta_\mu + i\omega\delta_\eta)\nabla^s u_0)||_{L^2(\Omega)}$$
$$\leq C\left(||\delta_\mu + i\omega\delta_\eta||_{L^\infty(\Omega)}||u_0||_{W^{2,2}} + ||\nabla(\delta_\mu + i\omega\delta_\eta)||_{L^4(\Omega)}||\nabla u_0||_{L^4(\Omega)}\right)$$
$$\leq C\left(||\delta_\mu||_{W^{2,2}(\Omega)} + ||\delta_\eta||_{W^{2,2}(\Omega)}\right)||u_0||_{W^{2,2}(\Omega)}.$$

This completes the proof.   □

Now we are ready to prove Theorem 21.2.

Proof.   [Proof of Theorem 21.2] From the definition of $J[\mu,\eta]$ in (21.5), we have

$$J[\mu + \delta_\mu, \eta + \delta_\eta] = J[\mu,\eta] + \Re\int_\Omega u_1\overline{(u_0 - u^{(m)})}dx + \Upsilon,$$

where Υ is

$$\Upsilon = \Re\int_\Omega (\delta u - u_1) \cdot \overline{(u_0 - u^{(m)})}dx + \frac{1}{2}\int_\Omega |\delta u|^2 dx. \qquad (21.14)$$

Using the adjoint problem (21.11), (21.14) can be expressed as

$$\Upsilon = \frac{1}{2}\int_\Omega |\delta u|^2 dx + \Re\int_\Omega (\delta u - u_1) \cdot \overline{(2\nabla \cdot (\mu - i\omega\eta)\nabla^s v + \nabla q + \rho\omega^2 v)}dx.$$

Using $\nabla \cdot \delta u = \nabla \cdot (u_0 + \delta u) - \nabla \cdot u_0 = 0$ and homogeneous boundary conditions for u_1 and δu, we have

$$\Upsilon = \frac{1}{2}\int_\Omega |\delta u|^2 dx - \Re\int_\Omega (2\nabla \cdot (\delta_\mu + i\omega\delta_\eta)\nabla^s \delta u) \cdot \bar{v}dx. \qquad (21.15)$$

Applying Hölder's inequality, Υ is estimated by

$$|\Upsilon| \leq \frac{1}{2}||\delta u||_{L^2(\Omega)}^2 + (||\delta_\mu||_{L^\infty(\Omega)} + ||\omega\delta_\eta||_{L^\infty(\Omega)})||\nabla\delta u||_{L^2(\Omega)}||\nabla\bar{v}||_{L^2(\Omega)},$$

$$\leq C||\nabla\delta u||_{L^2(\Omega)}\left(\frac{1}{2}||\nabla\delta u||_{L^2(\Omega)} + (||\delta_\mu||_{L^\infty(\Omega)} + ||\omega\delta_\eta||_{L^\infty(\Omega)})||\nabla\bar{v}||_{L^2(\Omega)}\right).$$

Now we apply Proposition 21.1 to get

$$|\Upsilon| \leq C \left(||\delta_\mu||_{W^{2,2}(\Omega)} + ||\delta_\eta||_{W^{2,2}(\Omega)} \right)^2 \left(||u_0||_{W^{2,2}(\Omega)} + ||\bar{v}||_{W^{2,2}(\Omega)} \right).$$

The proof is then completed.   □

Now, it remains to identify the Fréchet derivatives of $J[\mu, \eta]$. According to Theorem 21.2, the Fréchet derivatives $\frac{\partial}{\partial \mu} J[\mu, \eta]$ and $\frac{\partial}{\partial \eta} J[\mu, \eta]$ can be computed by expressing $\Re \int_\Omega u_1 \overline{(u_0 - u^{(m)})} dx$ in terms of δ_μ and δ_η. These are explained in the proof of Theorem 21.1.

Proof.   [Proof of Theorem 21.1]
We use the adjoint solution v in (21.11) to get

$$\int_\Omega u_1 \cdot \overline{(u_0 - u^{(m)})} dx = \int_\Omega u_1 \cdot \overline{(2\nabla \cdot ((\mu - i\omega\eta)\nabla^s v) + \nabla q + \rho\omega^2 v)} dx.$$
(21.16)

Using the vector identity $\nabla \cdot (q u_1) = \nabla q \cdot u_1$ and divergence free conditions ($0 = \nabla \cdot \delta u = \nabla \cdot u_1 = \nabla \cdot v$), the identity (21.16) can be rewritten as

$$\int_\Omega u_1 \cdot \overline{(u_0 - u^{(m)})} dx = - \int_\Omega 2(\mu + i\omega\eta)\nabla^s u_1 : \nabla^s \bar{v} dx + \int_\Omega \rho\omega^2 u_1 \cdot \bar{v} dx.$$

Since u_1 satisfies the equation (21.8), we have

$$\int_\Omega u_1 \cdot \overline{(u_0 - u^{(m)})} dx = \int_\Omega [2\nabla \cdot ((\mu + i\omega\eta)\nabla^s u_1) + \rho\omega^2 u_1] \cdot \bar{v} dx,$$

$$= \int_\Omega [-2\nabla \cdot ((\delta_\mu + i\omega\delta_\eta)\nabla^s u_0) + \nabla p_1] \cdot \bar{v} dx,$$

$$= \int_\Omega 2(\delta_\mu + i\omega\delta_\eta)\nabla^s u_0 : \nabla^s \bar{v} dx.$$

This proves the formula (21.9). The formula (21.10) can be obtained directly from Theorem 21.2 and the formula (21.9). This completes the proof.   □

Based on Theorem 21.1, the shear modulus and viscosity can be reconstructed by the following gradient descent iterative scheme.

21.2.3 Initial Guess

Numerous simulations show that the reconstruction from an adjoint-based optimization method may converge to some local minimum that is very different from the true solution when the initial guess is far from the true solution. We observed that different initial guesses produce different reconstructions, and thus a good initial guess is necessary for accurate reconstruction using the iterative method (21.17).

Algorithm 21.1 Gradient descent scheme.

---

1. Let $n = 0$. Start with an initial guess of shear modulus $\mu^{(0)}$ and shear viscosity $\eta^{(0)}$.

2. For $n = 0, 1, \ldots$, compute $u_0^{(n)}$ by solving the forward problem (21.4) with μ and η replaced by $\mu^{(n)}$ and $\eta^{(n)}$, respectively. Compute $v^{(n)}$ by solving the adjoint problem (21.11) with μ, η, u_0 replaced by $\mu^{(n)}, \eta^{(n)}, u_0^{(n)}$, respectively.

3. For $n = 0, 1, \ldots$, compute the Fréchet derivatives $\frac{\partial J}{\partial \mu}[\mu^{(n)}, \eta^{(n)}]$ and $\frac{\partial J}{\partial \eta}[\mu^{(n)}, \eta^{(n)}]$.

4. Update μ and η as follows:

$$
\begin{cases}
\mu^{(n+1)} = \mu^{(n)} - \delta \frac{\partial J}{\partial \mu}[\mu^{(n)}, \eta^{(n)}], \\
\eta^{(n+1)} = \eta^{(n)} - \delta \frac{\partial J}{\partial \eta}[\mu^{(n)}, \eta^{(n)}],
\end{cases}
\tag{21.17}
$$

where δ is the step size.

5. Repeat Steps 2, 3, and 4 until $||\mu^{(n+1)} - \mu^{(n)}|| \le \epsilon$ and $||\eta^{(n+1)} - \eta^{(n)}|| \le \epsilon$ for a given $\epsilon > 0$.

We examine the optimization method using the initial guess obtained by the direct inversion method (21.2). Numerical simulations with this initial guess showed that serious reconstruction errors occur near the interfaces of different materials in the same domain; the direct inversion method cannot probe those interfaces. We found empirically that it is important to find an initial guess capturing the interfaces of different materials for the effective use of the optimization method.

To develop a method of finding such a good initial guess, we adopt the hybrid one-step method [248] which considers the following simplified model ignoring the pressure term:

$$
2\nabla \cdot (\mu + i\omega\eta)\nabla^s u^\diamond + \rho\omega^2 u^\diamond = 0 \quad \text{in } \Omega,
\tag{21.18}
$$

where $u^\diamond$ is regarded as a good approximation of $u[\mu, \eta]$. To probe the discontinuity of $(\mu + i\omega\eta)\nabla^s u^\diamond$, we apply the Helmholtz decomposition

$$
(\mu + i\omega\eta)\nabla^s u^\diamond = \nabla f + \nabla \times W \quad \text{with } \nabla \cdot W = 0,
\tag{21.19}
$$

where f and W are vector and matrix, respectively. The curl of matrix is defined in column-wise sense: $\nabla \times W = \nabla \times (W_1, W_2, W_3) = (\nabla \times W_1, \nabla \times W_2, \nabla \times W_3)$, where W_j is the j-th column of matrix W for $j = 1, 2, 3$. Taking dot product of (21.19) with $\nabla^s u^\diamond$ gives the following formula

$$
\mu + i\omega\eta = \frac{\nabla f : \nabla^s \bar{u}^\diamond}{|\nabla^s u^\diamond|^2} + \frac{\nabla \times W : \nabla^s \bar{u}^\diamond}{|\nabla^s u^\diamond|^2}.
\tag{21.20}
$$

By taking the divergence to the equation (21.19), we have

$$
\Delta f = -\frac{1}{2}\rho\omega^2 u^\diamond \quad \text{in } \Omega.
\tag{21.21}
$$

By taking the curl operation to the equation (21.19), we have

$$\Delta W = \nabla \times ((\mu + i\omega\eta)\nabla^s u^\diamond) \quad \text{in } \Omega. \qquad (21.22)$$

Our proposed method for determining the initial guess is based on a modification of the hybrid one-step method. Using (21.21), an approximation of the vector potential f corresponding to the measurement $u^{(m)}$ can be computed by

$$\begin{cases} \Delta \widetilde{f} = -\frac{1}{2}\rho\omega^2 u^{(m)} & \text{in } \Omega, \\ \nabla\widetilde{f}\,\nu = (\mu_0 + i\omega\eta_0)\nabla^s u^{(m)}\,\nu & \text{on } \partial\Omega. \end{cases} \qquad (21.23)$$

On the other hand, W can not be computed directly from $u^{(m)}$ since (21.22) contains unknown terms μ and η. Regarding $\mu + i\omega\eta$ in (21.22) as $\frac{\nabla\widetilde{f}:\nabla^s\bar{u}^{(m)}}{|\nabla^s u^{(m)}|^2}$ (see (21.20)), we can compute a rough approximation of W by solving

$$\begin{cases} \Delta W_1 = \nabla \times \left(\frac{\nabla\widetilde{f}:\nabla^s\bar{u}^{(m)}}{|\nabla^s u^{(m)}|^2}\nabla^s u^{(m)}\right) & \text{in } \Omega, \\ W_1 = 0 & \text{on } \partial\Omega. \end{cases} \qquad (21.24)$$

Similarly, approximating $\mu + i\omega\eta$ by direct inversion formula (21.2), we can compute W by solving

$$\begin{cases} \Delta W_2 = \nabla \times \left(-\frac{\rho\omega^2(a\cdot u^{(m)})}{\nabla\cdot\nabla(a\cdot u^{(m)})}\nabla^s u^{(m)}\right) & \text{in } \Omega, \\ W_2 = 0 & \text{on } \partial\Omega, \end{cases} \qquad (21.25)$$

where a is any nonzero vector.

Now, we use the formula (21.20) to get the initial guess of shear modulus by substituting $f = \tilde{f}$, $W = (W_1 + W_2)/2$ and $u^\diamond = u^{(m)}$:

$$\mu^{(0)} + i\omega\eta^{(0)} = \frac{\nabla\widetilde{f} : \nabla^s\bar{u}^{(m)}}{|\nabla^s u^{(m)}|^2} + \frac{\nabla \times (W_1 + W_2) : \nabla^s\bar{u}^{(m)}}{2|\nabla^s u^{(m)}|^2}. \qquad (21.26)$$

In formula (21.26), the first term provides information in the wave propagation direction while the second term gives the information in the tangent direction of the wave propagation as shown in [248]. Note that if this initial guess is not satisfactory for the adjoint-based optimization problem, one can update the initial guess formula to obtain more accurate one by replacing $(\mu + i\omega\eta)$ in (21.22) by (21.26).

Numerical experiments demonstrate the possibility of probing the discontinuity of the shear modulus effectively. We emphasize that the initial guess plays an important role in Newton's iterative reconstruction algorithm based on the adjoint approach. By observing the adjoint problem (21.11), the load term $u_0 - u^{(m)}$ is related to the measured data and the initial guess in the first iteration step. If the initial guess ensure that $||u_0 - u^{(m)}||$ is small in certain norm, the iteration scheme will converge and give good results. Otherwise, the initial guess makes $||u_0 - u^{(m)}||$ far from 0 in certain norm, and the iteration scheme may not converge. This will be discussed in section 21.3.

21.2.4 Local Reconstruction

In MRE, the time-harmonic displacement, $u^{(m)}$, in the tissue is measured via phase-contrast-based MR imaging. Hence, the signal-to-noise ratio (SNR) of the data is related to that of the MR phase images, which varies from one region to another. For example, the SNR of data $u^{(m)}$ is very low in MR-defected regions, including the lungs, outer layers of bones, and some gas-filled organs. When the domain, Ω, contains such defected regions, the reconstructed image qualities may be seriously degraded by locally low SNR data in the defected regions. As a result, it would be desirable to exclude defected regions from Ω to prevent errors spreading in the image reconstruction.
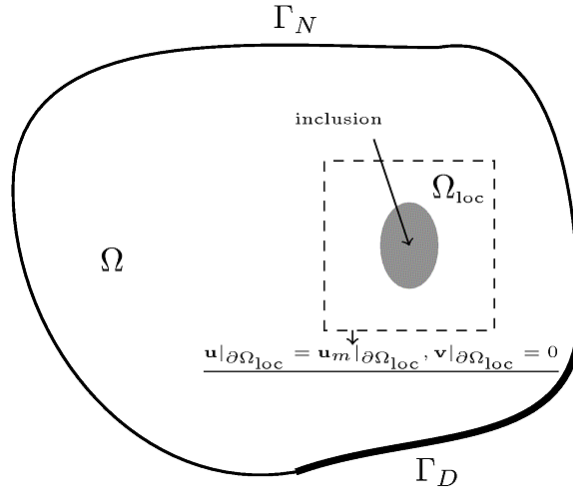
Fig. 21.2. Illustration of the localization of the small anomaly in certain subdomain.

The proposed method is capable of a local reconstruction by restricting to a local domain of the interest. To be precise, let Ω_{loc} be a subdomain of Ω in which $u^{(m)}$ has high SNR. Then, we consider the localized minimization problem

$$J_{\mathrm{loc}}[\mu, \eta] = \frac{1}{2} \int_{\Omega_{\mathrm{loc}}} |u_{\mathrm{loc}}[\mu, \eta] - u^{(m)}|^2 dx \qquad (21.27)$$

with $u_{\mathrm{loc}}[\mu, \eta]$ being the solution of

$$\begin{cases} 2\nabla \cdot ((\mu + i\omega\eta)\nabla^s u) + \nabla p + \rho\omega^2 u = 0 & \text{in } \Omega_{\mathrm{loc}}, \\ \nabla \cdot u = 0 & \text{in } \Omega_{\mathrm{loc}}, \\ u = u^{(m)} & \text{on } \partial\Omega_{\mathrm{loc}}. \end{cases} \qquad (21.28)$$

As before, we need to compute the corresponding adjoint problem to get Fréchet derivative:

$$\begin{cases} 2\nabla \cdot ((\mu - i\omega\eta)\nabla^s v) + \nabla q + \rho\omega^2 v = u_{\text{loc}} - u^{(m)} & \text{in } \Omega_{\text{loc}}, \\ \nabla \cdot v = 0 & \text{in } \Omega_{\text{loc}}, \\ v = 0 & \text{on } \partial\Omega_{\text{loc}}. \end{cases} \qquad (21.29)$$

There is no difference between the local reconstruction in Ω_{loc} and the global reconstruction with Ω, except the boundary conditions. As in (21.17), the local reconstruction can be done by solving (21.28) and (21.29) with the initial guess (21.26). Local reconstruction requires that neither the boundary conditions need to be used on the whole domain, Ω, nor that the exact shape of Ω needs to be known. Numerical simulations verify the effectiveness of this local reconstruction, and further discussion will be shown in section 21.3.

21.3 Numerical Illustrations

In this section, we perform several numerical experiments in dimension two to illustrate the effectiveness of the shear viscoelasticity reconstruction algorithm proposed in the previous section.

To implement the reconstruction algorithm (21.17) proposed in section 21.2, we use the algorithm (21.20) in section 21.2.3 to initialize the iteration scheme. For numerical experiments, we set the two dimensional domain as $\Omega = [0, 0.1] \times [0, 0.1]$ m^2 with a boundary denoted by $\partial\Omega = \Gamma_D \cup \Gamma_N$; see Figure 21.3 (a). We use a finite element method and discretize the rectangular domain Ω into 300×300 triangular elements with linear interpolation functions to solve the forward problem (21.4) as well as the adjoint problem (21.11) at each iteration step in the algorithm (21.17). Fixed iteration step size $\delta = 5 \times 10^6$ is used in the iterative reconstruction algorithm (21.17).

We set three different types of shear viscoelasticity distribution which are shown in the first column of Figures 21.4, 21.5, and 21.6 along with the true distribution of shear modulus and shear viscosity. For each model, the first row shows elasticity while the second row shows viscosity. Our numerical experiments are based on these three models. We generate two dimensional displacements $u^{(m)} = (u_1, u_2)^T$ by solving the problem (21.4) with frequency $\frac{\omega}{2\pi} = 70$Hz and area density $\rho = 1 kg \cdot m^{-2}$. We apply the vibration to Γ_D, and the other three sides boundaries are set to be traction free:

$$\begin{cases} u = (0.003, 0.003) & \text{on } \Gamma_D, \\ 2(\mu + i\omega\eta)\nabla^s u \, \nu + p\nu = 0 & \text{on } \Gamma_N. \end{cases} \qquad (21.30)$$

For example, Model 1 has the displacement fields shown in Figure 21.3 where (b) and (c) are real parts of u_1 and u_2, and (d) and (e) are imaginary parts of u_1 and u_2, respectively.

The next step is to implement our algorithm making use of these displacement fields with certain initial guesses of the distribution of viscoelasticity. We generate the initial guess by the direct inversion method (21.2) shown in the third column of Figures 21.4, 21.5 and 21.6 and the hybrid one-step
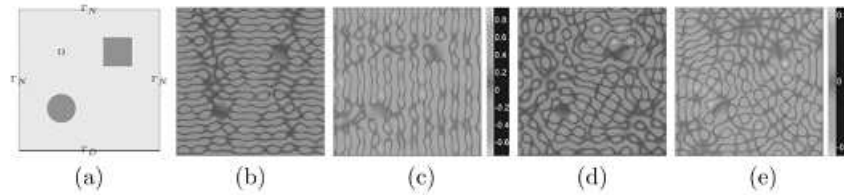
Fig. 21.3. Model 1 and the displacement fields. (a) Model 1; (b) and (c) are real parts of u_1 and u_2; (d) and (e) are imaginary parts of them, respectively.

method (21.20) shown in the fifth column of Figures 21.4, 21.5 and 21.6. From the generated initial guess, we can see that the reconstruction by the hybrid one-step method is much better than that of the direct inversion method in catching the inhomogeneous property of the medium. We have already explained the underlying mathematical reason for this phenomenon. We use the initial guesses from these two methods to initialize our proposed method, and the corresponding numerical results for each model are shown in the fourth column and last column of Figures 21.4, 21.5 and 21.6, respectively. For comparison, we also show the reconstruction with a homogeneous initial guess in each second column of Figures 21.4, 21.5 and 21.6.

The reconstruction results (see Figures 21.4, 21.5 and 21.6) show that the proposed method can reconstruct the viscoelasticity distribution with high accuracy (see (f) column) using a well-matched initial guess (see (e) column). Otherwise, poor initial guesses (for example, the homogeneous initial guess and (c)), leads to unsatisfactory reconstructed images (see (b) and (d) columns).

We also numerically evaluate the local reconstruction method proposed in section 21.2.4. We consider the rectangular domain, Ω, which is equally divided into four parts: top-left, top-right, bottom-left and bottom-right. It is assumed that the top-right part is contaminated by noise or defected data. For numerical simplicity, we add 3% white noise to the measured data in the top-right part. The reconstruction results in both the whole domain and the local domains are shown in Figure 21.7 where (a) is the true distribution of shear viscoelasticity, (b) the initial guess with hybrid method, (c) the reconstruction in whole domain using proposed method, (d) the local reconstruction.

21.4 Concluding Remarks

In this chapter, we have proposed a reconstruction algorithm for shear elasticity and shear viscosity in a viscoelastic tissue. The optimization-based approach involves introducing an adjoint problem to avoid taking any derivative
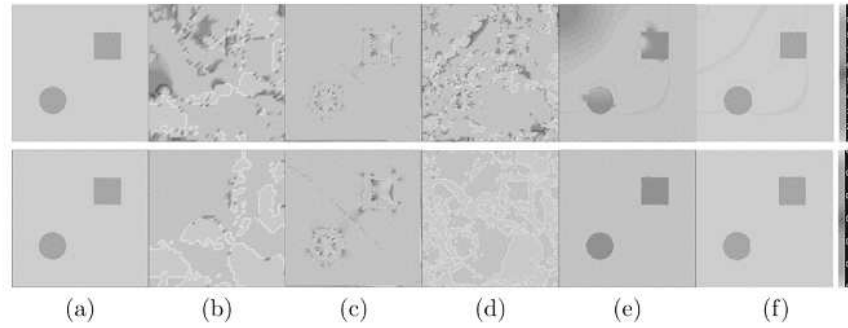
Fig. 21.4. Case 1: Simulation results for μ (first row) and η_μ (second row) image reconstruction. (a) True images; (c) direct inversion method; (e) hybrid one-step method; (b), (d) and (f) are reconstructed images by the adjoint-based optimization method (21.17) with initial guess of the constant $\mu_0 + i\omega\eta_{\mu_0}$, (c) and (e), respectively.
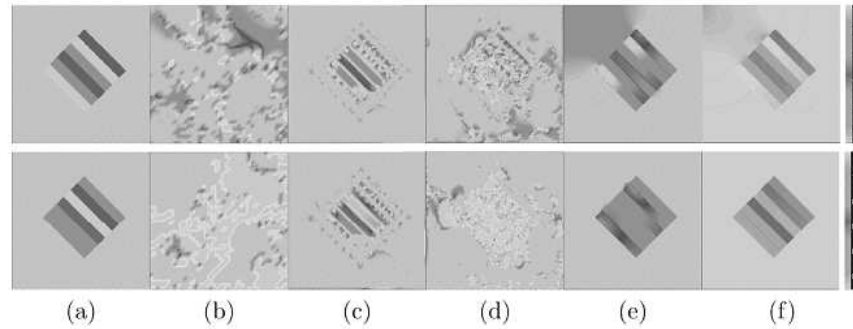
Fig. 21.5. Case 2: Simulation results for μ (first row) and η_μ (second row) image reconstruction. (a) True images; (c) direct inversion method; (e) hybrid one-step method; (b), (d) and (f) are reconstructed images by the adjoint-based optimization method (21.17) with initial guess of the constant $\mu_0 + i\omega\eta_{\mu_0}$, (c) and (e), respectively.

of the measured time-harmonic internal data. The proposed initial guess formula is particularly suitable for imaging viscoelastic anomalies. The stability estimates in [78] yield convergence of the proposed optimal control algorithm.
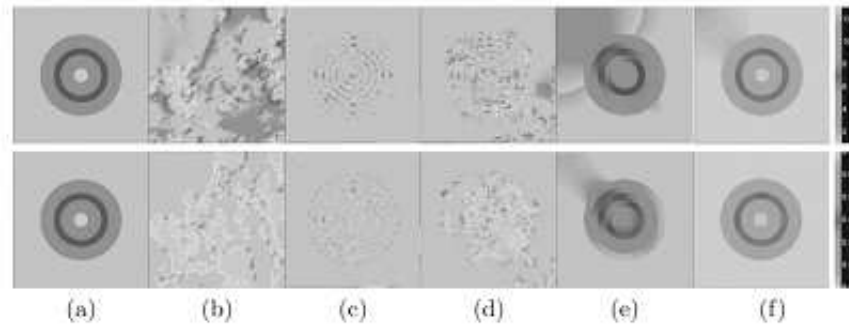
Fig. 21.6. Case 3: Simulation results for μ (first row) and η_μ (second row) image reconstruction. (a) True images; (c) direct inversion method; (e) hybrid one-step method; (b), (d) and (f) are reconstructed images by the adjoint-based optimization method (21.17) with initial guess of the constant $\mu_0 + i\omega\eta_{\mu_0}$, (c) and (e), respectively.
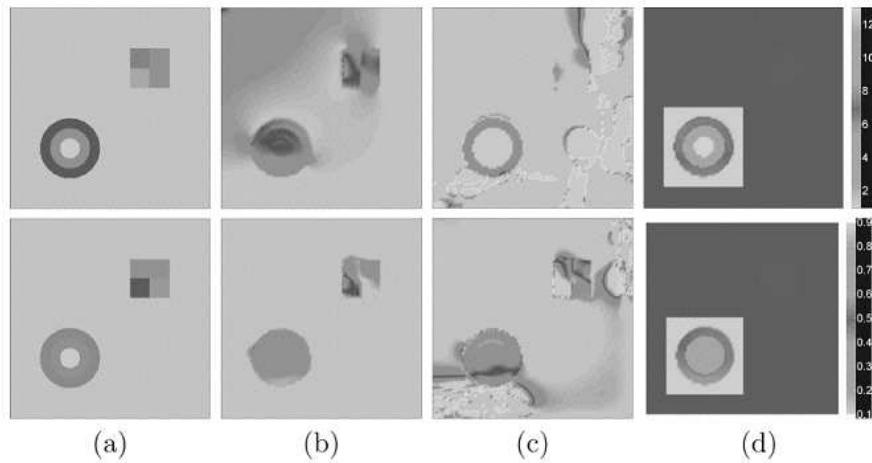
Fig. 21.7. Simulation results for local reconstruction. First row: images of μ. Second row: images of η_μ. (a) true image; (b) initial guess; (c) adjoint-based optimization method; (d) local reconstruction.

Full-Field Optical Coherence Elastography

22.1 Introduction

In this chapter, we provide a mathematical analysis of and a numerical framework for full-field optical coherence elastography, which has unique features including micron-scale resolution, real-time processing, and non-invasive imaging. We develop an algorithm for transforming volumetric optical images before and after the mechanical solicitation of a sample with sub-cellular resolution into quantitative shear modulus distributions. This has the potential to improve sensitivities and specificities in the biological and clinical applications of optical coherence tomography.

As seen in Chapter 10, optical coherence tomography (OCT) is a non-invasive and a non-ionizing imaging technique that produces high-resolution images of biological tissues. It performs optical slicing in the sample, to allow three-dimensional reconstructions of internal structures. Conventional optical coherence time-domain and frequency-domain tomographies require transverse scanning of the illumination spot in one or two directions to obtain cross-sectional or en face images, respectively.

Full-field OCT allows OCT to be performed without transverse scanning; the tomographic images are obtained by combining interferometric images acquired in parallel using an image sensor. Both the transverse and the axial resolutions are of the order of 1μm; see [154, 155].

In [279], elastographic contrast has been combined with full-field OCT with the aim of creating a virtual palpation map at the micrometer scale. The idea is to register a volumetric optical image before and after mechanical solicitation of the sample. Based on the assumption that the density of the optical scatterers is advected by the deformation, the displacement map can be first estimated. Then, using a quasi-incompressible model for the tissue elasticity, the shear modulus distribution can be reconstructed from the estimated displacement map.

The OCT elastography is able to perform displacement measurements with sub-cellular resolution. It enables a more precise characterization of tis-

sues than that achieved using ultrasound or magnetic resonance elastography; therefore, it provides a more accurate assessment of microscale variations of elastic properties. A map of mechanical properties added as a supplementary contrast mechanism to morphological images could aid diagnosis. The technique costs less than other elastography techniques.

The mapping of mechanical properties was first introduced to OCT imaging by Schmitt [316], who measured displacements as small as a few micrometers in heterogeneous gelatin phantoms containing scattering particles in addition to living skin. Various subsequent applications have employed OCT methods in elastography; these include dynamic and full-field optical coherence elastography (see [252, 303, 306]).

In all of the aforementioned techniques, transforming the OCT images before and after the application of a load into quantitative maps of the shear modulus is a challenging problem.

In this chapter we present a mathematical and numerical framework for the OCT-elastography experiment described in [279]. Using the set of images before and after mechanical solicitation we design a method to reconstruct the shear modulus distribution inside the sample.

To mathematically formulate the problem, let $\Omega_0 \subset \mathbb{R}^d, d = 2, 3$, and let ε_0 be the known piecewise smooth optical image of the medium, and μ be its shear modulus. In this chapter we consider heterogeneous (unknown) shear modulus distributions. The medium is solicited mechanically. Since compression modulus of biological media is four order of magnitude larger than the shear modulus, it can be shown that the displacement map u obeys the linearized equations of incompressible fluids or the Stokes system. As seen in Chapter 21, the model problem is then the following Stokes system in a heterogeneous medium which reads:

$$\begin{cases} \nabla \cdot \left(\mu (\nabla u + \nabla u^T) \right) + \nabla p = 0 & \text{in } \Omega_0 \,, \\ \qquad\qquad\qquad\quad \nabla \cdot u = 0 & \text{in } \Omega_0 \,, \\ \qquad\qquad\qquad\qquad\quad u = f & \text{on } \partial\Omega_0 \,, \end{cases} \tag{22.1}$$

where superposed T denotes the transpose and the real-valued vector f satisfies the compatibility condition $\int_{\partial\Omega_0} f \cdot \nu = 0$ with ν being the outward normal at $\partial\Omega_0$.

Throughout this chapter, we assume that $\mu \in \mathcal{C}^{0,1}(\overline{\Omega}_0)$ and $f \in \mathcal{C}^2(\partial\Omega_0)^d$. From [132, 183, 249], (22.1) has a unique solution $u \in \mathcal{C}^1(\overline{\Omega}_0)^d$. Moreover, there exists a positive constant C depending only on μ and Ω_0 such that

$$||u||_{\mathcal{C}^1(\overline{\Omega}_0)^d} \leq C ||f||_{\mathcal{C}^2(\partial\Omega_0)^d} \,.$$

Using a second OCT scan, one has access to the optical image of the deformed medium $\varepsilon_u(\widetilde{x})$, $\forall\, \widetilde{x} \in \Omega_u$, where Ω_u is defined by

$$\Omega_u = \{x + u(x),\ x \in \Omega_0\} \,.$$

The new optical image is linked to the original one by

$$\varepsilon(x) = \varepsilon_u \left(x + u(x) \right), \quad \forall\, x \in \Omega_0\,. \tag{22.2}$$

The goal is to reconstruct the shear modulus map μ on Ω_0 from the functions ε and ε_u. We first prove that, in two dimensions, if the direction of $\dfrac{\nabla \varepsilon}{|\nabla \varepsilon|}$ is not constant in a neighborhood of x, then the displacement field u at x can be approximately reconstructed. In three dimensions, one shall assume that the vectors $\dfrac{\nabla \varepsilon(y)}{|\nabla \varepsilon(y)|}$ are not coplanar for y a neighborhood of x. Hence, the reconstructed value of $u(x)$ serves as an initial guess for the minimization of the discrepancy between computed and measured changes in the optical image. Then, we compute an element of the subgradient [139] of the discrepancy functional. Finally, we implement a minimization scheme to retrieve the shear modulus map from the reconstructed displacements. Note that reconstructing the displacement field from $\varepsilon - \varepsilon_u$ is a registration problem and its linearization is an optical flow problem; see [194]. It is also worth mentioning that the approach developed in this chapter applies to other speckle imaging modalities.

The chapter is organized as follows. Section 22.2 is devoted to some mathematical preliminaries. In Section 22.3 we consider piecewise smooth ε functions and first derive a leading-order Taylor expansion of ε_u as $||u||_{\mathcal{C}^1}$ goes to zero. Then we provide an initial guess by linearization. Finally, we prove the Fréchet differentiability of the discrepancy functional between the measured and the computed advected images. The displacement field inside the sample can be obtained as the minimizer of such functional. Section 22.4 is devoted to the reconstruction of the shear modulus from the displacement measurements. In Section 22.5 we present some numerical results to highlight the viability and the performance of the proposed algorithm. The chapter ends with a short discussion. Our results in this chapter are from [40].

22.2 Preliminaries

Let Ω be a bounded smooth domain in $\mathbb{R}^d, d = 2, 3$. We start by defining a class of piecewise smooth functions.

Definition 22.1 *For any $k \in \mathbb{N}$, $\alpha \in (0, 1)$, for any curve S of class $\mathcal{C}^{1,\alpha}$ for some $0 < \alpha < 1$ such that $\Omega \setminus S$ is a union of connected domains $\Omega_i, i = 1, 2, \ldots, n$, we define $\mathcal{C}_S^{k,\alpha}\left(\overline{\Omega}\right)$ to be the class of functions $f : \Omega \longrightarrow \mathbb{R}$ satisfying*

$$f|_{\Omega_i} \in \mathcal{C}_S^{k,\alpha}\left(\overline{\Omega}_i\right) \quad \forall\, i = 1, \ldots, n\,. \tag{22.3}$$

Definition 22.2 *We define* $\mathrm{BV}(\Omega)$ *as the subspace of* $L^1(\Omega)$ *of all the functions* f *whose weak derivative* Df *is a finite Radon measure. In other terms,* f *satisfies*

$$\int_\Omega f \nabla \cdot F \leq C \sup_{x \in \Omega} |F|, \quad \forall\, F \in \mathcal{C}_0^1(\Omega)^d$$

for some positive constant C *with* $\mathcal{C}_0^1(\Omega)$ *being the set of compactly supported* $\mathcal{C}^1$ *functions.*

The derivative of a function $f \in \mathrm{BV}(\Omega)$ can be decomposed as

$$Df = \nabla f \mathcal{H}^d + [f]\nu_s \mathcal{H}_S^{d-1} + D_c f,$$

where $\mathcal{H}^d$ is the Lebesgue measure on Ω, $\mathcal{H}_S^{d-1}$ is the surface Hausdorff measure on a rectifiable surface S, ν_S is a normal vector defined a.e. on S, $\nabla f \in L^1(\Omega)$ is the smooth derivative of f, $[f] \in L^1(S, \mathcal{H}_S^{d-1})$ is the jump of f across S and $D_c f$ is a vector measure supported on a set of Hausdorff dimension less than $(d-1)$, which means that its $(d-1)$-Hausdorff-measure is zero; see [15, 22].

Definition 22.3 *We define* $\mathrm{SBV}(\Omega)$ *as the subspace of* $\mathrm{BV}(\Omega)$ *of all the functions* f *satisfying* $D_c f = 0$.

Definition 22.4 *For any* $1 \leq p \leq +\infty$, *we define*

$$\mathrm{SBV}^p(\Omega) = \left\{ f \in \mathrm{SBV}(\Omega) \cap L^p(\Omega),\ \nabla f \in L^p(\Omega)^d \right\}. \qquad (22.4)$$

Let $W^{1,p}(\Omega) = \{ f \in L^p(\Omega),\ \nabla f \in L^p(\Omega)^d \}$ for $p \geq 1$. Roughly speaking, a function $u \in SBV^p(\Omega)$ is a function of class $W^{1,p}$ admitting surface discontinuities. Note also that $\mathcal{C}_S^{k,\alpha}(\overline{\Omega}) \subset \mathrm{SBV}^p(\Omega)$; see [22].

From now on, we assume that the optical image in the medium ε belongs to $\mathcal{C}_S^{k,\alpha}(\overline{\Omega})$, which is a simple but good model for a discontinuous medium. Some of the following propositions are true for more general maps $\varepsilon \in \mathrm{SBV}(\Omega)$. In these propositions we only assume that ε is in $\mathrm{SBV}(\Omega)$.

22.3 Displacement Field Measurements

In this section we consider the problem of reconstructing the displacement u from the optical images before and after applying a load on the sample. Assuming that ε is piecewise smooth, we derive a leading-order Taylor expansion of ε_u as $||u||_{\mathcal{C}^1}$ goes to zero. Then we provide an initial guess by linearization. Finally, we prove the Fréchet differentiability of the discrepancy functional I between the measured and the computed advected images provided that ε is smooth. If ε has jumps, then I has a nonempty subgradient. Therefore, in both cases, the displacement field u inside the sample can be obtained as the minimizer of such functional.

22.3.1 First-Order Approximation

Let $\Omega \Subset (\Omega_0 \cap \Omega_u)$ be a smooth simply connected domain. On Ω, as in 20.4, we have

$$\begin{aligned} \varepsilon_u &= \varepsilon \circ (I + u)^{-1} \\ \varepsilon &= \varepsilon_u \circ (I + u) \,, \end{aligned}$$

where I is the $d \times d$ identity matrix.

Proposition 22.5 *Let $\varepsilon \in \mathrm{BV}(\Omega)$ and let $u \in \mathcal{C}^1(\overline{\Omega})^d$ be such that $\|u\|_{\mathcal{C}^1(\overline{\Omega})^d} < 1$. Then, for any $\psi \in \mathcal{C}_0^1(\Omega)$, we have*

$$\left| \int_\Omega (\varepsilon - \varepsilon_u)\,\psi - \int_\Omega \psi u \cdot D\varepsilon \right| \leq C \|u\|_{\mathcal{C}^0(\overline{\Omega})^d} \|u\|_{\mathcal{C}^1(\overline{\Omega})^d} \|\psi\|_{\mathcal{C}_0^1(\Omega)} |\varepsilon|_{\mathrm{TV}(\Omega)} \,, \tag{22.5}$$

where the constant C is independent of ψ and $|\ |_{\mathrm{TV}(\Omega)}$ denotes the total variation semi-norm. Estimate (22.5) yields that $\dfrac{\varepsilon_u - \varepsilon + u \cdot D\varepsilon}{\|u\|_{\mathcal{C}^0(\overline{\Omega})^d}}$ weakly converges to 0 in $\mathcal{C}_0^1(\Omega)$ when $\|u\|_{\mathcal{C}^1(\overline{\Omega})^d}$ goes to 0.

Proof. For each $t \in [0,1]$, define ϕ_t by $\phi_t^{-1}(x) = x + tu(x)$. Let $\eta > 0$ be a small parameter, and $\varepsilon^{(\eta)}$ be a smooth function such that $\|\varepsilon - \varepsilon^{(\eta)}\|_{L^1(\Omega)} \to 0$, and $|\varepsilon^{(\eta)}|_{\mathrm{TV}(\Omega)} \to |\varepsilon|_{\mathrm{TV}(\Omega)}$ as $\eta \to 0$. Analogously, we define $\varepsilon_u^{(\eta)}$ to be the smooth approximation of ε_u given by

$$\varepsilon_u^{(\eta)}(x) = \varepsilon^{(\eta)} \circ \phi_1(x) \,.$$

From

$$\varepsilon_u^{(\eta)}(x) - \varepsilon^{(\eta)}(x) = \left(\varepsilon^{(\eta)} \circ \phi_1 \right)(x) - \left(\varepsilon^{(\eta)} \circ \phi_0 \right)(x), \quad \forall\, x \in \Omega \,,$$

we have

$$\varepsilon_u^{(\eta)}(x) - \varepsilon^{(\eta)}(x) = \int_0^1 \nabla \varepsilon^{(\eta)}(\phi_t(x)) \cdot \partial_t \phi_t(x)\,dt, \quad \forall\, x \in \Omega \,.$$

Therefore, for $\psi \in \mathcal{C}_0^\infty(\Omega)$ with $\mathcal{C}_0^\infty(\Omega)$ being the set of compactly supported $\mathcal{C}^\infty$ functions,

$$\int_\Omega \left[\varepsilon_u^{(\eta)}(x) - \varepsilon^{(\eta)}(x) + \nabla \varepsilon^{(\eta)}(x) \cdot u(x) \right] \psi(x)\,dx =$$

$$\int_\Omega \left[\int_0^1 \nabla \varepsilon^{(\eta)}(\phi_t(x)) \cdot \partial_t \phi_t(x)\,dt \right] \psi(x)\,dx + \int_\Omega \nabla \varepsilon^{(\eta)}(x) \cdot u(x)\psi(x)\,dx, \quad \forall\, x \in \Omega \,. \tag{22.6}$$

By a change of variables in the first integral and using the fact that

$$\partial_t \phi_t(x) = -\partial_x \phi_t(x) \partial_t \phi_t^{-1}(y)|_{y=\phi_t(x)},$$

we get, $\forall\, x \in \Omega$,

$$\int_0^1 \left[\int_\Omega \nabla \varepsilon^{(\eta)}(\phi_t(x)) \cdot \partial_t \phi_t(x) \psi(x) dx \right] dt =$$
$$-\int_0^1 \int_\Omega \nabla \varepsilon^{(\eta)}(y) \cdot \left[\partial_x \phi_t(\phi_t^{-1}(y)) \partial_t \phi_t^{-1}(y) \right] |\det \partial_x \phi_t^{-1}(y)| \psi\left(\phi_t^{-1}(y) \right) dy dt\,.$$

Here, det denotes the determinant of a matrix. Since

$$\forall\, (y,t) \in \Omega \times [0,1], \quad \partial_t \phi_t^{-1}(y) = u(y),$$

$$\partial_y \phi_t^{-1}(y) = I + t \nabla u(y),$$

and

$$\partial_x \phi_t(\phi_t^{-1}(y)) \partial_y \phi_t^{-1}(y) = I\,,$$

we can write

$$\int_0^1 \int_\Omega \left[\nabla \varepsilon^{(\eta)}(\phi_t(x)) \cdot \partial_t \phi_t(x) \psi(x) dx \right] dt =$$
$$-\int_0^1 \int_\Omega \nabla \varepsilon^{(\eta)}(y) \cdot \left[(I + t \nabla u(y))^{-1} u(y) \right] |\det I + t \nabla u(y)| \psi\left(\phi_t^{-1}(y) \right) dy dt\,,$$

and hence

$$\int_\Omega \left[\varepsilon_u^{(\eta)}(x) - \varepsilon^{(\eta)}(x) + \nabla \varepsilon^{(\eta)}(x) \cdot u(x) \right] \psi(x) dx =$$
$$\int_0^1 \int_\Omega \nabla \varepsilon^{(\eta)}(x) \cdot u(x) \left[\psi(x) - \psi\left(\phi_t^{-1}(x) \right) \right] dx dt$$
$$+ \int_0^1 \int_\Omega \nabla \varepsilon^{(\eta)}(x) \cdot \left(\left[(I + t \nabla u(x))^{-1} |\det I + t \nabla u(x)| - I \right] u(x) \right) \psi\left(\phi_t^{-1}(x) \right) dx dt\,.$$
$$(22.7)$$

The first term in the right-hand side of (22.7) can be estimated as follows:

$$\left| \int_0^1 \int_\Omega \nabla \varepsilon^{(\eta)}(x) \cdot u(x) \left[\psi(x) - \psi\left(\phi_t^{-1}(x) \right) \right] dx dt \right| \leq \|u\|_{C^0(\overline{\Omega})^d}^2 \|\nabla \varepsilon^{(\eta)}\|_{L^1(\Omega)^d} \|\nabla \psi\|_{C^0(\Omega)^d}\,.$$

Let trace denote the trace of a matrix. Using the fact that

$$(I + t \nabla u)^{-1} = \sum_{i=0} (-1)^i (t \nabla u)^i\,,$$

which follows from $\|u\|_{C^1(\Omega)^d} < 1$, and

$$\det\left(I + t\nabla u\right) = \begin{cases} 1 - \operatorname{trace} t\nabla u + \det t\nabla u & \text{if } d = 2\,, \\ 1 + \operatorname{trace} t\nabla u - \dfrac{1}{2}\left[\left(\operatorname{trace} t\nabla u\right)^2 - \operatorname{trace}\left(t\nabla u\right)^2\right] + \det t\nabla u & \text{if } d = 3\,, \end{cases}$$

we get

$$\int_0^1 \int_\Omega \nabla\varepsilon^{(\eta)}(x)\cdot u(x)\left[\left(I + t\nabla u(x)\right)^{-1} |\det I + t\nabla u(x)| - I\right]\psi\left(\phi_t^{-1}(x)\right)dxdt$$

$$\leq \|u\|_{\mathcal{C}^0(\overline{\Omega})^d}\|u\|_{\mathcal{C}^1(\overline{\Omega})^d}\|\nabla\varepsilon^{(\eta)}\|_{L^1(\Omega)^d}\|\psi\|_{\mathcal{C}^0(\Omega)}\,,$$

which is the desired estimate for the second term in the right-hand side of (22.7).

Now, we can deduce the final result by density when $\eta \to 0$. Since $u \in \mathcal{C}^1(\Omega)^d$ and $\psi \in \mathcal{C}_0^1(\Omega)$, we can write

$$\int_\Omega \psi u \cdot \nabla\varepsilon^{(\eta)} = -\int_\Omega \nabla\cdot(\psi u)\varepsilon^{(\eta)}.$$

Since $\|\varepsilon^{(\eta)} - \varepsilon\|_{L^1(\Omega)} \to 0$, we have

$$\int_\Omega \nabla\cdot(\psi u)\varepsilon^{(\eta)} \to \int_\Omega \nabla\cdot(\psi u)\varepsilon\,.$$

As $\left|\varepsilon^{(\eta)}\right|_{\mathrm{TV}(\Omega)} \to \left|\varepsilon\right|_{\mathrm{TV}(\Omega)}$, we arrive at (22.5) and the proof of the proposition is complete. $\square$

22.3.2 Local Recovery Via Linearization

Assuming that $\varepsilon \in \mathrm{SBV}^2(\Omega)$, where $\mathrm{SBV}^2(\Omega)$ is defined by (22.4) for $p = 2$, we can write

$$D\varepsilon = \nabla\varepsilon\mathcal{H}^d + [\varepsilon]_S\nu_S\mathcal{H}_S^{d-1},$$

where ν_S is the outward normal at the oriented surface S of discontinuity of ε.

The data consists of ε and ε_u on Ω. In order to reconstruct u, we can use the first order approximation of $\varepsilon - \varepsilon_u$,

$$\varepsilon - \varepsilon_u \approx u \cdot D\varepsilon,$$

given by Proposition 22.5. These data can be decomposed into two parts:

$$u \cdot D\varepsilon(\cdot) = u \cdot \nabla\varepsilon\mathcal{H}^d + [\varepsilon]_S u \cdot \nu_S\mathcal{H}_S^{d-1} = d_{\mathrm{reg}}\mathcal{H}^d + d_{\mathrm{sing}}\mathcal{H}_S^{d-1}.$$

Let w be a mollifier supported on $[-1, 1]$. For any $\delta > 0$, we define

$$w_\delta = \frac{1}{\delta^d}w\left(\frac{\cdot}{\delta}\right),$$

and introduce

$$u_\delta(x) = \int_\Omega u(y)w_\delta(|x - y|)dy.$$

Since u is smooth, for any $x \in \Omega$, $u_\delta(x)$ is a good approximation of u on the ball with center x and radius δ.

We want to find an approximate value for u_δ from the optical measurements and use it as an initial guess in an optimization procedure. For doing so, we introduce the functional $J_x : \mathbb{R}^d \longrightarrow \mathbb{R}$ given by

$$u \longmapsto J_x(u) = \int_\Omega |\nabla\varepsilon(y) \cdot u - d_{\mathrm{reg}}(y)|^2 w_\delta(|x - y|)dy$$

$$+ \int_\Omega |[\varepsilon]_S u \cdot \nu_S - d_{\mathrm{sing}}(y)|^2 w_\delta(|x - y|)dy$$

and look for minimizers of J_x in $\mathbb{R}^d$. The gradient of J_x can be explicitly computed as follows:

$$\nabla J_x(u) = 2\int_\Omega (\nabla\varepsilon(y) \cdot u - d_{\mathrm{reg}}(y))\, \nabla\varepsilon(y)w_\delta(|x - y|)dy$$

$$+ 2\int_\Omega ([\varepsilon]_S(y)u \cdot \nu(y) - d_{\mathrm{sing}}(y))\, [\varepsilon]_S(y)\nu(y)w_\delta(|x - y|)dy\,.$$

In the case where ε has no jumps, J_x is a quadratic functional and we have

$$\nabla J_x(u) = 0 \tag{22.8}$$

if and only if

$$\left(\int_\Omega w_\delta(|x - y|)\nabla\varepsilon(y)\nabla\varepsilon^T(y)dy\right) u = \int_{x+\delta B} d_{\mathrm{reg}}(y)w_\delta(|x - y|)\nabla\varepsilon(y)dy\,,$$

$$\tag{22.9}$$

where B is the ball with center 0 and radius 1.

If the matrix $\int_\Omega w_\delta(|x - y|)\nabla\varepsilon(y)\nabla\varepsilon^T(y)$ is invertible, then the minimizer is given by

$$u = \left(\int_\Omega w_\delta(|x - y|)\nabla\varepsilon(y)\nabla\varepsilon^T(y)dy\right)^{-1}\int_{x+\delta B} d_{\mathrm{reg}}w_\delta(|x - y|)\nabla\varepsilon(y)dy\,.$$

$$\tag{22.10}$$

The following proposition gives a sufficient condition for the invertibilty of the matrix $\int_\Omega w_\delta(|x - y|)\nabla\varepsilon(y)\nabla\varepsilon^T(y)$.

Proposition 22.6 *Suppose that ε is smooth enough and $d = 2$. Assume $x + \delta B \subset \Omega$. Then, if all vectors $\nabla\varepsilon$ in $\{y \ : \ w_\delta(|y - x|) \neq 0\}$ are not collinear, the matrix*

$$\int_\Omega w_\delta(|x - y|)\nabla\varepsilon(y)\nabla\varepsilon^T(y)dy$$

is invertible.

Proof. Writing

$$\forall \, y \in x + \delta B, \quad \nabla \varepsilon(y) = u(y)e_1 + v(y)e_2,$$

where $\{e_1, e_2\}$ is the canonical basis of $\mathbb{R}^2$, it follows that

$$\nabla \varepsilon \nabla \varepsilon^T(y) = u^2(y)e_1 e_1^T + v^2(y)e_2 e_2^T + u(y)v(y)\left(e_1 e_2^T + e_2 e_1^T\right), \quad \forall \, y \in x + \delta B.$$

Computing the convolution with respect to w_δ, we get

$$\int_\Omega w_\delta(|y - y|)\nabla \varepsilon(y)\nabla \varepsilon^T(y)dy = \left(\int_\Omega u^2(y)w_\delta(|y - x|)dy\right)e_1 e_1^T$$

$$+ \left(\int_\Omega v^2(y)w_\delta(|y - x|)dy\right)e_2 e_2^T + \left(\int_\Omega u(y)v(y)w_\delta^T(|y - x|)dy\right)\left(e_1 e_2^T + e_2 e_1^T\right).$$

This matrix is not invertible if and only if

$$\left(\int_\Omega u^2(y)w_\delta(|y - x|)dy\right)\left(\int_\Omega v^2(y)w_\delta(|y - x|)dy\right) = \left(\int_\Omega u(y)v(y)w_\delta(|y - x|)dy\right)^2,$$

which is exactly the equality case in weighted Cauchy–Schwarz inequality. So, if there exist two points $y_1, y_2 \in \{y : \ w_\delta(|y - x|) \neq 0\}$ such that

$$\nabla \varepsilon(y_1) \times \nabla \varepsilon(y_2) \neq 0,$$

then u is not proportional to v, and the matrix is invertible.   □

Remark 22.7 *Assuming that $\nabla \varepsilon(y) \neq 0$ for $y \in x + \delta B \subset \Omega$, Proposition 22.6 gives that the direction of $\dfrac{\nabla \varepsilon}{|\nabla \varepsilon|}$ in not constant in $x + \delta B \subset \Omega$ if and only if*

$$\int_{x+\delta B} \nabla \varepsilon(y)\nabla \varepsilon^T(y)dy \quad \text{is invertible.}$$

Hence, under the above condition on ε in the neighborhood $x + \delta B$, the displacement field u at x can be approximately reconstructed.

Remark 22.8 *By exactly the same arguments as those in two dimensions, one can prove that in the three-dimensional case, if all vectors $\nabla \varepsilon$ in $\{y : \ w_\delta(|y - x|) \neq 0\}$ are not coplanar, then the matrix*

$$\int_\Omega w_\delta(|x - y|)\nabla \varepsilon(y)\nabla \varepsilon^T(y)dy$$

is invertible.

On the other hand, in the case where ε is piecewise smooth, one can first detect the surface of jumps of ε using, for example, an edge detection algorithm [121, 278] and then apply the proposed local algorithm in order to have a good approximation of u in the domains where ε is smooth.

22.3.3 Minimization of the Discrepancy Functional

Let $\varepsilon \in \mathcal{C}_S^{k,\alpha}(\overline{\Omega})$, where S is the surface of discontinuity. For the sake of simplicity we assume that $\Omega \setminus S$ is the union of two connected domains $\Omega_1 \cup \Omega_2$. Therefore, ε can be written as

$$\varepsilon = \varepsilon_1 \chi_{\Omega_1} + \varepsilon_2 \chi_{\Omega_2} \tag{22.11}$$

with $\varepsilon_i \in \mathcal{C}^1(\overline{\Omega}_i)$ for $i = 1, 2$.

Denote u^* the applied (true) displacement on Ω (as defined in (22.1)) and $\tilde{\varepsilon}$ the measured deformed optical image given by

$$\tilde{\varepsilon} = \varepsilon \circ (I + u^*)^{-1} \, .$$

Recall that a non-differentiable functional $u \mapsto I(u)$ has a nonempty subgradient if there exists ξ such that

$$I(u + h) - I(u) \geq (\xi, h) \, , \tag{22.12}$$

holds for $||h||$ small enough, which means that $\xi \in \partial I$ with ∂I being the subgradient of I. In order to minimize I, it is sufficient to find one $\xi \in \partial I$; see [139].

The following result holds.

Proposition 22.9 *Let ε verify (22.11), $u^* \in \mathcal{C}^1(\Omega)^d$ be the solution of (22.1), and $\tilde{\varepsilon} = \varepsilon \circ (I + u^*)^{-1}$. Suppose that $\Omega_2 \Subset \Omega$. Then, the functional I defined by*

$$I : \mathcal{C}^1(\Omega)^d \longrightarrow \mathbb{R},$$
$$u \longmapsto I(u) = \int_\Omega |\tilde{\varepsilon} \circ (I + u) - \varepsilon|^2 \, dx \tag{22.13}$$

has a nonempty subgradient. Let ξ in the dual of $\mathcal{C}^1(\Omega)^d$ be given by

$$\xi : h \mapsto 2 \int_\Omega [\tilde{\varepsilon}(x + u) - \varepsilon(x)] h(x) \cdot D\tilde{\varepsilon} \circ (I + u)(x) \, dx \, . \tag{22.14}$$

For $||h||_{\mathcal{C}^1(\Omega)^d}$ small enough, (22.12) holds with $(\,,\,)$ being the duality product between $\mathcal{C}^1(\Omega)^d$ and its dual.

Remark 22.10 *It is worth emphasizing that if ε has no jump, then I is Fréchet differentiable and ξ is its Fréchet derivative.*

Remark 22.11 *Under the assumptions of Proposition 22.9, if u^* is small enough (in $\mathcal{C}^1$-norm), then $\tilde{\varepsilon} = \varepsilon \circ (I + u^*)^{-1}$ can be written as*

$$\tilde{\varepsilon} = \tilde{\varepsilon}_1 + \tilde{\varepsilon}_2 \chi_{\widetilde{\Omega}_2} \tag{22.15}$$

with $\tilde{\varepsilon}_1 \in \mathcal{C}^1(\overline{\Omega})$ and $\tilde{\varepsilon}_2 \in \mathcal{C}_0^1(\Omega)$. In what follows, we shall define $\widetilde{\Omega}_i = (I + u^*)(\Omega_i)$ and $\tilde{f}_i = \varepsilon_i \circ (I + u^*)^{-1}$. To do so, we extend $\tilde{f}_1$ into a function

$\tilde{\varepsilon}_1$ *defined on the whole domain such that* $\tilde{\varepsilon}_1 \in \mathcal{C}^1(\overline{\Omega})$ *and* $\tilde{\varepsilon}_1|_{\widetilde{\Omega}_1} = \widetilde{f}_1$. *Then,* *we set* $\tilde{\varepsilon}_2 = \widetilde{f}_2 - \tilde{\varepsilon}_1$ *on* $\widetilde{\Omega}_2$. *Finally, we extend* $\tilde{\varepsilon}_2$ *into a compactly supported* $\mathcal{C}^1$-*function on the whole domain* Ω.

We first prove the following lemma.

Lemma 22.12 *Let* $u, h \in \mathcal{C}^1(\Omega)^d$ *and let* $\tilde{\varepsilon}$ *be as in (22.15). Then, for* $\|u - u^*\|_{\mathcal{C}^1(\Omega)^d}$ *and* $\|h\|_{\mathcal{C}^1(\Omega)^d}$ *small enough, we have*

$$\int_\Omega [\tilde{\varepsilon}(x + u + h) - \tilde{\varepsilon}(x + u)]^2 \, dx = \int_\Omega \tilde{\varepsilon}_2^2(x+u)|h\cdot\nu|\delta_{\partial\widetilde{\Omega}_2}(x+u) \, dx + o(\|h\|_{\mathcal{C}^1(\Omega)^d}) \,,$$

$$(22.16)$$

where $\delta_{\partial\widetilde{\Omega}_2}$ *is the Dirac distribution on* $\partial\widetilde{\Omega}_2$ *and* $\tilde{\varepsilon}_2$ *is defined in Remark 22.11.*

Proof. We start by decomposing $\tilde{\varepsilon}$ as follows:

$$\int_\Omega [\tilde{\varepsilon}(x + u + h) - \tilde{\varepsilon}(x + u)]^2 \, dx =$$

$$\int_\Omega \left[\left(\tilde{\varepsilon}_1(x+u+h) - \tilde{\varepsilon}_1(x+u)\right) + \left(\tilde{\varepsilon}_2(x+u+h)\chi_{\widetilde{\Omega}_2}(x+u+h) - \tilde{\varepsilon}_2(x+u)\chi_{\widetilde{\Omega}_2}(x+u)\right) \right]^2 \, dx \,.$$

Now, by developing the square, the first term can be estimated by

$$\left| \int_\Omega \left(\tilde{\varepsilon}_1(x + u + h) - \tilde{\varepsilon}_1(x + u) \right)^2 dx \right| \leq \|\tilde{\varepsilon}_1\|_{\mathcal{C}^1(\Omega)}^2 \|h\|_{\mathcal{C}^1(\Omega)^d}^2 \,.$$

Next, we write

$$\tilde{\varepsilon}_2(x+u+h)\chi_{\widetilde{\Omega}_2}(x+u+h) - \tilde{\varepsilon}_2(x+u)\chi_{\widetilde{\Omega}_2}(x+u) = [\tilde{\varepsilon}_2(x + u + h) - \tilde{\varepsilon}_2(x + u)] \chi_{\widetilde{\Omega}_2}(x+u+h)$$

$$+ \left[\chi_{\widetilde{\Omega}_2}(x + u + h) - \chi_{\widetilde{\Omega}_2}(x + u) \right] \tilde{\varepsilon}_2(x + u) \,.$$

Since $(\tilde{\varepsilon}_1(x + u + h) - \tilde{\varepsilon}_1(x + u)) \tilde{\varepsilon}_2(x + u) \in \mathcal{C}_0^1(\Omega)$, Proposition 22.5 yields

$$\left| \int_\Omega \left[\tilde{\varepsilon}_1(x + u + h) - \tilde{\varepsilon}_1(x + u) \right] \left[\chi_{\widetilde{\Omega}_2}(x + u + h) - \chi_{\widetilde{\Omega}_2}(x + u) \right] \tilde{\varepsilon}_2(x + u) \, dx \right|$$

$$\leq C \left(\int_\Omega [h \cdot \nabla\tilde{\varepsilon}_1(x + u)]^2 \, dx \right)^{1/2} \left(\left[\int_\Omega [h \cdot \nu\tilde{\varepsilon}_2(x + u)]^2 \, \delta_{\partial\widetilde{\Omega}_2}(x + u) \, dx \right] + o(\|h\|_{\mathcal{C}^1(\Omega)^d}) \right)^{1/2}$$

$$\leq C\|h\|_{\mathcal{C}^1(\Omega)^d}^2 \,.$$

We now need to handle the last term

$$\int_\Omega \left(\left[\chi_{\widetilde{\Omega}_2}(x + u + h) - \chi_{\widetilde{\Omega}_2}(x + u) \right] \tilde{\varepsilon}_2(x + u) \right)^2 dx$$

$$= \int_\Omega \left| \chi_{\widetilde{\Omega}_2}(x + u + h) - \chi_{\widetilde{\Omega}_2}(x + u) \right| \tilde{\varepsilon}_2(x + u)^2 \, dx \,.$$

Using Proposition 22.5, we obtain that

$$\int_\Omega \left(\left| \chi_{\widetilde{\Omega}_2}(x+u+h) - \chi_{\widetilde{\Omega}_2}(x+u) \right| \tilde{\varepsilon}_2(x+u) \right)^2 dx = \int_\Omega \tilde{\varepsilon}_2^2(x+u)|h\cdot\nu|\delta_{\partial\widetilde{\Omega}_2}(x+u)\, dx + o(\|h\|_{\mathcal{C}^1(\Omega)^d}),$$

which completes the proof of the lemma. $\quad\square$

We are now ready to prove Proposition 22.9.

Proof of Proposition 22.9. If $u \in \mathcal{C}^1(\Omega)^2$ and $h \in \mathcal{C}^1(\Omega)^2$, then we have

$$I(u+h)-I(u) = \int_\Omega [\tilde{\varepsilon}(x+u+h) + \tilde{\varepsilon}(x+u) - 2\varepsilon(x)]\,[\tilde{\varepsilon}(x+u+h) - \tilde{\varepsilon}(x+u)]\, dx,$$

and hence,

$$I(u+h) - I(u) = \int_\Omega [\tilde{\varepsilon}(x+u+h) - \tilde{\varepsilon}(x+u)]^2\, dx$$

$$+ 2\int_\Omega [\tilde{\varepsilon}(x+u) - \varepsilon(x)]\,[\tilde{\varepsilon}(x+u+h) - \tilde{\varepsilon}(x+u)]\, dx.$$

For any $\eta > 0$, let $g^{(\eta)}$ be a smooth, compactly supported function such that

$$\|g^{(\eta)} - [\tilde{\varepsilon} \circ (I + u) - \varepsilon]\|_{L^2(\Omega)} < \eta \quad \text{and} \quad \left| |g^{(\eta)}|_{\mathrm{TV}(\Omega)} - |\tilde{\varepsilon}\circ(I+u)-\varepsilon|_{\mathrm{TV}(\Omega)} \right| < \eta;$$

see [22].

Now, we write

$$\int_\Omega [\tilde{\varepsilon}(x+u) - \varepsilon(x)]\,[\tilde{\varepsilon}(x+u+h) - \tilde{\varepsilon}(x+u)]\, dx$$

$$= \int_\Omega g^\eta(x)\,[\tilde{\varepsilon}(x+u+h) - \tilde{\varepsilon}(x+u)]\, dx$$

$$+ \int_\Omega [\tilde{\varepsilon}(x+u) - \varepsilon(x) - g^\eta(x)]\,[\tilde{\varepsilon}(x+u+h) - \tilde{\varepsilon}(x+u)]\, dx.$$

Let τ_h be the translation operator. Then, τ_h satisfies, for any $h \in \mathcal{C}^1(\Omega)^d$,

$$\|\tau_h[f] - f\|_{L^p} \le C(f)\|h\|_{\mathcal{C}^1(\Omega)^d}, \quad \forall\, f \in \mathrm{SBV}^p(\Omega). \qquad (22.17)$$

Using the Cauchy–Schwarz inequality, we get

$$\left| \int_\Omega [\tilde{\varepsilon}(x+u) - \varepsilon(x) - g^\eta(x)]\,[\tilde{\varepsilon}(x+u+h) - \tilde{\varepsilon}(x+u)]\, dx \right| \le C\eta\|h\|_{\mathcal{C}^1(\Omega)^d},$$
$$(22.18)$$

where C is a constant depending on $\tilde{\varepsilon}$, u, and Ω.

We know that for a certain function ρ such that $\rho(s) \to 0$ when $s \to 0$,

$$\left| \int_\Omega g^\eta(x)\,[\tilde{\varepsilon}(x+u+h) - \tilde{\varepsilon}(x+u)]\, dx - \int_\Omega g^\eta(x)h(x) \cdot D\,(\tilde{\varepsilon}\circ(I+u))\, dx \right|$$
$$\le \|h\|_{\mathcal{C}^1(\Omega)^d}\rho(\|h\|_{\mathcal{C}^1(\Omega)^d}).$$
$$(22.19)$$

Now, we have the following estimate:

$$\left| \int_\Omega g^\eta(x) h(x) \cdot D\left(\tilde{\varepsilon} \circ (I + u)\right) \, dx - \int_\Omega [\tilde{\varepsilon}(x+u) - \varepsilon(x)] h(x) \cdot D\left(\tilde{\varepsilon} \circ (I + u)\right) \, dx \right| \le C'\eta \|h\|_{\mathcal{C}^1(\Omega)^d}.$$
$$(22.20)$$

Indeed, since $\tilde{\varepsilon} \in \mathcal{C}_S^{k,\alpha}\left(\overline{\Omega}\right) \subset \mathrm{SBV}(\Omega)$, $\tilde{\varepsilon} \circ (I + u) \in \mathrm{SBV}(\Omega)$ and we can write the following decomposition of $D\left(\tilde{\varepsilon} \circ (I + u)\right)$ into a continuous part and a jump part on a rectifiable surface S,

$$D\left(\tilde{\varepsilon} \circ (I + u)\right) = \nabla\left(\tilde{\varepsilon} \circ (I + u)\right) \mathcal{H}^d + [\tilde{\varepsilon} \circ (I + u)]\nu_S \mathcal{H}_S^{d-1},$$

we have that

$$\left| \int_\Omega \left[g^\eta(x) - [\tilde{\varepsilon}(x+u) - \varepsilon(x)]\right] h(x) \cdot \nabla\left(\tilde{\varepsilon} \circ (I + u)\right)(x) \, dx \right| \le C_1\eta \|h\|_{\mathcal{C}^1(\Omega)^d}.$$

For the jump part, since S is a rectifiable surface and the function $f^\eta = g^\eta - [\tilde{\varepsilon} \circ (I + u) - \varepsilon]$ is piecewise continuous, it is possible to define a trace $f^\eta|_S$ on the surface S satisfying

$$\|f^\eta|_S\|_{L^1(S)} \le C_2 \|f^\eta\|_{L^1(\Omega)}$$

for some positive constant C_2 depending only on S and Ω. Then we get

$$\left| \int_S f^\eta h(x) \cdot [\tilde{\varepsilon} \circ (I + u)]\nu_S \mathcal{H}_S^{d-1} \right| \le C_3\eta \|h\|_{\mathcal{C}^1(\Omega)^d}$$

for some positive constant C_3 independent of η and h.

Now, the last term $\int_\Omega [\tilde{\varepsilon}(x + u + h) - \tilde{\varepsilon}(x + u)]^2$ can be handled using Lemma 22.12. Doing so, we obtain

$$\int_\Omega [\tilde{\varepsilon}(x + u + h) - \tilde{\varepsilon}(x + u)]^2 = \int_\Omega \tilde{\varepsilon}_2^2(x+u)|h \cdot \nu|\delta_{\partial\widetilde{\Omega}_2}(x+u) + o(\|h\|_{\mathcal{C}^1(\Omega)^d}).$$
$$(22.21)$$

Combining (22.18), (22.19), (22.20), and (22.21), we get that for every $\eta > 0$,

$$\left| I(u+h) - I(u) - 2\int_\Omega [\tilde{\varepsilon}(x+u) - \varepsilon(x)] h(x) \cdot D\tilde{\varepsilon} \circ (I+u)(x) \, dx - \int_\Omega \tilde{\varepsilon}_2^2(x+u)|h\cdot\nu|\delta_{\partial\widetilde{\Omega}_2}(x+u) \, dx \right|$$

$$\le C_4 \|h\|_{\mathcal{C}^1(\Omega)^d}\left(\rho(\|h\|_{\mathcal{C}^1(\Omega)^d}) + \eta\right)$$

for some positive constant C_4 independent of h and η.

Finally, it follows that

$$I(u + h) - I(u) = (\xi, h) + \int_\Omega \tilde{\varepsilon}_2^2(x + u)|h \cdot \nu|\delta_{\partial\widetilde{\Omega}_2}(x + u) \, dx + o(\|h\|_{\mathcal{C}^1(\Omega)^d}),$$

where ξ is defined by (22.14). Hence, either $\int_\Omega \tilde{\varepsilon}_2^2(x + u)|h \cdot \nu|\delta_{\partial\widetilde{\Omega}_2}(x + u) \, dx$ is of order of $\|h\|_{\mathcal{C}^1(\Omega)^d}$ and we get

$$I(u + h) - I(u) \geq (\xi, h)$$

for $\|h\|_{\mathcal{C}^1(\Omega)^d}$ small enough or $\int_{\Omega} \tilde{\varepsilon}_2^2(x+u)|h \cdot \nu|\delta_{\partial \tilde{\Omega}_2}(x+u)\, dx = o(\|h\|_{\mathcal{C}^1(\Omega)^d})$ and in this case, I is Fréchet differentiable and ξ is its Fréchet derivative. The proof of Proposition 22.9 is then complete. $\qquad\square$

Remark 22.13 *The minimization of the functional I gives a reconstruction of u^* on a subdomain $\Omega \subset \Omega_0$. In practical conditions, since u^* is small, Ω is almost the whole domain Ω_0. The values of u^* on the boundary are known and, since u^* is of class $\mathcal{C}^1$, it is possible to deduce the values of u^* on $\Omega_0 \setminus \Omega$ by interpolation.*

22.4 Reconstruction of the Shear Modulus

The problem is now to recover the function μ the reconstructed internal data u. For doing so, we use the method described in Chapter 21. We introduce the operator $\mathcal{F}$

$$u = \mathcal{F}[\mu] = \begin{cases} \nabla \cdot \left(\mu(\nabla u + \nabla u^T)\right) + \nabla p = 0 & \text{in } \Omega_0\,, \\ \nabla \cdot u = 0 & \text{in } \Omega_0\,, \\ u = f & \text{on } \partial\Omega_0\,, \end{cases}$$

and minimize the function $\mathcal{K}$ given by

$$\mathcal{C}^{0,1}(\overline{\Omega_0}) \longrightarrow \mathbb{R}$$

$$\mu \longmapsto \mathcal{K}[\mu] = \int_{\Omega} |\mathcal{F}[\mu] - u|^2\, dx\,.$$

According to Theorem 21.1, $\mathcal{K}$ is Fréchet differentiable and its gradient can be explicitly computed. Let v be the solution of

$$\begin{cases} \nabla \cdot \left(\mu(\nabla v + \nabla v^T)\right) + \nabla q = (\mathcal{F}[\mu] - u) & \text{in } \Omega_0\,, \\ \nabla \cdot v = 0 & \text{in } \Omega_0\,, \\ v = 0 & \text{on } \partial\Omega_0\,. \end{cases}$$

Then,

$$\nabla\mathcal{K}(\mu)[h] = \int_{\Omega_0} h(\nabla v + \nabla v^T) : (\nabla u + \nabla u^T)\, dx\,.$$

The gradient descent method described in Algorithm 21.2.2 can be applied in order to reconstruct μ from u.

22.5 Numerical Illustrations

We take $\Omega = [0,1]^2$ and discretize it on a 300×300 grid, and use Algorithm 4.2 to generate a random Gaussian process to model the optical image ε of the medium as shown in Figure 22.1. Given a shear modulus μ map on Ω (see Figure 22.5 (left)), we solve (22.1) on Ω via a finite element method and compute the displacement field u. We then compute the displaced optical image ε_u by using a spline interpolation approach and proceed to recover the shear modulus from the data ε and ε_u on the grid by the method described in this chapter.

Using (22.10), we first compute the initial guess u_δ for the displacement field as the least-square solution to minimization of J_x. Figure 22.2 shows the kernel w_δ used to compute u_δ. As one can see, δ needs to be large enough so the matrix $w_\delta \star (\nabla \varepsilon \nabla \varepsilon^T)$ is invertible at each point x, which is basically saying that δ must be bigger than the correlation length of ε. Figure 22.3 shows the conditioning of the matrix $w_\delta \star (\nabla \varepsilon \nabla \varepsilon^T)$. Figure 22.4 shows the true displacement u^*, the result of the first order approximation (*i.e.*, the initial guess) u_δ and then the result of the optimization process using a gradient descent method to minimize the discrepancy functional I.

Once the displacement inside the domain is reconstructed, we can recover the shear modulus μ, as shown in Figure 22.5. We reconstruct μ by minimizing the functional $\mathcal{K}$ and using a gradient descent-type method. Note that gradient of $\mathcal{K}$ is computed with the adjoint state method, described previously. As it can be seen in Figure 22.5, the reconstruction is very accurate but not so perfect on the boundaries of Ω, which is due to the poor estimation of u on $\partial \Omega$.
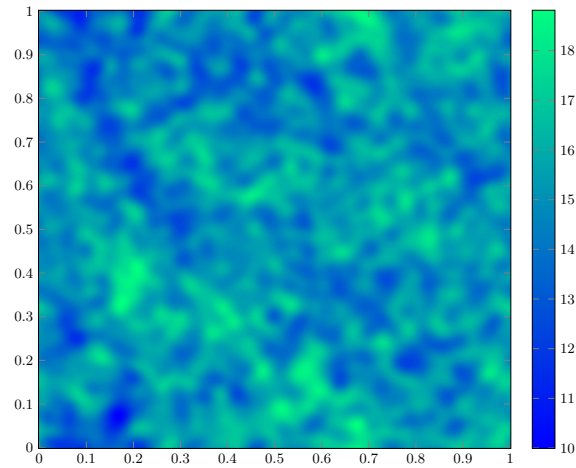
Fig. 22.1. Optical image ε of the medium.
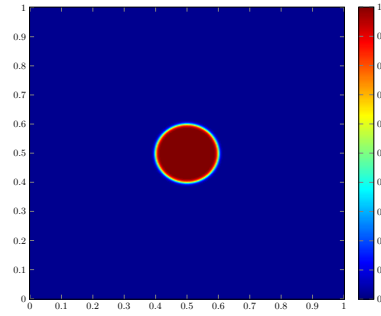
Fig. 22.2. Averaging kernel w_δ.
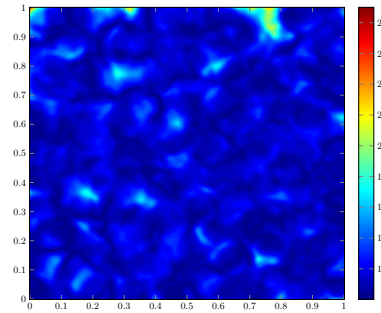
Fig. 22.3. Conditioning of the matrix $w_\delta \star \nabla \varepsilon \nabla \varepsilon^T$.

22.6 Concluding Remarks

In this chapter, we developed an efficient algorithm which gives access not only to stiffness quantitative information of biological tissues but also opens the way to other contrasts such as mechanical anisotropy. In the heart, the muscle fibers have anisotropic mechanical properties. It would be very interesting to detect a change in fiber orientation using OCT elastographic tomography.
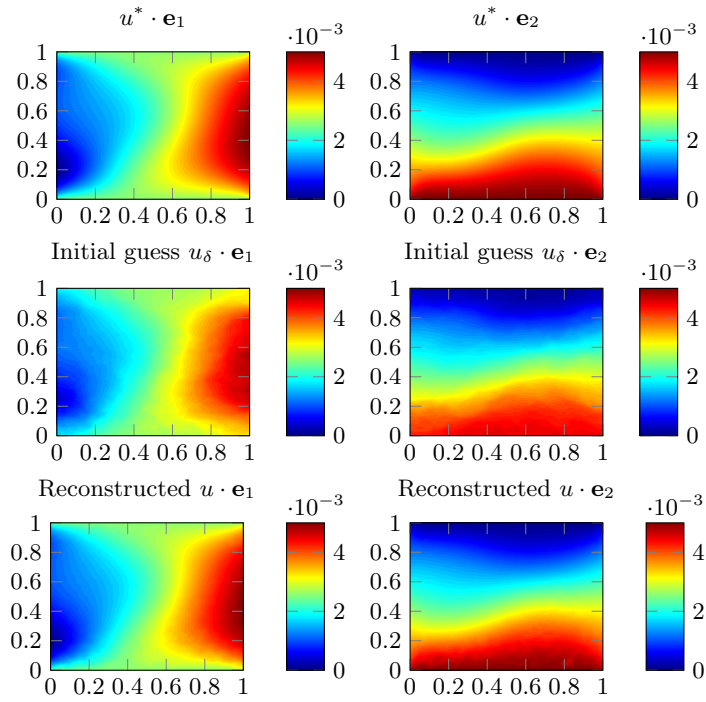
Fig. 22.4. Displacement field and its reconstruction.
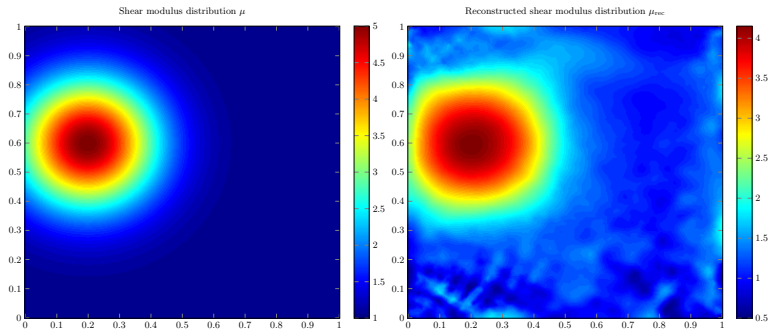
Fig. 22.5. Shear modulus reconstruction.

Part V

Spectroscopic and Nanoparticle Imaging

23

Effective Electrical Tissue Properties

23.1 Introduction

This chapter aims at analytically exhibiting the fundamental mechanisms underlying the fact that effective biological tissue electrical properties and their frequency dependence reflect the tissue composition and physiology. For doing so, a homogenization theory is derived to describe the effective admittivity of cell suspensions. A formula is reported for dilute cases that gives the frequency-dependent effective admittivity with respect to the membrane polarization. Different microstructures are shown to be distinguishable via spectroscopic measurements of the overall admittivity using the spectral properties of the membrane polarization. The Debye relaxation times associated with the membrane polarization tensor are shown to be able to give the microscopic structure of the medium. A natural measure of the admittivity anisotropy is introduced and its dependence on the frequency of applied current is derived. A Maxwell-Wagner-Fricke formula is given for concentric circular cells.

The electric behavior of biological tissue under the influence of an electric field at frequency ω can be characterized by its frequency-dependent effective admittivity $k_{ef} := \sigma_{ef}(\omega) + i\omega\varepsilon_{ef}(\omega)$, where σ_{ef} and ε_{ef} are respectively its effective conductivity and permittivity. Electrical impedance spectroscopy assesses the frequency dependence of the effective admittivity by measuring it across a range of frequencies from a few Hz to hundreds of MHz. Effective admittivity of biological tissues and its frequency dependence vary with tissue composition, membrane characteristics, intra-and extra-cellular fluids and other factors. Hence, the admittance spectroscopy provides information about the microscopic structure of the medium and physiological and pathological conditions of the tissue.

In this chapter, we consider a periodic suspension of identical cells of arbitrary shape. We apply at the boundary of the medium an electric field of frequency ω. The medium outside the cells has an admittivity of $k_0 := \sigma_0 + i\omega\varepsilon_0$. Each cell is composed of an isotropic homogeneous core of admittivity k_0 and a thin membrane of constant thickness δ and admittivity $k_m := \sigma_m + i\omega\varepsilon_m$.

The thickness δ is considered to be very small relative to the typical cell size and the membrane is considered very resistive, *i.e.*, $\sigma_m \ll \sigma_0$. In this context, the potential in the medium passes an effective discontinuity over the cell boundary; the jump is proportional to its normal derivative with a coefficient of the effective thickness, given by $\delta k_0 / k_m$. The normal derivative of the potential is continuous across the cell boundaries.

We use homogenization techniques with asymptotic expansions to derive a homogenized problem and to define an effective admittivity of the medium. We prove a rigorous convergence of the original problem to the homogenized problem via two-scale convergence. For dilute cell suspensions, we use layer potential techniques to expand the effective admittivity in terms of cell volume fraction. Through the effective thickness, $\delta k_0/k_m$, the first-order term in this expansion can be expressed in terms of a membrane polarization tensor, M, that depends on the operating frequency ω. We retrieve the Maxwell-Wagner-Fricke formula for concentric circular-shaped cells. This explicit formula has been generalized in many directions: in three dimension for concentric spherical cells; to include higher power terms of the volume fraction for concentric circular and spherical cells; and to include various shapes such as concentric, confocal ellipses and ellipsoids; see [83, 84, 172, 173, 174, 265, 317, 318, 320].

The imaginary part of M is positive for δ small enough. Its two eigenvalues are maximal for frequencies $1/\tau_i, i = 1, 2$, of order of a few MHz with physically plausible parameters values. This dispersion phenomenon well known by the biologists is referred to as the β-dispersion. The associated characteristic times τ_i correspond to Debye relaxation times. Given this, we show that different microscopic organizations of the medium can be distinguished via $\tau_i, i = 1, 2$, alone. The relaxation times τ_i are computed numerically for different configurations: one circular or elliptic cell, two or three cells in close proximity. The obtained results illustrate the viability of imaging cell suspensions using the spectral properties of the membrane polarization. The Debye relaxation times are shown to be able to give the microscopic structure of the medium.

The chapter is organized as follows. Section 23.2 introduces the problem settings and state our main results. Section 23.3 is devoted to the analysis of the problem. We prove existence and uniqueness results and establish useful *a priori* estimates. In section 23.4 we consider a periodic cell suspension and derive spectral properties of the overall conductivity. In section 23.5 we consider the problem of determining the effective property of a suspension of cells when the volume fraction goes to zero. In section 23.6 we provide numerical examples that support our findings. A few concluding remarks are given in the last section. For simplicity, we only treat the two-dimensional case. Our results in this chapter are from [48].

23.2 Problem Settings and Main Results

The aim of this section is to introduce the problem settings and state the main results of this chapter.

23.2.1 Periodic Domain

We consider the probe domain Ω to be a bounded open set of $\mathbb{R}^2$ of class $\mathcal{C}^2$. The domain contains a periodic array of cells whose size is controlled by ϵ. Let C be a $\mathcal{C}^{2,\eta}$ domain being contained in the unit square $Y = [0,1]^2$, see Figure 23.1. Here, $0 < \eta < 1$ and C represents a reference cell. We divide the domain Ω periodically in each direction in identical squares $(Y_{\epsilon,n})_n$ of size ϵ, where

$$Y_{\epsilon,n} = \epsilon n + \epsilon Y\,.$$

Here, $n \in N_\epsilon := \left\{ n \in \mathbb{Z}^2 : Y_{\epsilon,n} \cap \Omega \neq \emptyset \right\}$.

We consider that a cell $C_{\epsilon,n}$ lives in each small square $Y_{\epsilon,n}$. As shown in Figure 23.4, all cells are identical, up to a translation and scaling of size ϵ, to the reference cell C:

$$\forall n \in N_\epsilon, \quad C_{\epsilon,n} = \epsilon n + \epsilon\, C\,.$$

So are their boundaries $(\Gamma_{\epsilon,n})_{n \in N_\epsilon}$ to the boundary Γ of C:

$$\forall n \in N_\epsilon, \quad \Gamma_{\epsilon,n} = \epsilon n + \epsilon\, \Gamma\,.$$

Let us also assume that all the cells are strictly contained in Ω, that is for every $n \in N_\epsilon$, the boundary $\Gamma_{\epsilon,n}$ of the cell $C_{\epsilon,n}$ does not intersect the boundary $\partial\Omega$:

$$\partial\Omega \cap \Big(\bigcup_{n \in N_\epsilon} \Gamma_{\epsilon,n} \Big) = \emptyset.$$

23.2.2 Electrical Model of the Cell

In this section we consider the reference cell C immersed in a domain D. We apply a sinusoidal electrical current $g \in L_0^2(\partial D)$ with angular frequency ω at the boundary of D.

The medium outside the cell, $D \setminus \overline{C}$, is a homogeneous isotropic medium with admittivity $k_0 := \sigma_0 + i\omega\varepsilon_0$. The cell C is composed of an isotropic homogeneous core of admittivity k_0 and a thin membrane of constant thickness δ with admittivity $k_m := \sigma_m + i\omega\varepsilon_m$. We make the following assumptions :

$$\sigma_0 > 0, \sigma_m > 0, \varepsilon_0 > 0, \varepsilon_m \geq 0\,.$$

If we apply a sinusoidal current $\Re(g(x)e^{i\omega t})$ on the boundary ∂D in the low frequency range 10 MHz, the resulting potential has the form $\Re(\check{u}(x)e^{i\omega t})$ where the complex-valued time-harmonic field $\check{u}$ satisfies

$$\begin{cases} \nabla \cdot (k_0 + (k_m - k_0)\chi(\Gamma^\delta))\nabla \check{u}) = 0 \text{ in } D \,, \\[2mm] k_0 \dfrac{\partial \check{u}}{\partial \nu} = g \qquad\qquad\qquad\qquad\qquad \text{on } \partial D \,, \end{cases}$$

with $\Gamma^\delta := \{x \in C \ : \ \mathrm{dist}(x, \Gamma) < \delta\}$ and $\chi(\Gamma^\delta)$ is the characteristic function of the set Γ^δ.

The membrane thickness δ is considered to be very small compared to the typical size ρ of the cell, *i.e.*, $\delta/\rho \ll 1$. According to the transmission condition, the normal component of the current density $k_0 \dfrac{\partial \check{u}}{\partial \nu}$ can be approximately regarded as continuous across the thin membrane Γ.

We set $\beta := \dfrac{\delta}{k_m}$. Since the membrane is very resistive, *i.e.*, $\sigma_m/\sigma_0 \ll 1$, the potential $\check{u}$ in D undergoes a jump across the cell membrane Γ, which can be approximated at first order by $\beta k_0 \dfrac{\partial \check{u}}{\partial \nu}$.

More precisely, we approximate $\check{u}$ by u defined as the solution of the following equations [296, 297]:

$$\begin{cases} \nabla \cdot k_0 \nabla u = 0 & \text{in } D \setminus \overline{C} \,, \\[2mm] \nabla \cdot k_0 \nabla u = 0 & \text{in } C \,, \\[2mm] k_0 \dfrac{\partial u}{\partial \nu}\Big|_+ = k_0 \dfrac{\partial u}{\partial \nu}\Big|_- & \text{on } \Gamma \,, \\[2mm] u|_+ - u|_- - \beta k_0 \dfrac{\partial u}{\partial \nu} = 0 & \text{on } \Gamma \,, \\[2mm] k_0 \dfrac{\partial u}{\partial \nu}\Big|_{\partial D} = g, \quad \displaystyle\int_{\partial D} g(x)ds(x) = 0, \quad \int_{D \setminus \overline{C}} u(x)dx = 0 \,. \end{cases} \tag{23.1}$$

Equation (23.1) is the starting point of our analysis.

For any open set B in $\mathbb{R}^2$, we denote $\widetilde{W}^{1,2}(B)$ the Sobolev space $W^{1,2}(B)/\mathbb{C}$, which can be represented as

$$\widetilde{W}^{1,2}(B) = \left\{ u \in W^{1,2}(B) : \int_B u(x)dx = 0 \right\} \,.$$

Let $D^+ = D \setminus \overline{C}$ and $D^- = C$. The following result holds.

Lemma 23.1 *There exists a unique solution* $u := (u^+, u^-)$ *in* $\widetilde{W}^{1,2}(D^+) \times W^{1,2}(D^-)$ *to (23.1).*

Proof. To prove the well-posedness of (23.1) we introduce the following Hilbert space: $V := \widetilde{W}^{1,2}(D^+) \times W^{1,2}(D^-)$ equipped with the following natural norm for our problem:
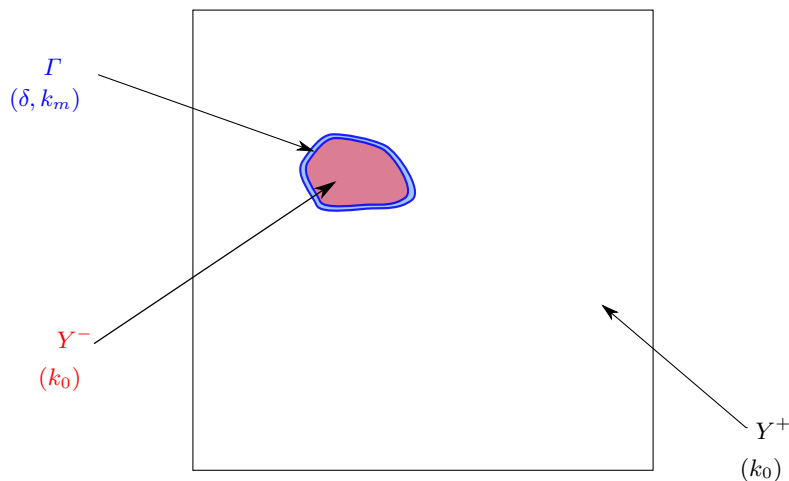
Fig. 23.1. Schematic illustration of a unit period Y.

$$\|u\|_V = \|\nabla u^+\|_{L^2(D^+)} + \|\nabla u^-\|_{L^2(D^-)} + \|u^+ - u^-\|_{L^2(\Gamma)}, \qquad \forall u \in V.$$

We write the variational formulation of (23.1) as follows:

Find $u \in V$ such that for all $v := (v^+, v^-) \in V$:

$$\begin{cases} \displaystyle\int_{D^+} k_0 \nabla u^+(x) \cdot \nabla \overline{v^-}(x)\, dx + \int_{D^-} k_0 \nabla u^+(x) \cdot \nabla \overline{v^-}(x)\, dx \\ \qquad\qquad + \dfrac{1}{\beta k_0} \int_\Gamma (u^+ - u^-)\overline{(v^+ - v^-)}\, d\sigma(x) = \dfrac{1}{k_0} \int_{\partial D} g\overline{v}\, d\sigma(x). \end{cases}$$

Since $\Re(k_0) = \sigma_0 > 0$ and $\Re(\dfrac{1}{\beta k_0}) = \dfrac{\sigma_m \sigma_0 + \varepsilon_m \varepsilon_0}{\delta |k_0|} > 0$, we can apply Lax-Milgram theory to obtain existence and uniqueness of a solution to problem (23.1). $\square$

We conclude this subsection with a few numerical simulations to illustrate the typical profile of the potential u. We consider an elliptic domain D in which lives an elliptic cell. We choose to virtually apply at the boundary of D an electrical current $g = e^{i30r}$.

We use for the different parameters the following realistic values:

- the typical size of eukaryotes cells: $\rho \simeq 10 - 100~\mu$m;
- the ratio between the membrane thickness and the size of the cell: $\delta/\rho = 0.7 \cdot 10^{-3}$;
- the conductivity of the medium and the cell: $\sigma_0 = 0.5$ S.m^{-1};
- the membrane conductivity: $\sigma_m = 10^{-8}$ S.m^{-1};
- the permittivity of the medium and the cell: $\varepsilon_0 = 90 \times 8.85 \cdot 10^{-12}$ F.m^{-1};
- the membrane permittivity: $\varepsilon_m = 3.5 \times 8.85 \cdot 10^{-12}$ F.m^{-1};
- the frequency: $\omega = 10^6$ Hz.

Note that the assumptions of our model $\delta \ll \rho$ and $\sigma_m \ll \sigma_0$ are verified.

The real and imaginary parts of u outside and inside the cell are represented in Figure 23.2.
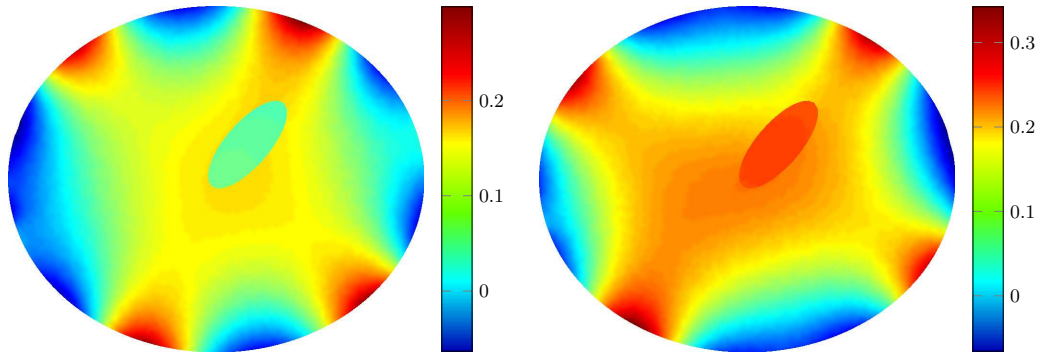
Fig. 23.2. Real and imaginary parts of the potential u outside and inside the cell.

We can observe that the potential jumps across the cell membrane. We plot the outside and inside gradient vector fields; see Figure 23.3.

23.2.3 Governing Equation

We denote by Ω_ϵ^+ the medium outside the cells and Ω_ϵ^- the medium inside the cells:

$$\Omega_\epsilon^+ = \Omega \cap \Big(\bigcup_{n \in N_\epsilon} Y_{\epsilon,n} \setminus \overline{C_{\epsilon,n}} \Big), \quad \Omega_\epsilon^- = \bigcup_{n \in N_\epsilon} C_{\epsilon,n}.$$

Set $\Gamma_\epsilon := \bigcup_{n \in N_\epsilon} \Gamma_{\epsilon,n}$. By definition, the boundaries $\partial\Omega_\epsilon^+$ and $\partial\Omega_\epsilon^-$ of respectively Ω_ϵ^+ and Ω_ϵ^- satisfy:

$$\partial\Omega_\epsilon^+ = \partial\Omega \cup \Gamma_\epsilon, \quad \partial\Omega_\epsilon^- = \Gamma_\epsilon.$$

We apply a sinusoidal current $g(x)\sin(\omega t)$ at $x \in \partial\Omega$, where $g \in L_0^2(\partial\Omega)$. The induced time-harmonic potential u_ϵ in Ω satisfies:
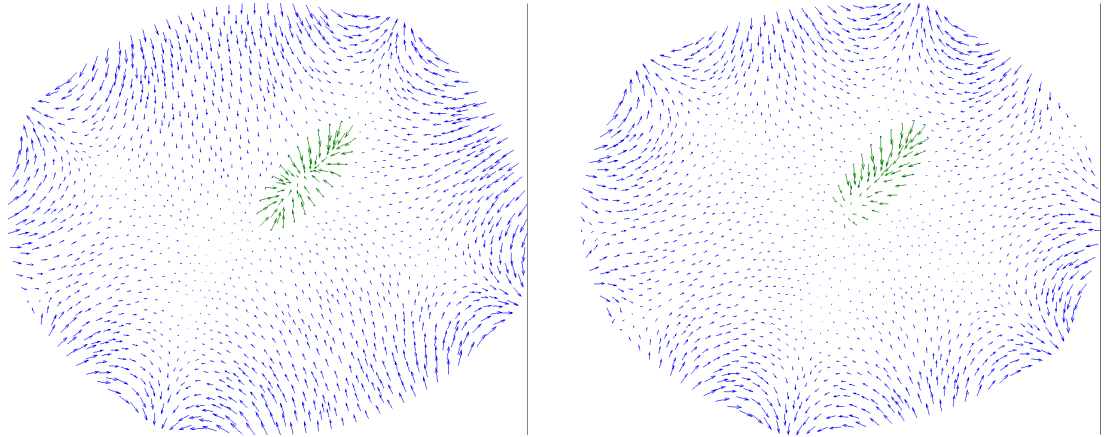
Fig. 23.3. Gradient vector fields of the real and imaginary parts of u.

$$
\begin{cases}
\nabla \cdot k_0 \nabla u_\epsilon^+ = 0 & \text{in } \Omega_\epsilon^+ , \\[2mm]
\nabla \cdot k_0 \nabla u_\epsilon^- = 0 & \text{in } \Omega_\epsilon^- , \\[2mm]
k_0 \dfrac{\partial u_\epsilon^+}{\partial \nu} = k_0 \dfrac{\partial u_\epsilon^-}{\partial \nu} & \text{on } \Gamma_\epsilon , \\[3mm]
u_\epsilon^+ - u_\epsilon^- - \epsilon \beta k_0 \dfrac{\partial u_\epsilon^+}{\partial \nu} = 0 & \text{on } \Gamma_\epsilon , \\[3mm]
k_0 \dfrac{\partial u_\epsilon^+}{\partial \nu}\Big|_{\partial \Omega} = g , \quad \displaystyle\int_{\partial \Omega} g(x)ds(x) = 0, \quad \int_{\Omega_\epsilon^+} u_\epsilon^+(x)dx = 0 ,
\end{cases}
\tag{23.2}
$$

where $u_\epsilon = \begin{cases} u_\epsilon^+ & \text{in } \Omega_\epsilon^+, \\[2mm] u_\epsilon^- & \text{in } \Omega_\epsilon^- . \end{cases}$

Note that the previously introduced constant β, *i.e.*, the ratio between the thickness of the membrane of C and its admittivity, becomes $\epsilon\beta$. Because the cells $(C_{\epsilon,n})_{n \in N_\epsilon}$ are in squares of size ϵ, the thickness of their membranes is given by $\epsilon\delta$ and consequently, a factor ϵ appears.

23.2.4 Main Results

We set $Y^+ := Y \setminus \overline{C}$ and $Y^- := C$ and assume that $\mathrm{dist}(Y^-, \partial Y) = O(1)$. We introduce some function spaces, which will be very useful in the following:
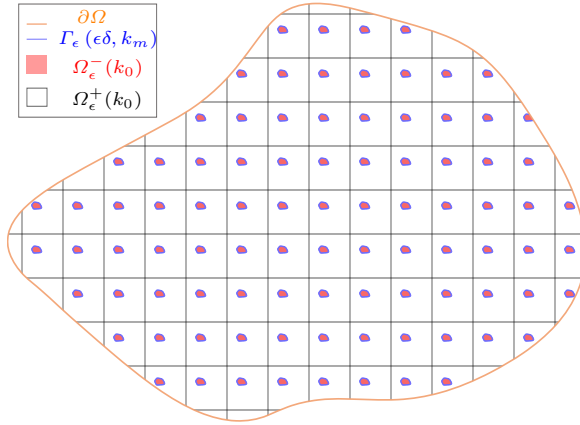
Fig. 23.4. Schematic illustration of the periodic medium Ω.

- $C_\sharp^\infty(D)$ is the space of functions, which are Y - periodic and in $C^\infty(D)$;
- $L_\sharp^2(D)$ is the completion of $C_\sharp^\infty(D)$ in the L^2-norm;
- $W_\sharp^{1,2}(D)$ is the completion of $C_\sharp^\infty(D)$ in the $W^{1,2}$-norm,
- $\widetilde{W}_\sharp^{1,2} = \left\{ u \in W_\sharp^{1,2}(D) : \int_D u = 0 \right\}$;
- $L^2(\Omega, W_\sharp^{1,2}(D))$ is the space of square integrable functions on Ω with values in the space $W_\sharp^{1,2}(D)$;
- $\mathcal{D}(\Omega)$ is the space of infinitely smooth functions with compact support in Ω;
- $\mathcal{D}(\Omega, C_\sharp^\infty(D))$ is the space of infinitely smooth functions with compact support in Ω and with values in the space $C_\sharp^\infty$,

where D is Y, Y^+, Y^- or Γ.

We write the solution u_ϵ as

$$\forall x \in \Omega \ \ u_\epsilon(x) = u_0(x) + \epsilon u_1(x, \frac{x}{\epsilon}) + o(\epsilon) \tag{23.3}$$

with

$$y \longmapsto u_1(x, y) \, Y\text{-periodic and } u_1(x, y) = \begin{cases} u_1^+(x, y) \text{ in } \Omega \times Y^+, \\ u_1^-(x, y) \text{ in } \Omega \times Y^-. \end{cases}$$

Recall the definition of two-scale convergence and a few results of this theory [17, 284].

Definition 23.2 *A sequence of functions u_ϵ in $L^2(\Omega)$ is said to* two-scale converge *to a limit u_0 belonging to $L^2(\Omega \times Y)$ if, for any function ψ in $L^2(\Omega, C_\sharp(Y))$, we have*

$$\lim_{\epsilon \to 0} \int_\Omega u_\epsilon(x)\psi(x, \frac{x}{\epsilon})dx = \int_\Omega \int_Y u_0(x,y)\psi(x,y)dxdy .$$

This notion of two-scale convergence makes sense because of the next compactness theorem.

Theorem 23.3 *From each bounded sequence u_ϵ in $L^2(\Omega)$, we can extract a subsequence, and there exists a limit $u_0 \in L^2(\Omega \times Y)$ such that this subsequence two-scale converges to u_0.*

The following result holds.

Theorem 23.4 (i) *The solution u_ε to (23.2) two-scale converges to u_0 and $\nabla u_\epsilon(x)$ two-scale converges to $\nabla u_0(x) + \chi(Y^+)(y)\nabla_y u_1^+(x,y) + \chi(Y^-)(y)\nabla_y u_1^-(x,y)$, where $\chi(Y^\pm)$ are the characteristic functions of $Y^\pm$.*

(ii) *The function u_0 in (23.3) is the solution in $\widetilde{W}^{1,2}(\Omega)$ to the following homogenized problem:*

$$\begin{cases} \nabla \cdot K^* \nabla u_0(x) = 0 & in\, \Omega\,, \\ \nu \cdot K^* \nabla u_0 = g & on\, \partial\Omega\,, \end{cases} \tag{23.4}$$

where K^*, the effective admittivity of the medium, is given by

$$\forall (i,j) \in \{1,2\}^2, \qquad K_{ij}^* = k_0\left(\delta_{ij} + \int_Y (\chi(Y^+)\nabla w_i^+ + \chi(Y^-)\nabla w_i^-) \cdot e_j\right), \tag{23.5}$$

and the function $(w_i)_{i=1,2}$ are the solutions of the following cell problems:

$$\begin{cases} \nabla \cdot k_0 \nabla(w_i^+(y) + y_i) = 0 & in\, Y^+\,, \\ \nabla \cdot k_0 \nabla(w_i^-(y) + y_i) = 0 & in\, Y^-\,, \\ k_0\dfrac{\partial}{\partial\nu}(w_i^+(y) + y_i) = k_0\dfrac{\partial}{\partial\nu}(w_i^-(y) + y_i) & on\, \Gamma\,, \\ w_i^+ - w_i^- - \beta k_0\dfrac{\partial}{\partial\nu}(w_i^+(y) + y_i) = 0 & on\, \Gamma\,, \\ y \longmapsto w_i(y) \, Y\text{-periodic.} \end{cases} \tag{23.6}$$

(iii) *Moreover, u_1 can be written as*

$$\forall (x,y) \in \Omega \times Y, \quad u_1(x,y) = \sum_{i=1}^2 \frac{\partial u_0}{\partial x_i}(x)w_i(y)\,. \tag{23.7}$$

We define the integral operator $\mathcal{L}_\Gamma : C^{2,\eta}(\Gamma) \to C^{1,\eta}(\Gamma)$, with $0 < \eta < 1$ by

$$\mathcal{L}_\Gamma[\varphi](x) = \frac{1}{2\pi} \int_\Gamma \frac{\partial^2 \log|x - y|}{\partial\nu(x)\partial\nu(y)}\varphi(y)ds(y), \quad x \in \Gamma\,. \tag{23.8}$$

$\mathcal{L}_\Gamma$ is the normal derivative of the double layer potential on $\Gamma = \partial Y^-$.

Since $\mathcal{L}_\Gamma$ is positive, one can prove that the operator $I + \alpha \mathcal{L}_\Gamma : \mathcal{C}^{2,\eta}(\Gamma) \to \mathcal{C}^{1,\eta}(\Gamma)$ is a bounded operator and has a bounded inverse provided that $\Re \alpha > 0$ [141, 283].

As the fraction f of the volume occupied by the cells goes to zero, we derive an expansion of the effective admittivity for arbitrary shaped cells in terms of the volume fraction. We refer to the suspension, as periodic dilute. The following theorem holds.

Theorem 23.5 *The effective admittivity of a periodic dilute suspension admits the following asymptotic expansion:*

$$K^* = k_0 \left(I + fM \left(I - \frac{f}{2}M \right)^{-1} \right) + o(f^2), \tag{23.9}$$

where $\rho = \sqrt{|Y^-|}$, $f = \rho^2$,

$$M = \left(M_{ij} = \beta k_0 \int_{\rho^{-1}\Gamma} \nu_j \psi_i^*(y) ds(y) \right)_{(i,j) \in \{1,2\}^2}, \tag{23.10}$$

and ψ_i^* is defined by

$$\psi_i^* = - \left(I + \beta k_0 \mathcal{L}_{\rho^{-1}\Gamma} \right)^{-1} [\nu_i]. \tag{23.11}$$

Note that $\rho^{-1}\Gamma$ is the rescaled membrane and therefore, M is independent of ρ.

23.3 Analysis of the Problem

For a fixed ϵ, recall that $\widetilde{W}^{1,2}(\Omega_\varepsilon^+)$ denotes the Sobolev space $\widetilde{W}^{1,2}(\Omega_\varepsilon^+)$, which can be represented as

$$\widetilde{W}^{1,2}(\Omega_\varepsilon^+) = \left\{ u \in W^{1,2}(\Omega_\varepsilon^+) : \int_{\Omega_\varepsilon^+} u(x) dx = 0 \right\}. \tag{23.12}$$

The natural functional space for (23.2) is

$$W_\varepsilon := \left\{ u = u^+ \chi(\Omega_\epsilon^+) + u^- \chi(\Omega_\epsilon^-), u^+ \in \widetilde{W}^{1,2}(\Omega_\varepsilon^+), u^- \in W^{1,2}(\Omega_\varepsilon^-) \right\}, \tag{23.13}$$

where $\chi(\omega_\epsilon^\pm)$ are the characteristic functions of the sets $\Omega_\varepsilon^\pm$. We can verify that

$$\|u\|_{W_\varepsilon} = \left(\|\nabla u^+\|_{L^2(\Omega_\varepsilon^+)}^2 + \|\nabla u^-\|_{L^2(\Omega_\varepsilon^-)}^2 + \epsilon \|u^+ - u^-\|_{L^2(\Gamma_\varepsilon)}^2 \right)^{\frac{1}{2}} \tag{23.14}$$

defines a norm on W_ε. In fact, as it will be seen in Proposition 23.7, this norm is equivalent to the standard norm on W_ε which is

$$\|u\|_{\widetilde{W}^{1,2}(\Omega_\varepsilon^+) \times W^{1,2}(\Omega_\varepsilon^-)} = \left(\|\nabla u^+\|_{L^2(\Omega_\varepsilon^+)}^2 + \|\nabla u^-\|_{L^2(\Omega_\varepsilon^-)}^2 + \|u^-\|_{L^2(\Omega_\varepsilon^-)}^2 \right)^{\frac{1}{2}}. \tag{23.15}$$

23.3.1 Existence and Uniqueness of a Solution

Problem (23.2) should be understood through its weak formulation as follows:
For a fixed $\epsilon > 0$, find $u_\varepsilon \in W_\varepsilon$ such that

$$\int_{\Omega_\varepsilon^+} k_0 \nabla u_\varepsilon^+(x) \cdot \nabla \overline{v^+}(x) dx + \int_{\Omega_\varepsilon^-} k_0 \nabla u_\varepsilon^-(x) \cdot \nabla \overline{v^-}(x) ds(x)$$

$$+ \frac{1}{\epsilon \beta} \int_{\Gamma_\varepsilon} (u_\varepsilon^+ - u_\varepsilon^-)(x) \overline{(v^+ - v^-)}(x) ds(x) \quad (23.16)$$

$$= \int_{\partial \Omega} g(x) \overline{v^+}(x) ds(x) \,,$$

for any function $v \in W_\varepsilon$.

Define the sesquilinear form $a_\epsilon(\cdot, \cdot)$ on $W_\epsilon \times W_\epsilon$ by

$$a_\epsilon(u, v) := \int_{\Omega_\varepsilon^+} k_0 \nabla u^+ \cdot \nabla \overline{v^+} dx + \int_{\Omega_\varepsilon^-} k_0 \nabla u^- \cdot \nabla \overline{v^-} dx$$

$$+ \frac{1}{\epsilon \beta} \int_{\Gamma_\varepsilon} (u^+ - u^-) \overline{(v^+ - v^-)} ds \,. \quad (23.17)$$

Associate the following antilinear form on W_ϵ to the boundary data g:

$$\ell(u) := \int_{\partial \Omega} g \overline{u^+} ds. \quad (23.18)$$

The forms a_ϵ and ℓ are bounded. Moreover, a_ϵ is coercive in the following
sense

$$\Re\, k_0^{-1} a_\epsilon(u, u) = \left(\int_{\Omega_\varepsilon^+} |\nabla u^+|^2 dx + \int_{\Omega_\varepsilon^-} |\nabla u^-|^2 dx \right) + \frac{1}{\epsilon \beta'} \int_{\Gamma_\varepsilon} |u^+ - u^-|^2 ds$$

$$\geq C \|u\|_{W_\varepsilon}^2 \,, \quad (23.19)$$

where $\beta' := \delta(\sigma_0 \sigma_m + \omega^2 \varepsilon_0 \varepsilon_m)/(\sigma_m^2 + \omega^2 \varepsilon_m^2)$. Consequently, due to the Lax–
Milgram theorem we have existence and uniqueness for (23.2) for each fixed
ϵ. Note that C can be chosen independent of ϵ.

Proposition 23.6 Let $g \in W_{-1/2}^2(\partial \Omega)$. There exists a unique $u_\epsilon \in W_\varepsilon$ so
that

$$a_\epsilon(u_\epsilon, \varphi) = \ell(\varphi), \quad \forall \varphi \in W_\varepsilon. \quad (23.20)$$

To end this subsection we remark that the two norms on W_ϵ are equivalent.

Proposition 23.7 The norm $\|\cdot\|_{W_\varepsilon}$ is equivalent with the standard norm on
$\widetilde{W}^{1,2}(\Omega_\varepsilon^+) \times W^{1,2}(\Omega_\varepsilon^-)$. Moreover, we can find two positive constants $C_1 < C_2$,
independent of ϵ, so that

$$C_1 \|u\|_{W_\varepsilon} \leq \|u\|_{\widetilde{W}^{1,2} \times W^{1,2}} \leq C_2 \|u\|_{W_\varepsilon} \,, \quad (23.21)$$

for any $u \in \widetilde{W}^{1,2}(\Omega_\varepsilon^+) \times W^{1,2}(\Omega_\varepsilon^-)$.

Similar equivalence relation was established by Monsurrò [276], whose method can be adapted easily to the current case. For the sake of completeness, we present the details in Section 23.7.3.

23.3.2 Energy Estimate

For any sequence of $\epsilon \to 0$, by solving (23.2) we obtain the sequence $u_\varepsilon = u_\varepsilon^+ \chi(\Omega_\epsilon^+) + u_\varepsilon^- \chi(\Omega_\epsilon^-)$. We obtain some *a priori* estimates for u_ε.

We first recall that the extension theorem (Theorem 23.26) yields a Poincaré–Wirtinger inequality in $\widetilde{W}^{1,2}(\Omega_\epsilon^+)$ with a constant independent of ϵ. Indeed, Corollary 23.28 shows that for all $v^+ \in \widetilde{W}^{1,2}(\Omega_\epsilon^+)$, there exists a constant C, independent of ϵ, such that

$$\|v^+\|_{L^2(\Omega_\epsilon^+)} \leq C\|\nabla v^+\|_{L^2(\Omega_\epsilon^+)}\,.$$

Similarly, we can find a constant, independent of ϵ, by applying the trace theorem in $W^{1,2}(\Omega_\epsilon^+)$. Using Corollary 23.29, the following result holds.

Proposition 23.8 *Let $g \in W_{-\frac{1}{2}}^2(\partial\Omega)$. Let $\Omega = \Omega_\varepsilon^+ \cup \Gamma_\varepsilon \cup \Omega_\varepsilon^-$. Then there exist constants C's, independent of ϵ, such that the solution u_ε to (23.2) satisfies the following estimates:*

$$\|\nabla u_\varepsilon^+\|_{L^2(\Omega_\varepsilon^+)} + \|\nabla u_\varepsilon^-\|_{L^2(\Omega_\varepsilon^-)} \leq C|k_0|^{-1}\|g\|_{W_{-1/2}^2(\partial\Omega)}\,, \tag{23.22}$$

$$\|u_\varepsilon^+ - u_\varepsilon^-\|_{L^2(\Gamma_\varepsilon)} \leq C|k_0|^{-1}\sqrt{\epsilon\beta'}\|g\|_{W_{-1/2}^2(\partial\Omega)}\,. \tag{23.23}$$

Proof. By taking $\varphi = u_\varepsilon$ in (23.20), and taking the real part of resultant equality, we get

$$\|\nabla u_\varepsilon^+\|_{L^2(\Omega_\varepsilon^+)}^2 + \|\nabla u_\varepsilon^-\|_{L^2(\Omega_\varepsilon^-)}^2 + (\epsilon\beta')^{-1}\|u_\varepsilon^+ - u_\varepsilon^-\|_{L^2(\Gamma_\varepsilon)}^2 = \Re k_0^{-1}(g, u_\varepsilon^+)\,. \tag{23.24}$$

Here $(g, u_\varepsilon^+) = \int_{\partial\Omega} g\overline{u_\varepsilon^+}\,ds$ is the pairing on $W_{-1/2}^2(\partial\Omega) \times W_{1/2}^2(\partial\Omega)$, for which we have the estimate

$$|(g, u_\varepsilon^+)| \leq \|g\|_{W_{-1/2}^2(\partial\Omega)}\|u_\varepsilon^+\|_{W_{1/2}^2(\partial\Omega)} \leq C_1\|g\|_{W_{-1/2}^2(\partial\Omega)}\|u_\varepsilon^+\|_{W^{1,2}(\Omega_\varepsilon^+)}\,.$$

thanks to the Cauchy–Schwarz inequality and Corollary 23.29. C_1 is here a constant which does not depend on ϵ.

Applying Proposition 23.7 yields

$$|(g, u_\varepsilon^+)| \leq C_2\|g\|_{W_{-1/2}^2(\partial\Omega)}\|u_\varepsilon\|_{W_\epsilon}\,,$$

with a constant C_2 independent of ϵ.

Using this in (23.24) along with the coercivity of a we get

$$\|u_\varepsilon\|_{W_\epsilon} \leq C_3 |k_0|^{-1} \|g\|_{W^2_{-1/2}(\partial\Omega)}\,,$$

where C_3 is still independent of ϵ.

It follows also that

$$|(g, u_\varepsilon^+)| \leq C_2 C_3 |k_0|^{-1} \|g\|_{W^2_{-1/2}(\partial\Omega)}\,.$$

Substituting this estimate into the right-hand side of (23.24), we get the desired estimates. $\square$

Next, we apply the extension theorem (Theorem 23.26) to obtain a bounded sequence in $W^{1,2}(\Omega)$ for which we can extract a converging subsequence.

Proposition 23.9 *Suppose that the same conditions of the previous proposition hold. Let $P^\epsilon : W^{1,2}(\Omega_\varepsilon^+) \to W^{1,2}(\Omega)$ be the extension operator of Theorem 23.26. Then we have*

$$\|P^\epsilon u_\varepsilon^+\|_{W^{1,2}(\Omega)} \leq C |k_0|^{-1} \|g\|_{W^2_{-1/2}(\partial\Omega)}\,, \tag{23.25}$$

and

$$\|P^\epsilon u_\varepsilon^+ - u_\varepsilon\|_{L^2(\Omega)} \leq C\epsilon |k_0|^{-1}(1 + \sqrt{\beta'}) \|g\|_{W^2_{-1/2}(\partial\Omega)}\,. \tag{23.26}$$

Proof. The first inequality is a direct result of (23.52), (23.54) and (23.22). For the second inequality, we have

$$\begin{aligned}
\|P^\epsilon u_\varepsilon^+ - u_\varepsilon\|_{L^2(\Omega)} &= \|P^\epsilon u_\varepsilon^+ - u_\varepsilon^-\|_{L^2(\Omega_\varepsilon^-)} \\
&\leq C\sqrt{\epsilon}\|P^\epsilon u_\varepsilon^+ - u_\varepsilon^-\|_{L^2(\Gamma_\varepsilon)} + C\epsilon\|\nabla(P^\epsilon u_\varepsilon^+ - u_\varepsilon^-)\|_{L^2(\Omega_\varepsilon^-)}\,.
\end{aligned}$$

Here, we have used estimate (23.59). Now, $\|P^\epsilon u_\varepsilon^+ - u_\varepsilon^-\|_{L^2(\Gamma_\varepsilon)} = \|u_\varepsilon^+ - u_\varepsilon^-\|_{L^2(\Gamma_\varepsilon)}$ is bounded in (23.23). The second term is bounded from above by

$$C\epsilon\|\nabla P^\epsilon u_\varepsilon^+\|_{L^2(\Omega_\varepsilon^-)} + C\epsilon\|\nabla u_\varepsilon^-\|_{L^2(\Omega_\varepsilon^-)} \leq C\epsilon(\|\nabla u_\varepsilon^+\|_{L^2(\Omega_\varepsilon^+)} + \|\nabla u_\varepsilon^-\|_{L^2(\Omega_\varepsilon^-)})\,,$$

where we have used again (23.52). This gives the desired estimates. $\square$

Remark 23.10 *As a consequence of the previous proposition, we get a sequence in $W^{1,2}(\Omega)$, namely $P^\epsilon u_\varepsilon^+$, which is a good estimate of u_ε in $L^2(\Omega)$ and from which we can extract a subsequence weakly converging in $W^{1,2}(\Omega)$ and strongly in $L^2(\Omega)$.*

23.4 Homogenization

We follow [20, 21] to derive a homogenized problem for the model with two-scale asymptotic expansions and to prove a rigorous two-scale convergence. In [276], the homogenization of an analogue problem is developed and proved with another method.

23.4.1 Two-Scale Asymptotic Expansions

We assume that the solution u_ϵ admits the following two-scale asymptotic expansion

$$\forall x \in \Omega \ \ u_\epsilon(x) = u_0(x) + \epsilon u_1(x, \frac{x}{\epsilon}) + o(\epsilon),$$

with

$$y \longmapsto u_1(x,y) \ Y\text{-periodic and } u_1(x,y) = \begin{cases} u_1^+(x,y) \text{ in } \Omega \times Y^+, \\ u_1^-(x,y) \text{ in } \Omega \times Y^-. \end{cases}$$

We choose a test function φ_ϵ of the same form as u_ϵ:

$$\forall x \in \Omega, \ \ \varphi_\epsilon(x) = \varphi_0(x) + \epsilon \varphi_1(x, \frac{x}{\epsilon})$$

with φ_0 smooth in Ω, $\varphi_1(x,.)$ Y-periodic,

$$\varphi_1(x,y) = \begin{cases} \varphi_1^+(x,y) \text{ in } \Omega \times Y^+, \\ \varphi_1^-(x,y) \text{ in } \Omega \times Y^-, \end{cases}$$

and $\varphi_1^\pm$ smooth in $\Omega \times Y^\pm$.

In order to prove items (ii) and (iii) in Theorem 23.4, we perform an asymptotic expansion of the variational formulation (23.20). We thus inject these Ansätze in the variational formulation and only consider the order 0 of the different integrals.

At order 0,

$$\nabla u_\epsilon(x) = \nabla u_0(x) + \nabla_y u_1(x, \frac{x}{\epsilon}) + o(\epsilon).$$

Thanks to Lemma 23.11, we then have for the two first integrals:

$$\int_{\Omega_\epsilon^+} k_0 \left(\nabla u_0(x) + \nabla_y u_1^+(x, \frac{x}{\epsilon}) \right) \cdot \left(\nabla \overline{\varphi}_0(x) + \nabla_y \overline{\varphi_1^+}(x, \frac{x}{\epsilon}) \right) dx$$

$$= \int_\Omega \int_{Y^+} k_0 \left(\nabla u_0(x) + \nabla_y u_1^+(x,y) \right) \cdot \left(\nabla \overline{\varphi_0}(x) + \nabla_y \overline{\varphi_1^+}(x,y) \right) dx dy + o(\epsilon)$$

and

$$\int_{\Omega_\epsilon^-} k_0 \left(\nabla u_0(x) + \nabla_y u_1^-(x, \frac{x}{\epsilon}) \right) \cdot \left(\nabla \overline{\varphi_0}(x) + \nabla_y \overline{\varphi_1^-}(x, \frac{x}{\epsilon}) \right) dx$$

$$= \int_\Omega \int_{Y^-} k_0 \left(\nabla u_0(x) + \nabla_y u_1^-(x,y) \right) \cdot \left(\nabla \overline{\varphi_0}(x) + \nabla_y \overline{\varphi_1^-}(x,y) \right) dx dy + o(\epsilon).$$

We write the third integral in (23.17) as the sum, over all squares $Y_{\epsilon,n}$, of integrals on the boundaries $\Gamma_{\epsilon,n}$. We have

$$\frac{1}{\beta\epsilon}\int_{\Gamma_\epsilon}\left(u_\epsilon^+(x,\frac{x}{\epsilon})-u_\epsilon^-(x,\frac{x}{\epsilon})\right)\left(\overline{\varphi_\epsilon^+}(x,\frac{x}{\epsilon})-\overline{\varphi_\epsilon^-}(x,\frac{x}{\epsilon})\right)ds(x)$$

$$=\frac{1}{\beta\epsilon}\sum_{n\in N_\epsilon}\int_{\Gamma_{\epsilon,n}}\left(u_\epsilon^+(x,\frac{x}{\epsilon})-u_\epsilon^-(x,\frac{x}{\epsilon})\right)\left(\overline{\varphi_\epsilon^+}(x,\frac{x}{\epsilon})-\overline{\varphi_\epsilon^-}(x,\frac{x}{\epsilon})\right)ds(x).$$

Let $x_{0,n}$ be the center of $Y_{\epsilon,n}$ for each $n\in N_\epsilon$. We perform Taylor expansions with respect to the variable x around $x_{0,n}$ for all functions $(u_i)_{i\in\{1,2\}}$ and $(\varphi_i)_{i\in\{1,2\}}$ on $Y_{\epsilon,n}$. After the change of variables $\epsilon(y-y_{0,n})=x-x_{0,n}$, we obtain that

$$u_\epsilon(x)=u_0(x_{0,n})+\epsilon u_1(x,y)+\epsilon(y-y_{0,n})\cdot\nabla u_0(x_{0,n})+o(\epsilon),$$

$$\varphi_\epsilon(x)=\varphi_0(x_{0,n})+\epsilon\varphi_1(x,y)+\epsilon(y-y_{0,n})\cdot\nabla\varphi_0(x_{0,n})+o(\epsilon).$$

Consequently, the third integral in the variational formulation (23.20) becomes

$$\frac{\epsilon^2}{\beta}\sum_{n\in N_\epsilon}\int_{\Gamma_n}\left(u_1^+(x_{0,n},y)-u_1^-(x_{0,n},y)\right)\left(\overline{\varphi_1^+}(x_{0,n},y)-\overline{\varphi_1^-}(x_{0,n},y)\right)ds(y).$$

Finally, Lemma 23.11 gives us that

$$\frac{1}{\epsilon\beta}\int_{\Gamma_\epsilon}\left(u_\epsilon^+-u_\epsilon^-\right)\left(\overline{\varphi_\epsilon^+}-\overline{\varphi_\epsilon^-}\right)ds$$

$$=\frac{1}{\beta}\int_\Omega\int_\Gamma\left(u_1^+(x,y)-u_1^-(x,y)\right)\left(\overline{\varphi_1^+}(x,y)-\overline{\varphi_1^-}(x,y)\right)dxds(y)+o(\epsilon).$$

Moreover, we can easily see that

$$\int_{\partial\Omega}g\overline{\varphi_\epsilon^+}ds=\int_{\partial\Omega}g\overline{\varphi_0}ds+o(\epsilon).$$

The order 0 of the variational formula is thus given by

$$\int_\Omega\int_{Y^+}k_0\left(\nabla u_0(x)+\nabla_yu_1^+(x,y)\right)\cdot\left(\nabla\overline{\varphi_0}(x)+\nabla_y\overline{\varphi_1^+}(x,y)\right)dxdy$$

$$+\int_\Omega\int_{Y^-}k_0\left(\nabla u_0(x)+\nabla_yu_1^-(x,y)\right)\cdot\left(\nabla\overline{\varphi_0}(x)+\nabla_y\overline{\varphi_1^-}(x,y)\right)dxdy$$

$$+\frac{1}{\beta}\int_\Omega\int_\Gamma\left(u_1^+(x,y)-u_1^-(x,y)\right)\left(\overline{\varphi_1^+}(x,y)-\overline{\varphi_1^-}(x,y)\right)dxds(y)$$

$$-\int_{\partial\Omega}g(x)\overline{\varphi_0}(x)ds(x)=0.$$

By taking $\varphi_0 = 0$, it follows that

$$\int_\Omega \int_{Y^+} k_0 \left(\nabla u_0(x) + \nabla_y u_1^+(x,y) \right) \cdot \nabla_y \overline{\varphi_1^+}(x,y) dx dy$$

$$+ \int_\Omega \int_{Y^-} k_0 \left(\nabla u_0(x) + \nabla_y u_1^-(x,y) \right) \cdot \nabla_y \overline{\varphi_1^-}(x,y) dx dy$$

$$+ \frac{1}{\beta} \int_\Omega \int_\Gamma \left(u_1^+(x,y) - u_1^-(x,y) \right) \left(\overline{\varphi_1^+}(x,y) - \overline{\varphi_1^-}(x,y) \right) dx ds(y) = 0,$$

which is exactly the variational formulation of the cell problem (23.6) and definition (23.7) of u_1.

By taking $\varphi_1 = 0$, we recover the variational formulation of the homogenized problem (23.4):

$$\int_\Omega \int_{Y^+} k_0 \left(\nabla u_0(x) + \nabla_y u_1^+(x,y) \right) \cdot \nabla \overline{\varphi_0}(x) dx dy$$

$$+ \int_\Omega \int_{Y^-} k_0 \left(\nabla u_0(x) + \nabla_y u_1^-(x,y) \right) \cdot \nabla \overline{\varphi_0}(x) dx dy$$

$$- \int_{\partial\Omega} g(x) \overline{\varphi_0}(x) ds(x) = 0.$$

The following lemma was used in the preceding proof. It follows from [20, Lemma 3.1].

Lemma 23.11 *Let f be a smooth function. We have*

$$(i) \quad \epsilon^2 \sum_{n \in N_\epsilon} \int_{\Gamma_{\epsilon,n}} f(x_{0,n}, y) ds(y) = \int_\Omega \int_\Gamma f(x,y) dx ds(y) + o(\epsilon);$$

$$(ii) \int_{\Omega_\epsilon^+} f(x, \frac{x}{\epsilon}) dx = \int_\Omega \int_{Y^+} f(x,y) dx dy + o(\epsilon)$$

$$and \quad \int_{\Omega_\epsilon^-} f(x, \frac{x}{\epsilon}) dx = \int_\Omega \int_{Y^-} f(x,y) dx dy + o(\epsilon).$$

We prove that the following lemmas hold.

Lemma 23.12 *The homogenized problem admits a unique solution in $\widetilde{W}^{1,2}(\Omega)$.*

Proof. The effective admittivity can be rewritten as

$$K_{ij}^* = k_0 \int_{Y^+} (\nabla w_i^+ + e_i) \cdot (\overline{\nabla w_j^+} + e_j) dx + k_0 \int_{Y^-} (\nabla w_i^- + e_i) \cdot (\overline{\nabla w_j^-} + e_j) dx$$

$$+ \frac{1}{\beta} \int_\Gamma (w_i^+ - w_i^-)(\overline{w_j^+} - \overline{w_j^-}) ds, \quad i,j = 1,2.$$

Therefore, it follows that, for $\xi = (\xi_1, \xi_2) \in \mathbb{R}^2$,

$$K^*\xi \cdot \xi = k_0 \int_{Y^+} |\nabla w^+ + \xi|^2 dx + k_0 \int_{Y^-} |\nabla w^- + \xi|^2 dx + \frac{1}{\beta} \int_{\Gamma} |w^+ - w^-|^2 ds,$$

where $w = \sum_i \xi_i w_i$. Since $\Re\beta \geq 0$,

$$K^*\xi \cdot \xi \geq k_0 \int_{Y^+} |\nabla w^+ + \xi|^2 dx + k_0 \int_{Y^-} |\nabla w^- + \xi|^2 dx.$$

Consequently, it follows from [18] that there exist two positive constants C_1 and C_2 such that

$$C_1|\xi|^2 \leq \Re K^*\xi \cdot \xi \leq C_2|\xi|^2.$$

Standard elliptic theory yields existence and uniqueness of a solution to the homogenized problem in $\widetilde{W}^{1,2}(\Omega)$. $\quad\square$

Lemma 23.13 *The cell problem (23.6) admits a unique solution in $\widetilde{W}_\sharp^{1,2}(Y^+) \times W_\sharp^{1,2}(Y^-)$.*

Proof. Let us introduce the Hilbert space

$$W_\sharp := \left\{ v := v^+\chi(Y^+) + v^-\chi(Y^-), (v^+, v^-) \in \widetilde{W}^{1,2}(Y^+) \times W^{1,2}(Y^-) \right\},$$

equipped with the norm

$$\|v\|_{W_\sharp}^2 = \|\nabla v^+\|_{L^2(Y^+)}^2 + \|\nabla v^-\|_{L^2(Y^-)}^2 + \|v^+ - v^-\|_{L^2(\Gamma)}^2.$$

We consider the following problem:

$$\begin{cases}
\text{Find } w_i \in W_\sharp \text{ such that for all } \varphi \in W_\sharp \\
\displaystyle\int_{Y^+} k_0 \nabla w_i^+(y) \cdot \nabla\overline{\varphi^+}(y) dy + \int_{Y^-} k_0 \nabla w_i^-(y) \cdot \nabla\overline{\varphi^-}(y) dy \\
\displaystyle\quad + \frac{1}{\beta} \int_{\Gamma} \left(w_i^+ - w_i^-\right)(y) \left(\overline{\varphi^+} - \overline{\varphi^-}\right)(y) ds(y) = \\
\displaystyle\quad\quad - \int_{Y^+} k_0 \nabla y_i \cdot \nabla\overline{\varphi^+}(y) dy - \int_{Y^-} k_0 \nabla y_i \cdot \nabla\overline{\varphi^-}(y) dy.
\end{cases} \quad (23.27)$$

Lax–Milgram theorem gives us existence and uniqueness of a solution. Moreover, one can show that this ensures the existence of a unique solution in $\widetilde{W}_\sharp^{1,2}(Y^+) \times W_\sharp^{1,2}(Y^-)$ for the cell problem (23.6). $\quad\square$

We present in the following numerical examples (Figures 23.5–23.8) the real and imaginary parts of the solutions w_1 and w_2 of the cell problems.
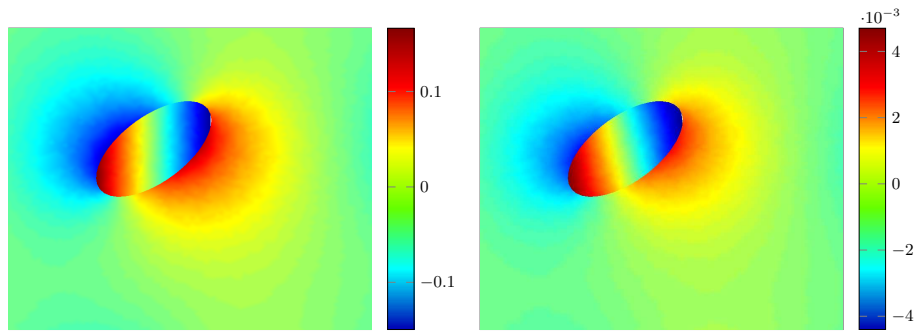
Fig. 23.5. Real and imaginary parts of the cell problem solution w_1.
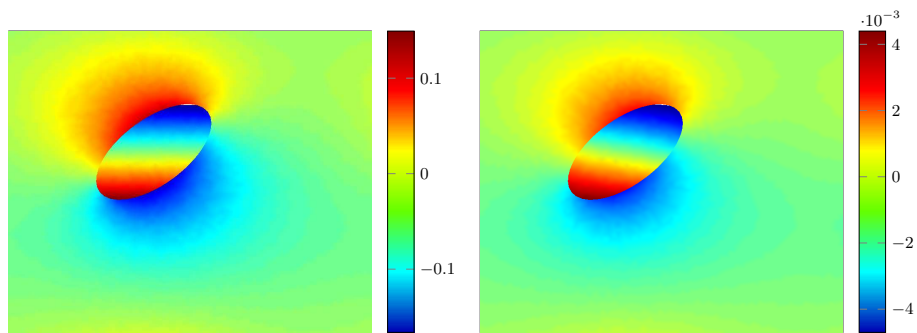
Fig. 23.6. Real and imaginary parts of the cell problem solution w_2.
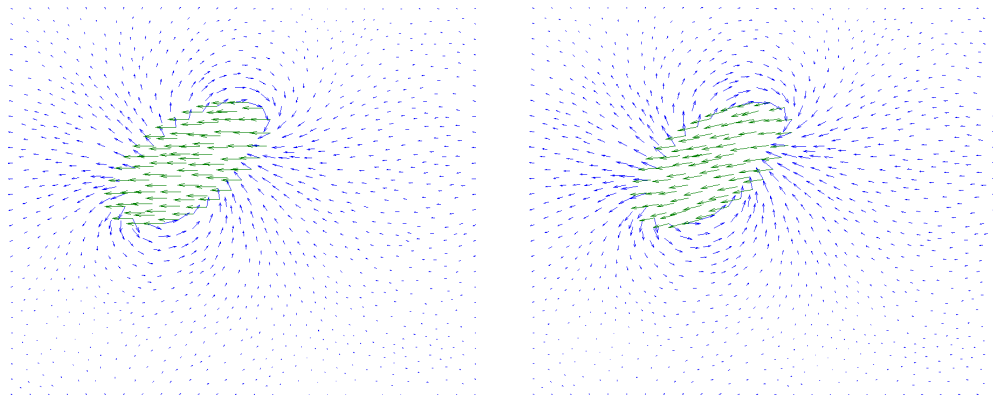
Fig. 23.7. Gradient vector field of the real and imaginary parts of w_1.
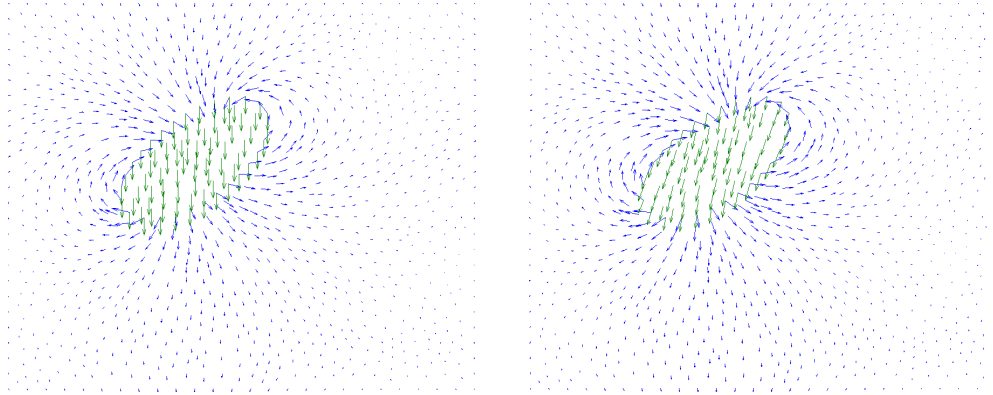
Fig. 23.8. Gradient vector field of the real and imaginary parts of w_2.

23.4.2 Convergence

We present in this section a rigorous proof of the convergence of the original problem to the homogenized one. We use for this purpose the two-scale convergence technique and hence need first of all some bounds on u_ϵ to ensure the convergence.

A Priori Estimates

Theorem 23.14 *The function u_ϵ^+ is uniformly bounded with respect to ϵ in $W^{1,2}(\Omega_\epsilon^+)$, i.e., there exists a constant C, independent of ϵ, such that*

$$\|u_\epsilon^+\|_{W^{1,2}(\Omega_\epsilon^+)} \leq C\,.$$

Proof. Combining (23.22) and Poincaré - Wirtinger inequality, we obtain immediately the wanted result. $\square$

The proof of the following result follows the one of Lemma 2.8 in [276].

Lemma 23.15 *There exists a constant C, which does not depend on ϵ, such that for all $v \in W_\varepsilon$:*
$$\|v^-\|_{L^2(\Omega_\epsilon^-)} \leq C\|v\|_{W_\varepsilon}\,.$$

Proof. We write the norm $\|v^-\|_{L^2(\Omega_\epsilon^-)}$ as a sum over all the cells.

$$\|v^-\|_{L^2(\Omega_\epsilon^-)}^2 = \sum_{n \in N_\epsilon} \|v^-\|_{L^2(Y_{\epsilon,n}^-)}^2 = \sum_{n \in N_\epsilon} \int_{Y_{\epsilon,n}^-} |v^-(x)|^2 dx\,.$$

We perform the change of variable $y = \dfrac{x}{\epsilon}$ and get

$$\|v^-\|^2_{L^2(\Omega_\epsilon^-)} = \epsilon^2 \sum_{n \in N_\epsilon} \int_{Y_n^-} |v_\epsilon^-(y)|^2 dy, \qquad (23.28)$$

where $v_\epsilon^-(y) := v^-(\epsilon y)$ for all $y \in Y^-$ and $Y_n^- = n + Y^-$ with $n \in N_\epsilon$.

Let W denote the following Hilbert space:

$$W := \left\{ v := v^+ \chi(Y^+) + v^- \chi(Y^-), (v^+, v^-) \in \widetilde{W}^{1,2}(Y^+) \times W^{1,2}(Y^-) \right\},$$

equipped with the norm:

$$\|v\|_W^2 = \|\nabla v^+\|^2_{L^2(Y^+)} + \|\nabla v^-\|^2_{L^2(Y^-)} + \|v^+ - v^-\|^2_{L^2(\Gamma)}.$$

We first prove that there exists a constant C_1, independent of ϵ, such that for every $v \in W$:

$$\|v^-\|_{L^2(Y^-)} \le C_1 \|v\|_W. \qquad (23.29)$$

We proceed by contradiction. Suppose that for any $n \in \mathbb{N}^*$, there exists $v_n \in W$ such that

$$\|v_n^-\|_{L^2(Y^-)} = 1 \quad \text{and} \quad \|v_n\|_W \le \frac{1}{n}.$$

Since $\|v_n^-\|_{L^2(Y^-)} = 1$ and $\|\nabla v_n^-\|_{L^2(Y^-)} \le \|v_n\|_W \le \frac{1}{n}$, v_n^- is bounded in $W^{1,2}(Y^-)$. Therefore it converges weakly in $W^{1,2}(Y^-)$. By weak compactness, we can extract a subsequence, still denoted v_n^-, such that v_n^- converges strongly in $L^2(Y^-)$. We denote by l its limit.

Besides, ∇v_n^- converges strongly to 0 in $L^2(Y^-)$. We thus have $\nabla l = 0$ and l constant in Y^-.

By applying in Y^+ the trace theorem and Poincaré–Wirtinger inequality to v_n^+, one also gets that

$$\|v_n^-\|_{L^2(\Gamma)} \le \|v_n^+ - v_n^-\|_{L^2(\Gamma)} + \|v_n^+\|_{L^2(\Gamma)} \le \|v_n^+ - v_n^-\|_{L^2(\Gamma)} + C\|v_n^+\|_{W^{1,2}(Y^+)} \le \frac{C'}{n}.$$

Consequently, v_n^- converges strongly to 0 in $L^2(\Gamma)$ and $l = 0$ on Γ.

We have then $l = 0$ in Y^-, which leads to a contradiction. This proves (23.29).

We can now find an upper bound to (23.28):

$$\|v^-\|^2_{L^2(\Omega_\epsilon^-)} \le \epsilon^2 C_1 \sum_{n \in N_\epsilon} \int_{Y_n^+} |\nabla v_\epsilon^+(y)|^2 dy + \int_{Y_n^-} |\nabla v_\epsilon^-(y)|^2 dy + \int_{\Gamma_n} |v_\epsilon^+(y) - v_\epsilon^-(y)|^2 ds(y).$$

After the change of variable $x = \epsilon y$, one gets

$$\|v^-\|^2_{L^2(\Omega_\epsilon^-)} \le \epsilon C_1 \left(\|\nabla v^+\|^2_{L^2(\Omega_\epsilon^+)} + \|\nabla v^-\|^2_{L^2(\Omega_\epsilon^-)} + \epsilon\|v^+ - v^-\|^2_{L^2(\Gamma_\epsilon)} \right).$$

Since $\epsilon < 1$, there exists a constant C_2, which does not depend on ϵ such that for every $v \in W_\varepsilon$,

$$\|v^-\|_{L^2(\Omega_\epsilon^-)} \leq C_2 \|v\|_{W_\varepsilon} \,,$$

which completes the proof. □

Theorem 23.16 u_ϵ^- *is uniformly bounded in ϵ in $W^{1,2}(\Omega_\epsilon^-)$, i.e., there exists a constant C independent of ϵ, such that*

$$\|u_\epsilon^-\|_{W^{1,2}(\Omega_\epsilon^-)} \leq C \,.$$

Proof. By definition of the norm on W_ε , $\|\nabla u_\epsilon^-\|_{L^2(\Omega_\epsilon^-)}^2 \leq \|u_\epsilon\|_{W_\varepsilon}^2$.
   We thus have with the result of Lemma 23.15:

$$\|u_\epsilon^-\|_{W^{1,2}(\Omega_\epsilon^-)}^2 \leq C_1 \|u_\epsilon\|_{W_\varepsilon}^2 \tag{23.30}$$

with a constant C_1 which does not depend on ϵ.
   Furthermore, using the result of Theorem 23.14, there exists a constant C_2 independent of ϵ such that

$$|a(u_\epsilon, u_\epsilon)| \leq C_2 \,.$$

We use the coercivity of a and get a uniform bound in ϵ of u_ϵ in W_ε. This bound and (23.30) complete the proof.   □

Two-Scale Convergence

We first extend two-scale convergence to sequences defined on periodic surfaces.

Proposition 23.17 *For any sequence u_ϵ in $L^2(\Gamma_\epsilon)$ such that*

$$\epsilon \int_{\Gamma_\epsilon} |u_\epsilon|^2 dx \leq C \,, \tag{23.31}$$

there exists a subsequence, still denoted u_ϵ, and a limit function $u_0 \in L^2(\Omega, L^2(\Gamma))$ such that u_ϵ two-scale converges to u_0 in the sense

$$\lim_{\epsilon \to 0} \epsilon \int_{\Gamma_\epsilon} u_\epsilon(x)\psi(x, \frac{x}{\epsilon})ds(x) = \int_\Omega \int_\Gamma u_0(x,y)\psi(x,y)dxds(y) \,,$$

for any function $\psi \in L^2(\Omega, C_\sharp(Y))$.

Remark 23.18 *If u_ϵ and ∇u_ϵ are bounded in $L^2(\Omega)$, one can prove by using for example [19, Lemma 2.4.9] that u_ϵ verifies the uniform bound (23.31). The two-scale limit on the surface is then the trace on Γ of the two-scale limit of u_ϵ in Ω.*

In order to prove item (i) in Theorem 23.4, we need the following results.

Lemma 23.19 *Let the functions $(u_\epsilon)_\epsilon$ be the sequence of solutions of (23.2). There exist functions $u(x) \in W^{1,2}(\Omega)$, $v^+(x,y) \in L^2(\Omega, W^{1,2}_\sharp(Y^+))$ and $v^-(x,y) \in L^2(\Omega, W^{1,2}_\sharp(Y^-))$ such that, up to a subsequence,*

$$
\begin{pmatrix}
u_\epsilon \\
\chi(\Omega^+_\epsilon)(\frac{x}{\epsilon})\nabla u^+_\epsilon \\
\chi(\Omega^-_\epsilon)(\frac{x}{\epsilon})\nabla u^-_\epsilon
\end{pmatrix}
\quad \text{two-scale converge to} \quad
\begin{pmatrix}
u(x) \\
\chi(\Omega_{Y^+})(y)\Big(\nabla u(x) + \nabla_y v^+(x,y)\Big) \\
\chi(\Omega_{Y^-})(y)\Big(\nabla u(x) + \nabla_y v^-(x,y)\Big)
\end{pmatrix} .
$$

Proof. We denote by $\widetilde{\cdot}$ the extension by zero of functions on Ω^+_ϵ and Ω^-_ϵ in the respective domains Ω^-_ϵ and Ω^+_ϵ.

From the previous estimates, $\widetilde{u}^\pm_\epsilon$ and $\widetilde{\nabla u}^\pm_\epsilon$ are bounded sequences in $L^2(\Omega)$. Up to a subsequence, they two-scale converge to $\tau^\pm(x,y)$ and $\xi^\pm(x,y)$. Since $\widetilde{u}^\pm_\epsilon$ and $\widetilde{\nabla u}^\pm_\epsilon$ vanish in $\Omega^\mp_\epsilon$, so do $\tau^\pm$ and $\xi^\pm$.

Consider $\varphi \in \mathcal{D}(\Omega, C^\infty_\sharp(Y))^2$ such that $\varphi = 0$ for $y \in \overline{Y^-}$. By integrating by parts, it follows that

$$
\epsilon \int_{\Omega^+_\epsilon} \nabla u^+_\epsilon(x) \cdot \overline{\varphi}(x, \frac{x}{\epsilon}) dx = - \int_{\Omega^+_\epsilon} u^+_\epsilon(x) \left(\nabla_y \cdot \overline{\varphi}(x, \frac{x}{\epsilon}) + \epsilon \nabla_x \cdot \overline{\varphi}(x, \frac{x}{\epsilon}) \right) dx .
$$

We take the limit of this equality as $\epsilon \to 0$:

$$
0 = - \int_\Omega \int_{Y^+} \tau^+(x,y) \nabla_y \cdot \overline{\varphi}(x,y) dx dy .
$$

Therefore, τ^+ does not depend on y in Y^+, *i.e.*, there exists a function $u^+ \in L^2(\Omega)$ such that $\tau^+(x,y) = \chi(Y^+)(y)u^+(x)$ for all $(x,y) \in \Omega \times Y$.

Take now $\varphi \in \mathcal{D}(\Omega, C^\infty_\sharp(Y))^2$ such that $\varphi = 0$ for $y \in \overline{Y^-}$ and $\nabla_y \cdot \varphi = 0$. Similarly, we have

$$
\int_{\Omega^+_\epsilon} \nabla u^+_\epsilon(x) \cdot \overline{\varphi}(x, \frac{x}{\epsilon}) dx = - \int_{\Omega^+_\epsilon} u^+_\epsilon(x) \nabla_x \cdot \overline{\varphi}(x, \frac{x}{\epsilon}) dx ,
$$

and thus

$$
\int_\Omega \int_{Y^+} \xi^+(x,y) \cdot \overline{\varphi}(x,y) dx dy = - \int_\Omega \int_{Y^+} u^+(x) \nabla_x \cdot \overline{\varphi}(x,y) dx dy . \quad (23.32)
$$

For φ independent of y, this implies that $u^+ \in W^{1,2}(\Omega)$. Furthermore, if we integrate by parts the right-hand side of (23.32), we get

$$
\int_\Omega \int_{Y^+} \xi^+(x,y) \cdot \overline{\varphi}(x,y) dx dy = \int_\Omega \int_{Y^+} \nabla u^+(x) \cdot \overline{\varphi}(x,y) dx dy ,
$$

for all $\varphi \in \mathcal{D}(\Omega, C_\sharp^\infty(Y^+))^2$ such that $\nabla_y \cdot \varphi = 0$ and $\varphi(x, y) \cdot \nu(y) = 0$ for y on Γ.

Since the orthogonal of the divergence-free functions are exactly the gradients, there exists a function $v^+ \in L^2(\Omega, W_\sharp^{1,2}(Y^+))$ such that

$$\xi^+(x, y) = \chi(Y^+)(y) \left(\nabla u^+(x) + \nabla_y v^+(x, y)\right) ,$$

for all $(x, y) \in \Omega \times Y$.

Likewise, there exist functions $u^- \in W^{1,2}(\Omega)$ and $v^- \in L^2(\Omega, W_\sharp^{1,2}(Y^-))$ such that

$$\tau^-(x, y) = \chi(Y^-)(y)u^-(x), \text{ and } \xi^-(x, y) = \chi(Y^-)(y)\left(\nabla u^-(x) + \nabla_y v^-(x, y)\right) ,$$

for all $(x, y) \in \Omega \times Y$.

Furthermore, thanks to Remark 23.18, we have also

$$\epsilon \int_{\Gamma_\epsilon} u_\epsilon^\pm(x) \overline{\varphi}(x, \frac{x}{\epsilon}) dx \xrightarrow[\epsilon \to 0]{} \int_\Omega \int_\Gamma u^\pm(x, y) \overline{\varphi}(x, y) dx dy ,$$

for all $\varphi \in L^2(\Omega, C_\sharp^\infty(\Gamma))$.

Recall that u_ϵ is a solution to the following variational form:

$$\int_{\Omega_\epsilon^+} k_0 \nabla u_\epsilon^+(x) \cdot \nabla \overline{\varphi_\epsilon^+}(x) dx + \int_{\Omega_\epsilon^-} k_0 \nabla u_\epsilon^-(x) \cdot \nabla \overline{\varphi_\epsilon^-}(x) dx$$

$$+ \frac{1}{\epsilon\beta} \int_{\Gamma_\epsilon} \left(u_\epsilon^+ - u_\epsilon^-\right) \left(\overline{\varphi_\epsilon^+} - \overline{\varphi_\epsilon^-}\right) ds - k_0 \int_{\partial\Omega} g\overline{\varphi_\epsilon^+} ds = 0 ,$$

for all $(\varphi_\epsilon^+, \varphi_\epsilon^-) \in (W^{1,2}(\Omega_\epsilon^+), W^{1,2}(\Omega_\epsilon^-))$.

We multiply this equality by ϵ^2 and take the limit when ϵ goes to 0. The first two terms disappear and we obtain, for all $(\varphi^+, \varphi^-) \in \mathcal{D}(\Omega, C_\sharp^\infty(Y^+)) \times \mathcal{D}(\Omega, C_\sharp^\infty(Y^-))$:

$$\frac{1}{\beta} \int_\Omega \int_\Gamma (u^+(x) - u^-(x))(\overline{\varphi^+}(x, y) - \overline{\varphi^-}(x, y)) dx dy = 0 .$$

Thus $u^+(x) = u^-(x)$ for all $x \in \Omega$, and u_ϵ two-scale converges to $u = u^+ = u^- \in W^{1,2}(\Omega)$. This completes the proof. $\square$

Now, we are ready to prove Theorem 23.4. For this, we need to show that $u = u_0$, that $v^+ - u_1^+$ is constant, and that $v^- - u_1^-$ is constant, where $u_1^\pm$ is defined in (23.7). The uniqueness of a solution for the homogenized problem and the cell problems will then allow us to conclude the convergence, not only up to a subsequence.

Proof of Theorem 23.4. We first want to retrieve the expression of u_1 as a test function of the derivatives of u_0 and the cell problem solutions w_i.

We choose in the variational formulation (23.16) a function φ_ϵ of the form

$$\varphi_\epsilon(x) = \epsilon\varphi_1(x, \frac{x}{\epsilon}),$$

where $\varphi_1 \in \mathcal{D}(\Omega, C_\sharp^\infty(Y^+)) \times \mathcal{D}(\Omega, C_\sharp^\infty(Y^-))$.

Lemma 23.19 shows the two-scale convergence of the following three terms:

$$\int_{\Omega_\epsilon^+} k_0 \nabla u_\epsilon^+(x) \cdot \nabla\overline{\varphi_\epsilon^+}(x)dx \xrightarrow[\epsilon \to 0]{} \int_\Omega\int_{Y^+} k_0 \left(\nabla u(x) + \nabla_y v^+(x,y)\right) \cdot \nabla_y\overline{\varphi_1^+}(x,y)dxdy$$

$$\int_{\Omega_\epsilon^-} k_0 \nabla u_\epsilon^-(x) \cdot \nabla\overline{\varphi_\epsilon^-}(x)dx \xrightarrow[\epsilon \to 0]{} \int_\Omega\int_{Y^-} k_0 \left(\nabla u(x) + \nabla_y v^-(x,y)\right) \cdot \nabla_y\overline{\varphi_1^-}(x,y)dxdy$$

$$\int_{\partial\Omega} g(x)\overline{\varphi_\epsilon^+}(x)ds(x) \xrightarrow[\epsilon \to 0]{} \qquad\qquad 0.$$

We can not take directly the limit as $\epsilon \to 0$ in the last term:

$$\frac{1}{\epsilon\beta}\int_{\Gamma_\epsilon}(u_\epsilon^+(x) - u_\epsilon^-(x))(\overline{\varphi_\epsilon^+}(x) - \overline{\phi_\epsilon^-}(x))ds(x)$$

$$= \frac{1}{\beta}\int_{\Gamma_\epsilon}(u_\epsilon^+(x) - u_\epsilon^-(x))\left(\overline{\varphi_1^+}(x, \frac{x}{\epsilon}) - \overline{\varphi_1^-}(x, \frac{x}{\epsilon})\right)ds(x).$$

Lemma 23.32 ensures the existence of a function $\theta \in (\mathcal{D}(\Omega, W_\sharp^{1,2}(Y^+)) \times \mathcal{D}(\Omega, W_\sharp^{1,2}(Y^-)))^2$ such that for all $\psi \in \widetilde{W}_\sharp^{1,2}(Y^+) \times W_\sharp^{1,2}(Y^-)$:

$$\int_{Y^+} \nabla\psi^+(y) \cdot \overline{\theta^+}(x,y)dy + \int_{Y^-} \nabla\psi^-(y) \cdot \overline{\theta^-}(x,y)dy$$

$$+ \int_\Gamma (\psi^+(y) - \psi^-(y))\left(\overline{\varphi_1^+}(x,y) - \overline{\varphi_1^-}(x,y)\right)ds(y) = 0.$$

$$(23.33)$$

We make the change of variables $y = \frac{x}{\epsilon}$, sum over all $(Y_{\epsilon,n})_{n\in N_\epsilon}$, and choose $\psi = u_\epsilon$ to get

$$\int_{\Gamma_\epsilon}(u_\epsilon^+(x) - u_\epsilon^-(x))\left(\overline{\varphi_1^+}(x, \frac{x}{\epsilon}) - \overline{\varphi_1^-}(x, \frac{x}{\epsilon})\right)ds(x) =$$

$$- \int_{\Omega_\epsilon^+} \nabla u_\epsilon^+(x, \frac{x}{\epsilon}) \cdot \overline{\theta^+}(x, \frac{x}{\epsilon})dx - \int_{\Omega_\epsilon^-} \nabla u_\epsilon^-(x, \frac{x}{\epsilon}) \cdot \overline{\theta^-}(x, \frac{x}{\epsilon})dx.$$

We can now take the limit as ϵ goes to 0:

$$\lim_{\epsilon \to 0}\int_{\Gamma_\epsilon}(u_\epsilon^+(x) - u_\epsilon^-(x))\left(\overline{\varphi_1^+}(x, \frac{x}{\epsilon}) - \overline{\varphi_1^-}(x, \frac{x}{\epsilon})\right)ds(x) =$$

$$- \int_{Y^+}\left(\nabla u(x) + \nabla_y v^+(x,y)\right) \cdot \overline{\theta^+}(x,y)dxdy - \int_{Y^-}\left(\nabla u(x) + \nabla_y v^-(x,y)\right) \cdot \overline{\theta^-}(x,y)dxdy.$$

Finally, the variational formula (23.33) gives us

$$\lim_{\epsilon \to 0} \int_{\Gamma_\epsilon} (u_\epsilon^+(x) - u_\epsilon^-(x)) \left(\overline{\varphi_1^+}(x, \frac{x}{\epsilon}) - \overline{\varphi_1^-}(x, \frac{x}{\epsilon}) \right) ds(x) =$$

$$\int_\Omega \int_\Gamma (v^+(y) - v^-(y)) \left(\overline{\varphi_1^+}(x, y) - \overline{\varphi_1^-}(x, y) \right) ds(y).$$

For $\varphi_\epsilon(x) = \epsilon \varphi_1(x, \frac{x}{\epsilon})$, with $\varphi_1 \in \mathcal{D}(\Omega, C_\sharp^\infty(Y^+)) \times \mathcal{D}(\Omega, C_\sharp^\infty(Y^-))$, the two-scale limit of the variational formula is

$$\int_\Omega \int_{Y^+} k_0 \left(\nabla u(x) + \nabla_y v^+(x, y) \right) \cdot \nabla_y \overline{\varphi_1^+}(x, y) dx dy$$

$$+ \int_\Omega \int_{Y^-} k_0 \left(\nabla u(x) + \nabla_y v^-(x, y) \right) \cdot \nabla_y \overline{\varphi_1^-}(x, y) dx dy$$

$$+ \frac{1}{\beta} \int_\Omega \int_\Gamma (v^+(y) - v^-(y)) \left(\overline{\varphi_1^+}(x, y) - \overline{\varphi_1^-}(x, y) \right) ds(y) = 0.$$

By density, this formula holds true for $\varphi_1 \in L^2(\Omega, W_\sharp^{1,2}(Y^+)) \times L^2(\Omega, W_\sharp^{1,2}(Y^-))$. One can recognize the formula verified by $u_1^\pm$ as the definition of the cell problems. Hence, separation of variables and uniqueness of the solutions of the cell problems in W give

$$v^-(x, y) = u_1^- = \sum_{i=1,2} \frac{\partial u_0}{\partial x_i}(x) w_i^-(y)$$

and, up to a constant:

$$v^+(x, y) = u_1^+ = \sum_{i=1,2} \frac{\partial u_0}{\partial x_i}(x) w_i^+(y).$$

We now choose in the variational formula verified by u_ϵ a test function $\varphi_\epsilon(x) = \varphi(x)$, with $\varphi \in C^\infty(\overline{\Omega})$.

The limit of (23.16) as ϵ goes to 0 is then given by

$$\int_\Omega \int_{Y^+} k_0 \left(\nabla u(x) + \nabla_y v^+(x, y) \right) \cdot \nabla \overline{\varphi}(x) dx dy$$

$$+ \int_\Omega \int_{Y^-} k_0 \left(\nabla u(x) + \nabla_y v^-(x, y) \right) \cdot \nabla \overline{\varphi}(x) dx dy$$

$$+ \int_{\partial \Omega} g(x) \overline{\phi}(x) ds(x) = 0.$$

By density, this formula hold true for $\varphi \in \widetilde{W}^{1,2}(\Omega)$, which leads exactly to the variational formula of the homogenized problem (23.4). Since the solution of this problem is unique in $\widetilde{W}^{1,2}(\Omega)$, u_ϵ converges to u_0, not only up to a subsequence. Likewise, ∇u_ϵ two-scale converges to $\nabla u_0 + \chi(Y^+) \nabla_y u_1^+ + \chi(Y^-) \nabla_y u_1^-$. $\square$

23.5 Effective Admittivity for a Dilute Suspension

In general, the effective admittivity given by formula (23.5) can not be computed exactly except for a few configurations. In this section, we consider the problem of determining the effective property of a suspension of cells when the volume fraction $|Y^-|$ goes to zero. In other words, the cells have much less volume than the medium surrounding them. This kind of suspension is called dilute. Many approximations for the effective properties of composites are based on the solution for dilute suspension.

23.5.1 Computation of the Effective Admittivity

We investigate the periodic double-layer potential used in calculating effective permittivity of a suspension of cells. We introduce the periodic Green function $G_\sharp$, for the Laplace equation in Y, given by

$$\forall x \in Y, \qquad G_\sharp(x) = \sum_{n \in \mathbb{Z}^2 \backslash \{0\}} \frac{e^{i2\pi n \cdot x}}{4\pi^2 |n|^2}.$$

Using the Poisson summation formula

$$\sum_{n \in \mathbb{Z}^2} e^{i2\pi n \cdot x} = \sum_{n \in \mathbb{Z}^2} \delta_0(x + n),$$

where δ_0 is the Dirac mass at 0, it follows that $G_\sharp$ satisfies

$$\Delta G_\sharp = - \sum_{n \in \mathbb{Z}^2} \delta_0(x + n) + 1. \tag{23.34}$$

The constant 1 is the surface of Y. An integration by parts shows that it should be there¡

The following lemma from [69, 66] plays an essential role in deriving the effective properties of a suspension in the dilute limit.

Lemma 23.20 *The periodic Green function $G_\sharp$ admits the following decomposition:*

$$\forall x \in Y, \qquad G_\sharp(x) = \frac{1}{2\pi} \log |x| + R_2(x), \tag{23.35}$$

where R_2 is a smooth function with the following Taylor expansion at 0:

$$R_2(x) = R_2(0) - \frac{1}{4}(x_1^2 + x_2^2) + O(|x|^4). \tag{23.36}$$

Let $L_0^2(\Gamma) := \left\{ \varphi \in L^2(\Gamma) : \int_\Gamma \varphi(x) ds(x) = 0 \right\}$.

We define the periodic double-layer potential $\widetilde{\mathcal{D}}_\Gamma$ of the density function $\varphi \in L_0^2(\Gamma)$:

$$\widetilde{\mathcal{D}}_\Gamma[\varphi](x) = \int_\Gamma \frac{\partial}{\partial\nu_y} G_\sharp(x-y)\varphi(y)ds(y) \, .$$

The double-layer potential has the following properties [66].

Lemma 23.21 *Let $\varphi \in L_0^2(\Gamma)$. $\widetilde{\mathcal{D}}_\Gamma[\varphi]$ verifies:*

$$(i) \qquad\qquad \Delta\widetilde{\mathcal{D}}_\Gamma[\varphi] = 0 \qquad\qquad in\, Y^+ \, ,$$

$$\Delta\widetilde{\mathcal{D}}_\Gamma[\varphi] = 0 \qquad\qquad in\, Y^- \, ,$$

$$(ii) \quad \left.\frac{\partial}{\partial\nu}\widetilde{\mathcal{D}}_\Gamma[\varphi]\right|_+ = \left.\frac{\partial}{\partial\nu}\widetilde{\mathcal{D}}_\Gamma[\varphi]\right|_- \quad on\, \Gamma \, ,$$

$$(iii) \; \left.\widetilde{\mathcal{D}}_\Gamma[\varphi]\right|_\pm = \left(\mp\frac{1}{2}I + \widetilde{\mathcal{K}}_\Gamma\right)[\varphi] \;\; on\, \Gamma \, ,$$

where $\widetilde{\mathcal{K}}_\Gamma : L_0^2(\Gamma) \mapsto L_0^2(\Gamma)$ is the periodic Neumann-Poincaré operator defined by

$$\forall x \in \Gamma, \qquad \widetilde{\mathcal{K}}_\Gamma[\varphi](x) = \int_\Gamma \frac{\partial}{\partial\nu_y} G_\sharp(x-y)\varphi(y)ds(y) \, .$$

The following integral representation formula holds.

Theorem 23.22 *Let w_i be the unique solution in W of (23.6) for $i = 1,2$. w_i admits the following integral representation in Y:*

$$w_i = -\beta k_0 \, \widetilde{\mathcal{D}}_\Gamma \left(I + \beta k_0 \widetilde{\mathcal{L}}_\Gamma\right)^{-1}[\nu_i] \, , \qquad\qquad (23.37)$$

where $\widetilde{\mathcal{L}}_\Gamma = \dfrac{\partial\widetilde{\mathcal{D}}_\Gamma}{\partial\nu}$ and $\nu = (\nu_i)_{i=1,2}$ is the outward unit normal to Γ.

Proof. Let $\varphi := -\beta k_0 \left(I + \beta k_0 \widetilde{\mathcal{L}}_\Gamma\right)^{-1}[\nu_i]$. φ verifies :

$$\int_\Gamma \varphi(y)ds(y) = -\beta k_0 \int_\Gamma \frac{\partial}{\partial\nu}(\widetilde{\mathcal{D}}_\Gamma[\varphi](y) + y_i)ds(y) = 0 \, .$$

The first equality comes from the definition of φ and the second from an integration by parts and the fact that $\widetilde{\mathcal{D}}_\Gamma[\varphi]$ and I are harmonic. Consequently, $\varphi \in L_0^2(\Gamma)$.

We now introduce $V_i := \widetilde{\mathcal{D}}_\Gamma[\varphi]$. V_i is solution to the following problem:

$$\begin{cases} \nabla \cdot k_0 \nabla V_i = 0 & in\, Y^+ \, , \\[2mm] \nabla \cdot k_0 \nabla V_i = 0 & in\, Y^- \, , \\[2mm] \left.k_0 \frac{\partial V_i}{\partial\nu}\right|_+ = \left.k_0 \frac{\partial V_i}{\partial\nu}\right|_- & on\, \Gamma \, , \\[2mm] V_i|_+ - V_i|_- = \varphi & on\, \Gamma \, , \\[2mm] y \longmapsto V_i(y) \; Y\text{-periodic.} \end{cases}$$

We use the definitions of φ and V_i and recognize that the last problem is exactly problem (23.6). The uniqueness of the solution in W gives us the wanted result. $\square$

From Theorem 23.4, the effective admittivity of the medium K^* is given by

$$\forall (i,j) \in \{1,2\}^2, \qquad K_{ij}^* = k_0 \left(\delta_{ij} + \int_Y \nabla w_i \cdot e_j \right).$$

After an integration by parts, we get

$$\forall (i,j) \in \{1,2\}^2, \qquad K_{ij}^* = k_0 \left(\delta_{ij} + \int_{\partial Y} w_i(y) \nu_j(y)\, ds(y) - \int_\Gamma \left(w_i^+ - w_i^- \right) \nu_j(y)\, ds(y) \right).$$

Because of the Y-periodicity of w_i, we have: $\displaystyle \int_{\partial Y} w_i(y) \nu_j\, ds(y) = 0.$

Finally, the integral representation (23.37) gives us that

$$\forall (i,j) \in \{1,2\}^2, \qquad K_{ij}^* = k_0 \left(\delta_{ij} - (\beta k_0) \int_\Gamma \left(I + \beta k_0 \widetilde{\mathcal{L}}_\Gamma \right)^{-1} [\nu_i]\nu_j\, ds(y) \right).$$

We consider that we are in the context of a dilute suspension, *i.e.*, the size of the cell is small compared to the square: $\left| Y^- \right| \ll |Y| = 1$. We perform the change of variable: $z = \rho^{-1} y$ with $\rho = |Y^-|^{\frac{1}{2}}$ and obtain that

$$\forall (i,j) \in \{1,2\}^2, \qquad K_{ij}^* = k_0 \left(\delta_{ij} - \rho^2 (\beta k_0) \int_{\rho^{-1}\Gamma} \left(I + \rho \beta k_0 \widetilde{\mathcal{L}}_\Gamma \right)^{-1} [\nu_i](\rho z) \nu_j(z)\, ds(z) \right),$$

where ν is the outward unit normal to Γ. Note that, in the same way as before, β becomes $\rho\beta$ when we rescale the cell.

Let us introduce $\varphi_i = - \left(I + \rho \beta k_0 \widetilde{\mathcal{L}}_\Gamma \right)^{-1} [\nu_i]$ and $\psi_i(z) = \varphi_i(\rho z)$ for all $z \in \rho^{-1}\Gamma$. From (23.35), we get, for any $z \in \rho^{-1}\Gamma$, after changes of variable in the integrals:

$$\widetilde{\mathcal{L}}_\Gamma[\varphi_i](\rho z) = \frac{\partial}{\partial \nu} \widetilde{\mathcal{D}}_\Gamma[\varphi_i](\rho z) = \rho^{-1} \frac{\partial}{\partial \nu} \mathcal{D}_{\rho^{-1}\Gamma}[\psi_i](z) + \frac{\partial}{\partial \nu(z)} \int_{\rho^{-1}\Gamma} \frac{\partial}{\partial \nu(y)} R_2(\rho z - \rho y) \varphi(\rho y) ds(y).$$

Besides, the expansion (23.36) gives us that the estimate

$$\nabla_y R_2(\rho(z-y)) \cdot \nu(y) = -\frac{\rho}{2}(z-y) \cdot \nu(y) + O(\rho^3),$$

holds uniformly in $z, y \in \rho^{-1}\Gamma$.

We thus get the following expansion:

$$\widetilde{\mathcal{L}}_\Gamma[\varphi_i](\rho z) = \rho^{-1} \mathcal{L}_{\rho^{-1}\Gamma}[\psi_i](z) - \frac{\rho}{2} \sum_{j=1,2} \nu_j \int_{\rho^{-1}\Gamma} \nu_j \psi_i(y) ds(y) + O(\rho^4).$$

Using ψ_i^* defined by (23.11) we get on $\rho^{-1}\Gamma$:

$$\psi_i = \psi_i^* + \beta k_0 \frac{\rho^2}{2} \sum_{j=1,2} \psi_j^* \int_{\rho^{-1}\Gamma} \nu_j(y)\psi_i(y)ds(y) + O(\rho^4). \qquad (23.38)$$

By iterating the formula (23.38), we obtain on $\rho^{-1}\Gamma$ that

$$\psi_i = \psi_i^* + \beta k_0 \frac{\rho^2}{2} \sum_{j=1,2} \psi_j^* \int_{\rho^{-1}\Gamma} \nu_j(y)\psi_i^*(y)ds(y) + O(\rho^4).$$

Therefore, one can easily see that Theorem 23.5 holds.

23.5.2 Case of Concentric Circular-Shaped Cells: the Maxwell-Wagner-Fricke Formula

We consider in this section that the cells are disks of radius r_0. $\rho^{-1}\Gamma$ becomes a circle of radius r_0.

For all $f \in L^2((0,2\pi))$, we introduce the Fourier coefficients:

$$\forall m \in \mathbb{Z}, \quad \hat{f}(m) = \frac{1}{2\pi} \int_0^{2\pi} f(\theta)e^{-im\theta}d\theta,$$

and have then for all $\theta \in (0,2\pi)$:

$$f(\theta) = \sum_{m=-\infty}^{\infty} \hat{f}(m)e^{im\theta}.$$

For $f \in \mathcal{C}^{2,\eta}(\rho^{-1}\Gamma)$ such that $\int_{\rho^{-1}\Gamma} f = 0$, we obtain after a few computations,

$$\forall \theta \in (0,2\pi), \quad (I+\beta k_0\mathcal{L}_{\rho^{-1}\Gamma})^{-1}[f](\theta) = \sum_{m\in\mathbb{Z}\backslash\{0\}} \left(1 + \beta k_0 \frac{|m|}{2r_0}\right)^{-1} \hat{f}(m)\,e^{im\theta}.$$

For $p = 1, 2$, $\psi_p^* = -(I + \beta k_0\mathcal{L}_{\rho^{-1}\Gamma})^{-1}[\nu_p]$ then have the following expression:

$$\forall \theta \in (0,2\pi), \quad \psi_p^* = -\left(1 + \frac{\beta k_0}{2r_0}\right)^{-1} \nu_p.$$

Consequently, we get for $(p,q) \in \{1,2\}^2$:

$$M_{pq} = -\delta_{pq} \frac{\beta k_0 \pi r_0}{1 + \dfrac{\beta k_0}{2r_0}},$$

and hence,

$$\Im M_{pq} = \delta_{pq} \frac{\pi r_0 \delta \omega (\varepsilon_m \sigma_0 - \varepsilon_0 \sigma_m)}{(\sigma_m + \sigma_0 \frac{\delta}{2r_0})^2 + \omega^2 (\varepsilon_m + \varepsilon_0 \frac{\delta}{2r_0})^2} . \tag{23.39}$$

Formula (23.39) is the two-dimensional version of the Maxwell-Wagner-Fricke formula, which gives the effective admittivity of a dilute suspension of spherical cells covered by a thin membrane.

An explicit formula for the case of elliptic cells can be derived by using the spectrum of the integral operator $\mathcal{L}_{\rho^{-1}\Gamma}$, which can be identified by standard Fourier methods [220].

23.5.3 Debye Relaxation Times

From (23.39), it follows that the imaginary part of the membrane polarization attains its maximum with respect to the frequency at

$$\frac{1}{\tau} = \frac{\sigma_m + \sigma_0 \frac{\delta}{2r_0}}{\varepsilon_m + \varepsilon_0 \frac{\delta}{2r_0}} .$$

This dispersion phenomenon due to the membrane polarization is well known and referred to as the β-dispersion. The associated characteristic time τ corresponds to a Debye relaxation time.

For arbitrary-shaped cells, we define the first and second Debye relaxation times, $\tau_i, i = 1, 2$, by

$$\frac{1}{\tau_i} := \arg \max_\omega |\lambda_i(\omega)|, \tag{23.40}$$

where $\lambda_1 \leq \lambda_2$ are the eigenvalues of the imaginary part of the membrane polarization tensor $M(\omega)$. Note that if the cell is of circular shape, $\lambda_1 = \lambda_2$.

As it will be shown later, the Debye relaxation times can be used for identifying the microstructure.

23.5.4 Properties of the Membrane Polarization Tensor and the Debye Relaxation Times

In this subsection, we derive important properties of the membrane polarization tensor and the Debye relaxation times defined respectively by (23.10) and (23.40). In particular, we prove that the Debye relaxation times are invariant with respect to translation, scaling, and rotation of the cell.

First, since the kernel of $\mathcal{L}_{\rho^{-1}\Gamma}$ is invariant with respect to translation, it follows that $M(C, \beta k_0)$ is invariant with respect to translation of the cell C.

Next, from the scaling properties of the kernel of $\mathcal{L}_{\rho^{-1}\Gamma}$ we have

$$M(sC, \beta k_0) = s^2 M(C, \frac{\beta k_0}{s})$$

for any scaling parameter $s > 0$.

Finally, we have

$$M(\mathcal{R}C, \beta k_0) = \mathcal{R}M(C, \beta k_0)\mathcal{R}^T \quad \text{for any rotation } \mathcal{R},$$

where T denotes the transpose.

Therefore, the Debye relaxation times are translation and rotation invariant. Moreover, for scaling, we have

$$\tau_i(hC, \beta k_0) = \tau_i(C, \frac{\beta k_0}{h}), \qquad i = 1, 2, \quad h > 0.$$

Since β is proportional to the thickness of the cell membrane, β/h is nothing else than the real rescaled coefficient β for the cell C. The Debye relaxation times (τ_i) are therefore invariant by scaling.

Since $\mathcal{L}_{\rho^{-1}\Gamma}$ is self-adjoint, it follows that M is symmetric. Finally, we show positivity of the imaginary part of the matrix M for δ small enough.

We consider that the cell contour Γ can be parametrized by polar coordinates. We have, up to $O(\delta^3)$,

$$M + \beta\rho^{-1}|\Gamma|\, I = -\beta^2 \int_{\rho^{-1}\Gamma} \nu \mathcal{L}_{\rho^{-1}\Gamma}[\nu]\, ds, \tag{23.41}$$

where again we have assumed that $\sigma_0 = 1$ and $\varepsilon_0 = 0$.

Recall that

$$\beta = \frac{\delta\sigma_m}{\sigma_m^2 + \omega^2\varepsilon_m^2} - i\frac{\delta\omega\varepsilon_m}{\sigma_m^2 + \omega^2\varepsilon_m^2}.$$

Hence, the positivity of $\mathcal{L}_{\rho^{-1}\Gamma}$ yields

$$\Im M \geq \frac{\delta\omega\varepsilon_m}{2\rho(\sigma_m^2 + \omega^2\varepsilon_m^2)}|\Gamma|I$$

for δ small enough, where I is the identity matrix.

Finally, by using (23.41) one can see that the eigenvalues of $\Im M$ have one maximum each with respect to the frequency. Let $l_i, i = 1, 2, l_1 \geq l_2$, be the eigenvalues of $\int_{\rho^{-1}\Gamma} \nu \mathcal{L}_{\rho^{-1}\Gamma}[\nu]ds$. We have

$$\lambda_i = \frac{\delta\omega\varepsilon_m}{\rho(\sigma_m^2 + \omega^2\varepsilon_m^2)}|\Gamma| - \frac{2\delta^2\omega\varepsilon_m\sigma_m}{(\sigma_m^2 + \omega^2\varepsilon_m^2)^2}l_i, \quad i = 1, 2. \tag{23.42}$$

Therefore, τ_i is the inverse of the positive root of the following polynomial in ω:

$$-\varepsilon_m^4|\Gamma|\omega^4 + 6\delta\varepsilon_m^2\sigma_m l_i\rho\omega^2 + \sigma_m^4|\Gamma|.$$

23.5.5 Anisotropy Measure

Anisotropic electrical properties can be found in biological tissues such as muscles and nerves. In this subsection, based on formula (23.9), we introduce a natural measure of the conductivity anisotropy and derive its dependence on the frequency of applied current. Assessment of electrical anisotropy of muscle may have useful clinical application. Because neuromuscular diseases produce substantial pathological changes, the anisotropic pattern of the muscle is likely to be highly disturbed [135, 178]. Neuromuscular diseases could lead to a reduction in anisotropy for a range of frequencies as the muscle fibers are replaced by isotropic tissue.

Let $\lambda_1 \leq \lambda_2$ be the eigenvalues of the imaginary part of the membrane polarization tensor $M(\omega)$. The function

$$\omega \mapsto \frac{\lambda_1(\omega)}{\lambda_2(\omega)}$$

can be used as a measure of the anisotropy of the conductivity of a dilute suspension. Assume $\varepsilon_0 = 0$. As frequency ω increases, the factor βk_0 decreases. Therefore, for large ω, using the expansions in (23.42) we obtain that

$$\frac{\lambda_1(\omega)}{\lambda_2(\omega)} = 1 + (l_1 - l_2)\frac{2\delta\sigma_m\rho}{(\sigma_m^2 + \omega^2\varepsilon_m^2)|\Gamma|} + O(\delta^2)\,, \qquad (23.43)$$

where $l_1 \leq l_2$ are the eigenvalues of $\int_{\rho^{-1}\Gamma} n\mathcal{L}_{\rho^{-1}\Gamma}[n]ds$.

Formula (23.43) shows that as the frequency increases, the conductivity anisotropy decreases. The anisotropic information can not be captured for

$$\omega \gg \frac{1}{\varepsilon_m}((l_1 - l_2)\frac{2\delta\sigma_m\rho}{|\Gamma|} - \sigma_m^2)^{1/2}\,.$$

23.6 Numerical Simulations

We present in this section some numerical simulations to illustrate the fact that the Debye relaxation times are characteristics of the microstructure of the tissue.

We take realistic values for our parameters, which are the same as those used in Subsection 23.2.2 and let the frequency $\omega \in [10^4, 10^9]$ Hz.

We first want to retrieve the invariant properties of the Debye relaxation times. We consider (Figure 23.9) an elliptic cell (in green) that we translate (to obtain the red one), rotate (to obtain the purple one) and scale (to obtain the dark blue one). We compute the membrane polarization tensor, its imaginary part, and the associated eigenvalues which are plotted as a function of the frequency (Figure 23.10). The frequency is here represented on a logarithmic scale. One can see that for the two eigenvalues the maximum of the curves

occurs at the same frequency, and hence that the Debye relaxation times are identical for the four elliptic cells. Note that the red and green curves are even superposed; this comes from the fact that M is invariant by translation.

Next, we are interested in the effect of the shape of the cell on the Debye relaxation times. We consider for this purpose, (Figure 23.11) a circular cell (in green), an elliptic cell (in red) and a very elongated elliptic cell (in blue). We compute similarly as in the preceding case, the polarization tensors associated to the three cells, take their imaginary part and plot the two eigenvalues of these imaginary parts with respect to the frequency. As shown in Figure 23.12, the maxima occur at different frequencies for the first and second eigenvalues. Hence, we can distinguish with the Debye relaxation times between these three shapes.

Finally, we study groups of one (in green), two (in blue) and three cells (in red) in the unit period (Figure 23.13) and the corresponding polarization tensors for the homogenized media. The associated relaxation times are different in the three configurations (Figure 23.14) and hence can be used to differentiate tissues with different cell density or organization.

These simulations prove that the Debye relaxation times are characteristics of the shape and organization of the cells. For a given tissue, the idea is to obtain by spectroscopy the frequency dependence spectrum of its effective admittivity. One then has access to the membrane polarization tensor and the spectra of the eigenvalues of its imaginary part. One compares the associated Debye relaxation times to the known ones of healthy and cancerous tissues at different levels. Then one would be able to know using statistical tools with which probability the imaged tissue is cancerous and at which level.
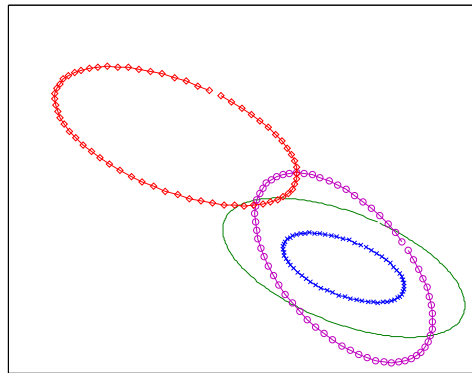
Fig. 23.9. An ellipse translated, rotated and scaled.
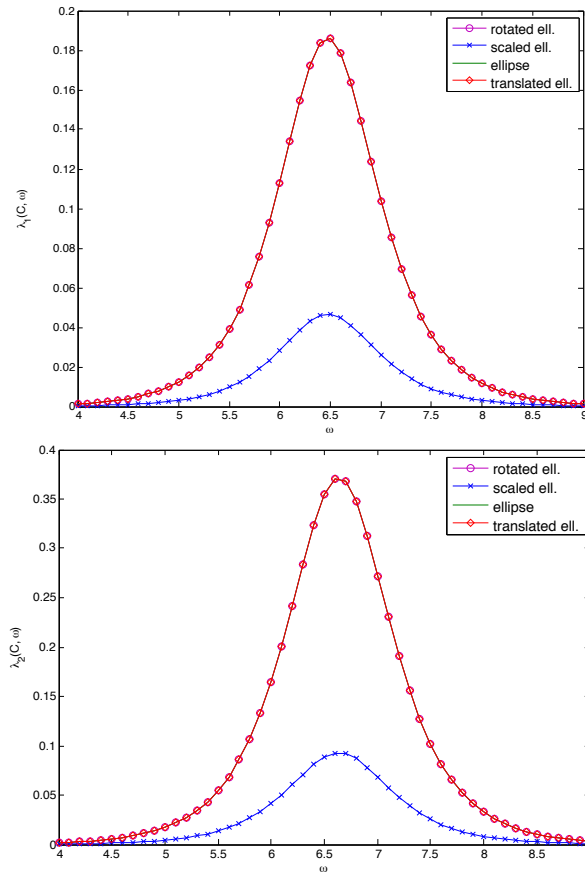
Fig. 23.10. Frequency dependence of the eigenvalues of $\Im M$ for the 4 ellipses in Figure 23.9.
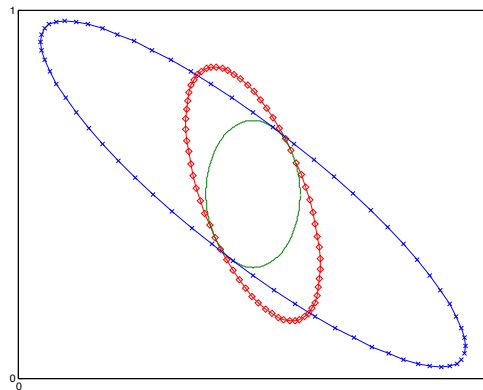
Fig. 23.11. A circle, an ellipse and a very elongated ellipse.
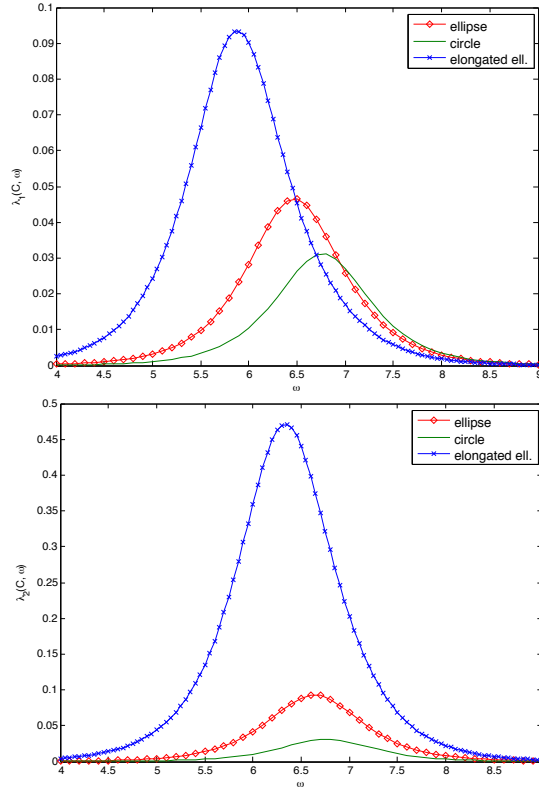
Fig. 23.12. Frequency dependence of the eigenvalues of $\Im M$ for the 3 different cell shapes in Figure 23.11.

23.7 Technical Results

23.7.1 Extension Lemmas

Consider two open sets $U, V \subset \mathbb{R}^2$ with the relation $U \subset V$, and two Sobolev spaces $W^{1,p}(U)$ and $W^{1,p}(V)$, $p \in [1, \infty]$. What we call an *extension operator* is a bounded linear map $P : W^{1,p}(U) \to W^{1,p}(V)$, such that $Pu = u$ a.e. on U for all $u \in W^{1,p}(U)$. In this section, we introduce several extension operators of this kind that are needed in this chapter. They extend functions that are defined on $Y^-, \mathbb{R}^2_+$ and Ω^+_ε, respectively.

Throughout this section, the notation $\mathcal{M}_A(f)$ for a measurable set $A \subset \mathbb{R}^2$ with positive volume and a function $f \in L^1(A)$ denotes the mean value of f in A, that is

$$\mathcal{M}_A(f) = \frac{1}{|A|} \int_A f(x)dx\,. \tag{23.44}$$

We start with an extension operator inside the unit cube Y. Since Y^- has smooth boundary, there exists an extension operator $S : W^{1,p}(Y^+) \to$
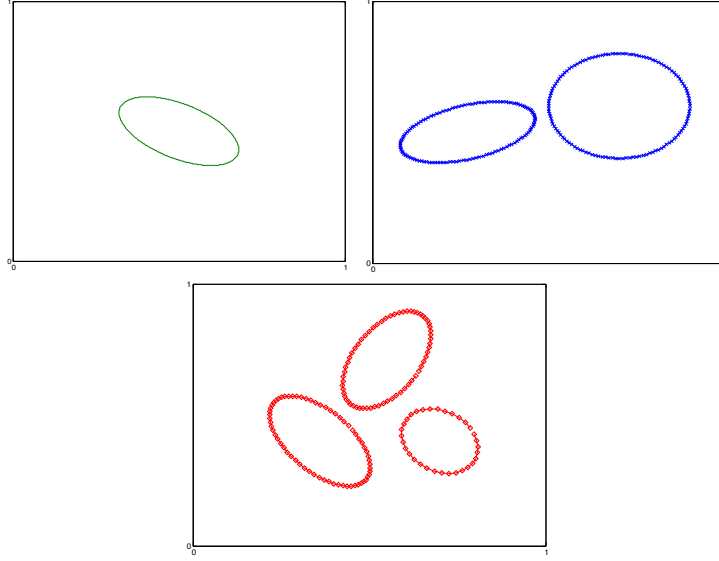
Fig. 23.13. Groups of one, two and three cells.

$W^{1,p}(Y)$ such that for all $f \in W^{1,p}(Y^+)$ and $p \in [1,\infty)$,

$$\|Sf\|_{L^p(Y)} \le C\|f\|_{L^p(Y^+)}, \quad \|Sf\|_{W^{1,p}(Y)} \le C\|f\|_{W^{1,p}(Y^+)}, \qquad (23.45)$$

where C only depends on p and Y^-. Such an S is given in [160, Section 5.4], where the second estimate above is given; the first estimate easily follows from their construction as well. Cioranescu and Saint Paulin [138] constructed another extension operator which refines the second estimate above. For the reader's convenience, we state and prove their result in the following. Similar results can be found in [204] as well.

Theorem 23.23 *Let Y, Y^+ and Y^- be as defined in Section 23.2; in particular, ∂Y^- is smooth. Then there exists an extension operator $P : W^{1,p}(Y^+) \to W^{1,p}(Y)$ satisfying that for any $f \in W^{1,p}(Y^+)$ and $p \in [1,\infty)$,*

$$\|\nabla Pf\|_{L^p(Y)} \le C\|\nabla f\|_{L^p(Y^+)}, \quad \|Pf\|_{L^p(Y)} \le C\|f\|_{L^p(Y^+)}, \qquad (23.46)$$

where C only depends on the dimension and the set Y^-.

Proof. Recall the mean operator $\mathcal{M}$ in (23.44) and the extension operator S in (23.45). Given f, we define Pf by

$$Pf = \mathcal{M}_{Y^+}(f) + S(f - \mathcal{M}_{Y^+}(f)). \qquad (23.47)$$

Then by setting $\psi = f - \mathcal{M}_{Y^+}(f)$, we have that

$$\|\nabla Pf\|_{L^p(Y)} = \|\nabla S\psi\|_{L^p(Y)} \le C\|\psi\|_{W^{1,p}(Y^+)} \le C\|\nabla \psi\|_{L^p(Y^+)} = C\|\nabla f\|_{L^p(Y^+)}.$$
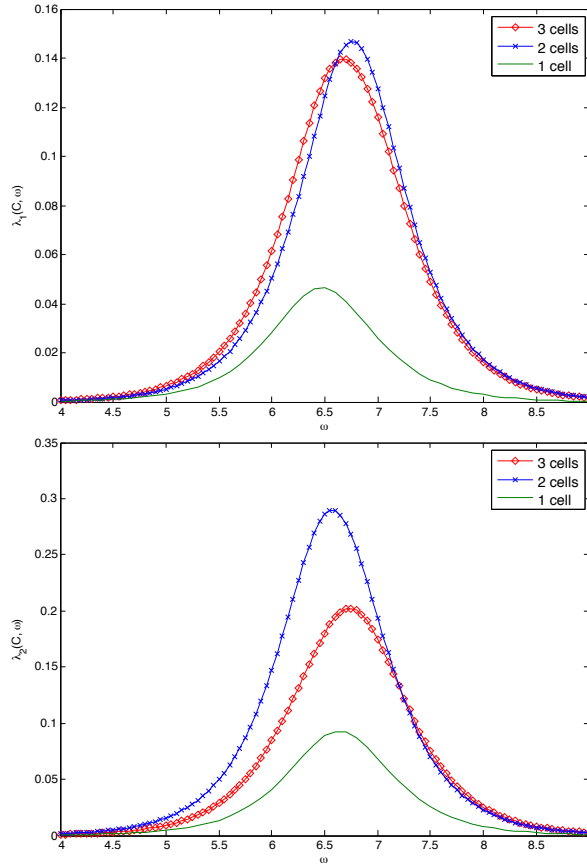
Fig. 23.14. Frequency dependence of the eigenvalues of $\Im M$ in the 3 different cases.

In the second inequality above, we used the Poincaré–Wirtinger inequality for ψ and the fact that ψ is mean-zero on Y^+. The L^2 bound of Pf follows from the observation

$$\|\mathcal{M}_{Y^+}(f)\|_{L^p(Y)} \leq \left(\frac{|Y|}{|Y^+|} \right)^{\frac{1}{p}} \|f\|_{L^p(Y^+)}$$

and the L^p estimate of Sf in (23.45). This completes the proof. □

Applying the extension operator on each translated cube in $\mathbb{R}_2^+$, we get the following.

Corollary 23.24 *Recall the definition of Y_n, Y_n^+ and Y_n^- in section 23.2. Abuse notations and define*

$$(Pu)|_{Y_n} = P(u|_{Y_n^+}), \quad n \in \mathbb{Z}^2, u \in W_{\mathrm{loc}}^{1,p}(\mathbb{R}_2^+). \tag{23.48}$$

Then P is an extension operator from $W_{\mathrm{loc}}^{1,p}(\mathbb{R}_2^+)$ to $W_{\mathrm{loc}}^{1,p}(\mathbb{R}^2)$. Further, with the same positive constant C in (23.46) and for any $n \in \mathbb{Z}^2$, we have

$$\|\nabla Pu\|_{L^p(Y_n)} \leq C\|\nabla u\|_{L^p(Y_n^-)}, \quad \|Pu\|_{L^p(Y_n)} \leq C\|u\|_{L^p(Y_n^-)}. \qquad (23.49)$$

Corollary 23.25 *For each $\epsilon > 0$, define P^ϵ as follows: for any $u \in W_{\mathrm{loc}}^{1,p}(\epsilon \mathbb{R}_2^+)$, $P^\epsilon u$ is defined on ϵY_n by*

$$P^\epsilon u(x) = \epsilon P\tilde{u}(\frac{x}{\epsilon}), \qquad (23.50)$$

where $\tilde{u}(x) = \epsilon^{-1}u(\epsilon x)$ and P is as in (23.49). Then P^ϵ is an extension operator from $W_{\mathrm{loc}}^{1,p}(\epsilon \mathbb{R}_2^+)$ to $W_{\mathrm{loc}}^{1,p}(\epsilon \mathbb{R}^2)$ which satisfies that for any $n \in \mathbb{Z}^2$,

$$\|\nabla P^\epsilon u\|_{L^p(\epsilon Y_n)} \leq C\|\nabla u\|_{L^p(\epsilon Y_n^-)}, \quad \|P^\epsilon u\|_{L^p(\epsilon Y_n)} \leq C\|u\|_{L^p(\epsilon Y_n^-)}, \quad (23.51)$$

where the constant C does not depend on ϵ.

Finally, we define the extension operator from $W^{1,p}(\Omega_\varepsilon^+)$ to $W^{1,p}(\Omega)$.

Theorem 23.26 *Let $\Omega_\varepsilon^\pm$ be defined as in Section 23.2. Define the linear operator P^ϵ as follows: for $u \in W^{1,p}(\Omega_\varepsilon^+)$, let $P^\epsilon u$ be given by (23.50) in $\Omega \setminus \overline{\Omega_\varepsilon^+}$, and let $P^\epsilon u = u$ in Ω_ε^+. Then P^ϵ is an extension operator from $W^{1,p}(\Omega_\varepsilon^+)$ to $W^{1,p}(\Omega)$ and it satisfies*

$$\|\nabla P^\epsilon u\|_{L^p(\Omega)} \leq C\|\nabla u\|_{L^p(\Omega_\varepsilon^+)}, \quad \|P^\epsilon u\|_{L^p(\Omega)} \leq C\|u\|_{L^p(\Omega_\varepsilon^+)}, \qquad (23.52)$$

where the constants C's do not depend on ϵ.

Proof. Since P^ϵ satisfies the estimates (23.51) uniformly in $\cup_n \epsilon Y_n$, we have the following:

$$\|\nabla P^\epsilon u\|_{L^p(\Omega)}^p = \|\nabla u\|_{L^p(K_\epsilon)}^p + \sum_n \|\nabla P^\epsilon u\|_{L^p(\epsilon Y_n)}^p$$

$$\leq C\|\nabla u\|_{L^p(\Omega_\varepsilon^+)}^p.$$

This completes the proof of the first estimate in (23.52). The second estimate follows in the same manner, completing the proof. □

23.7.2 Poincaré–Wirtinger Inequality

Our next goal is to derive a Poincaré–Wirtinger inequality for functions in $W^{1,2}(\Omega_\varepsilon^+)$ with a constant independent of ϵ. The following fact of the fluctuation of a function is useful.

Lemma 23.27 *Let $X \subset \mathbb{R}^2$ be an open bounded domain with positive volume and $f \in L^1(X)$. Assume that $X_1 \subset X$ is a subset with positive volume, then we have*

$$\|f - \mathcal{M}_{X_1}(f)\|_{L^2(X_1)} \leq \|f - \mathcal{M}_X(f)\|_{L^2(X)}. \qquad (23.53)$$

Proof. To simplify notations, let f_1 be the restriction of f on X_1, $m_1 = \mathcal{M}_{X_1}(f_1)$ and $\theta_1 = |X_1|/|X|$. Similarly, let f_2 be the restriction of f on $X_2 = X \setminus X_1$, $m_2 = \mathcal{M}_{X_2}(f_2)$. Let $m = \mathcal{M}_X(f)$. Then we have that

$$f - m = \begin{cases} f_1 - m_1 + (1 - \theta)(m_1 - m_2), & x \in X_1 \,, \\ f_2 - m_2 + \theta(m_2 - m_1), & x \in X_2 \,. \end{cases}$$

Then basic computation plus the observation that $f_i - m_i$ integrates to zero on X_i for $i = 1, 2$ yield the following:

$$\|f - m\|_{L^2(X)}^2 = \|f_1 - m_1\|_{L^2(X_1)}^2 + \|f_2 - m_2\|_{L^2(X_2)}^2 + (1 - \theta)\theta|X|(m_2 - m_1)^2 \,.$$

Since the items on the right-hand side are all non-negative, we obtain (23.53). □

Corollary 23.28 *Assume the same conditions as in Theorem 23.26. Then for any $u \in W^{1,2}(\Omega_\varepsilon^+)$, we have that*

$$\|u\|_{L^2(\Omega_\varepsilon^+)} \le C\|\nabla u\|_{L^2(\Omega_\varepsilon^+)} \,, \tag{23.54}$$

where the constant C does not depend on ϵ.

Proof. Thanks to Theorem 23.26, we extend u to $P^\epsilon u$ which is in $W^{1,2}(\Omega)$. Use (23.53) and the fact that $\mathcal{M}_{\Omega_\varepsilon^+}(u) = 0$ to get

$$\|u\|_{L^2(\Omega_\varepsilon^+)} \le \|P^\epsilon u - \mathcal{M}_\Omega(P^\epsilon u)\|_{L^2(\Omega)} \,.$$

Now apply the standard Poincaré–Wirtinger inequality for functions in $W^{1,2}(\Omega)$, and then use (23.52). We get

$$\|P^\epsilon u - \mathcal{M}_\Omega(P^\epsilon u)\|_{L^2(\Omega)} \le C\|\nabla P^\epsilon u\|_{L^2(\Omega)} \le C\|\nabla u\|_{L^2(\Omega_\varepsilon^+)} \,.$$

The constant C depends on Ω and the parameters stated in Theorem 23.26 but not on ϵ. The proof is now complete. □

Another corollary of the extension lemma is that we have the following uniform estimate when taking the trace of $u \in W_\varepsilon$ on the fixed boundary $\partial\Omega$.

Corollary 23.29 *Assume the same conditions as in Theorem 23.26. Then there exists a constant C depending on Ω and the parameters as stated in Theorem 23.26 but independent of ϵ such that*

$$\|u\|_{W_{1/2}^2(\partial\Omega)} \le C\|\nabla u\|_{L^2(\Omega_\varepsilon^+)} \,, \tag{23.55}$$

for any $u \in W^{1,2}(\Omega_\varepsilon^+)$.

Proof. Thanks to Theorem 23.26 we extend u to $P^\epsilon u$ which is in $W^{1,2}(\Omega)$. The trace inequality on Ω shows

$$\|P^\epsilon u\|_{W_{1/2}^2(\partial\Omega)} \le C(\Omega)\|P^\epsilon u\|_{W^{1,2}(\Omega)} \,. \tag{23.56}$$

The desired estimate then follows from (23.52) and (23.54). □

23.7.3 Equivalence of the Two Norms on W_ε

In this section, we prove Proposition 23.7 which establishes the equivalence between the two norms on W_ε. We essentially follow [276].

The first inequality of the proposition is proved by the following lemma together with the Poincaré–Wirtinger inequality (23.54):

Lemma 23.30 *There exists a constant C independent of ϵ, such that*

$$\|v^\pm\|_{L^2(\Gamma_\varepsilon)}^2 \leq C(\epsilon^{-1}\|v^\pm\|_{L^2(\Omega_\varepsilon^\pm)}^2 + \epsilon\|\nabla v^\pm\|_{L^2(\Omega_\varepsilon^\pm)}^2) \tag{23.57}$$

for any $v^+ \in W^{1,2}(\Omega_\varepsilon^+)$ and $v^- \in W^{1,2}(\Omega_\varepsilon^-)$.

Proof. Let us consider the case of $v^+ \in W^{1,2}(\Omega_\varepsilon^+)$. Denote by v_i the restriction of v^+ on $\epsilon\Gamma_i$. We have the trace inequality

$$\|v_i\|_{L^2(\Gamma_i)}^2 \leq C(\|v_i\|_{L^2(Y_i^+)}^2 + \|\nabla v_i\|_{L^2(Y_i^+)}^2). \tag{23.58}$$

Note that this constant depends on Y^- but is uniform in i.

Consequently, we have

$$\|v^+\|_{L^2(\Gamma_\varepsilon)}^2 = \sum_{i=1}^{N(\epsilon)} \int_{\epsilon\Gamma_i} |v_i(x)|^2 ds(x) \leq C\epsilon \sum_{i=1}^{N(\epsilon)} \int_{\Gamma_i} |v_i(y)|^2 ds(y).$$

Apply (23.58) and change the variable back to get

$$\|v^+\|_{L^2(\Gamma_\varepsilon)}^2 \leq C\epsilon \sum_{i=1}^{N(\epsilon)} \int_{Y_i^+} |v_i(y)|^2 + |\nabla_y v(y)|^2 dy$$

$$\leq C\epsilon^{-1} \sum_{i=1}^{N(\epsilon)} \int_{\epsilon Y_i^+} |v_i(x)|^2 + \epsilon^2|\nabla v(x)|^2 dx.$$

This completes the proof of (23.57).   □

The other inequality in (23.21) is implied by the following lemma:

Lemma 23.31 *There exists a constant $C > 0$ independent of ϵ such that*

$$\|v\|_{L^2(\Omega_\varepsilon^-)} \leq C \left(\sqrt{\epsilon}\|v\|_{L^2(\Gamma_\varepsilon)} + \epsilon\|\nabla v\|_{L^2(\Omega_\varepsilon^-)} \right) \tag{23.59}$$

for all $v \in W^{1,2}(\Omega_\varepsilon^-)$.

Proof. We have that

$$\|v\|_{L^2(Y^-)}^2 \leq C \left(\|v\|_{L^2(\Gamma_0)}^2 + \|\nabla v\|_{L^2(Y^-)}^2 \right), \tag{23.60}$$

for any $v \in W^{1,2}(Y^-)$ where C only depends on Y^- and the dimension. Indeed, suppose otherwise, we could find a sequence $\{v_n\} \subset W^{1,2}(Y^-)$ such that $\|v_n\|_{L^2(Y^-)} \equiv 1$ but

$$\|v_n\|_{L^2(\Gamma_0)} + \|\nabla v_n\|_{L^2(Y^-)} \longrightarrow 0, \quad \text{as } n \to \infty.$$

Then since $\|v_n\|_{W^{1,2}}$ is uniformly bounded, there exists a subsequence, still denoted as $\{v_n\}$, and a function $v \in W^{1,2}(Y^-)$ such that

$$v_n \rightharpoonup v \text{ weakly in } W^{1,2}(Y^-), \quad \nabla v_n \rightharpoonup \nabla v \text{ weakly in } L^2(Y^-).$$

Consequently, $\|\nabla v\|_{L^2} \leq \liminf \|\nabla v_n\|_{L^2} = 0$, which implies that $v = C$ for some constant. Moreover, since the embedding $W^{1,2}(Y^-) \hookrightarrow L^2(\Gamma_0)$ is compact, the convergence $v_n \to v$ holds strongly in $L^2(\Gamma_0)$ and $\|v\|_{L^2(\Gamma)} \leq \lim \|v_n\|_{L^2(\Gamma_0)} = 0$. Consequently $v \equiv 0$. On the other hand, $v_n \to v$ holds strongly in $L^2(Y^-)$ and hence $\|v\|_{L^2(Y^-)} = \lim \|v_n\|_{L^2(Y^-)} = 1$. This contradicts with the fact that $v \equiv 0$.

Proof (Proof of Proposition 23.7). To prove the first inequality, we apply Lemma 23.30 to get

$$\epsilon\|u^+ - u^-\|_{L^2(\Gamma_\varepsilon)}^2 \leq 2(\epsilon\|u^+\|_{L^2(\Gamma_\varepsilon)}^2 + \epsilon\|u^-\|_{L^2(\Gamma_\varepsilon)}^2)$$
$$\leq C(\|u^+\|_{L^2(\Omega_\varepsilon^+)}^2 + \|u^-\|_{L^2(\Omega_\varepsilon^-)}^2 + \epsilon^2\|\nabla u^+\|_{L^2(\Omega_\varepsilon^+)}^2 + \epsilon^2\|\nabla u^+\|_{L^2(\Omega_\varepsilon^+)}^2).$$

Only the first term in (23.54) does not show in $\|\cdot\|_{W^{1,2}\times W^{1,2}}$, but it is controlled by $\|\nabla u^+\|_{L^2(\Omega_\varepsilon^+)}$ uniformly in ϵ thanks to (23.54).

For the second inequality, we only need to control $\|u^-\|_{L^2(\Omega_\varepsilon^-)}$. We apply Lemma 23.31 and the triangle inequality:

$$\|u^-\|_{L^2(\Omega_\varepsilon^-)}^2 \leq C\left(\epsilon\|u^+\|_{L^2(\Gamma_\varepsilon)}^2 + \epsilon\|u^+ - u^-\|_{L^2(\Gamma_\varepsilon)}^2 + \epsilon^2\|\nabla u^-\|_{L^2(\Omega_\varepsilon^-)}^2\right).$$

Only the first term does not appear in $\|\cdot\|_{W_\varepsilon}$, but using Lemma 23.30 and (23.54) we can bound it by

$$\epsilon\|u^+\|_{L^2(\Gamma_\varepsilon)}^2 \leq C(\|u^+\|_{L^2(\Omega_\varepsilon^+)}^2 + \epsilon^2\|\nabla u^+\|_{L^2(\Omega_\varepsilon^+)}^2) \leq C\|\nabla u^+\|_{L^2(\Omega_\varepsilon^+)}^2.$$

This completes the proof. $\square$

23.7.4 Existence Result

Lemma 23.32 *Let φ_1 be a function in $\mathcal{D}(\Omega, C_\sharp^\infty(Y^+)) \times \mathcal{D}(\Omega, C_\sharp^\infty(Y^-))$. There exists at least one function θ in $(\mathcal{D}(\Omega, W_\sharp^{1,2}(Y^+)) \times \mathcal{D}(\Omega, W_\sharp^{1,2}(Y^-)))^2$ solution of the following problem:*

$$
\begin{cases}
-\nabla_y \cdot \theta^+(x,y) = 0 & in\ Y^+\,, \\[2mm]
-\nabla_y \cdot \theta^-(x,y) = 0 & in\ Y^-\,, \\[2mm]
\theta^+(x,y)\cdot n = \theta^-(x,y)\cdot n & on\ \Gamma\,, \\[2mm]
\theta^+(x,y)\cdot n = \varphi_1^+(x,y) - \varphi_1^-(x,y)\ on\ \Gamma\,, \\[2mm]
y \longmapsto \theta(x,y)Y - periodic.
\end{cases}
\qquad (23.61)
$$

Proof. We look for a solution under the form $\theta = \nabla_y \eta$. We hence introduce the following variational problem:

$$
\begin{cases}
\text{Find}\,\eta \in \widetilde{W}_\sharp^{1,2}(Y^+)\times\widetilde{W}_\sharp^{1,2}(Y^-)\,\text{such that} \\[2mm]
\displaystyle\int_{Y^+}\nabla\eta^+(y)\cdot\overline{\psi^+}(y)dy + \int_{Y^-}\nabla\eta^-(y)\cdot\overline{\psi^-}(y)dy \\[4mm]
\hspace{4cm} = \dfrac{1}{\beta k_0}\int_\Gamma(\varphi_1^+ - \varphi_1^-)(\overline{\psi^+} - \overline{\psi^-})(y)ds(y)\,, \\[4mm]
\text{for all}\,\psi \in \widetilde{W}_\sharp^{1,2}(Y^+)\times\widetilde{W}_\sharp^{1,2}(Y^-)\,,
\end{cases}
$$

for a fixed $x \in \Omega$. Lax-Milgram theorem gives us existence and uniqueness of such an η. Since $\varphi_1 \in \mathcal{D}(\Omega, C_\sharp^\infty(Y^+))\times\mathcal{D}(\Omega, C_\sharp^\infty(Y^-))$, there exists at least one function $\theta \in (\mathcal{D}(\Omega, W_\sharp^{1,2}(Y^+))\times\mathcal{D}(\Omega, W_\sharp^{1,2}(Y^-))^2$ solution of (23.61). Note that we do not have uniqueness of such a solution. $\square$

23.8 Concluding Remarks

In this chapter, we have explained how the dependence of the effective electrical admittivity measures the complexity of the cellular organization of the tissue. We have derived formulas for the effective admittivity of suspensions of cells and characterized their dependence with respect to the frequency in terms of membrane polarization tensors. We have presented numerical results to illustrate the use of the Debye relaxation times in classifying microstructures.

24

Plasmonic Nanoparticle Imaging

24.1 Introduction

Plasmon resonant nanoparticles have unique capabilities of enhancing the brightness of light and confining strong electromagnetic fields [313]. A thriving interest for optical studies of plasmon resonant nanoparticles is due to their recently proposed use as labels in molecular biology [202]. New types of cancer diagnostic nanoparticles are constantly being developed. Nanoparticles are also being used in thermotherapy as nanometric heat-generators that can be activated remotely by external electromagnetic fields [90].

This chapter is devoted to the mathematical modeling of plasmonic nanoparticles. Its aim is twofold: (i) to mathematically define the notion of plasmonic resonance and to analyze the shift and broadening of the plasmon resonance with changes in size and shape of the nanoparticles and (ii) to study the scattering and absorption enhancements by plasmon resonant nanoparticles and express them in terms of the polarization tensor of the nanoparticle. Optimal bounds on the enhancement factors are also derived. For simplicity, the Helmholtz equation is used to model electromagnetic wave propagation.

According to the quasi-static approximation for small particles, the surface plasmon resonance peak occurs when the particle's polarizability is maximized. Plasmon resonances in nanoparticles can be treated at the quasi-static limit as an eigenvalue problem for the Neumann-Poincaré integral operator, which leads to direct calculation of resonance values of permittivity and optimal design of nanoparticles that resonate at specified frequencies. At this limit, they are size-independent. However, as the particle size increases, they are determined from scattering and absorption blow up and become size-dependent. This was experimentally observed, for instance, in [181, 294, 314].

In this chapter, we first prove that, as the particle size increases and crosses its critical value for dipolar approximation, the plasmonic resonances become size-dependent. The resonance condition is determined from absorption and scattering blow up and depends on the shape, size and electromagnetic parameters of both the nanoparticle and the surrounding material. Then, we pre-

cisely quantify the scattering absorption enhancements in plasmonic nanoparticles. We derive new bounds on the enhancement factors given the volume and electromagnetic parameters of the nanoparticles. At the quasi-static limit, we prove that the averages over the orientation of scattering and extinction cross-sections of a randomly oriented nanoparticle are given in terms of the imaginary part of the polarization tensor. Moreover, we show that the polarization tensor blows up at plasmonic resonances and derive bounds for the absorption and scattering cross-sections. We also prove the blow-up of the first-order scattering coefficients at plasmonic resonances.

The chapter is organized as follows. In Section 24.2 we introduce a layer potential formulation for plasmonic resonances and derive asymptotic formulas for the plasmonic resonances and the near- and far-fields in terms of the size. In Section 24.3 we consider the case of multiple plasmonic nanoparticles. Section 24.4 is devoted to the study of the scattering and absorption enhancements. We also clarify the connection between the blow up of the scattering frequencies and the plasmonic resonances. As shown in Subsection 3.2.7, the scattering coefficients are simply the Fourier coefficients of the scattering amplitude. In Section 24.5 we investigate the behavior of the scattering coefficients at the plasmonic resonances. Section 24.6 is devoted to the derivation of asymptotic expansions with respect to the frequency of some boundary integral operators associated with the Helmholtz equation and a single particle. These results are generalized to the case of multiple particles in Section 24.7. In Section 24.8 we prove useful sum rules for the polarization tensor. The results of this chapter are from [45, 73, 75].

24.2 Layer Potential Formulation for Plasmonic Resonances

24.2.1 Problem Formulation and Some Basic Results

We consider the scattering problem of a time-harmonic wave incident on a plasmonic nanoparticle. For simplicity, we use the Helmholtz equation instead of the full Maxwell equations. The homogeneous medium is characterized by electric permittivity ε_m and magnetic permeability μ_m, while the particle occupying a bounded and simply connected domain $D \Subset \mathbb{R}^3$ of class $\mathcal{C}^{1,\alpha}$ for some $0 < \alpha < 1$ is characterized by electric permittivity ε_c and magnetic permeability μ_c, both of which may depend on the frequency. Assume that $\Re\varepsilon_c < 0, \Im\varepsilon_c > 0, \Re\mu_c < 0, \Im\mu_c > 0$ and define

$$k_m = \omega\sqrt{\varepsilon_m\mu_m}, \quad k_c = \omega\sqrt{\varepsilon_c\mu_c}\,,$$

and

$$\varepsilon_D = \varepsilon_m\chi(\mathbb{R}^3\backslash\bar{D}) + \varepsilon_c\chi(\bar{D}), \quad \mu_D = \varepsilon_m\chi(\mathbb{R}^3\backslash\bar{D}) + \varepsilon_c\chi(D)\,,$$

where χ denotes the characteristic function. Let $u^i(x) = e^{ik_m d\cdot x}$ be the incident wave. Here, ω is the frequency and d is the unit incidence direction.

Throughout this paper, we assume that ε_m and μ_m are real and strictly positive and that $\Re k_c < 0$ and $\Im k_c > 0$.

Using dimensionless quantities, we assume that the following set of conditions holds.

Condition 24.1 *We assume that the numbers $\varepsilon_m, \mu_m, \varepsilon_c, \mu_c$ are dimensionless and are of order one. We also assume that the particle has size of order one and ω is dimensionless and is of order $o(1)$.*

It is worth emphasizing that in the original dimensional variables ω refers to the ratio between the size of the particle and the wavelength. Moreover, the operating frequency varies in a small range and hence, the material parameters ε_c and μ_c can be assumed independent of the frequency.

The scattering problem can be modeled by the following Helmholtz equation

$$
\begin{cases}
\nabla \cdot \dfrac{1}{\mu_D} \nabla u + \omega^2 \varepsilon_D u = 0 & \text{in } \mathbb{R}^3 \backslash \partial D\,, \\[2mm]
u_+ - u_- = 0 & \text{on } \partial D\,, \\[2mm]
\dfrac{1}{\mu_m} \dfrac{\partial u}{\partial \nu}\bigg|_+ - \dfrac{1}{\mu_c} \dfrac{\partial u}{\partial \nu}\bigg|_- = 0 & \text{on } \partial D\,, \\[2mm]
u^s := u - u^i \ \text{satisfies the Sommerfeld radiation condition.}
\end{cases}
\tag{24.1}
$$

Here, $\partial/\partial\nu$ denotes the normal derivative and the Sommerfeld radiation condition can be expressed in three dimensions as follows:

$$
\left| \frac{\partial u}{\partial |x|} - ik_m u \right| \leq C|x|^{-2}
$$

as $|x| \to +\infty$ for some constant C independent of x.

The model problem (24.1) is referred to as the transverse magnetic case. Note that all the results of this paper hold true in the transverse electric case where ε_D and μ_D are interchanged.

Let

$$
F_1(x) = -u^i(x) = -e^{ik_m d \cdot x},
$$

$$
F_2(x) = -\frac{1}{\mu_m} \frac{\partial u^i}{\partial \nu}(x) = -\frac{i}{\mu_m} k_m e^{ik_m d \cdot x} d \cdot \nu(x)
$$

with $\nu(x)$ being the outward normal at $x \in \partial D$. Let $\Gamma_k(x,y)$ be the Green function for the Helmholtz operator $\Delta + k^2$ satisfying the Sommerfeld radiation condition. By using the following single-layer potential and Neumann-Poincaré integral operator

$$
\mathcal{S}_D^k[\psi](x) = \int_{\partial D} \Gamma_k(x,y)\psi(y)d\sigma(y), \qquad x \in \mathbb{R}^3\,,
$$

$$
(\mathcal{K}_D^k)^*[\psi](x) = \int_{\partial D} \frac{\partial \Gamma_k(x,y)}{\partial \nu(x)} \psi(y)d\sigma(y), \quad x \in \partial D\,,
$$

we can represent the solution u in the following form

$$u(x) = \begin{cases} u^i + \mathcal{S}_D^{k_m}[\psi], & x \in \mathbb{R}^3 \backslash \bar{D}, \\ \mathcal{S}_D^{k_c}[\phi], & x \in D, \end{cases} \tag{24.2}$$

where $\psi, \phi \in W_{-1/2}^2(\partial D)$ satisfy the following system of integral equations on ∂D [50]:

$$\begin{cases} \mathcal{S}_D^{k_m}[\psi] - \mathcal{S}_D^{k_c}[\phi] & = F_1, \\ \frac{1}{\mu_m}\left(\frac{1}{2}I + (\mathcal{K}_D^{k_m})^*\right)[\psi] + \frac{1}{\mu_c}\left(\frac{1}{2}I - (\mathcal{K}_D^{k_c})^*\right)[\phi] = F_2, \end{cases} \tag{24.3}$$

where I denotes the identity operator. In the sequel, we set $\mathcal{S}_D^0 = \mathcal{S}_D$.

We are interested in the scattering in the quasi-static regime, *i.e.*, for $\omega \ll 1$. Note that for ω small enough, $\mathcal{S}_D^{k_c}$ is invertible [50]. We have $\phi = (\mathcal{S}_D^{k_c})^{-1}\left(\mathcal{S}_D^{k_m}[\psi] - F_1\right)$, whereas the following equation holds for ψ

$$\mathcal{A}_D(\omega)[\psi] = f, \tag{24.4}$$

where

$$\mathcal{A}_D(\omega) = \frac{1}{\mu_m}\left(\frac{1}{2}I + (\mathcal{K}_D^{k_m})^*\right) + \frac{1}{\mu_c}\left(\frac{1}{2}I - (\mathcal{K}_D^{k_c})^*\right)(\mathcal{S}_D^{k_c})^{-1}\mathcal{S}_D^{k_m}, \tag{24.5}$$

$$f = F_2 + \frac{1}{\mu_c}\left(\frac{1}{2}I - (\mathcal{K}_D^{k_c})^*\right)(\mathcal{S}_D^{k_c})^{-1}[F_1]. \tag{24.6}$$

It is clear that

$$\mathcal{A}_D(0) = \mathcal{A}_{D,0} = \frac{1}{\mu_m}\left(\frac{1}{2}I + \mathcal{K}_D^*\right) + \frac{1}{\mu_c}\left(\frac{1}{2}I - \mathcal{K}_D^*\right) = \left(\frac{1}{2\mu_m} + \frac{1}{2\mu_c}\right)I - \left(\frac{1}{\mu_c} - \frac{1}{\mu_m}\right)\mathcal{K}_D^*, \tag{24.7}$$

where the notation $\mathcal{K}_D^* = (\mathcal{K}_D^0)^*$ is used for simplicity.

We are interested in finding $\mathcal{A}_D(\omega)^{-1}$. We refer to Subsection 3.1.4 for some basic facts about the Neumann-Poincaré operator $\mathcal{K}_D^*$.

Let $\mathcal{H}^*$ be defined by (3.25). From (24.7), it is easy to see that

$$\mathcal{A}_{D,0}[\psi] = \sum_{j=0}^{\infty} \tau_j(\psi, \varphi_j)_{\mathcal{H}^*}\varphi_j, \tag{24.8}$$

where

$$\tau_j = \frac{1}{2\mu_m} + \frac{1}{2\mu_c} - \left(\frac{1}{\mu_c} - \frac{1}{\mu_m}\right)\lambda_j. \tag{24.9}$$

We now derive the asymptotic expansion of the operator $\mathcal{A}(\omega)$ as $\omega \to 0$. Using the asymptotic expansions in terms of k of the operators $\mathcal{S}_D^k$, $(\mathcal{S}_D^k)^{-1}$ and $(\mathcal{K}_D^k)^*$ proved in Section 24.6, we can obtain the following result.

Lemma 24.2 *Let $\mathcal{H}^*$ be defined by (3.25). As $\omega \to 0$, the operator $\mathcal{A}_D(\omega)$: $\mathcal{H}^*(\partial D) \to \mathcal{H}^*(\partial D)$ admits the asymptotic expansion*

$$\mathcal{A}_D(\omega) = \mathcal{A}_{D,0} + \omega^2 \mathcal{A}_{D,2} + O(\omega^3),$$

where

$$\mathcal{A}_{D,2} = (\varepsilon_m - \varepsilon_c)\mathcal{K}_{D,2} + \frac{\varepsilon_m \mu_m - \varepsilon_c \mu_c}{\mu_c}\left(\frac{1}{2}I - \mathcal{K}_D^*\right)\mathcal{S}_D^{-1}\mathcal{S}_{D,2}. \qquad (24.10)$$

Proof. Recall that

$$\mathcal{A}_D(\omega) = \frac{1}{\mu_m}\left(\frac{1}{2}I + (\mathcal{K}_D^{k_m})^*\right) + \frac{1}{\mu_c}\left(\frac{1}{2}I - (\mathcal{K}_D^{k_c})^*\right)(\mathcal{S}_D^{k_c})^{-1}\mathcal{S}_D^{k_m}. \qquad (24.11)$$

By a straightforward calculation, it follows that

$$\begin{aligned}
(\mathcal{S}_D^{k_c})^{-1}\mathcal{S}_D^{k_m} &= I + \omega\left(\sqrt{\varepsilon_c \mu_c}\mathcal{B}_{D,1}\mathcal{S}_D + \sqrt{\varepsilon_m \mu_m}\mathcal{S}_D^{-1}\mathcal{S}_{D,1}\right) + \\
&\quad \omega^2\left(\varepsilon_c \mu_c \mathcal{B}_{D,2}\mathcal{S}_D + \sqrt{\varepsilon_c \mu_c \varepsilon_m \mu_m}\mathcal{B}_{D,1}\mathcal{S}_{D,1} + \varepsilon_m \mu_m \mathcal{S}_D^{-1}\mathcal{S}_{D,2}\right) + O(\omega^3), \\
&= I + \omega\left(\sqrt{\varepsilon_m \mu_m} - \sqrt{\varepsilon_c \mu_c}\right)\mathcal{S}_D^{-1}\mathcal{S}_{D,1} + \\
&\quad \omega^2\left((\varepsilon_m \mu_m - \varepsilon_c \mu_c)\mathcal{S}_D^{-1}\mathcal{S}_{D,2} + \sqrt{\varepsilon_c \mu_c}(\sqrt{\varepsilon_c \mu_c} - \sqrt{\varepsilon_m \mu_m})\mathcal{S}_D^{-1}\mathcal{S}_{D,1}\mathcal{S}_D^{-1}\mathcal{S}_{D,1}\right) \\
&\quad + O(\omega^3),
\end{aligned}$$

where $\mathcal{B}_{D,1}$ and $\mathcal{B}_{D,2}$ are defined by (24.58). Using the facts that

$$\left(\frac{1}{2}I - \mathcal{K}_D^*\right)\mathcal{S}_D^{-1}\mathcal{S}_{D,1} = 0$$

and

$$\frac{1}{2}I - (\mathcal{K}_D^k)^* = \left(\frac{1}{2}I - \mathcal{K}_D^*\right) - k^2\mathcal{K}_{D,2} + O(k^3),$$

the lemma immediately follows. $\square$

We regard $\mathcal{A}_D(\omega)$ as a perturbation to the operator $\mathcal{A}_{D,0}$ for small ω. Using standard perturbation theory [304], we can derive the perturbed eigenvalues and their associated eigenfunctions. For simplicity, we consider the case when λ_j is a simple eigenvalue of the operator $\mathcal{K}_D^*$.

We let

$$R_{jl} = \left(\mathcal{A}_{D,2}[\varphi_j], \varphi_l\right)_{\mathcal{H}^*}, \qquad (24.12)$$

where $\mathcal{A}_{D,2}$ is defined by (24.10).

As ω goes to zero, the perturbed eigenvalue and eigenfunction have the following form:

$$\tau_j(\omega) = \tau_j + \omega^2 \tau_{j,2} + O(\omega^3), \qquad (24.13)$$

$$\varphi_j(\omega) = \varphi_j + \omega^2 \varphi_{j,2} + O(\omega^3), \qquad (24.14)$$

where

$$\tau_{j,2} = R_{jj}, \qquad (24.15)$$

$$\varphi_{j,2} = \sum_{l \neq j} \frac{R_{jl}}{\left(\frac{1}{\mu_m} - \frac{1}{\mu_c}\right)(\lambda_j - \lambda_l)}\varphi_l. \qquad (24.16)$$

24.2.2 First-Order Correction to Plasmonic Resonances and Field Behavior at the Plasmonic Resonances

We first introduce different notions of plasmonic resonance as follows.

Definition 24.1. *(i) We say that ω is a plasmonic resonance if*

$$|\tau_j(\omega)| \ll 1 \quad \text{and is locally minimal for some } j.$$

(ii) We say that ω is a quasi-static plasmonic resonance if $|\tau_j| \ll 1$ and is locally minimized for some j. Here, τ_j is defined by (24.9).
(iii) We say that ω is a first-order corrected quasi-static plasmonic resonance if $|\tau_j + \omega^2 \tau_{j,2}| \ll 1$ and is locally minimized for some j. Here, the correction term $\tau_{j,2}$ is defined by (24.15).

Note that quasi-static resonances are size independent and is therefore a zero-order approximation of the plasmonic resonance in terms of the particle size while the first-order corrected quasi-static plasmonic resonance depends on the size of the nanoparticle (or equivalently on ω in view of the non-dimensionalization adopted herein).

We are interested in solving the equation $\mathcal{A}_D(\omega)[\phi] = f$ when ω is close to the resonance frequencies, *i.e.*, when $\tau_j(\omega)$ is very small for some j's. In this case, the major part of the solution would be the contributions of the excited resonance modes $\varphi_j(\omega)$. We introduce the following definition.

Definition 24.2. *We call $J \subset \mathbb{N}$ index set of resonance if τ_j's are close to zero when $j \in J$ and are bounded from below when $j \in J^c$. More precisely, we choose a threshold number $\varepsilon_0 > 0$ independent of ω such that*

$$|\tau_j| \geq \varepsilon_0 > 0 \quad \text{for } j \in J^c.$$

Remark 24.3 *Note that for $j = 0$, we have $\tau_0 = 1/\mu_m$, which is of size one by our assumption. As a result, throughout this paper, we always exclude 0 from the index set of resonance J.*

From now on, we shall use J as our index set of resonances. For simplicity, we assume throughout that the following conditions hold.

Condition 24.4 *Each eigenvalue λ_j for $j \in J$ is a simple eigenvalue of the operator $\mathcal{K}_D^*$.*

Condition 24.5 *Let*

$$\lambda = \frac{\mu_m + \mu_c}{2(\mu_m - \mu_c)} . \tag{24.17}$$

We assume that $\lambda \neq 0$ or equivalently, $\mu_c \neq -\mu_m$.

Condition 24.5 implies that the set J is finite.

We define the projection $P_J(\omega)$ such that

$$P_J(\omega)[\varphi_j(\omega)] = \begin{cases} \varphi_j(\omega), & j \in J, \\ 0, & j \in J^c. \end{cases}$$

In fact, we have

$$P_J(\omega) = \sum_{j \in J} P_j(\omega) = \sum_{j \in J} \frac{1}{2\pi i} \int_{\gamma_j} (\xi - \mathcal{A}_D(\omega))^{-1} d\xi, \tag{24.18}$$

where γ_j is a Jordan curve in the complex plane enclosing only the eigenvalue $\tau_j(\omega)$ among all the eigenvalues.

To obtain an explicit representation of $P_J(\omega)$, we consider the adjoint operator $\mathcal{A}_D(\omega)^*$. By a similar perturbation argument, we can obtain its perturbed eigenvalue and eigenfunction, which have the following form

$$\widetilde{\tau}_j(\omega) = \overline{\tau_j(\omega)}, \tag{24.19}$$

$$\widetilde{\varphi}_j(\omega) = \varphi_j + \omega^2 \widetilde{\varphi}_{j,2} + O(\omega^2). \tag{24.20}$$

Using the eigenfunctions $\widetilde{\varphi}_j(\omega)$, we can show that

$$P_J(\omega)[x] = \sum_{j \in J} \left(x, \widetilde{\varphi}_j(\omega) \right)_{\mathcal{H}^*} \varphi_j(\omega). \tag{24.21}$$

Throughout this paper, for two Banach spaces X and Y, by $\mathcal{L}(X, Y)$ we denote the set of bounded linear operators from X into Y.

We are now ready to solve the equation $\mathcal{A}_D(\omega)[\psi] = f$. First, it is clear that

$$\psi = \mathcal{A}_D(\omega)^{-1}[f] = \sum_{j \in J} \frac{(f, \widetilde{\varphi}_j(\omega))_{\mathcal{H}^*}}{\tau_j(\omega)} + \mathcal{A}_D(\omega)^{-1}[P_{J^c}(\omega)[f]]. \tag{24.22}$$

The following lemma holds.

Lemma 24.6 *The norm* $\|\mathcal{A}_D(\omega)^{-1} P_{J^c}(\omega)\|_{\mathcal{L}(\mathcal{H}^*(\partial D), \mathcal{H}^*(\partial D))}$ *is uniformly bounded in* ω.

Proof. Consider the operator

$$\mathcal{A}_D(\omega)|_{J^c} : P_{J^c}(\omega)\mathcal{H}^*(\partial D) \to P_{J^c}(\omega)\mathcal{H}^*(\partial D).$$

For ω small enough, we can show that $\mathrm{dist}(\sigma(\mathcal{A}_D(\omega)|_{J^c}), 0) \geq \frac{\varepsilon_0}{2}$, where $\sigma(\mathcal{A}_D(\omega)|_{J^c})$ is the discrete spectrum of $\mathcal{A}_D(\omega)|_{J^c}$. Then, it follows that

$$\|\mathcal{A}_D(\omega)^{-1}(P_{J^c}(\omega)f)\| = \|\left(\mathcal{A}_D(\omega)|_{P_{J^c}}\right)^{-1}(P_{J^c}(\omega)f)\| \lesssim \frac{1}{\varepsilon_0} \exp(\frac{C_1}{\varepsilon_0^2})\|P_{J^c}(\omega)f\|,$$

where the notation $A \lesssim B$ means that $A \leq CB$ for some constant C.

On the other hand,

$$
\begin{aligned}
P_J(\omega)f &= \sum_{j \in J} \left(f, \widetilde{\varphi_j}(\omega)\right)_{\mathcal{H}^*} \varphi_j(\omega) = \sum_{j \in J} \left(f, \varphi_j + O(\omega)\right)_{\mathcal{H}^*} \left(\varphi_j + O(\omega)\right) \\
&= \sum_{j \in J} \left(f, \varphi_j\right)_{\mathcal{H}^*} \varphi_j(\omega) + O(\omega) \, .
\end{aligned}
$$

Thus,

$$
\|P_{J^c}(\omega)\| = \|(I - P_J(\omega))\| \lesssim (1 + O(\omega)) \, ,
$$

from which the desired result follows immediately. $\square$

Second, we have the following asymptotic expansion of f given by (24.6) with respect to ω.

Lemma 24.7 *Let*

$$
f_1 = -i\sqrt{\varepsilon_m \mu_m} e^{ik_m d \cdot z} \left(\frac{1}{\mu_m}[d \cdot \nu(x)] + \frac{1}{\mu_c}\left(\frac{1}{2}I - \mathcal{K}_D^*\right)\mathcal{S}_D^{-1}[d \cdot (x - z)] \right)
$$

and let z be the center of the domain D. In the space $\mathcal{H}^*(\partial D)$, as ω goes to zero, we have

$$
f = \omega f_1 + O(\omega^2) \, ,
$$

in the sense that, for ω small enough,

$$
\|f - \omega f_1\|_{\mathcal{H}^*} \leq C\omega^2
$$

for some constant C independent of ω.

Proof. A direct calculation yields

$$
\begin{aligned}
f &= F_2 + \frac{1}{\mu_c}\left(\frac{1}{2}I - (\mathcal{K}_D^{k_c})^*\right)(\mathcal{S}_D^{k_c})^{-1}[F_1] \\
&= -\omega \frac{i}{\mu_m}\sqrt{\varepsilon_m \mu_m}e^{ik_m d \cdot z}[d \cdot \nu(x)] + O(\omega^2) + \\
&\quad \frac{1}{\mu_c}\left(\left(\frac{1}{2}I - \mathcal{K}_D^*\right)\left((\mathcal{S}_D)^{-1} + \omega\mathcal{B}_{D,1}\right) + O(\omega^2)\right)\left[-e^{ik_m d \cdot z}\left(\chi(\partial D) + i\omega\sqrt{\varepsilon_m \mu_m}[d \cdot (x - z)]\right) + O(\omega^2)\right] \\
&= -\frac{e^{ik_m d \cdot z}}{\mu_c}\left(\frac{1}{2}I - \mathcal{K}_D^*\right)\mathcal{S}_D^{-1}[\chi(\partial D)] - \frac{\omega e^{ik_m d \cdot z}}{\mu_c}\left(\frac{1}{2}I - \mathcal{K}_D^*\right)\mathcal{B}_{D,1}[\chi(\partial D)] - \\
&\quad \omega i\sqrt{\varepsilon_m \mu_m}e^{ik_m d \cdot z}\left(\frac{1}{\mu_m}[d \cdot \nu(x)] + \frac{1}{\mu_c}\left(\frac{1}{2}I - \mathcal{K}_D^*\right)\mathcal{S}_D^{-1}[d \cdot (x - z)]\right) + O(\omega^2) \\
&= -\omega i\sqrt{\varepsilon_m \mu_m}e^{ik_m d \cdot z}\left(\frac{1}{\mu_m}[d \cdot \nu(x)] + \frac{1}{\mu_c}\left(\frac{1}{2}I - \mathcal{K}_D^*\right)\mathcal{S}_D^{-1}[d \cdot (x - z)]\right) \\
&\quad + O(\omega^2) \, ,
\end{aligned}
$$

where we have made use of the facts that

$$\left(\frac{1}{2}I - \mathcal{K}_D^*\right)\mathcal{S}_D^{-1}[\chi(\partial D)] = 0$$

and

$$\mathcal{B}_{D,1}[\chi(\partial D)] = c\mathcal{S}_D^{-1}[\chi(\partial D)]$$

for some constant c; see again Section 24.6.   □

Finally, we are ready to state our main result in this section.

Theorem 24.8 *Under Conditions 24.1–24.5 the scattered field $u^s = u - u^i$ due to a single plasmonic nanoparticle has the following representation in the quasi-static regime:*

$$u^s = \mathcal{S}_D^{k_m}[\psi],$$

where

$$\psi = \sum_{j \in J} \frac{\omega\big(f_1, \widetilde{\varphi}_j(\omega)\big)_{\mathcal{H}^*} \varphi_j(\omega)}{\tau_j(\omega)} + O(\omega),$$

$$= \sum_{j \in J} \frac{ik_m e^{ik_m d \cdot z}\big(d \cdot \nu(x), \varphi_j\big)_{\mathcal{H}^*} \varphi_j + O(\omega^2)}{\lambda - \lambda_j + O(\omega^2)} + O(\omega)$$

with λ being given by (24.17).

Proof. We have

$$\psi = \sum_{j \in J} \frac{\big(f, \widetilde{\varphi}_j(\omega)\big)_{\mathcal{H}^*} \varphi_j(\omega)}{\tau_j(\omega)} + \mathcal{A}_D(\omega)^{-1}(P_{J^c}(\omega)f),$$

$$= \sum_{j \in J} \frac{\omega\big(f_1, \varphi_j\big)_{\mathcal{H}^*} \varphi_j + O(\omega^2)}{\frac{1}{2\mu_m} + \frac{1}{2\mu_c} - \big(\frac{1}{\mu_c} - \frac{1}{\mu_m}\big)\lambda_j + O(\omega^2)} + O(\omega).$$

We now compute $\big(f_1, \varphi_j\big)_{\mathcal{H}^*}$ with f_1 given in Lemma 24.7. We only need to show that

$$\left(\left(\frac{1}{2}I - \mathcal{K}_D^*\right)\mathcal{S}_D^{-1}[d \cdot (x - z)]\right), \varphi_j\right)_{\mathcal{H}^*} = (d \cdot \nu(x), \varphi_j)_{\mathcal{H}^*}. \qquad (24.23)$$

Indeed, we have

$$\left((\frac{1}{2}I - \mathcal{K}_D^*)\mathcal{S}_D^{-1}[d \cdot (x - z)], \varphi_j \right)_{\mathcal{H}^*} = -\left(\mathcal{S}_D^{-1}[d \cdot (x - z)], (\frac{1}{2}I - \mathcal{K}_D)\mathcal{S}_D[\varphi_j] \right)_{-\frac{1}{2}, \frac{1}{2}}$$

$$= -\left(\mathcal{S}_D^{-1}[d \cdot (x - z)], \mathcal{S}_D(\frac{1}{2}I - \mathcal{K}_D^*)[\varphi_j] \right)_{-\frac{1}{2}, \frac{1}{2}}$$

$$= -\left(d \cdot (x - z), (\frac{1}{2}I - \mathcal{K}_D^*)[\varphi_j] \right)_{-\frac{1}{2}, \frac{1}{2}}$$

$$= -\left(d \cdot (x - z), -\frac{\partial \mathcal{S}_D[\varphi_j]}{\partial \nu}\Big|_- \right)_{-\frac{1}{2}, \frac{1}{2}}$$

$$= \int_{\partial D} \frac{\partial [d \cdot (x - z)]}{\partial \nu} \mathcal{S}_D[\varphi_j] d\sigma$$

$$\quad - \int_D \left(\Delta[d \cdot (x - z)]\mathcal{S}_D[\varphi_j] - \Delta\mathcal{S}_D[\varphi_j][d \cdot (x - z)] \right) dx$$

$$= -\left(d \cdot \nu(x), \varphi_j \right)_{\mathcal{H}^*},$$

where we have used the fact that $\mathcal{S}_D[\varphi_j]$ is harmonic in D. This proves the desired identity and the rest of the theorem follows immediately. $\square$

Corollary 24.9 *Assume the same conditions as in Theorem 24.8. Under the additional condition that*

$$\min_{j \in J} |\tau_j(\omega)| \gg \omega^3, \tag{24.24}$$

we have

$$\psi = \sum_{j \in J} \frac{ik_m e^{ik_m d \cdot z} \left(d \cdot \nu(x), \varphi_j \right)_{\mathcal{H}^*} \varphi_j + O(\omega^2)}{\lambda - \lambda_j + \omega^2 \left(\frac{1}{\mu_c} - \frac{1}{\mu_m} \right)^{-1} \tau_{j,2}} + O(\omega).$$

More generally, under the additional condition that

$$\min_{j \in J} \tau_j(\omega) \gg \omega^{m+1},$$

for some integer $m > 2$, we have

$$\psi = \sum_{j \in J} \frac{ik_m e^{ik_m d \cdot z} \left(d \cdot \nu(x), \varphi_j \right)_{\mathcal{H}^*} \varphi_j + O(\omega^2)}{\lambda - \lambda_j + \omega^2 \left(\frac{1}{\mu_c} - \frac{1}{\mu_m} \right)^{-1} \tau_{j,2} + \cdots + \omega^m \left(\frac{1}{\mu_c} - \frac{1}{\mu_m} \right)^{-1} \tau_{j,m}} + O(\omega).$$

Rescaling back to original dimensional variables, we suppose that the magnetic permeability μ_c of the nanoparticle is changing with respect to the operating angular frequency ω while that of the surrounding medium, μ_m, is independent of ω. Then we can write

$$\mu_c(\omega) = \mu'(\omega) + i\mu''(\omega). \tag{24.25}$$

Because of causality, the real and imaginary parts of μ_c obey the following Kramer–Kronig relations:

$$\mu''(\omega) = -\frac{1}{\pi} \text{p.v.} \int_{-\infty}^{+\infty} \frac{1}{\omega - s} \mu'(s) ds,$$

$$\mu'(\omega) = \frac{1}{\pi} \text{p.v.} \int_{-\infty}^{+\infty} \frac{1}{\omega - s} \mu''(s) ds, \tag{24.26}$$

where p.v. stands for the principle value.

The magnetic permeability $\mu_c(\omega)$ can be described by the Drude model; see, for instance, [313]. We have

$$\mu_c(\omega) = \mu_0 \Big(1 - F \frac{\omega^2}{\omega^2 - \omega_0^2 + i\tau^{-1}\omega} \Big), \tag{24.27}$$

where $\tau > 0$ is the nanoparticle's bulk electron relaxation rate (τ^{-1} is the damping coefficient), F is a filling factor, and ω_0 is a localized plasmon resonant frequency. When

$$(1 - F)(\omega^2 - \omega_0^2)^2 - F\omega_0^2(\omega^2 - \omega_0^2) + \tau^{-2}\omega^2 < 0,$$

the real part of $\mu_c(\omega)$ is negative.

We suppose that $D = z + \delta B$. The quasi-static plasmonic resonance is defined by ω such that

$$\Re \frac{\mu_m + \mu_c(\omega)}{2(\mu_m - \mu_c(\omega))} = \lambda_j$$

for some j, where λ_j is an eigenvalue of the Neumann-Poincaré operator $\mathcal{K}_D^*(= \mathcal{K}_B^*)$. It is clear that such definition is independent of the nanoparticle's size. In view of (24.13), the shifted plasmonic resonance is defined by

$$\text{argmin} \Big| \frac{1}{2\mu_m} + \frac{1}{2\mu_c(\omega)} - \Big(\frac{1}{\mu_c(\omega)} - \frac{1}{\mu_m} \Big) \lambda_j + \omega^2 \delta^2 \tau_{j,2} \Big|,$$

where $\tau_{j,2}$ is given by (24.15) with D replaced by B.

24.3 Multiple Plasmonic Nanoparticles

24.3.1 Layer Potential Formulation in the Multi-Particle Case

We consider the scattering of an incident time harmonic wave u^i by multiple weakly coupled plasmonic nanoparticles in three dimensions. For ease of exposition, we consider the case of L particles with an identical shape. We assume that the following condition holds.

Condition 24.10 *All the identical particles have size of order δ which is a small parameter and the distances between neighboring ones are of order one.*

We write $D_l = z_l + \delta\widetilde{D}$, $l = 1, 2, \ldots, L$, where $\widetilde{D}$ has size one and is centered at the origin. Moreover, we denote $D_0 = \delta\widetilde{D}$ as our reference nanoparticle. Denote by

$$D = \bigcup_{l=1}^{L} D_l, \quad \varepsilon_D = \varepsilon_m \chi(\mathbb{R}^3 \backslash \bar{D}) + \varepsilon_c \chi(\bar{D}), \quad \mu_D = \mu_m \chi(\mathbb{R}^3 \backslash \bar{D}) + \mu_c \chi(D).$$

The scattering problem can be modeled by the following Helmholtz equation:

$$\begin{cases} \nabla \cdot \dfrac{1}{\mu_D} \nabla u + \omega^2 \varepsilon_D u = 0 & \text{in } \mathbb{R}^3 \backslash \partial D, \\ u_+ - u_- = 0 & \text{on } \partial D, \\ \dfrac{1}{\mu_m} \dfrac{\partial u}{\partial \nu}\bigg|_+ - \dfrac{1}{\mu_c} \dfrac{\partial u}{\partial \nu}\bigg|_- = 0 & \text{on } \partial D, \\ u^s := u - u^i \text{ satisfies the Sommerfeld radiation condition.} \end{cases} \quad (24.28)$$

Let

$$u^i(x) = e^{ik_m d \cdot x},$$

$$F_{l,1}(x) = -u^i(x)\big|_{\partial D_l} = -e^{ik_m d \cdot x}\big|_{\partial D_l},$$

$$F_{l,2}(x) = -\frac{\partial u^i}{\partial \nu}(x)\bigg|_{\partial D_l} = -ik_m e^{ik_m d \cdot x} d \cdot \nu(x)\big|_{\partial D_l},$$

and define the operator $\mathcal{K}^k_{D_p, D_l}$ by

$$\mathcal{K}^k_{D_p, D_l}[\psi](x) = \int_{\partial D_p} \frac{\partial \Gamma_k(x, y)}{\partial \nu(x)} \psi(y) d\sigma(y), \quad x \in \partial D_l.$$

Analogously, we define

$$\mathcal{S}^k_{D_p, D_l}[\psi](x) = \int_{\partial D_p} \Gamma_k(x, y) \psi(y) d\sigma(y), \quad x \in \partial D_l.$$

The solution u of (24.28) can be represented as follows:

$$u(x) = \begin{cases} u^i + \displaystyle\sum_{l=1}^{L} \mathcal{S}^{k_m}_{D_l}[\psi_l], & x \in \mathbb{R}^3 \backslash \bar{D}, \\ \displaystyle\sum_{l=1}^{L} \mathcal{S}^{k_c}_{D_l}[\phi_l], & x \in D, \end{cases}$$

where $\phi_l, \psi_l \in W^2_{-1/2}(\partial D_l)$ satisfy the following system of integral equations

$$
\begin{cases}
\mathcal{S}_{D_l}^{k_m}[\psi_l] - \mathcal{S}_{D_l}^{k_c}[\phi_l] + \sum_{p \neq l} \mathcal{S}_{D_p, D_l}^{k_m}[\psi_p] = F_{l,1}\,, \\[2mm]
\dfrac{1}{\mu_m}\Big(\dfrac{1}{2}I + (\mathcal{K}_{D_l}^{k_m})^*\Big)[\psi_l] + \dfrac{1}{\mu_c}\Big(\dfrac{1}{2}I - (\mathcal{K}_{D_l}^{k_c})^*\Big)[\phi_l] \\[2mm]
\qquad + \dfrac{1}{\mu_m}\sum_{p \neq l} \mathcal{K}_{D_p, D_l}^{k_m}[\psi_p] = F_{l,2}\,,
\end{cases}
$$

and

$$
\begin{cases}
F_{l,1} = -u^i \quad \text{on } \partial D_l\,, \\[2mm]
F_{l,2} = -\dfrac{1}{\mu_m}\dfrac{\partial u^i}{\partial \nu} \quad \text{on } \partial D_l\,.
\end{cases}
$$

24.3.2 First-Order Correction to Plasmonic Resonances and Field Behavior at Plasmonic Resonances in the Multi-Particle Case

We consider the scattering in the quasi-static regime, *i.e.*, when the incident wavelength is much greater than one. With proper dimensionless analysis, we can assume that $\omega \ll 1$. As a consequence, $\mathcal{S}_D^{k_c}$ is invertible. Note that

$$
\phi_l = (\mathcal{S}_{D_l}^{k_c})^{-1}\Big(\mathcal{S}_{D_l}^{k_m}[\psi_l] + \sum_{p \neq l} \mathcal{S}_{D_p, D_l}^{k_m}[\psi_p] - F_{l,1}\Big)\,.
$$

We obtain the following equation for ψ_l's,

$$
\mathcal{A}_D(w)[\psi] = f\,,
$$

where

$$
\mathcal{A}_D(w) =
\begin{pmatrix}
\mathcal{A}_{D_1}(\omega) & & & \\
& \mathcal{A}_{D_2}(\omega) & & \\
& & \ddots & \\
& & & \mathcal{A}_{D_L}(\omega)
\end{pmatrix}
+
\begin{pmatrix}
0 & \mathcal{A}_{1,2}(\omega) & \cdots & \mathcal{A}_{1,L}(\omega) \\
\mathcal{A}_{2,1}(\omega) & 0 & \cdots & \mathcal{A}_{2,L}(\omega) \\
\vdots & \cdots & 0 & \vdots \\
\mathcal{A}_{L,1}(\omega) & \cdots & \mathcal{A}_{L,L-1}(\omega) & 0
\end{pmatrix}\,,
$$

$$
\psi = \begin{pmatrix} \psi_1 \\ \psi_2 \\ \vdots \\ \psi_L \end{pmatrix}\,, \quad
f = \begin{pmatrix} f_1 \\ f_2 \\ \vdots \\ f_L \end{pmatrix}\,,
$$

and

$$
\mathcal{A}_{l,p}(\omega) = \frac{1}{\mu_c}\Big(\frac{1}{2}I - (\mathcal{K}_{D_l}^{k_c})^*\Big)(\mathcal{S}_{D_l}^{k_c})^{-1}\mathcal{S}_{D_p, D_l}^{k_m} + \frac{1}{\mu_m}\mathcal{K}_{D_p, D_l}^{k_m}\,,
$$

$$
f_l = F_{l,2} + \frac{1}{\mu_c}\Big(\frac{1}{2}I - (\mathcal{K}_{D_l}^{k_c})^*\Big)(\mathcal{S}_{D_l}^{k_c})^{-1}[F_{l,1}]\,.
$$

The following asymptotic expansions hold.

Lemma 24.11 *(i) Regarded as operators from $\mathcal{H}^*(\partial D_p)$ into $\mathcal{H}^*(\partial D_l)$, we have*

$$\mathcal{A}_{D_j}(\omega) = \mathcal{A}_{D_j,0} + O(\delta^2\omega^2)\,,$$

(ii) Regarded as operators from $\mathcal{H}^*(\partial D_l)$ into $\mathcal{H}^*(\partial D_j)$, we have

$$\mathcal{A}_{l,p}(\omega) = \frac{1}{\mu_c}\Big(\frac{1}{2}I - \mathcal{K}_{D_l}^*\Big)\mathcal{S}_{D_l}^{-1}\big(\mathcal{S}_{p,l,0,1} + \mathcal{S}_{p,l,0,2}\big) + \frac{1}{\mu_m}\mathcal{K}_{p,l,0,0} + O(\delta^2\omega^2) + O(\delta^4)\,.$$

Moreover,

$$\Big(\frac{1}{2}I - \mathcal{K}_{D_l}^*\Big) \circ \mathcal{S}_{D_l}^{-1} \circ \mathcal{S}_{p,l,0,1} = O(\delta^2),$$

$$\Big(\frac{1}{2}I - \mathcal{K}_{D_l}^*\Big) \circ \mathcal{S}_{D_l}^{-1} \circ \mathcal{S}_{p,l,0,2} = O(\delta^3),$$

$$\mathcal{K}_{p,l,0,0} = O(\delta^2)\,.$$

Proof. The proof of (i) follows from Lemmas 24.2 and 24.37. We now prove (ii). Recall that

$$\frac{1}{2}I - (\mathcal{K}_{D_l}^{k_c})^* = \frac{1}{2}I - \mathcal{K}_{D_l}^* + O(\delta^2\omega^2)\,,$$

$$(\mathcal{S}_{D_l}^{k_c})^{-1} = \mathcal{S}_{D_l}^{-1} - k_c\mathcal{S}_{D_l}^{-1}\mathcal{S}_{D_l,1}\mathcal{S}_{D_l}^{-1} + O(\delta^2\omega^2)\,,$$

$$\mathcal{S}_{D_p,D_l}^{k_m} = \mathcal{S}_{p,l,0,0} + \mathcal{S}_{p,l,0,1} + \mathcal{S}_{p,l,0,2} + k_m\mathcal{S}_{p,l,1} + k_m^2\mathcal{S}_{p,l,2,0} + O(\delta^4) + O(\omega^2\delta^2)$$

$$\mathcal{K}_{D_p,D_l}^{k_m} = \mathcal{K}_{p,l,0,0} + O(\omega^2\delta^2)\,.$$

Using the identity

$$\Big(\frac{1}{2}I - \mathcal{K}_{D_l}^*\Big)\mathcal{S}_{D_l}^{-1}[\chi(D_l)] = 0\,,$$

we can derive that

$$\mathcal{A}_{l,p}(\omega) = \frac{1}{\mu_c}\Big(\frac{1}{2}I - \mathcal{K}_{D_l}^*\Big)(\mathcal{S}_{D_l}^{k_c})^{-1}\mathcal{S}_{D_p,D_l}^{k_m} + \frac{1}{\mu_m}\mathcal{K}_{p,l,0,0} + O(\delta^2\omega^2)$$

$$= \frac{1}{\mu_c}\Big(\frac{1}{2}I - \mathcal{K}_{D_l}^*\Big)\mathcal{S}_{D_l}^{-1}\mathcal{S}_{D_p,D_l}^{k_m} + \frac{1}{\mu_m}\mathcal{K}_{p,l,0,0} + O(\delta^2\omega^2)$$

$$= \frac{1}{\mu_c}\Big(\frac{1}{2}I - \mathcal{K}_{D_l}^*\Big)\mathcal{S}_{D_l}^{-1}\big(\mathcal{S}_{p,l,0,0} + \mathcal{S}_{p,l,0,1} + \mathcal{S}_{p,l,0,2} + k_m\mathcal{S}_{p,l,1} + k_m^2\mathcal{S}_{p,l,2,0} + O(\delta^4)\big)$$

$$+ \frac{1}{\mu_m}\mathcal{K}_{p,l,0,0} + O(\delta^2\omega^2)$$

$$= \frac{1}{\mu_c}\Big(\frac{1}{2}I - \mathcal{K}_{D_l}^*\Big)\mathcal{S}_{D_l}^{-1}\big(\mathcal{S}_{p,l,0,1} + \mathcal{S}_{p,l,0,2}\big) + \frac{1}{\mu_m}\mathcal{K}_{p,l,0,0} + O(\delta^2\omega^2) + O(\delta^4)\,.$$

The rest of the lemma follows from Lemmas 24.37 and 24.40. $\square$

Denote by $\mathcal{H}^*(\partial D) = \mathcal{H}^*(\partial D_1) \times \ldots \times \mathcal{H}^*(\partial D_L)$, which is equipped with the inner product

$$(\psi, \phi)_{\mathcal{H}^*} = \sum_{l=1}^{L} (\psi_l, \phi_l)_{\mathcal{H}^*(\partial D_l)} \,.$$

With the help of Lemma 24.11, the following result is obvious.

Lemma 24.12 *Regarded as an operator from $\mathcal{H}^*(\partial D)$ into $\mathcal{H}^*(\partial D)$, we have*

$$\mathcal{A}(\omega) = \mathcal{A}_{D,0} + \mathcal{A}_{D,1} + O(\omega^2 \delta^2) + O(\delta^4) \,,$$

where

$$\mathcal{A}_{D,0} = \begin{pmatrix} \mathcal{A}_{D_1,0} & & & \\ & \mathcal{A}_{D_2,0} & & \\ & & \ddots & \\ & & & \mathcal{A}_{D_L,0} \end{pmatrix}, \quad \mathcal{A}_{D,1} = \begin{pmatrix} 0 & \mathcal{A}_{D,1,12} & \mathcal{A}_{D,1,13} & \cdots \\ \mathcal{A}_{D,1,21} & 0 & \mathcal{A}_{D,1,23} & \cdots \\ & & \ddots & \\ \mathcal{A}_{D,1,L1} & \cdots & \mathcal{A}_{D,1,LL-1} & 0 \end{pmatrix}$$

with

$$\mathcal{A}_{D_l,0} = \Big(\frac{1}{2\mu_m} + \frac{1}{2\mu_c}\Big) I - \Big(\frac{1}{\mu_c} - \frac{1}{\mu_m}\Big) \mathcal{K}^*_{D_l} \,,$$

$$\mathcal{A}_{D,1,pq} = \frac{1}{\mu_c} \Big(\frac{1}{2} I - \mathcal{K}^*_{D_p}\Big) \mathcal{S}^{-1}_{D_p} \big(\mathcal{S}_{q,p,0,1} + \mathcal{S}_{q,p,0,2}\big) + \frac{1}{\mu_m} \mathcal{K}_{q,p,0,0} \,.$$

It is evident that

$$\mathcal{A}_{D,0}[\psi] = \sum_{j=0}^{\infty} \sum_{l=1}^{L} \tau_j (\psi, \varphi_{j,l})_{\mathcal{H}^*} \varphi_{j,l} \,, \tag{24.29}$$

where

$$\tau_j = \frac{1}{2\mu_m} + \frac{1}{2\mu_c} - \Big(\frac{1}{\mu_c} - \frac{1}{\mu_m}\Big) \lambda_j \,, \tag{24.30}$$

$$\varphi_{j,l} = \varphi_j e_l \tag{24.31}$$

with e_l being the standard basis of $\mathbb{R}^L$.

We take $\mathcal{A}(\omega)$ as a perturbation to the operator $\mathcal{A}_{D,0}$ for small ω and small δ. Using a standard perturbation argument, we can derive the perturbed eigenvalues and eigenfunctions. For simplicity, we assume that the following conditions hold.

Condition 24.13 *Each eigenvalue λ_j, $j \in J$, of the operator $\mathcal{K}^*_{D_1}$ is simple. Moreover, we have $\omega^2 \ll \delta$.*

In what follows, we only use the first order perturbation theory and derive the leading order term, *i.e.*, the perturbation due to the term $\mathcal{A}_{D,1}$. For each l, we define an $L \times L$ matrix R_l by letting

$$R_{l,pq} = \big(\mathcal{A}_{D,1}[\varphi_{l,p}], \varphi_{l,q}\big)_{\mathcal{H}^*},$$
$$= \big(\mathcal{A}_{D,1}[\varphi_l e_p], \varphi_l e_q\big)_{\mathcal{H}^*},$$
$$= \big(\mathcal{A}_{D,1,pq}[\varphi_l], \varphi_l\big)_{\mathcal{H}^*}.$$

Lemma 24.14 *The matrix* $R_l = (R_{l,pq})_{p,q=1,\ldots,L}$ *has the following explicit expression:*

$$R_{l,pp} = 0,$$
$$R_{l,pq} = \frac{3}{4\pi\mu_c}(\lambda_j - \frac{1}{2}) \sum_{|\alpha|=|\beta|=1} \int_{\partial D_0}\int_{\partial D_0} \frac{(z_p - z_q)^{\alpha+\beta}}{|z_p - z_q|^5} x^\alpha y^\beta \varphi_l(x)\varphi_l(y) d\sigma(x)d\sigma(y)$$
$$+\big(\frac{1}{4\pi\mu_c} - \frac{1}{4\pi\mu_m}\big)(\lambda_j - \frac{1}{2})\int_{\partial D_0}\int_{\partial D_0} \frac{x \cdot y}{|z_p - z_q|^3}\varphi_l(x)\varphi_l(y)d\sigma(x)d\sigma(y)$$
$$= O(\delta^3), \quad p \neq q.$$

Proof. It is clear that $R_{l,pp} = 0$. For $p \neq q$, we have

$$R_{l,pq} = R_{l,pq}^I + R_{l,pq}^{II} + R_{l,pq}^{III},$$

where

$$R_{l,pq}^I = \frac{1}{\mu_c}\Big(\big(\frac{1}{2}I - \mathcal{K}_{D_p}^*\big)\mathcal{S}_{D_p}^{-1}\mathcal{S}_{q,p,0,1}[\varphi_l], \varphi_l\Big)_{\mathcal{H}^*(\partial D_l)},$$
$$R_{l,pq}^{II} = \frac{1}{\mu_c}\Big(\big(\frac{1}{2}I - \mathcal{K}_{D_p}^*\big)\mathcal{S}_{D_p}^{-1}\mathcal{S}_{q,p,0,2}[\varphi_l], \varphi_l\Big)_{\mathcal{H}^*(\partial D_l)},$$
$$R_{l,pq}^{III} = \frac{1}{\mu_m}\big(\mathcal{K}_{q,p,0,0}[\varphi_l], \varphi_l\big)_{\mathcal{H}^*(\partial D_l)}.$$

We first consider $R_{l,pq}^I$. By the following identity

$$\big(\frac{1}{2}I - \mathcal{K}_{D_p}^*\big)\mathcal{S}_{D_l}[\varphi_l] = \mathcal{S}_{D_l}\big(\frac{1}{2}I - \mathcal{K}_{D_p}\big)[\varphi_l] = (\lambda_j - \frac{1}{2})\varphi_l,$$

we obtain

$$R_{l,pq}^I = -\frac{1}{\mu_c}\Big(\big(\frac{1}{2}I - \mathcal{K}_{D_p}^*\big)\mathcal{S}_{D_p}^{-1}\mathcal{S}_{q,p,0,1}[\varphi_l], \mathcal{S}_{D_l}[\varphi_l]\Big)_{L^2(\partial D_l)},$$
$$= \frac{1}{\mu_c}(\lambda_j - \frac{1}{2})\big(\mathcal{S}_{q,p,0,1}[\varphi_l], \mathcal{S}_{D_l}[\varphi_l]\big)_{L^2(\partial D_l)}.$$

Using the explicit representation of $\mathcal{S}_{q,p,0,1}$ and the fact that $(\chi(\partial D_j), \phi_l)_{L^2(\partial D_j)} = 0$ for $j \neq 0$, we further conclude that

$$R_{l,pq}^I = 0.$$

Similarly, we have

$$R^{II}_{l,pq} = \frac{1}{\mu_c}(\lambda_j - \frac{1}{2})\big(\mathcal{S}_{q,p,0,2}[\varphi_l], \mathcal{S}_{D_l}[\varphi_l]\big)_{L^2(\partial D_l)},$$

$$= \frac{1}{\mu_c}(\lambda_j - \frac{1}{2}) \sum_{|\alpha|=|\beta|=1} \int_{\partial D_0} \int_{\partial D_0} \Big(\frac{3(z_p - z_q)^{\alpha+\beta}}{4\pi|z_p - z_q|^5}x^\alpha y^\beta + \frac{\delta_{\alpha\beta}x^\alpha y^\beta}{4\pi|z_p - z_q|^3}\Big)\varphi_l(x)\varphi_l(y)d\sigma(x)d\sigma(y)$$

$$= \frac{3}{4\pi\mu_c}(\lambda_j - \frac{1}{2}) \sum_{|\alpha|=|\beta|=1} \int_{\partial D_0} \int_{\partial D_0} \frac{(z_p - z_q)^{\alpha+\beta}}{|z_p - z_q|^5}x^\alpha y^\beta \varphi_l(x)\varphi_l(y)d\sigma(x)d\sigma(y)$$

$$+ \frac{1}{4\pi\mu_c}(\lambda_j - \frac{1}{2}) \sum_{|\alpha|=1} \int_{\partial D_0} \int_{\partial D_0} \frac{1}{|z_p - z_q|^3}x^\alpha y^\alpha \varphi_l(x)\varphi_l(y)d\sigma(x)d\sigma(y).$$

Finally, note that

$$\mathcal{K}_{q,p,0,0}[\varphi_l] = \frac{1}{4\pi|z_p - z_q|^3}a \cdot \nu(x) = \frac{1}{4\pi|z_p - z_q|^3}\sum_{m=1}^{3} a_m\nu_m(x),$$

where $a_m = \big((y - z_q)_m, \varphi_l\big)_{L^2(\partial D_q)}$, and $a = (a_1, a_2, a_3)^T$.

By identity (24.23), we have

$$R^{III}_{l,pq} = -\frac{1}{\mu_m}\big(\mathcal{K}_{q,p,0,0}[\varphi_l], \varphi_l\big)_{\mathcal{H}^*(\partial D_l)}$$

$$= -\frac{1}{4\pi|z_p - z_q|^3\mu_m}\big(a \cdot \nu(x), \varphi_l\big)_{\mathcal{H}^*(\partial D_l)}$$

$$= -\frac{1}{4\pi|z_p - z_q|^3\mu_m}\Big((\frac{1}{2}I - \mathcal{K}^*_{D_p})\mathcal{S}^{-1}_{D_p}(a \cdot (x - z_p)), \varphi_l\Big)_{\mathcal{H}^*(\partial D_l)}$$

$$= -\frac{1}{4\pi|z_p - z_q|^3\mu_m}(\lambda_j - \frac{1}{2})\big(a \cdot (x - z_p), \varphi_l\big)_{L^2(\partial D_p)}$$

$$= -\frac{1}{4\pi|z_p - z_q|^3\mu_m}(\lambda_j - \frac{1}{2}) \int_{\partial D_0} \int_{\partial D_0} x \cdot y\varphi_l(x)\varphi_l(y)d\sigma(x)d\sigma(y).$$

This completes the proof of the lemma.

We now have an explicit formula for the matrix R_l. It is clear that R_l is symmetric, but not self-adjoint. For ease of presentation, we assume the following condition.

Condition 24.15 R_l *has L-distinct eigenvalues.*

We remark that Condition 24.15 is not essential for our analysis. Without this condition, the perturbation argument is still applicable, but the results may be quite complicated. We refer to [215] for a complete description of the perturbation theory.

Let $\tau_{j,l}$ and $X_{j,l} = (X_{j,l,1}, \cdots, X_{j,l,L})^T$, $l = 1, 2, \ldots, L$, be the eigenvalues and normalized eigenvectors of the matrix R_j. Here, T denotes the transpose. We remark that each $X_{j,l}$ may be complex valued and may not be orthogonal to other eigenvectors.

Under perturbation, each τ_j is splitted into the following L eigenvalues of $\mathcal{A}(\omega)$,

$$\tau_{j,l}(\omega) = \tau_j + \tau_{j,l} + O(\delta^4) + O(\omega^2\delta^2)\,. \tag{24.32}$$

The associated perturbed eigenfunctions have the following form

$$\varphi_{j,l}(\omega) = \sum_{p=1}^{L} X_{j,l,p} e_p \varphi_j + O(\delta^4) + O(\omega^2\delta^2)\,. \tag{24.33}$$

We are interested in solving the equation $\mathcal{A}_D(\omega)[\psi] = f$ when ω is close to the resonance frequencies, $i.e.$, when $\tau_j(\omega)$ are very small for some j's. In this case, the major part of the solution would be based on the excited resonance modes $\varphi_{j,l}(\omega)$. For this purpose, we introduce the index set of resonance J as we did in the previous section for a single particle case.

We define

$$P_J(\omega)\varphi_{j,m}(\omega) = \begin{cases} \varphi_{j,m}(\omega), & j \in J\,, \\ 0, & j \in J^c\,. \end{cases}$$

In fact,

$$P_J(\omega) = \sum_{j\in J} P_j(\omega) = \sum_{j\in J} \frac{1}{2\pi i} \int_{\gamma_j} (\xi - \mathcal{A}_D(\omega))^{-1} d\xi\,, \tag{24.34}$$

where γ_j is a Jordan curve in the complex plane enclosing only the eigenvalues $\tau_{j,l}(\omega)$ for $l = 1, 2, \ldots, L$ among all the eigenvalues.

To obtain an explicit representation of $P_J(\omega)$, we consider the adjoint operator $\mathcal{A}_D(\omega)^*$. By a similar perturbation argument, we can obtain its perturbed eigenvalue and eigenfunctions. Note that the adjoint matrix $\bar{R}_j^T = \bar{R}_j$ has eigenvalues $\overline{\tau_{j,l}}$ and corresponding eigenfunctions $\overline{X_{j,l}}$. Then the eigenvalues and eigenfunctions of $\mathcal{A}_D(\omega)^*$ have the following form

$$\widetilde{\tau}_{j,l}(\omega) = \tau_j + \overline{\tau_{j,l}} + O(\delta^4) + O(\omega^2\delta^2)\,,$$
$$\widetilde{\varphi}_{j,l}(\omega) = \widetilde{\varphi}_{j,l} + O(\delta^4) + O(\omega^2\delta^2)\,,$$

where

$$\widetilde{\varphi}_{j,l} = \sum_{p=1}^{L} \widetilde{X}_{j,l,p} e_p \varphi_j$$

with $\widetilde{X}_{j,l,p}$ being a multiple of $\overline{X_{j,l,p}}$.

We normalize $\widetilde{\varphi}_{j,l}$ in a way such that the following holds

$$(\varphi_{j,p}, \widetilde{\varphi}_{j,q})_{\mathcal{H}^*(\partial D)} = \delta_{pq}\,,$$

which is also equivalent to the following condition

$$\overline{X_{j,p}}^T \widetilde{X}_{j,q} = \delta_{pq}\,.$$

Then, we can show that the following result holds.

Lemma 24.16 *In the space $\mathcal{H}^*(\partial D)$, as ω goes to zero, we have*

$$f = \omega f_0 + O(\omega^2 \delta^{\frac{3}{2}}),$$

where $f_0 = (f_{0,1}, \ldots, f_{0,L})^T$ with

$$f_{0,l} = -i\sqrt{\varepsilon_m \mu_m} e^{ik_m d \cdot z_l} \left(\frac{1}{\mu_m} d \cdot \nu(x) + \frac{1}{\mu_c} \left(\frac{1}{2} I - \mathcal{K}_{D_l}^* \right) \mathcal{S}_{D_l}^{-1} [d \cdot (x - z)] \right) = O(\delta^{\frac{3}{2}}).$$

Proof. We first show that

$$\|u\|_{\mathcal{H}^*(\partial D_0)} = \delta^{\frac{3}{2}+m} \|u\|_{\mathcal{H}^*(\partial \widetilde{D})}, \quad \|u\|_{\mathcal{H}(\partial D_0)} = \delta^{\frac{1}{2}+m} \|u\|_{\mathcal{H}(\partial \widetilde{D})}$$

for any homogeneous function u such that $u(\delta x) = \delta^m u(x)$. Indeed, we have $\eta(u)(x) = \delta^m u(x)$. Since $\|\eta(u)\|_{\mathcal{H}^*(\partial \widetilde{D})} = \delta^{-\frac{3}{2}} \|u\|_{\mathcal{H}^*(\partial D_0)}$ (see Section 24.7), we obtain

$$\|u\|_{\mathcal{H}^*(\partial D_0)} = \delta^{\frac{3}{2}} \|\eta(u)\|_{\mathcal{H}^*(\partial \widetilde{D})} = \delta^{\frac{3}{2}+m} \|u\|_{\mathcal{H}^*(\partial \widetilde{D})},$$

which proves our first claim. The second claim follows in a similar way. Using this result, by a similar argument as in the proof of Lemma 24.7 we arrive at the desired asymptotic result.   □

Denote by $Z = (Z_1, \ldots, Z_L)$, where $Z_j = ik_m e^{ik_m d \cdot z_j}$. We are ready to present our main result in this section.

Theorem 24.17 *Under Conditions 24.1, 24.4, 24.5, 24.10, and 24.15, the scattered field by L plasmonic particles in the quasi-static regime has the following representation*

$$u^s = \mathcal{S}_D^{k_m}[\psi],$$

where

$$\psi = \sum_{j \in J} \sum_{l=1}^{L} \frac{\left(f, \widetilde{\varphi}_{j,l}(\omega) \right)_{\mathcal{H}^*} \varphi_{j,l}(\omega)}{\tau_{j,l}(\omega)} + \mathcal{A}_D(\omega)^{-1} (P_{J^c}(\omega) f)$$

$$= \sum_{j \in J} \sum_{l=1}^{L} \frac{(d \cdot \nu(x), \varphi_j)_{\mathcal{H}^*(\partial D_0)} Z \overline{\widetilde{X}_{j,l}} \varphi_{j,l} + O(\omega^2 \delta^{\frac{3}{2}})}{\lambda - \lambda_j + \left(\frac{1}{\mu_c} - \frac{1}{\mu_m} \right)^{-1} \tau_{j,l} + O(\delta^4) + O(\delta^2 \omega^2)} + O(\omega \delta^{\frac{3}{2}}).$$

Proof. The proof is similar to that of Theorem 24.8.   □

As a consequence, the following result holds.

Corollary 24.18 *With the same notation as in Theorem 24.17 and under the additional condition that*

$$\min_{j \in J} |\tau_{j,l}(\omega)| \gg \omega^q \delta^p,$$

for some integer p and q, and

$$\tau_{j,l}(\omega) = \tau_{j,l,p,q} + o(\omega^q \delta^p) \, ,$$

we have

$$\psi = \sum_{j \in J} \sum_{l=1}^{L} \frac{(d \cdot \nu(x), \varphi_j)_{\mathcal{H}^*(\partial D_0)} Z \overline{\widetilde{X}_{j,l}} \, \varphi_{j,l} + O(\omega^2 \delta^{\frac{3}{2}})}{\tau_{j,l,p,q}} + O(\omega \delta^{\frac{3}{2}}) \, .$$

24.4 Scattering and Absorption Enhancements

In this section we analyze the scattering and absorption enhancements. We prove that, at the quasi-static limit, the averages over the orientation of scattering and extinction cross-sections (see Definition 3.41) of a randomly oriented nanoparticle are given by (24.37) and (24.38), where M given by (11.5) is the polarization tensor associated with the nanoparticle D and the magnetic contrast $\mu_c(\omega)/\mu_m$, *i.e.*, with λ be defined by (24.17). In view of (24.42), the polarization tensor M blows up at the plasmonic resonances, which yields scattering and absorption enhancements. A bound on the extinction cross-section is derived in (24.44). As shown in (24.47) and (24.49), it can be sharpened for nanoparticles of elliptical or ellipsoidal shapes.

24.4.1 The Quasi-Static Limit

We start by recalling the small volume expansion in the far-field. The following asymptotic expansion holds.

Proposition 24.19 *Assume that $D = \delta B + z$. As δ goes to zero the scattered field u^s can be written as follows:*

$$u^s(x) = -k_m^2 \left(\frac{\varepsilon_c}{\varepsilon_m} - 1 \right) |D| \Gamma_{k_m}(x, z) u^i(z) - \nabla_z \Gamma_{k_m}(x, z) \cdot M(\lambda, D) \nabla u^i(z)$$

$$+ O \left(\frac{\delta^4}{\mathrm{dist}(\lambda, \sigma(\mathcal{K}_D^*))} \right)$$

(24.35)

for x away from D. Here, $\mathrm{dist}(\lambda, \sigma(\mathcal{K}_D^*))$ denotes $\min_j |\lambda - \lambda_j|$ with λ_j being the eigenvalues of $\mathcal{K}_D^*$.

Assume for simplicity that $\varepsilon_c = \varepsilon_m$. Let the scattering amplitude A_∞ be defined by (3.110). We explicitly compute A_∞. Take $u^i(x) = e^{ik_m d \cdot x}$ and assume again for simplicity that $z = 0$. Equation (24.35) yields, for $|x| \gg \frac{1}{\omega}$,

$$u^s(x) = \frac{e^{ik_m |x|}}{4\pi |x|} ik_m \left(ik_m \frac{x}{|x|} - \frac{x}{|x|^2} \right) \cdot M(\lambda, D)d + O(\frac{\delta^4}{\mathrm{dist}(\lambda, \sigma(\mathcal{K}_D^*))}) \, .$$

Since we are in the far-field region, we can write that, up to an error of order $\delta^4/\mathrm{dist}(\lambda, \sigma(\mathcal{K}_D^*))$,

$$u^s(x) = -k_m^2 \frac{e^{ik_m|x|}}{4\pi|x|}\left(\frac{x}{|x|}\cdot M(\lambda, D)d\right) + O\left(\frac{1}{|x|^2}\right). \tag{24.36}$$

In the next proposition we write the extinction and scattering cross-sections, Q_m^{ext} and Q_m^s, in terms of the polarization tensor.

Proposition 24.20 *The leading-order term (as δ goes to zero) of the average over the orientation of the extinction cross-section of a randomly oriented nanoparticle is given by*

$$Q_m^{ext} = -\frac{4\pi k_m}{3}\Im\left[\mathrm{trace}M(\lambda, D)\right], \tag{24.37}$$

where trace *denotes the trace of a matrix. The leading-order term of the average over the orientation scattering cross-section of a randomly oriented nanoparticle is given by*

$$Q_m^s = \frac{k_m^4}{9\pi}\left|\mathrm{trace}M(\lambda, D)\right|^2. \tag{24.38}$$

Proof. Remark from (24.36) that the scattering amplitude A_∞ in the case of a plane wave illumination is given by

$$A_\infty\left(\frac{x}{|x|}, d\right) = -\frac{k_m^2}{4\pi}\frac{x}{|x|}\cdot M(\lambda, D)d. \tag{24.39}$$

Using Theorem 3.42, we can see that for a given orientation

$$Q^{ext} = -4\pi k_m\Im\left[d\cdot M(\lambda, D)d\right].$$

Therefore, if we integrate Q^{ext} over all illuminations we find that

$$Q_m^{ext} = -k_m\Im\left[\int_S d\cdot M(\lambda, D)d\,d\sigma(d)\right].$$

Since $\Im M(\lambda, D)$ is symmetric, it can be written as $\Im M(\lambda, D) = P^t N(\lambda)P$, where P is unitary and N is diagonal and real. Then, by the change of variables $d = P^t x$ and using spherical coordinates, it follows that

$$Q_m^{ext} = -k_m\left[\int_S x\cdot N(\lambda)x\,d\sigma(x)\right],$$

and therefore,

$$Q_m^{ext} = -\frac{4\pi k_m}{3}\left[\mathrm{trace}N(\lambda)\right] = -\frac{4\pi k_m}{3}\Im\left[\mathrm{trace}M(\lambda, D)\right]. \tag{24.40}$$

Now, we compute the averaged scattering cross-section. Let $\Re M(\lambda, D) = \widetilde{P}^t \widetilde{N}(\lambda)\widetilde{P}$ where $\widetilde{P}$ is unitary and $\widetilde{N}$ is diagonal and real. We have

$$Q_m^s = \frac{k_m^4}{16\pi^2} \iint_{S\times S} |x \cdot M(\lambda, D)d|^2 \, d\sigma(x) \, d\sigma(d),$$

$$= \frac{k_m^4}{16\pi^2} \left[\iint_{S\times S} \left|\widetilde{x} \cdot N(\lambda)\widetilde{d}\right|^2 \, d\sigma(\widetilde{x})d\sigma(\widetilde{d}) + \iint_{S\times S} \left|\widetilde{x} \cdot \widetilde{N}(\lambda)\widetilde{d}\right|^2 \, d\sigma(\widetilde{x}) \, d\sigma(\widetilde{d}) \right].$$

Then a straightforward computation in spherical coordinates gives

$$Q_m^s = \frac{k_m^4}{9\pi} \left|\mathrm{trace} M(\lambda, D)\right|^2 ,$$

which completes the proof. $\square$

From Theorem 3.42, we obtain that the averaged absorption cross-section is given by

$$Q_m^a = -\frac{4\pi k_m}{3}\Im\left[\mathrm{trace} M(\lambda, D)\right] - \frac{k_m^4}{9\pi}\left|\mathrm{trace} M(\lambda, D)\right|^2 .$$

Therefore, under the condition (24.24), Q_m^a blows up at plasmonic resonances.

24.4.2 An Upper Bound for the Averaged Extinction Cross-Section

The goal of this section is to derive an upper bound for the modulus of the averaged extinction cross-section Q_m^{ext} of a randomly oriented nanoparticle. Recall that the entries $M_{lm}(\lambda, D)$ of the polarization tensor $M(\lambda, D)$ are given by

$$M_{lm}(\lambda, D) := \int_{\partial D} x_l(\lambda I - \mathcal{K}_D^*)^{-1}[\nu_m](x) \, d\sigma(x). \qquad (24.41)$$

For a $\mathcal{C}^{1,\alpha}$ domain D in $\mathbb{R}^d$, $\mathcal{K}_D^*$ is compact and self-adjoint in $\mathcal{H}^*$ (defined in Lemma 3.14 for $d = 3$ and in Lemma 3.17 for $d = 2$). Thus, we can write

$$(\lambda I - \mathcal{K}_D^*)^{-1}[\psi] = \sum_{j=0}^{\infty} \frac{(\psi, \varphi_j)_{\mathcal{H}^*} \otimes \varphi_j}{\lambda - \lambda_j} ,$$

with (λ_j, φ_j) being the eigenvalues and eigenvectors of $\mathcal{K}_D^*$ in $\mathcal{H}^*$ (see Lemma 3.14). Hence, the entries of the polarization tensor M can be decomposed as

$$M_{lm}(\lambda, D) = \sum_{j=1}^{\infty} \frac{\alpha_{lm}^{(j)}}{\lambda - \lambda_j} , \qquad (24.42)$$

where $\alpha_{lm}^{(j)} := (\nu_m, \varphi_j)_{\mathcal{H}^*}(\varphi_j, x_l)_{-\frac{1}{2}, \frac{1}{2}}$. Note that $(\nu_m, \chi(\partial D))_{-\frac{1}{2}, \frac{1}{2}} = 0$. So, considering the fact that $\lambda_0 = 1/2$, we have $(\nu_m, \varphi_0)_{\mathcal{H}^*} = 0$ and so, $\alpha_{lm}^{(0)} = 0$.

The following lemmas are useful for us.

Lemma 24.21 *We have*

$$\alpha_{l,l}^{(j)} \geq 0, \quad j \geq 1 \,.$$

Proof. For $d = 3$, we have

$$
\begin{aligned}
(\varphi_j, x_l)_{-\frac{1}{2},\frac{1}{2}} &= \left(\left(\frac{1}{2} - \lambda_j \right)^{-1} \left(\frac{1}{2}I - \mathcal{K}_D^* \right) [\varphi_j], x_l \right)_{-\frac{1}{2},\frac{1}{2}} \\
&= \frac{-1}{1/2 - \lambda_j} \left(\frac{\partial \mathcal{S}_D[\varphi_j]}{\partial \nu} \Big|_-, x_l \right)_{-\frac{1}{2},\frac{1}{2}} \\
&= \int_{\partial D} \frac{\partial x_l}{\partial \nu} \mathcal{S}_D[\varphi_j] d\sigma - \int_D \left(\Delta x_l \mathcal{S}_D[\varphi_j] - x_l \Delta \mathcal{S}_D[\varphi_j] \right) dx \\
&= \frac{(\nu_l, \varphi_j)_{\mathcal{H}^*}}{1/2 - \lambda_j} \,,
\end{aligned}
$$

where we used the fact that $\mathcal{S}_D[\varphi_j]$ is harmonic in D. Since $|\lambda_j| < 1/2$ for $j \geq 1$, we obtain the result. $\square$

Lemma 24.22 *Let*

$$M_{lm}(\lambda, D) = \sum_{j=1}^{\infty} \frac{\alpha_{l,m}^{(j)}}{\lambda - \lambda_j}$$

be the (l, m)-entry of the polarization tensor M associated with a $\mathcal{C}^{1,\alpha}$ domain $D \Subset \mathbb{R}^d$. Let δ_{lm} denote the Kronecker symbol. Then, the following properties hold:

(i)

$$\sum_{j=1}^{\infty} \alpha_{l,m}^{(j)} = \delta_{lm}|D| \,;$$

(ii)

$$\sum_{j=1}^{\infty} \lambda_i \sum_{l=1}^{d} \alpha_{l,l}^{(j)} = \frac{(d-2)}{2}|D| \,;$$

(iii)

$$\sum_{j=1}^{\infty} \lambda_j^2 \sum_{l=1}^{d} \alpha_{l,l}^{(j)} = \frac{(d-4)}{4}|D| + \sum_{l=1}^{d} \int_D |\nabla \mathcal{S}_D[\nu_l]|^2 dx \,.$$

Proof. The proof can be found in Section 24.8. $\square$

Let $\lambda = \lambda' + i\lambda''$. We have

$$\left|\Im(\text{trace}(M(\lambda, D)))\right| = \sum_{j=1}^{\infty} \frac{|\lambda''| \sum_{l=1}^{d} \alpha_{l,l}^{(j)}}{(\lambda' - \lambda_j)^2 + \lambda''^2}. \tag{24.43}$$

For $d = 2$ the spectrum $\sigma(\mathcal{K}_D^*)\backslash\{1/2\}$ is symmetric. For $d = 3$ this is no longer true. Nevertheless, for our purposes, we can assume that $\sigma(\mathcal{K}_D^*)\backslash\{1/2\}$ is symmetric by defining $\alpha_{l,l}^{(j)} = 0$ if λ_j is not in the original spectrum.

Without loss of generality we assume for ease of notation that Conditions 24.4 and 24.5 hold. Then we define the bijection $\rho : \mathbb{N}^+ \to \mathbb{N}^+$ such that $\lambda_{\rho(j)} = -\lambda_j$ and we can write

$$\begin{aligned}
\left|\Im(\text{trace}(M(\lambda, D)))\right| &= \frac{1}{2}\left(\sum_{j=1}^{\infty} \frac{|\lambda''|\beta_j}{(\lambda' - \lambda_j)^2 + \lambda''^2} + \sum_{j=1}^{\infty} \frac{|\lambda''|\beta^{(\rho(j))}}{(\lambda' + \lambda_j)^2 + \lambda''^2} \right) \\
&= \frac{|\lambda''|}{2} \sum_{j=1}^{\infty} \frac{(\lambda'^2 + \lambda''^2 + \lambda_j^2)(\beta^{(j)} + \beta^{(\rho(j))}) + 2\lambda'\lambda_j(\beta^{(j)} - \beta^{(\rho(j))})}{\left((\lambda' - \lambda_j)^2 + \lambda''^2\right)\left((\lambda' + \lambda_j)^2 + \lambda''^2\right)},
\end{aligned}$$

where $\beta_j = \sum_{l=1}^{d} \alpha_{l,l}^{(j)}$.

From Lemma 24.21 it follows that

$$\frac{(\lambda'^2 + \lambda''^2 + \lambda_j^2)(\beta^{(j)} + \beta^{(\rho(j))}) + 2\lambda'\lambda_j(\beta^{(j)} - \beta^{(\rho(j))})}{\left((\lambda' - \lambda_j)^2 + \lambda''^2\right)\left((\lambda' + \lambda_j)^2 + \lambda''^2\right)} \geq 0.$$

Moreover,

$$\frac{(\lambda'^2 + \lambda''^2 + \lambda_j^2)(\beta^{(j)} + \beta^{(\rho(j))}) + 2\lambda'\lambda_j(\beta^{(j)} - \beta^{(\rho(j))})}{\left((\lambda' - \lambda_j)^2 + \lambda''^2\right)\left((\lambda' + \lambda_j)^2 + \lambda''^2\right)} \leq$$

$$\frac{(\lambda'^2 + \lambda''^2 + \lambda_j^2)(\beta^{(j)} + \beta^{(\rho(j))}) + 2\lambda'\lambda_j(\beta^{(j)} - \beta^{(\rho(j))})}{\lambda''^2(4\lambda'^2 + \lambda''^2)}$$

$$+ O\left(\frac{\lambda''^2}{4\lambda'^2 + \lambda''^2}\right).$$

Hence,

$$\left|\Im(\text{trace}(M(\lambda, D)))\right| \leq \frac{|\lambda''|}{2} \sum_{j=1}^{\infty} \frac{(\lambda'^2 + \lambda''^2 + \lambda_j^2)(\beta^{(j)} + \beta^{(\rho(j))}) + 2\lambda'(\lambda_j\beta^{(j)} + \lambda_{\rho(j)}\beta^{(\rho(j))})}{\lambda''^2(4\lambda'^2 + \lambda''^2)} + O\left(\frac{\lambda''^2}{4\lambda'^2 + \lambda''^2}\right).$$

Using Lemma 24.22 we obtain the following result.

Theorem 24.23 *Let $M(\lambda, D)$ be the polarization tensor associated with a $\mathcal{C}^{1,\alpha}$ domain $D \Subset \mathbb{R}^d$ with $\lambda = \lambda' + i\lambda''$ such that $|\lambda''| \ll 1$ and $|\lambda'| < 1/2$. Then,*

$$\left|\Im(\text{trace}(M(\lambda, D)))\right| \leq \frac{d|\lambda''||D|}{\lambda''^2 + 4\lambda'^2}$$

$$+ \frac{1}{|\lambda''|(\lambda''^2 + 4\lambda'^2)}\left(d\lambda'^2|D| + \frac{(d-4)}{4}|D| + \sum_{l=1}^{d}\int_D |\nabla \mathcal{S}_D[\nu_l]|^2 dx + 2\lambda'\frac{(d-2)}{2}|D|\right)$$

$$+ O(\frac{\lambda''^2}{4\lambda'^2 + \lambda''^2}).$$

The bound in the above theorem depends not only on the volume of the particle but also on its geometry. Nevertheless, we remark that, since $|\lambda_j| < \frac{1}{2}$,

$$\sum_{j=1}^{\infty} \lambda_j^2 \sum_{l=1}^{d} \alpha_{l,l}^{(j)} < \frac{d|D|}{4}.$$

Hence, we can find a geometry independent, but not optimal, bound.

Corollary 24.24 *We have*

$$\left|\Im(\text{trace}(M(\lambda, D)))\right| \leq \frac{1}{|\lambda''|(\lambda''^2 + 4\lambda'^2)}\left(d|D|\left(\lambda'^2 + \frac{1}{4}\right) + 2\lambda'\frac{(d-2)}{2}|D|\right) + \frac{d|\lambda''||D|}{\lambda''^2 + 4\lambda'^2} + O(\frac{\lambda''^2}{4\lambda'^2 + \lambda''^2}).$$

$$(24.44)$$

Bound for ellipses

If D is an ellipse whose semi-axes are on the x_1- and x_2- axes and of length a and b, respectively, then its polarization tensor takes the form (11.11),

$$M(\lambda, D) = \begin{pmatrix} \dfrac{|D|}{\lambda - \frac{1}{2}\frac{a-b}{a+b}} & 0 \\ 0 & \dfrac{|D|}{\lambda + \frac{1}{2}\frac{a-b}{a+b}} \end{pmatrix}. \qquad (24.45)$$

On the other hand, in $\mathcal{H}^*(\partial D)$,

$$\sigma(\mathcal{K}_D^*)\backslash\{1/2\} = \left\{\pm\frac{1}{2}\left(\frac{a-b}{a+b}\right)^j, \quad j = 1, 2, \dots\right\}.$$

Then, from (24.42), we also have

$$M(\lambda, D) = \begin{pmatrix} \displaystyle\sum_{j=1}^{\infty} \frac{\alpha_{1,1}^{(j)}}{\lambda - \frac{1}{2}\left(\frac{a-b}{a+b}\right)^j} & \displaystyle\sum_{j=1}^{\infty} \frac{\alpha_{1,2}^{(j)}}{\lambda - \frac{1}{2}\left(\frac{a-b}{a+b}\right)^j} \\ \displaystyle\sum_{j=1}^{\infty} \frac{\alpha_{1,2}^{(j)}}{\lambda - \frac{1}{2}\left(\frac{a-b}{a+b}\right)^j} & \displaystyle\sum_{j=1}^{\infty} \frac{\alpha_{2,2}^{(j)}}{\lambda - \frac{1}{2}\left(\frac{a-b}{a+b}\right)^j} \end{pmatrix}.$$

Let $\lambda_1 = \dfrac{1}{2}\dfrac{a-b}{a+b}$ and $\mathcal{V}(\lambda_j) = \{i \in \mathbb{N} \text{ such that } \mathcal{K}_D^*[\varphi_i] = \lambda_j\varphi_i\}$. It is clear now that

$$\sum_{i\in\mathcal{V}(\lambda_1)} \alpha_{1,1}^{(i)} = \sum_{i\in\mathcal{V}(-\lambda_1)} \alpha_{2,2}^{(i)} = |D|, \quad \sum_{i\in\mathcal{V}(\lambda_j)} \alpha_{1,1}^{(i)} = \sum_{i\in\mathcal{V}(-\lambda_j)} \alpha_{2,2}^{(i)} = 0 \quad (24.46)$$

for $j \geq 2$ and

$$\sum_{i\in\mathcal{V}(\lambda_j)} \alpha_{1,2}^{(i)} = 0$$

for $j \geq 1$.

In view of (24.46), we have

$$\frac{\beta^{(j)}}{(\lambda' - \lambda_j)^2 + \lambda''^2} + \frac{\beta^{(\rho(j))}}{(\lambda' + \lambda_j)^2 + \lambda''^2} \leq \frac{4\lambda'^2\beta^{(j)} + \lambda''^2(\beta^{(j)} + \beta^{(j)})}{\lambda''^2(4\lambda'^2 + \lambda''^2)} + O\left(\frac{\lambda''^2}{4\lambda'^2 + \lambda''^2}\right).$$

Hence,

$$|\Im(\mathrm{Tr}(M(\lambda, D)))| \leq \frac{|\lambda''|}{2} \sum_{j=1}^{\infty} \frac{4\lambda'^2\beta^{(j)} + \lambda''^2(\beta^{(j)} + \beta^{(j)})}{\lambda''^2(4\lambda'^2 + \lambda''^2)} + O\left(\frac{\lambda''^2}{4\lambda'^2 + \lambda''^2}\right).$$

Note that for for any ellipse $\widetilde{D}$ of semi-axes of length a and b, $\Im(\mathrm{trace}(M(\lambda, \widetilde{D}))) = \Im(\mathrm{trace}(M(\lambda, D)))$. Then using Lemma 24.22 we obtain the following result.

Corollary 24.25 *For any ellipse $\widetilde{D}$ of semi-axes of length a and b, we have*

$$|\Im(\mathrm{trace}(M(\lambda, \widetilde{D})))| \leq \frac{|\widetilde{D}|4\lambda'^2}{|\lambda''|(\lambda''^2 + 4\lambda'^2)} + \frac{2|\lambda''||\widetilde{D}|}{\lambda''^2 + 4\lambda'^2} + O\left(\frac{\lambda''^2}{4\lambda'^2 + \lambda''^2}\right).$$
$$(24.47)$$

Figure 24.1 shows (24.47) and the average extinction of two ellipses of semi-axis a and b, where the ratio $a/b = 2$ and $a/b = 4$, respectively.

We can see from (24.43), Lemma 24.21 and the first sum rule in Lemma 24.22 that for an arbitrary shape B, $|\Im(\mathrm{trace}(M(\lambda, B)))|$ is a convex combination of $\frac{|\lambda''|}{(\lambda' - \lambda_j)^2 + \lambda''^2}$ for $\lambda_j \in \sigma(\mathcal{K}_B^*)\backslash\{1/2\}$. Since ellipses put all the weight of this convex combination in $\pm\lambda_1 = \pm\frac{1}{2}\frac{a-b}{a+b}$, we have for any ellipse $\widetilde{D}$ and any shape B such that $|B| = |\widetilde{D}|$,

$$|\Im(\mathrm{trace}(M(\lambda^*, B)))| \leq |\Im(\mathrm{trace}(M(\lambda^*, \widetilde{D})))|$$

with

$$\lambda^* = \pm\frac{1}{2}\frac{a-b}{a+b} + i\lambda''.$$

Thus, bound (24.47) applies for any arbitrary shape B in dimension two. This implies that, for a given material and a given desired resonance frequency ω^*, the optimal shape for the extinction resonance (in the quasi-static limit) is an ellipse of semi-axis a and b such that $\lambda'(\omega^*) = \pm\frac{1}{2}\frac{a-b}{a+b}$.
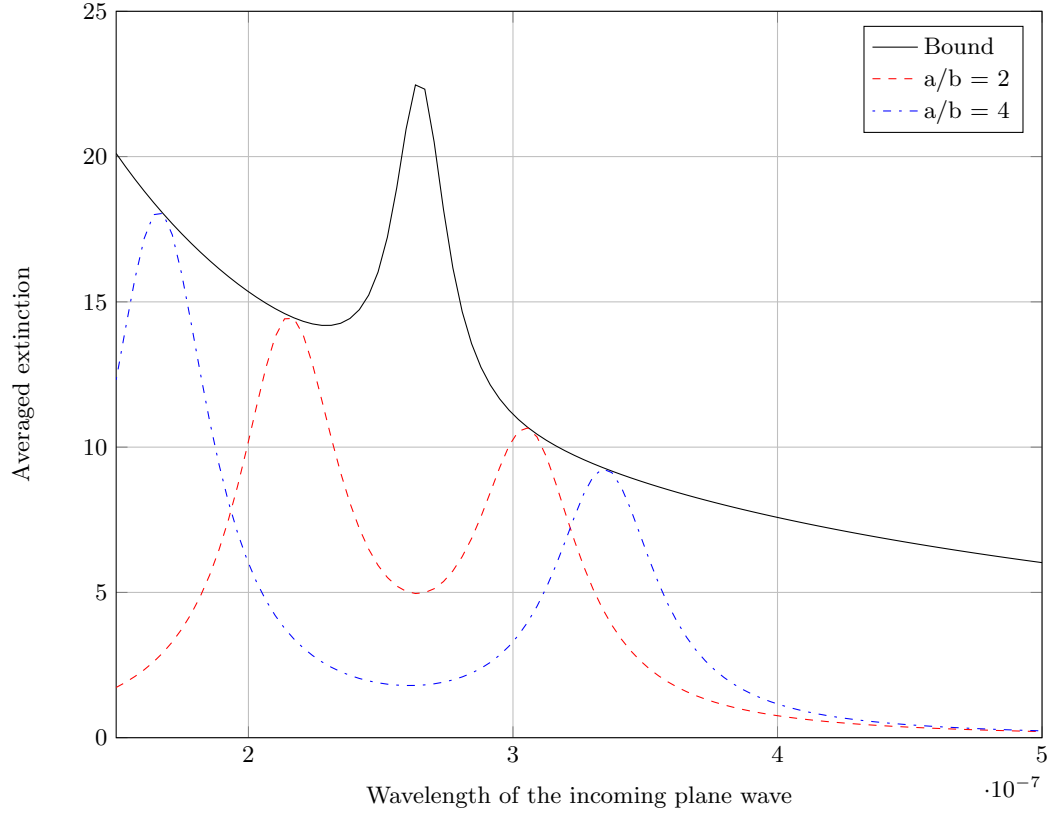
Fig. 24.1. Optimal bound for ellipses.

Bound for ellipsoids

Let D be an ellipsoid given by

$$\frac{x_1^2}{p_1^2} + \frac{x_2^2}{p_2^2} + \frac{x_3^2}{p_3^2} = 1. \tag{24.48}$$

The following holds [50].

Lemma 24.26 *Let D be the ellipsoid defined by* (24.48). *Then, for $x \in D$,*

$$\mathcal{S}_D[\nu_l](x) = s_l x_l, \quad l = 1, 2, 3,$$

where

$$s_l = -\frac{p_1 p_2 p_3}{2} \int_0^\infty \frac{1}{(p_l^2 + s)\sqrt{(p_1^2 + s)(p_2^2 + s)(p_3^2 + s)}} ds.$$

Then we have

$$\sum_{l=1}^{3} \int_D |\nabla \mathcal{S}_D[\nu_l]|^2 dx = (s_1^2 + s_2^2 + s_3^2)|D|\,.$$

For a rotated ellipsoid $\widetilde{D} = \mathcal{R}D$ with $\mathcal{R}$ being a rotation matrix, from Theorem 11.4, we have $M(\lambda, \widetilde{D}) = \mathcal{R}M(\lambda, D)\mathcal{R}^T$ and so $\mathrm{trace}(M(\lambda, \widetilde{D})) = \mathrm{trace}(M(\lambda, D))$. Therefore, for any ellipsoid $\widetilde{D}$ of semi-axes of length p_1, p_2 and p_3 the following result holds.

Corollary 24.27 *For any ellipsoid $\widetilde{D}$ of semi-axes of length p_1, p_2 and p_3, we have*

$$\Im(\mathrm{trace}(M(\lambda, \widetilde{D}))) \leq \frac{|\widetilde{D}|\left(3\lambda'^2 + \lambda' - \frac{1}{4} + (s_1^2 + s_2^2 + s_3^2)\right)}{|\lambda''|(\lambda''^2 + 4\lambda'^2)} + \frac{3|\lambda''||\widetilde{D}|}{\lambda''^2 + 4\lambda'^2} + O(\frac{\lambda''^2}{4\lambda'^2 + \lambda''^2})\,,$$
$$(24.49)$$

where for $j = 1, 2, 3$,

$$s_j = -\frac{p_1 p_2 p_3}{2} \int_0^\infty \frac{1}{(p_j^2 + s)\sqrt{(p_1^2 + s)(p_2^2 + s)(p_3^2 + s)}} ds\,.$$

24.5 Link with the Scattering Coefficients

Our aim in this section is to exhibit the mechanism underlying plasmonic resonances in terms of the scattering coefficients corresponding to the nanoparticle. The concept of scattering coefficients was first introduced in Subsection 3.2.7. The scattering coefficients are simply the Fourier coefficients of the scattering amplitude A_∞. In Theorem 24.31 we provide an asymptotic expansion of the scattering amplitude in terms of the scattering coefficients of order ± 1. Our formula shows that, under physical conditions, the scattering coefficients of orders ± 1 are the only scattering coefficients inducing the scattering cross-section enhancement. For simplicity we only consider here the two-dimensional case.

24.5.1 Scattering coefficients of plasmonic nanoparticles

We fiesr recall the notion of scattering coefficients. From Graf's addition formula [50] and (24.2) the following asymptotic formula holds as $|x| \to \infty$

$$u^s(x) = (u - u^i)(x) = -\frac{i}{4} \sum_{n \in \mathbb{Z}} H_n^{(1)}(k_m|x|)e^{in\theta_x} \int_{\partial D} J_n(k_m|y|)e^{-in\theta_y} \psi(y)d\sigma(y)\,,$$

where $x = (|x|, \theta_x)$ in polar coordinates, $H_n^{(1)}$ is the Hankel function of the first kind and order n, J_n is the Bessel function of order n and ψ is the solution

to (24.4).

For $u^i(x) = e^{ik_m d \cdot x}$ we have

$$u^i(x) = \sum_{m \in \mathbb{Z}} a_m(u^i) J_m(k_m |x|) e^{im\theta_x} \,,$$

where $a_m(u^i) = e^{im(\frac{\pi}{2} - \theta_d)}$. By the superposition principle, we get

$$\psi = \sum_{m \in \mathbb{Z}} a_m(u^i) \psi_m \,,$$

where ψ_m is solution to (24.4) replacing f by

$$f^{(m)} := F_2^{(m)} + \frac{1}{\mu_c} \left(\frac{1}{2} I - (\mathcal{K}_D^{k_c})^* \right) (\mathcal{S}_D^{k_c})^{-1} [F_1^{(m)}]$$

with

$$F_1^{(m)}(x) = -J_m(k_m|x|) e^{im\theta_x} \,,$$
$$F_2^{(m)}(x) = -\frac{1}{\mu_m} \frac{\partial J_m(k_m|x|) e^{im\theta_x}}{\partial \nu} \,.$$

We have

$$u^s(x) = (u - u^i)(x) = -\frac{i}{4} \sum_{n \in \mathbb{Z}} H_n^{(1)}(k_m|x|) e^{in\theta_x} \sum_{m \in \mathbb{Z}} W_{nm} e^{im(\frac{\pi}{2} - \theta_d)} \,,$$

where

$$W_{nm} = \int_{\partial D} J_n(k_m|y|) e^{-in\theta_y} \psi_m(y) d\sigma(y) \,. \tag{24.50}$$

The coefficients W_{nm} were called the scattering coefficients.

Lemma 24.28 *In the space* $\mathcal{H}^*(\partial D)$, *as* ω *goes to zero, we have*

$$f^{(0)} = O(\omega^2) \,,$$
$$f^{(\pm 1)} = \omega f_1^{(\pm 1)} + O(\omega^2) \,,$$
$$f^{(m)} = O(\omega^m), \quad |m| > 1 \,,$$

where

$$f_1^{(\pm 1)} = \mp \frac{\sqrt{\varepsilon_m \mu_m}}{2} \left(\frac{1}{\mu_m} e^{i \pm \theta_\nu} + \frac{1}{\mu_c} \left(\frac{1}{2} I - \mathcal{K}_D^* \right) \widetilde{\mathcal{S}}_D^{-1} [|x| e^{i \pm \theta_x}] \right) \,.$$

Proof. Recall that $J_0(x) = 1 + O(x^2)$. By virtue of the fact that

$$\left(\frac{1}{2} I - (\mathcal{K}_D^{k_c})^* \right) (\mathcal{S}_D^{k_c})^{-1} [\chi(\partial D)] = O(\omega^2),$$

we arrive at the estimate for $f^{(0)}$. Moreover,

$$J_{\pm 1}(x) = \pm \frac{x}{2} + O(x^3)$$

together with the fact that

$$\left(\frac{1}{2}I - (\mathcal{K}_D^{k_c})^*\right)(\mathcal{S}_D^{k_c})^{-1} = \left(\frac{1}{2}I - \mathcal{K}_D^*\right)\widetilde{\mathcal{S}}_D^{-1} + O(\omega^2 \log \omega)$$

gives the expansion of $f^{(\pm 1)}$ in terms of ω.

Finally, $J_m(x) = O(x^m)$ immediately yields the desired estimate for $f^{(m)}$.
□

It is easy to see that

$$\psi_m = \sum_{j \in J} \frac{\left(f^{(m)}, \widetilde{\varphi}_j(\omega)\right)_{\mathcal{H}^*} \varphi_j(\omega)}{\tau_j(\omega)} + \mathcal{A}_D(\omega)^{-1}(P_{J^c}(\omega)f). \qquad (24.51)$$

Hence, from the definition of the scattering coefficients,

$$W_{nm} = \sum_{j \in J} \frac{\left(f^{(m)}, \widetilde{\varphi}_j(\omega)\right)_{\mathcal{H}^*} \left(\varphi_j(\omega), J_n(k_m|x|)e^{-in\theta_x}\right)_{-\frac{1}{2}, \frac{1}{2}}}{\tau_j(\omega)} + \int_{\partial D} J_n(k_m|y|)e^{-in\theta_y} O(\omega) d\sigma(y).$$

$$(24.52)$$

Since

$$J_m(x) \sim \frac{(-1)^m}{\sqrt{2\pi|m|}} \left(\frac{ex}{2|m|}\right)^{|m|}$$

as $m \to \infty$, we have

$$|f^{(m)}| \le \frac{C^{|m|}}{|m|^{|m|}}.$$

Using the Cauchy–Schwarz inequality and Lemma 24.28, we obtain the following result.

Proposition 24.29 *For* $|n|, |m| > 0$, *we have*

$$|W_{nm}| \le \frac{O(\omega^{|n|+|m|})}{\min_{j \in J} |\tau_j(\omega)|} \frac{C^{|n|+|m|}}{|n|^{|n|}|m|^{|m|}}$$

for a positive constant C *independent of* ω.

24.5.2 The Leading-Order Term in the Expansion of the Scattering Amplitude

In the following, we analyze the first-order scattering coefficients.

Lemma 24.30 *Assume that Conditions* 1 *and* 2 *hold. Then,*

$$\psi_0 = \sum_{j \in J} \frac{O(\omega^2)}{\tau_j(\omega)} + O(\omega),$$

$$\psi_{\pm 1} = \sum_{j \in J} \frac{\pm \omega \frac{\sqrt{\varepsilon_m \mu_m}}{2}\left(\frac{1}{\mu_m} - \frac{1}{\mu_c}\right)(e^{\pm i\theta_\nu}, \varphi_j)_{\mathcal{H}^*} \varphi_j + O(\omega^3 \log \omega)}{\tau_j(\omega)} + O(\omega).$$

Proof. The expression of ψ_0 follows from (24.51) and Lemma 24.28. Changing $\mathcal{S}_D$ by $\widetilde{\mathcal{S}}_D$ in Theorem 24.8 gives $\left((\frac{1}{2}I - \mathcal{K}_D^*)\widetilde{\mathcal{S}}_D^{-1}[|x|e^{i\theta_x}], \varphi_j\right)_{\mathcal{H}^*} = -(e^{i\theta_\nu}, \varphi_j)_{\mathcal{H}^*}$. Using now Lemma 24.28 in (24.51) yields the expression of $\psi_{\pm 1}$. $\square$

Recall that in two dimensions,

$$\tau_j(\omega) = \frac{1}{2\mu_m} + \frac{1}{2\mu_c} - \left(\frac{1}{\mu_c} - \frac{1}{\mu_m}\right)\lambda_j + O(\omega^2 \log \omega),$$

where λ_j is an eigenvalue of $\mathcal{K}_D^*$ and $\lambda_0 = 1/2$. Recall also that for $0 \in J$ we need $\tau_j \to 0$ and so $\mu_m \to \infty$, which is a limiting case that we can ignore. In practice, $P_J(\omega)[\varphi_0(\omega)] = 0$. We also have $(\varphi_j, \chi(\partial D))_{-\frac{1}{2};\frac{1}{2}} = 0$ for $j \neq 0$.
It follows then from the above lemmas and the expression of the scattering coefficients that

$$W_{00} = \sum_{j \in J} \frac{O(\omega^4 \log \omega)}{\tau_j(\omega)} + O(\omega),$$

$$W_{0 \pm 1} = \sum_{j \in J} \frac{O(\omega^3 \log \omega)}{\tau_j(\omega)} + O(\omega),$$

$$W_{\pm 1 0} = \sum_{j \in J} \frac{O(\omega^3)}{\tau_j(\omega)} + O(\omega^2).$$

Note that $W_{\pm 1 \pm 1}$ has a special structure. Indeed, from Lemma 24.30 and equation (24.52), we have

$$W_{\pm 1 \pm 1} = \sum_{j \in J} \frac{\pm \pm \omega \frac{\sqrt{\varepsilon_m \mu_m}}{2}\left(\frac{1}{\mu_m} - \frac{1}{\mu_c}\right)(\varphi_j, J_1(k_m|x|)e^{\mp i\theta_x})_{-\frac{1}{2},\frac{1}{2}}\left(e^{\pm i\theta_\nu}, \varphi_j\right)_{\mathcal{H}^*} + O(\omega^4 \log \omega)}{\tau_j(\omega)} + O(\omega^2),$$

$$= \sum_{j \in J} \frac{\pm \pm \omega^2 \frac{\varepsilon_m \mu_m}{4}\left(\frac{1}{\mu_m} - \frac{1}{\mu_c}\right)(\varphi_j, |x|e^{\mp i\theta_x})_{-\frac{1}{2},\frac{1}{2}}\left(e^{\pm i\theta_\nu}, \varphi_j\right)_{\mathcal{H}^*} + O(\omega^4 \log \omega)}{\tau_j(\omega)} + O(\omega^2),$$

$$= \frac{k_m^2}{4}\left(\sum_{j \in J} \frac{\pm \pm (\varphi_j, |x|e^{\mp i\theta_x})_{-\frac{1}{2},\frac{1}{2}}\left(e^{\pm i\theta_\nu}, \varphi_j\right)_{\mathcal{H}^*} + O(\omega^2 \log \omega)}{\lambda - \lambda_j + O(\omega^2 \log \omega)} + O(1)\right),$$

where λ is defined by (24.17). Now, assume that $\min_{j \in J} |\tau_j(\omega)| \gg \omega^2 \log \omega$. Then,

$$W_{\pm 1 \pm 1} = \frac{k_m^2}{4} \left(\sum_{j \in J} \frac{\pm \pm \left(\varphi_j, |x| e^{\mp i\theta_x} \right)_{-\frac{1}{2},\frac{1}{2}} \left(e^{\pm i\theta_\nu}, \varphi_j \right)_{\mathcal{H}^*}}{\lambda - \lambda_j} + O(1) \right). \quad (24.53)$$

Define the contracted polarization tensors by

$$N_{\pm, \pm}(\lambda, D) := \int_{\partial D} |x| e^{\pm i\theta_x} (\lambda I - \mathcal{K}_D^*)^{-1} [e^{\pm i\theta_\nu}](x) \, d\sigma(x).$$

It is clear that

$$\begin{aligned}
N_{+,+}(\lambda, D) &= M_{11}(\lambda, D) - M_{22}(\lambda, D) + i2M_{1,2}(\lambda, D), \\
N_{+,-}(\lambda, D) &= M_{11}(\lambda, D) + M_{22}(\lambda, D), \\
N_{-,+}(\lambda, D) &= M_{11}(\lambda, D) + M_{22}(\lambda, D), \\
N_{-,-}(\lambda, D) &= M_{11}(\lambda, D) - M_{22}(\lambda, D) - i2M_{12}(\lambda, D),
\end{aligned}$$

where $M_{lm}(\lambda, D)$ is the (l, m)-entry of the polarization tensor given by (11.5).

Finally, considering the above we can state the following result.

Theorem 24.31 *Let A_∞ be the scattering amplitude for the incoming plane wave $u^i(x) = e^{ik_m d \cdot x}$. Assume Conditions 1 and 2 and*

$$\min_{j \in J} |\tau_j(\omega)| \gg \omega^2 |\log \omega|.$$

Then, A_∞ admits the following asymptotic expansion

$$A_\infty \left(\frac{x}{|x|}, d \right) = \frac{x}{|x|}^T W_1 d + O(\omega^2),$$

where

$$W_1 = \begin{pmatrix} W_{-11} + W_{1-1} - 2W_{1,1} & i\left(W_{1-1} - W_{-11} \right) \\ i\left(W_{1-1} - W_{-11} \right) & -W_{-11} - W_{1-1} - 2W_{11} \end{pmatrix}.$$

Here, W_{nm} are the scattering coefficients defined by (24.50).

Proof. From (24.39), we have

$$A_\infty \left(\frac{x}{|x|}, d \right) = -k_m^2 \frac{x}{|x|}^T M(\lambda, D) d.$$

Since $\mathcal{K}_D^*$ is compact and self-adjoint in $\mathcal{H}^*$, we have

$$\begin{aligned}
N_{\pm, \pm}(\lambda, D) &= \sum_{j=1}^\infty \frac{\left(\varphi_j, |x| e^{\pm i\theta_x} \right)_{-\frac{1}{2},\frac{1}{2}} \left(e^{\pm i\theta_\nu}, \varphi_j \right)_{\mathcal{H}^*}}{\lambda - \lambda_j} \\
&= \sum_{j \in J} \frac{\left(\varphi_j, |x| e^{\pm i\theta_x} \right)_{-\frac{1}{2},\frac{1}{2}} \left(e^{\pm i\theta_\nu}, \varphi_j \right)_{\mathcal{H}^*}}{\lambda - \lambda_j} + O(1).
\end{aligned}$$

We have then from (24.53) that

$$-\frac{k_m^2}{4}N_{+,+}(\lambda, D) = W_{-11} + O(\omega^2)\,,$$

$$-\frac{k_m^2}{4}N_{+,-}(\lambda, D) = -W_{11} + O(\omega^2)\,,$$

$$-\frac{k_m^2}{4}N_{-,+}(\lambda, D) = -W_{11} + O(\omega^2)\,,$$

$$-\frac{k_m^2}{4}N_{-,-}(\lambda, D) = W_{1-1} + O(\omega^2)\,.$$

In view of

$$M_{11} = \frac{1}{4}\left(N_{+,+} + N_{-,-} + 2N_{+,-}\right)\,,$$

$$M_{22} = \frac{1}{4}\left(-N_{+,+} - N_{-,-} + 2N_{+,-}\right)\,,$$

$$M_{12} = \frac{-i}{4}\left(N_{+,+} - N_{-,-}\right)\,,$$

we get the result.   □

24.6 Asymptotic Expansion of the Integral Operators: Single Particle

In this section, we derive asymptotic expansions with respect to k of some boundary integral operators defined on the boundary of a bounded and simply connected smooth domain D in dimension three whose size is of order one.

We first consider the single layer potential

$$\mathcal{S}_D^k[\psi](x) = \int_{\partial D} \Gamma_k(x, y)\psi(y)d\sigma(y), \quad x \in \partial D\,,$$

where

$$\Gamma_k(x, y) = -\frac{e^{ik|x-y|}}{4\pi|x-y|}$$

is the Green function of Helmholtz equation in $\mathbb{R}^3$, subject to the Sommerfeld radiation condition. Note that

$$\Gamma_k(x, y) = -\sum_{j=0}^{\infty}\frac{(ik|x-y|)^j}{j!4\pi|x-y|} = -\frac{1}{4\pi|x-y|} - \frac{ik}{4\pi}\sum_{j=1}^{\infty}\frac{(ik|x-y|)^{j-1}}{j!}\,.$$

We get

$$\mathcal{S}_D^k = \mathcal{S}_D + \sum_{j=1}^{\infty}k^j\mathcal{S}_{D,j}\,, \tag{24.54}$$

where

$$\mathcal{S}_{D,j}[\psi](x) = -\frac{i}{4\pi}\int_{\partial D}\frac{(i|x-y|)^{j-1}}{j!}\psi(y)d\sigma(y)\,.$$

In particular, we have

$$\mathcal{S}_{D,1}[\psi](x) = -\frac{i}{4\pi}\int_{\partial D}\psi(y)d\sigma(y)\,, \tag{24.55}$$

$$\mathcal{S}_{D,2}[\psi](x) = -\frac{1}{4\pi}\int_{\partial D}|x-y|\psi(y)d\sigma(y)\,. \tag{24.56}$$

Lemma 24.32 $\|\mathcal{S}_{D,j}\|_{\mathcal{L}((\mathcal{H}^*(\partial D),\mathcal{H}(\partial D))}$ *is uniformly bounded with respect to* j. *Moreover, the series in (24.54) is convergent in* $\mathcal{L}(\mathcal{H}^*(\partial D),\mathcal{H}(\partial D))$.

Proof. It is clear that

$$\|\mathcal{S}_{D,j}\|_{\mathcal{L}(L^2(\partial D),W^{1,2}(\partial D))} \leq C\,,$$

where C is independent of j. On the other hand, a similar estimate also holds for the operator $\mathcal{S}_{D,j}^*$. It follows that

$$\|\mathcal{S}_{D,j}\|_{\mathcal{L}(W^{-1,2}(\partial D),L^2(\partial D))} \leq C\,.$$

Thus, we can conclude that $\|\mathcal{S}_{D,j}\|_{\mathcal{L}(W^2_{-1/2}(\partial D),W^2_{1/2}(\partial D))}$ is uniformly bounded by using interpolation theory. By the equivalence of norms in the $W^2_{-1/2}(\partial D)$ and $W^2_{1/2}(\partial D)$, the lemma follows immediately.   □

Note that $\mathcal{S}_D$ is invertible in dimension three, so is $\mathcal{S}_D^k$ for small k. By formally writing

$$(\mathcal{S}_D^k)^{-1} = \mathcal{S}_D^{-1} + k\mathcal{B}_{D,1} + k^2\mathcal{B}_{D,2} + \dots, \tag{24.57}$$

and using the identity $(\mathcal{S}_D^k)^{-1}\mathcal{S}_D^k = I$, we can derive that

$$\mathcal{B}_{D,1} = -\mathcal{S}_D^{-1}\mathcal{S}_{D,1}\mathcal{S}_D^{-1}, \quad \mathcal{B}_{D,2} = -\mathcal{S}_D^{-1}\mathcal{S}_{D,2}\mathcal{S}_D^{-1} + \mathcal{S}_D^{-1}\mathcal{S}_{D,1}\mathcal{S}_D^{-1}\mathcal{S}_{D,1}\mathcal{S}_D^{-1}\,. \tag{24.58}$$

We can also derive other lower-order terms $\mathcal{B}_{D,j}$.

Lemma 24.33 *The series in (24.57) converges in* $\mathcal{L}(\mathcal{H}(\partial D),\mathcal{H}^*(\partial D))$ *for sufficiently small* k.

Proof. Using the identity

$$(\mathcal{S}_D^k)^{-1} = (I + \mathcal{S}_D^{-1}\sum_{j=1}^{\infty}k^j\mathcal{S}_{D,j})^{-1}\mathcal{S}_D^{-1}\,,$$

the proof follows immediately.   □

We now consider the expansion for the boundary integral operator $(\mathcal{K}_D^k)^*$. We have

$$(\mathcal{K}_D^k)^* = \mathcal{K}_D^* + k\mathcal{K}_{D,1} + k^2\mathcal{K}_{D,2} + \dots, \qquad (24.59)$$

where

$$\mathcal{K}_{D,j}[\psi](x) = -\frac{i}{4\pi}\int_{\partial D}\frac{\partial(i|x-y|)^{j-1}}{j!\partial\nu(x)}\psi(y)d\sigma(y) = -\frac{i^j(j-1)}{4\pi j!}\int_{\partial D}|x-y|^{j-3}(x-y)\cdot\nu(x)\psi(y)d\sigma(y).$$

In particular, we have

$$\mathcal{K}_{D,1} = 0, \quad \mathcal{K}_{D,2}[\psi](x) = \frac{1}{4\pi}\int_{\partial D}\frac{(x-y)\cdot\nu(x)}{|x-y|}\psi(y)d\sigma(y). \qquad (24.60)$$

Lemma 24.34 *The norm $\|\mathcal{K}_{D,j}\|_{\mathcal{L}(\mathcal{H}^*(\partial D),\mathcal{H}^*(\partial D))}$ is uniformly bounded for $j \geq 1$. Moreover, the series in (24.59) is convergent in $\mathcal{L}(\mathcal{H}^*(\partial D), \mathcal{H}^*(\partial D))$.*

24.7 Asymptotic Expansion of the Integral Operators: Multiple Particles

In this section, we consider the three-dimensional case. We assume that the particles have size of order δ which is a small number and the distance between them is of order one. We write $D_j = z_j + \delta\widetilde{D}$, $j = 1, 2, \ldots, M$, where $\widetilde{D}$ has size one and is centered at the origin. Our goal is to derive estimates for various boundary integral operators considered in the paper that are defined on small particles in terms of their size. For this purpose, we denote by $D_0 = \delta\widetilde{D}$. For each function f defined on ∂D_0, we define a corresponding function on $\widetilde{D}$ by

$$\eta(f)(\widetilde{x}) = f(\delta\widetilde{x}).$$

We first state some useful results.

Lemma 24.35 *The following scaling properties hold:*

(i) $\|\eta(f)\|_{L^2(\partial\widetilde{D})} = \delta^{-1}\|f\|_{L^2(\partial D_0)}$;

(ii) $\|\eta(f)\|_{\mathcal{H}(\partial\widetilde{D})} = \delta^{-\frac{1}{2}}\|f\|_{\mathcal{H}(\partial D_0)}$;

(iii) $\|\eta(f)\|_{\mathcal{H}^*(\partial\widetilde{D})} = \delta^{-\frac{3}{2}}\|f\|_{\mathcal{H}^*(\partial D_0)}$.

Proof. The proof of (i) is straightforward and we only need to prove (ii) and (iii). To prove (iii), we have

$$\|f\|_{\mathcal{H}^*(\partial D_0)}^2 = \int_{\partial D_0}\int_{\partial D_0}\frac{f(x)f(y)}{4\pi|x-y|}d\sigma(x)d\sigma(y)$$
$$= \delta^3\int_{\partial\widetilde{D}}\int_{\partial\widetilde{D}}\frac{\eta(f)(\widetilde{x})\eta(f)(\widetilde{y})}{4\pi|\widetilde{x}-\widetilde{y}|}d\sigma(\widetilde{x})d\sigma(\widetilde{x})$$
$$= \delta^3\|\eta(f)\|_{\mathcal{H}^*(\partial\widetilde{D})}^2,$$

whence (iii) follows. To prove (ii), recall that

$$\|f\|_{\mathcal{H}(\partial D_0)} = \|\mathcal{S}_{D_0}^{-1}f\|_{\mathcal{H}^*(\partial D_0)}\,.$$

Let $u = \mathcal{S}_{D_0}^{-1}[f]$. Then $f = \mathcal{S}_{D_0}[u]$. We can show that

$$\eta(f) = \delta \mathcal{S}_{\widetilde{D}}(\eta(u))\,.$$

As a result, we have

$$\|\eta(f)\|_{\mathcal{H}(\partial\widetilde{D})} = \delta\|\mathcal{S}_{\widetilde{D}}(\eta(u))\|_{\mathcal{H}(\partial\widetilde{D})} = \delta\|\eta(u)\|_{\mathcal{H}^*(\partial\widetilde{D})} = \delta^{-\frac{1}{2}}\|u\|_{\mathcal{H}^*(\partial D_0)} = \delta^{-\frac{1}{2}}\|f\|_{\mathcal{H}(\partial D_0)}\,,$$

which proves (ii). □

Lemma 24.36 *Let X and Y be bounded and simply connected smooth domains in $\mathbb{R}^3$. Assume $0 \in X,Y$ and $X = \delta\widetilde{X}$, $Y = \delta\widetilde{Y}$. Let $\mathcal{R}$ and $\widetilde{\mathcal{R}}$ be two boundary integral operators from $\mathcal{D}'(\partial Y)$ to $\mathcal{D}'(\partial X)$ and $\mathcal{D}'(\partial\widetilde{Y})$ to $\mathcal{D}'(\partial\widetilde{X})$, respectively. Here, $\mathcal{D}'$ denotes the Schwartz space. Assume that both operators have the same Schwartz kernel R with the following homogeneous scaling property*

$$R(\delta x, \delta y) = \delta^m R(x,y)\,.$$

Then,

$$\|\mathcal{R}\|_{\mathcal{L}(\mathcal{H}^*(\partial Y),\mathcal{H}^*(\partial X))} = \delta^{2+m}\|\widetilde{\mathcal{R}}\|_{\mathcal{L}(\mathcal{H}^*(\partial\widetilde{Y}),\mathcal{H}^*(\partial\widetilde{X}))}\,,$$

$$\|\mathcal{R}\|_{\mathcal{L}(\mathcal{H}^*(\partial Y),\mathcal{H}(\partial X))} = \delta^{1+m}\|\widetilde{\mathcal{R}}\|_{\mathcal{L}(\mathcal{H}^*(\partial\widetilde{Y}),\mathcal{H}(\partial\widetilde{X}))}\,.$$

Proof. Lemma 24.35 together with the following identity

$$\mathcal{R} = \delta^{2+m}\eta^{-1}\circ\widetilde{\mathcal{R}}\circ\eta\,,$$

yields the desired result. □

We first consider the operators $\mathcal{S}_{D_j}^k$ and $(\mathcal{K}_{D_j}^k)^*$. The following asymptotic expansions hold.

Lemma 24.37 *(i) Regarded as operators from $\mathcal{H}^*(\partial D_j)$ into $\mathcal{H}(\partial D_j)$, we have*

$$\mathcal{S}_{D_j}^k = \mathcal{S}_{D_j} + k\mathcal{S}_{D_j,1} + k^2\mathcal{S}_{D_j,2} + O(k^3\delta^3)\,,$$

where $\mathcal{S}_{D_j} = O(1)$ and $\mathcal{S}_{D_j,m} = O(\delta^m)$;
(ii) Regarded as operators from $\mathcal{H}(\partial D_j)$ into $\mathcal{H}^*(\partial D_j)$, we have

$$(\mathcal{S}_{D_j}^k)^{-1} = \mathcal{S}_{D_j}^{-1} + k\mathcal{B}_{D_j,1} + k^2\mathcal{B}_{D_j,2} + O(k^3\delta^3)\,,$$

where $\mathcal{S}_{D_j}^{-1} = O(1)$ and $\mathcal{B}_{D_j,m} = O(\delta^m)$;
(iii) Regarded as operators from $\mathcal{H}^*(\partial D_j)$ into $\mathcal{H}^*(\partial D_j)$, we have

$$(\mathcal{K}_{D_j}^k)^* = \mathcal{K}_{D_j}^* + k^2 O(\delta^2)\,,$$

where $\mathcal{K}_{D_j}^* = O(1)$.

Proof. The proof immediately follows from Lemmas 24.36, 24.32, and 24.34.
□

We now consider the operator $\mathcal{S}_{D_j,D_l}^k$. By definition,

$$\mathcal{S}_{D_j,D_l}^k[\psi](x) = \int_{\partial D_j} \Gamma_k(x,y)\psi(y)d\sigma(y), \quad x \in \partial D_l.$$

Using the expansion

$$\Gamma_k(x,y) = \sum_{m=0}^{\infty} k^m Q_m(x,y),$$

where

$$Q_m(x,y) = -\frac{i^m |x-y|^{m-1}}{4\pi},$$

we can derive that

$$\mathcal{S}_{D_j,D_l}^k = \sum_{m\geq 0} k^m \mathcal{S}_{j,l,m},$$

where

$$\mathcal{S}_{j,l,m}[\psi](x) = \int_{\partial D_j} Q_m(x,y)\psi(y)d\sigma(y).$$

We can further write

$$\mathcal{S}_{j,l,m} = \sum_{n\geq 0} \mathcal{S}_{j,l,m,n},$$

where $\mathcal{S}_{j,l,m,n}$ is defined by

$$\mathcal{S}_{j,l,m,n}[\psi](x) = \int_{\partial D_j} \sum_{|\alpha|+|\beta|=n} \frac{1}{\alpha!\beta!} \frac{\partial^{|\alpha|+|\beta|}}{\partial x^\alpha \partial y^\beta} Q_m(z_l,z_j)(x-z_l)^\alpha (y-z_j)^\beta \psi(y)\, d\sigma(y).$$

In particular, we have

$$\mathcal{S}_{j,l,0,0}[\psi](x) = -\frac{1}{4\pi|z_j-z_l|}(\psi, \chi(\partial D_j))_{W^2_{-1/2}(\partial D_j), W^2_{1/2}(\partial D_j)}\chi(D_l),$$

$$\mathcal{S}_{j,l,0,1}[\psi](x) = \sum_{|\alpha|=1} \frac{(z_l-z_j)^\alpha}{4\pi|z_l-z_j|^3}\left((x-z_l)^\alpha(\psi, \chi(\partial D_l))_{W^2_{-1/2}(\partial D_j), W^2_{1/2}(\partial D_j)} + ((y-z_j)^\alpha, \psi)\chi(D_l)\right),$$

$$\mathcal{S}_{j,l,0,2}[\psi](x) = \sum_{|\alpha|+|\beta|=2} \frac{1}{\alpha!\beta!}\frac{\partial^2 Q_0(z_l,z_j)}{\partial x^\alpha \partial y^\beta}(x-z_l)^\alpha(y-z_j)^\beta \psi(y)d\sigma(y),$$

$$\mathcal{S}_{j,l,1}[\psi](x) = -\frac{i}{4\pi}(\psi, \chi(\partial D_j))_{W^2_{-1/2}(\partial D_j), W^2_{1/2}(\partial D_j)}\chi(D_l),$$

$$\mathcal{S}_{j,l,2,0}[\psi](x) = \frac{1}{4\pi}|z_l-z_j|(\psi, \chi(\partial D_j))_{W^2_{-1/2}(\partial D_j), W^2_{1/2}(\partial D_j)}\chi(D_l).$$

The following estimate holds.

Lemma 24.38 *We have* $\|\mathcal{S}_{j,l,m,n}\|_{\mathcal{L}(\mathcal{H}^*(\partial D),\mathcal{H}(\partial D))} \lesssim O(\delta^{n+1})$.

Proof. After a translation of coordinates, the stated estimate immediately follows from Lemma 24.36. $\square$

Similarly, for the operator $\mathcal{K}^{k_m}_{D_j,D_l}$ defined in the following way

$$\mathcal{K}^k_{D_j,D_l}[\psi](x) = \int_{\partial D_j} \frac{\partial \Gamma_k(x,y)}{\partial \nu(x)} \psi(y)d\sigma(y), \quad x \in \partial D_l,$$

we have

$$\mathcal{K}^k_{D_j,D_l} = \sum_{m \geq 0} k^m \sum_{n \geq 0} \mathcal{K}_{j,l,m,n},$$

where

$$\mathcal{K}_{j,l,m,n}[\psi](x) = \int_{\partial D_j} \sum_{|\alpha|+|\beta|=n} \frac{1}{\alpha!\beta!} \frac{\partial^n K_m(z_l,z_j)}{\partial x^\beta \partial y^\alpha}(x-z_l)^\beta(y-z_j)^\alpha(x-y)\cdot\nu(x)\psi(y)d\sigma(y)$$

with

$$K_m(x,y) = -\frac{i^m(m-1)|x-y|^{m-3}}{4\pi m!}.$$

In particular, we have

$$\mathcal{K}_{j,l,0,0}[\psi](x) = \frac{1}{4\pi|z_l-z_j|^3}\Big[(x-z_l)\cdot\nu(x)\big(\psi,\chi(\partial D_j)\big)_{W^2_{-1/2}(\partial D_j),W^2_{1/2}(\partial D_j)}$$

$$-\big(\psi,(y-z_j)\cdot\nu(x)\big)_{W^2_{-1/2}(\partial D_j),W^2_{1/2}(\partial D_j)}$$

$$+(z_l-z_j)\cdot\nu(x)\big(\psi,\chi(\partial D_j)\big)_{W^2_{-1/2}(\partial D_j),W^2_{1/2}(\partial D_j)}\Big], \quad (24.61)$$

$$\mathcal{K}_{j,l,1,m}[\psi] = 0 \quad \text{for all } m. \tag{24.62}$$

Lemma 24.39 *We have* $\|\mathcal{K}_{j,l,m,n}\|_{\mathcal{L}(\mathcal{H}^*(\partial D_j),\mathcal{H}^*(\partial D_l))} \lesssim O(\delta^{n+2})$.

Proof. Note that

$$\mathcal{K}_{j,l,m,n}[\psi](x) = \int_{\partial D_j} \sum_{|\alpha|+|\beta|=n} \frac{1}{\alpha!\beta!} \frac{\partial^n K_m(z_l,z_j)}{\partial x^\beta \partial y^\alpha}(x-z_l)^\beta(y-z_j)^\alpha(x-z_l)\cdot\nu(x)\psi(y)d\sigma(y),$$

$$-\int_{\partial D_j} \sum_{|\alpha|+|\beta|=n} \frac{1}{\alpha!\beta!} \frac{\partial^n K_m(z_l,z_j)}{\partial x^\beta \partial y^\alpha}(x-z_l)^\beta(y-z_j)^\alpha(y-z_j)\cdot\nu(x)\psi(y)d\sigma(y),$$

$$+\int_{\partial D_j} \sum_{|\alpha|+|\beta|=n} \frac{1}{\alpha!\beta!} \frac{\partial^n K_m(z_l,z_j)}{\partial x^\beta \partial y^\alpha}(x-z_l)^\beta(y-z_j)^\alpha(z_l-z_j)\cdot\nu(x)\psi(y)d\sigma(y).$$

After a translation of coordinates, we can apply Lemma 24.36 to each one of the three terms above to conclude that $\mathcal{K}_{j,l,m,n} = O(\delta^{n+3}) + O(\delta^{n+2})$. This completes the proof of the lemma. $\square$

To summarize, we have proven the following results.

Lemma 24.40 *(i) Regarded as an operator from $\mathcal{H}^*(\partial D_j)$ into $\mathcal{H}(\partial D_l)$ we have,*

$$\mathcal{S}_{D_j,D_l}^k = \mathcal{S}_{j,l,0,0} + \mathcal{S}_{j,l,0,1} + \mathcal{S}_{j,l,0,2} + k\mathcal{S}_{j,l,1} + k^2\mathcal{S}_{j,l,2,0} + O(\delta^4) + O(k^2\delta^2).$$

Moreover,

$$\mathcal{S}_{j,l,m,n} = O(\delta^{n+1}).$$

(ii) Regarded as an operator from $\mathcal{H}^*(\partial D_j)$ into $\mathcal{H}^*(\partial D_l)$, we have

$$\mathcal{K}_{D_j,D_l}^k = \mathcal{K}_{j,l,0,0} + O(k^2\delta^2).$$

Moreover,

$$\mathcal{K}_{j,l,0,0} = O(\delta^2).$$

24.8 Sum Rules for the Polarization Tensor

Let f be a holomorphic function defined in an open set $U \subset \mathbb{C}$ containing the spectrum, $\sigma(\mathcal{K}_D^*)$, of $\mathcal{K}_D^*$. Then, we can write $f(z) = \sum_{j=0}^{\infty} a_j z^j$ for every $z \in U$.

Definition 24.3. *Let*

$$f(\mathcal{K}_D^*) := \sum_{j=0}^{\infty} a_j (\mathcal{K}_D^*)^j,$$

where $(\mathcal{K}_D^*)^j := \underbrace{\mathcal{K}_D^* \circ \mathcal{K}_D^* \circ .. \circ \mathcal{K}_D^*}_{j\ times}$.

Lemma 24.41 *We have*

$$f(\mathcal{K}_D^*) = \sum_{j=1}^{\infty} f(\lambda_j)(\cdot, \varphi_j)_{\mathcal{H}^*} \varphi_j.$$

Proof. We have

$$
\begin{aligned}
f(\mathcal{K}_D^*) &= \sum_{i=0}^{\infty} a_i (\mathcal{K}_D^*)^i = \sum_{i=0}^{\infty} a_i \sum_{j=1}^{\infty} \lambda_j^i (\cdot, \varphi_j)_{\mathcal{H}^*} \varphi_j \\
&= \sum_{j=1}^{\infty} \left(\sum_{i=0}^{\infty} a_i \lambda_j^i \right) (\cdot, \varphi_j)_{\mathcal{H}^*} \varphi_j \\
&= \sum_{j=1}^{\infty} f(\lambda_j)(\cdot, \varphi_j)_{\mathcal{H}^*} \varphi_j,
\end{aligned}
$$

which yields the desired result.   □

From Lemma 24.41, we can deduce that

$$\int_{\partial D} x_l f(\mathcal{K}_D^*)[\nu_m](x)\, d\sigma(x) = \sum_{j=1}^{\infty} f(\lambda_j)\alpha_{l,m}^{(j)}\,. \qquad (24.63)$$

Equation (24.63) yields the summation rules for the entries of the polarization tensor.

In order to prove that $\sum_{j=1}^{\infty} \alpha_{l,m}^{(j)} = \delta_{lm}|D|$, we take $f(\lambda) = 1$ in (24.63) to get

$$\sum_{j=1}^{\infty} \alpha_{l,m}^{(j)} = \int_{\partial D} x_l \nu_m(x)\, d\sigma(x) = \delta_{lm}|D|.$$

Next, we prove that

$$\sum_{j=1}^{\infty} \lambda_j \sum_{l=1}^{d} \alpha_{l,l}^{(j)} = \frac{(d-2)}{2}|D|\,.$$

Taking $f(\lambda) = \lambda$ in (24.63), we obtain

$$\sum_{j=1}^{\infty} \lambda_j \sum_{l=1}^{d} \alpha_{l,l}^{(j)} = \sum_{l=1}^{d} \int_{\partial D} x_l \mathcal{K}_D^*[\nu_l](x)\, d\sigma(x)\,,$$

$$\int_{\partial D} x_l \mathcal{K}_D^*[\nu_l](x)\, d\sigma(x) = \int_{\partial D} x_l \left(\frac{1}{2}\nu_l(x) + \frac{\partial \mathcal{S}_D[\nu_l]}{\partial \nu}\Big|_{-}(x) \right) d\sigma(x)\,,$$

$$= \frac{|D|}{2} + \int_{\partial D} x_l \frac{\partial \mathcal{S}_D[\nu_l]}{\partial \nu}\Big|_{-}(x) d\sigma(x)\,. \qquad (24.64)$$

Integrating by parts we arrive at

$$\int_{\partial D} x_l \frac{\partial \mathcal{S}_D[\nu_l]}{\partial \nu}\Big|_{-}(x) d\sigma(x) = \int_{D} e_l(x) \cdot \nabla \mathcal{S}_D[\nu_l](x) dx + \int_{D} x_l \Delta \mathcal{S}_D[\nu_l](x) dx\,,$$

where $(e_1, \ldots, e_d)$ is an orthonormal basis of $\mathbb{R}^d$. Since the single-layer potential is harmonic on D,

$$\int_{\partial D} x_l \frac{\partial \mathcal{S}_D[\nu_l]}{\partial \nu}\Big|_{-}(x) d\sigma(x) = \int_{D} e_l(x) \cdot \left(\int_{\partial D} \nabla_x \Gamma(x, x')\nu_l(x') d\sigma(x') \right) dx\,.$$

Summing on l and using $\nabla_x \Gamma(x, x') = -\nabla_{x'}\Gamma(x, x')$, we get

$$\sum_{l=1}^{d} \int_{\partial D} x_l \frac{\partial \mathcal{S}_D[\nu_l]}{\partial \nu}\Big|_{-}(x) d\sigma(x) = -\int_{D} \left(\int_{\partial D} \nu(x') \cdot \nabla_{x'}\Gamma(x, x') d\sigma(x') \right) dx\,,$$

$$= -\int_{D} \mathcal{D}_D[1](x) dx,$$

$$= -|D|, \qquad (24.65)$$

where $\mathcal{D}_D$ is the double-layer potential. Hence, summing equation (24.64) for $l = 1, \ldots, d$, we get the result.

Finally, we show that

$$\sum_{j=1}^{\infty} \lambda_j^2 \sum_{l=1}^{d} \alpha_{l,l}^{(j)} = \frac{d-4}{4}|D| + \sum_{l=1}^{d} \int_D |\nabla \mathcal{S}_D[\nu_l]|^2 dx \,.$$

Taking $f(\lambda) = \lambda^2$ in (24.63) yields

$$\sum_{j=1}^{\infty} \lambda_j^2 \sum_{l=1}^{d} \alpha_{l,l}^{(j)} = \sum_{l=1}^{d} \int_{\partial D} x_l (\mathcal{K}_D^*)^2 [\nu_l](x) \, d\sigma(x)$$

$$= \sum_{l=1}^{d} \int_{\partial D} \mathcal{K}_D[y_l](x) \mathcal{K}_D^*[\nu_l](x) \, d\sigma(x)$$

$$= \sum_{l=1}^{d} \int_{\partial D} \mathcal{K}_D[y_l] \frac{\nu_l}{2} d\sigma + \sum_{l=1}^{d} \int_{\partial D} \mathcal{K}_D[y_l] \frac{\partial \mathcal{S}_D[\nu_l]}{\partial \nu}\Big|_- d\sigma$$

$$= \frac{(d-2)}{4}|D| - \underbrace{\sum_{l=1}^{d} \int_{\partial D} \frac{y_l}{2} \frac{\partial \mathcal{S}_D[\nu_l]}{\partial \nu}\Big|_- d\sigma}_{I_1} + \underbrace{\sum_{l=1}^{d} \int_{\partial D} \mathcal{D}_D[y_l]\Big|_- \frac{\partial \mathcal{S}_D[\nu_l]}{\partial \nu}\Big|_- d\sigma}_{I_2} \,.$$

From (24.65) it follows that

$$I_1 = -\frac{|D|}{2}.$$

Since x_l is harmonic, we have $x_l = \mathcal{D}_D[y_l](x)|_- - \mathcal{S}_D[\nu_l](x)$ on ∂D, and thus,

$$I_2 = \sum_{l=1}^{d} \int_{\partial D} (x_l + \mathcal{S}_D[\nu_l](x)) \frac{\partial \mathcal{S}_D[\nu_l]}{\partial \nu}\Big|_- (x) d\sigma(x) \,,$$

$$= -|D| + \sum_{l=1}^{d} \int_{\partial D} \mathcal{S}_D[\nu_l] \frac{\partial \mathcal{S}_D[\nu_l]}{\partial \nu}\Big|_- d\sigma \,,$$

$$= -|D| + \sum_{l=1}^{d} \int_D |\nabla \mathcal{S}_D[\nu_l]|^2 dx \,.$$

Replacing I_1 and I_2 by their expressions gives the desired result.

24.9 Concluding Remarks

In this chapter, based on perturbation arguments, we studied the scattering by plasmonic nanoparticles when the frequency is close to a resonant frequency. We have derived the shift and broadening of the plasmon resonance

with changes in size. We have also consider the case of multiple nanoparticles under the weak interaction assumption. The localization algorithms developed in Chapter 12 can be extended to the problem of imaging plasmonic nanoparticles. We have precisely quantified the scattering and absorption cross-section enhancements and gave optimal bounds on the enhancement factors. We have also linked the plasmonic resonances to the scattering coefficients and showed that the leading-order term of the scattering amplitude can be expressed in terms of the $\pm$-one order of the scattering coefficients.

25

Nonlinear Harmonic Holography

25.1 Introduction

In this chapter, the detection of a small reflector in a randomly heterogeneous medium using second-harmonic generation is investigated. The medium is illuminated by a time-harmonic plane wave at frequency ω. It is assumed that the reflector has a non-zero second-order nonlinear susceptibility, and thus emits a wave at frequency 2ω in addition to the fundamental frequency linear scattering. It is shown how the fundamental frequency signal and the second-harmonic signal propagate in the medium. A statistical study of the images obtained by migration the boundary data is performed. It is proved that the second-harmonic image is more stable with respect to medium noise than the one obtained with the fundamental signal. Moreover, the signal-to-noise ratio for the second-harmonic image does not depend either on the second-order susceptibility tensor or on the volume of the particle.

Second-harmonic microscopy is a promising imaging technique based on a phenomenon called second-harmonic generation (SHG) or frequency-doubling. SHG requires an intense laser beam passing through a material with nonvanishing second-order polarizability [187]. A second electromagnetic field is emitted at exactly twice the frequency of the incoming field. Roughly speaking,

$$E_{2\omega} \sim E_\omega \chi^{(2)} E_\omega \,, \tag{25.1}$$

where $\chi^{(2)}$ is the second-order polarization tensor. A condition for an object to have nonvanishing second-order polarizability tensor is to have a noncentrosymmetric structure. Thus SHG occurs in nanoparticles [348, 198]. This makes SHG a very good contrast mechanism for microscopy, and has been used in biomedical imaging. SHG signals have a very low intensity because the coefficients in $\chi^{(2)}$ have a typical size of picometer$/V$. This is the reason why a high intensity laser beam is required in order to produce a second-harmonic field that is large enough to be detected by the microscope.

The coherent nature of the SHG signal allows us to use nonlinear holography for measuring the complex two-dimensional (amplitude and phase) SHG signal [190, 301]. On the other hand, since only the nanoparticle produces the second-harmonic signal, SHG microscopy allows a precise localization of the nanoparticle, clear of any scattering from the surrounding medium, contrary to the fundamental frequency image, where the signal measured is produced by both the reflector and the medium.

In this chapter, we study the case of a nanoparticle with non vanishing second-order polarizability tensor $\chi^{(2)}$ embedded in a randomly heterogeneous medium illuminated by an incoming electromagnetic field at a fixed frequency ω. We give asymptotic formulas for the electromagnetic field diffracted by the nanoparticle, at the fundamental frequency and at the second-harmonic frequency. Then we use a backpropagation algorithm in order to recover the position of the nanoparticle from boundary measurements of the fields. We study the images obtained by backpropagation both in terms of resolution and stability. In particular, we elucidate that the second-harmonic field provides a more stable image than that from fundamental frequency imaging, with respect to medium noise, and that the signal-to-noise ratio for the second-harmonic image does not depend either on $\chi^{(2)}$ or on the volume of the particle.

The chapter is organized as follows. In Section 25.2 we formulate the problem of SHG. In Section 25.3, asymptotic expansions in terms of the size of the small reflector (the nanoparticle) of the scattered field at the fundamental frequency and the second-harmonic generated field are derived. In Section 25.4, we introduce backpropagation imaging functions for localizing the point reflector using the scattered field at the fundamental frequency as well as the second-harmonic field. In Section 25.5, we perform a stability and resolution analysis of the backpropagation imaging functions. We show that the medium noise affects the stability and resolution of the imaging functions in different ways. We prove that using the second-harmonic field renders enhanced stability for the reconstructed image. This finding is delineated by a few numerical examples in Section 25.6. The chapter ends with a short discussion. The main results of this chapter are from [55].

25.2 Problem Formulation

Consider a small electric reflector Ω_r with a nonvanishing second-order susceptibility tensor embedded in a randomly heterogeneous medium in $\mathbb{R}^2$. We assume that the randomly heterogeneous medium has random fluctuations described by a bounded random process μ with mean zero. Furthermore, we assume that μ is compactly supported in $\mathbb{R}^2$ and let $\Omega_\mu := \operatorname{supp}(\mu)$. We also assume that the refractive index of the background homogeneous medium $\mathbb{R}^2 \setminus \overline{\Omega_\mu}$ is 1. The medium is illuminated by a plane wave at frequency $\omega > 0$, intensity $U_I > 0$, and direction $\theta \in S$:

$$U_0(x) = U_I e^{i\omega\theta \cdot x}, \tag{25.2}$$

with S being the unit circle. We assume that the incoming plane wave is polarized in the transverse magnetic mode. The small reflector Ω_r is in Ω_μ and has a refractive index given by

$$[\sigma_r - 1]\chi(\Omega_r)(x), \tag{25.3}$$

where σ_r is the refractive index contrast of the reflector, Ω_r is compactly supported in Ω_μ with volume $|\Omega_r|$, and $\chi(\Omega_r)$ is the characteristic function of Ω_r. The squared refractive index $n(x)$ in the whole space then has the following form:

$$\frac{1}{n(x)} = 1 + \mu(x) + [\sigma_r - 1]\chi(\Omega_r)(x). \tag{25.4}$$

The scattered field u_s generated by the plane wave satisfies the Helmholtz equation

$$\begin{cases} \nabla \cdot \left(([\sigma_r - 1]\chi(\Omega_r) + \mu + 1)\nabla(u_s + U_0)\right) + \omega^2(u_s + U_0) = 0 & \text{in } \mathbb{R}^2, \\ \lim_{|x|\to\infty} \sqrt{|x|}\left(\frac{\partial u_s}{\partial|x|} - i\omega u_s\right) = 0. \end{cases} \tag{25.5}$$

The point reflector also scatters a second field v at frequency 2ω. The field v satisfies, up to $O(\|\mu\|_{L^\infty(\Omega_\mu)}^2)$, the following Helmholtz equation [187]:

$$\begin{cases} \left(\Delta + \frac{(2\omega)^2}{[\sigma_r - 1]\chi(\Omega_r) + 1}\left(1 - \frac{\mu}{[\sigma_r - 1]\chi(\Omega_r) + 1}\right)\right) v = \sum_{k,l=1,2} \chi_{kl}^{(2)}\partial_{x_k}U\partial_{x_l}U\chi(\Omega_r) & \text{in } \mathbb{R}^2, \\ \lim_{|x|\to\infty} \sqrt{|x|}\left(\frac{\partial v}{\partial|x|} - 2i\omega v\right) = 0, \end{cases} \tag{25.6}$$

where $\chi^{(2)}$ is the electric polarization of the reflector, and can be written as $\chi^{(2)}(x) = (\chi_{ij}^{(2)})_{i,j=1,2}\chi(\Omega_r)(x)$ and $U = u_s + U_0$ is the total field.

Let us consider Ω to be a domain large enough so that $\Omega_\mu = \text{supp}(\mu) \Subset \Omega$ and measure the fields u_s and v on its boundary $\partial\Omega$. The goal of the imaging problem is to locate the reflector from the far-field measurements of the scattered field u_s at the fundamental frequency and/or the second-harmonic generated field v. It will be shown in this chapter that, in the presence of medium noise, the use of the second-harmonic field yields a better stability properties for imaging the small reflector than the use of the scattered field at the fundamental frequency.

25.3 Small-Volume Expansions

In this section, we establish small-volume expansions for the solutions of problems (25.5) and (25.6) similar to those derived in Chapter 11 . We assume that

the reflector is of the form $\Omega_r = z_r + \delta B$, where its characteristic size δ is small, z_r is its location, and B is a smooth domain. We derive asymptotic expansions of u_s and v as δ goes to zero.

25.3.1 Fundamental Frequency Problem

Let $U^{(\mu)} = u_s^{(\mu)} + U_0$ be the total field that would be observed in the absence of any reflector. The scattered field $u_s^{(\mu)}$ satisfies

$$
\begin{cases}
\nabla \cdot \left((1+\mu)\nabla(u_s^{(\mu)} + U_0) \right) + \omega^2(u_s^{(\mu)} + U_0) = 0 \quad \text{in } \mathbb{R}^2 , \\
\lim_{|x|\to\infty} \sqrt{|x|}(\dfrac{\partial u_s^{(\mu)}}{\partial |x|} - i\omega u_s^{(\mu)}) = 0 .
\end{cases}
\tag{25.7}
$$

Therefore,

$$
\nabla \cdot (1+\mu)\nabla u_s^{(\mu)} + \omega^2 u_s^{(\mu)} = -\nabla \cdot \mu \nabla U_0 \quad \text{in } \mathbb{R}^2 .
$$

Since $\Omega_\mu \Subset \Omega$, the estimate

$$
||u_s^{(\mu)}||_{W^{1,2}(\Omega)} \le C||\mu||_{L^\infty}
\tag{25.8}
$$

holds for some positive constant C independent of μ. We refer to Section 25.7 for a proof of (25.8). Actually, one can prove that

$$
u_s^{(\mu)}(x) = -\int_{\Omega_\mu} \mu(y)\nabla U_0(y) \cdot \nabla G_\omega^{(0)}(x,y)dy + O(||\mu||_{L^\infty}^2), \quad x \in \Omega .
$$

Moreover, writing

$$
\nabla \cdot \left((1+\mu)\nabla(u_s^{(\mu)} + U_0) \right) = -\omega^2(u_s^{(\mu)} + U_0) ,
$$

it follows by using Meyers' theorem [273] that there exists $\eta > 0$ such that for all $0 \le \eta' \le \eta$,

$$
\begin{aligned}
||\nabla u_s^{(\mu)}||_{L^{2+\eta'}(\Omega')} &\le ||\nabla(u_s^{(\mu)} + U_0)||_{L^{2+\eta'}(\Omega)} + ||\nabla U_0||_{L^{2+\eta'}(\Omega)} \\
&\le C||u_s^{(\mu)} + U_0||_{L^{2+\eta'}(\Omega)} + ||\nabla U_0||_{L^{2+\eta'}(\Omega)} \\
&\le C||u_s^{(\mu)}||_{L^{2+\eta'}(\Omega)} + C'
\end{aligned}
$$

for some positive constants C and C', where $\Omega' \Subset \Omega$. From the continuous embedding of $W^{1,2}(\Omega)$ into $L^{2+\eta'}(\Omega)$ and (25.8) we obtain

$$
||u_s^{(\mu)}||_{L^{2+\eta'}(\Omega)} \le C''
$$

for some constant C'' independent of μ. Therefore,

$$||\nabla u_s^{(\mu)}||_{L^{2+\eta'}(\Omega')} \le C \qquad (25.9)$$

for some constant C independent of μ.

Now, we turn to the derivation of an asymptotic expansion of u_s as δ goes to zero. On one hand, by subtracting (25.5) from (25.7), we get

$$\nabla \cdot \left(([\sigma_r - 1]\chi(\Omega_r) + \mu + 1)\nabla(u_s - u_s^{(\mu)}) \right) + \omega^2(u_s - u_s^{(\mu)})$$
$$= -\nabla \cdot [\sigma_r - 1]\chi(\Omega_r)\nabla U_0 - \nabla \cdot [\sigma_r - 1]\chi(\Omega_r)\nabla u_s^{(\mu)} \quad \text{in } \mathbb{R}^2 . \qquad (25.10)$$

On the other hand, we have

$$||[\sigma_r - 1]\chi(\Omega_r)\nabla u_s^{(\mu)}||_{L^2(\Omega)} \le C|\Omega_r|^{\frac{1+\frac{\eta}{2}}{2+\frac{\eta}{2}}}||\nabla u_s^{(\mu)}||_{L^{2+\frac{\eta}{2}}(\Omega)}$$
$$\le C|\Omega_r|^{\frac{1+\frac{\eta}{2}}{2+\frac{\eta}{2}}}||\nabla u_s^{(\mu)}||_{L^2(\Omega)}^{\frac{1}{4+\eta}}||\nabla u_s^{(\mu)}||_{L^{2+\eta}(\Omega)}^{\frac{1}{4+\eta}} ,$$

and hence, by (25.8) and (25.9), we arrive at

$$||[\sigma_r - 1]\chi(\Omega_r)\nabla u_s^{(\mu)}||_{L^2(\Omega)} \le C|\Omega_r|^{\frac{1+\frac{\eta}{2}}{2+\frac{\eta}{2}}}||\mu||_{L^\infty}^{\frac{2}{4+\eta}} .$$

Therefore, we can neglect in (25.10) the term $\nabla \cdot [\sigma_r - 1]\chi(\Omega_r)\nabla u_s^{(\mu)}$ as $||\mu||_{L^\infty} \to 0$.

Let $w^{(\mu)}$ be defined by

$$\nabla \cdot (1 + \mu + [\sigma_r - 1]\chi(\Omega_r))\nabla w^{(\mu)} + \omega^2 w^{(\mu)} = \nabla \cdot [\sigma_r - 1]\chi(\Omega_r)\nabla(x - z_r) \quad \text{in } \mathbb{R}^2 ,$$

subject to the Sommerfeld radiation condition

$$\lim_{|x|\to\infty} \sqrt{|x|}(\frac{\partial w^{(\mu)}}{\partial|x|} - i\omega w^{(\mu)}) = 0 .$$

Using the Taylor expansion

$$U_0(x) = U_0(z_r) + (x - z_r) \cdot \nabla U_0(z_r) + O(|x - z_r|^2) ,$$

one can derive the inner expansion

$$(u_s - u_s^{(\mu)})(x) = w^{(\mu)}(x) \cdot \nabla U_0(z_r) + O(\delta^2) \qquad (25.11)$$

for x near z_r. The following estimate holds. We refer the reader to Section 25.8 for its proof.

Proposition 25.1. *There exists a positive constant C independent of δ such that*

$$||u_s - u_s^{(\mu)} - w^{(\mu)}(x) \cdot \nabla U_0(z_r)||_{W^{1,2}(\Omega)} \le C\delta^2 .$$

Let $G_\omega^{(\mu)}$ be the outgoing Green function in the random medium, that is, the solution to

$$(\nabla \cdot (1 + \mu)\nabla + \omega^2)G_\omega^{(\mu)}(., z) = -\delta_z \quad \text{in } \mathbb{R}^2 , \tag{25.12}$$

subject to the Sommerfeld radiation condition

$$\lim_{|x| \to \infty} \sqrt{|x|}(\frac{\partial G_\omega^{(\mu)}}{\partial |x|} - i\omega G_\omega^{(\mu)}) = 0 .$$

An important property satisfied by $G_\omega^{(\mu)}$ is the reciprocity property (see Subsection 3.2.4):

$$G_\omega^{(\mu)}(x, z) = G_\omega^{(\mu)}(z, x), \qquad x \neq z . \tag{25.13}$$

Let us denote by $G_\omega^{(0)}$ the outgoing background Green function, that is, the solution to

$$(\Delta + \omega^2)G_\omega^{(0)}(., z) = -\delta_z \qquad \text{in } \mathbb{R}^2 , \tag{25.14}$$

subject to the Sommerfeld radiation condition. Note that $G_\omega^{(0)} = -\Gamma_\omega$ where Γ_ω is defined by (3.52) with k replaced by ω.

The Lippmann-Schwinger representation formula

$$
\begin{aligned}
(G_\omega^{(\mu)} - G_\omega^{(0)})(x, z_r) &= \int_{\Omega_\mu} \mu(y)\nabla G_\omega^{(\mu)}(y, z_r) \cdot \nabla G_\omega^{(0)}(x, y)\, dy \\
&= \int_{\Omega_\mu} \mu(y)\nabla G_\omega^{(0)}(y, z_r) \cdot \nabla G_\omega^{(0)}(x, y)\, dy \\
&\quad + \int_{\Omega_\mu} \mu(y)\nabla (G_\omega^{(\mu)} - G_\omega^{(0)})(y, z_r) \cdot \nabla G_\omega^{(0)}(x, y)\, dy
\end{aligned}
$$

holds for $x \in \partial\Omega$. Since $\Omega_\mu \Subset \Omega$, we have

$$\left|(G_\omega^{(\mu)} - G_\omega^{(0)})(x, z_r) - \int_{\Omega_\mu} \mu(y)\nabla G_\omega^{(0)}(y, z_r) \cdot \nabla G_\omega^{(0)}(x, y)\, dy\right|$$
$$\leq ||\mu||_{L^\infty}||\nabla G_\omega^{(0)}(x, \cdot)||_{L^\infty(\Omega_\mu)}||\nabla(G_\omega^{(\mu)} - G_\omega^{(0)})(\cdot, z_r)||_{L^2(\Omega_\mu)} .$$

Similarly to (25.8), one can prove that

$$||\nabla(G_\omega^{(\mu)} - G_\omega^{(0)})(\cdot, z_r)||_{L^2(\Omega_\mu)} \leq C||\mu||_{L^\infty} , \tag{25.15}$$

and hence there exists a positive constant C independent of μ such that

$$\left|(G_\omega^{(\mu)} - G_\omega^{(0)})(x, z_r) - \int_{\Omega_\mu} \mu(y)\nabla G_\omega^{(0)}(y, z_r) \cdot \nabla G_\omega^{(0)}(x, y)\, dy\right| \leq C||\mu||_{L^\infty}^2$$
$$\tag{25.16}$$

uniformly in $x \in \partial\Omega$.

Since

$$||\nabla\nabla G_\omega^{(0)}(x,\cdot)||_{L^\infty(\Omega_\mu)} \le C \qquad (25.17)$$

uniformly in $x \in \partial\Omega$, the estimate

$$\left|\nabla(G_\omega^{(\mu)} - G_\omega^{(0)})(x,z_r) - \nabla\int_{\Omega_\mu}\mu(y)\nabla G_\omega^{(0)}(y,z_r)\cdot\nabla G_\omega^{(0)}(x,y)\,dy\right| \le C||\mu||_{L^\infty}^2,$$

$$(25.18)$$

holds in exactly the same way as in (25.16). Therefore, the following Born approximation holds.

Proposition 25.2. *We have*

$$G_\omega^{(\mu)}(x,z_r) \quad = G_\omega^{(0)}(x,z_r) - \int_{\Omega_\mu}\mu(y)\nabla G_\omega^{(0)}(y,z_r)\cdot\nabla G_\omega^{(0)}(x,y)\,dy + O(||\mu||_{L^\infty}^2),$$

$$\nabla G_\omega^{(\mu)}(x,z_r) = \nabla G_\omega^{(0)}(x,z_r) - \nabla\int_{\Omega_\mu}\mu(y)\nabla G_\omega^{(0)}(y,z_r)\cdot\nabla G_\omega^{(0)}(x,y)\,dy + O(||\mu||_{L^\infty}^2)$$

uniformly in $x \in \partial\Omega$.

We now turn to an approximation formula for $w^{(\mu)}$ as $||\mu||_{L^\infty} \to 0$. By integrating by parts we get

$$w^{(\mu)}(x) = (1-\sigma_r)\int_{\Omega_r}\nabla(w^{(\mu)}(y) - (y-z_r))\cdot\nabla G_\omega^{(\mu)}(x,y)\,dy, \quad x \in \mathbb{R}^2.$$

Using (25.17) we have, for x away from Ω_r,

$$w^{(\mu)}(x) = (1-\sigma_r)[\int_{\Omega_r}\nabla(w^{(\mu)}(y)-(y-z_r))\,dy]\cdot[\nabla G_\omega^{(\mu)}(x,z_r)+O(\delta)]. \quad (25.19)$$

Let $\widetilde{w}$ be the solution to

$$\begin{cases} \nabla\cdot(1 + [\sigma_r - 1]\chi(B))\nabla\widetilde{w} = 0 & \text{in } \mathbb{R}^2, \\ \widetilde{w}(\widetilde{x}) - \widetilde{x} \to 0 & \text{as } |\xi| \to +\infty. \end{cases} \qquad (25.20)$$

The following result holds. We refer the reader to Section 25.9 for its proof.

Proposition 25.3. *We have*

$$w^{(\mu)}(y) - (y-z_r) = \delta\widetilde{w}(\widetilde{y}) + O(\delta[||\mu||_{L^\infty} + (\delta\omega)^2]), \qquad (25.21)$$

with the scaled variable

$$\widetilde{y} = \frac{y - z_r}{\delta}.$$

From (25.21), it follows that

$$\int_{\Omega_r}\nabla(w^{(\mu)}(y) - (y-z_r))\,dy = \delta^2\int_B\nabla\widetilde{w}(\widetilde{x})\,d\widetilde{x} + O(\delta^3[||\mu||_{L^\infty} + (\delta\omega)^2]).$$

$$(25.22)$$

Define the polarization tensor associated to σ_r and B by

$$M(\sigma_r, B) := (\sigma_r - 1) \int_B \nabla \widetilde{w}(\widetilde{x}) \, d\widetilde{x} \,, \tag{25.23}$$

where $\widetilde{w}$ is the solution to (25.20). Definition (25.23) is equivalent to (11.5) with $\lambda = (\sigma_r + 1)/(2(\sigma_r - 1))$. Recall from Theorem 11.4 that the matrix $M(\sigma_r, B)$ is symmetric definite (positive if $\sigma_r > 1$ and negative if $\sigma_r < 1$). Moreover, if B is a disk, then $M(\sigma_r, B)$ takes the form:

$$M(\sigma_r, B) = \frac{2(\sigma_r - 1)}{\sigma_r + 1} |B| I \,.$$

To obtain an asymptotic expansion of $u_s(x) - u_s^{(\mu)}(x)$ in terms of the characteristic size δ of the scatterer, we take the far-field expansion of (25.11). Plugging formula (25.22) into (25.19), we obtain the following small-volume asymptotic expansion.

Proposition 25.4. *We have*

$$u_s(x) = u_s^{(\mu)}(x) - \delta^2 M(\sigma_r, B) \nabla U_0(z_r) \cdot \nabla G_\omega^{(\mu)}(x, z_r) + O(\delta^3[1 + ||\mu||_{L^\infty} + (\delta\omega)^2]) \,, \tag{25.24}$$

uniformly in $x \in \partial\Omega$.

Finally, using (25.18) we arrive at the following result.

Theorem 25.1 *We have as δ goes to zero*

$$(u_s - u_s^{(\mu)})(x) = -\delta^2 M(\sigma_r, B) \nabla U_0(z_r) \cdot \left[\nabla G_\omega^{(0)}(x, z_r) + \nabla \int_{\Omega_\mu} \mu(y) \nabla G_\omega^{(0)}(y, z_r) \cdot \nabla G_\omega^{(0)}(x, y) \, dy \right]$$
$$+ O(\delta^3[1 + ||\mu||_{L^\infty} + (\delta\omega)^2] + \delta^2 ||\mu||_{L^\infty}^2) \,, \tag{25.25}$$

uniformly in $x \in \partial\Omega$.

Theorem 25.1 shows that the asymptotic expansion (25.25) is uniform with respect to ω and μ, provided that $\omega \leq C/\delta$ and $||\mu||_{L^\infty} \leq C'\sqrt{\delta}$ for two positive constants C and C'.

25.3.2 Second-Harmonic Problem

We apply similar arguments to derive a small-volume expansion for the second-harmonic field at frequency 2ω.

Introduce $G_{2\omega}^{(\sigma_r, \mu)}(., z)$ the outgoing solution of

$$\left(\Delta + \frac{(2\omega)^2}{[\sigma_r - 1]\chi(\Omega_r) + 1} \left(1 - \frac{\mu}{[\sigma_r - 1]\chi(\Omega_r) + 1}\right) \right) G_{2\omega}^{(\sigma_r, \mu)}(., z) = -\delta_z \qquad \text{in } \mathbb{R}^2 \,.$$

Let $G_{2\omega}^{(0)}$ be the outgoing solution to (25.14) with ω replaced by 2ω.

Similarly to (25.25), an asymptotic expansion for $G_{2\omega}^{(\sigma_r,\mu)}$ in terms of δ can be derived. We have

$$(G_{2\omega}^{(\sigma_r,\mu)} - G_{2\omega}^{(\mu)})(x,z) = O(\delta^2)$$

for $x \neq z$ and x,z away from z_r. Here $G_{2\omega}^{(\mu)}$ is the solution to (25.12) with ω replaced by 2ω. Moreover, the Born approximation

$$(G_{2\omega}^{(\sigma_r,\mu)} - G_{2\omega}^{(0)})(x,z) = -(2\omega)^2 \int_{\Omega_\mu} \mu(y)G_{2\omega}^{(0)}(y,z)G_{2\omega}^{(0)}(x,y)dy + O(\delta^2 + ||\mu||_{L^\infty}^2)$$

yields for $x \neq z$ and x,z away from z_r. From the integral representation formula

$$v(x) = -\int_{\Omega_r} \sum_{k,l=1,2} \chi_{kl}^{(2)} \partial_{x_k} U(y)\partial_{x_l} U(y)G_{2\omega}^{(\sigma_r,\mu)}(x,y)dy,$$

it follows that

$$v(x) = -\delta^2|B| \left(\sum_{k,l} \chi_{kl}^{(2)} \partial_{x_k} U(z_r)\partial_{x_l} U(z_r) \right) G_{2\omega}^{(\sigma_r,\mu)}(x,z_r) + O(\delta^3), \quad (25.26)$$

where $|B|$ denotes the volume of B, and hence, keeping only the terms of first-order in μ and in second-order in δ,

$$v(x) = -\delta^2|B| \left(\sum_{k,l} \chi_{kl}^{(2)} \partial_{x_k} U(z_r)\partial_{x_l} U(z_r) \right)$$

$$\left[G_{2\omega}^{(0)}(x,z_r) - 4\omega^2 \int_\Omega \mu(y)G_{2\omega}^{(0)}(x,y)G_{2\omega}^{(0)}(y,z_r)dy + O(||\mu||_{L^\infty}^2) \right] + O(\delta^3).$$

$$(25.27)$$

We denote by $(S)^\theta$ the source term, which depends on the angle θ of the incoming plane wave,

$$(S)^\theta = \left(\sum_{k,l} \chi_{kl}^{(2)} \partial_{x_k} U(z_r)\partial_{x_l} U(z_r) \right). \quad (25.28)$$

Now, since

$$U(x) = U_I e^{i\omega\theta\cdot x} + \int_\Omega \mu(y)\nabla G_\omega^{(0)}(x,y) \cdot \nabla U_0(y)dy + O(||\mu||_{L^\infty}^2 + \delta), \quad (25.29)$$

which follows by using the Born approximation and the inner expansion (25.11), we can give an expression for the partial derivatives of U. We have

$$\partial_{x_k} U(x) = i\omega\theta_k U_I e^{i\omega\theta\cdot x} - i\omega\theta\cdot\int_\Omega \nabla(\mu(y)e^{i\omega\theta\cdot y})\partial_{x_k} G_\omega^{(0)}(x,y)dy + O(||\mu||_{L^\infty}^2 + \delta)\,.$$

$$(25.30)$$

We can rewrite the source term as

$$\left(\sum_{k,l}\chi_{k,l}^{(2)}\partial_{x_k}U(z_r)\partial_{x_l}U(z_r)\right) = -\omega^2\sum_{k,l}\chi_{kl}^{(2)}\bigg[U_I^2\theta_k\theta_l e^{i\omega\theta\cdot z_r}$$

$$-\theta_k\theta\cdot\int_\Omega\nabla(\mu(y)e^{i\omega\theta\cdot y})\partial_{x_l}G_\omega^{(0)}(z_r,y)dy - \theta_l\theta\cdot\int_\Omega\nabla(\mu(y)e^{i\omega\theta\cdot y})\partial_{x_k}G_\omega^{(0)}(z_r,y)dy$$

$$+\theta\cdot\int_\Omega\nabla(\mu(y)e^{i\omega\theta\cdot y})\partial_{x_l}G_\omega^{(0)}(z_r,y)dy\theta\cdot\int_\Omega\nabla(\mu(y)e^{i\omega\theta\cdot y})\partial_{x_k}G_\omega^{(0)}(z_r,y)dy\bigg]$$

$$+ O(||\mu||_{L^\infty}^2 + \delta)\,.\quad(25.31)$$

Assume that $\mu\in\mathcal{C}^{0,\alpha}$ for $0<\alpha<1/2$ (see Section 25.5.1). From

$$\int_\Omega\nabla(\mu(y)e^{i\omega\theta\cdot y})\partial_{x_l}G_\omega^{(0)}(z_r,y)dy = \int_\Omega\nabla(\mu(y)e^{i\omega\theta\cdot y} - \mu(z_r)e^{i\omega\theta\cdot z_r})\partial_{x_l}G_\omega^{(0)}(z_r,y)dy$$

$$= -\int_\Omega\nabla\partial_{x_l}G_\omega^{(0)}(z_r,y)(\mu(y)e^{i\omega\theta\cdot y} - \mu(z_r)e^{i\omega\theta\cdot z_r})dy\,,$$

one can show that there exists a positive constant C independent of μ such that

$$\left|\theta\cdot\int_\Omega\nabla(\mu(y)e^{i\omega\theta\cdot y})\partial_{x_l}G_\omega^{(0)}(z_r,y)dy\theta\cdot\int_\Omega\nabla(\mu(y)e^{i\omega\theta\cdot y})\partial_{x_k}G_\omega^{(0)}(z_r,y)dy\right| \le C||\mu||_{\mathcal{C}^{0,\alpha}}^2\,.$$

So, if we split $(S)^\theta$ into a deterministic part and a random part,

$$(S)^\theta = (S)_{det}^\theta + (S)_{rand}^\theta + O(||\mu||_{\mathcal{C}^{0,\alpha}}^2 + \delta)\,,$$

we get

$$(S)_{det}^\theta = -\omega^2 U_I^2 e^{i2\omega\theta\cdot z_r}\sum_{k,l}\chi_{k,l}^{(2)}\theta_k\theta_l \qquad (25.32)$$

and

$$(S)_{rand}^\theta = \omega^2\sum_{k,l}\chi_{k,l}^{(2)}\bigg[\theta_k\theta\cdot\int_\Omega\nabla(\mu(y)e^{i\omega\theta\cdot y})\partial_{x_l}G_\omega^{(0)}(z_r,y)dy$$

$$+\theta_l\theta\cdot\int_\Omega\nabla(\mu(y)e^{i\omega\theta\cdot y})\partial_{x_k}G_\omega^{(0)}(z_r,y)dy\bigg]\,.$$

$$(25.33)$$

Finally, we obtain the following result.

Theorem 25.2 *Assume that $\mu\in\mathcal{C}^{0,\alpha}$ for $0<\alpha<1/2$. The following asymptotics for v:*

$$v(x) = -\delta^2 |B| \left((S)_{det}^\theta \left[G_{2\omega}^{(0)}(x, z_r) - 4\omega^2 \int_\Omega \mu(y) G_{2\omega}^{(0)}(x, y) G_{2\omega}^{(0)}(y, z_r) dy \right] \right.$$

$$\left. + (S)_{rand}^\theta G_{2\omega}^{(0)}(x, z_r) \right) + O(\delta^3 + \delta^2 ||\mu||_{\mathcal{C}^{0,\alpha}}^2) \quad (25.34)$$

holds uniformly in $x \in \partial\Omega$.

25.4 Imaging Functional

In this section, we use two imaging functionals introduced in Chapter 12 for locating small reflectors. For the sake of simplicity, we assume that B and Ω are disks centered at 0 with radius 1 and R, respectively.

25.4.1 The Fundamental Frequency Case

We assume that we are in possession of the following data: $\{(u_s - u_s^{(\mu)})(x), \ x \in \partial\Omega\}$. We introduce the reverse-time imaging functional

$$\forall z^S \in \Omega, \ I(z^S) = \int_{\partial\Omega \times S} \frac{1}{i\omega} e^{-i\omega\theta \cdot z^S} \theta^T \overline{\nabla G_\omega^{(0)}(x, z^S)} (u_s - u_s^{(\mu)})(x) d\sigma(x) d\sigma(\theta),$$

$$(25.35)$$

where T denotes the transpose. Introduce the matrix

$$R_\omega(z_1, z_2) = \int_{\partial\Omega} \overline{\nabla G_\omega^{(0)}(x, z_1)} \nabla G_\omega^{(0)}(x, z_2)^T d\sigma(x), \qquad z_1, z_2 \in \Omega' \Subset \Omega.$$

$$(25.36)$$

Using (25.25), we have the following expansion for $I(z^S), z^S \in \Omega'$:

$$I(z^S) = -\frac{2\pi\delta^2(\sigma_r - 1)}{\sigma_r + 1} U_I \int_S e^{-i\omega\theta \cdot (z^S - z_r)} \theta^T \left[R_\omega(z^S, z_r) \right.$$

$$+ \int_{\partial\Omega} \overline{\nabla G_\omega^{(0)}(x, z^S)} \cdot \nabla \int_{\Omega_\mu} \mu(y) \nabla G_\omega^{(0)}(y, z_r) \cdot \nabla G_\omega^{(0)}(x, y) dy d\sigma(x) \right] \theta d\sigma(\theta)$$

$$+ O(\delta^3 + \delta^2 ||\mu||_{L^\infty}^2). \quad (25.37)$$

Note that

$$\int_{\partial\Omega} \overline{\nabla G_\omega^{(0)}(x, z^S)} \cdot \nabla \int_{\Omega_\mu} \mu(y) \nabla G_\omega^{(0)}(y, z_r) \cdot \nabla G_\omega^{(0)}(x, y) dy d\sigma(x)$$

$$= \int_{\Omega_\mu} \mu(y) \int_{\partial\Omega} \overline{\nabla G_\omega^{(0)}(x, z^S)}^T \nabla \nabla G_\omega^{(0)}(y, z_r) \nabla G_\omega^{(0)}(x, y) d\sigma(x) dy.$$

Remark 25.3 *Here, the fact that not only do we backpropagate the boundary data, but we also average it over all the possible illumination angles in S, has two motivations. As will be shown later in Section 25.5, the first reason is to*

increase the resolution and make the peak at the reflector's location isotropic. If we do not sum over equidistributed illumination angles over S, we get more an "8-shaped" spot, as shown in Figure 25.7. The second reason is that an average over multiple measurements increases the stability of the imaging functional with respect to measurement noise.

25.4.2 Second-Harmonic Backpropagation

If we write a similar imaging functional for the second-harmonic field v, assuming that we are in possession of the boundary data $\{v(x), \ x \in \partial\Omega\}$, we get

$$\forall z^S \in \Omega, \ J_\theta(z^S) = \int_{\partial\Omega \times S} v(x)\overline{G^{(0)}_{2\omega}(x, z^S)}e^{-2i\omega\theta \cdot z^S} d\sigma(x)d\sigma(\theta). \quad (25.38)$$

As before, using (25.34) we can expand J in terms of δ and μ. Considering first-order terms in δ and μ we get

$$J(z^S) = -\pi\delta^2 \int_S e^{-2i\omega\theta \cdot z^S} \left[(S)^\theta_{det} \left(\int_{\partial\Omega} \overline{G^{(0)}_{2\omega}(x, z^S)}G^{(0)}_{2\omega}(x, z_r)d\sigma(x) \right. \right.$$
$$- 4\omega^2 \int_{\partial\Omega} \overline{G^{(0)}_{2\omega}(x, z^S)} \int_\Omega \mu(y)G^{(0)}_{2\omega}(y, x)G^{(0)}_{2\omega}(y, z_r)dyd\sigma(x) \Bigg)$$
$$\left. + (S)^\theta_{rand} \int_{\partial\Omega} \overline{G^{(0)}_{2\omega}(x, z^S)}G^{(0)}_{2\omega}(x, z_r)d\sigma(x) \right] d\sigma(\theta) + O(\delta^3 + \delta^2||\mu||^2_{\mathcal{C}^{0,\alpha}}).$$
$$(25.39)$$

Now, if we define $Q_{2\omega}$ as

$$Q_{2\omega}(x, z) = \int_{\partial\Omega} G^{(0)}_{2\omega}(y, x)\overline{G^{(0)}_{2\omega}(y, z)}d\sigma(y). \quad (25.40)$$

We have

$$J(z^S) = -\pi\delta^2 \int_S e^{-2i\omega\theta \cdot z^S} \left[(S)^\theta_{det} \left(Q_{2\omega}(z_r, z^S) - 4\omega^2 \int_{\Omega_\mu} \mu(y)G^{(0)}_{2\omega}(y, z_r)Q_{2\omega}(y, z^S)dy \right) \right.$$
$$\left. + (S)^\theta_{rand}Q_{2\omega}(z_r, z^S) \right] d\sigma(\theta) + O(\delta^3 + \delta^2||\mu||^2_{\mathcal{C}^{0,\alpha}}). \quad (25.41)$$

25.5 Statistical Analysis

In this section, we perform a resolution and stability analysis of both functionals. Since the image we get is a superposition of a deterministic image and of a random field created by the medium noise, we can compute the expectation and the covariance functions of those fields in order to estimate the signal-to-noise ratio. For the reader's convenience we give our main results in the following proposition.

Proposition 25.5. *Let l_μ and σ_μ be respectively the correlation length and the standard deviation of the process μ. Assume that l_μ is of order the wavelength $2\pi/\omega$. Let $(SNR)_I$ and $(SNR)_J$ be defined by*

$$(SNR)_I = \frac{\mathbb{E}[I(z_r)]}{(Var[I(z_r)])^{1/2}} \tag{25.42}$$

and

$$(SNR)_J = \frac{\mathbb{E}[J(z_r)]}{(Var[J(z_r)])^{\frac{1}{2}}} \,. \tag{25.43}$$

We have

$$(SNR)_I \approx \frac{\sqrt{2}\pi^{3/2}\omega\delta^2 U_I}{\sigma_\mu l_\mu \sqrt{\omega \, diam \, \Omega_\mu}} \frac{|\sigma_r - 1|}{\sigma_r + 1} \tag{25.44}$$

and

$$(SNR)_J \geq \frac{l_\mu^\alpha \left(\int_S \left(\sum_{k,l} \chi_{k,l}^{(2)} \theta_k \theta_l \right) d\theta \right)}{\sqrt{C}\sigma_\mu \min(\omega^{-\alpha}, 1) \max_{k,l} \left| \chi_{k,l}^{(2)} \right| \sqrt{(\omega \, diam \, \Omega_\mu)^{3+2\alpha} + 1}} \,. \tag{25.45}$$

Here, diam denotes the diameter and α is the upper bound for Holder-regularity of the random process μ.

25.5.1 Assumptions on the Random Process μ

Let $z(x)$, $x \in \mathbb{R}^2$ be a stationary random process with Gaussian statistics, zero mean, and a covariance function given by $R(|x - y|)$ satisfying $R(0) = 1$, $|R(0) - R(s)| \leq \frac{s^{2\alpha}}{l_\mu^{2\alpha}}$ and R is decreasing. Then, z is a $\mathcal{C}^{0,\alpha'}$ process for any $\alpha' < \alpha$ ([4, Theorem 8.3.2]). Let $\overline{\mu} > 0$ and F be a smooth odd bounded function, with derivative bounded by one. For example $F = \arctan$ is a suitable choice. Take

$$\mu(x) = \overline{\mu} F[z(x)] \,.$$

Then μ is a bounded stationary process with zero mean. It is bounded by $||F||_{L^\infty}\overline{\mu}$. Its standard deviation is

$$\sigma_\mu = \overline{\mu}\Big(\int F^2(s) \frac{1}{\sqrt{2\pi}} e^{-s^2/2} \, ds \Big)^{1/2} \,.$$

Its trajectories belong to $\mathcal{C}^{0,\alpha'}$ for any $\alpha' < \alpha$. We want to compute the expectation of its norm. Introduce

$$p(h) = \max_{\|x-y\| \leq \sqrt{2}h} \mathbb{E}|z(x) - z(y)| \,. \tag{25.46}$$

One can also write $p(u) = \sqrt{2}\sqrt{R(0) - R(\sqrt{2}u)}$. According to [4], for all $h, t \in \Omega_\mu$, almost surely,

$$|z(t+h) - z(t)| \leq 16\sqrt{2}[\log(B)]^{1/2}p(\frac{|h|}{l_\mu}) + 32\sqrt{2}\int_0^{\frac{|h|}{l_\mu}} (-\log u)^{1/2}\, dp(u)\,,$$

$$\tag{25.47}$$

where B is a positive random variable with $\mathbb{E}[B^n] \leq (4\sqrt{2})^n$ ([4, Formula 3.3.23]). We have that

$$p(|h|) \leq \sqrt{2}^{1+\alpha}\frac{|h|^\alpha}{l_\mu^\alpha}\,. \tag{25.48}$$

By integration by parts we find that

$$\int_0^{\frac{|h|}{l_\mu}} (-\log u)^{1/2}\, dp(u) = \left[(-\log u)^{1/2}p(u)\right]_0^{\frac{|h|}{l_\mu}} + \frac{1}{2}\int_0^{\frac{|h|}{l_\mu}} (-\log u)^{-1/2}u^{-1}p(u)du\,. \tag{25.49}$$

For any $\varepsilon > 0$, since $s^\varepsilon\sqrt{-\log s} \leq \frac{1}{\sqrt{\varepsilon}}e^{1/2}$ on $[0,1]$, we have, as $|h|$ goes to 0, that

$$\left[(-\log u)^{1/2}p(u)\right]_0^{\frac{|h|}{l_\mu}} \leq e^{\frac{1}{2}}\frac{\sqrt{2}^{1+\alpha}}{\sqrt{\varepsilon}}\frac{|h|^{\alpha-\varepsilon}}{l_\mu^\alpha}\,. \tag{25.50}$$

Similarly, when $|h| < \frac{1}{2e}$, for every $0 < u < |h|$,

$$(-\log u)^{-1/2}s^{-1}p(u) \leq \sqrt{2}^{1+\alpha}\frac{u^{\alpha-1}}{l_\mu^\alpha}\,.$$

So we get, when $|h|$ goes to 0, for every $\varepsilon > 0$,

$$\int_0^{\frac{|h|}{l_\mu}} (-\log u)^{1/2}\, dp(u) \leq \frac{e^{\frac{1}{2}}\sqrt{2}^{1+\alpha}}{\sqrt{\varepsilon}}\frac{|h|^{\alpha-\varepsilon}}{l_\mu^\alpha} + \frac{\sqrt{2}^{1+\alpha}}{\alpha}\frac{|h|^\alpha}{l_\mu^\alpha}\,. \tag{25.51}$$

Therefore, when $|h|$ goes to zero, we have for any $\varepsilon > 0$:

$$|z(t+h) - z(t)| \leq 32\sqrt{2}^\alpha \log(B)^{1/2}\frac{|h|^\alpha}{l_\mu^\alpha} + 64e^{\frac{1}{2}}\sqrt{2}^\alpha\frac{1}{l_\mu^\alpha}\left[\frac{1}{\sqrt{\varepsilon}}|h|^{\alpha-\varepsilon} + \frac{1}{2}|h|^\alpha\right]\,. \tag{25.52}$$

Since $F' \leq 1$, composing by F yields, for any $x, y \in \mathbb{R}^2$,

$$|\mu(x) - \mu(y)| \leq \overline{\mu}|z(x) - z(y)|\,. \tag{25.53}$$

We get the following estimate on $\|\mu\|_{\mathcal{C}^{0,\alpha'}}$, for any $\alpha' \in (0,\alpha)$, almost surely

$$\sup_{\substack{x,y\in\Omega_\mu \\ |x-y|\leq h}} \frac{|\mu(x) - \mu(y)|}{|x-y|^{\alpha'}} \leq 32\sqrt{2}^\alpha \log(B)^{1/2}\overline{\mu}\frac{h^{\alpha-\alpha'}}{l_\mu^\alpha} + 64e^{\frac{1}{2}}\sqrt{2}^\alpha\overline{\mu}\frac{1}{l_\mu^\alpha}\left[\frac{1}{\sqrt{\alpha-\alpha'}} + \frac{1}{2}h^{\alpha-\alpha'}\right]$$

$$\tag{25.54}$$

$$\|\mu\|_{\mathcal{C}^{0,\alpha'}} \leq 64\sqrt{2}^\alpha\frac{e^{\frac{1}{2}}\left[\log(B)^{1/2} + 1\right]}{\sqrt{\alpha-\alpha'}}\frac{\overline{\mu}}{l_\mu^\alpha}\,, \tag{25.55}$$

which gives, since $\mathbb{E}[\log B] \leq \mathbb{E}[B] - 1 \leq 4\sqrt{2} - 1$

$$\mathbb{E}[\|\mu\|_{\mathcal{C}^{0,\alpha'}}^2] \leq 64^2 2^{4+\alpha}\frac{e}{\alpha-\alpha'}\frac{\overline{\mu}}{l_\mu^{2\alpha}}\,. \tag{25.56}$$

25.5.2 Standard Backpropagation

Expectation

We use (25.37) and the fact that $\mathbb{E}(\mu)(x) = 0, \ \forall x \in \Omega$, to find that

$$\mathbb{E}[I(z^S)] = -2\pi\delta^2\frac{\sigma_r - 1}{\sigma_r + 1}U_I \int_S e^{-i\omega\theta\cdot(z^S - z_r)}\theta^T R_\omega(z^S, z_r)\theta d\theta\,. \qquad (25.57)$$

We now use the Helmholtz-Kirchhoff identity (3.80). Since

$$\lim_{R\to\infty}\int_{|x|=R}\nabla G_\omega^{(0)}(x, y)\overline{\nabla G_\omega^{(0)}(z, y)}^T dy = \frac{1}{\omega}\nabla_z\nabla_x\Im\left[G_\omega^{(0)}(x, z)\right] \qquad (25.58)$$

and

$$\Im\left[G_\omega^{(0)}(x, z)\right] = \frac{1}{4}J_0(\omega|x - z|)\,, \qquad (25.59)$$

we can compute an approximation of R_ω:

$$\begin{aligned}
\frac{1}{\omega}\nabla_z\nabla_x\Im\left[G_\omega^{(0)}(x, z)\right] = \frac{1}{4}\Bigg[&\omega J_0(\omega|x - z|)\left(\frac{(x - z)}{|x - z|}\frac{(x - z)^T}{|x - z|}\right) \\
&- \frac{2J_1(\omega|x - z|)}{|x - z|}\left(\frac{(x - z)}{|x - z|}\frac{(x - z)^T}{|x - z|}\right) \\
&+ \frac{J_1(\omega|x - z|)}{|x - z|}I\Bigg]\,, \quad (25.60)
\end{aligned}$$

where I is the 2×2 identity matrix. We can see that R_ω decreases as $|z_r - z^S|^{-\frac{1}{2}}$. The imaging functional has a peak at location $z^S = z_r$. Evaluating R_ω at $z^S = z_r$ we get

$$R_\omega(z_r, z_r) = \frac{\omega}{8}I\,. \qquad (25.61)$$

So we get the expectation of I at point z_r:

$$\mathbb{E}[I(z_r)] \approx -\frac{\pi^2(\sigma_r - 1)}{2(\sigma_r + 1)}\omega\delta^2 U_I\,. \qquad (25.62)$$

Covariance

Let

$$\mathrm{Cov}\left(I(z^S), I(z^{S'})\right) = \mathbb{E}\left[\left(I(z^S) - \mathbb{E}[I(z^S)]\right)\overline{\left(I(z^{S'}) - \mathbb{E}[I(z^{S'})]\right)}\right]. \qquad (25.63)$$

Define

$$\widetilde{R}_\omega(z^S, z_r, y) = \int_{\partial\Omega}\overline{\nabla G_\omega^{(0)}(x, z^S)}\left(\nabla\nabla G_\omega^{(0)}(x, y)\nabla G_\omega^{(0)}(y, z_r)\right)^T d\sigma(x)\,. \qquad (25.64)$$

Using (25.37) and (25.62), we get

$$
I(z^S) - \mathbb{E}[I(z^S)] = \int_{\partial\Omega\times S} \frac{1}{i\omega} e^{-i\omega\theta\cdot z^S} \theta^T \overline{\nabla G^{(0)}_\omega(x,z^S)^T} u_s^{(\mu)}(x)dxd\theta
$$

$$
- 2\pi\delta^2 \frac{\sigma_r - 1}{\sigma_r + 1} U_I \int_S e^{-i\omega\theta\cdot(z^S-z_r)} \left[\int_\Omega \mu(y)\theta^T \widetilde{R}_\omega(z^S, z_r, y)\theta dy \right] d\theta. \quad (25.65)
$$

The computations are a bit tedious. For brevity, we write the quantity above as

$$
I(z^S) - \mathbb{E}[I(z^S)] = A_I(z^S) + B_I(z^S), \quad (25.66)
$$

with

$$
A_I(z^S) = \int_{\partial\Omega\times S} \frac{1}{i\omega} e^{-i\omega\theta\cdot z^S} \theta^T \overline{\nabla G^{(0)}_\omega(x,z^S)} u_s^{(\mu)}(x)dxd\theta \quad (25.67)
$$

and

$$
B_I(z^S) = -2\pi\delta^2 \frac{\sigma_r - 1}{\sigma_r + 1} U_I \int_S e^{-i\omega\theta\cdot(z^S-z_r)} \left[\int_\Omega \mu(y)\theta^T \widetilde{R}_\omega(z^S, z_r, y)\theta dy \right] d\theta.
$$
$$
(25.68)
$$

We now compute each term of the product in (25.63) separately.

Main speckle term:

We need to estimate the typical size of A_I. From (25.8), keeping only terms of first-order in μ yields

$$
A_I(z^S) = -\int_{\partial\Omega\times S} \frac{1}{i\omega} e^{-i\omega\theta\cdot z^S} \theta^T \overline{\nabla G^{(0)}_\omega(x,z^S)} \int_\Omega \mu(y)\nabla G^{(0)}_\omega(x,y)\cdot\nabla U_0(y)dydxd\theta + o(|\mu|),
$$
$$
(25.69)
$$

so we have

$$
A_I(z^S) = -U_I \int_{\Omega\times S} e^{-i\omega\theta\cdot(z^S-y)} \mu(y)\theta^T R_\omega(z^S, y)\theta dyd\theta, \quad (25.70)
$$

and hence

$$
A_I(z^S)\overline{A_I(z^{S'})} = U_I^2 \int_S e^{-i\omega\theta\cdot(z^S-z^{S'})}
$$

$$
\left[\int\int_{\Omega\times\Omega} e^{i\omega\theta\cdot(y-y')} \mu(y)\mu(y')\theta^T R_\omega(z^S, y)\overline{R_\omega(z^{S'}, y')}\theta dydy' \right] d\theta. \quad (25.71)
$$

We assume that the medium noise is localized and stationary on its support Ω_μ. We also assume that the correlation length l_μ is smaller than the wavelength. We denote by σ_μ the standard deviation of the process μ. We can then write

$$\mathbb{E}\left[A_I(z^S)\overline{A_I(z^{S'})}\right] = U_I^2\sigma_\mu^2 l_\mu^2 \int_S e^{i\omega\theta\cdot(z^S-z^{S'})} \int_{\Omega_\mu} \theta^T R_\omega(z^S,y)\overline{R_\omega(z^{S'},y)}\theta dy d\theta\,.$$

$$(25.72)$$

We introduce

$$P_\omega(z^S,y,z^{S'}) := \int_S e^{i\omega\theta\cdot(z^S-z^{S'})}\theta^T R_\omega(z^S,y)\overline{R_\omega(z^{S'},y)}\theta d\theta\,, \qquad (25.73)$$

where R_ω is defined by (25.36). Therefore, we have

$$\mathbb{E}\left[A_I(z^S)\overline{A_I(z^{S'})}\right] = U_I^2\sigma_\mu^2 l_\mu^2 \int_{\Omega_\mu} P_\omega(z^S,y,z^{S'})dy\,. \qquad (25.74)$$

Hence, A_I is a complex field with Gaussian statistics of mean zero and covariance given by (25.74). It is a speckle field and is not localized.

We compute its typical size at point $z^S = z^{S'} = z_r$, in order to get signal-to-noise estimates. Using (25.60) and (25.59), we get for $|x-z| \gg 1$,

$$\lim_{R\to\infty} \int_{|x|=R} \nabla G_\omega^{(0)}(x,y)\overline{\nabla G_\omega^{(0)}(z,y)}^T dy = \frac{\omega}{4} J_0(\omega|x-z|)\left(\frac{(x-z)}{|x-z|}\frac{(x-z)^T}{|x-z|}\right)\,,$$

and

$$\Im\left[G_\omega^{(0)}(x,z)\right] = \frac{1}{4}J_0(\omega|x-z|)\,.$$

Since we have, for $|x-z| \gg 1$,

$$J_0(\omega|x-z|) \sim \frac{\sqrt{2}\cos(\omega|x-z| - \frac{\pi}{4})}{\sqrt{\pi\omega|x-z|}}\,, \qquad (25.75)$$

we obtain that

$$R_\omega(x,z) \approx \frac{\sqrt{\omega}\cos(\omega|x-z| - \pi/4)}{2\sqrt{2\pi}}|x-z|^{-1/2}\left(\frac{(x-z)}{|x-z|}\frac{(x-z)^T}{|x-z|}\right) \text{ for } |x-z| \gg 1\,.$$

$$(25.76)$$

Now we can write

$$\mathbb{E}\left[A_I(z_r)\overline{A_I(z_r)}\right] \approx U_I^2\sigma_\mu^2 l_\mu^2 \int_{\Omega_\mu} \left(\frac{\sqrt{\omega}}{2\sqrt{2\pi}}\right)^2 \frac{1}{2}|y-z_r|^{-1} \int_S \theta^T\left(\frac{(y-z_r)}{|y-z_r|}\frac{(y-z_r)^T}{|y-z_r|}\right)\theta d\theta dy\,.$$

$$(25.77)$$

If we compute the term

$$\int_S \theta^T\left(\frac{(y-z_r)}{|y-z_r|}\frac{(y-z_r)^T}{|y-z_r|}\right)\theta d\theta = \int_0^{2\pi}\left[\left(\frac{(y-z_r)_1}{|y-z_r|}\right)^2\cos^2\theta + \left(\frac{(y-z_r)_2}{|y-z_r|}\right)^2\sin^2\theta\right]d\theta\,,$$

$$(25.78)$$

then, after linearization and integration, we get

$$\int_S \theta^T\left(\frac{(y-z_r)}{|y-z_r|}\frac{(y-z_r)^T}{|y-z_r|}\right)\theta d\theta = \pi\,. \qquad (25.79)$$

So we have

$$\mathbb{E}\left[A_I(z_r)\overline{A_I(z_r)}\right] \approx \pi U_I^2 \sigma_\mu^2 l_\mu^2 \int_{\Omega_\mu} \left(\frac{\sqrt{\omega}}{4\sqrt{\pi}}\right)^2 |y - z_r|^{-1} dy, \qquad (25.80)$$

and therefore

$$\mathbb{E}\left[A_I(z_r)\overline{A_I(z_r)}\right] \approx \pi \frac{\omega}{8} U_I^2 \sigma_\mu^2 l_\mu^2 \mathrm{diam}\ \Omega_\mu. \qquad (25.81)$$

Secondary speckle term:

We have

$$B_I(z^S)\overline{B_I(z^{S'})} = \left(2\pi\delta^2 \frac{\sigma_r - 1}{\sigma_r + 1} U_I\right)^2 \int_S e^{-i\omega\theta\cdot(z^S - z^{S'})}$$
$$\left[\int_\Omega \mu(y)\mu(y')\theta^T \widetilde{R}_\omega(z^S, z_r, y)\overline{\widetilde{R}_\omega(z^{S'}, z_r, y')}\theta dy dy'\right] d\theta. \qquad (25.82)$$

So we get the expectation

$$\mathbb{E}\left[B_I(z^S)\overline{B_I(z^{S'})}\right] = \left(2\pi\delta^2 \frac{\sigma_r - 1}{\sigma_r + 1} U_I\right)^2 \sigma_\mu^2 l_\mu^2$$
$$\int_S e^{-i\omega\theta\cdot(z^S - z^{S'})}\theta^T \left[\int_{\Omega_\mu} \widetilde{R}_\omega(z^S, z_r, y)\overline{\widetilde{R}_\omega(z^{S'}, z_r, y)}dy\right]\theta d\theta. \qquad (25.83)$$

This term also creates a speckle field on the image. As before, we compute the typical size of this term at z_r. We first get an estimate on $\widetilde{R}_\omega$:

$$\left|\left(\widetilde{R}_\omega(z^S, z_r, y)\right)_{i,j}\right| \leq |\partial_j G_\omega^{(0)}(y, z_r)| |\sum_{k=1,2} \int_{\partial\Omega} \partial_{y_i}\overline{G_\omega^{(0)}(x, z^S)}\partial_{y_i}\partial_{y_k}G_\omega^{(0)}(x, y)d\sigma(x)|. \qquad (25.84)$$

From the Helmholtz-Kirchoff identity

$$\int_{\partial\Omega} \overline{G_\omega^{(0)}(x, y)}G_\omega^{(0)}(x, z)d\sigma(x) \sim \frac{1}{4\omega} J_0(\omega|y - z|) \quad \text{as } R \to \infty, \qquad (25.85)$$

it follows that

$$\int_{\partial\Omega} \partial_{y_i}\overline{G_\omega^{(0)}(x, z^S)}\partial_{y_i}\partial_{y_k}G_\omega^{(0)}(x, y)d\sigma(x) = \frac{1}{4\omega}\left(\partial_i\partial_i\partial_k f\right)(z^S - y), \qquad (25.86)$$

where f is defined by $f(x) = J_0(\omega|x|)$. We have

$$\partial_i\partial_j\partial_k f(x) = \omega\left(\frac{3\left(a_{i,j,k}(x) - b_{i,j,k}(x)\right)}{|x|^2}\left[J_0'(\omega|x|) - \omega|x|J_0''(\omega|x|)\right] + a_{i,j,k}(x)\omega^2 J_0^{(3)}(\omega|x|)\right), \qquad (25.87)$$

where $a_{i,j,k}$ and $b_{i,j,k}$ are rational fractions in the coefficients of x bounded by 1. Now, recall the power series of J_0:

$$J_0(z) = \sum_k (-1)^k \frac{\left(\frac{1}{4}z^2\right)^k}{(k!)^2} \,. \tag{25.88}$$

We can write

$$J_0'(\omega|x|) - \omega|x|J_0''(\omega|x|) = -\frac{\omega^3}{4}|x|^3 + o(|x|^3) \,. \tag{25.89}$$

Hence, since $J_0^{(3)}(x) \sim \frac{3}{4}x$ when $x \to 0$, we can prove the following estimate for x around 0:

$$\frac{1}{4\omega}(\partial_i\partial_j\partial_k f)(x) \sim \frac{3b_{i,j,k}(x)}{16}\omega^3|x| \,. \tag{25.90}$$

In order to get the decay of $\widetilde{R}_\omega$ for large arguments we use the following formulas: $J_0' = -J_1$, $J_0'' = \frac{1}{x}J_1 - J_0$, and $J_0^{(3)} = J_1 - \frac{1}{x^2}J_1 + \frac{1}{x}J_0$. We get

$$\frac{1}{4\omega}|\partial_i\partial_j\partial_k f(x)| \le \omega^2(\omega|x|)^{-1/2} \quad \text{as } x \to \infty \,. \tag{25.91}$$

We also have the following estimate:

$$|\nabla G_\omega^{(0)}(y, z_r)| \le \left(\frac{2}{\pi}\right)^{1/2} \max\left(\frac{1}{|y - z_r|}, \frac{\omega}{\sqrt{\omega|y - z_r|}}\right) \,. \tag{25.92}$$

We can now write the estimate on $\widetilde{R_{\omega i,j}}$:

$$|\widetilde{R_\Omega}(z^S, z_r, y)_{i,j}| \le \omega^2\left(\frac{2}{\pi}\right)^{1/2} \min\left(\omega|y - z_r|, \frac{1}{\sqrt{\omega|y - z^S|}}\right) \max\left(\frac{1}{\omega|y - z_r|}, \frac{1}{\sqrt{\omega|y - z_r|}}\right) \,. \tag{25.93}$$

We can now go back to estimating the term B_I. We split the domain of integration $\Omega_\mu = B(z_r, \omega^{-1}) \cup \Omega_\mu \backslash B(z_r, \omega^{-1})$ to get

$$\left|\mathbb{E}\left[B_I(z_r)\overline{B_I(z_r)}\right]\right| \le \left(2\pi\delta^2\frac{\sigma_r - 1}{\sigma_r + 1}U_I\right)^2 \sigma_\mu^2 l_\mu^2$$
$$4\pi\omega^4\frac{2}{\pi}\left[\int_{\Omega_\mu\backslash B(z_r, \omega^{-1})} \frac{1}{|y - z_r|^2}dy + \int_{B(z_r, \omega^{-1})} \omega^2 dy\right]. \tag{25.94}$$

Hence,

$$\left|\mathbb{E}\left[B_I(z_r)\overline{B_I(z_r)}\right]\right| \le 8\left(2\pi\delta^2\frac{\sigma_r - 1}{\sigma_r + 1}U_I\right)^2 \omega^4\sigma_\mu^2 l_\mu^2 \log(\omega \text{ diam } \Omega_\mu). \tag{25.95}$$

Double products:

The double products $A_I\overline{B_I}$ and $B_I\overline{A_I}$ have a typical amplitude that is the geometric mean of the typical amplitudes of A_I and B_I. So they are always smaller than one of the main terms $|A_I|^2$ or $|B_I|^2$.

Signal-to-Noise Ratio Estimates

We can now give an estimate of the signal-to-noise ratio $(SNR)_I$ defined by (25.42). Using (25.62), (25.81), and (25.95) we get

$$(SNR)_I \approx \frac{\frac{\pi^2(\sigma_r-1)}{2(\sigma_r+1)}\omega\delta^2 U_I}{\sigma_\mu l_\mu \left(\pi\frac{\omega}{8} \text{ diam } \Omega_\mu + 8\left(2\pi\delta^2\frac{\sigma_r-1}{\sigma_r+1}U_I\right)^2 \omega^4 \log(\omega \text{ diam } \Omega_\mu)\right)^{1/2}}.$$

(25.96)

Since $\delta \ll \frac{2\pi}{\omega}$ we have that $\delta\omega \ll 1$, so we can estimate $(SNR)_I$ as follows:

$$(SNR)_I \approx \frac{\sqrt{2}\pi^{3/2}\frac{\sigma_r-1}{\sigma_r+1}\omega\delta^2 U_I}{\sigma_\mu l_\mu\sqrt{\omega \text{ diam } \Omega_\mu}}.$$

(25.97)

The perturbation in the image I comes from different phenomena. The first one and most important one is the fact that we image not only the field scattered by the reflector, but also the field scattered by the medium's random inhomogeneities. This is why the signal-to-noise ratio depends on the volume and the contrast of the particle we are trying to locate. It has to stand out from the background. The other terms in the estimate (25.96) of $(SNR)_I$ are due to the phase perturbation of the field scattered by the particle when it reaches the boundary of Ω, which can be seen as a travel time fluctuation of the scattered wave by the reflector. Both terms are much smaller than the first one. $(SNR)_I$ depends on the ratio ω/l_μ. If the medium noise has a shorter correlation length, then the perturbation induced in the phase of the fields will more likely self-average.

25.5.3 Second-Harmonic Backpropagation

Expectation

We have

$$\mathbb{E}[J(z^S)] = -\pi\delta^2 \int_S e^{-2i\omega\theta\cdot z^S}\left[(S)_{det}^\theta \int_{\partial\Omega} \overline{G_{2\omega}^{(0)}(x,z^S)}G_{2\omega}^{(0)}(x,z_r)dx\right.$$
$$\left.+ \mathbb{E}[(S)_{rand}^\theta] \int_{\partial\Omega} \overline{G_{2\omega}^{(0)}(x,z^S)}G_{2\omega}^{(0)}(x,z_r)dx\right]d\theta. \quad (25.98)$$

Since $\mathbb{E}[(S)_{rand}^\theta] = 0$ we obtain by using (25.32) that

$$\mathbb{E}[J(z^S)] = \pi\delta^2\omega^2 U_I^2 \int_S \left(\sum_{k,l}\chi_{k,l}^{(2)}\theta_k\theta_l\right)e^{2i\omega\theta\cdot(z_r-z^S)}d\theta \int_{\partial\Omega} \overline{G_{2\omega}^{(0)}(x,z^S)}G_{2\omega}^{(0)}(x,z_r)dx.$$

(25.99)

If we define $\widetilde{Q}_{2\omega}$ as

$$\widetilde{Q}_{2\omega}(x,y) = \int_S \left(\sum_{k,l} \chi_{k,l}^{(2)} \theta_k \theta_l \right) e^{2i\omega\theta\cdot(x-y)} d\theta \,, \qquad (25.100)$$

then it follows that

$$\mathbb{E}[J(z^S)] = \delta^2 \omega^2 U_I^2 \widetilde{Q}_{2\omega}(z_r, z^S) Q_{2\omega}(z_r, z^S) \,, \qquad (25.101)$$

where $Q_{2\omega}$ is given by (25.40). To get the typical size of this term we first use the Helmholtz-Kirchhoff identity (3.80):

$$Q_{2\omega}(z_r, z^S) \sim \frac{1}{2\omega} \Im \left(G_{2\omega}^{(0)}(z_r, z^S) \right) \,. \qquad (25.102)$$

Therefore, we obtain that

$$\mathbb{E}[J(z_r)] = \frac{\pi}{8} \delta^2 \omega U_I^2 \int_S \left(\sum_{k,l} \chi_{k,l}^{(2)} \theta_k \theta_l \right) d\theta \,. \qquad (25.103)$$

Covariance

We have

$$J(z^S) - \mathbb{E}[J](z^S) = \pi\delta^2 \int_S e^{-2i\omega\theta\cdot z^S} \left[(S)_{det}^\theta 4\omega^2 \int_\Omega G_{2\omega}^{(0)}(s, z_r)\mu(s)Q_{2\omega}(s, z^S)ds \right.$$
$$\left. - (S)_{rand}^\theta Q_{2\omega}(z_r, z^S) \right] d\theta \,. \quad (25.104)$$

Denote

$$A_J(z^S) = 4\pi\delta^2\omega^2 \int_S e^{-2i\omega\theta\cdot z^S} (S)_{det}^\theta \int_\Omega G_{2\omega}^{(0)}(s, z_r)\mu(s)Q_{2\omega}(s, z^S)dsd\theta$$
$$(25.105)$$

and

$$B_J(z^S) = \pi\delta^2 \int_S e^{-2i\omega\theta\cdot z^S} (S)_{rand}^\theta Q_{2\omega}(z_r, z^S)d\theta \,. \qquad (25.106)$$

Then we can write the covariance function

$$\mathrm{Cov}\left(J(z^S), J(z^{S'}) \right) = \mathbb{E}\left[\left(J(z^S) - \mathbb{E}[J(z^S)] \right) \overline{\left(J(z^{S'}) - \mathbb{E}[J(z^{S'})] \right)} \right]$$
$$(25.107)$$

in the form

$$\mathrm{Cov}\left(J(z^S), J(z^{S'}) \right) = \mathbb{E}\left[A(z^S)\overline{A(z^{S'})} + B(z^S)\overline{B_J(z^{S'})} + A_J(z^S)\overline{B_J(z^{S'})} + \overline{A_J(z^S)}B_J(z^{S'}) \right].$$
$$(25.108)$$

We will now compute the first two terms separately and then deal with the double products.

The speckle term $A_J\overline{A_J}$:

From

$$A_J(z^S)\overline{A_J(z^{S'})} = 16\pi^2\delta^4\omega^4 \int_S e^{-2i\omega\theta\cdot(z^S-z^{S'})}|(S)_{det}^\theta|^2$$

$$\int\int_{\Omega\times\Omega} G_{2\omega}^{(0)}(s,z_r)\overline{G_{2\omega}^{(0)}(s',z_r)}\mu(s)\overline{\mu(s')}Q_{2\omega}(s,z^S)\overline{Q_{2\omega}(s',z^{S'})}dsds'd\theta\,,$$

(25.109)

it follows by using (25.32) that

$$A_J(z^S)\overline{A_J(z^{S'})} = 16\pi^2\delta^4\omega^8U_I^4 \int_S e^{-2i\omega\theta\cdot(z^S-z^{S'})}|\sum_{k,l}\chi_{k,l}^{(2)}\theta_k\theta_l|^2 d\theta$$

$$\int\int_{\Omega\times\Omega} G_{2\omega}^{(0)}(s,z_r)\overline{G_{2\omega}^{(0)}(s',z_r)}\mu(s)\overline{\mu(s')}Q_{2\omega}(s,z^S)\overline{Q_{2\omega}(s',z^{S'})}dsds'\,.$$

(25.110)

If we write $C_\mu(s,s') = \mathbb{E}[\mu(s)\mu(s')]$, then we find that

$$\mathbb{E}[A_J(z^S)\overline{A_J(z^{S'})}] = 16\pi^2\delta^4\omega^8U_I^4 \int_S e^{-2i\omega\theta\cdot(z^S-z^{S'})}|\sum_{k,l}\chi_{k,l}^{(2)}\theta_k\theta_l|^2 d\theta$$

$$\int\int_{\Omega\times\Omega} G_{2\omega}^{(0)}(s,z_r)\overline{G_{2\omega}^{(0)}(s',z_r)}C_\mu(s,s')Q_{2\omega}(s,z^S)\overline{Q_{2\omega}(s',z^{S'})}dsds'\,,$$

(25.111)

since μ is real.

As previously, we assume that the medium noise is localized and stationary on its support (which is Ω_μ). We denote by σ_μ the standard deviation of the process μ and by l_μ its correlation length. We can then write

$$\mathbb{E}[A_J(z^S)\overline{A_J(z^{S'})}] = 16\pi^2\delta^4\omega^8U_I^4\sigma_\mu^2 l_\mu^2 \int_S e^{-2i\omega\theta\cdot(z^S-z^{S'})}|\sum_{k,l}\chi_{k,l}^{(2)}\theta_k\theta_l|^2 d\theta$$

$$\int_{\Omega_\mu} |G_{2\omega}^{(0)}(s,z_r)|^2 Q_{2\omega}(s,z^S)\overline{Q_{2\omega}(s,z^{S'})}ds\,. \quad (25.112)$$

The term $\mathbb{E}[A_J(z^S)\overline{A_J(z^{S'})}]$ shows the generation of a non localized speckle image, creating random secondary peaks. We will later estimate the size of those peaks in order to find the signal-to-noise ratio. We compute the typical size of this term. We get, using (25.102),

$$\mathbb{E}[A_J(z^S)\overline{A_J(z^{S'})}] \approx 4\pi^2U_I^4\delta^4\omega^6\sigma_\mu^2 l_\mu^2$$

$$\int_S |\sum_{k,l}\chi_{k,l}^{(2)}\theta_k\theta_l|^2 d\theta \int_{\Omega_\mu} |G_{2\omega}^{(0)}(s,z_r)|^2 \Im G_{2\omega}^{(0)}(s,z^S)\Im G_{2\omega}^{(0)}(s,z^{S'})ds\,. \quad (25.113)$$

Then we use the facts that

$$|G_{2\omega}^{(0)}(x,y)| \approx \frac{1}{4\sqrt{\pi 2\omega}}|x-y|^{-1/2}$$

and

$$\Im G_{2\omega}^{(0)}(x,y) = \frac{1}{4}J_0(2\omega|x-y|) \approx \frac{\cos(2\omega|x-y|-\pi/4)}{4\sqrt{\pi\omega}}|x-y|^{-1/2}$$

if $|x-y| \gg 1$. Then, as previously, we write $\Omega_\mu = \Omega_\mu\backslash B(z_r,\omega^{-1})\cup B(z_r,\omega^{-1})$. Using (25.113), we arrive at

$$\mathbb{E}[A_J(z_r)\overline{A_J(z_r)}] \approx 4\pi^2 U_I^4\delta^4\omega^6\sigma_\mu^2 l_\mu^2 \int_S |\sum_{k,l}\chi_{k,l}^{(2)}\theta_k\theta_l|^2 d\theta$$

$$\left(\frac{1}{512\pi^2\omega^2}\int_{\Omega_\mu\backslash B(z_r,\omega^{-1})} \frac{\cos^2(2\omega|s-z_r|-\pi/4)}{|s-z_r|^2}ds + \frac{1}{16}\int_{B(z_r,\omega^{-1})}|G_{2\omega}^{(0)}(s,z_r)|^2 J_0(2\omega|s-z_r|)^2 ds\right),$$

$$(25.114)$$

which yields

$$\mathbb{E}[A_J(z_r)\overline{A_J(z_r)}] \approx \frac{\pi}{128}U_I^4\delta^4\omega^4\sigma_\mu^2 l_\mu^2 \log(\omega\ \text{diam}\ \Omega_\mu)\int_S |\sum_{k,l}\chi_{k,l}^{(2)}\theta_k\theta_l|^2 d\theta.$$

$$(25.115)$$

The localized term $B_J\overline{B_J}$:

We have

$$B_J(z^S)\overline{B_J(z^{S'})} = \pi^2\delta^4 Q_{2\omega}(z_r,z^S)\overline{Q_{2\omega}(z_r,z^{S'})}\int_S e^{-2i\omega\theta\cdot(z^S-z^{S'})}|(S)_{rand}^\theta|^2 d\theta.$$

$$(25.116)$$

Using (25.33) we have that $(S)_{rand}^\theta$ can be rewritten as

$$(S)_{rand}^\theta = -\omega^2 U_I^2 \int_\Omega \left(\mu(y)e^{i\omega\theta\cdot y} - \mu(z_r)e^{i\omega\theta\cdot z_r}\right)$$

$$\left[\sum_{k,l}\chi_{k,l}^{(2)}\left(\theta_k\theta\cdot\nabla\partial_{x_l}G_\omega^{(0)}(z_r,y) + \theta_l\theta\cdot\nabla\partial_{x_k}G_\omega^{(0)}(z_r,y)\right)\right]dy. \quad (25.117)$$

We need to get an estimate on S_{rand}^θ's variance. As in Section 25.2 we have the following estimate for any $0 < \alpha' < 1/2$:

$$\frac{1}{4}|y-z_r|^{\alpha'}|\partial_{x_k}\partial_{x_l}H_0^1(\omega|y-z_r|)| \leq \frac{1}{2}\min\left(1,\sqrt{\frac{2}{\pi}}\omega^{3/2}|y-z_r|^{\alpha'-1/2}\right)\max\left(1,|y-z_r|^{\alpha'-2}\right).$$

$$(25.118)$$

We get, for any $\alpha' < \min(\alpha, \frac{1}{2})$,

$$|S_{rand}^{\theta}| \leq \omega^2 U_I^2 \|\mu\|_{\mathcal{C}^{0,\alpha'}} \max_{k,l} \left|\chi_{k,l}^{(2)}\right| \omega^{2-2\alpha'} \left[\frac{8\sqrt{2\pi}}{3/2+\alpha'} \left(\omega\text{diam } \Omega_{\mu}\right)^{3/2+\alpha'} + \frac{\pi}{\alpha'}\right]$$
(25.119)

and

$$\left|\mathbb{E}[B_J(z^S)\overline{B_J(z^{S'})}]\right| \leq \frac{128\pi^3}{(3/2+\alpha')^2} \omega^{4-2\alpha'} \delta^4 U_I^4 \max_{k,l} \left|\chi_{k,l}^{(2)}\right|^2 \mathbb{E}\left[\|\mu\|_{\mathcal{C}^{0,\alpha'}}^2\right]$$
$$\left[\left(\omega\text{diam } \Omega_{\mu}\right)^{3+2\alpha'} + \frac{1}{\alpha'}\right] Q_{2\omega}(z_r, z^S)\overline{Q_{2\omega}(z_r, z^{S'})}. \quad (25.120)$$

Note that $Q_{2\omega}(z_r, z^S)$, defined in (25.40), behaves like $\frac{1}{8\omega}J_0(2\omega|z_r - z^S|)$, which decreases like $|z_r - z^S|^{-1/2}$ as $|z_r - z^S|$ becomes large. The term B_J is localized around z_r. It may shift, lower or blur the main peak but it will not contribute to the speckle field on the image. We still need to estimate its typical size at z_r in order to get the signal-to-noise ratio at z_r. Using (25.102) and (25.56), we get

$$\mathbb{E}[B_J(z_r)\overline{B_J(z_r)}] \leq \frac{2^{17+\alpha}\pi^3}{(3/2+\alpha')^2} \frac{e}{\alpha-\alpha'} \omega^{2-2\alpha'} \delta^4 U_I^4 \max_{k,l} \left|\chi_{k,l}^{(2)}\right|^2 \left[\left(\omega\text{diam } \Omega_{\mu}\right)^{3+2\alpha'} + \frac{1}{\alpha'}\right] \frac{\sigma_{\mu}^2}{l_{\mu}^{2\alpha}}.$$
(25.121)

We can write $(\omega\text{diam } \Omega_{\mu})^{3+2\alpha'} \leq (\omega\text{diam } \Omega_{\mu})^{3+2\alpha} + 1$. We can take $\alpha' = \frac{\alpha}{2}$. Let $C = \frac{2^{18+1/2}\pi^3 e}{(3/2)^2}$. We get that

$$\mathbb{E}[B_J(z_r)\overline{B_J(z_r)}] \leq C\omega^2 \min\left(\omega^{-2\alpha}, 1\right) \delta^4 U_I^4 \max_{k,l} \left|\chi_{k,l}^{(2)}\right|^2 \frac{\sigma_{\mu}^2}{l_{\mu}^{2\alpha}} \left[\left(\omega\text{diam } \Omega_{\mu}\right)^{3+2\alpha} + 1\right].$$
(25.122)

Remark 25.4 *We note that even though the term B_J is localized, meaning it would not create too much of a speckle far away from the reflector, it is still the dominant term of the speckle field around the reflector's location.*

The double products $A_J\overline{B_J}$ and $\overline{A_J}B_J$:

This third term has the size of the geometric mean of the first two terms A_J and B_J. So we only need to concentrate on the first two terms. Also this term is still localized because of $Q(z_r, z^S)$ that decreases as $|z_r - z^S|^{-1/2}$.

Signal-to-Noise Ratio

As before, we define the signal-to-noise ratio $(SNR)_J$ by (25.43). Using (25.103), (25.115) and (25.122),

$$\frac{\mathbb{E}[J(z_r)]}{(Var(J(z_r)))^{\frac{1}{2}}} \geq \frac{l_\mu^\alpha \left(\int_S \left(\sum_{k,l} \chi_{k,l}^{(2)} \theta_k \theta_l\right) d\theta\right)}{\sqrt{C}\sigma_\mu \min(\omega^{-\alpha}, 1) \max_{k,l} \left|\chi_{k,l}^{(2)}\right| \sqrt{(\omega \mathrm{diam}\ \Omega_\mu)^{3+2\alpha} + 1}} \cdot$$

(25.123)

The difference here with the standard backpropagation is that the (SNR) does not depend on neither the dielectric contrast of the particle, the nonlinear susceptibility or even the particle's volume. All the background noise created by the propagation of the illuminating wave in the medium is filtered because the small inhomogeneities only scatter waves at frequency ω. The nanoparticle is the only source at frequency 2ω so it does not need to stand out from the background. The perturbations seen on the image J are due to travel time fluctuations of the wave scattered by the nanoparticle (for the speckle field) and to the perturbations of the source field at the localization of the reflector (for the localized perturbation). The second-harmonic image is more resolved than the fundamental frequency image.

25.5.4 Stability with Respect to Measurement Noise

We now compute the signal-to-noise ratio in the presence of measurement noise without any medium noise ($\mu = 0$). The signals u_s and v are corrupted by an additive noise $\nu(x)$ on $\partial\Omega$. In real situations it is of course impossible to achieve measurements for an infinity of plane wave illuminations. So in this subsection we assume that the functional J is calculated as an average over n different illuminations, uniformly distributed in S. We consider, for each $j \in [0, n]$, an independent and identically distributed random process $\nu^{(j)}(x)$, $x \in \partial\Omega$, representing the measurement noise. If we assume that the surface of Ω is covered with sensors half a wavelength apart and that the additive noise has variance σ and is independent from one sensor to another one, we can model the additive noise process by a Gaussian white noise with covariance function:

$$\mathbb{E}(\nu(x)\overline{\nu(x')}) = \sigma_\nu^2 \delta(x - x'),$$

where $\sigma_\nu = \sigma^2 \frac{\lambda}{2}$.

Standard Backpropagation

We write, for each $j \in [0, n]$, $u_s^{(j)}$ as

$$u_s^{(j)}(x) = -2\pi\delta^2 \frac{\sigma_r - 1}{\sigma_r + 1} U_I e^{i\omega\theta^{(j)} \cdot z_r} \nabla G_\omega^{(0)}(x, z_r) \cdot (i\omega\theta^{(j)}) + o(\delta^2) + \nu^{(j)}(x),$$

(25.124)

where $\nu^{(j)}$ is the measurement noise associated with the j-th illumination. We can write I as

$$I(z^S) = \frac{1}{n} \sum_{j=1}^n \int_{\partial\Omega} \frac{1}{i\omega} e^{-i\omega\theta^{(j)} \cdot z^S} (\theta^{(j)})^T \overline{\nabla G_\omega^{(0)}(x, z^S)} u_s(x) dx.$$

(25.125)

Further,

$$I(z^S) = -2\pi\delta^2 \frac{\sigma_r - 1}{\sigma_r + 1} U_I \frac{1}{n} \sum_{j=1}^{n} e^{i\omega\theta^{(j)}\cdot(z_r - z^S)}(\theta^{(j)})^T R_\omega(z_r, z^S)\theta^{(j)}$$

$$+ \frac{1}{n}\sum_{j=1}^{n}\int_{\partial\Omega}\frac{1}{i\omega}e^{-i\omega\theta^{(j)}\cdot z^S}(\theta^{(j)})^T\overline{\nabla G_\omega^{(0)}(x, z^S)}\nu^{(j)}(x)dx. \quad (25.126)$$

We get that

$$\mathbb{E}[I(z^S)] = -2\pi\delta^2\frac{\sigma_r - 1}{\sigma_r + 1}U_I\frac{1}{n}\sum_{j=1}^{n}e^{i\omega\theta^{(j)}\cdot(z_r - z^S)}(\theta^{(j)})^T R_\omega(z_r, z^S)\theta^{(j)},$$

$$(25.127)$$

so that, using (25.60) and (25.59),

$$\mathbb{E}[I(z_r)] \sim -\frac{\pi(\sigma_r - 1)}{4(\sigma_r + 1)}\omega\delta^2 U_I. \quad (25.128)$$

We compute the covariance

$$Cov(I(z^S), I(z^{S'})) = \mathbb{E}\left[\frac{1}{n^2}\left(\sum_{j=1}^{n}\frac{1}{i\omega}e^{-i\omega\theta^{(j)}\cdot z^S}\int_{\partial\Omega}\nu^{(j)}(x)(\theta^{(j)})^T\overline{\nabla G_\omega^{(0)}(x, z^S)}dx\right)\right.$$

$$\left.\left(\sum_{l=1}^{n}\frac{-1}{i\omega}e^{i\omega\theta^{(l)}\cdot z^{S'}}\int_{\partial\Omega}\nu^{(l)}(x')(\theta^{(l)})^T\nabla G_\omega^{(0)}(x', z^{S'})dx'\right)\right] \quad (25.129)$$

and obtain that

$$Cov(I(z^S), I(z^{S'})) = \sigma^2\frac{\lambda}{2}\frac{1}{\omega^2 n^2}\sum_{j=1}^{n}e^{-i\omega\theta^{(j)}\cdot(z^S - z^{S'})}(\theta^{(j)})^T R_\omega(z^S, z^{S'})\theta^{(j)}. $$

$$(25.130)$$

The signal-to-noise ratio is given by

$$(SNR)_I = \frac{\mathbb{E}[I(z_r)]}{(Var(I(z_r))^{\frac{1}{2}}}. \quad (25.131)$$

If we compute

$$Var(I(z_r)) \sim \sigma^2\frac{\pi}{8\omega^2 n}, \quad (25.132)$$

then $(SNR)_I$ can be expressed as

$$(SNR)_I = \frac{\sqrt{\pi n}\delta^2\omega^2[\sigma_r - 1]U_I}{[\sigma_r + 1]\sigma}. \quad (25.133)$$

The backpropagation functional is very stable with respect to measurement noise. Of course, the number of measurements increases the stability because the measurement noise is averaged out. We will see in the following that the second-harmonic imaging is also pretty stable with respect to measurement noise.

Second-Harmonic Backpropagation

We write, for each $j \in [0, n]$, v_j as

$$v^{(j)}(x) = -\delta^2(2\omega)^2 \left(\sum_{k,l} \chi_{k,l}^{(2)} \partial_{x_k} U^{(j)}(z_r) \partial_{x_l} U^{(j)}(z_r) \right) G_{2\omega}^{(0)}(x, z_r) + \nu^{(j)}(x),$$

(25.134)

where ν_j is the measurement noise at the j-th measurement. Without any medium noise the source term (S) can be written as

$$(S)^{\theta^{(j)}} = \sum_{k,l} \chi_{k,l}^{(2)} \partial_{x_k} U^{(j)}(z_r) \partial_{x_l} U^{(j)}(z_r) = -\omega^2 U_I^2 e^{2i\omega\theta^{(j)} \cdot z_r} \sum_{k,l} \chi_{k,l}^{(2)} \theta_k^{(j)} \theta_l^{(j)}.$$

(25.135)

So we can write J as

$$J(z^S) = \frac{1}{n} \sum_{j=1}^{n} \int_{\partial\Omega} v^{(j)}(x) \overline{G_{2\omega}^{(0)}(x, z^S)} e^{-2i\omega\theta^{(j)} \cdot z^S} dx,$$

(25.136)

or equivalently

$$J(z^S) = -\delta^2(2\omega)^2 \frac{1}{n} \sum_{j=1}^{n} (S)^{\theta^{(j)}} \int_{\partial\Omega} G_{2\omega}^{(0)}(x, z_r) \overline{G_{2\omega}^{(0)}(x, z^S)} e^{-2i\omega\theta^{(j)} \cdot z^S} dx$$

$$+ \frac{1}{n} \sum_{j=1}^{n} \int_{\partial\Omega} \nu^{(j)}(x) \overline{G_{2\omega}^{(0)}(x, z^S)} e^{-2i\omega\theta^{(j)} \cdot z^S} dx. \quad (25.137)$$

We get that

$$\mathbb{E}[J(z^S)] = -\delta^2(2\omega)^2 \frac{1}{n} \sum_{j=1}^{n} (S)^{\theta^{(j)}} e^{-2i\omega\theta^{(j)} \cdot z^S} Q_{2\omega}(z_r, z^S),$$

(25.138)

so that, using (25.102),

$$\mathbb{E}[J(z_r)] \sim \delta^2 U_I^2 \frac{\omega^3}{2n} \sum_{k,l,j} \chi_{k,l}^{(2)} \theta_k^{(j)} \theta_l^{(j)}.$$

(25.139)

We can compute the covariance

$$Cov(J(z^S), J(z^{S'})) = \mathbb{E}\left[\frac{1}{n^2} \left(\sum_{j=1}^{n} e^{-2i\omega\theta^{(j)} \cdot z^S} \int_{\partial\Omega} \nu^{(j)}(x) \overline{G_{2\omega}^{(0)}(x, z^S)} dx \right) \right.$$

$$\left. \left(\sum_{l=1}^{n} e^{2i\omega\theta^{(l)} \cdot z^{S'}} \int_{\partial\Omega} \nu^{(l)}(x) G_{2\omega}^{(0)}(x', z^{S'}) dx' \right) \right], \quad (25.140)$$

which yields

$$Cov(J(z^S), J(z^{S'})) = \sigma^2 \frac{\lambda}{2} Q_{2\omega}(z^{S'}, z^S) \frac{1}{n^2} \sum_{j=1}^{n} e^{-2i\omega\theta^{(j)}\cdot(z^S - z^{S'})} . \quad (25.141)$$

Now we have

$$Var(J(z_r))^{1/2} \sim \frac{\sigma}{2\omega} \sqrt{\frac{\pi}{2n}} . \quad (25.142)$$

The signal-to-noise ratio,

$$(SNR)_J = \frac{\mathbb{E}[J(z_r)]}{(Var(J(z_r))^{\frac{1}{2}}} , \quad (25.143)$$

is given by

$$(SNR)_J = \frac{2\delta^2\omega^2 U_I \left(\sum_j \sum_{k,l} \chi_{k,l}^{(2)} \theta_k^{(j)} \theta_l^{(j)} \right)}{\pi\sigma\sqrt{n}} . \quad (25.144)$$

Even though it appears that the (SNR) is proportional to $\frac{1}{\sqrt{n}}$, the term $\sum_j \theta_k^{(j)} \theta_l^{(j)}$ is actually much bigger. In fact, if we pick $\theta^{(j)} = \frac{2j\pi}{n}$, we get that

$$\sum_{k,l} \chi_{k,l}^{(2)} \sum_j \theta_k^{(j)} \theta_l^{(j)} = \sum_{j=1}^{n} \left(\chi_{1,1}^{(2)} \cos^2 \frac{2j\pi}{n} + \chi_{2,2}^{(2)} \sin^2 \frac{2j\pi}{n} + 2\chi_{1,2}^{(2)} \sin \frac{2j\pi}{n} \cos \frac{2j\pi}{n} \right) ,$$

$$(25.145)$$

and hence

$$\sum_{k,l} \chi_{k,l}^{(2)} \sum_j \theta_k^{(j)} \theta_l^{(j)} \sim \frac{n}{2} \max[\chi_{1,1}^{(2)}, \chi_{2,2}^{(2)}] . \quad (25.146)$$

Therefore, we can conclude that

$$(SNR)_J = \frac{\delta^2\omega^2 U_I^2 \sqrt{n} \max[\chi_{1,1}^{(2)}, \chi_{2,2}^{(2)}]}{\pi\sigma_\nu} . \quad (25.147)$$

The signal-to-noise ratio is very similar to the one seen in the classic back-propagation case. So the sensitivity with respect to relative measurement noise should be similar. It is noteworthy that in reality, due to very small size of the (SHG) signal ($\chi^{(2)}$ has a typical size of 10^{-12} m/V), the measurement noise levels will be higher for the second-harmonic signal.

25.6 Numerical Results

25.6.1 The Direct Problem

We consider the medium to be the square $[-1, 1]^2$. The medium has an average propagation speed of 1, with random fluctuations with Gaussian statistics (see

Figure 25.2). To simulate μ we use the algorithm described in Section 4.4.2 which generates random Gaussian fields with Gaussian covariance function and take a standard deviation equal to 0.02 and a correlation length equal to 0.25. We consider a small reflector in the medium $\Omega_r = z_r + \delta B(0, 1)$ with $z_r = (-0.2, 0.5)$ and $\delta = 0.004/\pi$, represented in Figure 25.1. The contrast of the reflector is $\sigma_r = 2$. We fix the frequency to be $\omega = 8$. We get the boundary data u_s when the medium is illuminated by the plane wave $U_I(x) = e^{i\omega\theta \cdot x}$. The correlation length of the medium noise was picked so that it has a similar size as the wavelength of the illuminating plane wave. We get the boundary data by using an integral representation for the field $u_{s,\theta}$. We also compute the boundary data for the second-harmonic field v. We compute the imaging functions I and J, respectively, defined in (25.35) and (25.38), averaged over two different lightning settings. (see Figures 25.7 and 25.8, for instance).
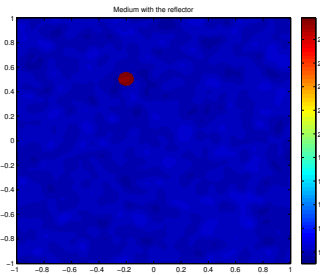
Fig. 25.1. Medium with the reflector.
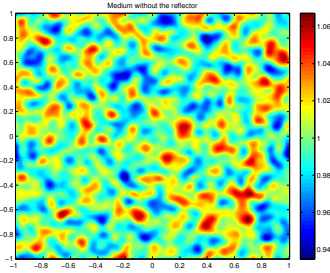
Fig. 25.2. Medium without the reflector (permittivity variations zoomed out).
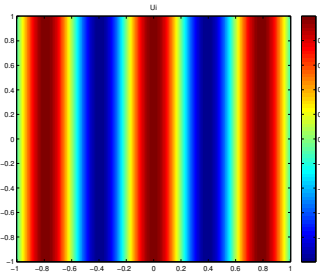
Fig. 25.3. Incoming field U_I.
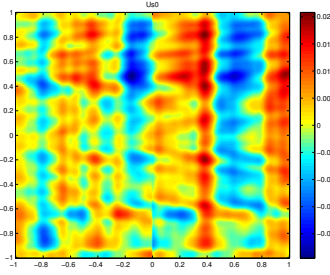
Fig. 25.4. Background field in the absence of a reflector $u_s^{(\mu)}$.
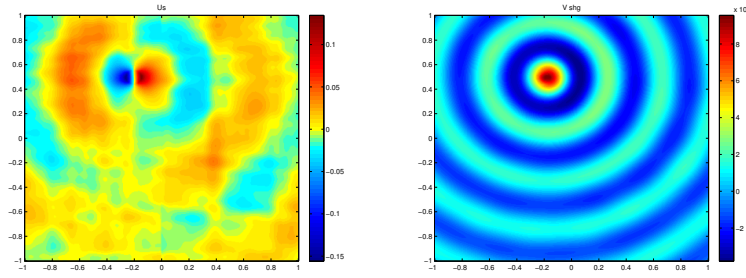
Fig. 25.5. Total scattered field u_s. **Fig. 25.6.** Second-harmonic field v.

25.6.2 The Imaging Functionals and the Effects of the Number of Plane Wave Illuminations

We compute the imaging functionals I and J, respectively, defined in (25.35) and (25.38), averaged over four different illuminations settings. We fix the noise level ($\sigma_\mu = 0,02$), the volume of the particle ($v_r = 10^{-2}$), and the contrast $\sigma_r = 2$. In Figures 25.7 and 25.8 the image is obtained after backpropagating the boundary data from one illumination ($\theta = 0$). On the following graphs, we average over several illumination angles:

- 4 uniformly distributed angles for Figures 25.9 and 25.10.
- 8 uniformly distributed angles for Figures 25.11 and 25.12.
- 32 uniformly distributed angles for Figures 25.13 and 25.14.

As predicted, the shape of the spot on the fundamental frequency imaging is very dependent on the illumination angles, whereas with second-harmonic imaging we get an acceptable image with only one illumination. In applications, averaging over different illumination is useful because it increases the stability with respect to measurement noise. It is noteworthy that, as expected, the resolution of the second-harmonic image is twice higher than the regular imaging one.

25.6.3 Statistical analysis

Stability with respect to medium noise

Here we show numerically that the second-harmonic imaging is more stable with respect to medium noise. In Figure 25.15, we plot the standard deviation of the error $|z_{est} - z_r|$, where z_{est} is the estimated location of the reflector. For each level of medium noise we compute the error over 120 realizations of the medium, using the same parameters as above. The functional imaging J is clearly more robust than earlier.
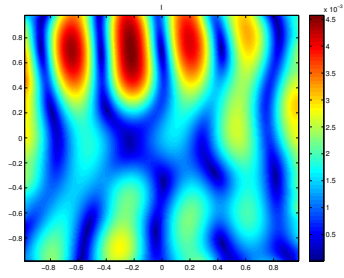
Fig. 25.7. *I* with 1 illumination.
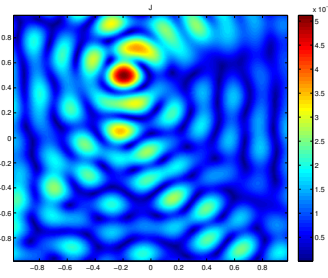
Fig. 25.8. *J* with 1 illumination.
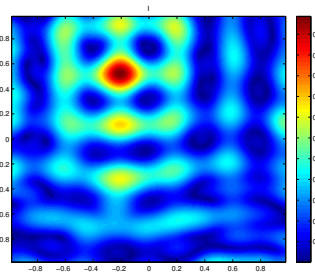
Fig. 25.9. *I* with 4 illuminations.
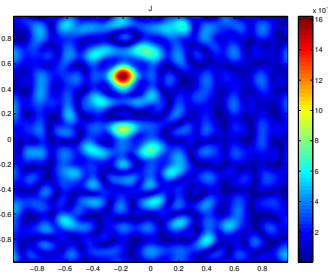
Fig. 25.10. *J* with 4 illuminations.
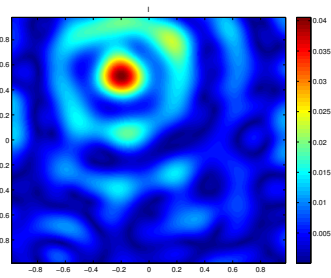
Fig. 25.11. *I* with 8 illuminations.
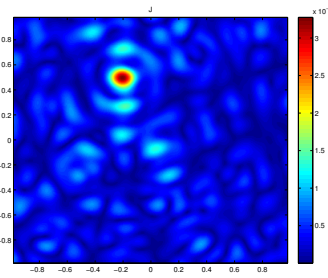
Fig. 25.12. *J* with 8 illuminations.

Effect of the Volume of the Particle

We show numerically that the quality of the second-harmonic image does not depend on the volume of the particle. We fix the medium noise level ($\sigma_\mu = 0.02$) and plot the standard deviation of the error with respect to the volume of the particle (Figure 25.16). We can see that if the particle is too small, the fundamental backpropagation algorithm cannot differentiate the reflector from the medium and the main peak gets buried in the speckle
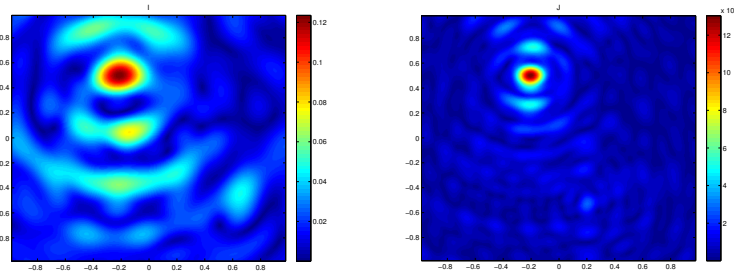
Fig. 25.13. I with 32 illuminations. **Fig. 25.14.** J with 32 illuminations.
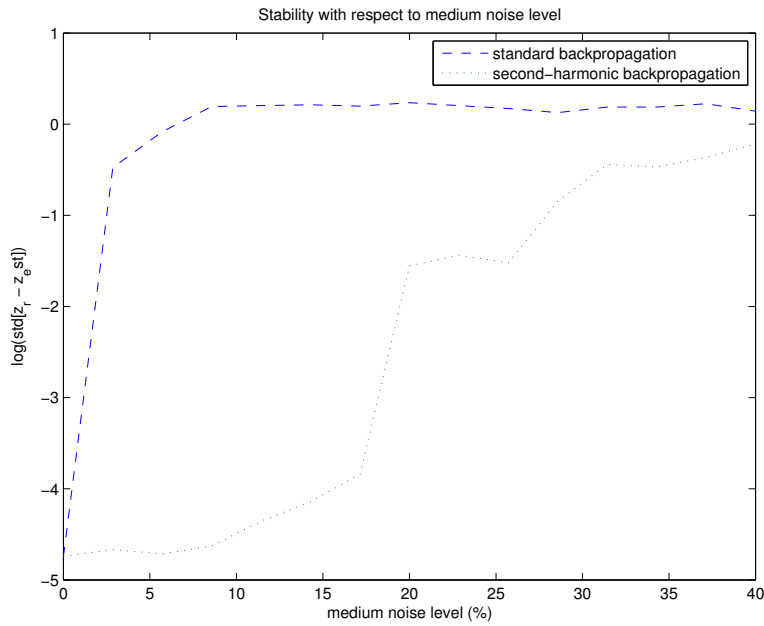
Fig. 25.15. Standard deviation of the localization error with respect to the medium noise level for standard backpropagation (top) and second-harmonic image (bottom).

field. The volume of the particle does not have much influence on the second-harmonic image quality.

Stability with Respect to Measurement Noise

We compute the imaging functionals with a set of data obtained without any medium noise and perturbed with a Gaussian white noise for each of 8
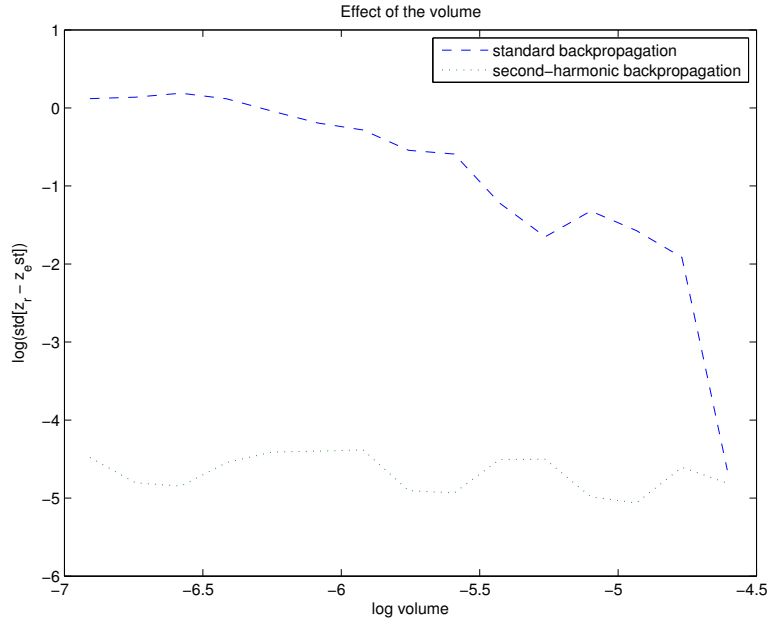
Fig. 25.16. Standard deviation of the localization error with respect to the reflector's volume (log scale) for standard backpropagation (top) and second-harmonic image (bottom).

different illuminations. For each noise level, we average the results over 100 images. Figure 25.17 shows that both functionals have similar behaviors.

As mentioned before, in applications, the weakness of the SHG signal will induce a much higher relative measurement noise than in the fundamental data. Since the model we use for measurement noise has a zero expectation, averaging measurements over different illuminations can improve the stability significantly, as shown in Figure 25.18, where the images have been obtained with 16 illuminations instead of 8.

25.7 Proof of Estimate (25.8)

Let R be large enough so that $\Omega_\mu \Subset B_R$, where B_R is the ball of radius R and center 0. Let $S_R = \partial B_R$ be the sphere of radius R, and introduce the Dirichlet-to-Neumann operator $\mathcal{T}$ on S_R:

$$\begin{aligned} \mathcal{T} \; : \; W^2_{1/2}(S_R) &\longrightarrow W^2_{-1/2}(S_R) \\ u &\longmapsto \mathcal{T}[u]\,. \end{aligned} \tag{25.148}$$

According to [283], $\mathcal{T}$ is continuous and satisfies
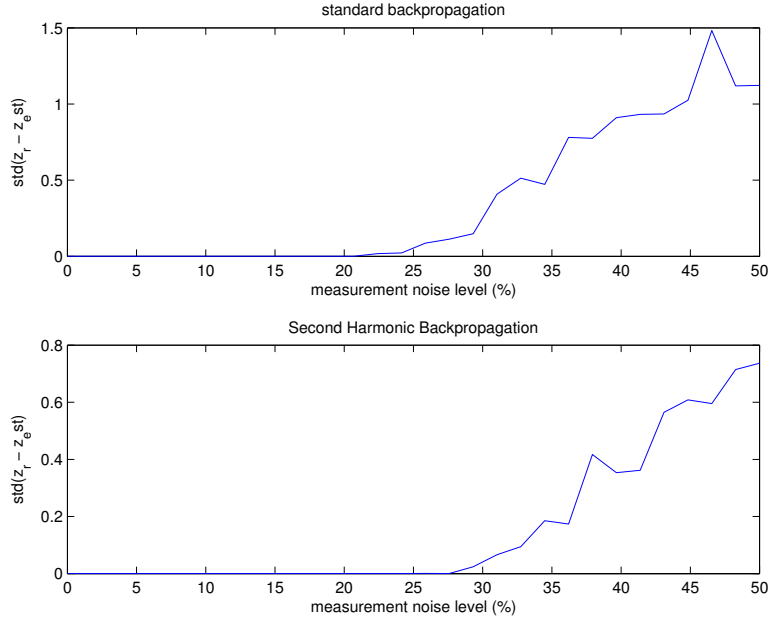
Fig. 25.17. Standard deviation of the localization error with respect to measurement noise level for standard backpropagation (top) and second-harmonic image (bottom).

$$-\Re(\mathcal{T}[u], u) \geq \frac{1}{2R}\|u\|^2_{L^2(S_R)}, \quad \forall u \in W^2_{1/2}(S_R), \tag{25.149}$$

and

$$\Im(\mathcal{T}[u], u) > 0 \text{ if } u \neq 0. \tag{25.150}$$

Here, $(\,,\,)$ denotes the duality pair between $W^2_{1/2}(S_R)$ and $W^2_{-1/2}(S_R)$. Now introduce the continuous bilinear form a:

$$W^{1,2}(B_R) \times W^{1,2}(B_R) \longrightarrow \mathbb{C}$$
$$(u,v) \longmapsto a(u,v) = \int_{B_R} (1+\mu)\nabla u \cdot \overline{\nabla v} - \omega^2 \int_{B_R} u\bar{v} - (\mathcal{T}[u], v),$$
$$\tag{25.151}$$

as well as the continuous bilinear form b:

$$W^{1,2}(B_R) \longrightarrow \mathbb{C}$$
$$v \longmapsto b(v) = \int_{B_R} \mu\nabla U_0 \cdot \overline{\nabla v}. \tag{25.152}$$

Problem (25.5) has the following variational formulation: Find $u \in W^{1,2}(B_R)$ such that
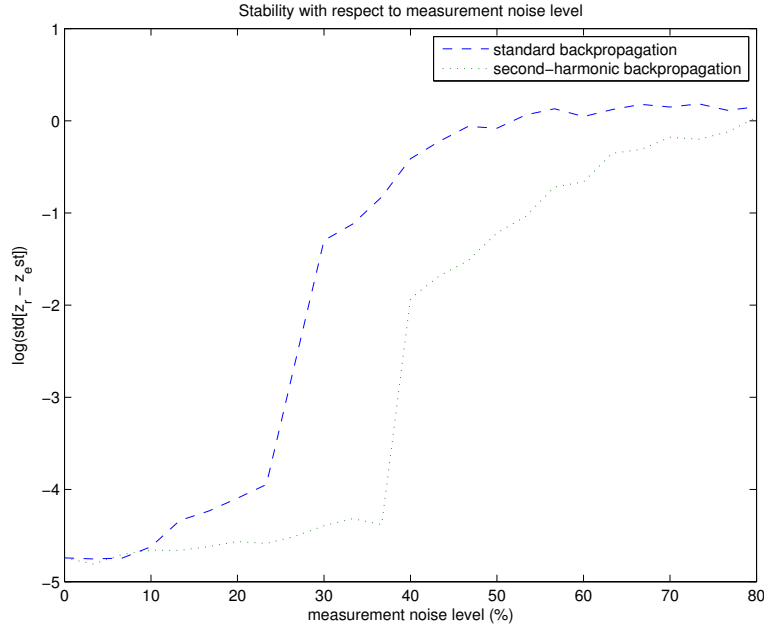
Fig. 25.18. Standard deviation of the localization error with respect to measurement noise level, when averaged over 16 illuminations of angles uniformly distributed between 0 and 2π for standard backpropagation (top) and second-harmonic image (bottom).

$$a(u, v) = b(v) \quad \forall v \in W^{1,2}(B_R) \,. \tag{25.153}$$

With (25.149) one can show that

$$\Re a(u, u) \geq C_1 \|\nabla u\|^2_{L^2(B_R)} - C_2 \|u\|^2_{L^2(B_R)} \,, \tag{25.154}$$

so that a is weakly coercive with respect to the pair $\left(W^{1,2}(B_R), L^2(B_R) \right)$. Since the embedding of $W^{1,2}(B_R)$ into $L^2(B_R)$ is compact, we can apply Fredholm's alternative to problem (25.153). Hence, we deduce existence of a solution from uniqueness of a solution, which easily follows by using identity (25.150).

Now we want to prove that if u is the solution of (25.153), then

$$\|u\|_{W^{1,2}(B_R)} \leq \|\mu\|_\infty \,. \tag{25.155}$$

We proceed by contradiction. Assume that $\forall n \in \mathbb{N}$, there exists $\mu_n \in L^\infty(B_R)$ compactly supported and $u_n \in W^{1,2}(B_R)$ solution of (25.153) such that

$$\|u_n\|_{W^{1,2}(B_R)} \geq nC\|\mu_n\|_\infty. \tag{25.156}$$

Consider the sequence

$$v_n = \frac{u_n}{\|u_n\|_{W^{1,2}(B_R)}}. \tag{25.157}$$

$(v_n)_{n \in \mathbb{N}}$ is bounded in $W^{1,2}(B_R)$ so there exists a subsequence still denoted by v_n and $v^* \in W^{1,2}(B_R)$ such that $v_n \rightharpoonup v^*$ in $W^{1,2}(B_R)$ and $v_n \to v^*$ in $L^2(B_R)$. Now since u_n is a solution of (25.153), we have

$$\int_{B_R} (1+\mu_n)\nabla v_n \cdot \overline{\nabla v_n} - \omega^2 \int_{B_R} v_n \overline{v_n} - (\mathcal{T}v_n, v_n) = \int_{B_R} \mu_n \nabla U_0 \cdot \overline{\nabla v_n}. \tag{25.158}$$

Using (25.156) we obtain that

$$\int_{B_R} (1+\mu_n)|\nabla v_n|^2 - \omega^2 \int_{B_R} |v_n|^2 - (\mathcal{T}v_n, v_n) \longrightarrow 0 \ (n \to \infty). \tag{25.159}$$

Since $\int_{B_R} \mu_n |\nabla v_n|^2 \longrightarrow 0$, we get that $\widetilde{a}(v_n, v_n) \longrightarrow 0$, where

$$\widetilde{a}(u, v) = \int_{B_R} \nabla u \cdot \overline{\nabla v} - \omega^2 \int_{B_R} u\overline{v} - (\mathcal{T}u, v). \tag{25.160}$$

We want to prove that v_n converges strongly in $W^{1,2}(B_R)$ to v^* and that $v^* = 0$. This will contradict the fact that $\forall n, \ \|v_n\|_{W^{1,2}(B_R)} = 1$.

Now we decompose $\widetilde{a} = \widetilde{a}_c + \widetilde{a}_w$ into a coercive part,

$$\widetilde{a}_c(u, v) = \int_{B_R} \nabla u \cdot \overline{\nabla v} - (\mathcal{T}u, v) \tag{25.161}$$

and a weakly continuous part,

$$\widetilde{a_w}(u, v) = -\omega^2 \int_{B_R} u\overline{v}. \tag{25.162}$$

So $\widetilde{a}(v_n - v^*, v_n - v^*) = \widetilde{a}_c(v_n - v^*, v_n - v^*) + \widetilde{a_w}(v_n - v^*, v_n - v^*)$. We write $\widetilde{a}_c(v_n - v^*, v_n - v^*) = \widetilde{a}_c(v_n - v^*) - \widetilde{a}_c(v_n - v^*, v^*)$. Now, since $v_n \rightharpoonup v$ in $W^{1,2}(B_R)$ and $\widetilde{a}_c$ is strongly continuous on $W^{1,2}(B_R)^2$, we have that $\widetilde{a}_c(v_n - v^*, v^*) \longrightarrow 0$, and $\widetilde{a}_c(v_n - v^*, v_n) = \widetilde{a}_c(v_n, v_n) - \widetilde{a}_c(v^*, v_n) \longrightarrow -\widetilde{a}_c(v^*, v^*)$, which is

$$\widetilde{a}_c(v_n - v^*, v_n - v^*) \longrightarrow -\widetilde{a}_c(v^*, v^*). \tag{25.163}$$

The coercivity of $\widetilde{a}_c$ gives

$$\widetilde{a}_c(v^*, v^*) = 0 \tag{25.164}$$

By a computation similar to the one just above, we also find that

$$\widetilde{a}(v_n - v^*, v_n - v^*) \longrightarrow -\widetilde{a}(v^*, v^*). \tag{25.165}$$

Since $\widetilde{a_w}(v_n - v^*, v_n - v^*) \longrightarrow 0$, we get that

$$\widetilde{a}(v^*, v^*) = 0. \tag{25.166}$$

So $v^* = 0$ and, since $\widetilde{a}$ satisfies (25.154), we get that $\|\nabla v_n\|^2_{L^2(B_R)} \longrightarrow 0$ as $n \to \infty$. We have

$$v_n \longrightarrow v = 0 \text{ in } W^{1,2}(B_R). \tag{25.167}$$

25.8 Proof of Proposition 25.1

Denote $V = u_s - u_s^{(\mu)} - w^{(\mu)} \cdot \nabla U_0(z_r)$. V is a solution on $\mathbb{R}^2$ of

$$\nabla \cdot (1 + \mu + [\sigma_r - 1]\mathbf{1}_{\Omega_r})\nabla V + \omega^2 V = -\nabla \cdot [\sigma_r - 1]\mathbf{1}_{\Omega_r}\nabla [U_0 - \nabla(x - z_r) \cdot \nabla U_0(z_r)]$$
(25.168)

subject to the Sommerfeld radiation condition. Now, define V_0 as the solution on $\mathbb{R}^2$ of

$$\nabla \cdot (1 + \mu + [\sigma_r - 1]\mathbf{1}_{\Omega_r})\nabla V_0 = -\nabla \cdot [\sigma_r - 1]\mathbf{1}_{\Omega_r}\nabla [U_0 - \nabla(x - z_r) \cdot \nabla U_0(z_r)] .$$
(25.169)

with the condition $V_0(x) \longrightarrow 0$ $(x \to \infty)$.

From [28, Lemma A.1], there exist three positive constants C, $\widetilde{C}$ and κ independent of μ and δ such that

$$\|\nabla V_0\|_{L^2(B_R)} \leq C\delta\|\nabla [U_0 - \nabla(x - z_r) \cdot \nabla U_0(z_r)]\|_{L^\infty(\Omega_r)}$$
(25.170)

and

$$\|V_0\|_{L^2(B_R)} \leq \widetilde{C}\delta^{1+\kappa}\|\nabla [U_0 - \nabla(x - z_r) \cdot \nabla U_0(z_r)]\|_{L^\infty(\Omega_r)} .$$
(25.171)

If we write $W = V - V_0$, we have that W solves

$$\nabla \cdot (1 + \mu + [\sigma_r - 1]\mathbf{1}_{\Omega_r})\nabla W + \omega^2 W = -\omega^2 V_0,$$
(25.172)

with the boundary condition $\frac{\partial W}{\partial \nu} - \mathcal{T}_\omega(W) = \mathcal{T}_\omega(V) - \mathcal{T}_0(V_0)$ on ∂B_R, where $\mathcal{T}_\omega$ is the Dirichlet-to-Neumann map on S_R defined in (25.148) associated with the frequency ω. The condition can be rewritten as $\frac{\partial W}{\partial \nu} - \mathcal{T}_\omega(W) = (\mathcal{T}_\omega - \mathcal{T}_0)(V_0)$. So, based on the well posedness of (25.172), there exist a constant C' independent of μ and δ such that

$$\|W\|_{W^{1,2}(B_R)} \leq C' \left(\|V_0\|_{L^2(B_R)} + \|[\mathcal{T}_\omega - \mathcal{T}_0](V_0)\|_{L^2(\partial B)}\right).$$
(25.173)

Now, we can write that, for some constant still denoted C independent of μ and δ,

$$\|V\|_{W^{1,2}(B_R)} \leq C \left(\|V_0\|_{W^{1,2}(B_R)} + \|V_0\|_{L^2(B_R)}\right) .$$
(25.174)

Since $\delta < 1$, using (25.170) and (25.171) we get

$$\|V\|_{W^{1,2}(B_R)} \leq C\delta^2 .$$
(25.175)

25.9 Proof of Proposition 25.3

Denote $\phi: y \longrightarrow \widetilde{y} = \phi(y) = \frac{y - z_r}{\delta}$. If we define $\forall \widetilde{y} \in B(0,1)$: $\widetilde{w}^{(\mu)}(\widetilde{y}) = \frac{1}{\delta}w^{(\mu)}(\phi^{-1}(\widetilde{y}))$, we want to prove the following:

$$\|\widetilde{w}^{(\mu)}(\widetilde{y}) - \widetilde{y} - \widetilde{w}(\widetilde{y})\|_{W^{1,2}(B(0,1))} \leq C \left(\|\mu\|_\infty + \delta\omega^2 \right) . \qquad (25.176)$$

Now, it is easy to see that $\widetilde{w}^{(\mu)}$ satisfies the following equation:

$$\nabla \cdot (1 + [\sigma_r - 1]\mathbf{1}_B + \widetilde{\mu}) \nabla\widetilde{w}^{(\mu)} + \omega^2\delta\widetilde{w}^{(\mu)} = \nabla \cdot ([\sigma_r - 1]\mathbf{1}_B\nabla\widetilde{y}) , \quad (25.177)$$

where $\widetilde{\mu} = \mu \circ \phi^{-1}$, equipped with the Sommerfeld radiation condition. Using equation (25.20) we get that

$$\nabla \cdot (1 + [\sigma_r - 1]\mathbf{1}_B + \widetilde{\mu}) \nabla \left(\widetilde{w}^{(\mu)} - \widetilde{y} - \widetilde{w} \right) = -\nabla \cdot \left(\widetilde{\mu}\nabla\widetilde{w}^{(\mu)} \right) - \omega^2\delta\widetilde{w}^{(\mu)} .$$
$$(25.178)$$

Now, using Meyer's theorem [273], we get the following estimate:

$$\|\nabla \left(\widetilde{w}^{(\mu)}(\widetilde{y}) - \widetilde{y} - \widetilde{w}(\widetilde{y}) \right) \|_{L^2(B)} \leq C \left(\|\widetilde{\mu}\nabla\widetilde{w}^{(\mu)}\|_{L^2(B)} + \omega\delta^2\|\widetilde{w}^{(\mu)}\|_{L^2(B)} \right) .$$
$$(25.179)$$

We need to estimate $\|\widetilde{w}^{(\mu)}\|_{W^{1,2}(B(0,1))}$. Introduce $\widetilde{w}_0^{(\mu)}$ as the solution of

$$\nabla \cdot (1 + [\sigma_r - 1]\mathbf{1}_B + \widetilde{\mu}) \nabla\widetilde{w}_0^{(\mu)} = \nabla \cdot ([\sigma_r - 1]\mathbf{1}_B\nabla\widetilde{y}) . \qquad (25.180)$$

with the condition $\widetilde{w}_0^{(\mu)}(\widetilde{y}) \longrightarrow 0$ as $\widetilde{y} \to \infty$. Meyers theorem gives

$$\|\widetilde{w}_0^{(\mu)}\|_{W^{1,2}(B(0,1))} \leq C\|[\sigma_r - 1]\nabla\widetilde{y}\|_{L^2(B(0,1))} . \qquad (25.181)$$

We can see that $\widetilde{w}^{(\mu)} - \widetilde{w}_0^{(\mu)}$ is a solution of

$$\nabla \cdot (1 + [\sigma_r - 1]\mathbf{1}_B + \widetilde{\mu}) \nabla \left(\widetilde{w}^{(\mu)} - \widetilde{w}_0^{(\mu)} \right) + \omega^2\delta \left(\widetilde{w}^{(\mu)} - \widetilde{w}_0^{(\mu)} \right) = -\omega^2\delta\widetilde{w}_0^{(\mu)} .$$
$$(25.182)$$

We get that

$$\|\widetilde{w}^{(\mu)} - \widetilde{w}_0^{(\mu)}\|_{W^{1,2}(B(0,1))} \leq C\omega^2\delta\|\widetilde{w}_0^{(\mu)}\|_{L^2(B(0,1))} .$$

So, using (25.181) we obtain

$$\|\widetilde{w}^{(\mu)}\|_{W^{1,2}(B(0,1))} \leq C \left(1 + \omega^2\delta \right) . \qquad (25.183)$$

Since $\|\widetilde{\mu}\nabla\widetilde{w}^{(\mu)}\|_{L^2(B(0,1))} \leq \|\widetilde{\mu}\|_{L^\infty(B(0,1))}\|\widetilde{w}^{(\mu)}\|_{W^{1,2}(B(0,1))}$ and $\|\widetilde{\mu}\|_{L^\infty(B(0,1))} \leq \|\mu\|_\infty$, using (25.179) and (25.181) we get

$$\|\nabla \left(\widetilde{w}^{(\mu)}(\widetilde{y}) - \widetilde{y} - \widetilde{w}(\widetilde{y}) \right) \|_{L^2(B(0,1))} \leq C \left(\|\mu\|_\infty + \delta\omega^2(1 + \|\mu\|_\infty + \delta\omega^2) \right) ,$$

which is exactly, as $\|\mu\|_\infty \to 0$ and $\delta \to 0$, for $y \in \Omega_r$

$$\nabla \left(w^{(\mu)}(y) - (y - z_r) \right) = \delta\nabla\widetilde{w}(\frac{y - z_r}{\delta}) + O \left(\delta\|\mu\|_\infty + (\delta\omega)^2 \right) . \qquad (25.184)$$

25.10 Concluding Remarks

We have studied how second-harmonic imaging can be used to locate a small reflector in a noisy medium, gave asymptotic formulas for the second-harmonic field, and investigated statistically the behavior of the classic and second-harmonic backpropagation functionals. We have proved that the backpropagation algorithm is more stable with respect to medium noise. Our results can also be extended to the case of multiple scatterers as long as they are well-separated.

References

1. T. Abboud and H. Ammari, Diffraction at a curved grating: TM and TE cases, homogenization, J. Math. Anal. Appl., 202 (1996), 995–1026.
2. T. Abboud and H. Ammari, Diffraction at a curved grating: Approximation by an infinite plane grating, J. Math. Anal. Appl., 202 (1996), 1076–1100.
3. M. Abramowitz and I. Stegun (editors), *Handbook of Mathematical Functions*, National Bureau of Standards, Washington D.C., 1964.
4. R. Adler, The Geometry of Random Fields, SIAM, Philadelphia, 2010.
5. R. Adler and J. Taylor, Random Fields and Geometry, Springer, New York, 2007.
6. M.S. Agranovich, B.A. Amosov, and M. Levitin, Spectral problems for the Lamé system with spectral parameter in boundary conditions on smooth or nonsmooth boundary, Russ. J. Math. Phys., 6 (1999), 247–281.
7. J.F. Ahner and G.C. Hsiao, On the two-dimensional exterior boundary-value problems of elasticity, SIAM J. Appl. Math., 31 (1976), 677–685.
8. K. Aki and P. G. Richards, *Quantitative Seismology*, Vol. 1, W. H. Freeman & Co., San Francisco, 1980.
9. G.S. Alberti, On multiple frequency power density measurements, Inverse Problems 29 (2013), 115007, 25 pp.
10. G.S. Alberti, On multiple frequency power density measurements II. The full Maxwell's equations. J. Differential Equations 258 (2015), no. 8, 27672793.
11. G.S. Alberti, Enforcing local non-zero constraints in PDEs and applications to hybrid imaging problems, Comm. Partial Differential Equations, 40 (2015), 1855–1883.
12. G.S. Alberti and H. Ammari, Disjoint sparsity for signal separation and applications to hybrid inverse problems in medical imaging, J. Appl. Comput. Harmonic Anal., DOI:10.1016/j.acha.2015.08.013.
13. G.S. Alberti, H. Ammari, B. Jin, J.-K. Seo, and W. Zhang, The Linearized inverse problem in multifrequency electrical impedance tomography, arXiv: 1602.04312.
14. G.S. Alberti, H. Ammari, and K. Ruan, Multi-frequency acousto-electromagnetic tomography, Contemp. Math., 658 (2016), 67–79.
15. G. Alberti and C. Mantegazza, A note on the theory of SBV functions, Boll. Un. Mat. Ital., B 11 (1997), 375–382.

16. M.S. Aliroteh, G. Scott and A. Arbabian, Frequency-modulated magneto-acoustic detection and imaging, Elect. Lett., 50 (2014), 790–792.

17. G. Allaire, Homogenization and two-scale convergence, SIAM J. Math. Anal., 23 (1992), 1482–1518.

18. G. Allaire, *Shape Optimization by the Homogenization Method*, Applied Mathematical Sciences, 146. Springer-Verlag, New York, 2002.

19. G. Allaire and K. El Ganaoui, Homogenization of a conductive and radiative heat transfer problem, Multiscale Model. Simul., 7 (2008), 1148–1170.

20. G. Allaire and Z. Habibi, Second order corrector in the homogenization of a conductive-radiative heat transfer problem, Discrete Contin. Dyn. Syst. Ser. B, 18 (2013), 1–36.

21. G. Allaire and Z. Habibi, Homogenization of a Conductive, Convective and radiative heat transfer problem in a heterogeneous domain, SIAM J. Math. Anal., 45 (2013), 1136–1178.

22. L. Ambrosio, N. Fusco, and D. Pallara, *Functions of Bounded Variation and Free Discontinuity Problems*, Clarendon Press Oxford, 2000.

23. H. Ammari, An inverse initial boundary value problem for the wave equation in the presence of imperfections of small volume, SIAM J. Control Optim., 41 (2002), 1194–1211.

24. H. Ammari, *An Introduction to Mathematics of Emerging Biomedical Imaging*, Math. & Appl., Vol. 62, Springer-Verlag, Berlin, 2008.

25. H. Ammari, M. Asch, L. Guadarrama Bustos, V. Jugnon, and H. Kang, Transient wave imaging with limited-view data, SIAM J. Imag. Sci., 4 (2011), 1097–1121.

26. H. Ammari, E. Beretta, E. Francini, H. Kang, and M. Lim, Optimization algorithm for reconstructing interface changes of a conductivity inclusion from modal measurements, Math. Comp., 79 (2010), 1757–1777.

27. H. Ammari, E. Beretta, E. Francini, H. Kang, and M. Lim, Reconstruction of small interface changes of an inclusion from modal measurements II: The elastic case, J. Math. Pures Appl., 94 (2010), 322–339.

28. H. Ammari, E. Bonnetier, Y. Capdeboscq, M. Tanter, and M. Fink, Electrical impedance tomography by elastic deformation, SIAM J. Appl. Math., 68 (2008), 1557–1573.

29. H. Ammari, E. Bossy, J. Garnier, L.H. Nguyen, and L. Seppecher, A reconstruction algorithm for ultrasound-modulated diffuse optical tomography, Proc. Amer. Math. Soc., 142 (2014), 3221–3236.

30. H. Ammari, E. Bossy, J. Garnier, and L. Seppecher, Acousto-electromagnetic tomography, SIAM J. Appl. Math., 72 (2012), 1592–1617.

31. H. Ammari, E. Bossy, V. Jugnon, and H. Kang, Mathematical modelling in photo-acoustic imaging of small absorbers, SIAM Rev., 52 (2010), 677–695.

32. H. Ammari, E. Bossy, V. Jugnon, and H. Kang, Quantitative photo-acoustic imaging of small absorbers, SIAM J. Appl. Math., 71 (2011), 676–693.

33. H. Ammari, T. Boulier, and J. Garnier, Modeling active electrolocation in weakly electric fish, SIAM J. Imag. Sci., 5 (2013), 285–321.

34. H. Ammari, T. Boulier, J. Garnier, and H. Wang, Shape identification and classification in electrolocation, Proc. Natl. Acad. Sci. USA 111 (2014), 11652–11657.

35. H. Ammari, S. Boulmier, and P. Millien, A mathematical and numerical framework for magnetoacoustic tomography with magnetic induction, J. Differential Equations, 259 (2015), 5379–5405.

36. H. Ammari, E. Bretin, J. Garnier, and A. Wahab, Time reversal in attenuating acoustic media, Contemp. Math., 548 (2011), 151–163.
37. H. Ammari, E. Bretin, J. Garnier, and V. Jugnon, Coherent interferometry algorithms for photoacoustic imaging, SIAM J. Num. Anal., 50 (2012), 2259–2280.
38. H. Ammari, E. Bretin, J. Garnier, H. Kang, H. Lee, and A. Wahab, *Mathematical Methods in Elasticity Imaging*, Princeton Series in Applied Mathematics, Princeton University Press, Princeton, 2015.
39. H. Ammari, E. Bretin, V. Jugnon, and A. Wahab, Photo-acoustic imaging for attenuating acoustic media, in *Mathematical Modeling in Biomedical Imaging II*, Lecture Notes in Mathematics, Vol. 2035, 57–84, Springer-Verlag, Berlin, 2011.
40. H. Ammari, E. Bretin, P. Millien, L. Seppecher, and J.K. Seo, Mathematical modeling in full-field optical coherence elastography, SIAM J. Appl. Math., 75 (2015), 1015–1030.
41. H. Ammari, P. Calmon, and E. Iakovleva, Direct elastic imaging of a small inclusion, SIAM J. Imag. Sci., 1 (2008), 169–187.
42. H. Ammari, Y. Capdeboscq, F. de Gournay, A. Rozanova-Pierrat, and F. Triki, Microwave imaging by elastic deformation, SIAM J. Appl. Math., 71 (2011), 2112–2130.
43. H. Ammari, G. Ciraolo, H. Kang, H. Lee, and G. Milton, Spectral theory of a Neumann-Poincaré-type operator and analysis of cloaking due to anomalous localized resonance, Arch. Rat. Mech. Anal., 208 (2013), 667–692.
44. H. Ammari, G. Ciraolo, H. Kang, H. Lee, and K. Yun, Spectral analysis of the Neumann-Poincaré operator and characterization of the stress blow-up in anti-plane elasticity, Arch. Rat. Mech. Anal., 208 (2013), 275–304.
45. H. Ammari, Y. Deng, and P. Millien, Surface plasmon resonance of nanoparticles and applications in imaging, Arch. Ration. Mech. Anal., 220 (2016), 109–153.
46. H. Ammari, P. Garapon, L. Guadarrama Bustos, and H. Kang, Transient anomaly imaging by the acoustic radiation force, J. Diff. Equat., 249 (2010), 1579–1595.
47. H. Ammari, P. Garapon, H. Kang, and H. Lee, A method of biological tissues elasticity reconstruction using magnetic resonance elastography measurements, Quart. Appl. Math., 66 (2008), 139–175.
48. H. Ammari, J. Garnier, L. Giovangigli, W. Jing, and J.K. Seo, Spectroscopic imaging of a dilute cell suspension, J. Math. Pures Appl., 105 (2016), 603–661.
49. H. Ammari, J. Garnier, and W. Jing, Resolution and stability analysis in acousto-electric imaging, Inverse Problems 28 (2012), 084005, 20 pp.
50. H. Ammari, J. Garnier, W. Jing, H. Kang, M. Lim, K. Sølna, and H. Wang, *Mathematical and Statistical Methods for Multistatic Imaging*, Lecture Notes in Mathematics, Volume 2098, Springer, Cham, 2013.
51. H. Ammari, J. Garnier, W. Jing, and L.H. Nguyen, Quantitative thermo-acoustic imaging: an exact reconstruction formula, J. Differential Equations, 254 (2013), 1375–1395.
52. H. Ammari, J. Garnier, and V. Jugnon, Detection, reconstruction, and characterization algorithms from noisy data in multistatic wave imaging, submitted.
53. H. Ammari, J. Garnier, V. Jugnon, and H. Kang, Direct reconstruction methods in ultrasound imaging of small anomalies, in *Mathematical Modeling in Biomedical Imaging II*, Lecture Notes in Mathematics, Vol. 2035, 31–55, Springer-Verlag, Berlin, 2011.

508   References

54. H. Ammari, J. Garnier, V. Jugnon, and H. Kang, Stability and resolution analysis for a topological derivative based imaging functional, SIAM J. Control Optim., 50 (2012), 48–76.

55. H. Ammari, J. Garnier, and P. Millien, Backpropagation imaging in nonlinear harmonic holography in the presence of measurement and medium noises, SIAM J. Imaging Sci., 7 (2014), 239–276.

56. H. Ammari, J. Garnier, L.H. Nguyen, and L. Seppecher, Reconstruction of a piecewise smooth absorption coefficient by an acousto-optic process, Comm. Partial Differential Equations, 38 (2013), 1737–1762.

57. H. Ammari, J. Garnier, H. Kang, W.K. Park, and K. Sølna, Imaging schemes for perfectly conducting cracks, SIAM J. Appl. Math., 71 (2011), 68–91.

58. H. Ammari, J. Garnier, and K. Sølna, A statistical approach to target detection and localization in the presence of noise, Waves Random Complex Media, 22 (2012), 40–65.

59. H. Ammari, J. Garnier, and K. Sølna, Resolution and stability analysis in full-aperature, linearized conductivity and wave imaging, Proc. Amer. Math. Soc., 141 (2013), 3431–3446.

60. H. Ammari, P. Grasland-Mongrain, P. Millien, L. Seppecher, and J.K. Seo, A mathematical and numerical framework for ultrasonically-induced Lorentz force electrical impedance tomography, J. Math. Pures Appl., 103 (2015), 1390–1409.

61. H. Ammari, E. Iakovleva, and D. Lesselier, Two numerical methods for recovering small electromagnetic inclusions from scattering amplitude at a fixed frequency, SIAM J. Sci. Comput., 27 (2005), 130–158.

62. H. Ammari, E. Iakovleva, and D. Lesselier, A MUSIC algorithm for locating small inclusions buried in a half-space from the scattering amplitude at a fixed frequency, Multiscale Model. Simul., 3 (2005), 597–628.

63. H. Ammari, E. Iakovleva, D. Lesselier, and G. Perrusson, A MUSIC-type electromagnetic imaging of a collection of small three-dimensional inclusions, SIAM J. Sci. Comput., 29 (2007), 674–709.

64. H. Ammari and H. Kang, *Reconstruction of Small Inhomogeneities from Boundary Measurements*, Lecture Notes in Mathematics, Vol. 1846, Springer-Verlag, Berlin, 2004.

65. H. Ammari and H. Kang, Boundary layer techniques for solving the Helmholtz equation in the presence of small inhomogeneities, J. Math. Anal. Appl., 296 (2004), 190–208.

66. H. Ammari and H. Kang, *Polarization and Moment Tensors: with Applications to Inverse Problems and Effective Medium Theory*, Applied Mathematical Sciences, Vol. 162, Springer-Verlag, New York, 2007.

67. H. Ammari, H. Kang, and H. Lee, A boundary integral method for computing elastic moment tensors for ellipses and ellipsoids, J. Comput. Math., 25 (2007), 2–12.

68. H. Ammari, H. Kang, G. Nakamura, and K. Tanuma, Complete asymptotic expansions of solutions of the system of elastostatics in the presence of an inclusion of small diameter and detection of an inclusion, J. Elasticity, 67 (2002), 97–129.

69. H. Ammari, H. Kang, and K. Touibi, Boundary layer techniques for deriving the effective properties of composite materials, Asymp. Anal., 41 (2005), 119–140.

70. H. Ammari and A. Khelifi, Electromagnetic scattering by small dielectric inhomogeneities, J. Math. Pures Appl., 82 (2003), 749–842.

71. H. Ammari, O. Kwon, J.K. Seo, and E.J. Woo, Anomaly detection in T-scan trans-admittance imaging system, SIAM J. Appl. Math., 65 (2004), 252–266.

72. H. Ammari, E. Lee, H. Kwon, J.K. Seo, and E.J. Woo, Mathematical modeling of mechanical vibration-assisted conductivity imaging, SIAM J. Appl. Math., 75 (2015), 1031–1046.

73. H. Ammari, P. Millien, M. Ruiz, and H. Zhang, Mathematical analysis of plasmonic nanoparticles: the scalar case, arXiv:1506.00866.

74. H. Ammari, L.H. Nguyen, and L. Seppecher, Laurent Reconstruction and stability in acousto-optic imaging for absorption maps with bounded variation, J. Funct. Anal., 267 (2014), 4361–4398.

75. H. Ammari, M. Ruiz, S. Yu, and H. Zhang, Mathematical analysis of plasmonic resonances for nanoparticles: the full Maxwell equations, arXiv:1511.06817.

76. H. Ammari and J.K. Seo, An accurate formula for the reconstruction of conductivity inhomogeneities, Adv. Appl. Math., 30 (2003), 679–705.

77. H. Ammari, J.K. Seo, and L. Zhou, Viscoelastic modulus reconstruction using time harmonic vibrations, Math. Model. Anal. 20 (2015), 836–851.

78. H. Ammari, A. Waters, and H. Zhang, Stability analysis for magnetic resonance elastography, J. Math. Anal. Appl., 430 (2015), 919–931.

79. C. Amrouche, C. Bernardi, M. Dauge, and V. Girault, Vector potentials in three-dimensional non-smooth domains, Math. Meth. Appl. Sci., 21 (1998), 823–864.

80. K. Ando and H. Kang, Analysis of plasmon resonance on smooth domains using spectral properties of the Neumann-Poincaré operator, J. Math. Anal. Appl., 435 (2016), 162–178.

81. S.R. Arridge, Optical tomography in medical imaging, Inverse Probl., 15 (1999), R41–R93.

82. S.R. Arridge and J.C. Schotland, Optical tomography: forward and inverse problems, Inverse Problems, 25 (2009), 123010.

83. K. Asami, Characterization of biological cells by dielectric spectroscopy, J. Non-Crystal. Solids, 305 (2002), 268–277.

84. K. Asami, Characterization of heterogeneous systems by dielectric spectroscopy, Prog. Polym. Sci., 27 (2002) 1617–1659.

85. M. Assenheimer, O. Laver-Moskovitz, D. Malonek, D. Manor, U. Nahliel, R. Nitzan, and A. Saad, The T-scan technology: Electrical impedance as a diagnostic tool for breast cancer detection, Physiol. Meas., 22 (2001), 1–8.

86. P.W. Atkins, *The Elements of Physical Chemistry*, Oxford University Press, Oxford, 2001.

87. A. Aubry and A. Derode, Random matrix theory applied to acoustic backscattering and imaging in complex media, Phys. Rev. Lett., 102 (2009), 084301.

88. A. Aubry and A. Derode, Singular value distribution of the propagation matrix in random scattering media, Waves Random Complex Media, 20 (2010), 333–363.

89. A. Aubry and A. Derode, Detection and imaging in a random medium: A matrix method to overcome multiple scattering and aberration, J. Appl. Phys., 106 (2009), 044903.

90. G. Baffou, C. Girard, and R. Quidant, Mapping heat origin in plasmonic structures, Phys. Rev. Lett., 104 (2010), 136805.

91. J. Baik and J.W. Silverstein, Eigenvalues of large sample covariance matrices of spiked population models, J. Multivariate Anal., 97 (2006), 1382–1408.

92. G. Bal, E. Bonnetier, F. Monard, and F. Triki, Inverse diffusion from knowledge of power densities, Inverse Probl. Imaging, 7 (2013), 353–375.

510　　　References

93. C. Bardos, A mathematical and deterministic analysis of the time-reversal mirror in *Inside out: Inverse Problems and Applications*, 381–400, Math. Sci. Res. Inst. Publ., Vol. 47, Cambridge Univ. Press, Cambridge, 2003.

94. C. Bardos and M. Fink, Mathematical foundations of the time reversal mirror, Asymptot. Anal., 29 (2002), 157182.

95. C. Bardos, G. Lebeau, and J. Rauch, Sharp sufficient conditions for the observation, control, and stabilization of waves from the boundary, SIAM J. Control Optim., 30 (1992), 1024–1065.

96. A.T. Basford, J.R. Basford,T.J. Kugel, and R.L. Ehman, Lorentz-force-induced motion in conductive media, Magn. Res. Imag., 23 (2005), 647–651.

97. A. Beck and M. Teboulle, A fast iterative shrinkage-thresholding algorithm for linear inverse problems, SIAM J. Imaging Sci., 2 (2009), 183–202.

98. F. Benaych-Georges and R.R. Nadakuditi, The eigenvalues and eigenvectors of finite, low rank perturbations of large random matrices, Adv. Math., 227 (2011), 494–521.

99. Y. Benveniste, A new approach to the application of Mori-Tanka's theory in composite materials, Mech. Mater. 6 (1987), 147–157.

100. J. Bercoff, M. Tanter, and M. Fink, Supersonic shear imaging: a new technique for soft tissue elasticity mapping, IEEE Trans. Ultrasonics, Ferro., Freq. Control, 51 (2004), 396–409.

101. J. Bercoff, M. Tanter, and M. Fink, The role of viscosity in the impulse diffraction field of elastic waves induced by the acoustic radiation force, IEEE Trans. Ultrasonics, Ferro., Freq. Control, 51 (2004), 1523–1536.

102. A.P. Berens, NDE reliability data analysis, ASM Handbook, Vol. 17, 689-701, 1989.

103. E. Beretta and E. Francini, Asymptotic formulas for perturbations in the electromagnetic fields due to the presence of thin inhomogeneities, Contemp. Math., 333 (2003), 49–62.

104. J. Bergh and J. Löfström, *Interpolation Spaces. An Introduction,* Grundlehren der Mathematischen Wissenschaften, 223, Springer-Verlag, Berlin-New York, 1976.

105. N. Bleistein, J.K. Cohen, and J.W. Stockwell Jr., *Mathematics of Multidimensional Seismic Imaging, Migration, and Inversion*, Springer, New York, 2001.

106. L. Borcea, Electrical impedance tomography, Inverse Probl., 18 (2002), R99–R136.

107. L. Borcea, G. Papanicolaou, and C. Tsogka, Theory and applications of time reversal and interferometric imaging, Inverse Problems, 19 (2003), 134–164.

108. L. Borcea, G. Papanicolaou, and C. Tsogka, Interferometric array imaging in clutter, Inverse Problems, 21 (2005), 1419–1460.

109. L. Borcea, G.C. Papanicolaou, C. Tsogka, and J.G. Berrymann, Imaging and time reversal in random media, Inverse Problems, 18 (2002), 1247–1279.

110. L. Borcea, G. Papanicolaou, and F.G. Vasquez, Edge illumination and imaging of extended reflectors, SIAM J. Imag. Sci., 1 (2008), 75–114.

111. W. Borchers and H. Sohr, On the equations rot $\mathbf{v} = \mathbf{g}$ and div $\mathbf{u} = f$ with zero boundary conditions, Hokkaido Math. J., 19 (1990), 67–87.

112. M. Born and E. Wolf, *Principles of Optics: Electromagnetic Theory of Propagation, Interference and Diffraction of Light*, Cambridge University Press, 6 edition, Cambridge, 1997.

113. L. Breiman, *Probability*, Addison-Wesley, Reading, 1968; reprinted by Society for Industrial and Applied Mathematics, Philadelphia, 1992.

114. A. Bressan and W. Shen, On discontinuous differential equations, in *Differential Inclusions and Optimal Control*, J. Andres, L. Gorniewicz and P. Nistri Eds., Julius Schauder Center, Lecture Notes in Nonlinear Analysis 2 (1998), 73–87.

115. W.L. Briggs and V.E. Henson, *The DFT: An Owner Manuel for the Discrete Fourier Transform*, SIAM, Philadelphia, 1995.

116. B. H. Brown, J. Tidy, K. Boston, A. D. Blackett, R. H. Smallwood, and F. Sharp, The relationship between tissue structure and imposed electrical current flow in cervical neoplasia, The Lancet, 355 (2000), 892–895.

117. M. Brühl, M. Hanke, and M.S. Vogelius, A direct impedance tomography algorithm for locating small inhomogeneities, Numer. Math., 93 (2003), 635–654.

118. K. Bryan and T. Leise, Impedance Imaging, inverse problems, and Harry Potter's Cloak, SIAM Rev., 52 (2010), 359–377.

119. A. Buffa, M. Costabel, and D. Sheen, On traces for $H(\mathrm{curl}, \Omega)$ in lipschitz domains. J. Math. Anal. Appl., 276 (2002), 845–867.

120. M. Burger and S.J. Osher, A survey on level set methods for inverse problems and optimal design, European J. Appl. Math., 16 (2005), 263–301.

121. J.F. Canny, A computational approach to edge detection, IEEE Trans. Pattern Anal. Mach. Intell., 8 (1986), 679–697.

122. Y. Capdeboscq, On the scattered field generated by a ball inhomogeneity of constant index, Asymp. Anal., 77 (2012), 197–246.

123. Y. Capdeboscq, J. Fehrenbach, F. de Gournay, and O. Kavian, Imaging by modification: numerical reconstruction of local conductivities from corresponding power density measurements, SIAM J. Imaging Sci., 2 (2009), 1003–1030.

124. Y. Capdeboscq and H. Kang, Improved Hashin-Shtrikman bounds for elastic moment tensors and an application, Appl. Math. Optim. 57 (2008), 263–288.

125. Y. Capdeboscq and M.S. Vogelius, A general representation formula for the boundary voltage perturbations caused by internal conductivity inhomogeneities of low volume fraction, Math. Model. Num. Anal., 37 (2003), 159–173.

126. Y. Capdeboscq and M.S. Vogelius, Optimal asymptotic estimates for the volume of internal inhomogeneities in terms of multiple boundary measurements, Math. Model. Num. Anal., 37 (2003), 227–240.

127. D.J. Cedio-Fengya, S. Moskow, and M.S. Vogelius, Identification of conductivity imperfections of small diameter by boundary measurements: Continuous dependence and computational reconstruction, Inverse Problems, 14 (1998), 553–595.

128. A. Chai, M. Moscoso, and G. Papanicolaou, Array imaging using intensity-only measurements, Inverse Problems, 27 (2011), 015005.

129. A. Chai, M. Moscoso, and G. Papanicolaou, Robust imaging of localized scatterers using the singular value decomposition and l_1 minimization, Inverse Problems, 29 (2013), 025016.

130. D.H. Chambers and J.G. Berryman, Analysis of the time-reversal operator for a small spherical scatterer in an electromagnetic field, IEEE Trans. Antennas and Propagation, 52 (2004), 1729–1738.

131. D.H. Chambers and J.G. Berryman, Time-reversal analysis for scatterer characterization, Phys. Rev. Lett., 92 (2004), 023902-1.

132. Y.Z. Chen and L.C. Wu, *Second Order Elliptic Equations and Elliptic Systems*, Translated from the 1991 Chinese original by Bei Hu. Translations of Mathematical Monographs, 174. American Mathematical Society, Providence, RI, 1998.

133. M. Cheney, D. Isaacson, and J.C. Newell, Electrical impedance tomography, SIAM Rev., 41 (1999), 85–101.
134. M. Cheney, The linear sampling method and the MUSIC algorithm, Inverse Problems, 17 (2001), 591–595.
135. A. B. Chin, L. P. Garmirian, R. Nie, and S. B. Rutkove, Optimizing measurement of the electrical anisotropy of muscle, Muscle Nerve, 37 (2008), 560–565.
136. M. Choulli and F. Triki, New stability estimates for the inverse medium problem with internal data, SIAM J. Math. Anal. 47 (2015), no. 3, 17781799.
137. P.G. Ciarlet, *Mathematical Elasticity*, Vol. I, Norh-Holland, Amsterdam (1988).
138. D. Cioranescu and J. Saint Jean Paulin, Homogenization in open sets with holes, J. Math. Anal. Appl., 71 (1979), 590–607.
139. F.H. Clarke, Yu. S. Ledyaev, R.J. Stern, and P.R. Wolenski, *Nonsmooth Analysis and Control Theory*, Graduate Texts in Mathematics, Springer-Verlag, New York, 1998.
140. D. Colton and R. Kress, *Inverse Acoustic and Electromagnetic Scattering Theory*, Applied Mathematical Sciences, Vol. 93, 2nd Ed., Springer-Verlag, New York, 1998.
141. D. Colton and R. Kress, *Integral Equation Methods in Scattering Theory*, Vol. 72. SIAM, 2013.
142. B.T. Cox, S.R. Arridge, and P.C. Beard, Gradient-based quantitative photoacoustic image reconstruction for molecular imaging, Proc. of SPIE, 6437 (2007), 64371T.
143. B.T. Cox, J.G. Laufer, and P.C. Beard, The challenges for quantitative photoacoustic imaging, Proc. of SPIE, 7177 (2009), 717713.
144. J.L. Crassidis and J.L. Junkins, *Optimal Estimation of Dynamic Systems*, CRC Press, Boca Raton, 2004.
145. G. Dassios and R.E. Kleinman, *Low Frequency Scattering*, Oxford Science Publications, The Clarendon Press, Oxford University Press, New York, 2000.
146. B.E. Dahlberg, C.E. Kenig, and G. Verchota, Boundary value problem for the systems of elastostatics in Lipschitz domains, Duke Math. J., 57 (1988), 795–818.
147. I. Daubechies, *Ten Lectures on Wavelets*, SIAM, Philadelphia, 1992.
148. R. Dautray and J.L. Lions, *Mathematical Analysis and Numerical Methods for Science and Technology*, Vol. 3, *Spectral Theory and Applications*, Springer-Verlag, Berlin, 1990.
149. A.C. Davison, *Statistical Models*, Cambridge University Press, Cambridge, 2003.
150. J.A. Decker Jr., Hadamard-transform image scanning, Appl. Opt., 9 (1970), 1392–1395.
151. T. Deffieux, G. Montaldo, M. Tanter, and M. Fink, Shear wave spectroscopy for in vivo quantification of human soft tissues viscoelasticity, IEEE Trans. Med. Im., 28 (2009), 313–322.
152. A.J. Devaney, A filtered backpropagation algorithm for diffraction tomography, Ultrasonic Imaging, 4 (1982), 336–350.
153. A.J. Devaney, Time reversal imaging of obscured targets from multistatic data, IEEE Trans. Antennas Propagat., 523 (2005), 1600–1610.
154. A. Dubois and A.C. Boccara, Full-field optical coherence tomography, in *Optical Coherence Tomography*, 565–591, Biological and Medical Physics, Biomedical Engineering, Springer, 2008.

155. A. Dubois, K. Grieve, G. Moneron, R. Lecaque, L. Vabre, and C. Boccara, Ultrahigh-resolution full-field optical coherence tomography, Appl. Optics, 43 (2004), 2874–2883.

156. I. Ekeland and R. Temam, *Convex analysis and variational problems*, North Holland, 1976.

157. H.W. Engl, M. Hanke, and A. Neubauer, *Regularization of Inverse Problems*, Kluwer, Dordrecht, 1996.

158. B. Engquist and A. Majda, Absorbing boundary conditions for the numerical simulation of waves, Math. Comp. 31 (1977), 629–651.

159. A. Erdélyi, W. Magnus, F. Oberhettinger, and F.G. Tricomi (editors), *Higher Transcendental Functions, Vol. II*, McGraw-Hill, New York, 1953.

160. L. C. Evans, *Partial differential equations*, Graduate Studies in Mathematics, Vol. 19, American Mathematical Society, Providence, RI, 1998.

161. C. Fabre and G. Lebeau, Régularité et unicité pour le problème de Stokes, Comm. Partial Diff. Equat., 27 (2002), 437–475.

162. C. Fabre and G. Lebeau, Prolongement unique des solutions de l'quation de Stokes, Comm. Partial Diff. Equat., 21 (1996), 573–596.

163. R. Farwig, H. Kozono, and H. Sohr, On the Helmholtz decomposition in general unbounded domains, Arch. Math., 88 (2007), 239–248.

164. A. F. Fercher, W. Drexler, C. K. Hitzenberger, and T. Lasser, Optical coherence tomography - principles and applications, Rep. Prog. Phys. **66**, 239–303 (2003).

165. D. Finch, M. Haltmeier, and Rakesh, Inversion of spherical means and the wave equation in even dimensions, SIAM J. Appl. Math., 68 (2007), 392–412.

166. D. Finch and Rakesh, The spherical mean value operator with centers on a sphere, Inverse Problems, 23 (2007), S37–S49.

167. M. Fink, Time-reversal acoustics, Contemp. Math., 408 (2006), 151–179.

168. G.B. Folland, *Introduction to Partial Differential Equations*, Princeton University Press, Princeton, NJ, 1976.

169. G.B. Folland, *Real Analysis: Modern Techniques and Their Applications* (1st ed.), John Wiley & Sons, New York, 1984.

170. J.P. Fouque, J. Garnier, G. Papanicolaou, and K. Sølna, *Wave Propagation and Time Reversal in Randomly Layered Media,* Springer-Verlag, New York, 2007.

171. A. Friedman and M.S. Vogelius, Identification of small inhomogeneities of extreme conductivity by boundary measurements: a theorem on continuous dependence, Arch. Rat. Mech. Anal., 105 (1989), 299–326.

172. H. Fricke, A mathematical treatment of the electrical conductivity of colloids and cell suspensions, J. General Physio., 4 (1924), 375–383.

173. H. Fricke, A mathematical treatment of the electric conductivity and capacity of disperse systems. I. The electric conductiivty of a suspension of homogeneous spheroids, Phys. Rev., 24 (1924), 575–587.

174. H. Fricke, A mathematical treatment of the electrical conductivity and capacity of disperse systems. II. The capacity of a suspension of conducting spheroids surrounded by a non-conducting membrane for a current of low frequency, Phys. Rev., 26 (1925), 678–681.

175. H. Fricke, The Maxwell-Wagner dispersion in a suspension of ellipsoids, J. Phys. Chem., 57 (1953), 934–937.

176. H. Fricke and S. Morse, The electric capacity of tumors of the breast, J. Cancer Res., 16 (1926), 340–376.

514   References

177. G.P. Galdi, *An Introduction to the Mathematical Theory of the Navier-Stokes Equations, Vol. I, Linearized Steady Problems*, Springer-Verlag, New York, 1994.

178. L. P. Garmirian, A. B. Chin, and S. B. Rutkove, Discriminating neurogenic from myopathic disease via measurement of muscle anisotropy, Muscle Nerve, 39 (2009), 16–24.

179. J. Garnier, Use of random matrix theory for target detection, localization, and reconstruction, Contemp. Math., 548 (2011), 1–19.

180. J. Garnier and G. Papanicolaou, Resolution analysis for imaging with noise, Inverse Problems, 26 (2010), 074001.

181. R. Giannini, C.V. Hafner, and J.F. Löffler, Scaling behavior of individual nanoparticle plasmon resonances, J. Phys. Chem. C, 119 (2015), 6138–6147.

182. M. Giaquinta and E. Giusti, Global $C^{1,\alpha}$ - regularity for second-order quasi-linear elliptic equations in divergence form, Research Report. Centre for Mathematical Analysis, Australian National University, 1983.

183. M. Giaquinta and L. Martinazzi, *An Introduction to the Regularity Theory for Elliptic Systems, Harmonic Maps and Minimal Graphs*, Second edition. Appunti. Scuola Normale Superiore di Pisa (Nuova Serie), 11. Edizioni della Normale, Pisa, 2012.

184. D. Gilbarg and N. S. Trudinger, *Elliptic partial differential equations of second order*, Springer-Verlag, Berlin, 1977.

185. P. Grasland-Mongrain, J.-M. Mari, J.-Y. Chapelon, and C. Lafon, Lorentz force electrical impedance tomography, IRBM, 34 (2013), 357-360.

186. D. Grieser, The plasmonic eigenvalue problem, Rev. Math. Phys. 26 (2014), 1450005.

187. P. Guyot-Sionnest, W. Chen and Y.R. Shen, General consideration on optical second-harmonic generation from surfaces and interfaces, Phys. Rev. B, 33 (1986), 8254–8263.

188. J. Hadamard, Résolution d'une question relative aux déterminants, Bull. Sci. Math., 17 (1893), 30–31.

189. M. Hanke, A. Neubauer, and O. Scherzer, A convergence analysis of the Landweber iteration for nonlinear ill-posed problems, Numer. Math., 72 (1995), 21–37.

190. C.L. Hsieh, R. Grange, Y. Pu, and D. Psaltis, Three-dimensional harmonic holographic microcopy using nanoparticles as probes for cell imaging, Optics Express, 17 (2009), 2880–2891.

191. M.V. de Hoop, L. Qiu, and O. Scherzer, Local analysis of inverse problems: Hölder stability and iterative reconstruction, Inverse Problems, 28 (2012), 045001.

192. C.D. Hopkins and G.W.M. Westby, Time domain processing of electrical organ discharge waveforms by pulse-type electric fish, Brain Behav. Evol., 29 (1986), 77–104.

193. R.A. Horn and C.R. Johnson, *Matrix Analysis*, Cambridge University Press, Cambridge, 1985.

194. B.K.P. Horn and B. Schunk, Determining optical flow, Artificial Intellig., 17 (1981), 185–204.

195. S. Hou, K. Sølna, and H. Zhao, A direct imaging algorithm for extended targets, Inverse Problems, 22 (2006), 1151–1178.

196. S. Hou, K. Sølna, and H. Zhao, Imaging of location and geometry for extended targets using the response matrix, J. Comput. Phys., 199 (2004), 317–338.

197. D. Huang, E. A. Swanson, C. P. Lin, J. S. Schuman, W. G, Stinson, W, Chang, M. R. Hee, T. Flotte, K. Gregory, C. A. Puliafito, and J. G. Fujimoto, Optical coherence tomography, Science **254**, 1178–1181 (1991).

198. P.M. Hui, C. Xu, and D. Stroud, Second-harmonic generation for a dilute suspension of coated particles, Phys. Rev. B, 69 (2004), 014203.

199. Y. Huo, R. Bansal, and Q. Zhu, Modeling of noninvasive microwave characterization of breast tumors, IEEE Trans. Biomedical Eng., 51 (2004), 1089–1094.

200. V. Isakov, *Inverse Source Problems*, AMS, Providence, RI, 1990.

201. V. Isakov, *Inverse Problems for Partial Differential Equations*, Applied Mathematical Sciences, Vol. 127, Springer-Verlag, New York, 1998.

202. P.K. Jain, K.S. Lee, I.H. El-Sayed, and M.A. El-Sayed, Calculated absorption and scattering properties of gold nanoparticles of different size, shape, and composition: Applications in biomedical imaging and biomedicine, J. Phys. Chem. B, 110 (2006), 7238–7248.

203. L. Ji and J. McLaughlin, Recovery of the Lamé parameter μ in biological tissues, Inverse Probl., 20 (2014), 1–24.

204. V. V. Jikov, S. M. Kozlov, and O. A. Oleunik, *Homogenization of Differential Operators and Integral Functionals*, Springer-Verlag, Berlin, 1994.

205. D.J. Jobson, S.J. Katzberg, and R.B. Spiers, Jr., Signal-to-noise analysis and evaluation of the Hadamard imaging technique, NASA Technical Note, D-8377, 1977.

206. I.M. Johnstone, On the distrbution of the largest eigenvalue in principal components analysis, Ann. Statist., 29 (2001), 295–327.

207. J. Jossinet, The impedivity of freshly excised human breast tissue, Physiol. Meas., 19 (1998), 61–75.

208. J. Jossinet, B. Lavandier, and D. Cathignol, The phenomenology of acousto-electric interaction signals in aqueous solutions of electrolytes, Ultrasonics, 36 (1998), 607–613.

209. J. Kaipio and E. Somersalo, *Statistical and Computational Inverse Problems*, Applied Mathematical Sciences, Vol. 160, Springer-Verlag, New York, 2005.

210. K. Kalimeris and O. Scherzer, Photoacoustic imaging in attenuating acoustic media based on strongly causal models, Math. Meth. Appl. Sci., 36 (2013), 2254–2264.

211. H. Kang and J.K. Seo, Layer potential technique for the inverse conductivity problem, Inverse Problems, 12 (1996), 267–278.

212. H. Kang and J.K. Seo, Identification of domains with near-extreme conductivity: Global stability and error estimates, Inverse Problems, 15 (1999), 851–867.

213. H. Kang and J.K. Seo, Inverse conductivity problem with one measurement: Uniqueness of balls in R^3, SIAM J. Appl. Math., 59 (1999), 1533–1539.

214. H. Kang and J.K. Seo, Recent progress in the inverse conductivity problem with single measurement, in *Inverse Problems and Related Fields*, CRC Press, Boca Raton, FL, 2000, 69–80.

215. T. Kato, *Perturbation Theory for Linear Operators* (2nd ed.), Springer-Verlag, Berlin, 1980.

216. S.M. Kay, *Fundamentals of Statistical Signal Processing, Detection Theory*, Englewood Cliffs, Prentice-Hall, 1998.

217. J. B. Keller and D. Givoli, Exact nonreflecting boundary conditions, J . Comput. Phys., 82 (1989), 172–192.

218. J.B. Keller and R.M. Lewis, Asymptotic methods for partial differential equations: the reduced wave equation and Maxwell's equations, in *Surveys in Applied Mathematics, Volume 1*, 1–82, edited by J.B. Keller, D.W. McLaughlin, and G.C. Papanicolaou, Plenum Press, New York, 1995.

219. O.D. Kellogg, *Foundations of Potential Theory*, Dover, New York, 1953.

220. D. Khavinson, M. Putinar, and H.S. Shapiro, Poincaré's variational problem in potential theory, Arch. Ration. Mech. Anal., 185 (2007), 143–184.

221. Y.J. Kim, O. Kwon, J.K. Seo, and E.J. Woo, Uniqueness and convergence of conductivity image reconstruction in magnetic resonance electrical impedance tomography, Inverse Problems, 19 (2003), 1213–1225.

222. S. Kim, O. Kwon, J.K. Seo, and J.R. Yoon, On a nonlinear partial differential equation arising in magnetic resonance electrical impedance imaging, SIAM J. Math. Anal., 34 (2002), 511–526.

223. A. Kirsch, *An Introduction to the Mathematical Theory of Inverse Problems*, Applied Mathematical Sciences, Vol. 120, Springer-Verlag, New York, 1996.

224. A. Kirsch, The MUSIC algorithm and the factorisation method in inverse scattering theory for inhomogeneous media, Inverse Problems, 18 (2002), 1025–1040.

225. L. Klimes, Correlation functions of random media, Pure Appl. Geophys., 159 (2002), 1811–1831.

226. T. Kotnik, D. Miklavcic, and T. Slivnik, Time course of transmembrane voltage induced by time-varying electric fields-a method for theoretical analysis and its application, Bioelectrochemistry and Bioenergetics, 45 (1998), 3–16.

227. R. Kowar, Integral equation models for thermoacoustic imaging of dissipative tissue, Inverse Problems, 26 (2010), 095005 (18pp).

228. R. Kowar, O. Scherzer, and X. Bonnefond, Causality analysis of frequency dependent wave attenuation, Math. Meth. Appl. Sci., 34 (2011), 108–124.

229. S.M. Kozlov, On the domain of variations of added masses, polarization and effective characteristics of composites, J. Appl. Math. Mech., 56 (1992), 102–107.

230. P. Kuchment and L. Kunyansky, Mathematics of photoacoustics and thermoacoustic tomography, in *Handbook of Mathematical Methods in Imaging* (ed: O. Scherzer), Springer-Verlag, New York, 2011.

231. P. Kunchment and L. Kunyansky, Mathematics of thermoacoustic tomography, Europ. J. Appl. Math., 19 (2008), 191–224.

232. L.A. Kunyansky, Explicit inversion formulae for the spherical mean Radon transform, Inverse Probl., 23 (2007), 373–383.

233. L. Kunyansky, A mathematical model and inversion procedure for magneto-acousto-electric tomography, Inverse Problems, 28 (2012), 035002.

234. V.D. Kupradze, *Potential Methods in the Theory of Elasticity*, Daniel Davey & Co., New York, 1965.

235. V.D. Kupradze, T.G. Gegelia, M.O. Basheleishvili, and T.V. Burchuladze, *Three-Dimensional Problems of the Mathematical Theory of Elasticity and Thermoelasticity*, North-Holland Publishing Co., Amsterdam-New York, 1979.

236. O. Kwon, J. Lee and J. Yoon, Equipotential line method for magnetic resonance electrical impedance tomography, Inverse Problems, 18 (2002), 1089–1100.

237. O. Kwon and J.K. Seo, Total size estimation and identification of multiple anomalies in the inverse electrical impedance tomography, Inverse Problems, 17 (2001), 59–75.

238. O. Kwon, J.K. Seo, and J.R. Yoon, A real-time algorithm for the location search of discontinuous conductivities with one measurement, Comm. Pure Appl. Math., 55 (2002), 1–29.

239. O. Kwon, E.J. Woo, J.R. Yoon, and J.K. Seo, Magnetic resonance electrical impedance tomography (MREIT): simulation study of J-substitution algorithm, IEEE Trans. Biomed. Eng., 49 (2002), 160–167.

240. O. Kwon, J.R. Yoon, J.K. Seo, E.J. Woo, and Y.G. Cho, Estimation of anomaly location and size using impedance tomography, IEEE Trans. Biomed. Engr., 50 (2003), 89–96.

241. O.A. Ladyzhenskaya, *The Mathematical Theory of Viscous Incompressible Flow*, Second English Edition, Gordon and Breach, New York, 1969.

242. O. A. Ladyzhenskaya and N. N. Ural'tseva, *Linear and Quasilinear Elliptic Equations*, Translated from the Russian by Scripta Technica, Inc. Translation editor: Leon Ehrenpreis, Academic Press, New York - London, 1968.

243. L.D. Landau and E.M. Lifshitz, *Theory of Elasticity*, Pergamon, London, 1959.

244. H.J. Landau and H. Widom, The eigenvalue distribution of time and frequency limiting, J. Math. Anal. Appl., 77 (1980), 469–481.

245. L. Landweber, An iteration formula for Fredholm integral equations of the first kind, American J. Math., 73 (1951), 615–624.

246. C.L. Lawson and R.J. Hanson, *Solving Least Squares Problems*, vol. 15 of Classics in Applied Mathematics, Society for Industrial and Applied Mathematics (SIAM), Philadelphia, PA, 1995. Revised reprint of the 1974 original.

247. N.N. Lebedev, *Special Functions and Their Applications*, Prentice-Hall, Englewood Cliffs, 1965.

248. T.G. Lee, C.Y. Ahn, O.I. Kwon, and J.K. Seo, A hybrid one-step inversion method for shear modulus imaging using time-harmonic vibrations, Inverse Problems, 26 (2010), 085014.

249. Y.Y. Li and L. Nirenberg, Estimates for elliptic systems from composite material. Dedicated to the memory of Jürgen K. Moser, Comm. Pure Appl. Math., 56 (2003), 892–925.

250. X. Li and B. He, Multi-excitation magnetoacoustic tomography with magnetic induction for bioimpedance imaging, IEEE Trans. Med. Imag., 29 (2010), 1759–1767.

251. X. Li, Y. Xu, and B. He, Imaging electrical impedance from acoustic measurements by means of magnetoacoustic tomography with magnetic induction (MAT-MI), IEEE Trans. Bio. Eng., 54 (2007), 323–330.

252. X. Liang, V. Crecea, and S. Boppart, Dynamic optical coherence elastography: A review, J. Innov. Opt. Health Sci., 3 (2010), 221–233.

253. G. M. Lieberman, Boundary regularity for solutions of degenerate elliptic equations, Nonlinear Anal., 12 (1988), 1203–1219.

254. G. M. Lieberman, The natural generalization of the natural conditions of Ladyzhenskaya and Ural'tseva for elliptic equations, Comm. Partial Differential Equations, 16 (1991), 311–361.

255. M. Lim, *Reconstruction of Inhomogeneities via Boundary Measurements*, Ph.D. thesis, Seoul National University, 2003.

256. S. Link and M.A. El-Sayed, Shape and size dependence of radiative, nonradiative and photothermal properties of gold nanocrystals, Int. Rev. Phys. Chem., 19 (2000), 409–453.

257. C.M. Linton, The Green's function for the two-dimensional Helmholtz equation in periodic domains, J. Eng. Math., 33 (1998), 377–402.

258. J. L. Lions, *Contrôlabilité Exacte, Perturbations et Stabilisation de Systèmes Distribués*, Tome 1, Contrôlabilité exacte, Masson, Paris, 1988.

259. R. Lipton, Inequalities for electric and elastic polarization tensors with applications to random composites. J. Mech. Phys. Solids, 41 (1993), 809–833.

260. J.J. Liu, H.C. Pyo, J.K. Seo, and E.J. Woo, Convergence properties and stability issues in MREIT algorithm, Contemp. Math., 408 (2006), 201–218.

261. S. Mallat, *A Wavelet Tour of Signal Processing*, Academic Press, San Diego, 1998.

262. A. Manduca, T.E. Oliphant, M.A. Dresner, J.L. Mahowald, S.A. Kruse, E. Amromin, J.P. Felmlee, J.F. Greenleaf, and R.L. Ehman, Magnetic resonance elastography: Non-invasive mapping of tissue elasticity, Med. Imag. Anal., 5 (2001), 237–254.

263. L. Mariappan and B. He, Magnetoacoustic tomography with magnetic induction: bioimpedance reconstruction through vector source imaging, IEEE Trans. Med. Imag., 32 (2013), doi:10.1109/TMI.2013.2239656.

264. L. Mariappan, G. Hu, and B. He, Magnetoacoustic tomography with magnetic induction for high-resolution bioimpedance imaging through vector source reconstruction under the static field of MRI magnet, Med. Phys., 41 (2014), 0222902.

265. O.G. Martinsen, S. Grimnes, and H.P. Schwan, Interface phenomena and dielectric properties of biological tissue, Encyclopedia Surface Colloid Sci., 2643–2652, Marcel Dekker, 2002.

266. K. Maslov, H. F. Zhang, and L. V. Wang, Effects of wavelength-dependent fluence attenuation on the noninvasive photoacoustic imaging of hemoglobin oxygen saturation in subcutaneous vasculature in vivo, Inverse Problems, 23 (2007), S113–S122.

267. T.D. Mast, A. Nachman, and R.C. Waag, Focusing and imagining using eigenfunctions of the scattering operator, J. Acoust. Soc. Am., 102 (1997), 715–725.

268. I.D. Mayergoyz, D.R. Fredkin, and Z. Zhang, Electrostatic (plasmon) resonances in nanoparticles, Phys. Rev. B, 72 (2005), 155412.

269. I.D. Mayergoyz and Z. Zhang, Numerical analysis of plasmon resonances in nanoparticules, IEEE Trans. Mag., 42 (2006), 759–762.

270. W. McLean, *Strongly Elliptic Systems and Boundary Integral Equations*, Cambridge University Press, Cambridge, 2000.

271. J. McLaughlin and J.-R. Yoon, Unique identifiability of elastic parameters from time-dependent interior displacement measurement, Inverse Probl., 20 (2004), 25–45.

272. J. McLaughlin, N. Zhang, and A. Manduca, Calculating tissue shear modulus and pressure by $2D$ log-elastographic methods, Inverse Probl., 26:085007, 2010.

273. N.G. Meyers, An l^p-estimate for the gradient of solutions of second order elliptic divergence equations, Ann. Scuola Norm. Sup. Pisa, 3 (1963), 189–206.

274. O.D. Miller, C.W. Hsu, M.T.H. Reid, W. Qiu, B.G. DeLacy, J.D. Joannopoulos, M. Soljacić, and S. G. Johnson, Fundamental limits to extinction by metallic nanoparticles, Phys. Rev. Lett., 112 (2014), 123903.

275. G.W. Milton, *The Theory of Composites*, Cambridge Monographs on Applied and Computational Mathematics, Cambridge University Press, 2001.

276. S. Monsurrò, Homogenization of a two-component composite with interfacial thermal barrier, Adv. Math. Sci. Appl., 13 (2003), 43–63.

277. R. Muthupillai and R.L. Ehman, Magnetic resonance elastography, Nat. Med., 2 (1996), 601–603.

278. W. Naetar and O. Scherzer, Quantitative photoacoustic tomography with piecewise constant material parameters, SIAM J. Imaging Sci. 7 (2014), 1755–1774.

279. A. Nahas, M. Bauer, S. Roux, and A.C. Boccara, 3D static elastography at the micrometer scale using Full Field OCT, Biomedical Opt. Expr., 4 (2013), 2138–2149.

280. F. Natterer, *The Mathematics of Computerized Tomography*, Classics in Applied Mathematics, SIAM, Philadelphia, 2001.

281. F. Natterer and F. Wübbeling, *Mathematical Methods in Image Reconstruction*, SIAM Monographs on Mathematical Modeling and Computation, SIAM, Philadelphia, 2001.

282. J. Nevcas, *Les Méthodes Directes en Théorie des Équations Elliptiques*, Academia, Prague, 1967.

283. J.C. Nédélec, *Acoustic and Electromagnetic Equations. Integral Representations for Harmonic Problems*, Applied Mathematical Sciences, Vol. 144, Springer-Verlag, New-York, 2001.

284. G. Nguestseng, A general convergence result for a functional related to the theory of homogenization, SIAM J. Math. Anal., 20 (1989), 608–623.

285. L.V. Nguyen, A family of inversion formulas in thermoacoustic tomography, Inverse Problems and Imaging, 3 (2009), 649–675.

286. H.L. Nguyen and K. Schmitt, On positive solutions of quasilinear elliptic equations, Differ. Integral Equat., 22 (2009), 829–842.

287. H. Nguyen and M. Vogelius, A representation formula for the voltage perturbations caused by diametrically small conductivity inhomogeneities. Proof of uniform validity, Ann. I. H. Poincaré-AN, 26 (2009), 2283–2315.

288. K. Nightingale, M.S. Soo, R. Nightingale, and G. Trahey, Acoustic radiation force impulse imaging: In vivo demonstration of clinical feasibility, Ultrasound Med. Biol., 28 (2002), 227–235.

289. J. Nocedal and S.J. Wright, *Numerical Optimization*, Springer-Verlag, New York, 1999.

290. H.J. Nussbaumer, *Fast Fourier Transform and Convolution Algorithms*, Springer-Verlag, New York, 1982.

291. K. Patch and M. Haltmeier, Thermoacoustic tomography - ultrasound attenuation artifacts, IEEE Nuclear Science Symposium Conference, 4 (2006), 2604–2606.

292. S. Osher and J.A. Sethian, Fronts propagating with curvature-dependent speed: algorithms based on Hamilton-Jacobi formulations, J. Comput. Phys., 79 (1988), 12–49.

293. V. Palamodov, Remarks on the general Funk transform and thermoacoustic tomography, Inverse Probl. Imaging, 4 (2010), 693–702.

294. S. Palomba, L. Novotny, and R.E. Palmer, Blue-shifted plasmon resonance of individual size-selected gold nanoparticles, Optics Commun., 281 (2008), 480–483.

295. I.G. Petrovsky, *Lectures on Partial Differential Equations*, Dover, New York, 1954.

296. C. Poignard, Asymptotics for steady state voltage potentials in a bidimensional highly contrasted medium with thin layer, Math. Meth. Appl. Sci., 31 (2008), 443–479.

297. C. Poignard, About the transmembrane voltage potential of a biological cell in time-harmonic regime, ESAIM:Proceedings, 26 (2009), 162–179.

298. C. Prada and M. Fink, Eigenmodes of the time-reversal operator: A solution to selective focusing in multiple-target media, Wave Motion, 20 (1994), 151–163.

299. C. Prada, J.L. Thomas, and M. Fink, The iterative time reversal process: Analysis of the convergence, J. Acoust. Soc. Amer., 97 (1995), 62–71.

300. M. H. Protter and H. F. Weinberger, *Maximum Principles in Differential Equations*, Prentice-Hall, 1967.

301. Y. Pu, M. Centurion, and D. Psaltis, Harmonic holography: a new holographic principle, Applied Optics, 47 (2008), A103–A110.

302. C.W. Qiu, L. Hu, B. Zhang, B.I. Wu, S.G. Johnson, and J.D. Joannopoulos, Spherical cloaking using nonlinear transformations for improved segmentation into concentric isotropic coatings, Optics Express, 17 (2009), 13467–13478.

303. M. Razami, A. Mariampillai, C. Sun, V.X.D. Yang, and M.C. Kolios, Biomechanical properties of soft tissue measurement using optical coherence elastography, Proc. SPIE, 8207 (2012), 820758.

304. M. Reed and B. Simon, *Methods of Modern Mathematical Physics. IV Analysis of Operators*, Academic Press, New York, 1970.

305. P.J. La Rivière, J. Zhang, and M.A. Anastasio, Image reconstruction in optoacoustic tomography for dispersive acoustic media, Opt. Lett., 31 (2006), 781–783.

306. J. Rogowska, N.A. Patel, J.G. Fujimoto, and M.E. Brezinski, Optical coherence tomographic elastography technique for measuring deformation and strain of atherosclerotic tissues, Heart, 90 (2004), 556–562.

307. M.W. van Rossum and T.W. Nieuwenhuizen, Multiple scattering of classical waves: microscopy, mesoscopy, and diffusion, Rev. Mod. Phys., 71 (1999), 313–371.

308. B.J. Roth, The role of magnetic forces in biology and medicine, Exp. Biol. Med., 236 (2011), 132–137.

309. B.J. Roth, P.J. Basser, and J.P. Wikswo, Jr., A theoretical model for magneto-acoustic imaging of bioelectric currents, IEEE Trans. Bio. Eng., 41 (1994), 123–728.

310. B.J. Roth and K. Schalte, Ultrasonically-induced Lorentz force tomography, Medical Bio. Eng. Comp., 47 (2009), 573–577.

311. F. Santosa, A level-set approach for inverse problems involving obstacles, ESAIM: COCV, 1 (1996), 17–33.

312. F. Santosa and M.S. Vogelius, A backprojection algorithm for electrical impedance imaging, SIAM J. Appl. Math., 50 (1990), 216–243.

313. D. Sarid, W. A. Challener, *Modern Introduction to Surface Plasmons: Theory, Mathematica Modeling, and Applications*, Cambridge University Press, New York, 2010.

314. L.B. Scaffardi and J.O. Tocho, Size dependence of refractive index of gold nanoparticles, Nanotech., 17 (2006), 1309–1315.

315. O. Scherzer, M. Grasmair, H. Grossauer, M. Haltmeier, F. Lenzen, *Variational Methods in Imaging*, Applied Mathematical Sciences, Vol. 167, Springer-Verlag, New York, 2009.

316. J.M. Schmitt, OCT elastography: imaging microscopic deformation and strain in tissue, Opt. Express, 3 (1998), 199–211.

317. H. P. Schwan, Electrical properties of tissue and cell suspensions, in Advances in Biological and Medical Physics, Lawrence, J.H., Tobias, C.A., Eds.; Acad. Press: New York, vol V, 147–209, 1957.

318. H. P. Schwan, Mechanism responsible for electrical properties of tissues and cell suspensions, Med. Prog. Technol., 19 (1993), 163–165.

319. J. Seberry, B.J. Wysocki, and T.A. Wysocki, On some applications of Hadamard matrices, Metrika, 62 (2005), 221–239.

320. J. K. Seo, T. K. Bera, H. Kwon, and R. Sadleir, Effective admittivity of biological tissues as a coefficient of elliptic PDE, Comput. Math. Meth. Medicine, 2013, Article ID 353849, 10 pages.

321. J.K. Seo, O. Kwon, H. Ammari, and E.J. Woo, Mathematical framework and anomaly estimation algorithm for breast cancer detection using TS2000 configuration, IEEE Trans. Biomedical Eng., 51 (2004), 1898–1906.

322. J.K. Seo and E.J. Woo, *Nonlinear Inverse Problems in Imaging*, Wiley, 2013.

323. A. Shabalin and A. Nobel, Reconstruction of a low-rank matrix in the presence of Gaussian noise, J. Multivariate Anal., 118 (2013), 67–76.

324. D. Slepian, Some comments on Fourier analysis, uncertainty and modeling, SIAM Rev., 25 (1983), 379–393.

325. N.J.A. Sloane, T. Fine, P.G. Phillips, and M. Harwit, Codes for multiplex spectrometry, Appl. Opt., 8 (1969), 2103–2106.

326. D.R. Smith, D.G. Winters, and R.A. Bartels, Submillisecpnd second harmonic holographic imaging of biological specimens in three dimensions, Proc. Natl. Acad. Sci. USA, 110 (2013), 18391–18396.

327. H. Sohr, *The Navier-Stokes Equations: An Elementary Functional Analytic Approach*, Springer, 2012.

328. G.W. Stewart, Perturbation theory for the singular value decomposition, in *SVD and Signal Processing, II: Algorithms, Analysis and Applications*, Elsevier, 1990, 99–109.

329. N.V. Sushilov and R.S.C. Cobbold, Frequency-domain wave equation and its time-domain solutions in attenuating media, J. Acoust. Soc. Am., 115 (2004), 1431–1436.

330. T. L. Szabo. Causal theories and data for acoustic attenuation obeying a frequency power law, J. Acoust. Soc. Amer., 97 (1995), 14–24.

331. M.E. Taylor, *Partial Differential Equations I. Basic Theory*, Applied Mathematical Sciences, Vol. 115, Springer-Verlag, New York, 1996.

332. C.W. Therrien, *Discrete Random Signals and Statistical Signal Processing*, Englewood Cliffs, NJ, Prentice-Hall, 1992.

333. B.E. Treeby and B.T. Cox, Fast, tissue-realistic models of photoacoustic wave propagation for homogeneous attenuating media, Proc. of SPIE, 7177 (2009), 717716.

334. N. Tseng and B.J. Roth, The potential induced in anisotropic tissue by the ultrasonically-induced Lorentz force, Med. Bio. Eng. Compt., 46 (2008), 195–197.

335. M.S. Vogelius and D. Volkov, Asymptotic formulas for perturbations in the electromagnetic fields due to the presence of inhomogeneities, Math. Model. Numer. Anal., 34 (2000), 723–748.

336. L.V. Wang and X. Yang, Boundary conditions in photoacoustic tomography and image reconstruction, J. Biomed. Optics, 12 (2007), 014027.

337. G.N. Watson, *Theory of Bessel Functions*, 2nd edition, Cambridge University Press, Cambridge, 1944.

338. A. Webb, *Introduction to Biomedical Imaging*, IEEE Press Series in Biomedical Engineering, Wiley-Interscience, New Jersey, 2003.

339. P.-A. Wedin, Perturbation bounds in connection with singular value decomposition, BIT Numer. Math., 12 (1972), 99–111.

340. G. Welch and G. Bishop, An introduction to the Kalman filter, (Technical Report 95-041), University of North Carolina at Chapel Hill, 2001 & SIGGRAPH 2001, Los Angeles, CA, August 12–17, ACM.

341. H. Wen, J. Shah, and R.S. Balaban, Hall effect imaging, IEEE Trans. Biomedical Eng., 45 (1998), 119–124.

342. T. Widlak and O. Scherzer, Hybrid tomography for conductivity imaging, Inverse Problems, 28 (2012), 084008.

343. T. Wildak and O. Scherzer, Stability in the linearized problem of quantitative elastography, Inverse Problems, 31 (2015), 035005.

344. R. Wong, Asymptotic expansion of $\int_0^{\pi/2} J_\nu^2(\lambda \cos\theta)d\theta$, Math. Comp., 50 (1988), 229–34.

345. M. Xu and L.V. Wang, Photoacoustic imaging in biomedicine, Rev. Scient. Instrum., 77 (2006), 041101.

346. Y. Xu and B. He, Magnetoacoustic tomography with magnetic induction (MAT-MI), Phys. Med. Bio, 50 (2005), 5175,

347. Y. Xu and L.V. Wang, Reconstructions in limited-view thermoacoustic tomography, Medical Phys., 31 (2004), 724–733.

348. M. Zavelani-Rossi, M. Celebrano, P. Biagioni, D. Polli, M. Finazzi, L. Duò, G. Cerullo, M. Labardi, M. Allegrini, and J. Grand, Near-field second-harmonic generation in single gold nanoparticles, Appl. Phys. Lett., 92 (2008), 093119–093119.

349. L. Zhao, J. Yang, K.W. Wang, and F. Semperlotti, Structural damage detection via impediographic tomography, Proc. SPIE, 9435 (2015), 94350F-1.

350. L. Zhao, J. Yang, K.W. Wang, and F. Semperlotti, An application of impediography to the high sensitivity and high resolution identification of structural damage, Smart Mater. Struct., 24 (2015), 065044.

351. L. Zhou, S. Zhu, and B. He, A reconstruction algorithm of magnetoacoustic tomography with magnetic induction for an acoustically inhomogeneous tissue, IEEE Trans. Bio. Eng., 61 (2014), 1739–1746.

352. J.M. Ziman, *Principles of the Theory of Solids*, Cambridge, 1972.

Index

0–Laplacian, 294, 297

absorption coefficient, 6
absorption cross-section, 75, 444
acoustic wave equation, 273
acousto-electric effect, 11, 293
aliasing artifact, 27
anisotropy, 381, 412
anticausal Green function, 121
asymptotic expansion, 156, 159
attenuation, 207
attenuation coefficient, 208
attenuation law, 208

backprojection algorithm, 114
backpropagation, 177, 182, 188, 476
Banach fixed point theorem, 324
band-limited function, 27
Bessel function, 17
Bessel's equation, 19
Born approximation, 68, 117, 118, 127,
    156, 274, 316, 322, 471, 473

Calderón identity, 48, 55
causal Dirichlet Green function, 120
causality, 28, 208
cell membrane, 383
central limit theorem, 94
CINT algorithm, 188, 189
circular symmetry, 97
closure relation, 22
cluttered medium, 102, 103
Cole-Cole model, 3
compact operator, 32, 50, 88

completeness relation, 22
conditioning formula, 95
conjugate gradient method, 39
conormal derivative, 85
contracted polarization tensor, 454
correlation length, 100, 184, 187, 480
cross correlation, 188
current density, 12, 247, 250, 269, 283,
    335

Debye model, 3, 381, 410
Debye relaxation time, 382, 410, 413
decomposition formula, 60, 65, 66
diffuse optical tomography, 315
diffusion approximation, 7
dilute suspension, 406, 410
dipole, 48
direct imaging, 178, 180, 187
Dirichlet function, 166
discrepancy principle, 37
dispersion relations, 2, 29
displacement field, 78
double-layer potential, 85

effective admittivity, 381
elastic moment tensor, 162, 167
elastic wave equation, 79
elastography, 335, 347, 361
electric permittivity, 159
electrical energy density, 297
electrical impedance tomography, 111,
    294
electrical model of the cell, 383
electrode model, 116